Gas Explosions in Dwellings

The Effects of Interconnected Rooms and Obstacles, and the Interpretation of Thermal Damage

Gary Brian Tomlin

Submitted in accordance with the requirements for the degree of

Doctor of Philosophy

The University of Leeds

Energy Research Institute

School of Chemical and Process Engineering

September 2015

Dedicated to family and friends

my time is yours

INTELLECTUAL PROPERTY

The candidate confirms that the work submitted is his own, except where work which has formed part of jointly-authored publications has been included. The contribution of the candidate and the other authors to this work has been explicitly indicated below. The candidate confirms that appropriate credit has been given within the thesis where reference has been made to the work of others.

The experimental work in this study was carried out in five distinct experimental programmes:

1 Large-scale vented gas explosion tests in a multiple compartment chamber. Conducted in 1984 by the Fire Research Station (FRS) on behalf of Midland Research Station (MRS), this experimental programme was concerned with the propagation of flames from one room to another and the characterisation of thermal damage following a gas explosion.
2 Large-scale vented explosion tests in a 180 m^3 explosion chamber with obstacle arrays. Conducted in 1993 by MRS to characterise an explosion chamber.
3 Large-scale vented explosion tests in a 70 m^3 explosion chamber. Conducted in 2000 by Advantica. The explosion tests carried out in this programme were concerned with the characterisation of thermal damage.
4 Large-scale vented explosion tests carried out in a 70 m^3 explosion chamber. I conducted the explosion tests in this programme, which were concerned with the effects of furniture on vented explosions and the characterisation of thermal damage.
5 Small-scale confined explosion tests carried out in a 1 m^3 explosion vessel located at the University of Leeds. I carried out the explosion tests in this programme, with the assistance of Miss C Huéscar. The tests were concerned with the characterisation of thermal damage.

The results of the experimental work are presented and discussed in Chapters 4, 5 and 6 of the thesis.

Chapter 4

The results of experimental programme 1 are presented in Chapter 4 and Chapter 6 of this thesis.

The experimental work was undertaken by Dr Skippon (MRS) and Mr P Field (FRS). I was responsible for the analysis and interpretation of the experimental results based on a notebook compiled by Dr Skippon and a printed copy of each of the overpressure-time profiles. Dr Skippon provided assistance in the analysis.

Part of the work in Chapter 4 of this thesis has appeared in publication as follows:

Pedersen, H.H., G. Tomlin, P Middha, H.N. Phylaktou and G.E. Andrews. Modelling large-scale vented gas explosions in a twin compartment enclosure. *Journal of Loss Prevention in the Process Industries,* Volume 26 (6), 2013.

Pedersen, H.H., G. Tomlin, P Middha, H.N. Phylaktou and G.E. Andrews. Comparison of FLACS simulations against large-scale vented gas explosion experiments in a twin compartment enclosure. In: *Proc of the Ninth International Symposium on Hazard, Prevention and Mitigation of Industrial Explosions (ISHPMIE)*, 2012, 26pp, Cracow, Poland.

I was responsible for the analysis and interpretation of the experimental work, and co-wrote these publications. H.H. Pedersen carried out CFD analysis using FLACS and co-wrote these publications. The remaining authors discussed the interpretation of results and proof read the publications.

Chapter 5

The results of experimental programmes 2 and 4 are reported in Chapter 5 of this thesis.

The experimental work in programme 2 was carried out by Mr P Cronin (MRS), Mr M Rogers (MRS) and Mr S.G Trim (MRS). I was responsible for the analysis and interpretation of the results in respect of the effects of congestion on pressure generation and flame speed.

I carried out the experimental work in programme 4 and was responsible for the analysis and interpretation of the results.

Part of the work in Chapter 5 of the thesis has appeared in publication as follows:

Tomlin, G.B. and D.M. Johnson. A Large Scale Study of the Venting of Confined Explosions into Unobstructed and Congested Flammable Vapour Clouds. In: *Proc of the Seventh International Symposium on Fire and Explosion Hazards (ISFEH)*, 2013, pp.679-688, Providence, USA.

Tomlin, G.B., D.M. Johnson, P. Cronin, H.N. Phylaktou and G.E. Andrews. The Effect of Vent Size and Congestion in Large-Scale Vented Natural Gas/Air Explosions. *Journal of Loss Prevention in the Process Industries, Volume 35, 2015.*

In the 2013 publication, the analysis and interpretation of the experimental work was undertaken jointly by me and the co-author (2013 publication). In the 2015 publication, I was responsible for the analysis and interpretation of the experimental work, and was the main author. The remaining authors discussed the interpretation of results and proof read the publications.

Chapter 6

The results of experimental programmes 1, 3, 4 and 5 are reported in Chapter 6 of this thesis.

The experimental work in programme 1 was undertaken by Dr Skippon (MRS) and Mr P Field (FRS). The photographing of the marker boards was undertaken by Dr S Skippon of MRS. I was responsible for the analysis and interpretation of the results based on a notebook compiled by Dr Skippon and on an assessment of the archived experimental photographs.

The experimental work in programme 3 was carried out by Mr P Cronin (Advantica) and Dr Walker (Advantica). I was responsible for the analysis and interpretation of the results.

I carried out the experimental work in programme 4. I was also responsible for the analysis and interpretation of the results.

I carried out the experimental work in programme 5 with the assistance of Miss C Huéscar (University of Leeds). I was responsible for the analysis and interpretation of the results. Operation of the SEM was undertaken by Miss C Huéscar.

Part of the work in Chapter 6 of the thesis has appeared in publication as follows:

Tomlin, G.B., H. N. Phylaktou and G. E. Andrews. The Interpretation of Thermal Damage Sustained by a Building and its Décor as a Consequence of a Gas Explosion. In: *Proc of the Seventh International Symposium on Fire and Explosion Hazards (ISFEH)*, 2013, pp.595–604, Providence, USA.

I was responsible for the analysis and interpretation of the experimental work and was the main author of the publication. The co-authors contributed to the analysis and interpretation of the results.

LIST OF PUBLICATIONS AND AWARDS

This research has resulted in the publication of papers in journals and the proceedings of conferences.

Journal Publications:

Pedersen, H.H., G. Tomlin, P Middha, H.N. Phylaktou and G.E. Andrews. Modelling large-scale vented gas explosions in a twin compartment enclosure. *Journal of Loss Prevention in the Process Industries,* Volume 26 (6), 2013.

Johnson, D.M., G.B. Tomlin and D.G. Walker. Detonations and Vapor Cloud Explosions: Why it Matters. *Journal of Loss Prevention in the Process Industries,* 2015.

Tomlin, G.B., D.M. Johnson, P. Cronin, H.N. Phylaktou and G.E. Andrews. The Effect of Vent Size and Congestion in Large-Scale Vented Natural Gas/Air Explosions. *Journal of Loss Prevention in the Process Industries, Volume 35, 2015.*

Conference Publications:

Pedersen, H.H., G. Tomlin, P Middha, H.N. Phylaktou and G.E. Andrews. Comparison of FLACS simulations against large-scale vented gas explosion experiments in a twin compartment enclosure. In: *Proc of the Ninth International Symposium on Hazard, Prevention and Mitigation of Industrial Explosions (ISHPMIE)*, 2012, 26pp, Cracow, Poland.

Tomlin, G.B. and D.M. Johnson. A Large Scale Study of the Venting of Confined Explosions into Unobstructed and Congested Flammable Vapour Clouds. In: *Proc of the Seventh International Symposium on Fire and Explosion Hazards (ISFEH)*, 2013, pp.679-688, Providence, USA.

Tomlin, G.B., H. N. Phylaktou and G. E. Andrews. The Interpretation of Thermal Damage Sustained by a Building and its Décor as a Consequence of a Gas Explosion. In: *Proc of the Seventh International Symposium on Fire and Explosion Hazards (ISFEH)*, 2013, pp.595–604, Providence, USA.

MSc and Intensive CPD Courses:

G. Tomlin., The Investigation of gas explosions. In: *Fire and Explosion Investigation*. MSc Fire and Explosion Engineering, 2013. The University of Leeds.

G. Tomlin., The Investigation of gas explosions. In: *Fire and Explosion Investigation*. MSc Fire and Explosion Engineering, 2014. The University of Leeds.

Awards:

The author was the winner of the Institution of Gas Engineers and Managers (IGEM) 2010 Silver Medal for his contribution to the investigation of gas explosions in dwellings.

ACKNOWLEDGEMENTS

This PhD thesis is the culmination of what seems to have been a life-long interest in gas explosions, and for several years was as much a labour of love as a scientific study. The journey to the submission of this thesis however, has been a long one, perhaps too long, judging by the now all too frequent comments amongst colleagues and friends. I, like so many other PhD students before me, have found the writing-up stage of the study to be exhausting; particularly given that whilst studying, I have been fulfilling my role as Vice President of DNV GLs' Major Hazards Research and Testing group, a role which frequently involves long hours and much travelling. Consequently, this study would not have been possible without the support of many colleagues and friends. If you are reading this Thesis, you are more than likely one of them, and to you, I express my heartfelt thanks.

I would like to express my special appreciation to my supervisor Dr H.N. Phylaktou for his support and guidance throughout this period of research and beyond. He has been a tremendous support for me through some difficult times but also with many laughs along the way (I for one will never forget the attack of the 'midgets' at Spadeadam and the look on his face when he realised he had to surrender his mobile phone). I hope we will remain friends. I would also like to thank him for the countless times he accepted my calls during evenings, weekends and holidays (my study time), and apologise to his wife for the inconvenience I clearly caused (the flowers are on the way). My sincere appreciation also goes to Professor G. E. Andrews for his guidance, encouragement and meaningful debate. He will not know it, but he made me realise that I must have been successful in my field as I am not sure whether what I am doing is work or play.

I would like to thank all past and present colleagues at DNV GL for their valuable contributions to this study; in particular Olav R Hansen for his guidance, Jonathan Minnitt for his constant encouragement, and Alastair Chester and Darren Bird, for their help during the experimental work at Spadeadam. A special mention must go to Mike Johnson, Paul Cronin, Dr Martin Brown and Dr Dave Walker for the numerous discussions, insightful advice, encouragement and assistance; without which I would not have been able to complete this study.

I would also like to thank my co-authors, fellow PhD students and other individuals who have contributed so much to this study through their constructive comments, sharing of ideas and support. In particular, Dr Trygve Skjold , Dr Kees van Wingerden and Helene Hisken Pedersen (GexCon), Clara Huéscar and Professor Derek Bradley (University of

Leeds), Regis Bauwens (FM Global), Professor Elaine Oran (University of Maryland) and Professor Vincent Tam (Kingston University) for their generous assistance and co-operation.

Most importantly, I would like to give a special thanks to my family. This study has been a massive burden for them all and words cannot express how grateful I am for their understanding. Louisa, I know you have made many sacrifices on my behalf, I promise to do my best to make it up to you.

I would like to give a few words of encouragement to fellow PhD students. I am one of a growing ‘band of brothers’ commonly referred to as ‘mature students’. A quick look at a dictionary reveals that mature has several meanings; “complete in natural growth or development, ripe, fully aged, fully developed in body or mind, pertaining to or characteristic of full development, elaborated in full by the mind, no longer developing or expanding; having little or no potential for further growth or expansion; exhausted…..*”.* I hope that I do not match any of those definitions, save perhaps for the last one. During this study, I quickly discovered the paradox of Socrates; realising that the more I learnt, the more I realised how much there was still to learn. This realisation can be frustrating and daunting, particularly if you are studying part time, when each new thing you understand will lead you to another that you don’t, and so on. Don’t give up, PhD’s are not meant to be easy. I am sure, that like me, you will go through periods when you will wonder how you will ever complete the study. Winston Churchill once said; “if you're going through hell, keep going”. These words have helped me through this PhD; I hope they can help you.

ABSTRACT

There are, on average, over twenty-five accidental gas explosions every year in the UK, each requiring an investigation to determine the origin and cause, in order to satisfy regulatory requirements, or for the purposes of criminal or civil litigation. The most important conclusion to be drawn from the investigation is the identification of the source of the gas release. This is most often determined through interpretation of the severity of pressure and thermal damage to the building and its contents.

Guidance in reference books states that gas explosions exhibit characteristic pressure and thermal damage dependent upon the concentration of the fuel/air mixture prior to ignition. It is believed that a number of investigations have resulted in the incorrect apportion of blame as a consequence of the misinterpretation of forensic evidence.

The key objectives of the study were to answer three questions. Firstly, can ignition of a fuel lean or fuel rich mixture cause significant structural damage to a building? Secondly, is it possible to determine the gas concentration in a building, prior to ignition, from the severity of the thermal damage? Thirdly, do materials exposed to a transient flame front always exhibit thermal damage?

The results of four experimental programmes, and over one hundred and fifty explosion tests, are reported in this thesis. Explosion tests were conducted in explosion chambers ranging from 1 m^3 to 180 m^3. Experiments were conducted in single and interconnected enclosures, with and without obstacles (including furniture) and with a number of 'marker' boards to assess the severity of thermal damage. A number of parameters were varied; including, fuel type, concentration, distribution of gas, congestion, ignition position and vent size and failure pressure.

The results demonstrate that under the right conditions, fuel lean and fuel rich explosions can cause overpressures that have the potential to structurally damage buildings (> 200 mbar).

A number of mechanisms have been proposed, detailing the manner in which gas explosions propagate from one room to another. This knowledge provides a valuable new insight into how complex a vented explosion in a typical building can be, and how the design and construction of a building can affect the magnitude of the explosion.

Several causes of the development of high overpressures have been identified; the ignition of a flammable cloud outside the vent opening(s), the sudden increase in mass combustion as a turbulent mixture in a secondary compartment is ignited by a

propagating flame front passing through an interconnecting doorway, and the highly turbulent ‘jetting’ expanding flame, driven by the venting process, propagating through a doorway and towards a vent opening in a secondary enclosure.

Evidence is presented that shows it is possible to generate pressures capable of causing structural damage to buildings with volume blockages of as little as 0.57%, if vent openings do not allow sufficient outflow. However, the obstacle geometry, and its location to other obstacles and the enclosure, were found to be critical in the development, or otherwise, of damaging overpressures.

The experiments have demonstrated that it is possible to use the severity and extent of thermal damage to wall coverings and wood surfaces, sustained during a gas explosion, to provide useful information on the gas concentration, its distribution throughout the building prior to ignition and the depth of any flammable layer. It is demonstrated that it is possible to assess the severity of the thermal damage to various materials in order to estimate the natural gas concentration prior to the explosion to the nearest 2%.

The most suitable materials, in terms of forensic indicators, appear to be softwood covered with either gloss varnish or white oil based gloss paint. Such surfaces are common in buildings as door frames, window frames, etc. However, it is shown that quick drying paints are less susceptible to thermal damage and may cause the misinterpretation of evidence which could lead to an incorrect diagnosis of the origin and cause of an explosion.

In tests where a flammable gas/air layer was present, thermal damage may be observed above the nominal layer boundary (for natural gas), down to the lowest level where the concentration was originally above 8% ± 1%. It is shown to be possible to estimate the layer depth from the damage to an accuracy of approximately 15 cm.

The results of the experimental programmes presented in this thesis, provide new knowledge and understanding of the development of gas explosions in buildings and how this knowledge may be used to better interpret forensic evidence found in a gas explosion.

TABLE OF CONTENTS

LIST OF TABLES

LIST OF FIGURES

NOMENCLATURE

Symbols			
A	Area (m^2)	P_{ext}	Pressure peak due to external explosion (mbar)
C	Carbon number	P_{jeff}	Pressure peak due to jetting expanding flame front (mbar)
D	Diameter (m)	P_{lfo}	Pressure peak due to Helmholtz/Taylor instabilities (mbar)
e	Rate of energy dissipation	P_{mfa}	Pressure peak associated with maximum flame area (mbar)
E	Expansion factor	P_{red}	Maximum pressure in a vented explosion (mbar)
H_C	heat of combustion (MJ/m^3) or (MJ/kg)	P_{stat}	Vent failure pressure (mbar)
K_A	vent coefficient (A/A_V)	P_t	Pressure peak due to turbulent combustion (mbar)
k_s	Karlovitz flame stretch factor	P_V	Pressure peak due to vent opening (mbar)
K_G	cubic-law gas constant	Pe	Peclet number
K_V	vent coefficient ($V^{2/3}/A_V$)	R	Universal gas constant (J/K mol) or (L atm/K mol)
L	Length (m)	Re	Reynolds number
Le	Lewis number	S_f	flame speed (m/s)
Ma	Markstein number	S_g	induced gas velocity (m/s)
MW	Molecular weight (kg/kmol)	S_n	velocity of a curved flame (m/s)
m	Mass (kg)	S_u	burning velocity (m/s)
$\dot{m}$	Mass flow rate (kg/s)	T	Temperature (K)
N	Number of moles	U	Velocity (m/s)
P	Pressure (mbar) or (kN/m^2)	u'	velocity scale
P_{ac}	Pressure peak due to acoustic oscillations (mbar)	V	Volume (m^3)
P_b	Pressure peak due to onset of burnt gas venting (mbar)	$\dot{V}$	volumetric flow rate (m^3/s)

Subscripts		Greek Symbols	
A	Actual or area	ϕ	fuel/air equivalence ratio
a	air	ρ	Density (kg/m^3)
b	burnt	ξ	energy density (MJ/m^3) or (kJ/m^3)
f	fuel	μ	dynamic viscosity (Pa·s) or (kg/m s).
g	gas/air mixture	ν	kinematic viscosity (m^2/s)
l	laminar	ℓ	mean length scale
s	stoichiometric	λ	Taylor microscale
t	turbulent	δ	flame thickness
u	unburnt	η	Kolmogorov microscale
v	vent	β	Turbulence factor

Abbreviations	
AB	area blockage
ABR	Area blockage ratio
AFR	air/fuel ratio
ATEX	Directive for equipment intended for use in potentially explosive atmospheres
AWRE	Atomic Weapons Research Establishment
BCRA	British Ceramic Research Association
BRE	Building Research Establishment
CP	constant pressure
CV	constant volume
ECV	consumer emergency control valve
FAR	fuel/air ratio
fps	Frames per second
FRS	Fire Research Station
GIA	gas in air
GS(M)R	Gas Safety (Management) Regulations
HAZID	Hazard Identification Study
HSE	UK Health and Safety Executive
IGE	Institution of Gas Engineers
LNG	Liquefied Natural Gas
LPG	Liquefied Petroleum Gas
MOD	Ministry of Defence
MRS	Midlands Research Station
NIA	Network Innovation Allowance
NIC	Network Innovation Competition
NFPA	National Fire Protection Association
ONS	Office for National Statistics
OPSO	over pressure shut-off device
RAF	Royal Air Force
SCADA	system control and data acquisition
VB	volume blockage
VBR	volume blockage ratio

PREFACE

This research is related to the investigation of accidental gas explosions in dwellings. It is primarily concerned with the interpretation of forensic evidence found at the scene of an explosion such that the composition and distribution of a fuel/air mixture, prior to its ignition, may be estimated and used to correctly determine the origin and cause of the explosion.

To correctly interpret the forensic evidence presented through pressure generation and thermal damage requires knowledge and understanding of a wide range of scientific and engineering principles, which include, the properties and characteristics of hydrocarbons, the installation of gas distribution and consumer pipework and appliances, the distribution and build-up of flammable mixtures following a release of gas, flame propagation following ignition of a flammable gas/air mixture, the generation of pressure through flame propagation and the response of structures to flame and pressure. Consequently, it was recognised that whilst the task of completing such a broad literature review was a significant challenge, the main objective of the research would only be achievable if a significant part of the experimental work was conducted by others.

Fortunately, my role within the Major Hazards Research and Testing department at DNV GL meant I had access to the results of a number of extensive large-scale experimental programmes that had been undertaken by British Gas Research and Development (including MRS, BG Technology and Advantica), which for budgetary and/or political reasons had not been analysed or published. These research programmes were comprehensive and covered subject matter that still has not been reported in the literature to date. Accordingly, it was decided that it would be of benefit to the explosion research community and gas industry if the results of these experimental programmes were published as part of a wider PhD study. This research therefore consists of the analysis of five distinct experimental programmes to determine the effects of parametric variations on vented gas explosions and to characterise the evidential thermal damage that is a consequence of the exposure to a transient flame front. Of these experimental programmes, two were undertaken by MRS (one in collaboration with FRS), one was undertaken by Advantica and the remaining two were undertaken by me.

The experimental programmes carried out are listed as follows:

1 Large-scale vented gas explosion tests in a multiple compartment chamber. Conducted in 1984 by the Fire Research Station (FRS) on behalf of the Midlands Research Station (MRS). The explosion tests carried out in this programme considered both the effects of interconnected rooms and the characterisation of thermal damage.

2 Large-scale vented explosion tests in a 180 m^3 explosion chamber with obstacle arrays. Conducted in 1993 by MRS to characterise an explosion chamber, this experimental work has been analysed by the author with regard to the effects of congestion on pressure generation and flame speed.

3 Large-scale vented explosion tests in a 70 m^3 explosion chamber. Conducted in 2000 by Advantica. The explosion tests carried out in this programme were concerned with the characterisation of thermal damage.

4 Large-scale vented explosion tests carried out in a 70 m^3 explosion chamber. The explosion tests carried out in this programme were conducted by the author and were concerned with the effects of furniture on vented explosions and the characterisation of thermal damage.

5 Small-scale confined explosion tests carried out in a 1 m^3 explosion vessel located at the University of Leeds. The explosion tests carried out in this programme were conducted by the author and Clara Huéscar and were concerned with the characterisation of thermal damage.

CHAPTER 1
GAS EXPLOSIONS IN DWELLINGS

CHAPTER 1

GAS EXPLOSIONS IN DWELLINGS

1.1. Introduction

Natural gas and LPG are common fuels that have been used safely in the home for many decades. However, when there is a release of gas within a dwelling, or gas escaping from a leaking main or service migrates into a building, an explosion may occur, resulting in a rapid, uncontrolled liberation of energy. The sequence of events leading to an explosion in a dwelling are shown in Figure 1-1, which shows that specific conditions in respect of the concentration of gas are needed, together with a source of ignition, before an explosion can occur.

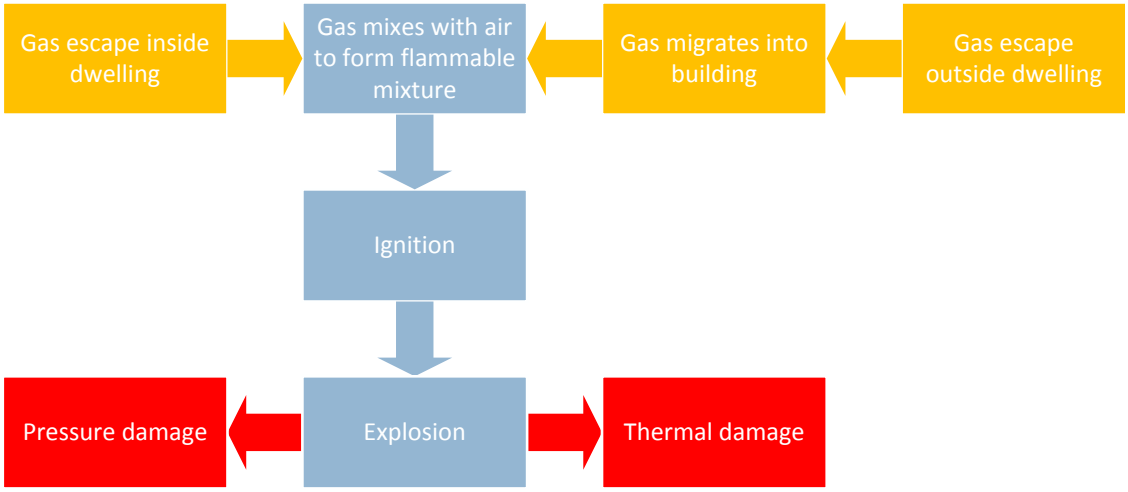

Figure 1-1 Sequence of events required to cause a gas explosion

To help prevent explosions, natural gas and LPG are odorised, which makes an escape of gas detectible at very small concentrations (20% of the lower flammability limit; i.e. 1% gas in air for natural gas and 0.4% gas in air for LPG). Furthermore, the UK gas industry has a dedicated emergency service that responds to reported gas escapes 24 hours/day and 365 days/year. This service, combined with a buried pipework replacement programme (replacing ageing metallic gas mains and service pipes) and the enforcement of stringent regulation and standards governing the correct installation and maintenance of gas pipework and appliances [1] means that the likelihood of a gas explosion is relatively low. In a 12 month period during 2012/13, there were twenty-six gas explosions in dwellings in the UK [2], with the number of households recorded at 26.4 million [3].

During the same period, there were over 16,000 public reported gas escapes, of which there were 686 occurrences where gas escaping from an outside gas main or service entered an adjacent building [4]. These gas-in-building events represent a significantly higher fire and explosion risk to members of the public than external gas escapes and are a strong indicator of the safety of the gas network.

The UK Health and Safety Executive (HSE) statistics on reported gas escapes, gas-in-building events and gas explosions [2, 4] demonstrate that only a small proportion of gas escapes (< 4%) have the potential to cause the build-up of a flammable layer within a dwelling, and of those only a fraction actually lead to an explosion. Ideally, the safety measures described above would eliminate the occurrence of explosions, but in practice it is not possible to guarantee that a hazardous situation will not arise (e.g. during the same 12 month period of 2012/13, 115 buried gas pipes were damaged by third parties during excavation works). Nevertheless, the overall risk of being killed in a gas explosion in a dwelling is very low, and this is reflected in a comparison of the relative hazard from different sources of risk in the UK given in Table 1-1. The risk values have been calculated using 2012/2013 Office for National Statistics (ONS) and HSE fatality data [2, 5, 6], and by assuming a UK population of 63.7 million [7].

Table 1-1 Comparison of gas explosions with some every day risks

Cause of Death	Annual Risk of Death	Annual Risk/Million People
Cancer	1 in 390	2564
Heart disease	1 in 404	2475
Respiratory disease	1 in 809	1236
Road traffic accident	1 in 35,280	28
Homicide	1 in 96,690	10
Accident at work	1 in 347,648	2.9
Lightning strike	1 in 20,627,133	0.05
Gas explosion	1 in 30,940,700	0.03

Whilst the risk of an explosion in the UK has been shown to be small, there are still, on average, over twenty-five accidental gas explosions every year. These explosions, on average each year, cause two fatalities, thirty-two non-fatal injuries [2], and cost the UK millions of pounds. Indeed, in 2005, Transco received the UK's largest fine, £15 million, for causing a gas explosion in a bungalow in Larkhall, Lanarkshire, which tragically killed four persons.

To reduce the number of gas explosions, the HSE have developed a legislative framework that requires conveyors of gas to investigate releases that could have resulted in a fire or an explosion, to determine the source of the release and the reason for it. This framework is enacted under the Health and safety at Work etc. Act 1974 [8] and enforced through the Gas Safety (Management) Regulations 1996 (GS(M)R) [9].

1.2. The Investigation of Gas Explosions

The investigation of explosions in buildings is undertaken by a number of parties including regulatory and enforcing bodies (e.g. HSE), fire investigators and forensic scientists and engineers working on behalf of gas conveyors and insurers. The range of activities carried out by such parties include extensive origin and cause investigations required for the purposes of criminal or civil litigation through to carrying out specific undertakings such as pipeline testing, failure analysis or solving complex technical issues.

Burgoyne [10, 11] detailed the preferred approach to the investigation of fires and explosions; recommending that ‘a proper investigation should be of the nature of a research project in which a hypothesis is formed, tested and refined until it is in the fullest possible conformity with the facts ascertained’. More recently, updated versions of NFPA 921: Guide for Fire and Explosion Investigations [12] and IGE/GL/8: Reporting and Investigating of Gas Related Incidents [13] have been published, further recommending the use of this ‘scientific method’ of investigating incidents.

NFPA 921 provides scientifically based guidance for the systematic investigation and/or analysis of fire and explosion incidents. As it is a guide, the recommendations are informative and advisory in nature and are not mandatory. However, courts in the USA are using NFPA 921 as the industry standard and benchmark to determine if the methodology used by an expert in conducting an investigation or forming a conclusion was reliable. In these courts, failure to use the scientific method jeopardises the conclusions of an investigation. An adaptation of the scientific method outlined in NFPA 921, as applied to explosion investigation, is shown in Figure 1-2.

In keeping with the philosophy of investigation outlined above, the investigation should normally proceed from a detailed examination of the damage caused by the explosion, through a scientific and logical interpretation of the evidence, to arrive at conclusions as to the cause of the incident that are consistent with the facts.

In some cases, the purpose of the investigation will not be to determine origin and cause but to solve a complex technical problem or answer specific questions as part of a wider investigation or regulatory requirement.

In these cases, the general principles outlined in Figure 1-2 still apply. However, the scope of the work would define the issues that need to be addressed during the investigation and the hypotheses that need to be tested against the available evidence.

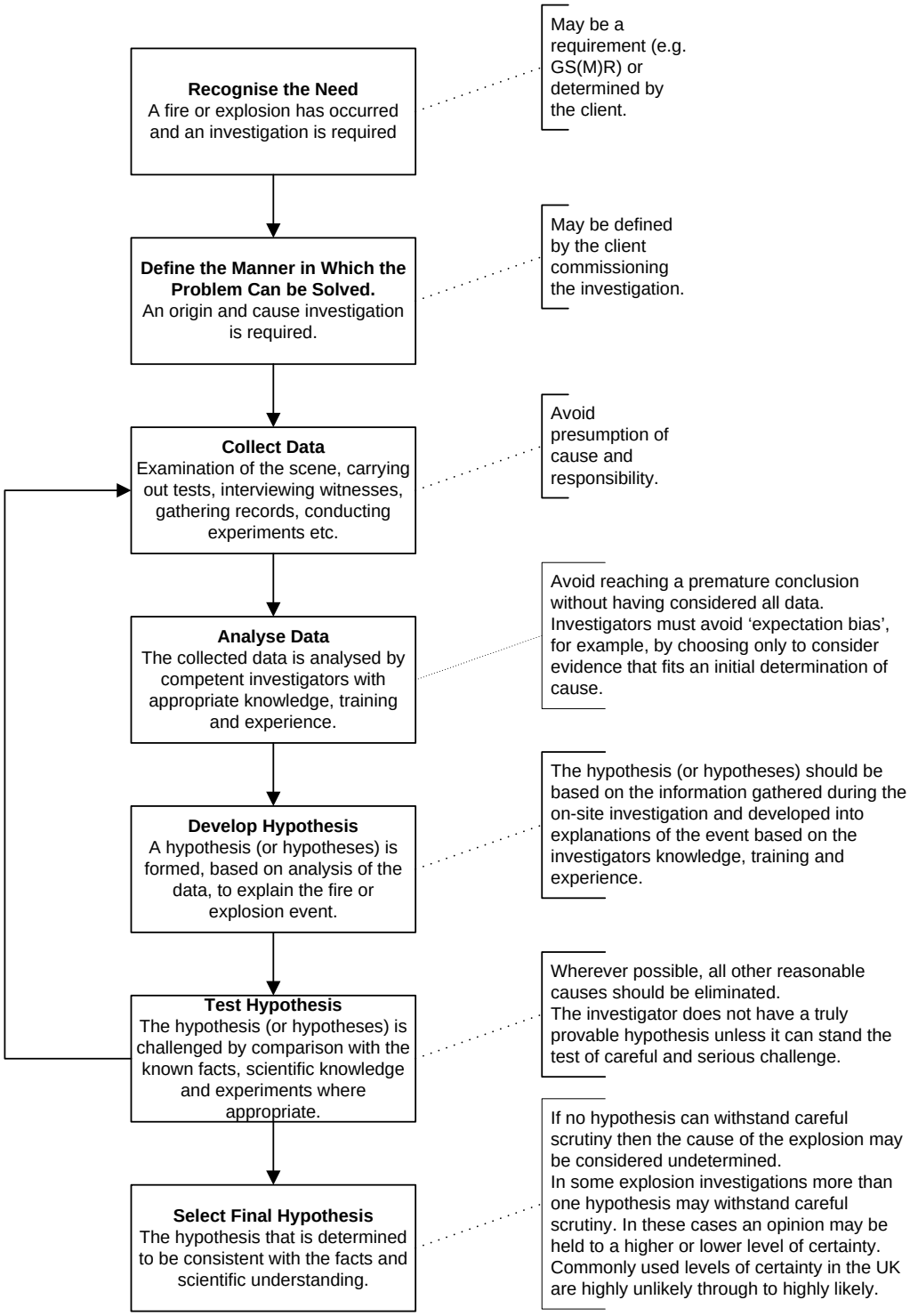

Figure 1-2 The Scientific Method (adapted from NFPA 921 [12])

A particular example of where an investigation may be limited in its scope arises from the UK GS(M)R [9]. These Regulations place requirements on the gas conveyor to carry out an investigation if an escape of gas has resulted in a fire or explosion. The investigation shall meet the following criteria:

- for a fire or explosion resulting from a gas escape downstream of the consumers emergency control valve (ECV), the scope of the investigation has to be sufficient to identify, so far as is reasonably practicable, whether the gas escape was from installation pipework or from an appliance and, if the latter, which appliance.
- for a fire or explosion resulting from a gas escape upstream of the ECV (i.e. from the gas main or services), the scope of the investigation has to be sufficient to establish the source of the gas escape, and so far as is reasonably practicable, the reason for it.

Therefore, the purpose of a GS(M)R investigation is to determine, so far as is reasonably practicable, the source of the escape and, where appropriate, the cause. There is no specific requirement to determine the source of ignition or the gas concentration at the time of ignition etc. The gas conveyor may therefore limit the investigation to answering questions relating to the gas tightness (or otherwise) of the network, installation pipework, meter and any appliance(s). In such cases the evidence should be tested against these questions.

In order to carry out an effective on-site investigation of a gas explosion it is necessary to have a thorough understanding of the following:

- gas industry legislation and standards,
- the properties and characteristics of hydrocarbons,
- fracture mechanics and material properties of pipes,
- metallurgy and corrosion mechanics,
- gas tracking/movement through soils,
- gas build-up in buildings and enclosures,
- ignition,
- explosion physics (flame propagation, pressure generation etc.),
- fire chemistry/physics, and
- response of structures to flame/pressure.

For the practicing gas explosion investigator, there are a number of textbooks [12-22] that provide guidance on some of the topics mentioned above. However, none really provide a comprehensive coverage of all of the required subjects, as well as equipping the reader with the necessary skills to undertake a gas explosion investigation in a dwelling.

The most widely used reference for investigating gas explosions is that written by Harris [16], in one of a series of British Gas Research and Development monographs. The monograph presents some of the results of experimental work carried out predominately by British Gas' Midlands Research Station (MRS), including information on the generation of pressure in confined vented explosions, the effect of explosion pressures on structures and structural components, and also providing guidance on how to investigate gas explosion incidents. Whilst it was published in 1983, it remains the most common reference for gas explosion investigators worldwide. Furthermore, the recently published edition of NFPA 921 [12], "Guide for Fire & Explosion Investigations", which has a completely revised chapter on explosions, and Foster [15], still make significant reference to the British Gas explosion monograph.

1.3. Explosions Propagating from One Room to Another

On the 16th of May 1968, an accidental gas explosion occurred at Ronan Point, a twenty-two storey tower block in Newham, East London [23]; that was to shape legislation for the gas industry, initiate a significant body of research into gas explosions and introduce new regulations relating to the construction of dwellings of five storeys or more.

The explosion occurred in a one-bedroom flat located on the south-east corner of the eighteenth floor of the twenty-two storey tower block, tragically killing four people and injuring seventeen others.

The subsequent Inquiry into the incident determined that a defective cooker connection in the kitchen of Flat 90 had allowed gas to escape, resulting in the build-up of a high level layer of flammable town gas/air mixture throughout the flat (perhaps excluding the bathroom as the door was known to have been closed) [23]. This mixture was ignited when the occupant attempted to light the cooker hob. The Inquiry reported that the damage to the tower block was caused by a pressure pulse of at least 205 mbar, with a maximum overpressure likely approaching 830 mbar in the hall of the flat where the explosion took place.

The explosion blew out the façade of the non-load bearing kitchen and living room walls and crucially, also removed the external load bearing flank walls of the living room and bedroom. Consequently, the floor slab above collapsed and the flank walls and floors followed, resulting in the progressive collapse of the south-east corner of the tower block (see Figure 1-3). It is worth noting that it was the collapse of the building and not the explosion itself that caused the fatality and the majority of the injuries. Indeed, the occupant of Flat 90 survived the incident.

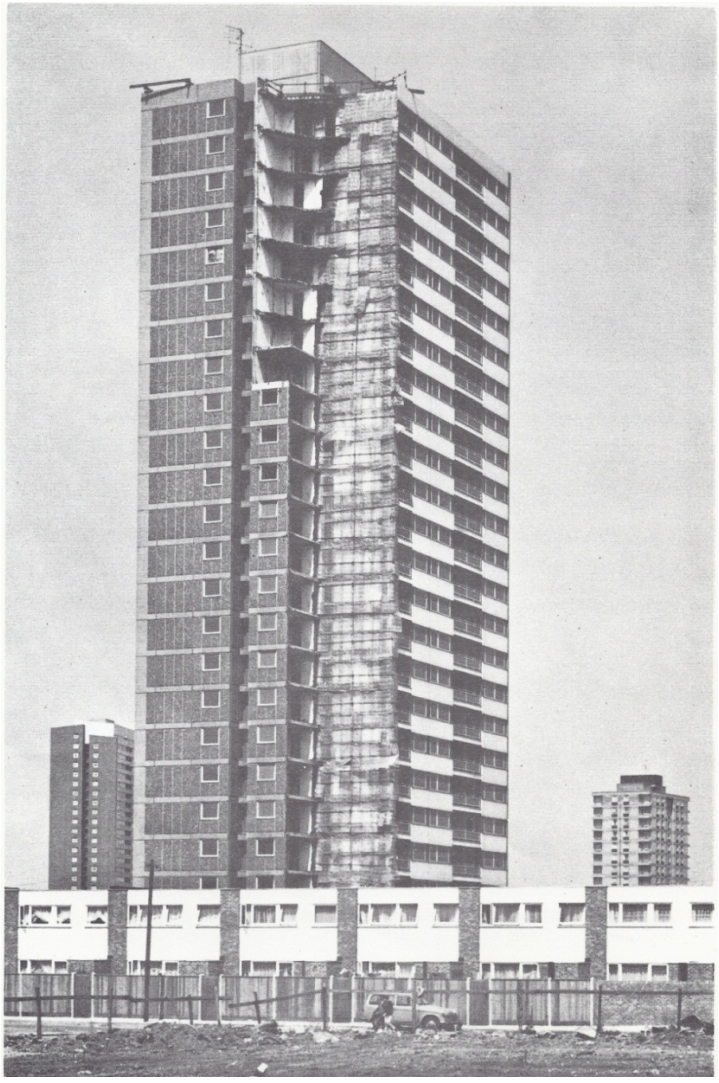

Figure 1-3 Ronan Point after the explosion (photo from DNV GL archive)

Whilst the potential for gas explosions to damage dwellings was understood prior to this explosion, little research into the causes, mechanisms and effects of such explosions had been undertaken. Indeed, much of the information used to estimate the damage an explosion could cause to a building, was gained from a series of nuclear tests undertaken by the US Atomic Energy Commission to determine the effects of nuclear weapons [24].

Consequently, an extensive experimental programme to investigate gas explosions in multi-storey load bearing brick structures was carried out by the British Ceramic Research Association (BCRA) in collaboration with the Midlands Research Station (British Gas Corporation Research & Development Division) and the Atomic Weapons Research Establishment (AWRE) [25]. The tests took place at Potters Marston in Leicestershire with the primary objective of determining the integrity of the load bearing brickwork when subjected to pressure pulses generated in accidental gas explosions. A limited number of tests were also undertaken to determine the effects of explosions propagating from one room to another.

The tests carried out to examine the effects of so called ‘cascade’ explosions proceeding from one room to another, were undertaken in a purpose built full-scale building designed to simulate the top three floors of a cross-wall tower block. During one of the tests, where both rooms had a high level gas/air layer of stoichiometric concentration, major damage was caused to the building structure. It was believed that the explosion in the first room, which developed a pressure of 90 mbar, passed through the door into the second room causing a ‘cascade effect’, which resulted in a significantly higher pressure of 228 mbar being recorded.

Because of the higher overpressure that was developed within the second room and the damage that was caused to the brickwork of the building, there was significant interest in the results of this test. As a consequence, two separate programmes of further tests were planned in order to improve understanding of explosions that propagate from one room to another. The first set of explosion tests was undertaken by the Fire Research Station (FRS) in a bunker containing two partitions, each with large openings [26].

In this series of tests, a high level layer, 0.9 m in depth from the ceiling was ignited. The results demonstrated that it was possible to generate substantially larger pressures in an explosion that propagated from one room to another than would be expected in an explosion in a single room, even if the single room was completely filled with a stoichiometric gas/air mixture. However, the enhanced explosion pressures were only attained over a narrow gas concentration range.

The second series of tests focussed on the effects of different layering conditions in the pair of rooms and was undertaken at Potters Marston by BCRA in collaboration with the Midlands Research Station (MRS), AWRE and FRS [27]. These tests were to include layers of both neat gas and gas/air mixtures. Due to time constraints, and because the building suffered extensive damage, the series of tests were not completed.

However, it was demonstrated that under certain conditions, it was possible to generate higher pressures in explosions where there was an interaction between adjoining rooms than that of an explosion in a single room [27].

Whilst the various programmes of experimental work had generated some data on ‘cascade’ explosions, only a limited number of conclusions were able to be drawn concerning the nature of this type of event.

By the early 1980’s, many more experimental and theoretical studies into confined gas explosions had been completed, for example Solberg et al. [28-32], MacFadyen and Tite [33], Tite [34, 35], Hammond [36] and Zalosh [37]. However, British Gas Research and Development were conscious that most of this work had been restricted to simple, single enclosures of cuboid or spherical geometry. Very few studies had been made of gas explosions in typical room sized enclosures, and still fewer of explosions in multiple compartments. The large multiple compartment case is clearly of importance, since it is typical of domestic, commercial and industrial premises.

Accordingly, in order to provide a more detailed understanding of the mechanism of gas explosions in large and multiple compartment enclosures, typical of a dwelling, a comprehensive experimental programme was begun by British Gas Research and Development and FRS. This programme was completed in 1983, but only a summary of the work was disseminated internally and the main body of the work was not analysed in detail or published. The results of this experimental programme will be analysed as part of this research.

Since this extensive programme of research was undertaken in the early 1980’s, no further large-scale vented gas explosion studies have been undertaken using enclosures that represent the conditions encountered in an accidental explosion in a dwelling.

1.4. The Effect of Furniture on Gas Explosions

When a gas explosion occurs in a confined enclosure or vessel, there is an associated pressure rise. The pressure rise is caused by the restriction, that the vessel or enclosure places on the expansion of the hot burnt gases. In accidental explosions, the dwelling is often inadvertently vented, when a weak part of the structure fails (i.e. a window), and the pressure is relieved. Up until this point the explosion may be considered as a confined explosion, but after venting begins, the rate of pressure rise, and hence the maximum pressure developed, is governed by the balance between the rate at which combustion products are produced and the rate of outflow through the venting process.

The rate at which hot combustion products are produced is directly related to the burning velocity of the fuel, and consequently, the rate of pressure rise in an accidental explosion is strongly dependent upon the fuels composition.

The laminar burning velocity for most stoichiometric hydrocarbon gas/air mixtures is in the order of 0.4 m/s, but will increase if the chemical reaction takes place in a turbulent flow field. The turbulence in the gas/air mixture can be developed by jet mixing prior to ignition or by interaction of the unburnt gas/air mixture, pushed ahead of the flame by the expanding flame front, with obstacles located within the enclosure (Figure 1-4).

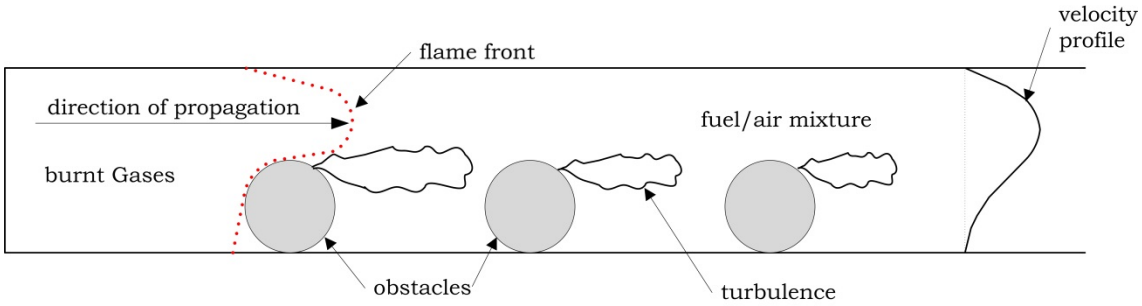

Figure 1-4 Turbulence generation due to obstacles in a vented explosion (taken from Bjerketvedt et al. [14])

It is widely accepted that the acceleration of a propagating flame is enhanced when a solid obstacle is located in its path [38-44], with the degree of enhancement being strongly dependent on the flow structure that is formed in the wake behind the obstruction. Moreover, data from large-scale experiments, for example, Bauwens et al. [45], Hjertager et al. [46], Moen et al. [47] and Bimson et al. [48] have demonstrated that flame speed and pressure also have a strong dependence on obstruction size and gas concentration. However, it is also clear from further experimental studies that are relevant to gas explosions in buildings [29, 31, 33, 37, 45, 46, 49-64], that the acceleration of the flame front is a consequence of a complex interaction of many factors, including the size and geometry of the enclosure, local obstructions, instabilities and pressure wave interactions.

Most flame acceleration studies to date (referenced above) have been undertaken using baffle-type or cylindrical obstacles that are representative of congested regions typically found in process plants (e.g. pipe racks etc.). Accidental explosions in dwellings are likely to be affected by obstructions that are non-uniform (furniture etc.) and may be sharp edged, and as a consequence the flame front is likely to interact in a different manner. A detailed review of large-scale vented explosion tests with obstacles will be presented in the next chapter.

The enhancement of the combustion process, and hence increased overpressure, as a consequence of the generation of turbulence is of great significance and determines the degree of damage that a building sustains during a gas explosion. Current guidance suggests that extensive pressure damage is not usually associated with either lean or rich mixtures [12, 16, 65]. Consequently, a better understanding of the mechanism of flow interaction through interconnected rooms, and of the interaction of the induced flow with furniture in a dwelling (both of which topics are explicitly addressed in this project), would greatly assist explosion investigators and may contribute to changes to building codes and gas safety standards that would improve public safety.

1.5. Thermal Damage Sustained During Explosions

Following an accidental gas explosion, a detailed examination of the thermal damage (scorching, blistering etc.) caused by the explosion, can provide critical evidence to the investigator [16]. The investigator will be able to determine the rooms through which the flame propagated (and hence where a flammable gas/air mixture was present prior to ignition), whether the flammable gas involved was more or less dense than air, and the depth of any flammable layer. This information may then be used to determine any credible sources of gas by calculating or measuring the release rate and estimating whether an escape of this magnitude is capable of mixing with air to form a flammable layer, or completely full mixture, which is in agreement with the scorching patterns.

Following the release of a lighter than air gas, such as natural gas, a layer of flammable gas/air mixture will accumulate extending downwards from the ceiling to the location of the release source [66-71]. If the flammable mixture is subsequently ignited, the flame will propagate through the gas/air mixture at high level, and, because of high temperature and low density, the hot gases will rise and preferentially stay at high level. Consequently, evidence of the passage of the flame is expected to be found at high rather than low level.

In contrast, explosions involving layers of heavier than air gases, such as LPG, will exhibit thermal damage at low level, from the point of leakage down to floor level. In these situations, more burning should be evident at low level, such as scorching to carpets, furniture etc., than at ceiling level.

Figure 1-5 Evidence of thermal damage following a layered LPG explosion (photo taken by the author)

Other evidence as to the nature of the gas involved (e.g. its relative density) might be provided by the pattern of burn injuries suffered by individuals in the room through which the flame propagates. Although ordinary clothing provides some degree of short term protection against a transient explosion flame. Burns to the head and upper part of the body, but not the legs and lower torso, are indications that a layer of a buoyant gas had been involved (e.g. natural gas). If burns were restricted to the lower part of the body, this provides an indication that the explosion involved a heavier than air gas such as LPG or petrol vapour. However, caution should be taken when using this type of information, as hot combustion products are much more buoyant than air and may cause burn injuries to the upper part of the body, potentially providing a false indication that the fuel involved is lighter than air.

1.6. Forensic Evidence

The damage sustained by a building, and its decor, during an explosion can provide useful forensic evidence in the subsequent investigation. In particular, the pressure generated and the thermal damage sustained in an explosion can provide information in terms of the composition and distribution of the fuel/air mixture prior to ignition. This information is critical to the success of the investigation in determining the origin and cause of the explosion.

The level of damage a building sustains following a gas explosion is dependent upon the magnitude of the pressure generated and the relationship between the duration of the imposed pressure load and the natural period of vibration of the structure. Studies have shown that an overpressure generated by a gas explosion, in the region of 200 mbar, has the potential to cause significant structural damage to a properly designed and constructed building. [16, 25, 72-75]. Guidance in the most widely used reference material [12, 15, 16] states that extensive thermal damage to decor, furnishings etc. is associated with fuel/air mixtures of stoichiometric or greater concentrations, whilst an explosion involving a fuel lean concentration will exhibit little signs of thermal damage. Consequently, the following interpretation of evidence is given by Harris [16] and Foster [15] for use during accidental gas explosion investigations:

i. minimal structural damage (i.e. a low overpressure) and little evidence of thermal damage is indicative of an ignition of a lean fuel/air mixture.
ii. significant structural damage (i.e. a high overpressure) and extensive scorching, blistering etc. is indicative of an ignition of a near stoichiometric fuel/air mixture.
iii. minimal structural damage (i.e. a low overpressure) and significant evidence of burning is indicative of an ignition of a rich fuel/air mixture.

A number of gas explosions investigated by the author of this study and other members of the DNV GL incident investigation team, have exhibited forensic evidence that has not been in agreement with the information given above. In particular, there have been incidents where the building has suffered significant structural damage (i.e. indicative of a near stoichiometric mixture) but there has been very little, and in some cases, no evidence of thermal damage (see Figure 1-6).

It was believed that this apparent discrepancy in forensic evidence may be attributed to one or more of the following:

i. the effects of turbulence caused by flame propagation through a dwelling with interconnected rooms;
ii. the effects of turbulence caused by non-uniform obstacles such as furniture etc. that are commonly found in occupied buildings;
iii. the use of paints and other construction materials that are not susceptible to thermal damage during an explosion.

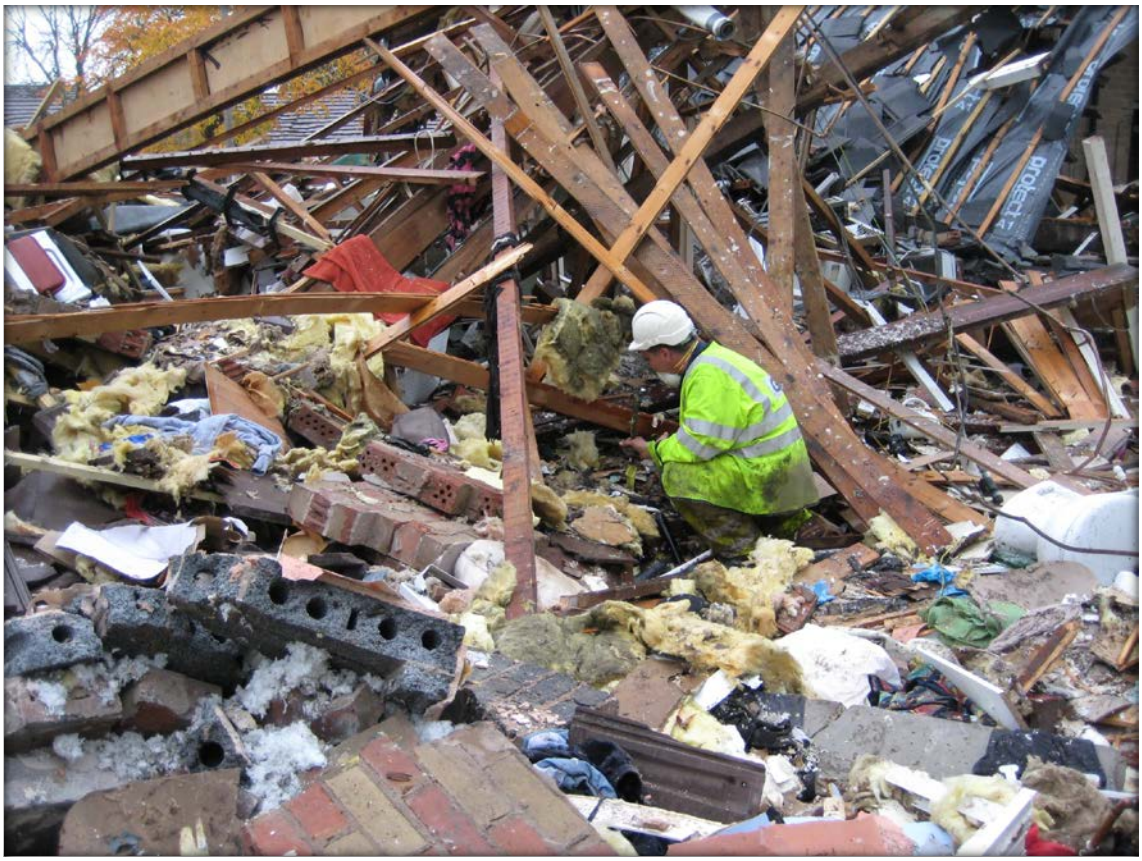

Figure 1-6 The author at the scene of a gas explosion

1.7. Aims of the Research

Whilst much experimental work has now been conducted into confined vented explosions in empty enclosures and flame acceleration by obstacles and other means (e.g. bends in ducts etc.) that are associated with vapour cloud explosions, little work has been undertaken on flame acceleration mechanisms of explosions that occur in typical occupied buildings. Furthermore, to the authors' knowledge, other than the very brief coverage in the British Gas explosion monograph, no other experimental studies have been published concerning thermal damage sustained during a gas explosion in a dwelling. Therefore, the main aims of this research were to investigate and improve understanding of the following:

1. the effects of interconnected rooms on gas explosions;
2. the effects of furniture on gas explosions;
3. the thermal damage sustained during a gas explosion in a dwelling.

The main purpose of the work was to assist investigators with the interpretation of forensic evidence found at the scene of an explosion such that the composition and distribution of a fuel/air mixture, prior to its ignition, could be estimated and used to correctly determine the origin and cause of the explosion.

CHAPTER 2
LITERATURE REVIEW

CHAPTER 2

LITERATURE REVIEW

2.1. Introduction

The purpose of this chapter is to provide an overview of the fundamental parameters associated with gas explosions in dwellings and to discuss the influence of multiple compartments and obstacles (typically found in dwellings) on pressure generation. The interpretation of forensic evidence found at the scene of an accidental gas explosion is also discussed.

An abundance of research has been published regarding confined vented explosions and the effects of turbulence on the combustion process. However, much of this work has been conducted using empty single chambers of cuboid or spherical geometries, which are not representative of those conditions encountered in accidental gas explosions in dwellings. Few studies have been carried out in large (room sized) enclosures and even fewer still have been conducted in multiple compartments. As it is not practical to present all the information available relating to confined vented explosions, and consequently, explosions in dwellings, this chapter outlines the important parameters of vented explosions but concentrates on research concerning:

- the effects of multiple compartments with interconnecting doorways,
- the effects of obstacles typically found in dwellings, and
- the thermal damage associated with the exposure to a transient flame front.

2.2. Fundamentals of Gas Explosion Theory

An explosion in a building may be considered as an exothermic reaction that gives rise to a rapid increase in pressure. Explosions require a level of premixing of the fuel with an oxidant (typically oxygen from air) and confinement or congestion in order for pressure to be generated. Before considering the mechanisms involved in the development of accidental gas explosions and the important forensic evidence which may be used by the explosion investigator to determine the origin and cause of the explosion, it is beneficial to describe some of the fundamental explosion parameters.

Some values for relevant combustion parameters of different gas/air mixtures are also given. This information is required in order to understand some of the principles and interpret some of the analysis described in later chapters.

Combustion may be described as a chemical reaction involving a fuel and air which emits energy and light. Flame is the visible oxidation process of the fuel gas. For combustion to take place, the following conditions must be satisfied:

1. the fuel must be in its gaseous phase (liquid fuels must vaporise and solids pyrolyze);
2. sufficient air must be available, and adequately mixed with the fuel;
3. adequate energy must be available to initiate ignition.

Combustion of gas/air mixtures has been studied extensively for decades and consequently there is a wealth of information available. For a detailed consideration of combustion, reference should be made to standard reference texts such as Lewis and von Elbe [76], Griffiths and Barnard [77], Williams [78], Strehlow [79], Mishra [80], Drysdale [81], Kuo [82] and Kuo and Acharya [83].

2.2.1. Flammability Limits

For gas/air mixtures there are limits of composition between which flame propagation can occur but outside which self-sustaining flames cannot exist. These limits are known as the 'flammability limits' and are usually expressed as percentages of gas in air by volume.

The lower flammability limit (LFL), also known as the lower explosive limit (LEL), is the fuel lean concentration below which a flame will not propagate. The upper flammability limit (UFL), also known as the upper explosive limit (UEL), is the fuel rich concentration above which a flame will not propagate.

Increasing the temperature of a gas/air mixture has the effect of widening the limits of flammability. This is an important concept to understand as a gas/air mixture which is non-flammable at ambient conditions may become flammable if the mixture temperature is increased. This effect is highlighted in Figure 2-1. Furthermore, increasing the pressure widens the limits of flammability but decreasing the pressure narrows the limits.

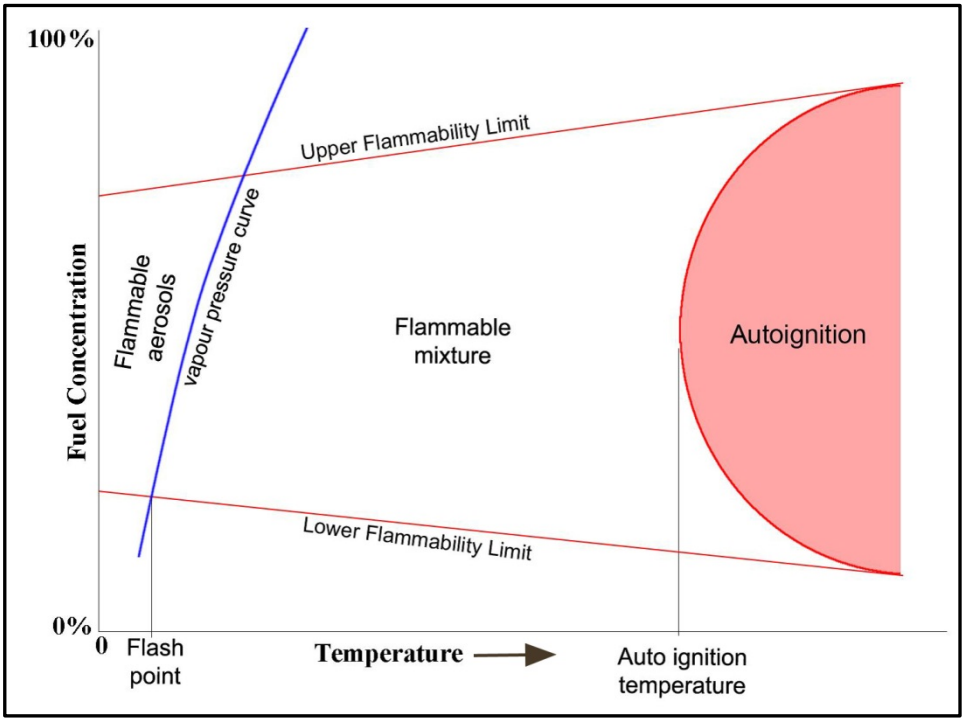

Figure 2-1 Schematic of the effects of temperature on the limits of flammability (taken from Zabetakis [84])

Values for flammability limits are usually quoted for mixtures of gases with air. Air typically consists of 21% oxygen, 78% nitrogen and 1% other gases. Altering the composition of air, for example by vitiation (i.e. reducing the oxygen concentration through the recirculation of products of combustion), can have a significant effect on the flammability limits and other combustion characteristics. Likewise, if the air composition consists of a sufficient concentration of 'non-reacting' components the gas/air mixture may not burn at all, even if it appears to be within its quoted flammable range.

The most widely used data concerning the flammable limits of fuel gases is that taken from studies conducted by the US Bureau of Mines in the 1950's and 60's [84, 85]. Flammability data should be used with caution as UK natural gas reserves are declining and supplies are increasingly being sourced from Europe and further afield. In order to ensure security of supply, new import pipelines and three new LNG terminals have been constructed. Consequently, the specification of natural gas is altering. Additionally, the government focus on 'green' energy is seeing biogas being injected into the natural gas distribution system, which also has the potential to alter the specification of the gas within the distribution network.

2.2.2. Stoichiometry

Stoichiometry is the branch of chemistry concerned with the proportions in which elements in compounds are combined. Thus, with reference to combustion associated with accidental gas explosions, there are several contexts in which the term stoichiometric may be used, including:

- the stoichiometric air requirement - meaning the minimum (or theoretical) air requirement for complete combustion;
- a stoichiometric mixture - the theoretically optimum mixture (i.e. there is just enough oxygen in the air to burn all the fuel).

Stoichiometric combustion refers to the burning of a fuel under precise conditions; that is, there is the exact amount of oxygen for complete combustion to take place (for example, five moles of oxygen for each mole of propane).

In accidental explosions the fuel is usually burned in oxygen from the air; which itself, for simplicity, may be considered to consist of approximately 79.1% nitrogen and 20.9% oxygen. A general formula for the combustion of any hydrocarbon (C_nH_m) in air may be written using terms m, n and z (where $z = n + \frac{m}{4}$).

It is commonly known as the 'general equation of the combustion of hydrocarbons in air' and is shown below:

$$C_nH_m + zO_2 + z(3.78)N_2 \Rightarrow nCO_2 + \left(\frac{m}{2}\right)H_2O + z(3.78)N_2 \qquad \textbf{(2-1)}$$

Air-Fuel Ratio

The volumetric air/fuel ratio (AFR) for the combustion of any hydrocarbon may be given by:

$$AFR = \left(\frac{V_a}{V_f}\right) \qquad \textbf{(2-2)}$$

Where:

V_a = amount of air required for stoichiometric combustion (m^3).

V_f = amount of fuel required for stoichiometric combustion (m^3).

The amount of air is obtained by adding the amount of oxygen to the amount of nitrogen.

The mass air/fuel ratio (AFR) for the combustion of any hydrocarbon may be given by:

$$AFR = \left(\frac{m_a}{m_f}\right) \quad \textbf{(2-3)}$$

Where:

m_a = amount of air required for stoichiometric combustion (kg).

m_f = amount of fuel required for stoichiometric combustion (kg).

When conducting on-site gas investigations, equipment used by emergency responders most commonly expresses the gas concentration as a percentage in air, or a percentage of the LEL. The percentage of gas in air (GIA) required for a stoichiometric concentration can easily be determined by:

$$\%\ GIA_s = \frac{(V_f)_s}{(V_a+V_f)_s} \times 100 = \frac{1}{\left(\frac{V_a}{V_f}\right)_s + 1} \times 100 \quad \textbf{(2-4)}$$

Fuel/Air Ratio

The volumetric fuel/air ratio (FAR) for the combustion of any hydrocarbon may be given by:

$$FAR = \left(\frac{V_f}{V_a}\right) \quad \textbf{(2-5)}$$

The mass fuel/air ratio (FAR) for the combustion of any hydrocarbon may be given by:

$$FAR = \left(\frac{m_f}{m_a}\right) \quad \textbf{(2-6)}$$

In the literature there is often reference to the air to fuel ratio (AFR) which is effectively the inverse of FAR.

Non-Stoichiometric Combustion

Non-stoichiometric combustion simply refers to conditions under which the exact amount of oxygen is not available; that is, it can mean either too much or too little oxygen.

If excess air (and hence excess oxygen) is present the gas/air mixture is said to be 'lean'; and conversely, if there is less than the stoichiometric amount of oxygen available, the mixture is said to be 'rich'.

Normalised Hydrocarbon Composition

It is useful to represent the combustion of hydrocarbons in an equation where the hydrocarbon composition has been normalised with respect to the number of carbon atoms [86]. Let a, b, e, m, n and y be convenient algebraic notation for stoichiometric combustion:

$$CH_y + n(O_2+3.78N_2) \Rightarrow aCO_2 + bH_2O + n(3.78)N_2 \quad \textbf{(2-7)}$$

Where:

$y = \frac{\text{No.hydrogen atoms}}{\text{No.carbon atoms}}$.

a = 1 from a carbon balance.

b = $\frac{y}{2}$ from a hydrogen balance.

n = a + $\frac{b}{2}$ or 1 + $\frac{y}{4}$ from an oxygen balance.

The normalised equation may now be written as:

$$CH_y + \left(1+\frac{y}{4}\right)(O_2+3.78N_2) \Rightarrow CO_2 + \frac{y}{2}H_2O + \left(1+\frac{y}{4}\right)(3.78)N_2 \quad \textbf{(2-8)}$$

The air/fuel ratio equation (by volume) may be expressed as:

$$(AFR)_V = C\left[4.78\left(1+\frac{y}{4}\right)\right] \quad \textbf{(2-9)}$$

Where:

C = Carbon number (e.g. 3 for propane, 4 for butane etc.).

The air/fuel ratio equation (by mass) may be expressed as:

$$(AFR)_m = \left[4.78\left(1+\frac{y}{4}\right)\right]\frac{MW_a}{(12+y)} \quad \textbf{(2-10)}$$

Where:

The molecular weight of air, MW_a ≈ 29 kg/kmol.

Using the above technique, the air fuel ratio and the stoichiometric gas concentration have been calculated for several hydrocarbon fuels and are given, in addition to some other important parameters, in Table 2-1.

Table 2-1 Stoichiometric gas concentration and air/fuel ratio for a range of fuels (ΔH taken from Harris [16])

Fuel	$\left(\frac{V_a}{V_f}\right)_s$	$\left(\frac{m_a}{m_f}\right)_s$	% GIA_s	ΔH_c (Gross) (MJ/kg)	ΔH_c (Net) (MJ/kg)	$\Delta H_{c,\ air}$ (MJ/kg)	$\Delta H_{c,\ air}$ (MJ/m^3)
Methane (CH_4)	9.56	17.26	9.5	55.50	50.03	2.90	3.57
Propane (C_3H_8)	23.82	15.69	4.0	50.35	46.36	2.95	3.63
n-Butane (C_4H_{10})	30.96	15.47	3.1	49.50	45.72	2.96	3.63
n-Hexane (C_6H_{14})	45.18	15.24	2.2	48.31	44.74	2.94	3.61
n-Decane ($C_{10}H_{22}$)	73.80	15.07	1.3	47.64	44.24	2.94	3.61
Cyclohexane (C_6H_{12})	42.84	14.79	2.3	46.58	43.45	2.94	3.61

In Table 2-1, ΔH_c air is calculated by dividing the net ΔH_c by the either the volume or mass based AFR. Table 2-1 highlights some useful stoichiometric combustion relationships:

- the air/fuel ratio (by mass) for hydrocarbons (except methane) is approximately constant at 15:1;
- the ΔHc, (air) for hydrocarbons is approximately constant at 3 MJ/kg; and
- the ΔHc, (air) for hydrocarbons is approximately constant at 3.6 MJ/m^3.

This is because the calorific value of a fuel is proportional to the air requirement for its stoichiometric combustion [86].

Equivalence Ratio

The equivalence ratio is a convenient non-dimensional combustion parameter that may be expressed in terms of mass or volume with the same result and is often used to analyse fundamental theoretical concepts in explosion science. The fuel/air equivalence ratio, ϕ, is defined by the relationship of the actual fuel/air ratio of a mixture to that of its fuel/air ratio at stoichiometric conditions. It may be expressed, in volume terms, as:

$$\phi = \frac{(V_f/V_a)_A}{(V_f/V_a)_s} = \frac{(V_a/V_f)_s}{(V_a/V_f)_A} \qquad \textbf{(2-11)}$$

Or, in mass terms:

$$\phi = \frac{(m_f/m_a)_A}{(m_f/m_a)_s} = \frac{(m_a/m_f)_s}{(m_a/m_f)_A} \qquad \textbf{(2-12)}$$

Based on this definition of the equivalence ratio, the following gas concentration conditions are observed:

$\phi < 1$ = fuel lean.

$\phi > 1$ = fuel rich.

In some of the literature the inverse definition of the equivalence ratio is used, in which case, the concentration conditions indicated above are reversed.

2.2.3. Minimum Ignition Energy

In accidental gas explosions in dwellings, the temperature of the gas/air mixture is well below the autoignition temperature and ignition is usually initiated by contact with an open flame, hot surface or spark (for example by operation of a light switch etc.).

There is a minimum energy that is required to ignite a gas/air mixture by a spark. A spark with energy below this limiting level is not capable of establishing a flame above a critical minimum size such that the flame can propagate unsupported. This is because the heat losses to the unburnt gas around the flame kernel are relatively high and dissipate the heat of the reaction zone, quenching the chemical reaction and thus preventing the flame from propagating.

The minimum ignition values, usually quoted in millijoules (mJ), vary for different fuel gases and for differing concentrations, and may be as low as 0.1 mJ for some fuel gases. Some reference books (for example, Crowl [87]) quote that the minimum ignition energy for a particular fuel gas lies at, or close to, its stoichiometric concentration. Figure 2-2 shows the minimum ignition energy for a number of hydrocarbons and highlights that the minimum ignition energy does not necessarily occur at its stoichiometric concentration. The graph also demonstrates that the energy required for spark ignition is dependent upon the gas concentration; with a greater energy required to ignite the gas/air mixture as it diverges to its flammable limits.

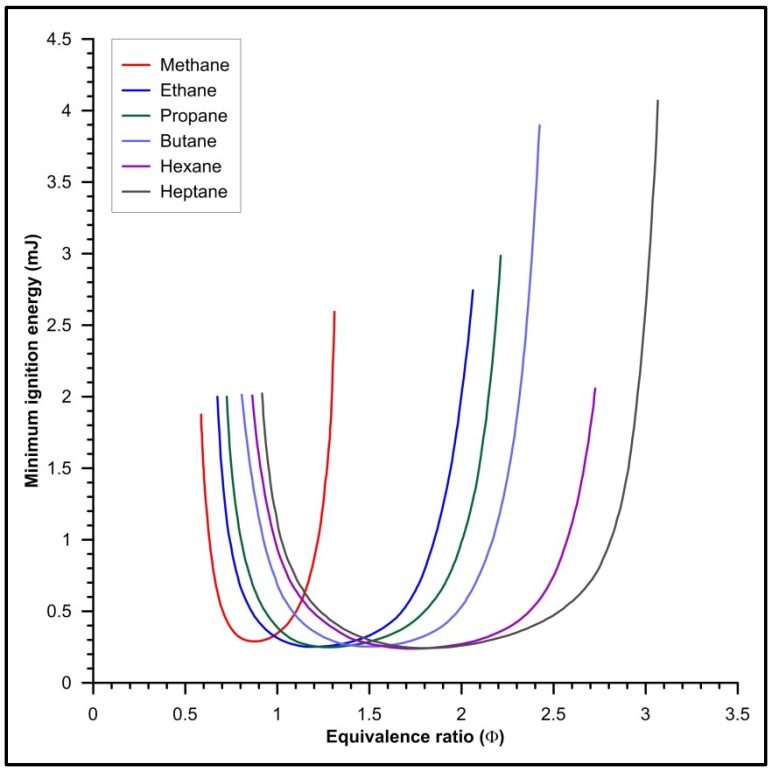

Figure 2-2 Variation of minimum ignition energy with fuel type and concentration (adapted from Lewis and von Elbe [76])

2.2.4. Flame Temperature

Stoichiometric hydrocarbon/air flames have an adiabatic flame temperature, at conditions of constant pressure, of approximately 2150 – 2250K (see Table 2-2), but the flame temperature decreases as the gas/air concentration diverges towards its flammable limits. Figure 2-3 shows the adiabatic flame temperatures for methane, ethane and propane, at conditions of constant pressure and constant volume, calculated using the chemical kinetic calculation software Gaseq [88]. Gaseq is a software program which was developed by Dr Morley of Cambridge University. It is intended primarily for gaseous phase calculations and solves chemical equilibrium problems based on the minimisation of free energy (NASA method).

Table 2-2 Combustion properties of some hydrocarbon fuel/air mixtures (taken from Harris [16])[a]

Fuel	Molecular weight	Flammability limits % GIA by volume)		% Gas at stoichiometric ratio	% Gas at maximum burning velocity	Maximum laminar burning velocity (m/s)	Adiabatic flame temperature (K)	Expansion ratio (T_i = 288K)	Maximum laminar flame speed (m/s)	Autoignition temp (K)	Minimum ignition energy (mJ)	Net calorific value (288K, 1atmos.) MJ/m^3
		Lower	Upper									
Hydrogen (H_2)	2	4	75	30	54	3.5	2318	8.0	28	847	0.02	10.2
Methane (CH_4)	16	5	15	9.5	10	0.45	2148	7.4	3.5	813	0.29	34
Ethane (C_2H_6)	30	3	12.5	5.6	6.3	0.53	2168	7.5	4.0	788	0.24	60.5
Propane (C_3H_8)	44	2.2	9.5	4.0	4.5	0.52	2198	7.6	4.0	723	0.25	86.4
Butane (C_4H_{10})	58	1.9	8.5	3.1	3.5	0.50	2168	7.5	3.7	678	0.25	112.4
Pentane (C_5H_{12})	72	1.5	7.8	2.6	2.9	0.52	2232	7.7	4.0	533	0.25	138.1
Hexane (C_6H_{14})	86	1.2	7.5	2.2	2.5	0.52	2221	7.7	4.0	498	0.25	164.4
Heptane (C_7H_{16})	100	1.2	6.7	1.9	2.3	0.52	2196	7.6	4.0	488	0.25	190.4
Acetylene (C_2H_2)	26	2.5	80	7.7	9.3	1.58	2598	9.0	14.2	578	0.02	51
Ethylene (C_2H_4)	28	3.1	32	6.5	7.4	0.83	2248	7.8	6.5	763	0.12	56
Propylene (C_3H_6)	42	2.4	10.3	4.4	5.0	0.66	2208	7.7	5.1	733	0.28	81.5
Butylene (C_4H_8)	56	1.7	9.5	3.4	3.9	0.57	2203	7.6	4.3	658	0.28	107.1
Benzene (C_6H_6)	78	1.4	7.1	2.7	3.3	0.62	2287	7.9	4.9	833	0.22	134
Cyclohexane (C_6H_{12})	84	1.3	8.0	2.3	2.7	0.52	2232	7.8	4.1	518	0.24	167.3

[a] The values given in this table are for comparative purposes and for consistency have been taken from one source. Some values of properties, that are widely accepted today, may differ from those shown. For example, the current accepted laminar burning velocity value for a stoichiometric methane/air mixture is 0.38 m/s [122].

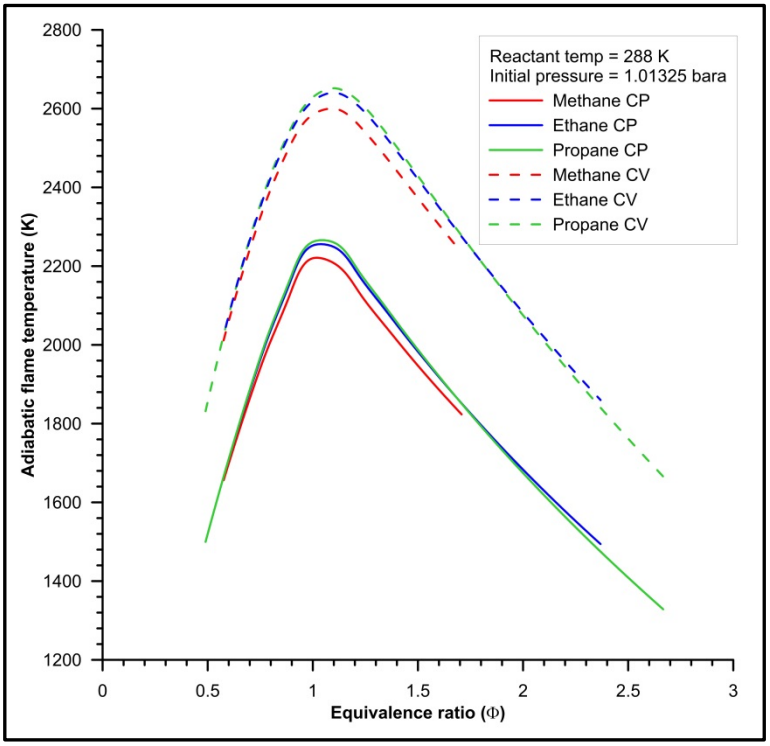

Figure 2-3 Variation in flame temperature with gas concentration (calculated using Gaseq [88])

The typically quoted adiabatic flame temperatures are measured, or calculated, at room temperature and atmospheric pressure (i.e. constant pressure). When considering accidental explosions in dwellings, the volume is constant (at least in the early stages of the explosion) and the pressure increases. In these conditions, the flame temperature increases because the unburnt gas/air mixture is heated by compression. This can be clearly seen in the flame temperature calculations shown in Figure 2-3.

2.2.5. Flame Propagation

Burning Velocity

A key characteristic of a flame is the burning velocity, which is defined as the velocity of a plane flame front in a direction normal to itself and relative to the unburnt reactants. It is independent of flame geometry, burner size and flow rate and depends only on the initial fuel composition and conditions of temperature and pressure.

Values for burning velocity are usually determined experimentally. Several reviews have been undertaken on the methods of measuring burning velocity, for example Linnett [89], Andrews and Bradley [90], and Rallis and Garforth [91], but there is no agreement as to precise laminar burning velocity values.

Andrews and Bradley [90] recommended a maximum laminar burning velocity of 0.45 ± 0.02 m/s for methane/air mixtures at (25°C and 1 atmosphere). This recommendation has been widely used in the gas industry, however, accepted values today are in the order of 0.38 m/s, but as discussed earlier, the composition of natural gas is changing so care should be taken when using any published value. Nonetheless, in terms of accidental gas explosions, the differences in published values are not significant and values of burning velocity appropriate for use in calculating explosion pressures are given in Table 2-2.

The burning velocity of a flammable gas is dependent upon the heat and mass transfer processes within the flame front. Methane, which is the largest constituent of natural gas, has the lowest laminar burning velocity of all the hydrocarbons. The term ‘laminar’ burning velocity indicates that the gas/air mixture is flowing into the flame under conditions of laminar flow. Conversely, the term ‘turbulent’ burning velocity indicates that the gas/air mixture is flowing into the flame in a turbulent motion. The turbulent movement has the effect of intensifying the heat and mass transfer processes in the vicinity of the reaction zone, such that higher velocities are produced than under laminar conditions [92].

In controlled combustion, stationary flames are required, for example for cooking and heating. In order to achieve a stationary flame, it is necessary to pass the reactants (e.g. gas/air mixture) into the flame at an efflux velocity equal to that of the burning velocity and in an opposite direction.

In uncontrolled combustion, a propagating flame (sometimes called an explosion flame) is observed as the burning velocity acts in the same direction as the flow of unburnt gas/air mixture (reactants) and the flame front is ‘pushed’ forward through the unburnt gases by the hot expanding gases behind it.

The burning velocity of a particular flammable gas is also strongly dependent upon the concentration of the gas/air mixture. As discussed earlier, it is only possible to sustain flame propagation if the concentration of the gas/air mixture is within its flammable limits. Within these limits, the maximum laminar burning velocity value for any fuel gas is usually found to be just on the ‘rich’ side of the stoichiometric concentration and reduces as the concentration diverges towards its flammable limits (Figure 2-4).

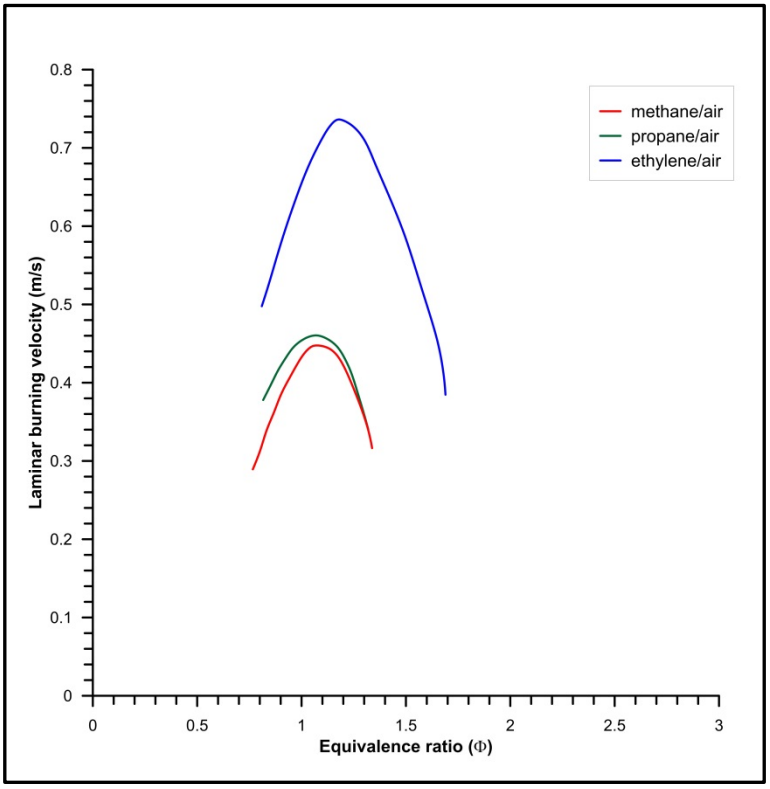

Figure 2-4 The effect of gas concentration on burning velocity (adapted from Gibbs and Calcote [93])

In addition to the strong dependence upon gas concentration, burning velocity also varies with the initial pressure and temperature of the gas/air mixture. Lewis [94], proposed that the burning velocity dependence on pressure could be determined by the following relationship:

$$S_u \propto P^n \qquad \textbf{(2-13)}$$

Where:

n = negative, for S_u < 0.45 m/s (i.e. burning velocity decreases).

n = 0, for 0.45 m/s ≤ S_u ≤ 1.0 m/s.

n = positive, for S_u > 1.0 m/s (i.e. burning velocity increases).

Egerton and Lefebvre [95] carried out research on the burning velocity of methane, propane, ethylene and propylene gas/air mixtures under increased pressure conditions. They found the pressure dependence could be expressed using the following relationship:

$$S_u = cP^{-x} \qquad \textbf{(2-14)}$$

Where:

c = a constant.

x = 0.46 (lean) to 0.5 (rich) for methane/air mixtures.

Generally, for the gas/air mixtures that are most commonly involved in accidental explosions, the burning velocity value decreases as the pressure increases (see Figure 2-5). However, although there is a decrease in the rate of combustion in volumetric terms, the mass burning rate is increased due to the increased density of the gas.

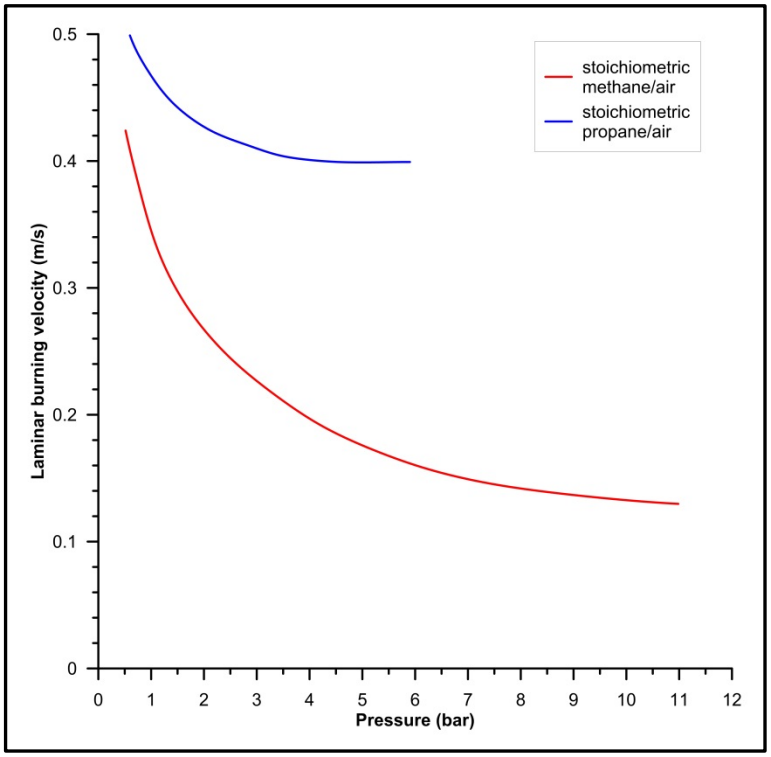

Figure 2-5 The pressure dependence of burning velocity (adapted from Egerton and Lefebvre [95])

In contrast to the dependence on pressure, the burning velocity value has been found to increase with increasing initial temperature.

Dugger [96] carried out research to determine burning velocities dependence upon the initial temperature of methane/ propane and ethylene gas/air mixtures. The findings of this work have been used to plot the estimated burning velocities over a range of temperature conditions that may be encountered in an accidental gas explosion (see Figure 2-6).

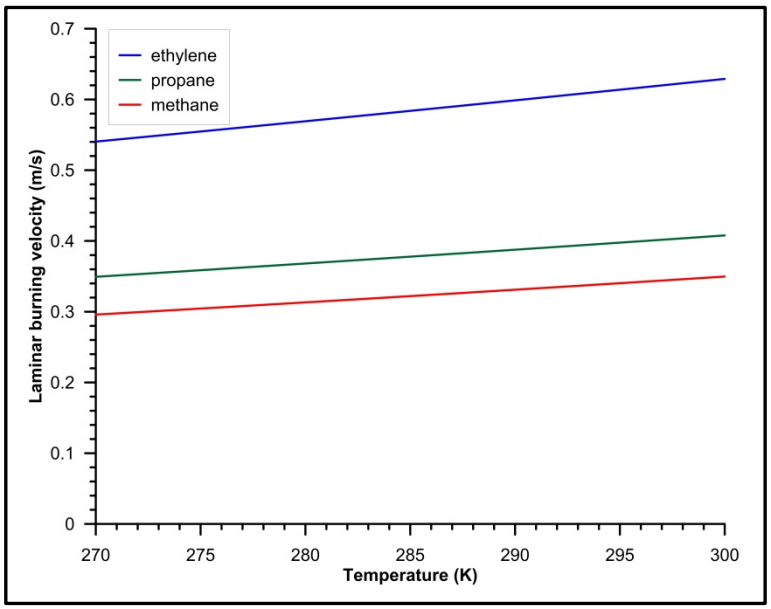

Figure 2-6 The effect of initial temperature on burning velocity (adapted from Dugger [96])

Andrews and Bradley [90] in comparing a number of experimentally determined burning velocities measured at different initial mixture temperatures corrected the measurements to a standard temperature of 298 K (≈ 25°C) by assuming that the burning velocity varies as the square of the absolute temperature. They also corrected experimental results for the major errors of flame thickness and quenching distance, deriving an equation for the temperature dependence of burning velocity (stoichiometric methane/air) [97]:

$$S_u = 10+0.000371T^2 \quad \textbf{(2-15)}$$

Where:

S_u = burning velocity (cm/s).

T = absolute temperature of the gas/air mixture (K).

In a later study, conducted by Dixon-Lewis and Islam [98], a computational one dimensional flame modelling method was used to derive burning velocity values for methane/air flames. The results of this study indicated that the best value for a stoichiometric methane/air flame at 25°C was 0.37 m/s.

Equation (2-15), derived by Andrews and Bradley [90], was used to plot the corrected experimentally measured burning velocities over the temperature range that may be encountered in an accidental gas explosion. Using Equation (2-15), the calculated laminar burning velocity at 25°C is 0.43 m/s in comparison to a value of 0.34 m/s observed by Dugger at 25°C.

Flame Thickness

Flame thickness is known to be affected by flame speed whilst being dependent upon temperature, pressure, density and concentration of the fuel/air mixture [99]. Heravi et al. [99] derived an equation to predict the flame thickness for stoichiometric methane/air mixtures against conditions of increasing pressure and temperature that was suitable for temperatures up to 700 K and pressures up to 30 bar:

$$X = 0.2643\left(\frac{T}{300}\right)^{-0.85}(P)^{-0.58} \qquad \textbf{(2-16)}$$

Where:

X = flame thickness (mm).

T = temperature (K).

P = pressure (bar).

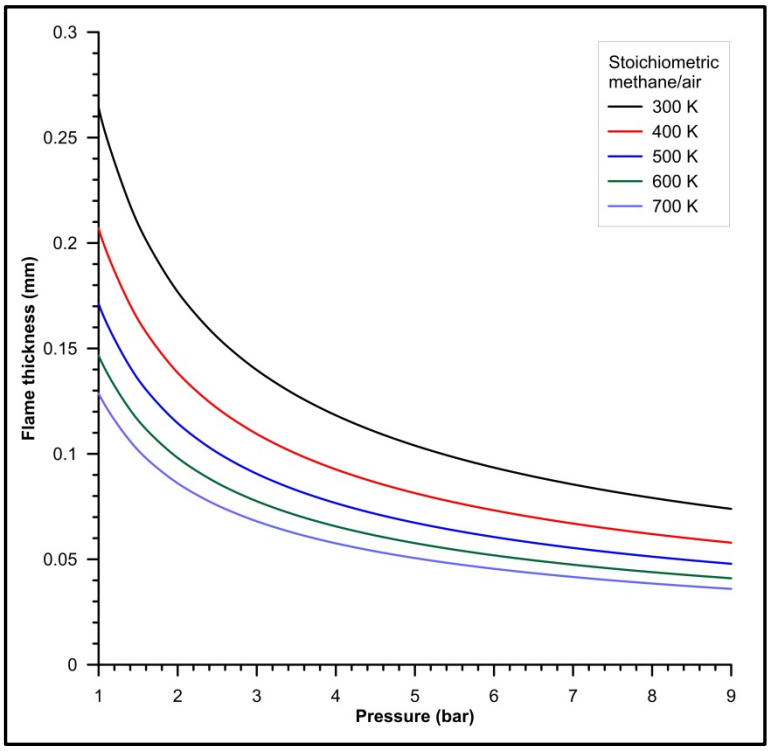

Figure 2-7 The effect of increasing pressure and temperature on flame thickness (calculated using Equation (2-16) Heravi et al. [99])

In Figure 2-7, curves have been plotted using Equation (2-16) to demonstrate the effect of increasing pressure and temperature on flame thickness. It can be seen that the flame thickness decreases with increasing pressure and temperature; the dependency on pressure being larger than that of temperature.

Andrews and Bradley [97] measured the flame thickness of methane/air mixtures of differing concentration using fine wire thermocouples (12.5 μm) and a schlieren interferometer. Values of flame thickness obtained during these experiments are shown, for different values of equivalence ratio, by the curve in Figure 2-8. It can be seen that the flame thickness increases as the concentration diverges towards the flammable limits. For the stoichiometric concentration the flame thickness is to be of the order of 1.2mm, significantly higher than the values indicated in Figure 2-7.

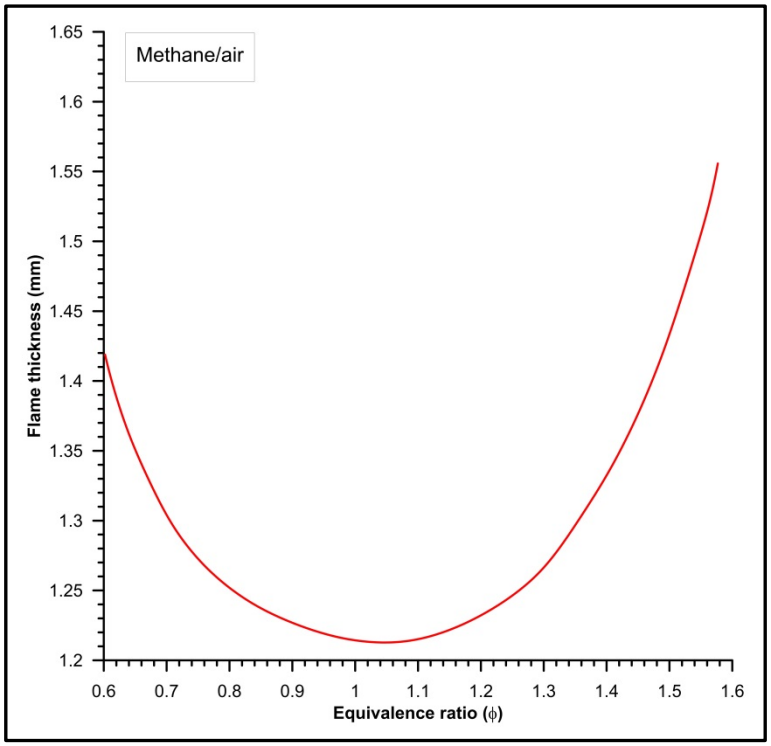

Figure 2-8 The effect of gas concentration on flame thickness (adapted from Andrews and Bradley [97])

Flame Speed

Some gas engineering text books confuse flame speed with burning velocity [100-102]. It is important to understand that burning velocity is not usually the same as the observed speed of flame propagation or flame speed. However, whilst flame speed is a very useful concept, and is used widely to describe explosion mechanisms, it is not a fundamental property of flame propagation.

Flame speed may be defined as the speed at which the flame front travels through a flammable gas/air mixture, measured with respect to a fixed position. When considering a gas explosion, the flame speed is always greater than the burning velocity as the flame front is pushed forward by the motion of the expanding hot gases trapped behind it.

However, in terms of controlled combustion, for example a cooker burner, the flame speed would be zero, as the flame is stationary in relation to a fixed point (i.e. the burner), whilst the burning velocity would be in the region of 0.4 m/s (natural gas). The laminar flame speed is therefore a function of the burning velocity and the expansion of the gases as their temperature changes during combustion.

As discussed, flame speed is measured with respect to some fixed reference point; consequently, it is possible that prior to ignition, the flammable gas/air mixture may be in motion in either a positive or negative direction. The velocity with which these gases flow will contribute to the flame speed, either increasing it or decreasing it depending upon their direction of flow.

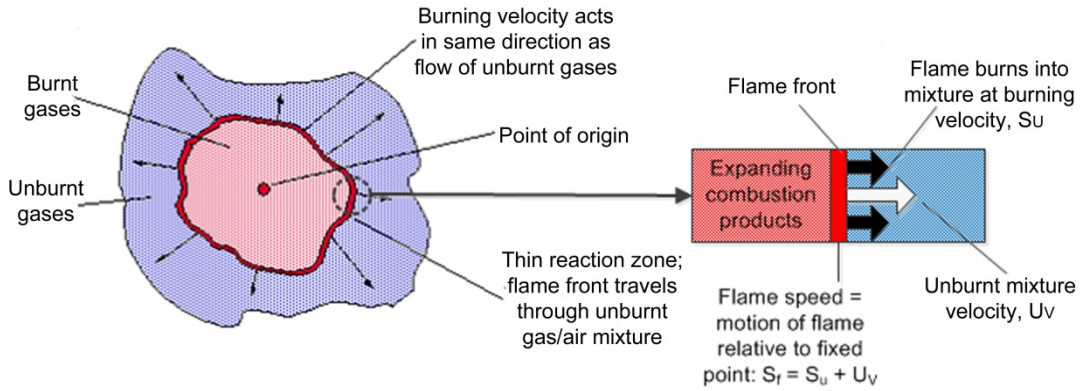

Figure 2-9 Propagating flame in uncontrolled combustion event (adapted from Harris [16])

In a laminar, spherical gas explosion, the flame speed may be given by:

$$S_f = S_u \frac{\rho_u}{\rho_b} \qquad \textbf{(2-17)}$$

Where:

S_f = laminar flame speed (m/s).

S_u= laminar burning velocity (m/s).

ρ_u = density unburnt gases (kg/m^3).

ρ_b = density burnt gases (kg/m^3).

Following combustion there is an associated increase in temperature and change in density of the burnt gases. The equation to determine the flame speed may also be expressed as:

$$S_f = S_u E \quad \textbf{(2-18)}$$

Where:

E = an expansion factor, given by the ratio of the densities of the unburnt and burnt gases.

The expansion factor may be determined by:

$$E = \frac{N_b}{N_u}\frac{T_b}{T_u} \quad \textbf{(2-19)}$$

Where:

N_b = the number of moles of products remaining after combustion.

N_u = the number of moles of reactants before combustion.

T_b = the temperature of the burnt gases (K) (≈ flame temperature).

T_u = the initial temperature of the gas/air mixture before combustion (K).

The mole number ratio (N_b/N_u) varies for different gases and for different gas/air mixture concentrations. However, the mole number ratio for the most common fuel gases involved in accidental explosions in dwellings is approximately 1.0 and consequently the expansion factor, E, may be approximated as T_b/T_u. Calculations show that the expansion factor, at stoichiometric concentration, is approximately 8 - 9 for hydrocarbons typically involved in accidental explosions. Care must be taken during calculations to ensure an appropriate flame temperature is used.

As discussed earlier, many quoted adiabatic flame temperatures are calculated or measured under conditions of constant pressure, whereas, at least for the early part of an explosion, the volume is constant and the pressure rises. Flame temperatures are higher under constant volume conditions due to compression, with expansion factors in the region of 9 – 10 for hydrocarbons.

Assuming the gas during combustion behaves as an ideal gas, the pressure and volume relationship is given by:

$$\frac{PV}{T} = nR \quad \textbf{(2-20)}$$

Where:

P = Absolute pressure (atm).

V = Volume (L).

T = Temperature (K).

n = no. moles.

R = Gas constant (0.0821 L atm / K mol).

If it is assumed that the quantity of gas remains constant, then the ideal gas law may be expressed as:

$$\frac{P_1V_1}{T_1} = \frac{P_2V_2}{T_2} \qquad \textbf{(2-21)}$$

Therefore, by observing the above equation, it can be seen that uncontrolled combustion will result in either a volume or pressure increase depending upon surroundings. In a fully confined explosion (e.g. in a closed vessel), where the volume may be considered as constant, there will be an associated increase in pressure, however, in an unconfined (and uncongested) area the pressure will remain constant and there will be an associated increase in volume.

Using Equation (2-18) it can be demonstrated that the maximum laminar flame speed for hydrocarbons is typically less than 10 m/s. This calculation assumes that the burnt gases are completely trapped behind the flame front. In situations where this is not the case; for example ignition at the edge of a pocket of flammable gas/air mixture in a dwelling, some of the burnt gases may escape away from the flame front and consequently the flame front will not be pushed forward at the same velocity. Whilst the burning velocity will remain unchanged, the flame speed will be less than that calculated above.

The initial expanding spherical or hemi-spherical flame, typical of a gas explosion in a dwelling, also pushes unburnt gas away from the flame front at a velocity S_g known as the ‘induced gas velocity’ (often called the explosion-induced wind). This is important in confined vented explosions and its effects on the maximum pressure generated will be discussed in later chapters. The induced gas velocity, S_g, may be determined by:

$$S_g = S_f - S_u \qquad \textbf{(2-22)}$$

Alternatively, the flame speed may be expressed as:

$$S_f = S_u + S_g \qquad \textbf{(2-23)}$$

By rearranging Equations (2-18), (2-19), and (2-22), S_g may be expressed as:

$$S_g = S_u (E - 1) \quad \textbf{(2-24)}$$

Or, in terms of the flame speed:

$$S_g = S_u(E - 1) = \frac{S_f}{E}(E - 1) = S_f\left(1 - \frac{1}{E}\right) \quad \textbf{(2-25)}$$

Considering a stoichiometric methane/air mixture at 288K, under adiabatic conditions, the induced gas velocity may be calculated as 87% of the flame speed. Results of experimental work carried out by MRS [103] has shown that 80 – 85% of the flame speed is the velocity of the gases accelerating the flame forward. The difference between the calculated and experimental values is due to heat losses.

Flame Instabilities

It has been observed in the literature that explosion flames are conducive to the development of a cellular flame structure [104-107]. It is known that in such cases, the flame instability is a consequence of both hydrodynamic and thermodiffusive effects; that is, an instability resulting from the competing effects of heat conduction from, and reactant diffusion toward, the flame.

The Lewis number (Le) is a dimensionless number used to characterize fluid flows where there is simultaneous heat and mass transfer. It may be defined as:

$$Le = \frac{\alpha}{D} \quad \textbf{(2-26)}$$

Where:

α = the thermal diffusivity of the bulk mixture.

D = the mass diffusivity of the scarce reactant in the bulk mixture.

The Lewis number can be interpreted as the ratio of the rate of diffusion of thermal enthalpy from the flame front to the unburned gas, to the rate of diffusion of chemical enthalpy (in the form of the scarce reactant) from the unburned gas to the flame front [108].

The seminal work of Darrieus [109] and Landau and Lifshitz [110] demonstrated that, a planar flame front is intrinsically unstable due to hydrodynamic effects connected with the expansion of the hot combustion products behind the flame front. If a flame is slightly curved, the streamlines in the combustion products converge behind the convex part of the flame front and diverge behind the concave parts leading to a torque that acts to encourage flame wrinkling [111].

These instabilities that cause wrinkling can either be stabilised or further destabilised by thermodiffusion effects, resulting in a cellular flame structure.

For a slightly wrinkled flame front, in addition to the hydrodynamic Darrieus-Landau (D-L) instabilities, molecular and thermal diffusive instabilities may also not be balanced. When Le differs from unity, flame stretch causes changes in the rates of transport of chemical and thermal enthalpy that in turn affects the temperature at the flame front. Since the combustion of flammable gas/air mixtures are strongly exothermic reactions with relatively high activation energies, changes in flame front temperature can lead to changes in the reaction rate at the flame front and thus changes in the local burning velocity and flame propagation rate [108]. Explosion flame fronts in mixtures with Le below a critical value, that are concave towards the products of combustion, will result in an increase in the rate of chemical enthalpy to the flame front that is greater than the increase in the rate of thermal energy loss, and thus the curved flame will burn more intensely than a planar flame in the same mixture (i.e. increased burning velocity) and the flame would become more wrinkled leading to a cellular flame structure. Conversely, a flame front in a flammable mixture with Le above the critical value, would result in a lower local burning velocity and, therefore, the smoothing out of wrinkles.

Cellular flame propagation has been widely researched by numerous authors including Markstein [112], Clavin and Williams [113], Joulin and Clavin [114], Pelce and Clavin [115], Abdel-Gayed et al. [116], Andrews et al. [117] and Bradley [118, 119]. It was recognised that whilst the flame is expanding, the hydrodynamic instability can be inhibited. This inhibition is governed by the Peclet number, which is defined as the ratio of the flame radius to the flame thickness:

$$Pe = \frac{R_f}{\delta} \qquad \textbf{(2-27)}$$

Where:

Pe = Peclet number.

R_f = radius of the flame.

δ = flame thickness.

For unstable flames (*Le* < 1), the cellular structure will develop when the radius became sufficiently large, such that the Peclet number exceeds a critical value, Pe_{cr} [120].

In the classic study on non-steady flame propagation, Markstein [112] suggested that the flame curvature is the main parameter that defines the flame structure and, consequently, the local speed of flame propagation. Markstein proposed that the normal propagation velocity of a curved flame, S_n, may be expressed as:

$$S_{u,l} - S_n = S_{u,l} \frac{L_M}{R_{f,c}} \quad \textbf{(2-28)}$$

Where:

L_M = the Markstein length.

$R_{f,c}$ = the radius of flame curvature.

The ratio of the Markstein length to the flame thickness is known as the Markstein number, Ma:

$$Ma = \frac{L_M}{\delta} \quad \textbf{(2-29)}$$

The values of the Markstein length, or number, are determined experimentally by measuring the propagation speed of spherical flames as a function of the flame radius [112].

Karlovitz et al. [121] proposed that it is the flame stretch rate that defines the local speed of flame propagation:

$$k_s = \frac{1}{A_f} \frac{dA_f}{dt} \quad \textbf{(2-30)}$$

Where:

k_s = Karlovitz flame stretch factor.

A_f = elementary area of the flame front.

Karlovitz et al. [121] proposed that flame stretch may be created by both flame curvature effects (α_c) and inhomogeneities of the upstream flow (strain rate, α_s) and by combining the two the following equation for the propagation velocity of a stretched flame is derived:

$$1 = \frac{S_n}{S_{u,l}} = Ma \frac{\delta}{S_{u,l}} \alpha \quad \textbf{(2-31)}$$

Authors, including Bradley et al.[122], Buckmaster [123], Matalon [124] and Chung and Law [125] separated the effects of curvature and strain rate, thereby allowing Equation (2-31) to be rewritten with two different Markstein numbers:

$$S_{u,l} - S_n = Ma_c \delta\alpha_c + Ma_s \delta\alpha_s \quad \textbf{(2-32)}$$

The sign of the Markstein number in Equation (2-32) defines the response of the flame front to stretch and strain [111]. For Ma > 0, flame stretch causes a decrease in the local burning velocity, whilst Ma < 0 flame stretch tends to increase the burning velocity. The detailed studies of Clavin and Williams [113] and Joulin and Clavin [114, 126] have demonstrated that for a positive Ma (i.e. Ma > 0), flame stretch works against the D-L hydrodynamic instability and has a stabilising effect on the flame wrinkling process.

D-L and diffusive instabilities are relatively weak and only play a significant role during the initial stages of a vented explosion. As the explosion develops, interaction with the enclosure and obstacles within the enclosure, in addition to the process of explosion relief, causes instabilities that are considerably more influential in the development of fast flames and the generation of pressure. Generally, if confinement and/or obstructions are present (and dwellings will typically have both of these), two powerful hydrodynamic instabilities, namely Kelvin–Helmholtz (K–H) [127, 128] and Rayleigh–Taylor (R–T) [129, 130], strongly influence flame propagation.

Both the K-H and R-T instabilities are hydrodynamic instabilities that occur when there is an interface between fluids of different density. The K-H instability occurs when there is a velocity shear in a single continuous fluid, or where there is a velocity difference across the interface between two fluids, and the R-T instability develops when a less dense fluid is accelerated towards a more dense fluid. The flame surface must be distorted by an initial perturbation in order to develop an instability. Both K–H and R–T instabilities are triggered when the flame is accelerated over an obstacle or through a vent. Solberg et al. [31] carried out a series of propane/air vented explosions in a 35 m^3 chamber and suggested that R-T instabilities were the predominant factor in the development of significant overpressures. During the tests it was observed that it was necessary for a significant part of the flame to propagate in a direction away from the vent opening in order to develop an R-T instability (e.g. centrally ignited), but the distance from the point of ignition to the vent was not as important (e.g. R-T instabilities would develop if the gas/air mixture was ignited close to the vent opening) [31]. R-T instabilities were seen to be developed at the rear of the flame propagating away from the vent opening when the flame front reached the vent opening and hot, less dense combustion products were vented at high velocities. For rear ignition tests no R-T

instabilities were observed and it was suggested that this was because the whole flame front propagates towards the vent, so that an R-T instability will not have the same possibility to develop when the flame reaches the vent opening.

Flame propagation in enclosures also generates acoustic waves that cause instabilities, but they are usually associated with relatively slow flames in enclosures that are free of obstacles [111]. The acoustic waves reflect off of the walls and obstacles within the enclosure and interact with the flame front to develop flame perturbations through a variety of instability mechanisms. These mechanisms include flame distortion caused by the flame acoustic wave interaction, and wave amplification caused by the coherence between the acoustic wave and the exothermic energy release [131].

Acoustic instabilities have been observed in vented explosions by authors including van Wingerden and Zeeuwen [132], Tamanini and Chaffee [63], Harrison and Eyre [133] and Zalosh [37]; with these instabilities enhancing the peak pressure by a factor of eight for fuel rich propane/air mixtures [132] and by a factor of between two and nine for stoichiometric methane/air and propane/air mixtures [63]. Tamanini and Chaffee [63] demonstrated that that the presence of sound-absorbing material can eliminate acoustically-induced combustion instabilities; under quiescent conditions, the sound-absorbing material decreased the explosion pressure by as much as a factor of ten but in turbulent explosions the reduction was typically by a factor of two.

Flame Self-Acceleration

Flame instabilities lead to a phenomena that many authors refer to as flame self-acceleration. When an initially quiescent flammable gas/air mixture is ignited in a confined enclosure, the flame initiates as a kernel and a smooth spherical flame is formed. As the flame front propagates into the unburnt gas/air mixture ahead of it, consuming the flammable gas, it converts chemical energy into heat and leaves a sphere of hot, loss dense combustion products behind it. These combustion products, as discussed earlier, may be up to eight times less dense than the unburnt gases ahead of them. Consequently, the less dense gases expand and push the flame front forward. The chemical reaction and the motion of the burnt gases accelerating the flame front into the more dense unburnt gases, create thermodiffusion and hydrodynamic instabilities that cause ‘cracks’ to propagate across the flame surface, resulting in a cellular or wrinkled flame surface.

The cellular structure of the flame surface (see Figure 2-10) creates a greater surface area in contact with the unburned gas, giving rise to an increased rate of combustion and hence increased flame speeds.

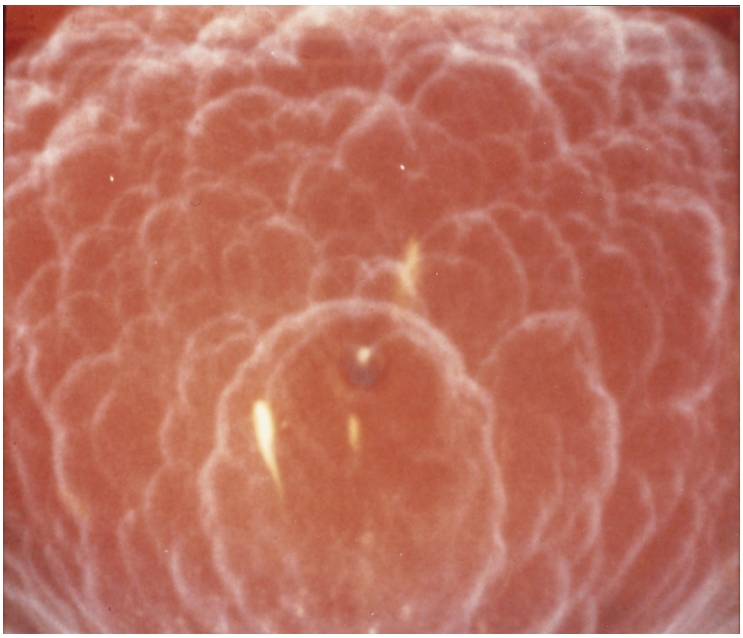

Figure 2-10 Cellular structure of a flame prior to venting (taken from DNV GL archive)

The mass combustion rate may be given by:

$$\frac{dm}{dt} = A_f \rho_u S_u \qquad \textbf{(2-33)}$$

Where:

A_f = Area of the flame.

Although Equation (2-18) can be used to estimate flame speeds under idealised conditions, it does not take account of the increased rate of combustion caused by increases in flame surface area.

A more accurate relationship between flame speed and burning velocity, for a centrally ignited gas/air mixture (hence spherical flame) in a dwelling, is therefore given by:

$$S_f = S_u E \left(\frac{A_c}{A_s}\right) \qquad \textbf{(2-34)}$$

Where:

A_c = the cellular flame surface area (including wrinkles) (m^2).

A_s = the area equivalent to a smooth spherical flame area (m^2).

For a flame propagating spherically, A_s will be given by $4\pi r^2$. For rear ignition of a flammable gas, where the flame initially propagates hemispherically, A_s will be given by $2\pi r^2$.

In practice, it is extremely difficult to account for, with any degree of accuracy, the cellular nature of the flames surface. When magnified, the wrinkles; which may be evident with spherical flames of radii of twenty to thirty centimetres, appear as individual peaks and troughs in the flame's surface, making it very difficult to calculate the surface area.

However, Bradley [134] has shown that, at the transition from cellular to self-turbulising flames, for the typical fuels and concentrations involved in accidental explosions, the turbulent to laminar burning velocity ratio may be estimated as:

$$\frac{S_{u,t}}{S_{u,l}} \approx 3.1 \qquad \textbf{(2-35)}$$

Where:

$S_{u,t}$ = the turbulent burning velocity (m/s).

$S_{u,l}$ = the laminar burning velocity (m/s).

Or, in terms of flame speed:

$$\frac{S_t}{S_l} \approx 3.1 \qquad \textbf{(2-36)}$$

Where:

S_t = the turbulent flame speed (m/s).

S_l = the laminar flame speed (m/s).

It can therefore be seen that the cellular nature of the flame surface increases the flame acceleration by a factor of approximately three. Consequently, a stoichiometric natural gas/air mixture would be expected to exhibit flame speeds in the region of 9 m/s. This value is similar to that observed in experiments conducted by MRS [34, 35].

Deflagration and Detonation

In explosions in air, flames propagate at speeds varying from a few centimetres per second to approximately two thousand metres per second. Flame propagation at velocities less than the speed of sound in air are termed subsonic, whilst flames propagating at velocities greater than that of the speed of sound are termed supersonic. In accidental explosions in dwellings, flames will initially propagate at low velocities in a laminar form but if the unburned gas becomes turbulent the propagation velocities will increase. Nonetheless, the velocities attained are still substantially lower than that of the speed of sound.

It has become convention to name a combustion process where the flame propagates at a subsonic speed as a deflagration and where the flame propagates at a supersonic speed as a detonation [92]. However, it is possible for a deflagration to propagate at a supersonic speed [103].

In a deflagration, combustion reactions occur through means of conduction and molecular diffusion of heat and species (laminar combustion) and through the turbulent mixing of the unburnt and burnt gases (turbulent combustion). In contrast, in a detonation, the reaction front is propagated by a strong shock wave that compresses the unburnt mixture ahead of it beyond its autoignition temperature. The energy released during the ensuing combustion reaction generates substantial heat which is sufficient to maintain the strength of the shock wave ahead of it, and the shock wave and flame front are coupled together to form a detonation wave [135].

2.2.6. The Effects of Scale

The influence of scale in explosion applications that typically involve no great variation in scale is relatively unimportant (e.g. combustion engines). Conversely, the large-scale factors involved in the prediction of pressure generation in a vented explosion in a building make scale dependence critical [136]. To achieve scaling of an explosion, the flame speeds that occur at large-scale must be reproduced at the same relative position in a geometrically equivalent small-scale experiment [137]. However, experimental work has demonstrated that the scale dependence of the combustion processes will result in the small-scale tests generating lower flame speeds and overpressures [37, 48, 138-147]. The simple volume scaling method based on the cube law, assuming spherical flame and constant flame velocity, can only be expected to give an approximate description of the pressure time history before the first peak [148].

In the MERGE experimental programme [149, 150] tests at ‘medium’ and ‘large’ scale were conducted with similar idealised pipework grids. The large-scale grids were twice the linear scale of the medium-scale grids. It was found that under otherwise identical conditions, the large-scale tests produced overpressures more than 50% greater than those at medium-scale.

To achieve scaling it is therefore necessary to compensate for scale effects in both the laminar and turbulent combustion phases of the explosion. This is achieved by increasing the reactivity of the mixture used in the small-scale experimental set-up either by using a more reactive fuel (fractal model) [151-153] or by oxygen enrichment of the gas/air mixture [137]. Due to the plethora of vented explosion research, and to avoid the complications of small scale effects, this literature review will concentrate on large-scale vented explosion research and only the most relevant small-scale studies.

2.3. Confined Explosions

When a gas explosion occurs in a confined enclosure or vessel, there is an associated pressure rise. The pressure rise is caused by the restriction, that the vessel or enclosure places, on the expansion of the hot burnt gases. As discussed earlier in the chapter, the expansion ratio (unburnt to burnt gases), for stoichiometric fuel/air mixtures, is approximately eight for hydrocarbons. This means, assuming adiabatic expansion, that the explosion of a flammable stoichiometric hydrocarbon gas/air mixture, which is initially at atmospheric pressure and temperature, completely confined in a vessel or enclosure, and ignited in the centre of the vessel or enclosure, will generate a pressure in the region of 8 bar. This is well in excess of that a dwelling is capable of withstanding and is the reason that dwellings sustain damage (often structural) when they are subject to an accidental gas explosion. Totally confined explosions that are initiated by an ignition source that is not located centrally will produce a lower maximum pressure. This is because the flame will touch the surfaces of the enclosure sooner than that of a centrally ignited propagating flame, which has the effect of 'cooling' the flame. Similarly, enclosures of L/D great than unity will also produce lower maximum pressures.

The relationship that determines the maximum pressure rise developed in a totally confined explosion, assuming adiabatic conditions, is given by:

$$P_{max} = P_i \frac{N_b}{N_u} \frac{T_b}{T_u} \qquad \textbf{(2-37)}$$

Where:

P_{max} = the maximum pressure (bar).

P_i = the initial pressure (bar).

N_b = the number of moles of products remaining after combustion.

N_u = the number of moles of reactants before combustion.

T_b = the adiabatic flame temperature (K).

T_u = the initial temperature of the gas/air mixture before combustion (K).

The maximum pressure that can be generated in a totally confined explosion occurs when a stoichiometric gas/air mixture completely fills the enclosure. This is not surprising, however, what may not seem so intuitive is that the pressure developed, when considering fuels typically involved in accidental explosions, is independent of fuel type. This is because the energy density of most stoichiometric fuel gas/air mixtures is approximately the same (3.6 MJ/m^3) [86], as tabulated earlier, Table 2-1.

When using Equation (2-37) to calculate the maximum overpressure in a totally confined explosion, care must be taken to use the correct adiabatic flame temperature value. The most commonly quoted adiabatic flame temperatures are measured or calculated at constant pressure and this would lead to an underprediction of the maximum overpressure. In experiments, common hydrocarbon fuels will generate maximum pressures in the region of 8 to 9 bar.

Figure 2-11 shows the calculated pressure-time curves for three different fuel gas/air mixtures that were ignited in a totally confined 1 m^3 vessel. Whilst it can be seen that the maximum overpressure is the same for the different fuel gases, the time taken for them to reach the maximum pressure varies (i.e. the rate of pressure rise is different). This is because the different fuel gases have different burning velocities and hence different flame speeds [16].

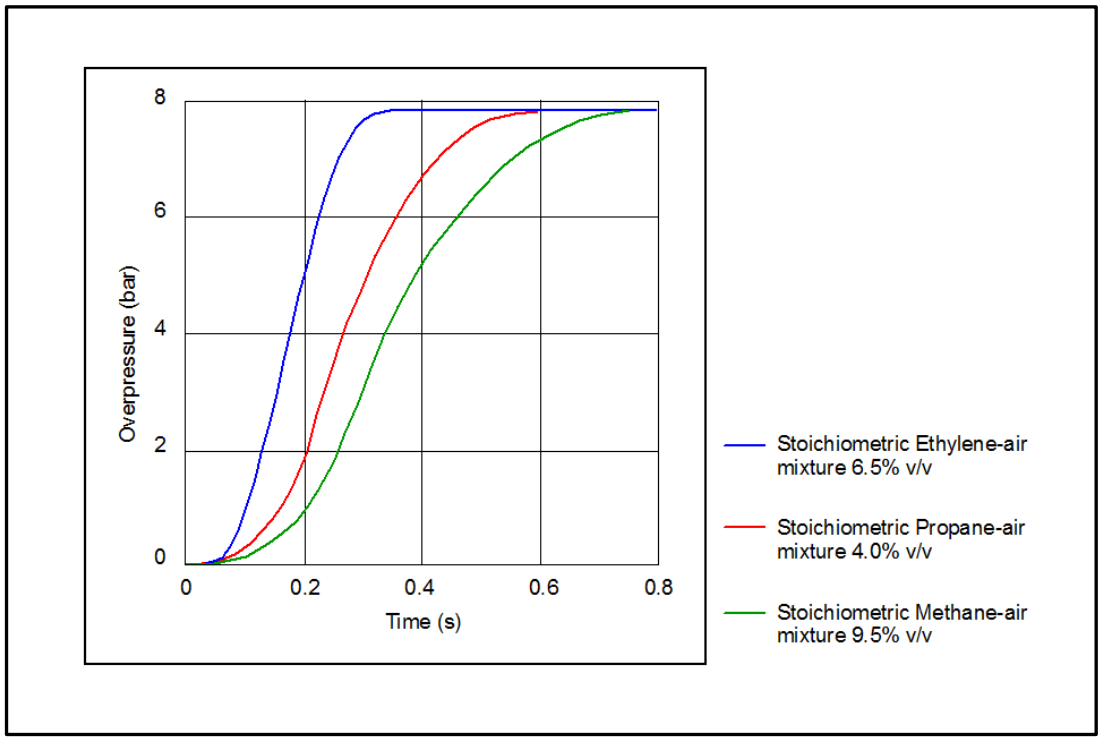

Figure 2-11 Pressure-time profiles for totally confined explosions in a 1 m^3 cubical vessel (taken from DNV GL archive)

The rate of pressure rise may be determined by:

$$\frac{dP}{dt} = \frac{\Delta P}{\Delta t} \text{ bar/s} \qquad \textbf{(2-38)}$$

Where dP/dt is the rate of pressure rise.

The variation in the rate of pressure rise highlighted in Figure 2-11 is a measure of the explosion severity and is an important factor when considering accidental gas explosions in dwellings. It can be seen that propane has a greater rate of pressure rise

than methane, and hence is capable of producing a more severe explosion. However, whilst some fuel gases are clearly capable of producing a more severe explosion than natural gas, it must be remembered that accidental explosions are inadvertently vented events that are subject to a number of other explosion parameters (construction of the building, number and size of inadvertent vents, density of flammable gas, fuel concentration, ignition position, turbulence etc.) that make it impossible for an investigator to determine the fuel type through assessment of the explosion pressure damage (or lack of it) alone.

The maximum pressure that can be developed in a confined explosion is independent of the volume of the enclosure. That is, if vessels of different volume are completely filled with a stoichiometric gas/air mixture they are capable of producing a pressure of 8 to 9 bar (constant volume adiabatic flame temperature). However, in addition to the fuel, the volume of the vessel will also have a significant effect upon the severity of the explosion [154].

Figure 2-12 shows explosions of a stoichiometric propane/air mixture in three vessels of differing volume. It can be seen that all three generate the same maximum pressure but the explosion propagates more rapidly as the vessel volume decreases. Consequently, there is an indirect correlation rate of pressure rise and vessel volume.

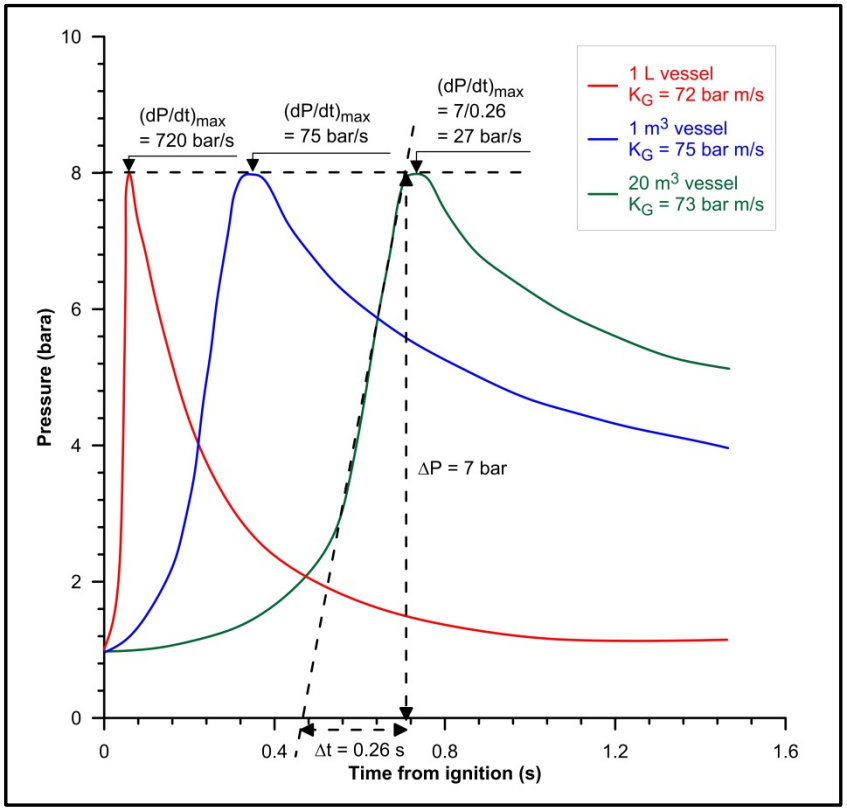

Figure 2-12 Influence of vessel volume on the development of a confined explosion (adapted from Bartknecht [154])

The influence of vessel volume on the maximum rate of pressure rise may be determined by the cube law:

$$\frac{dP}{dt} V^{\frac{1}{3}} = \text{constant } (K_G) \text{ bar m/s} \qquad \textbf{(2-39)}$$

Where V is the volume of the vessel.

The constant, which is referred to as K_G (for gases), is a fundamental characteristic of the given gas and is representative of its explosive nature. Values of K_G for stoichiometric methane and propane gas/air mixtures, ignited with zero turbulence and an ignition energy of approximately 10 J are given in Table 2-3.

Table 2-3 KG values for common fuel gases (taken from NFPA 68 [155])

`Hydrocarbon	**K_G (bar m/s)**
Methane	55
Propane	75

In Figure 2-12 it can be seen from the curve of the 20 m^3 vessel, that there are two stages in the growth period of the confined explosion. An initial period of low pressure rise and then a rapid pressure rise period. Consider a typical room sized enclosure of 3 m x 3 m x 2.5 m high, that is filled with a flammable gas/air mixture. If we consider a spherical flame of diameter equal to half the enclosure width (e.g. 1.5 m), then the volume of the spherical flame is approximately 1/12 of the enclosure volume. However, as the flame sphere contains burnt gases at approximately 1/8 of the density of the unburnt gas/air mixture, it contains only 1/96 of the mass and the pressure rise is a function of the mass burnt. Thus, in the time taken for the flame to grow to a diameter of approximately half the width of the enclosure, the pressure has only risen by approximately 1% of its maximum (i.e. ≈ 80 mbar).

If we apply the above theory to vented explosions, and assume that the very early stages of the explosion may be treated as totally confined, it is simple to predict that early failure of a weak part of the enclosure (windows and brick walls typically fail at pressures less than 80 mbar) would result in a considerable amount of unburnt gas/air mixture being vented to outside.

2.4. Gas Explosions in Dwellings

2.4.1. Vent Coefficients

One of the parameters used in characterising the size of the explosion relief, or vent opening, is the 'vent coefficient'. This term characterises the area of relief required in terms of the size of the enclosure or vessel. There are several methods of defining the vent coefficient (K), the most common of which are, the area vent coefficient, given by:

$$K_A = \frac{A_x}{A_v} \quad \textbf{(2-40)}$$

Where:

K_A = the vent (area) coefficient.

A_x = the cross-sectional area of the enclosure or vessel in the plane of the vent.

A_v = the area of the vent opening.

And, the volume vent coefficient, given by:

$$K_v = \frac{V^{\frac{2}{3}}}{A_v} \quad \textbf{(2-41)}$$

K_v = the vent (volume) coefficient.

V = the volume of the enclosure or vessel.

These two definitions of vent coefficient give the same value for cubical vessels but the value differs when applied to non-cubical vessels. When more than one vent opening is present in an enclosure, the total vent coefficient (K_{total}) can be expressed in terms of the individual vent coefficients, given by:

$$K_{total} = K_1 + K_2 + K_3 + \cdots\cdots \quad \textbf{(2-42)}$$

2.4.2. The Mechanism of Pressure Generation

Numerous studies have attempted to explain the mechanism for the development of a vented explosion [32, 37, 45, 48, 49, 133, 139, 140, 142, 156-165]; which in general has taken the form of identifying a number of pressure peaks on an overpressure-time profile and discussing the cause of them.

In the classic research conducted by Cubbage and Simmonds in the 1950's [164, 165], on explosion reliefs for industrial drying ovens, the researchers were somewhat surprised when analysis of the pressure development, for explosions in drying ovens, revealed two pressure peaks. They had been expecting a sharp pressure rise during

the confined stage of the explosion, followed by a rapid pressure decay once the explosion relief had opened, to produce a pressure peak, P_1.

They theorised that the second pressure peak, P_2, was due to the increased combustion rate as the flame continued to propagate following vent opening, and the imbalance between the rate of combustion and the outflow through the relief opening.

A joint industry project was carried out in Sweden in 1957 [166]. Vented explosion experiments using propane/air and acetylene/air mixtures of varying concentration were carried out in a 200 m^3 building with various sized vent openings. Meteorological balloons placed within the building were used to contain the gas/air mixtures such that the volume could be varied. Volumes of 15, 25, 40 and 70 m^3 were used in the experiments in addition to the full enclosure volume of 200 m^3 (no balloon).

In these experiments, the double pressure peak was observed in addition to oscillatory combustion. As balloons were used, the tests are not directly relevant to this study due to the artificial situation where turbulence is generated upon bursting of a full balloon of gas. However, the importance of this pioneering work lies in the observation that the generation of high overpressures was associated with the subsequent turbulent combustion of flammable gas/air mixture that is expelled during venting.

Butlin and Tonkin of FRS [160], undertook a number of vented layered explosion tests in a 28 m^3 chamber, as part of a larger research programme, following the Ronan Point explosion. The tests were mainly concerned with the maximum pressure generated outside the chamber but a typical pressure-time trace was included in the published report. The pressure-time graph clearly showed three pressure peaks and an oscillatory peak which commenced just after the third pressure peak and was present until the explosion ended. The first, small, pressure peak, P_1, occurred after 300 ms and was undoubtedly caused by the opening of the vent. After 540 ms there was a second pressure peak, P_2, followed shortly afterwards, at 600 ms, by a third sharp pressure peak, P_3, which was immediately followed by the oscillations, P_4. The pressure peaks were likened to the two peaks described by Cubbage and Simmonds [164, 165]. However, the second peak was likely to be caused by the onset of burnt gas venting, whereas the second peak in the Cubbage and Simmonds tests is a function of the maximum flame area.

Solberg et al. [28, 29, 31]; undertook a number of large-scale experimental studies on vented gas explosions in which they concluded that Taylor instabilities following the onset of burnt gas venting may be the dominant mechanism in terms of generating high pressures within an enclosure. They noticed that the instability develops at the rear of

the flame (i.e. the furthest point from the vent), when the hot combustion gases exit the opening at high velocities.

Solberg et al. [30] discussed a series of large-scale explosion tests undertaken in a 35 m^3 prismatic steel explosion chamber. They proposed that the dominating mechanism governing pressure development during a vented explosion is R-T instabilities. Observations of flame development from high speed video of centrally ignited tests showed that, prior to the first significant pressure peak, the flame was smooth and almost spherical. As the flame front reached the vent opening, the volumetric flow of gases through the vent opening increased by a factor of approximately three, giving rise to a pressure peak that the authors considered P_1.

At this point, the combustion gases attain correspondingly higher flow velocities through the vent opening and the backward flame propagation of the rear part of the spherical flame is slowed down causing the flame to become R-T instabilised and highly turbulent giving rise to the second and maximum pressure peak P_2 [30].

Mercx et al. [147] and van Wingerden [156] carried out a large-scale experimental programme in a 38.5 m^3 explosion chamber (4.0 m x 3.7 m x 2.6 m). A number of methane/air explosions were conducted in order to consider the effects of vent size and failure pressure and ignition position. In general, two pressure peaks were exhibited; the first pressure peak was generally attributed to the opening of the vent and the second, and maximum, pressure peak was due to acoustic oscillations. In a test where no vent cover was employed, it was recognised that the first pressure peak was caused by a minor external explosion of unburned gas/air mixture expelled from the enclosure after the vent had opened. As no video cameras were located externally, the cause of this pressure peak was determined by the authors by calculating the time that an externally generated pressure wave would take to reach the pressure transducers located within the enclosure ($\approx$ 5 to 10 ms to travel a distance of 4 m through hot combustion gases).

In two separate studies [156, 157], van Wingerden analysed the results of a number of vented explosion tests undertaken in a 38.5 m^3 concrete enclosure and a 5.2 m^3 enclosure. Both studies produced multi-peak pressure-time profiles, with increased pressures inside the enclosure attributed to minor combustion outside the enclosure. The first pressure peak was found to be due to the vent failure and the second, dominating pressure peak resulted from oscillatory combustion. In some experiments acoustic driven flame instabilities gave rise to a third pressure peak [157].

Bimson et al. [48] discuss a series of vented explosion tests carried out in a 550 m^3 [6.25 m (h) x 8.75 m (w) x 10 m (l)] steel explosion chamber; each wall lined with

Rockwool to dampen acoustic oscillations, and with a vent opening of K_A = 2 in the front face of the chamber which was covered with a thin polythene sheet to contain the gas/air mixture prior to ignition. The tests involved methane/air and propane/air mixtures at 10% above stoichiometric concentration. The authors determined that the inclusion of Rockwool eliminated resonant wall interactions and greatly simplified the interpretation of the pressure-time traces. In all explosions, two significant pressure peaks were observed. The first pressure peak, P_1, was observed when the flame front reached the plane of the vent opening (signalling the onset of burnt gas venting), whilst the second pressure peak, P_2, occurred as a consequence of the external explosion. The external explosion was considered extremely important as it increased the internal pressure by a factor of four above the P_1 peak.

The Stages of a Confined Vented Explosion

Extensive large-scale experimental research carried out by MRS [33-36, 51, 54, 62, 144, 167] has identified a number of distinct ‘stages’ that occur during a vented gas explosion. This work, which was summarised in a paper by Cooper et al. [64], demonstrated that each of the four critical stages of the explosion mechanism were capable of producing a local significant peak on a pressure-time graph, which depending on the circumstances of the explosion, could represent the maximum overpressure peak. Whilst the experiments summarised by Cooper et al. typically identified four significant pressure peaks, the authors recognised that, depending upon the situation, it was possible during a vented explosion to develop between one and six pressure peaks.

By analysing the development of a vented explosion in terms of these four critical stages, it is possible to make a direct comparison of large-scale studies where differing numbers of pressure peaks were identified and/or where the pressure peak was identified as having being caused by a different explosion phenomena. A diagram detailing the four critical stages that were identified by MRS is given in Figure 2-13.

The four stages of a vented explosion may be described as:

- stage 1: confined explosion and vent opening,
- stage 2: burnt gas venting and external combustion,
- stage 3: low frequency oscillatory combustion and maximum flame area,
- stage 4: high frequency acoustic oscillations.

Figure 2-13 shows that there are potentially six pressure peaks that can occur during a vented explosion, each of which may be the maximum depending upon circumstances. However, it should be noted that most gas explosions in dwellings would not exhibit six

pressure peaks. Indeed, many vented explosion pressure–time profiles, representative of realistic accidental explosion scenarios, would only exhibit two or three pressure peaks. This is reflected in the most relevant large-scale research programmes that have been conducted to date [32, 37, 45, 48, 49, 133, 139, 140, 142, 156-163] (see Table 2-4). These pressure peaks have generally been identified in the literature, in the order in which they were observed on the pressure-time profile (i.e. P_1, P_2, etc.). Fakandu et al. [168], analysed the results of some vented explosion experiments and attempted to develop a standard terminology in order to better compare the various pressure peaks identified by vented explosion researchers.

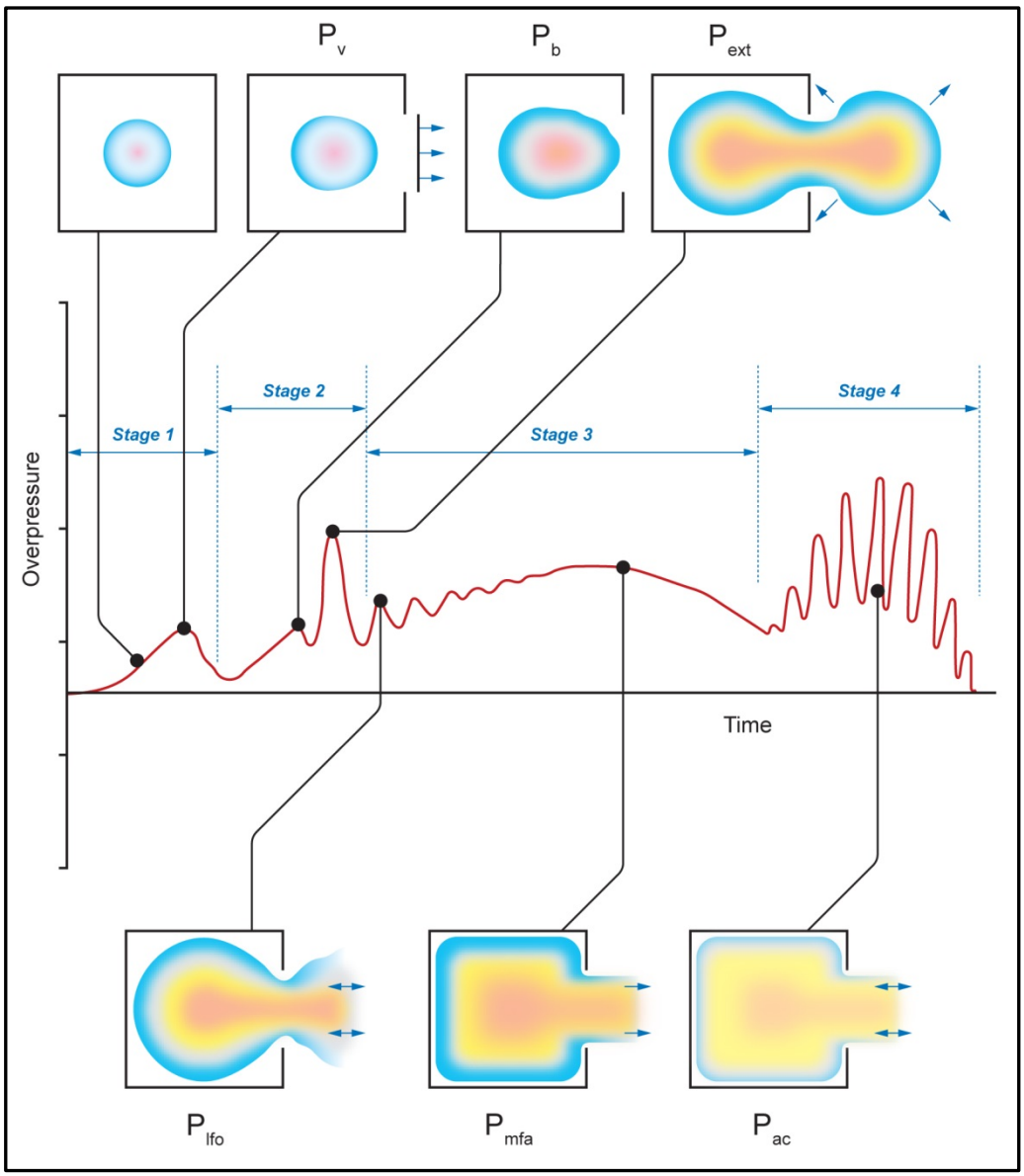

Figure 2-13 Pressure-time profile showing the four stages of a vented explosion

The approach developed by Fakandu et al. has been extended in this study to the most relevant large-scale experimental work and the terminology has been amended to

better identify the pressure peaks. The following terminology is used to describe the pressure-time profile peaks, listed in the order in which they will typically occur:

- P_v – Peak due to vent opening.
- P_b – Peak due to the onset of burnt gas venting.
- P_{ext} – Peak due to the external explosion.
- P_{lfo} – Peak due to Helmholtz oscillatory/Taylor instabilities.
- P_{mfa} – Peak due to maximum flame surface area.
- P_{ac} – Peak due to high frequency acoustic oscillations.

Table 2-4 Potential pressure peaks in a vented explosion and the corresponding stages of the explosion in which they occur

Experimental Programme	Pressure Peak Identified					
	Stage 1	Stage 2		Stage 3		Stage 4
	P_v	P_b	P_{ext}	P_{lfo}	P_{mfa}	P_{ac}
Bauwens et al. [45]			P_1		P_3	P_2
Bimson et al. [48]		P_1	P_2			
Cooper et al. [64]	P_1		P_2		P_3	P_4
Fakandu et al. [168]	P_1	P_2	P_3	P_5	P_4	P_6
Harrison & Eyre [133]	P_1	P_2	P_3			
Mercx et al. [147]	P_1	P_2 (rear ign)	P_3 (rear ign)			P_2 (cent ign)
Pappas et al. [142]		P_1		P_2		
van Wingerden [156]	P_1			P_2		
van Wingerden [169]	P_1	P_2				P_3
van Wingerden & Zeeuwen [157]	P_1	P_2				P_3
Zalosh [37]	P_1			P_2[a]		

[a] Attributed to flame instabilities, but likely caused by the external explosion.

Fakandu et al. [170] and Fakandu [171] considered the development of a vented gas explosion in a 10 litre explosion vessel. The pressure-time results of a slightly richer than stoichiometric methane/air explosion (10% gas in air, $\phi \approx 1.05$), undertaken as part of this work are shown in Figure 2-14. The pressure peaks (labelled 1 to 6 in the original work) have been labelled using the proposed terminology. Fakandu et al. [170], originally described the P_{lfo} pressure peak as having been caused by flow reversal back into the chamber following the external explosion. The authors did not have the benefit of high speed cameras when determining the cause of this pressure peak but the results are identical to those attributed by Cooper et al. [64] and Bauwens et al. [45] as being due to low frequency oscillatory combustion.

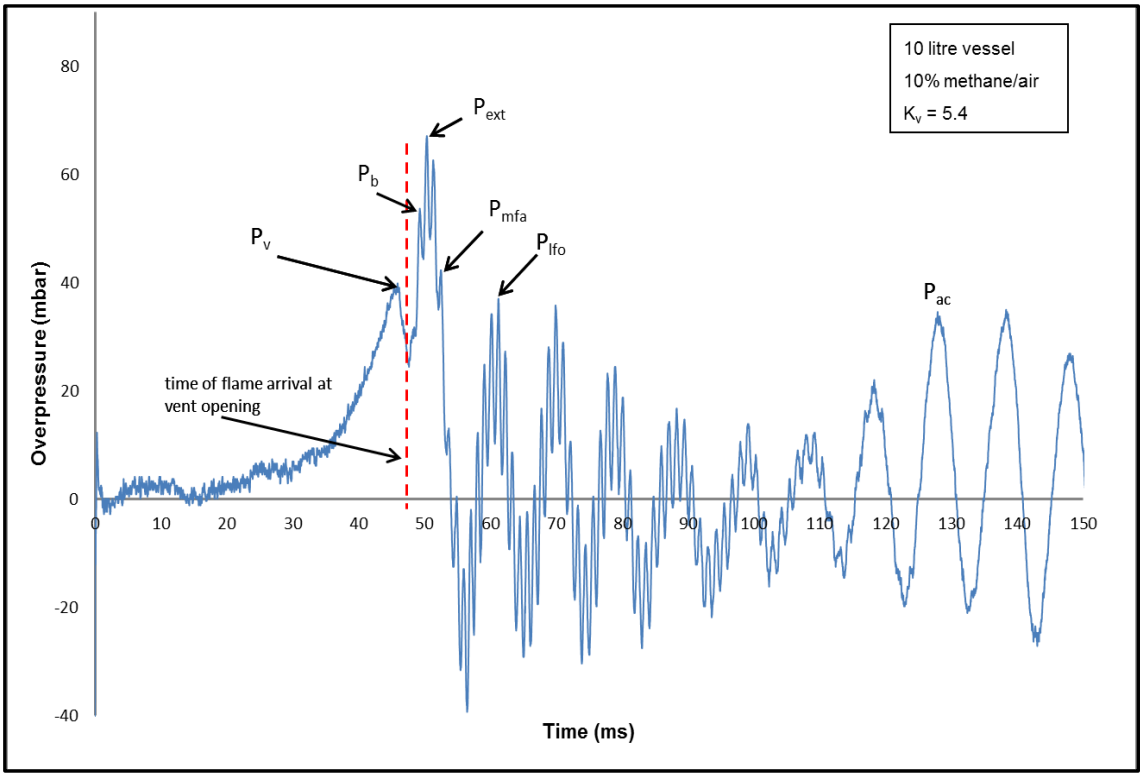

Figure 2-14 Pressure-time profile for vented gas explosion (adapted from Fakandu [171])

To better understand whether there are observed differences, or simply different terminology in the literature, it is beneficial to consider each of the stages of a vented explosion in turn.

Stage 1: Confined Explosion and Vent Opening

If a gas is released into a room, builds up to form a flammable gas/air mixture, and is ignited, the subsequent explosion will initially behave in the same manner as a totally confined explosion. Providing the mixture is quiescent, the flame will originate as a flame kernel at the point of ignition and initially propagate as a laminar spherical flame (largely smooth at this time; see Figure 2-15 A).

Because of the confinement of the room, the expanding hot combustion products are contained and the pressure will begin to rise relatively slowly (at this early stage), with the rate of pressure rise determined by the flame speed, which is dependent on the fuel type and concentration.

Figure 2-15 Confined explosion and vent opening stage (adapted from DNV GL archive)

The flame will continue to grow spherically (for central ignition) and the pressure will continue to rise until it reaches the failure pressure of the weakest component of the room (usually the window), at which point the component fails allowing some of the unburnt gas/air mixture to vent to outside (see Figure 2-15 B). The vent opening phase of this stage should be considered with two different scenarios, the outcome of which will determine whether a pressure peak occurs, and if so, the magnitude of the peak. Consider scenario 1, where the room has a component that has a very low failure pressure (e.g. a single glazed window). In this case, the component will fail very early in the explosion, when the pressure is very low, allowing unburnt gas/air mixture to vent.

If the flow through a vent opening is assumed to be incompressible, and the opening is treated as an orifice, the rate of volume flow through the opening may be calculated by:

$$Q = C_d A_v \sqrt{\frac{2\Delta P}{\rho}} \qquad \textbf{(2-43)}$$

Where:

Q = the volume flow rate (m^3/s).

C_d = the discharge coefficient.

A_v = the area of the vent opening (m^2).

ΔP = the difference in pressure across the opening (Pa) or ($kg/m \cdot s^2$).

ρ = the density of the gas flowing through the opening (kg/m^3).

The venting process commences, typically causing the pressure within the enclosure to fall, producing a pressure peak, P_v. At this stage, in a low pressure vent failure scenario, there will not be a significant pressure gradient across the vent opening and consequently, the rate of outflow will be low, with P_v exhibiting itself as a low pressure peak (Figure 2-16).

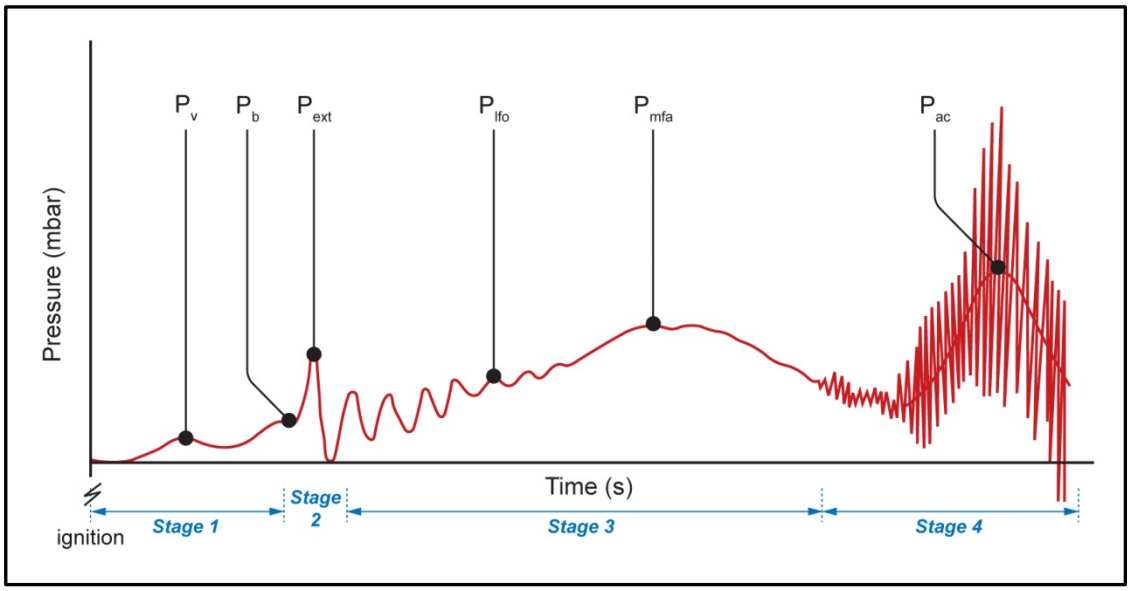

Figure 2-16 Pressure-time profile with a low failure pressure vent showing the four stages of a vented explosion (adapted from DNV GL archive)

In certain instances, the flame propagates at a speed such that the combustion gases are produced at a rate greater than gases can be relieved through the vent. In these situations, the pressure may continue to rise, causing P_v to exhibit itself as a shoulder on an increasing pressure gradient (Figure 2-17).

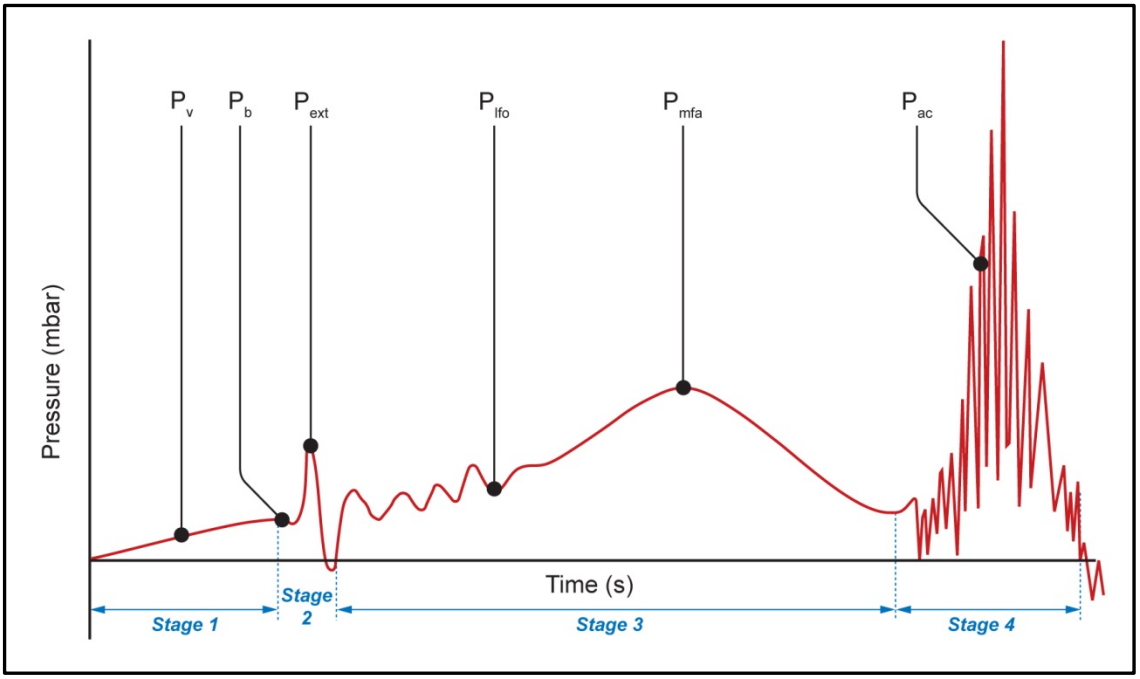

Figure 2-17 Further pressure-time profile with a low failure pressure vent showing the four stages of a vented explosion (adapted from DNV GL archive)

Consider now scenario 2, where the room has a component with a high failure pressure. In this case, the component will fail at a later stage in the explosion when the pressure is higher and consequently the pressure gradient across the vent opening will be greater. This facilitates a greater initial outflow through the vent opening and the pressure in the room will drop more significantly, producing a more noticeable pressure peak (see Figure 2-13). These effects have also been identified in early studies, for example Lunn [172], Burgoyne and Wilson [173] and Cubbage and Simmonds [164, 165]. It should also be noted that with higher failure pressure vent openings, the flame may have become cellular in structure prior to the vent opening, whereas with low failure pressure vent openings this does not occur until stage two of the explosion.

At this stage of the explosion, the pressure generated is proportional to the cube of both the flame speed and time, and consequently, the maximum rate of pressure rise is proportional to the cube of the flame speed and the square of time [16]. Therefore, more volatile fuels, with faster flame speeds, will have a greater rate of pressure rise and will reach a given pressure in a shorter duration. In addition, as the flame speed is a function of the burning velocity, changes in the concentration of the gas/air mixture, which alter the burning velocity, will affect the rate of pressure rise. It follows that explosions involving near stoichiometric concentrations generate higher pressures than those with lean or rich concentrations. Observing Figure 2-15 B, it can be seen that the vent has just opened (right edge of the photograph) and the diameter of the flame is approximately $^{3}/_{8}$ of the diameter of the enclosure. By applying a similar analysis to that

carried out earlier in the chapter, the volume of the spherical flame can be found to be occupying approximately $^1/_{13}$ of the volume of the enclosure and the resulting pressure (assuming the explosion is totally confined at this stage) at vent failure would be in the region of 70 mbar. This simple calculation predicts a pressure greater than a typical component failure in a dwelling (e.g. windows etc.) but is explained by the effects of inertia. The vent will begin to open at its failure pressure, but the outflow of gases will not begin immediately because of the inertia of the confined gases, resulting in a small time lag before venting becomes established.

In addition, because the vent panel has mass, it also has inertia, and it takes a period of time for the vent panel to be moved a sufficient distance to allow full venting through the opening. As a consequence of the effects of inertia, there is a pressure 'overshoot', albeit, at a slightly reduced rate to that prior to commencement of vent opening.

The effects of the weight of relief panels has been studied extensively and the reader should consult references such as Lunn [172], Bartknecht [154], Donat [174] and NFPA [155] for further information.

In order to minimise the damage to a building involved in an explosion, it is therefore necessary to limit the pressure developed by some means. In industrial applications this is often achieved by the use of appropriately designed 'vent panels or reliefs', which are designed to reduce the maximum overpressure to a value, P_{red}, that can be withstood by the protected vessel or enclosure (typically set at 2/3 of the vessel or enclosure design strength) [155]. However, clearly these explosion protection systems would not be desirable in a habitable property. Fortunately, components used in the construction of dwellings are relatively weak, in terms of withstanding explosion loads, and often fail to provide an inadvertent vent opening (see Figure 2-18).

In summary, the P_v pressure peak depends on the failure pressure of the vent opening (P_{stat}), and in non-turbulent environments may be taken to be approximately equal to P_{stat}. Whether there is any pressure overshoot (i.e. $P_v - P_{stat} > 0$), depends upon the inertia of the vent, the rate of pressure rise (i.e. the reactivity of the fuel) and the rate at which the unburnt gas/air mixture is expelled.

Figure 2-18 Accidental gas explosion where early failure of the window has provided adequate vent relief and prevented structural damage to the property

Figure 2-19 Accidental gas explosion where inadvertant venting has failed to prevent structural damage to the property

Stage 2: Burnt Gas Venting and External Combustion

At this stage, due to selective diffusion and hydrodynamic instabilities, the flame surface has adopted a cellular structure. The outflow of gases, both unburnt and burnt, causes the spherical flame to distort towards the vent, adopting a 'pear' like shape (see Figure 2-20 C). The flame continues to increase in size and cellular like structure and consequently the rate of production of burnt gases is also increasing. If the rate of production of these gases increases at a faster rate than the unburnt (and potentially some burnt) gases can be expelled, the pressure will increase still further even though the vent is fully open.

Although venting commenced in stage 1 of the explosion mechanism, the gases vented at that stage were unburnt gases. With the onset of burnt gas venting, the volumetric outflow rate increases dramatically. As the hot combustion products are approximately eight times less dense than the unburnt gases, the volumetric outflow rate increases by a factor of approximately three (i.e. $\sqrt{8} = 2.8$). This significant increase in outflow can manifest itself as a drop in pressure on a pressure-time profile resulting in a pressure peak P_b. However, in the case of a low pressure vent opening, it may be observed as a slight drop in pressure, as shown just before the P_{ext} pressure peak in Figure 2-17. Furthermore, in the case of a higher pressure vent opening, the onset of burnt gas venting will occur much sooner after the vent opens, and coupled with the already increased venting due to the raised pressure gradient across the vent, the pressure drop caused by the increased venting may be superimposed on the already reducing pressure gradient [54]. It should be noted that in the conditions described for a high failure pressure vent, it is possible for a very small P_{ext} pressure peak to be observed on the decreasing pressure gradient, immediately after burnt gas venting and before the low frequency oscillations.

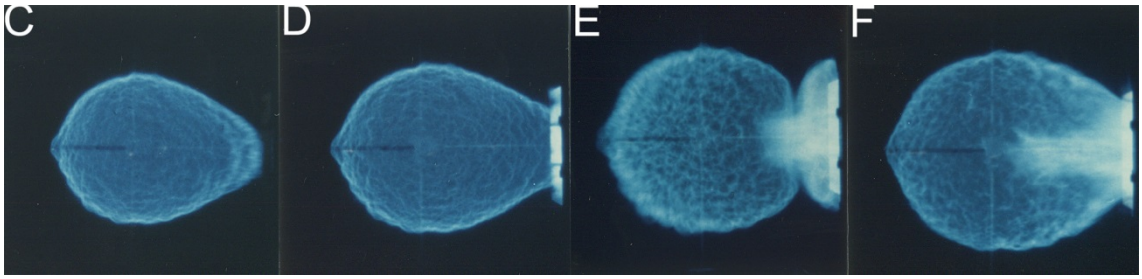

Figure 2-20 Burnt gas venting and external combustion stage (adapted from DNV GL archive)

In Figure 2-20 D, the distorted flame can be seen as it reaches the plane of the vent opening. It is this point when the onset of burnt gas venting generally commences but up until this point the vented gases have consisted of unburnt gas/air mixture. This unburnt gas/air mixture can form a turbulent flammable cloud outside the vent which is ignited when the flame front reaches the vent opening, giving rise to rapid external combustion which creates a pressure wave that, as well as causing a pressure pulse outside the vent, can be observed as a pressure peak of relatively short duration inside the room or enclosure. Figure 2-20 E & F show that the pressure wave generated as a consequence of the external combustion was of sufficient magnitude to push the burnt gases back through the vent opening and into the enclosure. Figure 2-21 shows a photograph of the external combustion stage taken by MRS during an experimental research programme [54].

The effects of the so called ‘external explosion’ have been subject to numerous studies [54, 59, 64, 133, 162, 167, 175-177]. Cooper et al. [64], hypothesise that the P_{ext} peak is caused by the propagation of the external pressure wave into the enclosure. In a few of the tests, wooden boards were placed outside the enclosure and perpendicular to the vent opening, in order to create a partial confinement, and thereby maximising the size of the flammable gas/air mixture outside of the vent. The results of these tests showed a significant increase in the P_{ext} peak whilst the other pressure peaks were unaffected [64]. Contrastingly, they also observed, that in some cases the pressure generated inside the enclosure was greater than that generated by the external pressure pulse. This effect was explained by a temporary restriction to the outflow of gases caused by the reduced pressure differential across the vent opening following the external combustion.

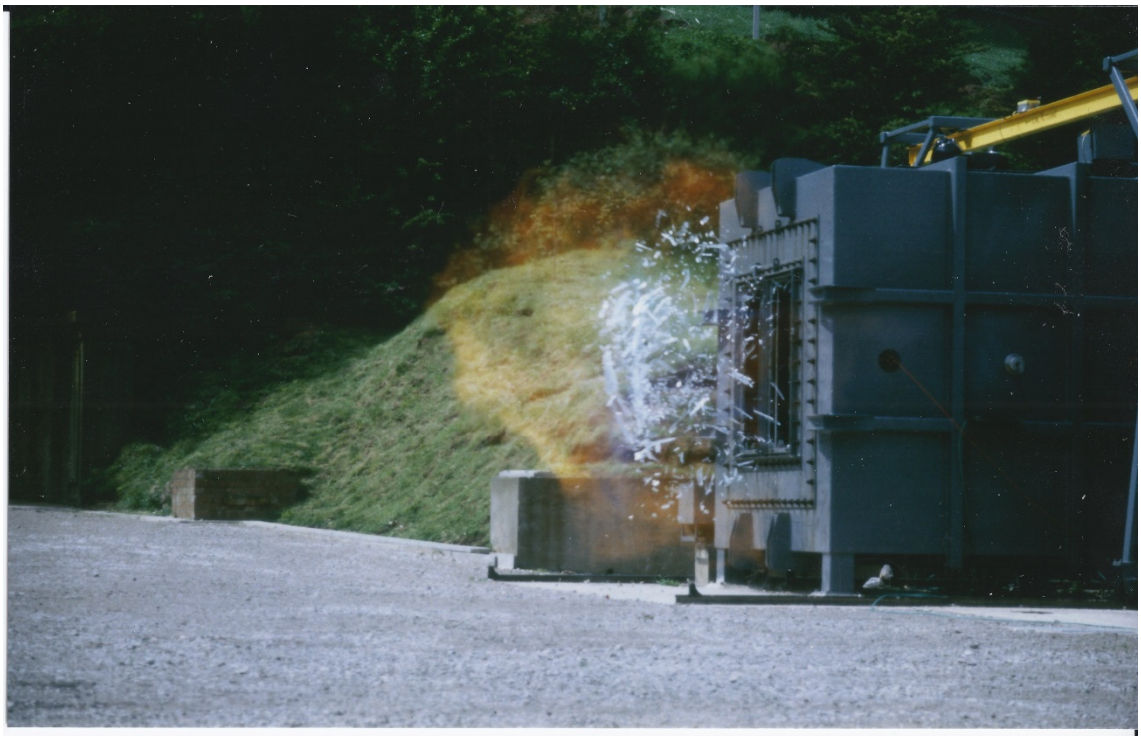

Figure 2-21 Photograph of external combustion at the second stage of a gas explosion (photo from DNV GL archive)

MRS research [54, 167] has demonstrated that whilst the P_{ext} peak is caused by the pressure wave generated by the external explosion, and that its magnitude may be enhanced by restriction of outflow through the vent opening; increases in the rate of combustion caused by turbulence and Taylor instabilities also contribute to the P_{ext} pressure peak. To confirm that the external explosion was the origin of the P_{ext} peak, Greening and Tite [54], examined video footage of several explosions, frame by frame, to determine the time at which the internal and external combustion rate was the greatest. The times at which the P_{ext} pressure pulse was detected on the internal transducer and the external transducer nearest the vent were then also recorded. By comparing the time of peak combustion rate and arrival of the pressure pulse, Greening and Tite determined the time delay between the potential origin of the source and the time at which the pressure pulse arrived at the transducer. For each transducer, they then calculated the distance to the centre of the P_{ext} reaction using the time delay and an appropriate value for the speed of sound in the atmosphere through which the pressure wave would have been travelling (i.e. for internally located transducers, with the speed of sound for hot combustion products). These distances were then used to triangulate the point of origin of the source pressure pulse. In all cases, the source was found to be outside the vessel, even if the calculations for the internal transducer were made using a value for the speed of sound in air.

Notwithstanding the above, results of an experimental programme undertaken by British Gas Research and Technology [178], where the external explosion was prevented by the use of a flame arrestor on the vent opening, provided further evidence that the P_{ext} peak was not solely attributable to the external explosion. The availability of suitable flame arrestors meant the experimental explosion work was undertaken using Perspex tubes, 0.2 and 0.3 m in diameter, with L/D ratios of 2:1 and 3:1 respectively. The 2:1 tube contained a single baffle and the 3:1 tube contained two 6 mm baffles (50% blockage ratio). The vent opening on both tubes was covered with a flame arrester. Up until the flame front reached the vent opening, video records and overpressure-time profiles were found to be similar to tests undertaken without a flame arrestor. Consequently, the flame arrester was determined to have had no visible effect on the flame development within the tube. However the features occurring after the onset of burnt gas venting differed significantly. Firstly, the external flammable cloud was not ignited, and secondly, repeated oscillations of the gas flow within the tube, associated with the onset of burnt gas venting and rapid combustion within the enclosure, were observed. The oscillations were attributed, largely, to the inclusion of the flame arrestor. The magnitude of overpressures generated in the second stage of the explosions were similar to those developed with external combustion events, with the addition of the flame arrestor increasing the prominence of the pressure peak associated with the onset of burnt gas venting. The results of these tests suggested that the external combustion event did not necessarily cause the P_{ext} peak and that turbulent combustion and flame instabilities could also be dominant factors.

The P_{ext} peak is more likely to be evident with low failure pressure vent openings (due to the relatively late arrival of the flame front), rear ignition (as more unburnt gas will be pushed through the vent opening) and possibly with richer gas concentrations (as the turbulent unburnt gas/air mixture expelled through the vent may mix further with available air, thus developing a large cloud of near stoichiometric concentration). These effects, in addition to the effects of interconnecting rooms will be explored in later chapters.

Harrison and Eyre [133], carried out a series of eighteen explosion experiments using natural gas/air and propane/air mixtures in a 30 m^3 explosion chamber [5.92 m (l) x 2.38 m (w) x 2.16 m (h)] to investigate the effects of the external combustion stage of a vented explosion.

The pressure-time profiles from the tests presented a variety of characteristics including single, multiple and oscillatory pressure peaks. All the pressure-rime profiles exhibited a small amplitude (10 – 20 mbar) P_v peak associated with the removal of the thin polythene sheet covering the vent opening. P_b peaks associated with the onset of

burnt gas venting were observed during experiments with rear and central ignition, with a P_{ext} peak caused by the external explosion following almost immediately. In central ignition tests, low frequency R-T instabilities were triggered by the external explosion producing a P_{lfo} peak which was followed by a P_{ac} peak related to higher frequency acoustic oscillations.

An important observation was that for any given fuel and vent size, greater pressures were observed for rear ignition than those with central ignition. Furthermore, the amplitude of the pressure peak for near vent ignition was very small (circa 10 mbar) except for those produced by acoustic pressure oscillations close to the end of the explosion. The reason for the increased overpressure for rear ignition tests was due to the increased amount of unburnt gas that was expelled from the vent. It was also noted that, in a number of tests, the external explosion influenced the magnitude of the pressure within the chamber. The reasoning for this conclusion was the restriction that the external event placed on the outflow of gases through the vent and the propagation of an acoustic pressure wave into the enclosure. Importantly, in all eighteen tests the magnitude of the pressure inside the enclosure was greater than that recorded outside. Consequently, the authors determined, in agreement with the findings of MRS [54, 167, 178], that external combustion could not be solely attributable to the pressure peak generated by external combustion.

Harrison and Eyre [133] also observed that in tests conducted with a larger vent, the flame typically emerged from the vent as a narrow jet and a few metres from the plane of the vent opening the flame propagated rapidly in all directions, giving rise to the peak external overpressure. For the small vent opening tests, the emerging jet velocity was very high and the unburnt gas/air mixture, by the time of flame arrival, was distributed a long way from the vent opening. In these instances, external flame propagation was elongated and not spherical. For large vent areas, the internally generated pressures were correspondingly lower and the peak external pressure typically exceeded the internal pressure at the time of the external explosion. For small vents, the reverse was found to be true. For this reason, and because the size of pressure wave that can propagate into the enclosure is limited by the size of the vent, the influence of the external explosion was found to be greater with larger vent areas. For small vents, the centre of the external explosion was typically several metres from the vent opening and it was noted to occur well before the normal maximum internal pressure was attained.

This meant that in practice, for large vents, the external explosion was the dominating influence on the internal pressure whereas for small vents the effects of the external explosion were likely to be less significant.

The authors discussed the manner in which the external explosion influenced the pressure within the enclosure; recognising that three different effects were evident:

i. The pressure generated outside the chamber by the external explosion reduces or reverses the pressure gradient across the vent opening, impeding the flow through the vent and thereby increasing the internal pressure.
ii. The acoustic pressure wave generated by the external explosion may propagate into the enclosure thereby affecting the internal pressure. The acoustic wave was found to reflect from the rear face of the enclosure producing larger, narrower pressure peaks at the rear than the front of the enclosure as a consequence of the incident and reflected acoustic pressure waves. A negative phase, which is not expected from an 'internal' explosion, was also observed in the internally measured pressure traces, which was reasoned to be triggered by the external explosion.
iii. The external explosion triggers low frequency oscillations (instabilities).

Harrison and Eyre [133] analysed the earlier work of Zalosh [37] and reasoned that the pressure peaks attributed to flame instabilities by the author were likely caused by the external explosion.

Stage 3: Low Frequency Oscillatory Combustion and Maximum Flame Area

Cooper et al. [64], identified another effect that was evident in a number of the experimental tests that were undertaken. They observed the motion, of pockets of burnt gas within the vessel, towards and away from the vent opening. This type of motion is known as a Helmholtz, or organ-pipe, oscillation and is visible in Figure 2-16 & Figure 2-17 as a low frequency oscillation just after the P_{ext} pressure peak, giving rise to a pressure peak P_{lfo}. Helmholtz oscillations can become more influential in large L/D ratio enclosures.

Once the external combustion process is complete, the venting of both unburnt and burnt gases is re-established and the flame continues to propagate; increasing in area and hence combustion rate. The Helmholtz oscillations that were initiated in stage two are gradually damped out as the flame surface continues to expand. However, they can induce Taylor instabilities at the flame surface furthest from the vent opening (where the rear of the flame is propagating towards the rear of the enclosure, and in the direction of the unburnt, denser gases).

It can be seen from Figure 2-22 G, that the whilst the flame surface area is increasing, it is beginning to be affected by the interaction of the walls of the enclosure, losing its spherical shape and taking on the shape of the enclosure (see Figure 2-22 G).

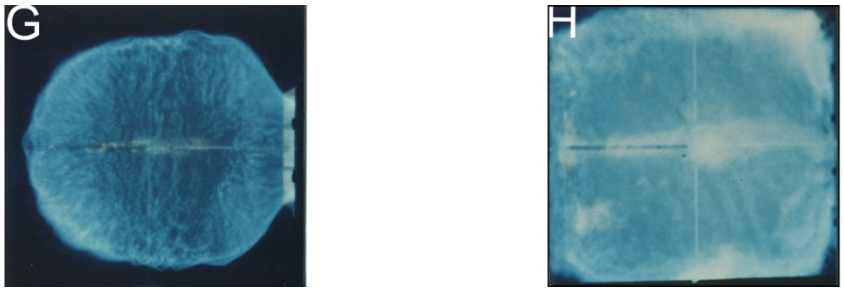

Figure 2-22 Maximum flame area (adapted from DNV GL archive)

The changing in shape of the flame surface means that, in terms of gas explosions in dwellings, where the enclosures are typically rectangular, the maximum flame area will occur later in the explosion and its maximum surface area will be greater than a corresponding spherical flame, so a higher maximum pressure will be attained than might otherwise be expected with a spherical container. As a consequence of the increasing flame surface area, the pressure within the room will either rise or fall, depending upon the balance between the rate of production of combustion products and the outflow through the vent opening. Where the production of gases is greater than the rate at which they are expelled, such as with smaller vent openings, the pressure will once again rise.

When the flame touches the surfaces of the enclosure it is cooled. The consequences of the flame cooling are twofold. Firstly, the combustion reaction is quenched, which results in a reduction in the flame surface area and hence a reduced combustion rate. Secondly, the reduced combustion rate causes a drop in the pressure within the enclosure which may be observed as the P_{mfa} peak on the pressure-time profile (see Figure 2-16 and Figure 2-17). It should be noted that the P_{mfa} pressure peak is typically broader and of longer duration than peaks P_v and P_{ext}.

Bauwens et al. [45] carried out large-scale vented explosion tests in a room sized enclosure of volume 63.7 m^3 to determine the effects of obstacles on pressure generation. A number of explosion tests were conducted without obstacles, the results of which exhibited two pressure peaks. The authors determined that the first pressure peak was associated with the combination of external combustion, Helmholtz oscillations and Taylor instabilities, whilst the second peak was produced as a consequence of interactions between the surface of the flame, acoustics and the structure of the enclosure .

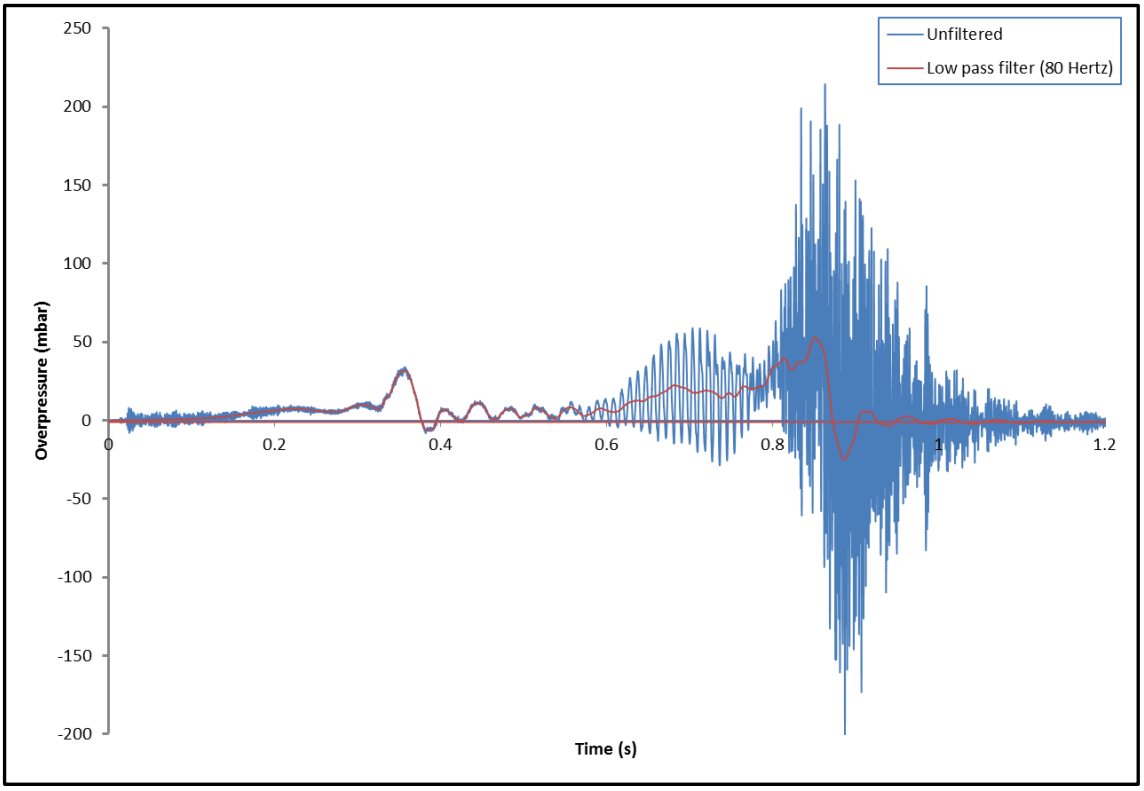

Figure 2-23 Pressure-time profile for a large-scale vented explosion (adapted from Bauwens et al. [45])

The evidence of research to date, conducted in single empty enclosures, suggests that a pressure-time profile for an accidental natural gas explosion would not be dominated by a P_{mfa} peak. This is because relatively large inadvertent vent openings are typical and the fuel has a low burning velocity. Furthermore, the P_{mfa} peak may be expected to be considerably lower than peaks P_v and P_{ext}. LPG, having a higher initial burning velocity, would be expected to produce a higher P_{mfa} pressure. However, these fuels are more susceptible to acoustic instabilities, which are often initiated before the flame has reached its maximum surface area, and which can mean that the pressure peak is not observed. Nevertheless, the conditions encountered in a typical dwelling mean the likelihood of acoustic stabilities occurring is significantly less than that of an experimental test which are typically carried out in metallic enclosures with thin walls and thus easily excitable acoustics.

In summary, the P_{mfa} pressure peak is only likely to be dominant in situations where there is a very low failure pressure vent but of insufficient area (hence the rate of venting is insufficient to prevent the pressure rising) or where there is significant turbulence. The effect of turbulence in gas explosions in dwellings is to be considered later in this chapter.

Stage 4: Acoustic Pressure Oscillations

Combustion derived pressure oscillations has been observed in large-scale experiments by Zalosh [37], van Wingerden and Zeeuwen [132, 157], Tamanini and Chaffee [63], Thorne et al. [179], Dragosavic [180] and McCann et al. [181]. The P_{ac} peak shown in Figure 2-16 and Figure 2-17 usually, but not always, occurs at a late stage in an explosion and is associated with high frequency acoustic oscillations of large amplitude. MRS [33-35, 54, 62] undertook a significant research programme to determine the effects of oscillatory flame instabilities having become aware of a number of vented explosion tests where oscillatory pressure peaks had been observed. Over 120 vented explosion tests were undertaken during this programme during which it became apparent that oscillatory combustion effects were strongly dependent on the geometry of the enclosure and its acoustic characteristics [33].

Accidental explosions occur in dwellings that have significant damping materials within them that are capable of absorbing the acoustic oscillations. Consequently, for the purposes of this study, the oscillatory stage of the explosion can be ignored. However, for completeness, there are a few fundamental observations that are worth noting:

1. The oscillatory stage of the explosion always occurred during the period when the flame was venting through the opening and the oscillations coincided with a sudden increase in luminosity [33].
2. The oscillatory pressure peaks were found to occur over a particular band of gas/air concentrations. For natural gas, this range was between 8 – 12% gas in air, with the highest pressures, perhaps not surprisingly, being recorded with near stoichiometric concentrations. However, other researchers reported that this peak occurs most frequently with fuel rich mixtures [132, 157].
3. The oscillatory peaks always marked the end of the explosion, that is, the combustion process ended and the mean pressure within the enclosure decreased to ambient shortly after the oscillations ceased.
4. The magnitude of the pressure peak generated during this stage of the explosion was found to increase with vent failure pressure [33].
5. Because of the acoustic nature of empty cubical chambers, the magnitude of the pressure peak is likely to be greater in them than non-cubical chambers or chambers with sound dampening materials (e.g. wall surface coverings, furniture etc.).

The Effect of Enclosure Volume

It has already been shown that the maximum pressure that can be developed in a totally confined explosion is independent of volume. However, in a vented explosion, the rate of pressure rise is a critical factor in pressure generation. So, given that the combustion rate is a key parameter in the development of pressure, and that the combustion rate is dependent upon the flame surface area (including the effects of flame disturbance), it follows that the enclosure volume should in some way affect the pressure generated in a vented explosion.

During the confined stage of a vented explosion it is important to consider the maximum pressure generated, the rate of pressure rise and the pressure difference between the maximum pressure attained and the failure pressure of the vent (sometimes called the overshoot). This difference in pressure is found to be inversely proportional to the cube root of the volume of the enclosure:

$$P_1 - P_V \propto \frac{1}{\sqrt[3]{V}} \qquad \textbf{(2-44)}$$

MRS [144] conducted research into the effects of enclosure volume during a number of large-scale experimental tests using cubical enclosures of volume ranging from 0.055 m^3 to 112 m^3. The results of these tests revealed, that to a certain extent, all of the potential pressure peaks were dependent upon the enclosure volume.

It was demonstrated that the pressure difference between the P_v maximum pressure and the failure pressure of the vent (P_{stat}) decreased with increasing enclosure volume. This is in agreement with the relationship shown in Equation (2-44). It was also shown that for small vent areas, the P_{ext} pressure peak increased with increasing vessel volume. However, for larger vent areas the pressure appeared to be unaffected by changes in the volume of the enclosure.

The pressure peak that occurs when the flame surface area has reached its maximum, P_{mfa}, was found to increase in proportion to the cube root of the enclosure volume [144]:

$$P_{mfa} \propto \sqrt[3]{V} \qquad \textbf{(2-45)}$$

Oscillatory pressure peaks were observed in large enclosures with small vent areas whereas they were rarely encountered in smaller enclosures with large vents, indicating that there is some dependence on enclosure volume. In addition, it was noticed that, in order to eliminate acoustic disturbances, more acoustic damping was required with enclosures of larger volume.

Zalosh [37] carried out vented explosion tests in small-scale and large-scale enclosures, and concluded that the amplitude of the second pressure peak was an order of magnitude greater for an explosion in a large enclosure than it was for an explosion in a small enclosure with comparable vent areas. The reason for this finding was explained by suddenly accelerated combustion caused by flame instabilities in the latter part of the explosion. This observation is supported by the study of McCann et al. [181], who observed that flame cellularity appeared at an earlier stage of the explosion in a larger enclosure; whereas in a smaller enclosure the onset of cellularity did not occur until just prior to vent failure and, consequently, did not have a significant effect on the flame size and hence pressure rise.

Kasmani et al. [182], and Kasmani [183] also investigated the influence of vessel volume on vented gas explosions by conducting tests in vessels of volume 0.2 m^3 and 0.0065 m^3. Their findings indicated that greater pressures were generated in explosions in enclosures of larger volume and that this was caused by flame self-acceleration and the development of larger flame surface areas within the enclosure.

The Effect of Vent Size

Rasbash and Rogowski [184, 185] undertook a series of propane/air and pentane/air vented explosion experiments in long ducts of L/D 6 to 48, in which the size of the vent was varied from K_A = 1 (i.e. completely open) to K_A = 64. It was found that the overpressure was directly proportional to K_A or inversely proportional to the vent size.

Sutton and Tite [62] carried out natural gas/air vented explosion experiments in vessels of volume 2.39 and 0.68 m^3 with an L/D ratio 3:1 and vent size that was varied between K_v = 3.2 to K_v 18.9. Reducing the vent size was found to affect not only the maximum pressure but also the mechanism responsible for the generation of the pressure. The authors found that as the vent size was increased, the magnitude of P_b decreased because unburnt gas venting was not significantly restricted by the vent opening and the external explosion, P_{ext}, was dominant. However, as the size of the vent was reduced, venting was restricted which increased the magnitude of P_b. and the external explosion became less significant and in some instances (i.e. very small vent) resulted in its pressure peak, P_{ext} merging with the pressure peak P_b, to produce a single broad peak.

Rogers and Tite [144] conducted natural gas/air vented explosions in a 112 m^3 vessel. They found, that for large volume vessels, whilst smaller vent areas generally resulted in greater P_b pressure peaks in comparison with larger vent areas, there was little significant difference in the pressure generated.

Alexiou et al. [186] reported on vented natural gas/air explosion tests carried out in a 76 mm diameter cylindrical vessel of L/D 13.6 with vent sizes of K_A = 1 to K_A = 5. They found that for smaller vent areas (K_A = 5), the P_1 pressure peak was found to be dominant. This pressure peak was attributed by the authors to be due to the maximum flame area (P_{mfa}). It was also observed that smaller vent areas resulted in lower maximum flame speeds. This was due to the impeding of the flow through the vent opening in comparison to that of the larger vent openings.

Bauwens et al. [45] observed, during explosion experiments in a cuboidal vessel of volume 63.7 m^3 with a low failure pressure vent openings of K_A = 5 and K_A = 2.5, in agreement with the findings of Rasbash and Rogowski, that reducing the size of the vent had the effect of increasing the peak pressure for all configurations and ignition locations.

Hammond [187] carried out research into multiple vents in enclosures. He observed that if the failure pressures of the vents were different, venting occurred predominantly through the single vent of lower failure pressure.

The Effect of a Gas Layer

In accidental gas explosions in dwellings, it is reasonably common for the escaping fuel gas to mix with air in a room and form a flammable layer. The position of the layer is dependent on the relative density of the gas, the location of the release and the type of ventilation pattern. The reader is referred to Harris [16], for detailed information relating to the build-up of gas in a dwelling. In very general terms, releases of natural gas (i.e. less dense than air) may form a high level layer from the point of release to the ceiling and escapes of LPG (more dense than air) may form a low level layer from the point of release to the floor.

Buckland [188], as part of a larger FRS study of vented explosions, presents work undertaken to consider the effects of explosions of gas layers in room sized enclosures. The conclusion of the study was that the explosion pressures produced by buoyant layered explosions should not cause any significant structural damage to a dwelling.

Earlier in the chapter, it has been shown that in a totally confined explosion, the maximum pressure that can be generated depends solely upon the energy density of the gas. Nonetheless, Cubbage and Marshall [189], demonstrated that the pressure generated in a vented layered explosion (i.e. the gas/air mixture does not fill the enclosure); can, under certain circumstances, be as high as when the enclosure is completely full of flammable gas/air mixture, even though the energy density is less. By plotting the pressure in the enclosure (at the time of vent opening), against energy

density, they were able to observe that, for large vent areas, it is necessary to fill as little as 1/E (i.e. 1/8 for typical hydrocarbons) times the volume of the enclosure to generate the same maximum pressure that would be produced if the enclosure were completely filled with a flammable mixture (see Figure 2-24). However, under most circumstances, greater maximum pressures will be produced by near stoichiometric concentrations that completely fill the enclosure. For clarity, it should be stressed that the pressure generated with layered explosions only has the potential to equal that of a completely full enclosure in the first stage of the explosion, in the later stages of the explosion the pressure generated by a layer will always be lower in comparison.

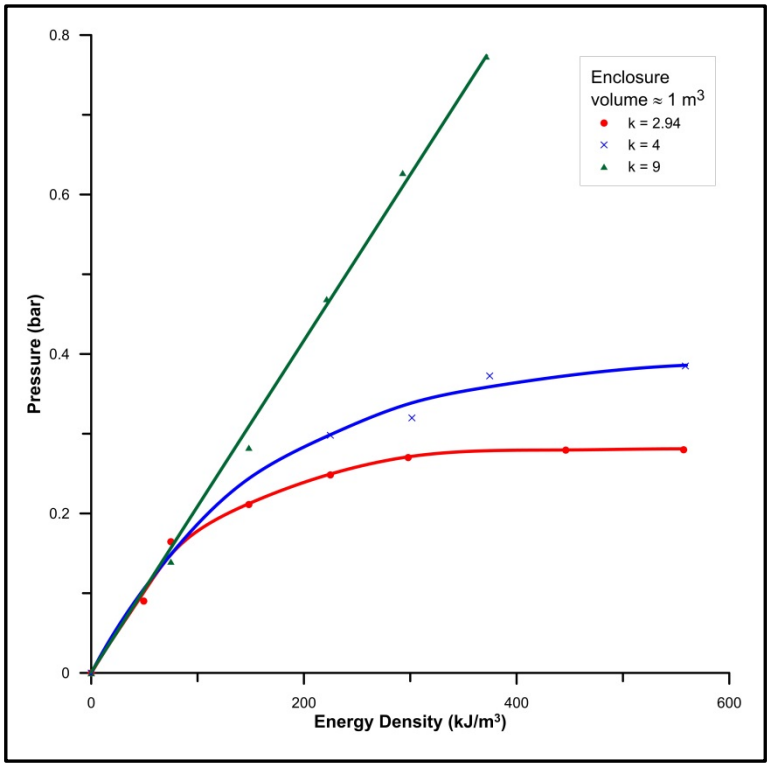

Figure 2-24 Pressure generated at time of vent opening during a layered natural gas explosion (adapted from Cubbage and Marshall [189])

Butlin and Tonkin [160], carried out a number of vented explosion experiments to determine the effect of layer depth on the pressure generated within a 28 m^3 enclosure with varying vent opening sizes. High level layers of stoichiometric natural gas/air mixture were ignited at the rear of the enclosure. The results are shown in Figure 2-25, where it can be seen, for a given vent size, that the pressure generated within the enclosure increases with layer depth.

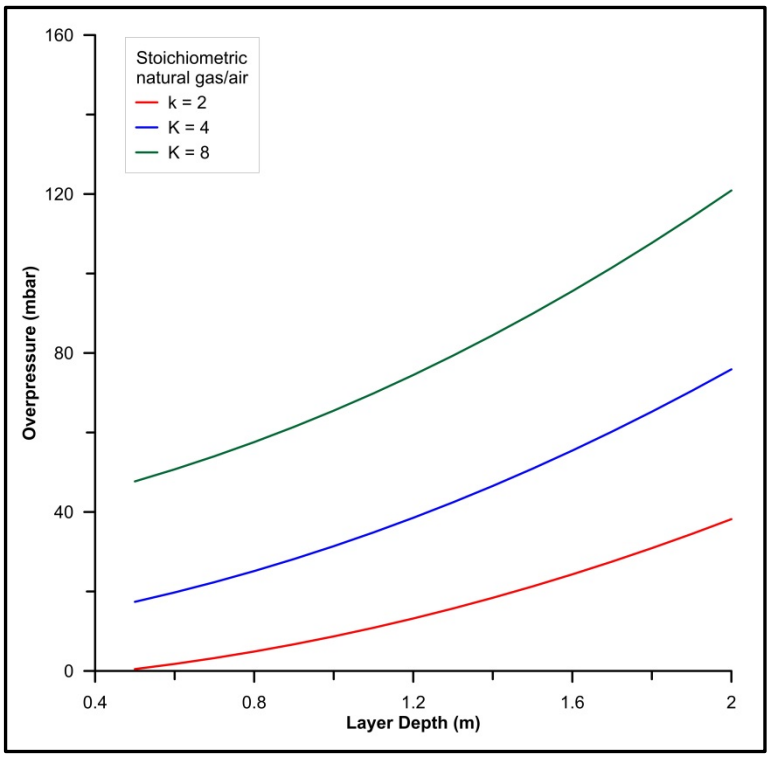

Figure 2-25 Effect of layer depth on pressure produced inside enclosure (adapted from Butlin & Tonkin [160])

Explosions Produced by Pockets of Flammable Gas-Air Mixtures

When investigating accidental explosions, it is sometimes necessary to determine if a 'pocket' of flammable gas/air mixture, filling a small fraction of the room or enclosure, was capable of causing the explosion.

Experimental work carried out by Cubbage and Marshall [189], demonstrated that the maximum pressure that could be generated in an enclosure by a pocket of gas, was a function of the energy contained within the pocket, relative to the volume of the enclosure (i.e. a function of the energy density). For explosions of pockets of gas where venting does not occur, the maximum pressure may be estimated by the following equation:

$$P = 1.87\xi + 0.8 \times 10^{-3}\xi^2 \qquad \textbf{(2-46)}$$

Where:

ξ = the energy density (kJ/m^3).

If the explosion was vented, and it is suspected that a pocket of flammable gas was involved, a modified equation is given in Cubbage and Marshall [189].

The Effect of Gas Concentration

In all of the confidential, large-scale vented explosion research programmes, carried out by MRS [33-36, 51, 54, 62, 144, 190], explosion tests were undertaken with gas concentrations across the natural gas flammable range. In addition, a number of the tests were repeated with varying concentrations of propane. Consequently, there is a wealth of information available regarding the effects, on pressure generation, of varying gas concentration.

There are two main effects of varying the concentration of a flammable gas/air mixture. It has already been shown earlier in the chapter that the burning velocity alters with gas concentration, with the value reducing from a maximum, that is slightly rich of stoichiometric, as the concentration diverges towards the flammable limits. This is of critical importance in vented explosions as it governs the rate of production of combustion products and if this is greater than the rate at which they can be vented from the enclosure, the pressure will rise. Consequently, whilst it was shown earlier that the burning velocity does not affect the maximum pressure generated in a totally confined explosion, it can affect the maximum pressure generated in a vented explosion. The effect of changing natural gas concentration on explosion pressure (in the early stages of a vented explosion) is shown in Figure 2-26.

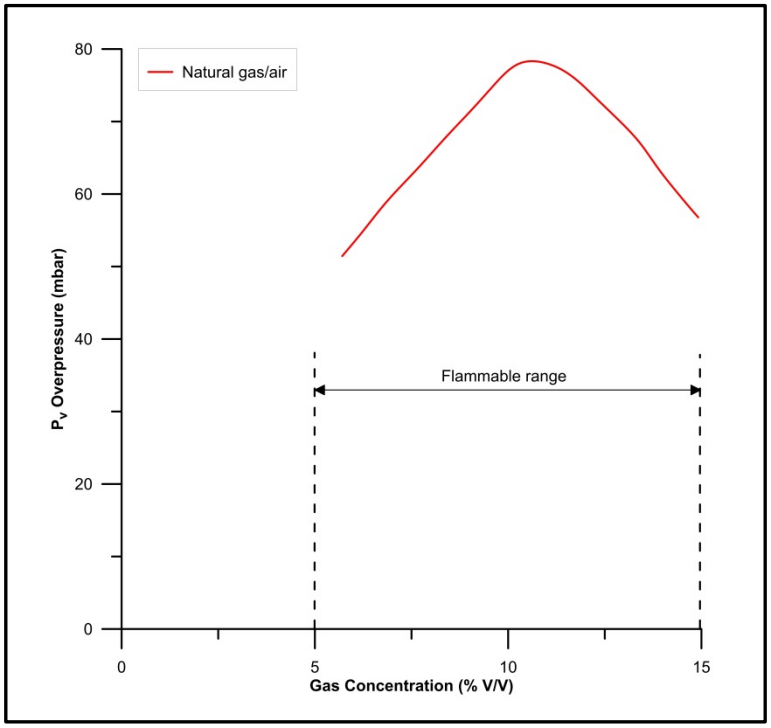

Figure 2-26 The variation in explosion pressure with gas concentration (stage 1 natural gas/air – adapted from Cubbage and Marshall [189])

Not surprisingly, the pressure-gas concentration curve is similar to the shape of the burning velocity-gas concentration curve, with the maximum pressure occurring near the stoichiometric concentration, and values reducing as the concentration diverges towards the flammable limits.

It was noted [34, 35], under certain circumstances, that the highest pressure generated in a vented explosion did not always occur when the burning velocity was at its maximum (i.e. the gas concentration was not just rich of stoichiometric). This was found to occur in situations where the most significant contributory factor to pressure generation was the external combustion and the dominant pressure peak was $P_{ext.}$ In these situations, fuel rich unburnt gases, which are expelled through the vent opening, mix with air to produce a flammable gas/air mixture that is close to stoichiometric concentration.

Figure 2-27 shows how the pressure produced within the enclosure, during stage 2 of the vented explosion, may vary with gas concentration prior to venting. Contrastingly, fuel lean and stoichiometric mixtures may be diluted to produce leaner gas/air mixtures and consequently lower pressures within the enclosure.

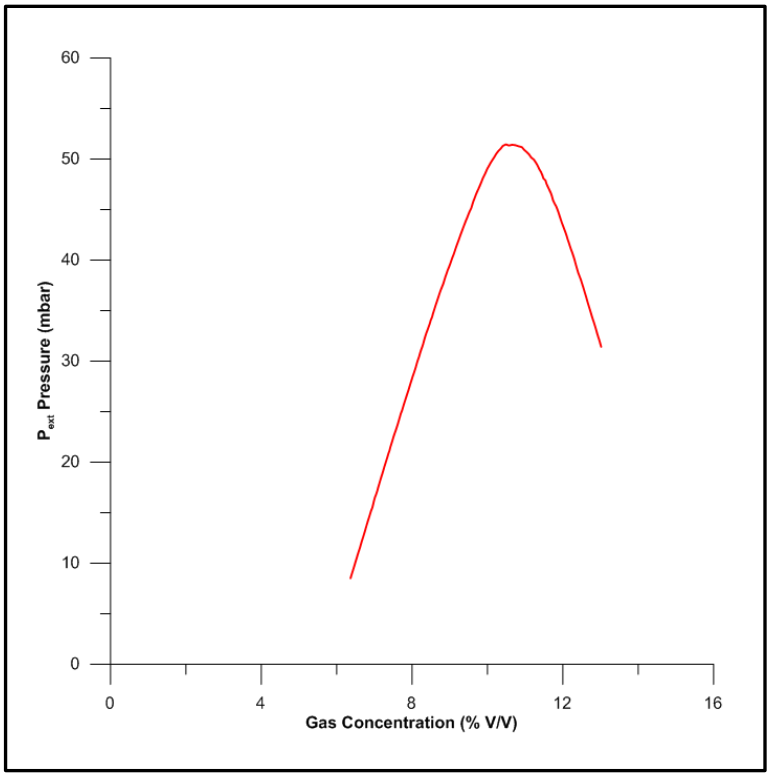

Figure 2-27 Variation in explosion pressure with gas concentration (stage 2 natural gas – adapted from Cubbage and Marshall) [34])

The second effect of gas concentration on pressure generation within the enclosure is caused by changes to the expansion factor. The expansion factor is largely dependent on the flame temperature and to a lesser extent the combustion chemistry (i.e. mole number ratio). It has been shown that the flame temperature reduces as the gas concentration diverges to its flammable limits, and consequently, the expansion factor is strongly dependent upon gas concentration.

Changes in gas concentration also affect the mole number ratio. For fuel lean mixtures, the effects of changing mole number ratio are insignificant. However, as the fuel/air mixture increases in concentration, the mole number ratio increases significantly. Calculations for the mole number ratio vs. equivalence ratio for methane, ethane and propane have been carried out using GASEQ [88] and are plotted in Figure 2-28 for comparison.

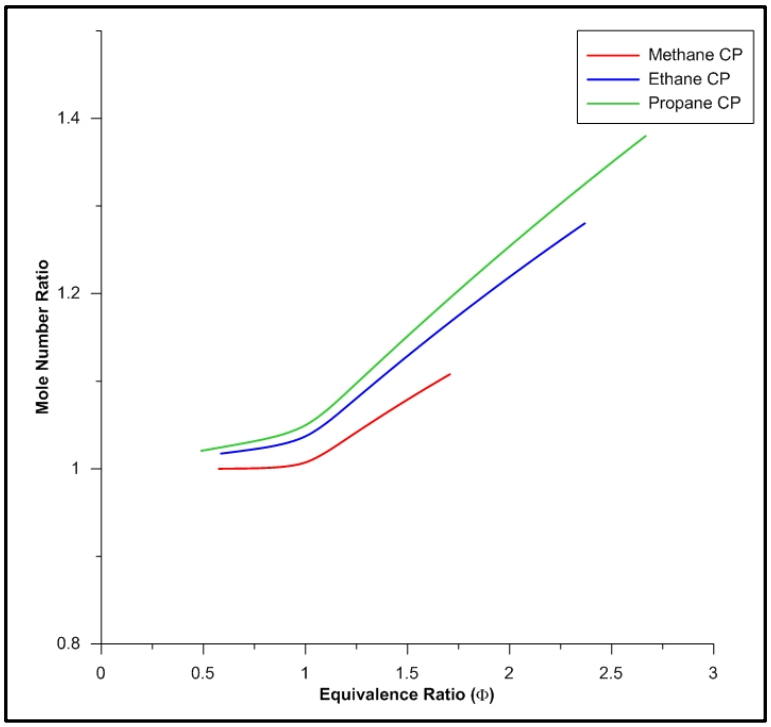

Figure 2-28 Variation in mole number ratio with gas concentration (calculated using GAEQ [88])

The effect of the increase in mole number ratio with increasing gas concentration, counteracts the effect of reduced flame temperature. Indeed, at the upper flammable limit, the mole number ratio increases the expansion factor of methane by over 20% and by approximately 30% for propane, offsetting to some degree, the reduction in expansion factor caused by changes to the flame temperature. The combined effects of flame temperature and combustion chemistry on the expansion factor are shown in Figure 2-29.

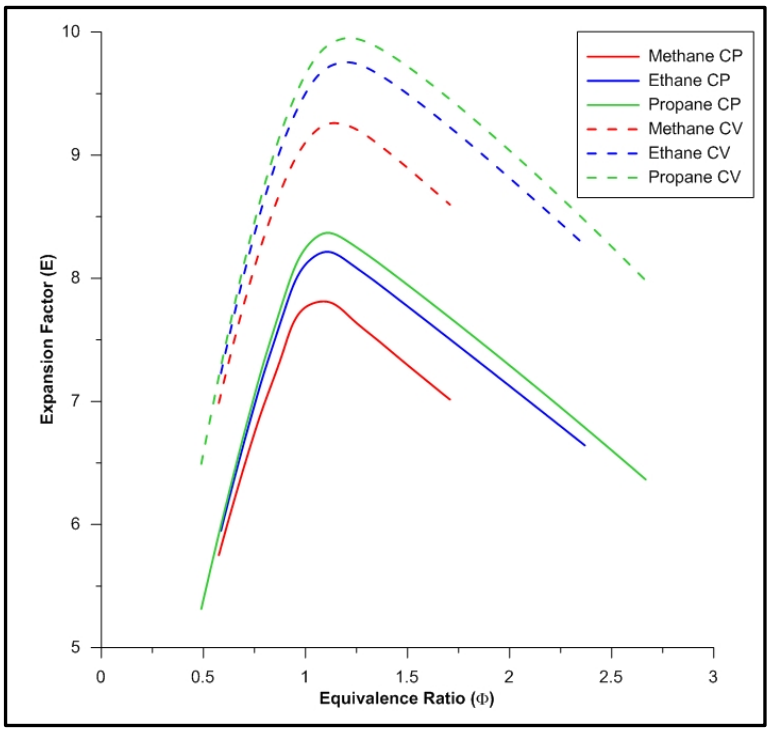

Figure 2-29 The variation of expansion factor with equivalence ratio (gas/air mixture temperature of 288 K)

Ferrara et al. [191], carried out a number of propane/air explosion tests using varying gas concentrations. Earlier in this chapter, it was shown that the burning velocity varies with gas concentration. Consequently, as the flame shape, for a given ignition position (e.g. central or rear), would be the same regardless of gas concentration, it would be logical to expect the maximum flame speeds to be recorded during tests involving near stoichiometric gas/air mixtures, and lower flame speeds to be observed during tests with fuel lean and fuel rich gas/air mixtures. However, whilst the results of Ferrara et al. [191], are in agreement for fuel lean mixtures, fuel rich mixtures were found to have considerably higher flame speeds than would be expected on the basis of the corresponding laminar burning velocity. These findings may be explained as fuel rich gas/air mixtures are known to be more susceptible to developing cellular flames, and furthermore, larger flames, such as those developed with rear ignition, are predisposed to instabilities that cause the flame to adopt a cellular structure. As a consequence of these two factors, rear ignition of fuel rich mixtures, will result in the propagation of fast cellular flames giving rise to higher overpressures.

The Effects of Ignition Location

In totally confined explosions in spherical vessels, the maximum pressure will be generated if the ignition source is located in the centre of the vessel [154, 155, 174]. An ignition source, located elsewhere in the vessel, would result in the flame front reaching the vessel walls sooner and being cooled.

Kindracki et al. [192] have undertaken a number of small-scale experiments in a closed vertical cylindrical vessel. Their findings, that centrally ignited explosions produce higher maximum pressures than explosions ignited at the top or bottom of the vessel, are in agreement with the work of Bartknecht [154], Donat [174] and NFPA [155].

Solberg et al. [30] ascertained that explosions ignited at the rear wall of the enclosure behaved differently to those ignited centrally or near the vent opening. A major part of the flame must be able to propagate in a direction away from the vent opening in order to develop a R-T instability, but the distance from the point of ignition to the vent is not important. With explosions ignited at the rear wall of the enclosure, the whole flame must propagate in a direction towards the vent opening, and consequently, R-T instabilities do not have the same opportunity to develop when the flame front reaches the vent opening and hot, less dense combustion gases, vent at high velocity. In the rear ignited explosion tests discussed by Solberg et al., two pressure peaks were still observed, the first of which was noted to be caused by the onset of burnt gas venting, but the second was attributed to the development of shear turbulence in the boundary layer between the unburnt gas/air mixture at low velocity and burnt gases at higher velocity. Consequently, according to Solberg et al. [30], R-T instabilities may be developed in all ignition locations except the rear wall (or very close to it). Interestingly, during this experimental programme, Solberg et al. observed that rear ignition tests exhibited lower maximum pressures than centrally ignited tests or those ignited close to the vent opening.

Mercx et al. [147] and van Wingerden [156] found that the pressure-time profiles for rear ignition experiments were completely different to those exhibited by central or near vent ignition locations. With ignition close to the vent, one significant oscillatory combustion pressure peak was observed, P_{ac}; and, whilst the maximum pressure for centrally ignited explosions was also found to be produced by oscillatory combustion, two further pressure peaks were noted. The first of these, P_1, was explained by the opening of the vent, P_v and the second was perceived as being caused by the onset of burnt gas venting, P_b. With rear ignited experiments, three pressure peaks were clearly visible; the first two of which were similar to those of centrally ignited explosions, but the third, and maximum pressure peak, which occurred almost immediately after P_b,

was caused by an external explosion as the unburnt gas/air mixture that had been expelled from the enclosure was ignited. It was also noted that in some instances, flame jets of up to 18 m in length exited the vent opening [156]. The results of this experimental programme suggested to the authors, that whilst the mechanism for developing the maximum overpressure during an explosion in an empty large-scale enclosure differed depending upon ignition position, the location of the ignition source had a limited effect on the maximum overpressure generated.

MRS work [33-36, 51, 54, 62, 144], has demonstrated that in vented explosions, the location of the ignition source can have a significant impact on the severity of the explosion, and consequently, the damage a building or dwelling sustains. However, in contrast to totally confined explosions, whilst non central ignition would result in the flame front reaching the walls of the enclosure sooner than with central ignition, higher pressures may be generated than with central ignition.

Notwithstanding cooling of the flame front, the main effect of the ignition position is to determine the time at which the flame front will reach the vent opening. This signifies the time at which burnt gas venting commences, which often determines the maximum pressure generated in the explosion. It follows that ignition sources located close to the vent opening will allow burnt gases to vent earlier in the explosion and consequently lower pressures will be observed inside the enclosure. Conversely, ignition sources located some distance from the vent opening (e.g. on the wall of a room furthest from the vent), will result in a delay in burnt gas venting, giving rise to higher pressures. Furthermore, if the enclosure has a considerable quantity of gas/air mixture within it (e.g. completely full or a considerable layer), and the ignition source is some distance from the vent opening, then a significant quantity of unburnt gas/air mixture will be expelled through the vent before the flame front reaches the plane of the vent opening. The accelerating flame front will exit the vent opening as a ‘jet’ of flame, igniting the unburnt gases, causing rapid combustion. This event is sometimes termed the ‘external jet explosion’. It follows that the greater the volume of unburnt gas outside the vent, the higher the potential overpressure within the enclosure.

Ponizy and Leyer [193, 194] carried out research on small-scale vented vessels connected to ducts with open vents of K_A between 9 and 45. They concluded that central ignition, even in cases of simply vented vessels, produces the highest pressure within the vessel. They argue that whilst rear ignition produces higher combustion rates due to flow disturbances and greater flame surface areas, the smaller amount of unburnt gas left in the vessel after vent opening, and heat losses to the walls, lead to lower maximum pressures than explosions with central ignition. This does not appear to be in agreement with the significant amount of large-scale research conducted by

MRS [33-36, 51, 54, 62, 144, 167, 195, 196]; and Bauwens et al. [45], possibly due to scaling difficulties.

Ferrara et al. [191] carried out vented propane/air explosion experiments using a 200 litre vessel connected to a large 'dump' vessel via a 1 m duct. The flame speeds measured during the experimental tests ranged from 5 to 10 m/s for central ignition to 15 (lean & rich mixtures) to 50 m/s (near stoichiometric) for rear ignition. The faster flame speeds observed with rear ignition are explained by that fact that the flame front is pushed forward in one direction, as opposed to being pushed spherically with central ignition. This results in an elongated flame with a greater increased surface area (compared to a spherical flame), and consequently a faster combustion rate than that associated with spherical flame propagation.

To investigate this effect further, the authors 'normalised' the flame speed by dividing by the laminar burning velocity, thus allowing them to determine the effective expansion ratio; and allowing comparison with typical laminar expansion factors determined earlier in this chapter. The effective expansion factors were in the order of 30 for central ignition and up to 130 for rear ignition, approximately 16 times greater than that for laminar spherical expansion.

As no turbulence was induced in the early stages of the explosions, and since the effective expansion ratio is correlated to the combustion rate (which is a function of the flame surface area and the burning velocity), the differences in the measured flame speed values (compared to laminar flames) were attributed to the elongated increased flame surface area caused by distortion effects.

Willacy et al. [197] carried out a number of vented explosion experiments in a vessel connected to a duct, using homogeneous and stratified propane/air mixtures. The duct was of similar size to the vent opening and was connected to a large 'dump' volume such that the experimental venting arrangement could be assumed as venting to atmosphere. The authors found that with end ignition the flame propagated in a unidirectional manner away from the end wall towards the vent. In a manner identical to the earlier work of Ferrara et al. [191], the flame front, which initially propagated in a hemispherical shape was pushed forward in one direction by the hot combustion products, causing the flame to elongate. This elongation of the flame results in a greater flame surface area, faster flame speeds and consequently higher pressures. In addition, the greater distance from the vent to the point of ignition provides additional distance for flame acceleration to take place.

Bauwens et al. [45], in addition to investigating the effects of obstacles on large-scale vented explosions, also determined the effects of ignition location. The results of their

tests showed that rear ignition produced higher pressures within the enclosure than centre or front ignition. These pressures were associated with external combustion and increased flame surface area. The oscillatory peak pressures were found to be lower with rear ignition. This is due to the fact that there is little unburned gas left within the enclosure at the time the acoustic oscillations develop.

High pressures may also be generated in rare occurrences when two or more sources of ignition are located simultaneously. In this instance, the separate flame kernels propagate and at some point merge to produce a larger flame surface area giving rise to higher pressures within an enclosure.

In accidental explosions, it is not typical for the origin of the explosion (i.e. point of ignition) to be in the centre of the room or enclosure. This is because, the most common sources of ignition are pilot lights on gas appliances, electrical switches or electrical appliances. All of the above are most commonly located around the periphery of the room.

It is also worth noting that dwellings often have appliances with a fixed source of ignition (e.g. pilot light etc.). Where these situations occur, the pressure generated in an accidental explosion is often minimised as any escape of gas is ignited immediately it reaches its LEL. This reduces the severity of the explosion and often prevents significant structural damage to the building.

Effects of Enclosure Geometry

In accidental explosions in dwellings, the most commonly encountered enclosures are rectangular and do not typically have significantly large L/D ratios. In such cases, the geometry does not have a significant effect on the magnitude of the pressure produced at the time of vent opening. This is because, as demonstrated earlier, the flame occupies only a small fraction of the volume of the enclosure at the time the vent fails (unless for some reason there is a vent with a particularly high failure pressure).

Explosion pressures generated within enclosures that are not cubical can be either higher or lower than the maximum in a cubical enclosure, depending upon circumstance. In some instances (e.g. when fuels with high burning velocities are involved), the greatest explosion pressure occurs when the flame surface area has reached its maximum. Where the L/D ratio is close to unity, and assuming central ignition, the flame will propagate spherically and its maximum surface area will occur when the diameter of the flame is equal to the second smallest dimension of the enclosure. It follows, that for enclosures that have L/D ratios that are increasingly greater than unity, but do not lead to significant flame acceleration, lower pressures could be realised. However, in enclosures where the flame is elongated due to

distortion effects, such as L/D greater than 3:1, flame acceleration will occur if the ignition is in the centre or rear of the enclosure, and higher explosion pressures will be realised [62]. This is a consequence of the increased surface area of the flame, the increased flame speed because of the unidirectional expansion and because for significant periods of the explosion, only cold unburnt gases are being expelled through the vent opening.

The Effect of Initial Pressure

In terms of accidental explosions in dwellings, typical changes in the initial (atmospheric) pressure will have little consequence on the magnitude of the maximum pressure generated during the explosion. Consequently, these effects can be ignored.

In totally confined explosions, however, increases in the initial pressure will result in an increased energy density and consequently a greater total energy within the enclosure. Therefore, the rate of pressure rise and the magnitude of the explosion pressure will be increased.

The Effect of Initial Temperature

Changes to the initial temperature will affect both confined and vented explosions. The critical explosion parameters of burning velocity and expansion factor are both affected by changes in temperature. The effects of these changes have been discussed earlier in this chapter.

2.5. Turbulence and Flame Acceleration

2.5.1. General

There is a wealth of literature concerning turbulent combustion, much of which is not directly applicable to this study and consequently it is beyond the scope of this project to review it in detail. However, it is necessary to gain an understanding of the principles of turbulent combustion and to critically appraise the current literature relating to the effects of obstacles in vented explosions in dwellings. For a thorough review of turbulent combustion, the reader is referred to the works of Andrews et al [117], Bray [198, 199], Clavin [200], Clavin et al. [201], Abdel-Gayed et al. [116, 202] and Kuo and Acharya [83].

It is the need to predict the flame speed during explosions that has driven the comprehensive body of turbulent combustion research over the past twenty five years. In order to predict the flame speed in a turbulent explosion it is necessary to have a thorough understanding of the local speed of flame propagation and the characteristics

of a turbulent flame that enable the local burning velocity to be related to the turbulent flame speed [203].

It is interesting to note that despite significant advancements in the theory of turbulent combustion, our present understanding is still essentially based on the classic study of Damköhler published in English in 1947 [203, 204]. It was Damköhler that first suggested that there are two distinct regimes of turbulent combustion that may be related to the flame thickness, namely small-scale and large-scale.

In the small-scale turbulent regime, the internal flame structure is disrupted by small-scale energetic motion, enhancing molecular diffusion and thermal conduction. In this regime the turbulent flame speed is governed by the following relationship:

$$\frac{S_t}{S_l} \approx \sqrt{\frac{D_t}{D}} \qquad \textbf{(2-47)}$$

Where:

S_t = turbulent flame speed.

S_l – laminar flame speed.

D_t = effective turbulent diffusivity.

D = molecular diffusivity.

In the large-scale regime, the flame structure is dependent on large-scale (i.e. greater than the flame thickness) turbulent motion. The motion stretches and folds the flame, thereby increasing its surface area and consequently the flame speed. The turbulent flame speed may therefore be determined by:

$$S_t = S_l \left(\frac{A_t}{A_l}\right) \qquad \textbf{(2-48)}$$

Where:

S_t = turbulent flame speed (m/s).

S_l – laminar flame speed (m/s).

A_t = surface area of the turbulent flame (m^2).

A_l = surface area of the laminar flame (m^2).

The laminar burning velocity for most stoichiometric hydrocarbon gas/air mixtures is in the order of 0.5 m/s, but will increase if the chemical reaction takes place in a turbulent flow field. The turbulence in the gas/air mixture can be developed by mixing prior to ignition or by interaction of the unburnt gas, pushed ahead of the flame by the

expanding flame front, with obstacles located within the enclosure. The latter of these turbulence mechanisms may be important in accidental explosions; by the interaction of flow through interconnected rooms and the interaction of the induced flow with furniture in a dwelling, thereby enhancing the combustion process.

As a flame propagates during an explosion, the expansion of hot combustion gases behind the propagating flame front sets up a flow in the unburnt gas/air mixture ahead of the reaction zone, thereby generating a turbulent flow field. If there are obstacles in the path of the induced gas flow, the turbulent flow field will be enhanced. When the flame encounters such turbulence it is affected in two ways [205]:

1. small-scale turbulence increases the local heat and mass transfer rates.
2. large-scale turbulence distorts the flame front and increases the flame area.

This flow in the unburnt gas/air mixture is a critical element in the combustion process. As the flame propagates into the turbulent flow field, its effective combustion rate is increased by stretching and folding of the flame, generating turbulence and initiating instabilities, causing the flow velocity and turbulence ahead of the flame to increase still further [206]. This enhanced combustion rate can be further influenced by obstacles, the geometry of the enclosure, ignition position and the interaction of adjoining rooms.

Consequently a ‘coupling’ is created which manifests as a strong positive feedback mechanism which is largely generated by the interaction with obstructions located in the path of the advancing flame front [207]. It is this coupling process (see Figure 2-30), known as the Schelkin mechanism, between flame acceleration and gas flow dynamics, that is the key problem in gas explosions, whether confined or unconfined [206]. Phylaktou and Andrews [40, 208, 209] demonstrated, during experiments in a long vessel with one or two orifice-plate obstacles in the path of a propagating flame, that the strength of this feedback loop can be extreme, causing the flame speed to increase by a factor of up to two hundred. Other studies [39, 42, 103] have demonstrated that very fast flame speeds, in excess of 600 m/s, may be generated when a flame propagates through a flammable gas/air mixture in the presence of repeated obstacles. To predict the pressure generated during these type of fast flame events, it is necessary to understand the role that the obstacle configuration, blockage ratio, and the parameters that affect the turbulent flow field, play in effecting the strength of the feedback mechanism.

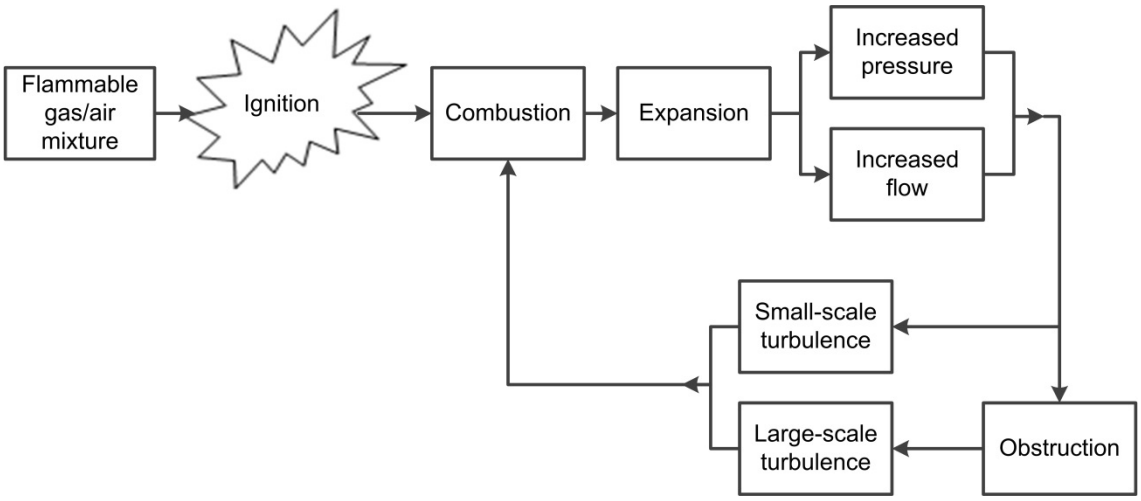

Figure 2-30 Positive feedback mechanism causing flame acceleration (adapted from Phylaktou et al. [39])

The Concepts of Turbulent Flow

In fluid dynamics, flow regimes are divided into laminar flow and turbulent flow. In laminar flow, the fluid flows in smooth layers, whilst in turbulent flow, the flow contains eddying motion of all sizes.

Turbulent flow may be considered as the random irregular motion of local masses of fluid superimposed over any uniform flow that exists, with its over-riding characteristic being its randomness and three dimensionality [76].

Turbulent flow in explosions may be generated by increasing the flow velocity, altering the geometry of the confining enclosure or by placing obstructions in the path of the fluid in motion.

Osborne Reynolds developed an expression to predict the change in flow regime for any fluid:

$$Re = \frac{\rho u l}{\mu} \qquad \textbf{(2-49)}$$

Where:

ρ = density of the fluid (kg/m^3).

u = the mean velocity (m/s).

l = length (m).

μ = the dynamic viscosity of the fluid (Pa·s or kg/m s).

It is often useful, to express Equation (2-49) in terms of the kinematic viscosity, $\left(\nu = \frac{\mu}{\rho}\right)$:

$$Re = \frac{ul}{\nu} \quad \textbf{(2-50)}$$

Where:

u = the mean velocity (m/s).

l = length (m).

ν = the kinematic viscosity of the fluid (m^2/s).

Osborne Reynolds demonstrated that the variable velocities which are part of turbulent flow, create much larger stresses than the already present viscous stresses caused by molecular motion [210, 211]. Turbulent energy is fed into the fluid in motion by virtue of the straining that takes place against such Reynold stresses [117].

Lighthill [212] showed that the ratio of the rate of production to the rate of dissipation of turbulent energy gives a turbulent Reynolds number:

$$R_\ell = \frac{u'\ell}{\nu} \quad \textbf{(2-51)}$$

Where:

R_ℓ = the turbulent Reynolds number.

u' = the velocity scale, taken to be the root mean square (rms) value of the fluctuating component of velocity (u), $\therefore\ u' = \sqrt{\overline{u^2}}$ (m/s).

ℓ = mean length scale of the large eddies (average distance over which the low frequency turbulent velocity fluctuations occur).

ν = the kinematic viscosity of the fluid (m^2/s).

Turbulent flow and combustion chemistry are each characterised by a broad spectrum of length and time scales [199]. The largest scales in a turbulent flow are related to the physical dimensions of the confinement and to the flow velocity, while the smallest scales characterise the dissipation of turbulence energy through viscosity.

The Reynolds stresses are predominantly generated from the larger eddies which are anisotropic and of large-scale, ℓ, are of the same order as the physical structure that induces the turbulence [117]. As the turbulent Reynolds number increases, vortex stretching effects increase rotational energy and consequently smaller, faster

dissipative eddies are created. Vortex stretching produces ever smaller scales of turbulence of ever increasing velocity and vorticity. This energy is eventually converted into randomised molecular motion through the effects of viscosity.

Because angular momentum is conserved during this flow process, the kinetic rotational energy increases and the vortex stretching eradicates the original anisotropy of the large eddies and creates isotropy amongst the small scale eddies [42]. It should be noted that this process of eddy decay from large to small scale only occurs in the free stream. At the origin of turbulence, for example jet mixing of a gas/air mixture, the reverse process occurs, where small scale eddies coalesce into large eddies.

Taylor [213] demonstrated that the kinetic energy associated with turbulent velocity fluctuations is related to their frequency. That is, large eddies are associated with velocities of low frequency and small scale eddies with velocities of high frequency.

Taylor [214] has also shown that for isotropic turbulence, the rate of energy dissipation per unit mass, may be expressed as:

$$e = 15\nu\overline{\left(\frac{du}{dx}\right)^2} \qquad \textbf{(2-52)}$$

Where:

e = rate of energy dissipation (m^2/s^3).

ν = the kinematic viscosity of the fluid (m^2/s).

u = fluctuating component of velocity (m/s).

x = distance between eddies (m).

Taylor also defined the Taylor microscale, λ, which is a length scale, such that:

$$\left(\frac{u'}{\lambda}\right)^2 = \overline{\left(\frac{du}{dx}\right)^2} \qquad \textbf{(2-53)}$$

Simplifying Equation (2-53) by substitution:

$$e = 15\nu\left(\frac{u'}{\lambda}\right)^2 \qquad \textbf{(2-54)}$$

The rate at which large eddies supply energy to small eddies may be considered to be proportional to the kinetic energy per unit mass of the large eddies divided by the time scale of the large eddies, $\left(\frac{l}{u'}\right)$, therefore, the rate of production of turbulent energy is

proportional to $\frac{(u')^3}{l}$ [117]. In the steady state, the production rate is equal to the rate of viscous dissipation; thus:

$$e \propto \frac{(u')^3}{\ell} \quad \textbf{(2-55)}$$

From Equations (2-54) and (2-55), it can be determined that the Taylor microscale is related to the macroscale, ℓ, by:

$$\frac{\lambda^2}{\ell} \propto \frac{\nu}{u'} \quad \textbf{(2-56)}$$

A number of researchers, including Abdel-Gayed and Bradley [202], and Dryden [215], have conducted experiments to determine the proportionality constant. Abdel-Gayed and Bradley [202] recommended a value of 40.4 giving:

$$\frac{\lambda^2}{\ell} = 40.4\frac{\nu}{u'} \quad \textbf{(2-57)}$$

The turbulent Reynolds number, R_λ, based on the microscale λ, is given by:

$$R_\lambda = \frac{u'\lambda}{\nu} \quad \textbf{(2-58)}$$

Combining the above equation with the equation of a turbulent Reynolds number given in Equation (2-51) gives:

$$R_\lambda = 6.36\sqrt{R_\ell} \quad \textbf{(2-59)}$$

In turbulence, a cascade of eddy sizes exist from macro to micro scales. These are the mechanism through which turbulent energy is dissipated. If the energy supply to generate turbulence is removed, the larger scales disappear first.

The isotropy of the dissipative eddies make their detailed structure independent of that of the large eddies. It has already been discussed that the Taylor microscale, λ, is primarily based upon large eddy parameters. However, in his universal equilibrium theory, Kolmogorov [216] derived microscale values for the isotropic regime:

$$\eta = \left(\frac{v^3}{e}\right)^{\frac{1}{4}} = 15^{-\frac{1}{4}}\lambda R_{\lambda}^{-\frac{1}{2}} \quad \textbf{(2-60)}$$

$${}^{v}\eta = (ev)^{\frac{1}{4}} = 15^{\frac{1}{4}}u'R_{\lambda}^{-\frac{1}{2}} \quad \textbf{(2-61)}$$

$${}^{\tau}\eta = \left(\frac{v}{e}\right)^{\frac{1}{2}} = \frac{\lambda}{15^{\frac{1}{2}}u'} \quad \textbf{(2-62)}$$

Where

η = Kolmogorov microscale – length.

${}^{v}\eta$ = Kolmogorov microscale – velocity.

${}^{\tau}\eta$= Kolmogorov microscale – time.

The Taylor and Kolmogorov microscales are theoretical parameters and consequently will not precisely describe the actual microstructure of the turbulence.

2.5.2. Turbulent Combustion Correlations

Fluid flows become turbulent as a result of flow instabilities that initially possess discrete characteristic length and time scales. A wider range of scales become involved as the turbulence is characterised by a broad continuous spectrum of essentially random velocity fluctuations. The large-scale motion depends on the size and nature of the mean flow field, whereas, at the smallest scales, the velocity fluctuations are found to be nearly isotropic and universal in character.

The Classical Correlation

This model was originally published by Damköhler [217]. The equation relates the turbulent burning velocity, $S_{u,t}$, to the Laminar burning velocity $S_{u,l}$ and the rms fluctuating velocity of the flow field. It is given by:

$$\frac{S_{u,t}}{S_{u,l}} = 1 + C\frac{u'}{S_{u,l}} \quad \textbf{(2-63)}$$

Where:

$S_{u,t}$ = turbulent burning velocity.

$S_{u,l}$ = laminar burning velocity.

C = a constant.

u' = the velocity scale, taken to be the root mean square (rms) value of the fluctuating component of velocity (u), $\therefore\ u' = \sqrt{u^2}$.

In his original work, Damköhler proposed that the constant C is 1. Phylaktou [42] suggests that a value of 2.0 provides a better fit to much of the experimental data available.

A number of researchers have proposed equations similar to Equation (2-63), often with different values for the constant. Detailed information on these equations may be found in the reviews of Andrews and Bradley [117] and Gülder [204]. Nonetheless, in all of the variations of Equation (2-63) above, the turbulent burning velocity, $S_{u,t}$, is found to be dependent only on u' and $S_{u,l}$. Furthermore, at high turbulence levels, $S_{u,t}$ is effectively dependent on u' only [42].

2.5.3. Interaction with Solid Obstructions

In an accidental explosion, the rise in burning rate and pressure occurs due to the propagation of the flame front travelling through a flammable gas/air mixture that is contained within the dwelling. It is widely accepted that the acceleration of a propagating flame is enhanced when a solid obstacle is located in its path [38-44], with the degree of enhancement being strongly dependent on the flow structure that is formed in the wake behind the obstruction. Moreover, data from large-scale experiments carried out by Moen et al. [47], and Hjertager et al. [46] have demonstrated that flame speed and pressure also have a strong dependence on obstruction size and gas concentration.

Bimson et al. [48] discuss a series of sixteen vented explosion tests carried out in a 550 m^3 [6.25 m (h) x 8.75 m (w) x 10 m (l)] steel explosion chamber; each wall lined with Rockwool to dampen acoustic oscillations, and with a vent opening of $K_A = 2$ in the front face of the chamber which was covered with a thin polythene sheet to contain the gas/air mixture prior to ignition. The tests involved methane/air and propane/air mixtures at 10% above stoichiometric concentration and utilised four internal configurations:

i. an empty chamber;
ii. a row of seven, vertically positioned, PE pipes of 0.5 m diameter, located 5.74 m from the vent;
iii. a row of seven, vertically positioned, PE pipes of 0.5 m diameter, located 2.78 m from the vent;
iv. a combination of ii and iii above (i.e. two rows of obstacles).

Bimson et al. [48] determined that the inclusion of Rockwool eliminated resonant wall interactions and greatly simplified the interpretation of the pressure-time traces. In all explosions, two significant pressure peaks were observed. The first pressure peak, P_b,

was observed when the flame front reached the plane of the vent opening (signalling the onset of burnt gas venting), whilst the second pressure peak, P_{ext}, occurred as a consequence of the external explosion. The pressure-time profile for explosions with obstacles typically followed the empty chamber curve until the flame front reached the obstacles (Figure 2-31). At this point, the flame speed increased and as soon as the flame front reached the vent opening a P_b peak was observed. This P_b peak; which was observed earlier than the corresponding peak in the empty chamber and was of significantly greater amplitude, was quickly followed by an external explosion which produced the maximum pressure peak, P_{ext}.

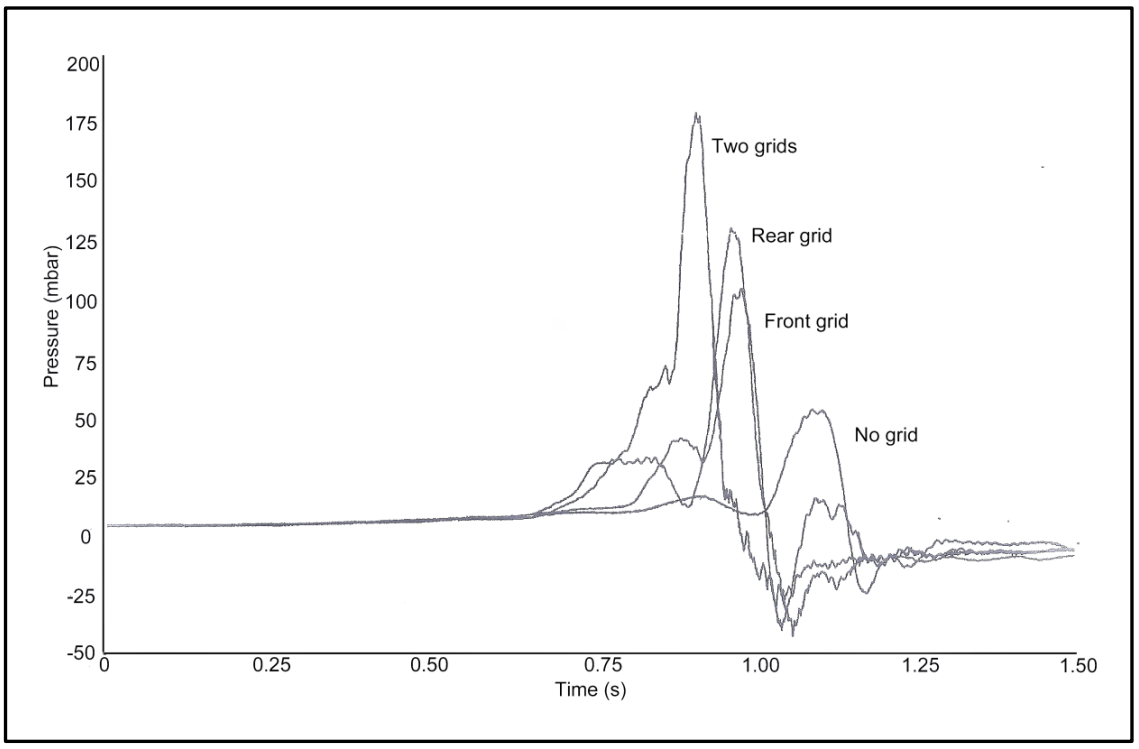

Figure 2-31 A pressure-time profile of Shell SOLVEX tests with differing internal configurations (taken from Bimson et al. [48])

Video and photographic records of the explosion tests allowed the authors to gain valuable insight into the explosion mechanism. The video showed the flame transition from the typical self-wrinkling behaviour to flame distortion as the flame front approached an obstacle, followed by rapid acceleration. Unburnt gas/air mixture is driven ahead of the expanding flame front and expelled through the vent opening to take the form of a mushroom shaped ring vortex, which is rapidly ignited by the flame front when it reaches the vent opening. The flame was seen to adopt the mushroom shape and was rapidly totally inflamed, producing a significant pressure pulse that registers as the P_{ext} peak within the explosion chamber This mechanism was found to be in agreement with the observations of other large-scale experimental programmes [133, 167]; an example of which is shown in Figure 2-32.

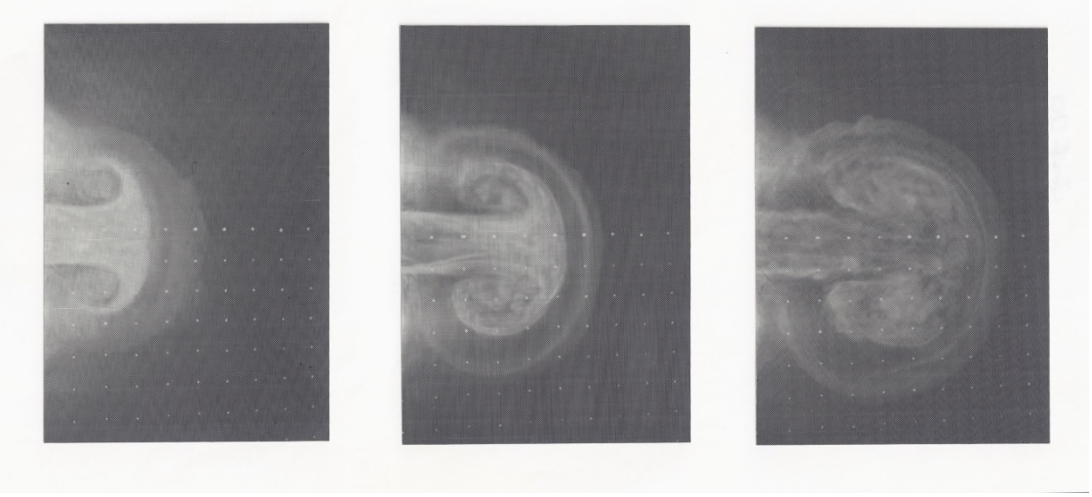

Figure 2-32 Expelled unburnt gas/air mixture forming a mushroom shaped vortex (taken from DNV GL archive)

A very interesting observation by the authors was that even at the time of maximum energy release of the external explosion, and for some duration following, burning gas continued to stream at high velocity (≈ 100 m/s) through the burning mushroom. This continued until flow reversal back into the explosion chamber had occurred.

Cates and Samuels [218] produced a simple theoretical model to predict overpressures in vented explosions. They argued that the worst case overpressures would be generated in explosions in the presence of obstacles, ignited at the farthest point from the vent. The work was based on the belief that the external explosion would dominate, but they also stated that this may not be the case in some situations. The results of this model were compared to the work of Pappas et al. [140, 163] and were found to be in broad agreement. However, the authors limited the scope of this model to single enclosures with aspect ratios close to one and scenarios where the external explosion dominates.

Chamberlain and Rowson [219] described a series of confined and unconfined experiments, considering the effect of partially filled congested environments and the effect of obstacles located near the ignition point. The confined vented explosion tests were undertaken in a steel explosion chamber measuring 2.5 m (l) x 1.5 m (h) x 2.25 m (w), with a K_A of 2. The explosion chamber was fitted with seven arrays of steel bars, each 50 mm thick and 6 mm wide providing a uniform area blockage at each array of 17% (one experiment was carried out with the last three arrays removed). The tests were carried out using methane, with an equivalence ratio of 1.1, and the ignition position was in the centre of the rear wall of the chamber. The distance from ignition to the 1st array was not altered during the confined vented tests.

For tests with a full volume of gas/air mixture, overpressures were generated between 315 and 473 mbar. In contrast, tests involving a partially filled chamber produced overpressures ranging from 10 mbar with a partial fill volume of 10.2% to 349 mbar with a fill volume of 41.2%. The partial volume was contained using a thin polythene sheet secured to an appropriate obstacle array. The authors observed that whilst the effect of increasing fill volume was correctly predicted by the Shell Code for Overpressure Predictions in Gas Explosions (SCOPE), the overpressures were overpredicted, particularly at lower levels of partial fill. They determined that this was due to the transient mixing of the pre-mixed fuel/air mixture with air in the chamber (as the polythene sheet was broken by the developing pressure) resulting in a weaker mixture overall. A similar trend was observed in the unconfined explosion tests.

The effects of obstacles located near to the ignition position were investigated during the unconfined explosion tests. Obstacles located close to the ignition source were found to have little effect on the maximum overpressure in experiments with a full gas/air volume, but the time taken to reach the peak was reduced. This behaviour is explained by the enhancement of combustion in the early stages of the explosion due to the initial turbulence induced by the obstacle arrays located close to the ignition source. However, the peak overpressure is dominated by the later stages of the explosion when the flame front is interacting with the outer obstacle arrays and flame speeds are greater. Consequently, the influence of the obstacles during the early stages of the explosion is less significant. However, the influence of the obstacles in the early stages of the explosion was far more significant in tests with a low partial fill volume, significantly enhancing the maximum overpressure. This was because the outer obstacle arrays were outside the flammable region and therefore had comparatively small or no influence.

Small-scale experiments conducted by Fairweather et al. [220, 221] to investigate turbulent flame interaction with obstacles revealed a strong link between the developed peak pressure and the amount of unburnt fuel/air mixture trapped behind the obstruction(s). In further small-scale experiments to study the flame interaction with baffle-type obstacles located within a chamber, Sakthitharan [222], and Lindstedt and Sakthitharan [223], witnessed the flame front pass over the obstacle and then interact with an eddy that was formed and remained behind the baffle. In a more accurate representation of an accidental gas explosion in a dwelling, the flame front will propagate around the obstruction and the interaction is likely to be different. As the flame structure and the amount of unburnt gas/air mixture trapped behind the obstruction will be liable to differ from the small-scale tests (due to the effects of scaling), the pressure-time history will also be different. Nevertheless, small-scale

experiments are still extremely useful in improving the understanding of turbulent explosions.

In a series of small-scale vented explosion experiments, Ibrahim et al. [43] considered the effects of a solid wall-type obstruction with methane/air mixtures of varying concentration. They found that for a variety of equivalence ratios (ϕ = 0.8, 1.0 & 1.2), three different phases of flame propagation appeared to exist. During phase 1, the flame accelerates as it interacts with the solid wall. The greatest rate of acceleration occurred with stoichiometric concentrations, showing an increase from 5 to 39 m/s. Lower flame acceleration was observed with non-stoichiometric concentrations, with the flame front accelerating from 5 to 32 m/s for a rich mixture and 5 to 27 m/s for a lean mixture. This initial flame acceleration may be attributed to the increase in flame surface area as a consequence of the interaction with the wall boundary. Furthermore, high momentum jetting through the gap between the obstruction and the enclosure walls further enhances flame propagation, by convecting heat from the flame farther downstream, before the flame front interacts with the flow vortices behind the obstruction.

In phase 2, the authors observed that the flame front starts to interact with the flow vortices behind the obstruction and the flame speed was found to decrease for all equivalence ratios. In phase 3, highly turbulent combustion was triggered in the wake of the obstruction as the flame front interacted with the flow vortices. The nature of the flow around solid obstacles was found to be critical as the vortices formed in the wake of the obstruction caused an amount of unburnt gas/air mixture to be trapped and subsequently burnt in a highly turbulent combustion phase leading to increased flame speeds and resultant pressure rise. The variations in the observed flame speeds correlate to the change in flame surface area as the flame front interacts with the obstacle.

Fairweather et al. [220] carried out a study of explosions in a cylindrical tube where obstruction rings were placed at various axial locations on the wall of the vessel. Flame visualisation studies revealed that unburnt gas/air mixture becomes ‘trapped’ behind the obstruction in vortices, which then reacts violently after the flame front was seen to exit the plane of the vessels vent opening.

Ibrahim and Masri [224] conducted a number of small-scale vented explosion experiments where cylindrical, square and diamond shaped obstructions, amongst others, were positioned within the enclosure. Most flame acceleration studies prior to this were undertaken using baffle-type obstacles. In real situations, accidental explosions in dwellings are likely to include obstacles of various size and geometry

(e.g. rectangular, sharp edged etc.), and the flame front is likely to interact in a different manner.

For tests carried out with walls/plates and squares, increasing the blockage ratio resulted in higher P_1 and P_2 pressures whilst the vent failure pressure remained constant. It was observed that as the obstruction ratio increased, the time taken to reach the peak pressure decreased.

As tests were undertaken with obstacles of different geometry, it was noticed that the shape of the obstruction had a direct influence on the flame speed and the pressure generated. The pressure was found to be greatest in enclosures with wall/plate type obstructions (≈ 90 mbar) whilst cylindrical objects caused the lowest pressure rises (≈ 30 mbar). Pressure rises from interaction with diamond (≈ 75 mbar), square (≈ 45 mbar) and triangular (≈ 40 mbar) shaped objects caused intermediate level pressure rises.

Not surprisingly, the time delay to reach the peak overpressure was shortest for wall/plate type obstructions, for similar blockage ratios, indicating the rate of flame acceleration was dependent upon both the obstruction geometry as well as the blockage ratio.

Whilst velocity and turbulence measurements were not recorded during the experiments, the authors speculated as to the nature of the flame dynamics during the explosions. As the flame approaches the 1st obstruction, it travels at laminar speeds since the flow field ahead of the flame is undisturbed. When the flame reaches the obstacle, it starts to interact with a modified flow field where the turbulence levels and length scales will vary depending on the obstacles geometry and size. When the blockage ratio increases, the gaps between the obstructions and the enclosure will decrease resulting in increased gas velocities around the obstacle. This increases the reaction rate, leading to faster flames and higher pressures, providing the gap is not of a sufficiently small size to quench the reaction.

The effect that the shape of the obstruction has on the overpressure in the enclosure is significant. It implies that the manner of the flow around the obstruction, the intensity of the re-circulation zone which is formed, and the amount of unburnt gas trapped in the wake of the obstruction are all critical in determining the overpressure. It seems logical that the wall/plate type obstruction that gave rise to the highest pressures caused the largest volume of unburnt gas/air mixture to be trapped. In contrast, it is expected that the cylindrical shaped obstruction would trap the least amount of gas.

As turbulent flame propagation is sensitive to obstacle geometry, the effects of shape may be considered by applying the following correlations for the coefficient of discharge [57]:

- C_D = 1.2 – cylinder,
- C_D = 2.0 – square,
- C_D = 2.2 – triangle.

Abdel-Gayed and Bradley [202] have produced a vast array of experimental data which allow the turbulent enhancement of burning velocity to be determined. However, in real situations, the acceleration of the flame front is a consequence of a complex interaction between the propagating flame front, the local obstruction and the size and geometry of the enclosure.

Such blockages set up a complex interaction between the propagating reaction front and the flow fields around the obstructions resulting in local flame acceleration in the form of jetting. The motion of gas movement around the obstacles creates both turbulence by vortex shedding and local wake/recirculation which can cause the flame to 'fold' on itself. This folding, increases the flame surface area available for combustion but may produce localised flame quenching.

The studies of Moen et al. [47], Phylaktou et al. [39] and others have produced conclusive evidence that the presence of repeated obstacles increases flame speed and hence pressure.

In considering the turbulence generated downstream of a grid plate obstacle by explosion induced flow [41], Phylaktou and Andrews presented a method for predicting the maximum turbulence levels. It was shown that the turbulence intensity, defined as the ratio of the rms turbulence velocity to the mean velocity of the induced gas flow, was given by:

$$\frac{u'}{S_g} = C_T\sqrt{K_o} \qquad \textbf{(2-64)}$$

Where:

u' = the rms turbulent velocity of the flow (m/s);

S_g = the induced gas flow (m/s);

C_T = a turbulence generation constant (Phylaktou and Andrews [41] recommmend 0.225 for thin or sharp edged obstacles and 0.076 for thick or round edged obstacles);

K_o = is the pressure loss coefficient of the obstacle;

The pressure loss coefficient, K_o, may be defined as:

$$K_o = \frac{\Delta P}{\frac{1}{2}\rho S_g^2} \quad \textbf{(2-65)}$$

Where:

ΔP = the difference in pressure across the obstacle (Pa) or (kg/m·s²);

ρ = the density of the fluid (kg/m^3).

For incompressible flow, K_o can also be expressed in terms of the geometry alone as a function of the area blockage ratio, ABR, and the coefficient of discharge, C_d [39]:

$$K_o = \left[\frac{1}{C_d\left(1 - ABR\right)} - 1\right]^2 \quad \textbf{(2-66)}$$

Phylaktou conducted a series of explosion experiments in long, closed vessels with grid plate obstacles [42] and developed a method that enabled the quantification of the turbulent burning velocity, S_T, directly from experimental measurements. The author subsequently investigated the variation of the turbulent burning velocity with the test parameters and derived a turbulent combustion model :

$$\frac{S_T}{S_L} = 1 + 0.67\left(\frac{u'}{S_L}\right)^{0.47} R_\ell^{0.31}\, Le^{-0.46}\left(\frac{\nu}{\nu_a}\right)^{0.95} \quad \textbf{(2-67)}$$

Where:

S_L is the laminar burning velocity;

R_ℓ = the turbulent Reynolds number;

Le = the Lewis number;

ν = the kinematic viscosity of the mixture;

ν_a = the viscosity of air.

This model was subsequently validated with a large set of experimental data (explosions with obstacles) from various sources shown to correlate well (correlation coefficient in excess of 90%) [42].

To confirm the suitability of this model to realistic industrial explosion problems, calculations were undertaken using Reynolds number in the range of 26 to 113000 (the upper end of which is comparable to the Reynolds numbers induced in large-scale

industrial explosions). Based on the turbulent combustion correlation given in Equation (2-67) an explosion-overpressure scaling model was derived:

$$P \propto \left[\left(C_T\sqrt{K}\right)^{1.56} \ell^{0.62}\right]\left[E^{3.56}\ S_L^{2.62}\ Le^{-0.92}\left(\frac{\nu}{\nu_a}\right)^{1.28}\right] \qquad \textbf{(2-68)}$$

Where:

ℓ = the characteristic length scale.

E = the expansion factor.

This equation demonstrates the dependence of the blast overpressure on the geometric configuration and gas/air mixture properties.

Masri et al. [44] carried out small-scale vented explosion tests (commercial propane in a 20 litre cuboidal chamber) in the presence of obstacles of differing geometry. They observed that in the early stages of the explosion, a very symmetrical flame develops, which is similar, regardless of the geometry of the obstruction ahead of it.

It is important to distinguish between the effects that direct and indirect obstructions have on the flame. Direct effects are those which occur when the flame impinges on the obstacle. The indirect effects are the complex effects that arise from changes in the flow field due to drag, turbulence and volume reduction induced by the obstacle. Masri et al. [44] observed that the shape and size of the obstruction determine the formation of vortex pairs of different size behind the obstacle and this greatly affects the distortion of the flame front. The volume of trapped flammable gas/air mixture in the wake of the obstacle was found to be proportional to the vortex size and was higher for obstacles of triangular cross-section. Rectangular and circular cross-sections were found, respectively, to have lower volumes of trapped unburnt gas. These pockets of trapped gas are the last to be combusted.

Dorofeev [225] comments that flame acceleration due to obstacles in large-scale vented explosion tests produces similar dynamics to flame acceleration in closed systems. However, there are a few specific characteristics of vented explosions that effect flame acceleration. These include Helmholtz oscillations, the external explosion and Rayleigh Taylor instabilities.

Hall et al. [226] carried out a series of small-scale tests to investigate the effect of position and frequency of obstacles on the pressure generated in a vented explosion. They concluded that increasing the blockage ratio, up to a critical value, increases the overpressure and that whilst increasing the number of obstacles generally increases flame speeds and overpressure, a limit is reached where the addition of more

obstacles results in a decrease in pressure. No explanation could be given, by the authors, for this finding.

They also observed that the location of the obstacles with respect to the ignition source can have a significant effect. Increasing the distance between the obstacles allows the turbulence to 're-laminarise' causing less distortion of the flame front and lowering the flame speeds. This is in agreement with the work carried out by Phylaktou [42].

Bauwens et al. [45] investigated the effect of obstacles for varying ignition position in a room sized enclosure of volume 63.7 m^3. They found the presence of obstacles greatly increased the amplitude of pressure peak P_1, particularly for back-wall ignition due to the increase in flame surface area and turbulence as unburned gas is forced around the obstacles (Figure 2-33). Surprisingly, the authors found that the addition of obstacles only increased the overall peak pressure in half of the tests, typically for tests where the pressure profile was dominated by either peaks P_1 or P_3.

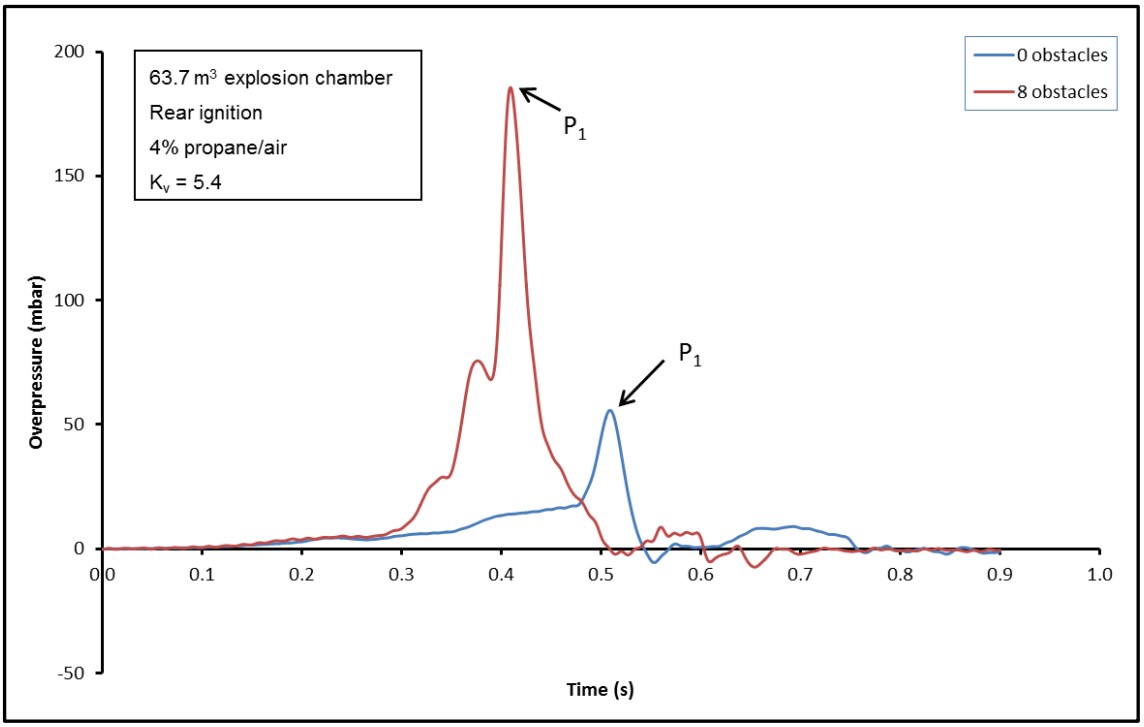

Figure 2-33 A pressure-time profile showing the effects of obstacles (taken from Bauwens et al. [45])

When obstacles were positioned in the enclosure a third peak was sometimes noticed. This peak is identical to the P_{mfa} peak determined by MRS and was observed to correspond to the time when the flame surface area was at its maximum. However, in this instance, the pressure was magnified by the acceleration effects of the obstacles, thus making the peak more noticeable. It was also identified that the presence of the

obstacles reduced the acoustic instabilities and significantly reduced the value of the second peak identified in the tests without obstacles.

Chao et al. [159] presented experimental data gathered from vented explosion tests carried out using methane/air mixtures in a 63.7 m^3 chamber. The purpose of this work was to present a simple model to estimate the peak pressure for each of the pressure transients encountered in a vented explosion. The authors noted some interesting characteristics of the explosion experiments when obstacles were placed in the enclosure.

In most instances, experiments without obstacles did not produce an obvious pressure peak associated with the maximum flame area. However, in agreement with the work of Bauwens et al. [45], the authors found the inclusion of obstacles, produced a pressure peak that correlated to the time of maximum flame area. Furthermore, the 1st pressure peak was of greater magnitude with explosions that included obstacles than those that did not.

Although obstacles enhanced the peak pressure associated with the maximum flame area, they interfered with the acoustics of the enclosure and consequently eliminated the acoustic peak. Surprisingly, Bauwens et al. [45] found that the addition of obstacles, due to the acoustic disrupting effect, did not always result in increased maximum overpressures, when compared to experiments without obstacles and in which the maximum pressure peak was caused by acoustic oscillations.

Park et al. [57] reviewed the experimental data obtained from vented explosions in various enclosures with obstacles and developed an empirical model for predicting the pressures associated with vented explosions. They developed the model as a two-stage method in order to consider the effects of obstacles. The 1st stage divided the chamber into two at the obstacles and applied existing correlations to each chamber section. In the 2nd stage they applied a correction in order to characterise the important turbulent parameters such as boundary conditions, L/D ratio and turbulence factor. This model seems of limited value when representing the conditions encountered in a real explosion situation.

Mercx et al. [147] and van Wingerden [156], in addition to tests in an empty chamber, carried out tests with a single large steel box shaped obstacle located within the enclosure (chosen to represent central heating plant). Its dimensions were 1.5 m (h) x 0.75 m (w) x 0.5 m (l). The pressure-time profiles from these tests also revealed three pressure peaks; P_1 due to vent opening, P_2 due to the external explosion and, contradictory to rear ignition tests without the obstacle, P_3 due to oscillatory combustion. In these tests, the magnitude of P_2 was found to increase as the distance

between the obstacle and ignition source was increased. It was noted that the presence of a single large obstacle had increased the overpressure when compared with similar tests in the empty enclosure but only when the distance between the obstacle and ignition source was large. Mercx et al. [147] concluded that the presence of a single large obstacle in an enclosure had only a minor influence on the explosion effect.

Mercx et al. [227], in an article concerning vapour cloud explosions, postulated that explosions involving homogeneous obstacle configurations could be characterised by only two parameters, volume blockage ratio and obstacle size; with a combination of these two parameters being a measure for the spacing between the obstacles. The number of obstacles met by the flame front was considered the most important factor for the development of pressure. The authors proposed that this is given by the ratio of flame path length and the spacing between obstacles. Because of the feedback coupling triggered by repeated obstacles, flame propagation develops in an approximately exponential manner. Consequently, the authors proposed the following correlation:

$$P \propto \left[\frac{VBR \times L_f}{D}\right]^b \qquad \textbf{(2-69)}$$

Where:

P = pressure generated.

VBR = volume blockage ratio (i.e. the proportion of volume occupied by obstacles).

L_f = flame path length.

D = average diameter of obstacle.

b = a constant.

Work by Taylor and Hirst [151] and Catlin [228], modelling the scale-effects on gas explosions suggested that the flame speed obtained in some gas explosion experiments was related to the laminar burning velocity and a scale factor (a linear dimension of the experiment) S_c, by the following approximation:

$$S_f \propto S_{u,l}^{1.35} S_c^{0.35} \qquad \textbf{(2-70)}$$

Mercx et al. [227] hypothesised, that if on the basis of acoustics, a quadratic relationship between overpressure and flame speed is assumed, the maximum explosion overpressure Po, can be considered to have the following dependence upon the laminar burning velocity and scale:

$$P_o \propto S_{u,l}^{2.7}\, S_c^{0.7} \quad \textbf{(2-71)}$$

Developing the concept, Mercx et al. [227] postulated that if the three factors of influence; namely, the boundary conditions, the mixture reactivity, and the scale, are considered together, a general approximate relation can be used to determine the maximum overpressure in an explosion with obstacles:

$$P_o = a\left[\frac{VBR \times L_f}{D}\right]^b S_{u,l}^{2.7}\, S_c^{0.7} \quad \textbf{(2-72)}$$

Where:

P_o = maximum overpressure (bar).

a = a constant (0.84 for conservative estimate).

VBR = volume blockage ratio.

L_f = flame path length - taken to be the longest distance from ignition to obstacle (m).

D = average obstacle diameter/width (m).

b = a constant (2.75 for conservative estimate).

$S_{u,l}$ = laminar burning velocity (m/s).

S_c = scale factor – assumed to be equal to the average obstacle diameter D (m).

Accidental gas explosions in dwellings are not idealised. However, it is possible to assume average volume blockage ratios for typical buildings such that the maximum overpressure could be predicted given knowledge of the fuel gas, building geometry, and potential ignition sources (and hence location).

2.5.4. The Conditions for Turbulence Generation in Gas Explosions in Dwellings

In 1969, Rasbash [229] suggested that explosions involving stationary fuel/air mixtures inside well vented enclosures would not develop serious turbulence, providing there were not too many obstacles present in the enclosure that would obstruct the motion of the flame towards the vent opening. As most dwellings will contain turbulence generating obstructions, it is important to understand their influence on turbulent combustion. Turbulence in accidental gas explosions in dwellings may be pre-existing or induced by combustion.

In the former case, the flammable mixture is already turbulent prior to ignition. This turbulence may occur, for example, as a result of cooling fans ‘stirring up’ the mixture or by the escape of high pressure gas into the room or enclosure. In the latter case, the

turbulence is generated by the interaction of the combustion driven flow with obstacles in the room, or through interconnected rooms.

In practical situations, all dwellings will contain obstructions such as furniture, appliances, cupboards, beds etc., which will produce turbulence in the unburnt gases as they flow ahead of the advancing flame, and they will all have a number of interconnected rooms that may, or may not have closable doors. The effect of these influences on the combustion process is typically modelled by the introduction of a turbulence factor β, to correlations used to predict flame speed or overpressure.

Turbulence factors are usually employed so that the design of explosion mitigation systems may be appropriately considered, with the explosion mitigation system being required to activate and respond much earlier in the explosion in order to suppress or relieve the pressure at a faster rate than that required in a laminar explosion. However, it is also important to understand the influence of turbulence generating scenarios when investigating a gas explosion in order to accurately determine the origin and cause of the explosion. This is because turbulence significantly enhances the rate of pressure rise, and consequently, the severity of damage sustained to the dwelling.

Rasbash et al. [230] suggested a turbulence factor of 1.5 be applied to assessments of buildings where furniture and other obstacles was restricted to one level or 5 where a flammable mixture would likely be distributed such that the flame front would propagate from one room to another or where furniture and other decorative items were distributed throughout the entire enclosure. In more severe turbulence generating events, such as where it was possible for a pre-turbulent gas/air mixture to be ignited in the presence of an obstacle congested room, Rasbash et al. [230] recommended a turbulence factor of 8 to 10 be considered. This was in agreement with the work of Phylaktou and Andrews [40] where a factor of 10 was recommended for enclosures with a high blockage ratio.

Phylaktou and Andrews [40] conducted an experimental programme to determine the effect of a single baffle on the characteristics of gas explosions in a closed vessel of large length to diameter ratio and demonstrated that the normalised rate of pressure rise (defined as the rate of pressure rise with the obstacle to that without the obstacle) is equal to the turbulence factor. Dorge et al. [231], conducted a series of experiments to study flame induced turbulence by locating wire mesh grids in the path of a propagating flame. The flame speed was measured either side of the grids through the use of a high speed camera, allowing the turbulence factor to be determined using the flame speed approach:

$$S_t = \beta \times S_l \quad \textbf{(2-73)}$$

2.6. The Effects of Interconnected Rooms

2.6.1. General

There have been very few large-scale experimental studies of the effects of interconnected rooms on gas explosions. To the author of this study's knowledge, the only published works are those conducted at the BCRA facility at Potters Marston [25-27] and by TNO in the Netherlands [180, 232]; both instigated as a consequence of the Ronan Point explosion in the UK. However, there have been a small number of theoretical studies and reviews of the BCRA experimental work. Rasbash et al. [230] hypothesised that the amount of explosion relief necessary to protect large enclosures could be calculated using an empirical formula based on experimental work on ducts and compact vessels. The effect of turbulence on explosion overpressures has been discussed earlier in this chapter, however in relation to interconnected rooms, using fans to generate turbulence, Burgoyne and Wilson [173], Harris [233], Andrews [234] and Andrews et al. [235], demonstrated that the greater the degree of turbulence, the greater the maximum pressure generated in the explosion. The source of the turbulence is of secondary importance [230]. Whilst there is a plethora of information relating to turbulence generated through the induced flow of unburnt gas/air mixture over and around obstacles, turbulence can also be generated by inducing flow over surfaces or through openings such as doorways [26].

The work of Cubbage and Simmonds [164, 165] on box ovens had shown that shelves positioned in the ovens provided a degree of blockage which resulted in higher pressures being generated in explosions than were the case when the shelves were absent. This situation was analogous to a multi-compartment experiment in which flame propagated through openings from one compartment to another or to a situation where furniture may be present.

Although no direct experiments had been carried out under conditions identical to those of a room in a domestic dwelling, Rasbash [229, 236] considered that the explosion relief work of the Swedish Committee for Explosion Testing [166], Cubbage and Simmonds [164, 165, 237] and Rasbash [238] had been undertaken in conditions that were roughly similar in one or more respects to provide an estimate of the maximum pressure developed in explosions in dwellings with rooms of L/D less than 3:1 and K_A between 1 and 5:

$$P_{max} = 1.5P_v + 3.5K_A \quad \textbf{(2-74)}$$

Where:

P_{max} = maximum overpressure (kPa).

P_v = vent opening pressure (kPa).

K_A = vent coefficient defined as the ratio of the area of the face containing the vent to the area of the vent itself (dimensionless).

Rasbash [236] recognised that combustion during an explosion in a dwelling is likely to be turbulent and therefore the equation presented in his work was likely to underpredict the maximum pressure generated, particular given that no research had been conducted on the effect of furniture. Rasbash hypothesised that due to the turbulence generated by flow through internal door openings and it's exacerbation by the use of 'strong' windows, the way to avoid high pressures in dwellings was to have some explosion relief that was open all the time, or that opened at very low pressure and before the flame propagated through an internal door to ignite a turbulent flammable mixture in an adjoining room. Rasbash referred to this type of relief as 'back relief' as it was relief provided in the room of ignition and was open prior to the flame propagating into an adjoining room (see Figure 2-34).

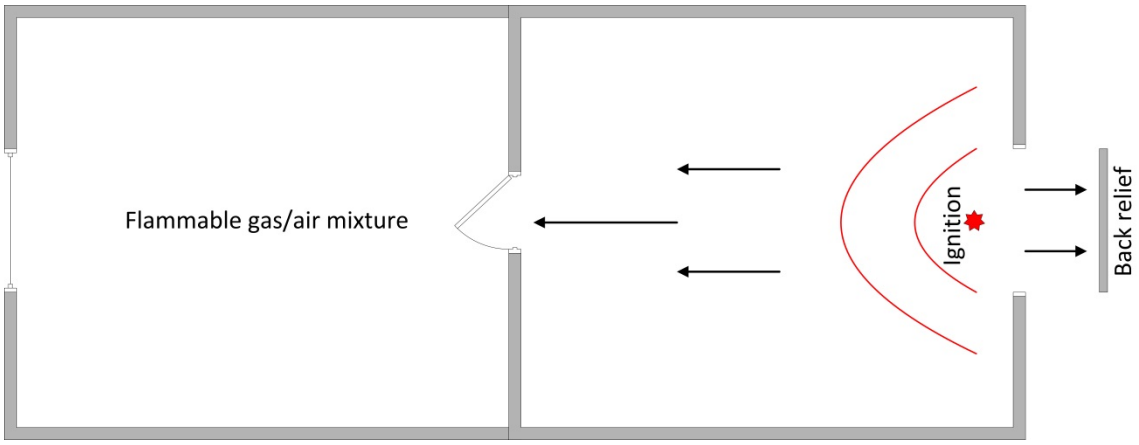

Figure 2-34 The concept of explosion back relief

Rasbashs' insightful paper concluded by stating that it should be practical to design dwellings to withstand gas explosions by using windows that were of generous proportion and designed with a low failure pressure. He also stated that back relief should also be provided by doors opening into open spaces, or if in the case of flats, into verandas or large open corridors. Where it was not possible to provide back relief in a room in which ignition of a flammable gas/air mixture could occur, Rasbash made

the following recommendations to prevent turbulent explosions propagating from one room to another:

i. Use self-closing doors which could withstand the maximum pressure of a low turbulence explosion in the room.
ii. Use sufficient mechanical ventilation to prevent the accumulation of a flammable mixture.
iii. Use flammable gas detectors which provide an audible warning and are interlocked to the gas system and mechanical ventilation.

Some of these recommendations are not practical and could actually enhance a gas explosion. For example, mechanical ventilation is a turbulence generator and a source of ignition. It is unlikely that a flame proof ventilation system would be cost effective in a dwelling. Self-closing doors could enhance explosions by isolating pre-turbulent areas which could be subsequently ignited as partition walls fail in an explosion; further work is needed to investigate this mechanism. Rasbash [236] concluded by stating that large-scale experimental work was required to determine pressure-time curves for single sets of rooms containing furniture. To the authors' knowledge, some forty-five years after the recommendation, this work has yet to be undertaken.

Rasbash et al. [230], developed a correlation to predict the maximum overpressure generated in a vented explosion in a building where turbulence was generated either from the effects of interconnected rooms or through turbulence:

$$P_{max} = 1.5P_v + f\left(\frac{S_u}{0.45}\right)\left(P_I + 2.5K_A\right) \quad \textbf{(2-75)}$$

Where:

P_{max} = maximum overpressure (KN/m^2).

P_v = vent opening pressure (KN/m^2).

f = a turbulence factor (1.5 where furniture is on one level of the building, 5 where there are interconnected rooms with furniture or furniture is located throughout the whole building).

The function P_I, represents the contribution to the increase in pressure due to inertia of the vent cover and is given by:

$$P_I = \frac{0.203K_A w + 1.17}{V^{1/3}} \quad \textbf{(2-76)}$$

Where:

P_I = the increased pressure due to inertia (KN/m^2).

w = the mass of the vent cover per unit area (KN/m^2).

V = volume of the enclosure (m^3).

Stretch [239] examined how gas explosions in dwellings are controlled by the particular features of the building. The author considers that the maximum pressure that could be attained in a gas explosion in a sealed container is approximately 7 bar, if the reaction occurred under adiabatic conditions (which is an underestimate). The author continues by reasoning that a dwelling could not withstand a pressure of this magnitude; a low failure component of the building will yield. Stretch stated that this not only relieves the pressure but also allows a major portion of the flammable mixture to escape the building before the combustion reaction is complete. The author states that this removal of potential energy before it can be released plays the main part in protecting the building from destruction. He reasoned that the extent to which the overpressure is minimised depends upon a number of variables, including the reactivity of the flammable mixture, the characteristics of the building, the degree to which internal building features, including furniture and room layouts, generate turbulence, restrict pressure relief and either connect or isolate different parts of the building. Stretch continued to argue however, whilst recognising that in accidental explosions vent relief is typically provided by windows and doors, that the most important factors of all, was the vent failure pressure, the weight of the vent cover and the vent area. It is these factors, he concluded, that govern the degree to which the reaction is completed within the building, and hence the degree of damage sustained to the structure.

The degree to which a building is damaged is dependent not only on the peak pressure but also on the duration of the pressure wave (i.e. the impulse). The requirement to ensure wind loadings did not damage buildings had resulted, at the time Stretch wrote the article, in windows that were capable of withstanding pressures in the order of 35 mbar. Stretch reasoned that the common practice of painting window frames and maintenance activities meant that it was unrealistic to expect or rely on the relief of dwellings at much less than 70 mbar. The author also makes the point that the pressure-time curves for explosions in enclosures demonstrates that the peak pressure is usually an order of magnitude greater than the vent failure pressure meaning that the more severe gas explosions expose the building to pressures of the order of 0.7 bar.

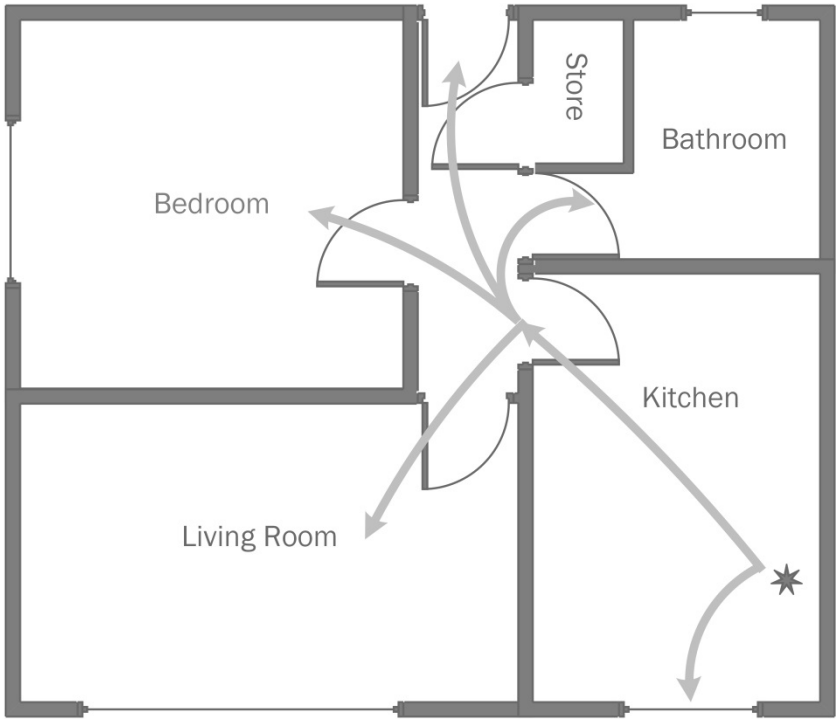

Figure 2-35 Explosion propagating through dwelling (adapted from Stretch [239])

Figure 2-35 is adapted from Stretch [239] with the arrows highlighting the path that the flame front might follow if a flammable mixture was ignited in the kitchen (assuming the flammable mixture was distributed throughout the dwelling). This illustration of the flame path is not particularly enlightening (it also assumes that the partition walls will not fail), but its importance is in the recognition, in 1969, that most dwellings had rooms with small interconnecting areas, partition walls, and windows of different vent area and failure pressure. Consequently, the maximum pressure developed in an explosion in a dwelling is dependent upon the individual characteristics of the building.

The work of Stretch is important as it recognises the role that both interconnected rooms and furniture play in the development of an accidental gas explosion and the necessity for research into their effects. However, there is also a miss-understanding of the mechanism of a vented explosion as there is a belief that the ejection of unburnt gas helps protect the building when the external explosion peak may be the dominant factor in a domestic explosion. In the conclusions, Stretch noted that full-scale experiments are difficult to carry out with a high degree of reliability, and are expensive; however, when the investment and risks involved are considered, further experimental work is quite clearly demanded. To date, no work of this nature has been published.

Molkov [240] analysed the Ronan Point explosion and simulated the overpressure-time profile using a simple mathematical model largely based on two parameters; namely the discharge coefficient, μ, and the turbulence factor, χ. Molkov, used data from the

Ronan Point explosion to establish values for the turbulence factor. The turbulence factor was described as the “real area of flame front surface to area of imaginable sphere to which the combustion products, being inside the vessel at the same moment, might be collected”. This designation makes the assumption that in accidental vented explosions, combustion is spherical; which, for many reasons, may not always be the case. Firstly, the fuel air mixture may be a layer; secondly, ignition may be initiated close to a wall (e.g. light switch etc.), making spherical propagation impossible, thirdly, once the vent opens, the flame is stretched towards the vent opening, assuming a ‘pear’ shape; and, fourthly, interaction between connecting rooms also alters the flame shape. Nonetheless, the ratio of actual flame area to hypothetical flame area may be used as an estimation of turbulence, providing the assumed flame shape is the same as the actual flame shape.

Molkov argued that because windows do not fail until the threshold pressure is reached, explosions in premises would be ‘aggravated’ due to venting through interconnecting doors into adjoining rooms, leading to conditions of high turbulence and pressure piling. Based on the maximum overpressure assumed to have been developed in the Ronan Point explosion, Molkov, calculated that for explosions in real domestic structures with internal obstacles, the turbulence factor would appear to be 11 $\pm$ 3. This is somewhat higher than the estimates of Rasbash [230] and Phylaktou and Andrews [40].

Figure 2-36 shows Molkovs’ predicted overpressure-time profile of the Ronan Point explosion based on a turbulence factor of 12. What is immediately apparent is that there are two predicted pressure peaks, P_V and P_{mfa}, and that the time profile appears to be very fast, even for Towns gas. In the discussion, Molkov states that the two pressure peaks are in agreement with the “well known” pressure peaks, related to vent opening and mixture burnout. It is assumed that the author, when talking of mixture burnout, is referring to the latter stages of combustion and maximum flame area. In addition, he added “that as the result of inertia the first pressure peak depends on the value of the turbulence factor. This means that after removal of the vent cover, the pressure continues to increase until the vent is open enough for the pressure to start to decrease. Clearly, the higher the turbulent burning velocity, the higher the first pressure peak”.

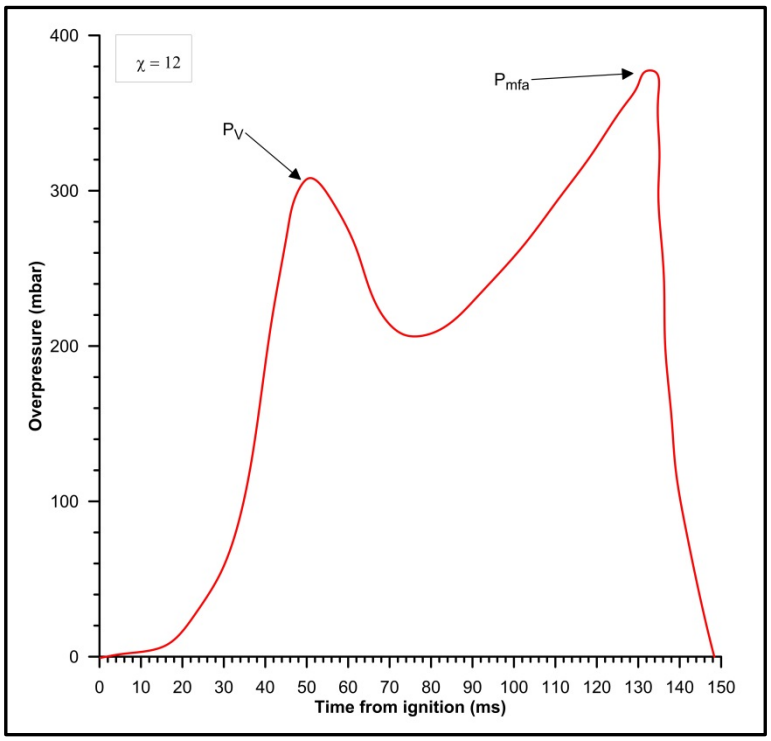

Figure 2-36 Predicted overpressure-time profile of Ronan Point explosion (taken from Molkov [240])

Whilst, very little work has been conducted into the effects of interconnected rooms, a number of studies have been published relating to interconnected process-type vessels [241-254], however, these do not have the same geometry as a room or an interconnecting door that can be either open or closed prior to the explosion. Furthermore, the inadvertent venting arrangements on dwellings make the comparison of experiments conducted in vessels, with interconnecting ducts or pipes, limited in value. Nonetheless, for completeness, the most important literature is reviewed.

2.6.2. Explosion Tests Conducted at Potters Marston

General

In 1968, in order to better understand the events of the Ronan Point gas explosion, an extensive experimental programme to investigate gas explosions in multi-storey load bearing brick structures was commenced by the British Ceramic Research Association in collaboration with MRS (British Gas Corporation Research & Development Division, now DNV GL) and the Atomic Weapons Research Establishment [25]. The tests took place at Potters Marston in Leicestershire with the primary objective of determining the integrity of the load bearing brickwork when subjected to pressure pulses generated in accidental gas explosions. A limited number of tests were also undertaken to determine the effects of explosions propagating from one room to another.

The phrase 'cascade effect' had been widely used after the Ronan Point explosion, and was used to describe the increase in pressure and rate of pressure rise in the progression of an explosion from one room or enclosure to another. However, as the explosion mechanism comprises the combined effects of turbulence and pre-compression of the gas air mixture in the secondary room or enclosure prior to ignition (pressure-piling), the phrase is a little misleading.

The most important tests carried out to examine the effects of so called ‘cascade’ explosions proceeding from one room to another, were undertaken in a purpose built, full scale building, designed to simulate the top three floors of a cross-wall tower block. The building is shown in Figure 2-37 and Figure 2-38.

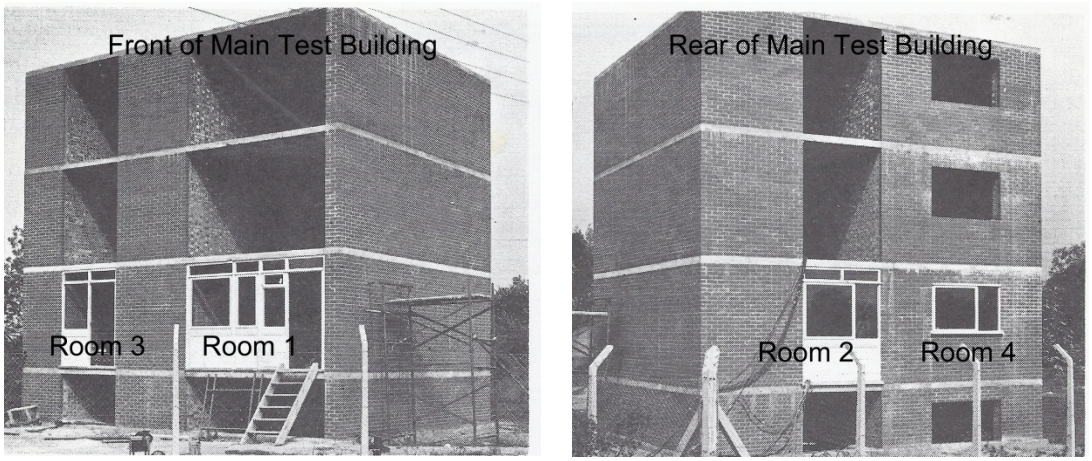

Figure 2-37 The main test building at Potters Marston
(adapted from photo from DNV GL archive)

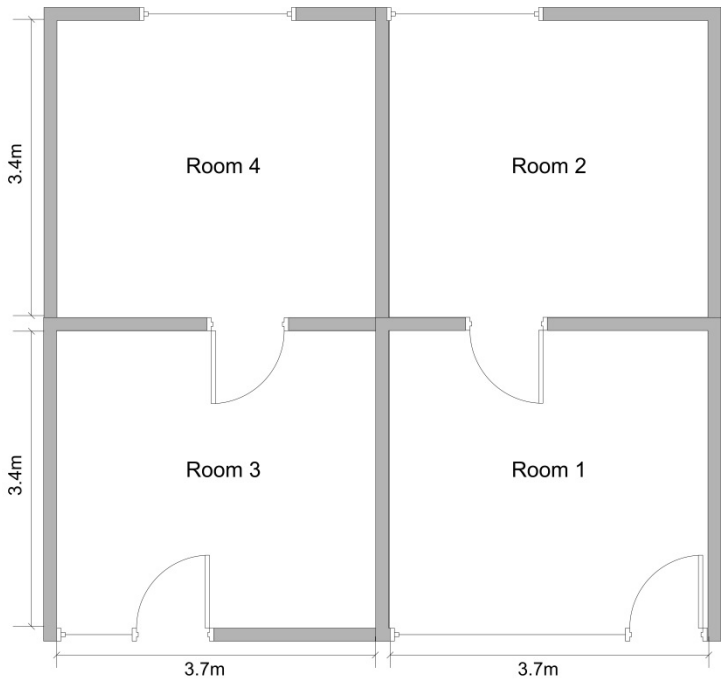

Figure 2-38 Plan view of the main test building at Potters Marston

The tests were undertaken in either rooms 1 and 2 or rooms 3 and 4. The volume of each of the rooms was approximately 25 m^3.

In addition, some cascade explosion tests were undertaken in a 'bunker' which had a volume of approximately 35 m^3 (see Figure 2-39).

Figure 2-39 The bunkers at Potters Marston (photo from DNV GL archive)

Phase I & II

The experimental tests undertaken in Phase I of the full scale research programme, had a specific set of objectives:

(a) to determine the effectiveness of venting provided by the cladding and windows, and to measure the pressure involved,
(b) to determine the pressure necessary to damage a load bearing-brick wall, and,
(c) to test the ability of the structure to withstand progressive collapse following the failure of the main structural wall.

In phase II of the tests some additional objectives were considered:

(d) to determine the pressure profiles of different types of explosions, and,
(e) to determine the effect of cascade explosions (i.e. explosions proceeding from one room to another through a doorway when both rooms contain flammable gas).

In Phase I of the tests, meteorological balloons were located in one of the rooms, filled with stoichiometric gas/air mixtures and ignited electrically. In Phase II of the experimental programme, more tests were undertaken using gas filled meteorological balloons, but in addition, explosion tests using layered gas/air mixtures of nominal stoichiometric concentration were also undertaken. Both natural gas and town gas were used in each phase of experimentation.

It was found that in all the balloon experiments in the building, the pressure in the room containing the balloon was much greater than the pressure in the adjoining room. However, where layers of flammable gas/air mixture were used, the pressure was always greater in the secondary room (i.e. the room in which ignition had not been initiated). The absence of high overpressures in these experiments was attributed to the presence of a large glass window acting as an explosion relief in the ignition room, which provided 'back relief'.

An empirical relationship for the pressures in the adjoining rooms was derived [25]:

$$\mathrm{P}_2 = 0.59\mathrm{P}_1 + 1.14\mathrm{P}_1^2 \qquad \textbf{(2-77)}$$

Where:

P_1 is the pressure developed in the room in which ignition is initiated (lb/in^2).

P_2 is the pressure developed in the secondary room (lb/in^2).

It should be noted that the equation was derived from data taken from just three of the experiments and information on the pressure developed in the kitchen of the Ronan Point explosion. No theoretical attempt was made to justify the relationship.

It was observed in some of the preliminary experiments that the rate of pressure rise was greater for tests involving town gas than natural gas. This was simply attributable to the greater burning velocity of town gas.

From the results of the Phase I and II tests it was maintained that because the pressure impulse (taken as the integral of the pressure-time profile $\int_o^t P(t)\,dt$) was found to be similar, for layered town gas and meteorological balloon-contained town gas, then the use of balloons to simulate layer explosions was justified. However, this assumption may not have been correct, as the method for forming layers of gas of uniform concentration in the rooms was of limited accuracy [255].

During phase II, test No. 49 was carried out in the main building with both rooms having a high level gas/air layer of stoichiometric concentration. The explosion caused major damage to the building structure. It was hypothesised that the explosion in the 1st

room, which developed a pressure of 90 mbar, passed through the door into the 2nd room with a cascade effect leading to a significantly higher pressure of 228 mbar being recorded.

Because of the higher overpressure that was developed within the 2nd room and the damage that was caused to the brickwork of the building, there was significant interest in the results of this test. As a consequence, two separate programmes of further tests were planned in order to improve understanding of explosions that propagate from one room to another.

Using the results of the Potters Marston experiments, Cubbage and Marshall [189] derived a correlation to determine the maximum pressure in the primary and secondary enclosures:

$$P_1 = P_V + \left(\frac{a(K_A w)_{avg} S_u^2}{V^{\frac{1}{3}}} \right) [F(E, E_0)] \quad \textbf{(2-78)}$$

Where:

P_1 = the maximum pressure in the compartment in which the explosion is ignited (lb/in^2).

P_V = the failure pressure of the vent (lb/in^2).

a = a constant (Cubbage and Marshall [189] recommend a value of 0.5).

K_A = the vent coefficient.

w = the weight of the vent per unit area (lb/ft^2).

S_u = the laminar burning velocity (ft/s).

V = the volume of the enclosure (ft^3).

E = energy density of the gas/air mixture (BTU/ft^3).

E_0 = energy density at which the vent is removed (BTU/ft^3).

$F(E,E_0)$ is therefore, a measure of the energy content of the gas/air mixture in excess of that required to remove the vent. Where the enclosures are full of stoichiometric gas/air mixtures, $F(E,E_0)$ may be taken as 1.

The average of the function (K_Aw) may be determined by:

$$\frac{1}{(K_A w)_{avg}} = \frac{1}{(K_A w)_i} + \frac{1}{(K_A w)_j} + \cdots\cdots \quad \textbf{(2-79)}$$

Where (i) and (j) refer to separate vents in a single room (e.g. doors and windows). N.B.: the averaging of vents in this manner is only valid if their failure pressures are approximately similar.

The maximum pressure in the secondary enclosure may be determined by:

$$P_2 = \left[\left(\frac{V_2}{V_1}\right)\left(\frac{Kw_{avg} {S_u}^2 P_1}{V_2^{\frac{1}{3}}} + \frac{K_{A,2} P_1^2}{K_{1,2}}\right)\right]^{0.5} \quad \textbf{(2-80)}$$

Where the subscripts refer to the primary and secondary enclosures and where the vent area coefficient subscripts are separated by a comma the subscripts refer to a vent that is common to both enclosures (e.g. an interconnecting door).

The Cubbage and Marshall correlation given in Equation (2-80) suggests that the maximum pressure developed in the secondary enclosure is a function of the enclosure volume ratio, the laminar burning velocity, the vent coefficient between the two enclosures and finally on the weight and vent coefficients for the vents on both the enclosures venting towards the external atmosphere. Whilst there is an account of the potential pre-compression through the use of the P_1 pressure there is no accounting for any additional turbulence that may be developed.

Phase III

The 1st set of explosion tests was undertaken by FRS, BCRA and MRS in a bunker containing two partitions each with large openings [26].

In order to better understand the effects of turbulence on explosions in interconnected rooms, which is generated by the propagation of the flame front, and the movement of unburnt gas, past obstacles and through restricted openings, nine experiments were carried out in the bunker at Potters Marston.

The tests were all undertaken using a high level layer, nominally 0.9 m in depth from the ceiling, of town gas or natural gas. The 35 m^3 bunker was divided into three compartments, by internal brick walls, with large openings between the compartments. The front face of the bunker was sealed using a polythene sheet.

Ignition was initiated in the compartment furthest from the vent, so ‘back relief’ was eliminated and higher pressures were generated than those measured in phases I and II. Measured flame speeds were found to be an order of magnitude higher in the secondary and tertiary compartments than the ignition compartment, with maximum overpressures of approximately 340 mbar using town gas as the fuel, and 205 mbar using natural gas. It was concluded that turbulence was created by the flow through the openings between compartments, induced by flame expansion in the ignition

compartment. This led to an increased burning velocity in the secondary and tertiary compartments, giving rise to pressures some 2 to 3 times higher than a comparable explosion in a single empty chamber.

The results demonstrated that it was possible to generate substantially larger pressures in an explosion that propagated from one room to another than would be expected in an explosion in a single room, even if the single room was completely filled with a stoichiometric gas/air mixture. However, the enhanced explosion pressures were only attained over a narrow gas concentration range.

Phase IV

The second, further set of experiments at Potters Marston, Phase IV [27], were conducted in both the main building and the bunker. The purpose of the tests carried out in the main building included the following:

(a) to gain further understanding of explosions of layered town gas/air and natural gas/air mixtures, where the explosion propagated from one room with vent(s), to an adjacent room with vent(s), via a doorway.
(b) to examine the effects of layer thickness, gas concentration and position of ignition on pressure-time profiles.
(c) to investigate the effect of the interconnecting door position before ignition (i.e. open or closed).

The test that caused structural damage to the building during Phase II (test 49) was also repeated during this phase of testing.

The purpose of the tests in the bunker was to measure the failure pressure of single and double glazed windows.

Due to difficulties in obtaining acceptable layering of gas mixtures, many of the experiments originally intended were abandoned. Consequently, it was not possible to make positive conclusions from the results of many of the experiments. Nonetheless, some general conclusions were made:

- Much higher pressures were generated with layered town gas explosions than layered natural gas.
- The direction in which the door connecting the two rooms opened was important, since:
    - when ignition took place in the room into which the door opened, gas was ‘sucked’ into the ignition room from the secondary room by a

rarefaction wave after an explosion and venting had already occurred, leading to low pressure generation.

- when the door opened into the secondary room (with ignition still in the primary room), the flame was able to enter the secondary room, via the doorway, before the vent had opened, leading to the generation of higher pressures.

- When there is a layer of flammable gas/air mixture in two adjoining rooms, both with vents, and with an inter-communicating open door, higher pressures are observed in the secondary room than in the room in which ignition took place.
- Three pressure peaks were observed during some of the experiments, comprising the common double-peak for a vented enclosure plus an extra peak corresponding to the vented explosion in the adjoining room.
- The experiments which measured the failure pressure of single and double-glazed windows showed, that in general terms, double glazed windows failed at pressures about 30 per cent higher than for the equivalent single sheet of glass.

2.6.3. Experimental Tests Carried out by TNO

TNO undertook large-scale experimental work in a one storey building consisting of two rooms of different size (2 m x 4 m and 3.5 m x 4 m) connected by an open doorway [180, 232]. Each room had an open front face so that the vent material and opening size could be varied.

Thirty four explosion tests were undertaken during this experimental programme. During the experimental tests, each room was filled with a stoichiometric natural gas/air mixture. The typical pressure-time traces were found to be very similar to those observed by Tite [34, 35], Greening and Tite [54], Cooper et al. [64] and Bauwens et al. [45] in single enclosure experiments (see Figure 2-16, Figure 2-17 and Figure 2-23). However, Dragosavic [180, 232] described the pressure-time histories as being generally characterised by two peaks, the first peak was associated with the failure of the vent and the venting of unburnt gas/air mixture and the second peak had a high frequency (200 Hz) oscillation superimposed (acoustic oscillations) and occurred near to the end of the explosion.

One interesting finding was that ignition at the centre of a room led to higher pressures being generated than ignition in locations adjacent to one of the walls. Very low overall pressures were recorded when the explosion propagated via an open doorway from the smaller to the larger room. In this instance, the vent in the smaller room had failed before the vent in the larger room.

Dragosavic summarised the findings of the experimental programme in terms of pressure generation as the following:

i. Even with a large vent of negligible strength, explosion overpressures of 30 mbar were possible.
ii. The first observed pressure peak increased proportionally to the vent failure pressure.
iii. The second observed pressure peak (as reported by Dragosavic) increased in accordance with the relationship $0.5P_v$.

Dragosavic developed correlations to predict the overpressure developed during an explosion in a building with interconnected rooms. For the first pressure peak:

$$P_1 = 3 + P_v \quad \textbf{(2-81)}$$

Where:

P_1 = the 1st peak pressure, caused by the vent opening and relief of unburnt gases (kN/m^2).

P_v = the vent failure pressure (kN/m^2).

For the second pressure peak:

$$P_2 = 3 + 0.5P_v + \frac{0.04}{\psi^2} \quad \textbf{(2-82)}$$

Where:

P_2 = the 2nd peak pressure (kN/m^2).

$\psi = \frac{A_{vent}\ (m^2)}{V_{room}\ (m^3)}$.

The larger of the two values must be adopted, such that:

$$P_{max} = 3 + 0.5P_v + \frac{0.04}{\psi^2} \geq 3 + 0.5P_v \quad \textbf{(2-83)}$$

2.6.4. Studies on Interconnected Vessels

The potential for pressure piling, when a flame propagates from one chamber into another, was first identified by Beyling [256], in 1906. The substantial increase in pressure in the secondary chamber was attributed to pre-compression, as the hot combustion gases from the ignition chamber were pushed ahead of the flame front into the adjoining chamber. After ignition in the primary vessel, the expanding flame front causes a rise in pressure in the vessel and sets-up a flow from the primary to the

secondary vessel, creating turbulent conditions and raising the pressure in the secondary vessel above atmospheric. When the propagating flame front reaches the secondary vessel, conditions may be intensely turbulent and, due to pre-compression, the maximum pressure may be significantly higher than the adiabatic value calculated thermodynamically from initial atmospheric conditions [244].

Despite a significant number of studies related to the phenomena of pressure piling [241-245, 247-251, 257-260], very few correlations have been published to predict the pressure peak in interconnected vessels.

Grice and Wheeler [261], in 1929, followed on from the work of Beyling and recognised that the rapid increase in pressure in the second chamber was not solely attributable to pressure piling. They concluded that there were three contributory factors:

1. Compression of the gas/air mixture, in the secondary chamber, before ignition.
2. Turbulence, created by the high velocity inrush of gases.
3. Jetted ignition as the flame rapidly propagates through the communicating passage.

Gleim and Marcy [262], of the US Bureau of Mines, investigated the effects of differing vessel size and ignition position. Their results indicated that higher peak pressures are attained as the vessel volume ratio $\left(V_1/V_2\right)$ increases. In addition, they found that the pressure piling was more pronounced when the distance between the ignition source and the secondary chamber was increased.

Brown [260], in 1959, investigated the effect that the length of the connecting pipe had on explosions propagating from one vessel into another. He concluded that the pressure generated in the secondary chamber was independent of the length of the pipe. This was because the pressure in the primary chamber is the ‘driving force’ causing flow into the secondary chamber and the pressure in the secondary chamber at the time of flame entry was likely to be similar to that when the flame entered the pipe [257]. Brown also observed that peak pressures were dependent on changes in the cross-sectional area of the interconnecting pipe. That is, the peak pressure in the vessels increased when the pipe diameter was decreased.

Bartknecht [154] reports on a range of experiments conducted in interconnected vessels. On experiments conducted with a vessel ratio of 1, he noted that, in agreement with Brown [260], the length of the connecting pipe did not alter the course of the explosion, but the diameter had a significant influence on the violence of the explosion in both vessels. Due to pressure oscillations, the rate of pressure rise in the primary (ignition) vessel was found to be 4 times as high as it would be for an

equivalent single vessel, but the maximum pressure was not increased. However, the rate of pressure rise in the secondary vessel was up to 10 times higher than an equivalent single vessel and the maximum pressure was found to have an increase of approximately 10%. The elevated pressure in the secondary chamber was attributed to jet ignition and turbulence.

Bartknecht also reported on experiments conducted on vessels of differing size, that is, $(V_1/V_2 \neq 1)$. In these experiments it was found that if the primary vessel was of lesser volume than the secondary vessel, it was possible for the peak pressure to be recorded in the primary vessel. However, in general terms, the pressure in both vessels was found to increase by approximately 40 to 50% of equivalent single vessel explosions. Contrastingly, if the primary vessel was of greater volume than the secondary vessel, a different explosion mechanism was observed. In these instances, there was a significant amplification of the violence of explosion (rate of pressure rise). Whilst the pressure recorded in the primary vessel was considerably lower than that recorded in the secondary vessel, there was an overall pressure increase of approximately 200%.

Of significant interest to this study, was the finding that the gas concentration; at which the maximum pressure was measured, varied, and was not in agreement with that of a single vessel explosion (i.e. close to stoichiometric). It was observed, that the gas concentration at which maximum pressure occurred, appeared to be influenced by the diameter of the interconnecting pipe and the location of the ignition source. The rate of pressure rise in the secondary vessel, in all cases, occurred when the distance between the ignition source and plane of the interconnecting pipe connection was at a maximum. On the basis of the experimental tests he conducted, Bartknecht concluded that excessive pressures may be avoided if the interconnecting vessels were of the same size, that is $(V_1/V_2 = 1)$, and the ratio of the cross-sectional area of the connecting pipe to the vessel volume did not exceed 0.002 m^2/m^3 or was greater than 0.4 m^2/m^3.

Solberg [207], in 1982, theorised that flame speeds, in explosions in interconnected compartments, may strongly accelerate as the flame propagates from compartment to compartment. He predicted that as the explosion becomes faster, the pre-compression in the next compartment will be less, which counteracts the energy release in this compartment as the flame arrives. He also suggested that the pressure increase would be greater for larger interconnecting openings.

Singh conducted several small-scale studies of pressure piling and its effects [251, 258, 259]. Of particular interest was the investigation of the effects of the volume and

size of the vessels, the ignition location, and the length and diameter of the interconnecting pipe. In general terms, Singh confirmed the findings of previous studies [260, 262]. He concluded that ignition at the rear of the primary vessel, or central ignition in a vessel of large L/D, resulted in a larger volume of unburnt gas being pushed into the secondary vessel, pre-compressing the flammable mixture in the second vessel, and thus producing a higher peak pressure. He also found that the peak pressure in the secondary vessel was independent of the length of the interconnecting pipe but dependent upon its diameter; and that increasing the vessel volume ratio had the effect of increasing the peak pressure, up to a point where back venting from the secondary vessel caused the pressure to level out or even decrease depending upon the gas concentration and pipe diameter. The main finding of importance to this study, was that the maximum developed pressure and peak rate of pressure rise were more pronounced in larger scale setups. However, although the conclusion may be right, the basis for it seems debatable, given that whilst Singh varied the vessel volume during the experiments, the opening into the secondary vessel was fixed. As a consequence, tests involving vessels of smaller volume would result in more efficient back venting of the explosion in the secondary vessel.

Singh developed a correlation for determining the maximum pressure in the secondary vessel. The correlation, which does not take into account the effect of turbulence on the pressure peak [244], is given by:

$$P_k = P_1 \left(E - \frac{2.31}{S_u} \frac{d_c^2}{V} \right) \qquad \textbf{(2-84)}$$

Where:

P_k = the maximum pressure in the secondary vessel (g/cm s^2).

P_1 = the pressure in the secondary vessel at the time the flame front reaches the linked vessel (g/cm s^2).

E = the expansion factor.

d_c = the diameter of the interconnecting duct (cm).

S_u = laminar burning velocity (cm/s).

V = volume of vessel (cm^3).

The use of this correlation requires the prediction of the P_1 pressure peak. Singh derived a series of further correlations and graphs to predict P_1. As the Singh correlation is based on small-scale studies in spherical or cylindrical vessels, and is dependent upon idealised conditions, it will not be further considered in this study.

Abdullin et al. [241], developed a model for predicting the mechanism of an explosion in interconnected vessels by focusing on the interaction of the combustion rate and the energy transferred during the flow of gases from vessel to vessel.

Phylaktou and Andrews [249], carried out a number of methane/air explosion tests in interconnected vessels of equal size (0.5 m diameter x 0.5 m length), that is $(V_1/V_2 = 1)$, that were connected by a 76 mm diameter pipe that was 1.7 m in length. By instrumenting the vessels and connecting pipe (using thermocouples and pressure transducers), the authors were able to measure the transient pressure-time data for the explosion and monitor flame propagation from vessel to vessel.

Following central ignition in the primary vessel, they observed an initial period of delay before any appreciable pressure rise was observed in the 1st vessel. From this point, the flame propagated in a spherical, laminar manner, and the pressure began to increase slowly. This created a difference in pressure between the two vessels and therefore initiated flow into the secondary vessel. As the rate of flame propagation increased, the pressure difference was increased and the flow through the interconnecting pipe accelerated. Just prior to the flame reaching the inlet of the interconnecting pipe, there was a pressure difference between the two vessels of approximately 80 mbar, creating flow into the secondary vessel at high velocity (≈ 80 m/s). This rapid flow of unburnt gas/air mixture ahead of the flame created turbulence in the pipe. The flame front, already accelerating due to the expansion of hot combustion products, underwent further rapid acceleration as the combustion rate was enhanced significantly due to the turbulent flow. When the flame front entered the second chamber, the pressure increased dramatically from approximately 200 mbar to 3.7 bar, with the maximum rate of pressure rise in the order of 584 bar/s. This very rapid increase in pressure was due to the jetted ignition (as the flame excited the pipe at high velocity) of the turbulent gas/air mixture. This abrupt pressure rise resulted in a reversal of flow (as the pressure in vessel two was greater than that of the primary vessel) back into the primary vessel, which up to this point had been burning in laminar manner. The consequence of this reversal of flow was to create turbulence in the primary vessel, which increased the combustion rate and increased the pressure in the 1st vessel. The pressure in this vessel was found to increase at a similar rate to the initial pressure increase in the secondary vessel and consequently the direction of flow altered again. The changes in flow direction set up oscillatory combustion. The maximum pressure recorded during this explosion was 6.7 bar in the primary vessel and 7.4 bar in the secondary vessel, the difference between the two being associated with pre-compression.

With end ignition, a different explosion mechanism was noted. In the initial laminar stage of the explosion, it took longer for the flame to reach the plane of the connecting pipe, simply because the flame front had farther to travel. However, by the time the flame front reached the pipe the pressure difference between the two vessels was 180 mbar (over twice the value for central ignition) and consequently a much higher flow regime was set up, resulting in a greater turbulence intensity. Accordingly, the combustion in this vessel was almost instantaneous, with a maximum rate of pressure rise of 2068 bar/s.

The results of the central ignition tests of Phylaktou and Andrews [249] are in broad agreement with the findings of Bartknecht [154] with a rate of pressure rise in the primary vessel approximately 4 times that of an explosion in equivalent sized single vessel and up to 10 times greater for the secondary vessel. However, when the results of end ignition are considered, the rate of pressure rise was found to have increased by a factor of 17. That is almost double the value predicted by Bartknecht [154]

In 1996 Lunn et al. [247], published a report on totally confined coal dust and toner dust explosions in interconnected vessels. The experimental arrangement consisted of several vessels with sizes ranging between 2 m^3 and 20 m^3 connected with a 5 m long pipe of varying diameter (15, 25 and 50 cm). The experimental work was focused mainly on the effects of vessel volume, vessel volume ratios and pipe diameter. The authors confirmed much of the findings of earlier work and noted that pressure piling did not occur for volume ratios less than 0.25.

In 1996 Holbrow et al. [245], published a report on vented coal dust, toner dust and anthraquinone dust explosions in interconnected vessels. The experimental setup consisted of several vented vessels with sizes ranging between 2 m^3 and 20 m^3 connected with pipes of varying diameter (15, 25 and 50 cm) and varying length (up to 15 m). Interestingly, the authors concluded that varying the pipe length had some effect on the maximum pressure and the pressure–time profile. The longer the pipe length, the greater the separation between the pressure peaks recorded in the individual vessels. Furthermore, the backflow also decreased as the pipe length was increased. These findings are not in agreement with the work of others [154, 251, 258, 259].

Maremonti, et al. [248] investigated the ability of a CFD program (AutoReaGas) to model gas explosions in linked vessels. They used the experimental data of Phylaktou et al. [249], and found reasonable agreement between the measured and calculated data with regard to the peak pressure but less agreement when comparing values for the rate of pressure rise and flame speed. The computed values of the turbulence intensity in both chambers demonstrated that turbulence induced in the secondary

vessel is a major factor affecting the explosion violence. With the interconnecting pipe diameter being a key influencing parameter.

Razus et al. [250] carried our small-scale experiments on two cylindrical interconnected vessels using stoichiometric propylene/air mixtures. The explosion transmission between the linked vessels was found to be strongly dependent on the vessels configuration, position of the ignition source, and length and diameter of the connecting pipe. The explosion was found to propagate from one vessel to another when the pressure in the primary vessel reached a critical value. This critical pressure increased with decreasing interconnecting pipe diameter.

The results showed that the initial pressure and the tube diameter were the major parameters in the development of explosions in interconnected vessels. Other factors, such as the vessel volume ratio and the location of ignition source were also important.

The effects of partially filled interconnected enclosures on vented gas explosions is of importance to investigators of accidental gas explosions, where there is a potential for the release of a flammable gas to fill only a single room because the door to an interconnecting room is closed. This situation was investigated by Willacy et al. [253] in 2006. The major purpose of this study was to gain a better understanding of how explosions develop in interconnected enclosures when one enclosure is full of flammable mixture and the adjoining enclosure is free of gas.

The results showed that the mechanism of flame propagation and pressure development of an explosion in a partially filled interconnected vessel, was similar to that of completely full interconnected systems. However, not surprisingly, the key difference was that, whilst the total explosion time was similar, a partially full explosion in an interconnected vessel did not generate maximum pressures of the same magnitude as that of a completely full interconnected system. However, there is the possibility that a pocket of rich gas/air mixture in the primary vessel, could get pushed into the secondary vessel at high velocity, whereupon it mixes turbulently with the air in the secondary vessel to produce a stoichiometric mixture. In this situation it may be possible to develop a pressure in the secondary chamber comparable to that of a completely full system.

Di Benedetto et al. [243] and Di Benedetto and Salzano [242], recognised that a universal chemical model had not been developed to fully consider the various combustion regimes present during an explosion in interconnected vessels (e.g. laminar, flamelet, corrugated, well mixed distributed regime) and developed a CFD model in which the combustion models adapt to the specific combustion regime arising. The model was directly validated by means of a blind test carried out with the

experimental findings of Singh [258]. Whilst the work was entitled “Modeling Explosion In Compartmented Vessels” [243], the work was related to equipment found in industrial applications (e.g. reactors, tanks, vessels etc.) where pressure piling due to pre-compression was important. Vented explosions through interconnected rooms present a different problem.

Di Benedetto et al. [244] when considering the effects of pressure piling in two interconnected vessels (they were considering buildings, mines, reactors and tanks as interconnecting vessels), evaluated empirical correlations to determine their suitability to predict the intensity of the pre-compression induced by flame propagation in the primary vessel and the flow of gases into the secondary chamber. The authors suggest that the correlation developed by Molkov [263] for vent sizing of a single vessel is the most appropriate correlation for predicting peak pressures in linked enclosures. The reason for this, it is argued, is because the correlation takes into account the initial pressure and turbulent flame propagation. The peak pressure is determined by:

$$\mathrm{P_{red}} = \frac{\pi_{\mathrm{red}}}{\pi_{\mathrm{v}}^{1.5}} = \mathrm{Br_t^{-2.4}}, \mathrm{P_{red}} \leq 1, \mathrm{Br_t} \geq 1 \qquad \textbf{(2-85)}$$

or:

$$\mathrm{P_{red}} = \frac{\pi_{\mathrm{red}}}{\pi_{\mathrm{v}}^{1.5}} = \mathrm{P_{red}^{*}} - 6\mathrm{Br_t^{0.5}}, \mathrm{P_{red}} > 1, \mathrm{Br_t} < 1 \qquad \textbf{(2-86)}$$

Where:

P_{red} = the reduced explosion pressure, which is lower than the maximum possible pressure (i.e. ≈ 8 bar) for example, through venting; but in the context of this work is equal to the maximum overpressure peak, $P_{max,abs} – P_{i,\,abs}$ (bar).

π_{red} = dimensionless reduced explosion overpressure ($\pi_{red} = P_{red,abs}/P_{i,abs}$).

π_v = dimensionless vent failure pressure ($\pi_v = P_{v,abs}/P_{i,abs}$).

$\mathrm{P_{red}^{*}}$= the reduced pressure when $Br_t = 0$, thus being the reduced pressure reached in the equivalent adiabatic closed vessel. Molkov [263] assumed this to be equal to 7, but the value would vary as different fuels are used (e.g. 6.7 for methane and 8.2 for propane).

Br_t = the turbulent Bradley number.

The turbulent Bradley number may be given by:

$$\mathrm{Br_t} = 0.21\sqrt{\frac{\mathrm{E}}{\gamma_{\mathrm{u}}}}\frac{\mu}{\chi}Br \qquad \textbf{(2-87)}$$

Where:

E = the expansion ratio.

γ_u = the specific heat ratio for the unburned fuel at initial conditions.

μ = a discharge coefficient.

χ = a turbulence factor after vent opening.

Br = the Bradley number.

The Bradley number may be determined by:

$$\mathrm{Br} = \frac{A_v c_0}{V^{2/3} S_u \left(E - 1\right)} \qquad \textbf{(2-88)}$$

Where:

A_v = the area of the vent (m^2).

V = volume of the vessel (m^3).

c_0 = the speed of sound at initial conditions of the explosion (m/s).

S_u = laminar burning velocity (m/s).

The turbulent Bradley number is a modification of the Bradley number to take account of turbulent conditions. This is achieved through the introduction of the deflagration outflow interaction (DOI) parameter, χ/μ, given by:

$$\frac{\chi}{\mu} = \alpha \left[\frac{\left(1 + 10\sqrt[3]{V_\#}\right)\left(1 + 0.5 Br^{\beta}\right)}{1 + \pi_v} \right]^{0.4} \pi_{1,\#}^{0.6} \qquad \textbf{(2-89)}$$

Where:

α = empirical coefficient (suggested value 1.75 [263]).

$V_\#$ = dimensionless volume (numerically equal to enclosure volume).

β = empirical coefficient (suggested value 0.5 [263]).

$\pi_{1,\#}$ = dimensionless initial pressure expressed as the ratio of absolute initial pressure to the pressure of 1bar.

Di Benedetto et al. [244] undertook a series of calculations using the Molkov correlation to compare the predictions with the results of Singh [251]. The authors found good agreement with the experimental results and suggested that this was because the pressure piling phenomenon is mainly dependent upon the turbulence within the

interconnected vessels and the initial pressure in the secondary vessel, both of which are accounted for in the correlation.

Konishi [264] undertook a programme of small-scale experimental testing and CFD modelling to attempt to understand the explosion mechanism of a ‘real’ accidental gasoline vapour explosion that occurred in a boat with multiple compartments. He concluded that the key contributor to the compartmental explosion was the transition from laminar to turbulent combustion as the flame propagated through the adjoining openings.

2.7. Thermal Damage in Explosions

2.7.1. General

Heat that is released as a consequence of the combustion process is transmitted to the surroundings by conduction, convection and thermal radiation. During the course of a gas explosion the flame front will propagate through the entire flammable mixture. As a gas explosion is a very short duration event, it is flame contact and thermal radiation that present the most significant hazard when the effects on humans, clothing and furnishings are considered; with the incident heat flux being at a maximum when the receiver is engulfed by the flame.

Following an accidental gas explosion, a detailed examination of the thermal damage (scorching, blistering etc.) caused by the explosion, can provide critical evidence [16]. The investigator will be able to determine the rooms through which the flame propagated, whether the flammable gas involved was more or less dense than air, and the depth of any layer. This information may then be used to determine any credible sources of gas by calculating or measuring the release rate and estimating whether an escape of this magnitude was capable of mixing with air to form a flammable layer, or completely full mixture, which is in agreement with the scorching patterns.

Following the release of a lighter than air gas, a layer of flammable gas/air mixture may accumulate, extending downwards from the ceiling to the location of the release source [66-71]. If the flammable mixture is subsequently ignited, the flame will propagate through the gas/air mixture at high level and consequently evidence of the passage of the flame is expected to be found at high level rather than at low level. In contrast to the location of thermal damage in a natural gas explosion, explosions involving layers of heavier than air gases, such as LPG, will exhibit thermal damage at low level, from the point of leakage down to floor level. In these situations, more burning should be evident at low level, such as scorching to carpets, furniture etc., than at ceiling level (see Figure 2-40).

Figure 2-40 Evidence of thermal damage following a layered LPG explosion (photo taken by the author)

Other evidence as to the nature of the gas involved (e.g. its relative density) might be provided by the pattern of burn injuries suffered by individuals in the room through which the flame propagates. Although ordinary clothing provides some degree of short term protection against a transient explosion flame. Burns to the head and upper part of the body, but not the legs and lower torso, are indications that a layer of a buoyant gas had been involved (e.g. natural gas). If burns were restricted to the lower part of the body, this provides an indication that the explosion involved a heavier than air gas such as LPG or petrol vapour. However, caution should be taken when using this type of information, as hot combustion products are more buoyant than air and may cause burn injuries to the upper part of the body, potentially providing a false indication that the fuel involved is lighter than air.

2.7.2. Thermal Radiation

Thermal radiation may be considered as the transfer of heat by electromagnetic waves, generated by the motion of charged particles. Electromagnetic waves travel at the speed of light and are typically described by the frequency, wavelength, or photon energy. However, in terms of thermal radiation they are most commonly described by their wavelength, given by:

$$f = \frac{c}{\lambda} \qquad \textbf{(2-90)}$$

Where:

f = frequency (Hz).

c = the speed of light in a vacuum (2.9979 x 10^8 m/s).

λ = wavelength (m).

The electromagnetic waves of thermal radiation have wavelengths of approximately 0.3 to 50 μm, depending on the radiating source temperature, and span the infrared and visible ranges of the electromagnetic spectrum [265].

The thermal radiation emitted from a flame is the net result of radiation emitted by radiating gases, particularly carbon dioxide and water vapour, and by carbon particles (i.e. soot). Consequently, it depends on the type of fuel and on the nature of the combustion. A flame in which the radiation is emitted solely from the gaseous constituents is termed non-luminous and one in which there is soot is termed luminous [265]. Natural gas flames contain relatively little soot and are generally termed non-luminous (in relative terms).

Gas explosions in buildings are very brief transient events with a typical duration of approximately 1 s. The emitted radiation of a vented gas explosion will depend on the actual distribution of flame temperatures, partial pressure of combustion products, geometry of the combustion zone, and absorption of radiation in the expanding flame front itself. The incident heat flux is therefore a function of flame temperature, emissivity, distance to receiver and view factor. As a consequence, the incident thermal radiation, received by a person or object located within the building, would vary as the flame propagated through the flammable mixture (i.e. depending upon location of the receiver) and would be a maximum when the flame is largest relative to the target (i.e. just before the flame arrives at the target). Thermal radiation decreases approximately by the square of the distance from the radiating source; meaning that a receiving object situated 2 m from the source would receive ¼ of the radiation than if it were sited 1 m from the source. It should be noted that the flame area (and hence the view factor) is at a maximum for a very short duration (i.e. tens of milliseconds).

The total emissive power at which radiation is emitted over all wavelengths may be determined by Stefan-Boltzmann Law:

$$E = \sigma \varepsilon T^4 \qquad \textbf{(2-91)}$$

Where:

E = total emissive power (kW/m^2).

σ = Stefan's constant, 5.67 x 10^{-11} kW/m^2 K^4.

ε = emissivity.

T = source temperature (K).

The use of the Stefan-Boltzmann law to estimate the thermal radiation effects from a gas explosion therefore require a detailed knowledge of the flame temperature and its emissivity. To calculate the emissive power, the flame temperature can be determined from adiabatic calculations at constant volume and the emissivity of gases formed during the combustion process (i.e. CO_2 and H_2O) are typically calculated using diagrams, such as that given by Hottel and Sarofim [266]. Leckner [267], gives empirical correlations for the total emittance for both water vapour and carbon dioxide. The correlations, for the emissivity of water vapour and carbon dioxide at atmospheric pressure, which are derived from calculations summing narrow band behaviour over the full spectrum [268], are given below:

$$\epsilon(T, pL_e) = \exp\left\{a_0 + \sum_{j=1}^{M} a_j [\log(pL_e)]^j\right\} \quad \textbf{(2-92)}$$

Where:

ϵ = emissivity.

p = partial pressure (bar).

L_e = mean beam length (cm).

The coefficient, a_j, is given by:

$$a_j = c_{0j} + \sum_{i=1}^{N} c_{ij} \left(\frac{T}{1000}\right)^i \quad \textbf{(2-93)}$$

The values of c_{ij}, for both water vapour and carbon dioxide, may be found in a table of coefficients published in Leckner [267] and Hottel and Sarofim [266]. A plot of emissivity using Equation (2-92) shows that the emittance increases with pressure-path length (pLe). However, observations for temperature show that emittance generally decreases with increasing temperature for water vapour, whilst in contrast, emissivity goes through a peak at approximately 1200 K for carbon dioxide and then decreases with increasing temperature.

The spectral average of the mean beam limit may be determined by an approximation given, for example, by Howell et al. [268] and Bejan and Kraus [269]:

$$L_e = 3.6\frac{V}{A} \quad \textbf{(2-94)}$$

Where:

V = volume of the flame (cm^3).

A = flame surface area (cm^2).

There are a number of simple geometric relationships that may also be used to determine the spectral average mean beam length. For example, the mean beam length for the flame given from a gas explosion ignited centrally in a room (i.e. an approximately spherical flame radiating to its surface), may be estimated from the relationship given by Howell et al. [268]:

$$L_e = 0.65D \quad \textbf{(2-95)}$$

Where D is the diameter of the spherical flame (cm).

The emissivity correlations given in Equation (2-92) are for carbon dioxide, water vapour and air with a total pressure of 1 atm. If the total pressure differs considerably from this pressure, a pressure correction needs to be applied. For water vapour, this correction is given by:

$$C_{H_2O} = 1 + (\Delta_{H_2O}\text{-}1)\Xi_{H_2O} \quad \textbf{(2-96)}$$

Where:

$$\Delta_{H_2O} = \frac{[1.888 - 2.053\log_{10}(T/1000)]P_{E,H_2O} + 1.10(T/1000)^{-1.4}}{P_{E,H_2O} + [1.888 - 2.053\log_{10}(T/1000)] + 1.10(T/1000)^{-1.4} - 1} \quad \textbf{(2-97)}$$

and:

$$P_{E,H_2O} = P_t\left[1 + 4.9(p_{H_2O}/P_t)\sqrt{(273/T)}\right] \quad \textbf{(2-98)}$$

Where: Pt is the total pressure of the air/H_2O mixture,

and:

$$\Xi_{H_2O} = \exp\left(-0.5\{\log_{10}[13.2(T/1000)^2] - \log_{10}(p_{H_2O}L_e)\}^2\right) \quad \textbf{(2-99)}$$

For carbon dioxide, the pressure correction is given by:

$$C_{CO_2} = 1 + (\Delta_{CO_2}\text{-}1)\Xi_{CO_2} \quad \textbf{(2-100)}$$

Where:

$$\Delta_{CO_2} = \frac{[1 + 0.1(T/1000)^{-1.45}]P_{E,CO_2} + 0.23}{P_{E,CO_2} + [1 + 0.1(T/1000)^{-1.45}] - 0.77} \quad \textbf{(2-101)}$$

and:

$$P_{E,CO_2} = P_t\left[1 + 0.28\left(p_{CO_2}/P_t\right)\right] \quad \textbf{(2-102)}$$

Where: P_t is the total pressure of the air/CO_2 mixture, and:

$$\Xi_{CO_2} = \exp\left(-1.47\left\{\log_{10}\left[0.225(T/1000)^2\right] - \log_{10}\left(p_{CO_2}L_e\right)\right\}^2\right) \quad \textbf{(2-103)}$$

The individual emittances for water vapour and carbon dioxide must be modified when both gases are in a mixture, such as that of an explosion in air, because the individual spectral lines and absorption for the two gases overlap in some spectral regions, and simple addition of the individual emittances would overpredict the total emittance of the mixture. Consequently, an 'overlap' correction must be applied:

$$\Delta_\epsilon = \left(\frac{\zeta}{10.7+101\zeta} - 0.0089\zeta^{10.4}\right)\left[\log_{10}(pL_e)\right]^{2.76} \quad \textbf{(2-104)}$$

Where:

$$\zeta = \left(\frac{p_{H_2O}}{p_{H_2O}+p_{CO_2}}\right) \quad \textbf{(2-105)}$$

and,

$$p = p_{H_2O} + p_{CO_2} \quad \textbf{(2-106)}$$

The total emissivity, including corrections for pressure and overlap may be calculated by:

$$\epsilon(pL_e) = C_{H_2O}\epsilon_{H_2O}\left(p_{H_2O}L_e\right) + C_{CO_2}\epsilon_{CO_2}\left(p_{CO_2}L_e\right) - \Delta\epsilon \quad \textbf{(2-107)}$$

Using the total emissivity correlation [Equation (2-107)], for a stoichiometric methane/air vented explosion in a typical dwelling (i.e. $L_e \approx 2.5$ m, $T \approx 2200$ K, and typical pressure P_t of 1.5 bara), the total emissivity is calculated to be 0.23. Using the Stefan-Boltzmann Law [Equation (2-91)] ($\epsilon = 0.23$ and $T \approx 2200$ K), the emissive power of a stoichiometric vented methane/air explosion is estimated to be in the order of 305 kW/m^2.

Table 2-5 shows the range of surface emissive powers measured from various hydrocarbon fire experiments. For a detailed study of the thermal effects of hydrocarbon fires, the reader is referred to Cowley [270, 271], Cowley and Johnson [272], Chamberlain [273-279], Drysdale [81], Lowesmith et al. [280] and Wickens and Lowesmith [281]. It should be noted that the most important radiative element in these values of surface emissive power for hydrocarbon fires is soot. Soot is not likely to be as significant in vented natural gas explosions.

Table 2-5 Emissive power from various types of hydrocarbon fire (taken from Mannan [265])

Fire Type	Surface Emissive Power (kW/m^2)
Flash Fire	173
Jet Fire	50 - 220
Pool Fire	60 - 200
Fireball	350

It can be seen from Table 2-5 that the estimated maximum surface emissive power of a vented explosion in a typical room (circa 305 kW/m^2) is greater than that of a flash, jet or pool fire, and similar to that of a fireball.

The level of thermal dose received in an explosion is determined by the intensity, duration and wavelength of the event as well as the exposure time. The thermal dose is therefore based on a combination of the radiation intensity and the exposure duration:

$$\mathrm{TD} = \mathrm{I}t \qquad \textbf{(2-108)}$$

Where:

TD = thermal dose (kW/m^2 s).

I = radiation intensity (kW/m^2).

t = duration of exposure (s).

Given that explosions are too fast for escape, the exposure time may be considered equivalent to the duration of the event. Equation (2-108) is the simplest form for estimating the impact of radiation on people, structures and materials. Lees [265] states that whilst this correlation is relatively accurate at predicting the effects of thermal radiation at low intensity with long exposure duration, it under-predicts the effect of thermal radiation at high intensity. Consequently, Lees suggests that a better correlation for higher intensity radiation events, such as explosions, is of the form:

$$\mathrm{TDU} = \mathrm{I}^{\mathrm{n}}t \qquad \textbf{(2-109)}$$

Where:

TDU = thermal dose units [(kW/m^2)^n s].

Eisenberg et al. [282], based on ultra-violet radiation data from nuclear explosions, proposed that the exponent, n, should take the value of 1.33 (4/3) for correlating fatality data and 1.15 for non-fatal injuries. Hymes et al. [283] reasoned that it was acceptable

to use n = 1.33 for both fatal and non-fatal situations, although it was accepted that in non-fatal cases the value was more approximate. Consequently, using a value of 1.33 for n in non-fatal cases may result in an over-prediction (but nonetheless conservative estimate) of the impact of thermal radiation.

2.7.3. Response of People and Materials Exposed to Heat

In order to estimate the response of persons and materials following an explosion, of a given gas concentration, in addition to estimating the thermal dose it is also necessary to have an understanding of the response of the persons and/or materials exposed to the explosion [284]. Whilst much work has been undertaken on the intensity of hydrocarbon fires (referenced above) and the behaviour of materials and people exposed to compartment fires [285-339], little work was found in the literature relating to the radiative heat flux of a vented explosion.

The full effect of radiation on humans and materials is outside the scope of this study and the reader is advised to consult Hymes et al. [283], Hockey and Rew [340], Stoll et al. [325-329], Backer et al. [341], Babrauskas [342], Burrell and Hare [343] and Horrocks and Anand [302] for a detailed analysis of the topic. However, with basic material and burn data it is possible to model and predict the thermal effects of a vented explosion. Table 2-6 lists the observed effects of people and materials exposed to varying levels of radiation but it should be noted that the exposure duration is much longer than that of a vented gas explosion for all of the situations referred to in this Table.

There are a number of factors that determine the likelihood of a person surviving the thermal effects of a vented explosion [340]. These include:

- The incident thermal dose.
- The degree and effectiveness of any protective clothing.
- The degree of burn sustained.
- The age of the person.
- Any inhalation injury.
- Any pre-existing medical condition.
- The speed and medical response and any medical complications.

Table 2-6 Observed effects of incident thermal radiation (taken from Technica Ltd. [344] and OGP [345])

Incident Flux (kW/m^2)	Observed Effect	
	Equipment	**People**
37.5	Sufficient to damage process equipment and cause collapse of mechanical structures.	100% lethality in 1 min. 1% lethality in 10 s.
35	Cellulosic material will pilot ignite within one minute's exposure.	
25.0	Minimum energy to ignite wood at indefinitely long exposure without a flame. Unprotected steel will reach thermal stress temperatures that can cause failure. Fully Insulated thin steel may lose mechanical integrity.	100% lethality in 1 min. Significant injury in 10 s.
12.5	Minimum energy to ignite wood with a flame or spark (piloted ign). Melts plastic tubing.	1% lethality in 1 min. 1st degree burns in 10 s.
11.7	Partly insulated steel may lose integrity.	
10.0	Certain polymers may ignite.	
7.0		Tolerance limit for persons completely covered by Nomex protective clothing.
6.5		Causes pain within 10 s. Escape is only possible if rapid.
4.7		Causes pain in 15-20 s and burns after 30 s.
4.0		Causes pain if duration is longer than 20 s but blistering of skin is unlikely.
1.6		Causes no discomfort for long exposure.
1.2		Received from the sun at noon in summer.

A dangerous thermal dose is defined by Rew [284] as the dose at which serious burns may be received or a small percentage of the population may die. The level at which serious burns may be obtained has been well defined by the UK medical profession as being a burn that covers more than 10% of the total body surface area in children and the elderly, and more than 15% in the average population. This definition only refers to partial-thickness burns, with full-thickness burns being classed as severe [346].

A superficial burn, that is one which does not penetrate the epidermis (outer layer of skin), is referred to as a first degree burn and is not considered to be serious. Partial-thickness or second-degree burns are those where the epidermis (which is approximately 0.1mm thick) and some of the underlying secondary skin layer, known as the dermis, are destroyed. The dermis, which contains blood vessels, hair follicles and sweat glands, can heal itself while some portion of the dermis remains. However, when all of the dermis is destroyed, the skin is unable to heal itself and serious medical treatment, such as skin grafts will be required. These burns are referred to as full-thickness or third-degree burns. The key factor that affecting the likelihood of fatality for a given burn is age [346]. This is largely due to the reduction in skin depth with age and the reduced tolerance to surgery.

Table 2-7 Effects on persons of increasing thermal dose (taken from Rew [347])

Thermal Dose Units $(kW/m^2)^{4/3}$ s	Injury Criterion
80 - 130	First degree burn
240 - 730	Second degree burn
1000 - 1400	Third degree burn
1000	1% probability of lethality
1800	Ignition of clothing[a]
2000	50% probability of lethality

[a] The lower bound ignition criterion corresponding to a duration of 10 s.

The criterion given in Table 2-7 have been derived for radiation incident on a target located outside the boundary of the flame front. Persons within a building that are subjected to a gas explosion would be engulfed by the flame and the above criterion for the probability of lethality would have to be modified (i.e. because all the unclothed skin area would be simultaneously exposed to heat flux). Rew and Spencer [348] recommend that the doses for the probability of lethality are halved for engulfment situations. In addition, when assessing the risks associated with fire or explosion events, it is typical to assume that ignition of clothing will result in 100% probability of fatality [284].

The earlier estimate of the emissive power ($\approx$ 305 kW/m^2), may be extended using Equation (2-109) to estimate the thermal dose from a typical vented stoichiometric methane/air explosion. Video records from vented explosion experiments (Chapter 5) showed that the flame front had expanded to approximately half the width of the enclosure, some 500 ms after ignition. Therefore, assuming that significant emissive

power occurs for a duration of approximately 500 ms (time taken from when the flame front is half the width of the enclosure to the end of the explosion), conservative estimates in the region of 360 $(kW/m^2)^{4/3}$ s for n = 1.15 to 1026 $(kW/m^2)^{4/3}$ s for n = 4/3 are calculated. Using the upper value of n suggests that following a stoichiometric methane/air explosion, people may sustain third degree burns and there is a greater than 1% probability of fatality (if the person is located in a room where the gas/air mixture is distributed). The calculated probability of fatality for persons involved in a gas explosion is less than the statistical average of 22% [2] (taken over the period 2009 to 2014). This is because fatalities in explosions are also caused by injuries sustained during the collapse of all or part of the building, by projectiles, by inhalation of hot combustion gases and by burns caused by flame engulfment. Consequently, as a person exposed to radiation from a vented explosion flame is most likely in an enclosure where a flammable mixture is present, burns due to radiation exposure are of less interest than those associated with flame engulfment.

In terms of materials, there are a number of different forms of thermal damage by radiation. If a cellulosic material (e.g. wood, fabric etc.) is exposed to a heat source its temperature will rise. If the intensity of the heat source is high enough, and the duration is long enough such that the net thermal dose is sufficient, pyrolytic decomposition of the material substrate will occur [341]. The products of this decomposition include combustible gases, non-combustible gases and carbonaceous char. The combustible gases will mix with air, and once flammable and above their ignition temperature, will ignite, yielding flame.

There is a plethora of literature regarding the ignition, pyrolysis, burning and charring behaviour of wood and other cellulosic materials. However, the literature is mainly concerned from a fire science perspective and little material is related to the scorching of fabrics and materials following an explosion. For a detailed review on the ignition of wood and cellulosic materials, the reader is referred to Babrauskas [342], Lawson and Simms [303], Simms [323], Simms and Law [324], Spearpoint and Quintiere [349], Thunman and Leckner [350], Wesson et al. [351], Shen and Fang [352], Shen et al. [353], Thomas et al. [333], Burrell and Hare [343] and Staggs et al. [354].

The ignition of solids cannot be characterised as easily as gases (auto ignition temperature) or liquids (flash point) because of their low thermal conductivity and lack of mass transfer [343]. However, the point of ignition can be measured as a surface temperature, a mass flux (pyrolysis) or a heat flux (radiation). The lowest radiative flux capable of ignition of the solid in the presence of a pilot flame is termed the minimum critical heat flux (after prolonged exposure).

The effect of heat on a cellulosic material can produce both physical and chemical effects. Physical changes are mainly exhibited by thermoplastic fibres (e.g. polyamide, polyester and polyolefin), which soften above a glass-transition temperature, T_g, and subsequently melt above a melting temperature, T_m, whilst chemical changes begin at a temperature at which pyrolysis (thermal degradation) occurs, T_p, and may proceed to oxidation and flaming combustion at a temperature, T_c, [301]. Consequently, the magnitude of the thermal transitions T_g, T_m, T_p, and T_c, provide an indication as to the resistance of a given fibre to heat and/or flame.

In terms of chemical action, the first action of heat on any fibre, once the fibre reaches the temperature T_P, is to pyrolyse it. If after pyrolysis, the temperature is equal to or above T_c, the volatiles and gases are combustible, and oxygen is present, then flaming combustion may take place producing products such as carbon dioxide and water vapour. Pyrolysis of cellulosic material is considered to occur via two competing reactions; the first one creates char via dehydration and the second, via depolymerisation generates the non-volatile 'liquid fuel' levoglucosan, which subsequently pyrolyses, producing highly flammable gases as well as secondary char formation [318]. Charring is the chemical process of incomplete combustion of certain solids when subjected to high heat, with the resulting residue being called char. Through this process of incomplete combustion, charring removes hydrogen and oxygen from the solid material, so that the remaining char is composed primarily of carbon (charcoal) [342]. Polymers like thermosets, or most solid organic compounds like wood or biological tissue, exhibit charring behaviour.

A convenient measure of the flammability of cellulosic material is the critical (or limiting) oxygen index (LOI) which is the volume percentage of oxygen required in the atmosphere for sustained combustion to occur [302]. As air contains about 21% oxygen by volume, fibres with LOI < 21 burn readily in air. It is generally considered that fabrics with LOI values in the range of ≈ 27 to 30 are flame resistant [341]. Table 2-8 provides the respective LOI values for some common fibres.

Non-thermoplastic fibres (thermosets) are often called heat-resistant because their physical properties do not change significantly at high temperatures. Table 2-8 shows that cotton, some other natural fibres and some speciality fibres, are non-thermoplastic with a low inherent flammability. This can be beneficial, in terms of thermal protection, since fabrics made from them do not recede from a flame and so offer protection to the wearer. The advantages of this property are shown by both flame-retardant cotton and wool, as well as the speciality synthetic fibres like Nomex, Kevlar and PBI [302].

Table 2-8 Thermal transitions of fibres (taken from Horrocks [301])

Material/Fibre	T_g (°C) softens	T_m (°C) melts	T_p (°C) pyrolysis	T_c (°C) combustion	Thermoplastic	LOI (%)
Wool			245	600	No	25
Cotton			350	350	No	18.4
Viscose rayon			350	420	No	18.9
Triacetate	172	290	305	540	Yes	18.4
Nylon 6	50	215	431	450	Yes	20-21.5
Nylon 6-6	50	265	403	530	Yes	20-21.5
Polyester	80-90	255	420-447	480	Yes	20-21
Acrylic	100	> 220	290	> 250	Yes	18.2
Polypropylene	-20	165	469	550	Yes	18.6
PVC	< 80	> 180	> 180	450	Yes	37-39
PVDC	-17	180-210	> 220	532	Yes	60
PTFE	126	≥ 327	400	560	Yes	95
Nomex	275	375	410	> 500	Yes	28.5-30
Kevlar	340	560	> 590	> 550	No	29
PBI	> 400		≥ 500	> 500	No	40-42

In certain situations, such as when subjected to stationary flames, thermoplastic fibres can give the impression of low flammability due to the softening and melting of the fabric which causes the structure to shrink away from the flame [302]. In those fibres that melt, molten drips help to extinguish the flame by removing the flaming regions from the textile. As a consequence of this tendency to melt and ‘drip’, these fibres (e.g. nylon 6-6 and polyester) may pass certain standard tests (e.g. BS 3119 and BS 5438). However, such fabrics, not only expose the wearer to the direct heat from the igniting source but also have the potential to cause burns through contact with flaming drips [301].

Of the few studies in the literature concerning thermal damage from an explosion, the most relevant work is that of Wąs [355], and Wąs-Gubala and Krauß [356-358]. The authors attempted to identify fibres after their thermal alteration using infrared spectroscopy, optical microscopy and scanning electron microscopy (SEM) with energy dispersive X-ray microanalysis (EDX). Thermally altered fibres are commonly the focus of crime scene investigators who are required to determine the original type of the fibre and the conditions through which the fibre underwent the thermal alteration, in order to determine whether it was possible to link clothing (textile fibres) and hence people to a

possible crime [355]. Whilst this work is primarily related to murder or arson investigations, it is of some relevance to investigators of accidental gas explosions.

In a study subjecting a variety of fibres to two different types of heat; an electric heating plate set to 350°C (to ensure the fabric melting point was exceeded) and a gas burner, Wąs-Gubala and Krauß [357] exposed fibre samples to the heat sources for a duration of 30 s, except for acrylic, polyester, silk and wool where the duration was shortened to 15 s due to the very rapid melting/charring of the fibre samples. The samples were subsequently analysed through an optical microscope and SEM.

The initial change in the fibre, that occurred with either heat source, and which was particularly prevalent in cellulosic materials, was a discolouration from yellowish initially through to brown. The fibre ends of nylon, polyester, acrylic and wool were found to have melted and fused together to form ‘bulb-like’ ends (Figure 2-41). Cotton fibres, after contact with the flame were found to lose their normal appearance and take on a lacelike, delicate charred consistency. Whilst these results are of relevance to this study, they need to be treated with caution as the experiments are not fully representative of the conditions of an explosion, particularly in terms of duration and flame temperature.

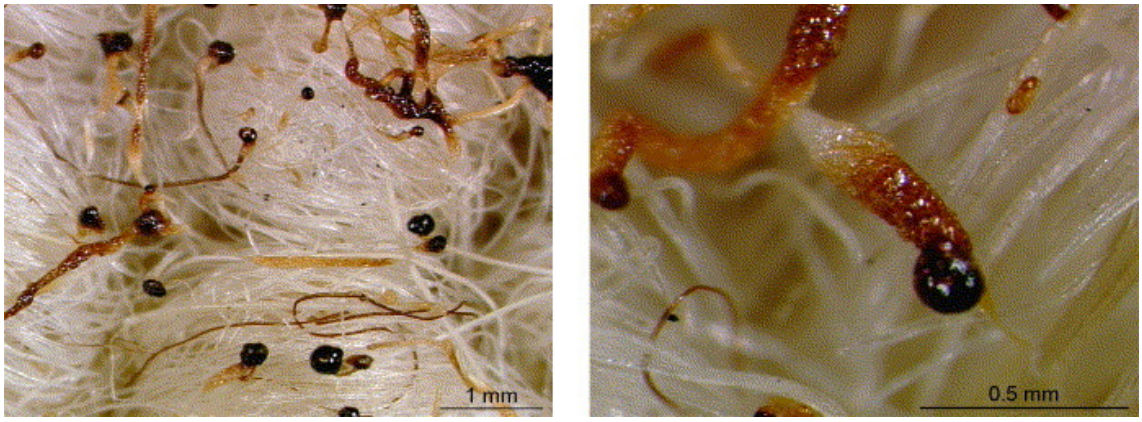

Figure 2-41 Woolen carpet fibres showing bulb ends after flame contact (taken from Wąs-Gubala [356])

The titles of two of the published articles of particular interest [356, 358] indicate that the work was specifically concerned with the damage caused to textiles by vapour cloud explosions. However, the authors have confused vapour cloud explosions with confined vented explosions involving petrol/air mixtures; with their main interest being related to crime scene investigation of arson or murder. In recent years, arson cases resulting in explosions of petrol/air mixtures have become more prevalent [359]. A variety of clothing and household garments, differing in colour, fibre composition and textile construction were subjected to vented petrol/air explosions in a small metal tin.

The tin had a volume of 850 ml, with 0.17 ml of petrol being used to provide a petrol vapour concentration of 2.9%. The authors concluded that whilst the degree of thermal damage was very dependent upon the garment construction, explosions cause very specific damage to textiles and single fibres. In general terms, the following was observed:

- Areas of affected and unaffected fibre material were evident, corresponding to areas of different textile construction.
- Textiles discoloured, generally from a yellowish colour through to brown.
- Often the fibres would have melted to leave bulb shaped ends (acrylics, polyesters, wool, Figure 2-41).
- Single natural fibres (e.g. cotton and wool) in contact with the flame front became burned, exhibiting brownish or blackish ends (Figure 2-42).
- Cellulosic textile (of cotton, viscose) composed of thermoset fibre polymer, appears to burn exhibiting black fibres and black ends.
- Synthetic fibres (acrylics, polyamide, polyester) melted to form conglomerates and their fibre ends fused together to form bulb or shovel like shapes.
- The yarns of garments become more clearly visible, due to some fibre destruction.

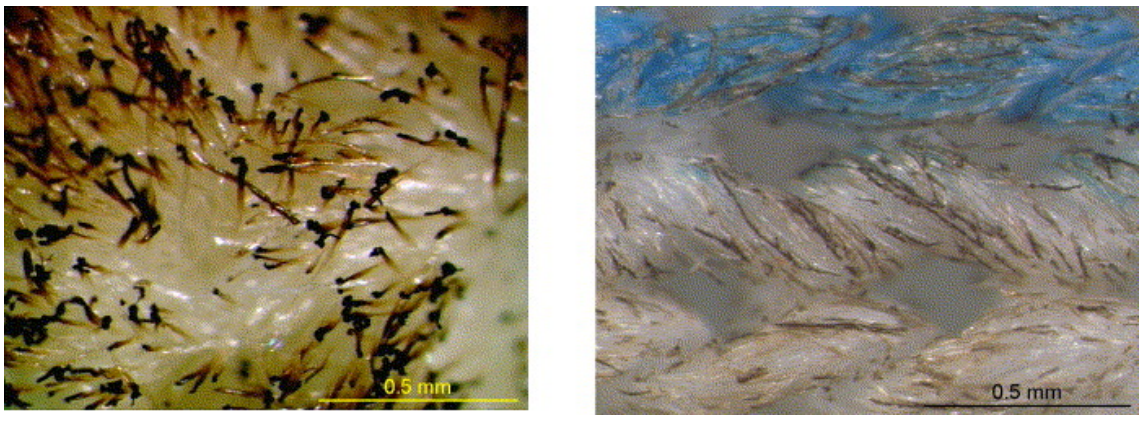

Figure 2-42 Cotton fibres showing brown and black ends (taken from Wąs-Gubala [356])

The objective of a gas explosion investigation is to use the forensic evidence and information gathered from witnesses to determine the origin and cause of the explosion, and consequently the most credible source of gas that led to the build-up of a flammable mixture prior to ignition. In terms of thermal damage, most of the literature was found to have been concerned with the ignition, pyrolysis, burning and charring behaviour of wood and textiles, that are associated with compartment fires. Few studies were found that were directly relevant to the scorching of fabrics and materials following an explosion.

The most relevant studies are those of Harris [16] and Wąs-Gubala and Krauß [356, 357, 360]. The work of Harris is still the most widely used guide to explosion investigators but provides scant information to assist in the determination of the concentration of the flammable mixture prior to ignition. The studies of Wąs-Gubala and Krauß considered whether thermal damage to clothing could be used to determine if arson had been committed. Whilst this work provides very useful guidance on how textiles behave when exposed to flame, its use is limited to explosion investigators as it was restricted to the ignition of stoichiometric petrol/air mixtures in a small container.

2.8. Objectives of the Research

In Chapter 1, it was highlighted that there are over twenty-five gas explosions in buildings in the UK each year; which on average, cause two fatalities, thirty-five non-fatal injuries and cost the UK millions of pounds.

The investigation of these incidents is undertaken by a number of parties including regulatory bodies, fire investigators and forensic scientists and engineers who may undertake an extensive origin and cause investigation, or a more basic investigation to answer specific questions as part of a wider investigation or for the purposes of meeting specific regulatory requirements.

In order to carry out an effective on-site investigation of a gas explosion, in addition to having a detailed knowledge of the physical and chemical characteristics of hydrocarbons and gas engineering practices, it is necessary to have a thorough understanding of the mechanism by which pressure is generated in an explosion and the response of structures to the passage of a transient flame front.

In Chapter 2, a comprehensive literature review was carried out to determine the current understanding relating to accidental gas explosions in buildings and the investigative techniques that can be used to determine their origin and cause. This review included the fundamentals of gas explosion theory, the mechanisms through which pressure is generated in confined vented explosions and the thermal damage caused by a propagating flame front.

It was found that the vast majority of confined vented explosion research has been conducted using empty single chambers of cuboid or spherical geometries, which are not representative of the conditions encountered in accidental gas explosions. Dwellings differ in that they consist of a series of furnished, interconnected rooms joined by doors and this highlights a problem that has received little attention. It is not possible to keep the flame and pressure effects of an explosion contained in one room, either because the flammable gas/air mixture may be distributed in more than one

room prior to ignition, or because it is pushed from one room to another during the course of the explosion. Consequently, whilst the mechanisms for generating pressure in idealised vented explosions are relatively well understood [45, 48, 64, 147, 156, 157, 171, 183], there is little information in the published literature relating to pressure generation in accidental explosions in buildings.

In gas explosions, pressure is generated either through confinement, or through the production of turbulence enhanced 'fast flames', or as a combination of the two. The structural damage that a building sustains, as a consequence of a gas explosion, is dependent upon the magnitude of the pressure pulse and the relationship between the duration of the imposed pressure load and the natural period of vibration of the structure [16, 25, 65, 72-74, 190, 232, 361-369]. In a vented gas explosion, the peak overpressure is a function of the rate at which combustion gases are produced and the rate at which they are vented, whilst the duration of the various pressure peaks is dependent upon many factors, including the fuel type, concentration, distribution of flammable mixture, ignition position, geometry of the enclosure(s) (including vent size and location) and turbulence.

The role of turbulence has been discussed as a mechanism for increasing the burning velocity by distorting the flame front, thereby increasing its surface area and burning rate. There have been numerous studies of flame acceleration due to the presence of circular or flat obstacles in the path of a propagating flame [40-42, 45, 46, 103, 145, 192, 205, 206, 208, 209, 226, 370-387]. In an accidental explosion in a dwelling, following ignition, the flame will propagate through the enclosure, interacting with the interconnecting area and doorways, and obstructions of various size and cross-section such as cylinders, squares, flat objects and sharp edges, all in the form of furniture. The propagating flame front is likely to interact in a different manner with these non-idealised obstacles. Consequently, it is important to understand and predict the effects of turbulent combustion in this situation. This is usually achieved by the introduction of a turbulence factor.

The tragic gas explosion at Ronan Point in 1968 shaped current gas safety legislation and initiated a significant body of research into the causes, mechanisms and effects of gas explosions in buildings that was unprecedented in its scale. It was believed that the cause of the widespread damage to the tower block was largely produced by the propagation of a flame from one room to another, generating higher overpressures than would have been expected if the explosion had been confined to a single room. Whilst the research [25-27, 160, 180, 232, 255] demonstrated that higher pressures could be generated in these so called 'cascade' explosions, the mechanism for producing these overpressures was not fully understood. However, Astbury et al.

[Equation (2-77)], Cubbage and Marshall [Equation (2-78) to (2-80)] and Dragosavic [Equations (2-81) to (2-83)] developed correlations for predicting the pressure in an adjoining room.

Although no direct experiments had been carried out under conditions identical to those of a room in a domestic dwelling, Rasbash et al. [230] and Rasbash [229, 236] developed a correlation for predicting the maximum pressure in an accidental explosion [Equation (2-74)] and suggested a turbulence factor of 1.5 for furniture and other obstacles restricted to one room and 5.0 where the flame propagates from one room to another through an open door or where furniture and other decorative items were distributed throughout the entire enclosure. In more severe turbulence generating events, such as pre-turbulent gas/air mixtures, which are subsequently ignited in the presence of an obstacle congested room, the authors recommended a factor of 8 to 10 be considered. Molkov [240] estimated that for explosions in real domestic structures with internal obstacles, the turbulence factor would be in the range 8 to 14 for the most dangerous near stoichiometric mixtures.

Whilst studies concerning ‘pressure piling’ are analogous to explosions propagating from one room to another, there are a number of significant differences between an explosion propagating from one vessel to another through an interconnecting duct and an accidental explosion in a building (e.g. inadvertent venting, the presence of a door, size and geometry of enclosures, furniture etc.). However, Di Benedetto [244] suggested that the correlation developed by Molkov, for vent sizing of a single vessel [Equations (2-85) to (2-89)] was the most appropriate correlation for predicting peak pressures in linked enclosures.

The insightful work of Stretch [239] and Rasbash [229, 236] is especially important to this study as it recognised the role that both interconnected rooms and furniture play in the development of an accidental gas explosion and the necessity for research into their effects. The authors identified in 1969, that as most dwellings had rooms with small interconnecting areas, partition walls, and windows of different vent area and failure pressure, the maximum pressure developed in an explosion would be dependent upon the individual characteristics of the dwelling. They also realised, that the effect of self-closing doors (e.g. fire doors) which are now commonly used in buildings of three storeys or more, could enhance an explosion in which there is high turbulence (e.g. a room cluttered with furniture).

Rasbash and Stretch concluded that large-scale experimental work was required to determine pressure-time curves for single sets of rooms containing furniture. They noted that whilst full-scale experiments are difficult to carry out with a high degree of

reliability, and are expensive, when the investment and risks involved are considered, further experimental work is quite clearly demanded. To date, some forty-five years after this recommendation, no work of this nature has been published.

Following a gas explosion, a detailed examination of the thermal damage may provide critical evidence to determine the rooms through which the flame propagated, whether the flammable gas involved was more or less dense than air, and the depth of any layer. This information may then be used to determine the most credible source of gas that caused the explosion. However, most of the literature related to thermal damage has been conducted in terms of fire investigation and is concerned with the ignition, pyrolysis, burning and charring behaviour of wood and textiles. Consequently, there is little directly relevant material regarding the scorching of fabrics and materials following an explosion. The most relevant studies are those of Harris [16] and Wąs-Gubala and Krauß [356, 357, 360]. The former reference source is the most widely used guide to explosion investigators and states that the degree of scorching, along with the degree of pressure damage, may be used to determine the gas concentration prior to ignition, such that:

i. minimal structural damage and little evidence of thermal damage is indicative of an ignition of a lean fuel/air mixture.
ii. significant structural damage and extensive scorching, blistering etc. is indicative of an ignition of a near stoichiometric fuel/air mixture.
iii. minimal structural damage and significant evidence of burning is indicative of an ignition of a rich fuel/air mixture.

The studies of Wąs-Gubala and Krauß considered whether thermal damage to clothing could be used to determine if arson had been committed. Whilst this work provides very useful guidance on how textiles behave when exposed to flame, its use is of limited value to explosion investigators, as it was restricted to the ignition of stoichiometric petrol/air mixtures in a small container.

The author of this study and other members of the DNV GL incident investigation team, have investigated explosions where the building has suffered significant structural damage but there has been very little, and in some cases, no evidence of thermal damage. No information was found during the literature review to relate the degree of thermal damage to the gas concentration prior to ignition or the depth of any layer of flammable mixture.

In view of the above information, this research will address some of the gaps in the current understanding of accidental explosions in buildings, through the following objectives:

1 To develop a better understanding of the effects of multiple compartments with interconnecting doorways; by
   a. determining the mechanism of pressure generation in gas explosions in large and multiple compartment enclosures, representative of a dwelling, through the analysis of an unpublished, comprehensive, large-scale experimental programme conducted by MRS and FRS in the early 1980's.
   b. comparing existing correlations to the results of the experimental programme.

2 To develop a better understanding of the effects of obstacles typically found in dwellings; by
   a. determining the pressure and flame speeds generated by idealised obstacle arrays in a large-scale enclosure (representative of the degree of congestion typically found in a dwelling), through the analysis of a series of unpublished, large-scale vented explosion experiments, conducted by MRS in the early 1990's.
   b. determining the pressure and flame speeds generated by furniture through a series of large-scale vented explosion experiments.

3 To develop a better understanding of the behaviour of common building materials (e.g. wood) and furnishings when involved in a gas explosion; by
   a. determining whether the severity of thermal damage to building materials and décor associated with the passage of a transient flame front can be used to estimate the gas concentration prior to ignition through the analysis of a series of unpublished, large-scale vented explosion experiments, conducted by MRS and FRS in the early 1980's and by Advantica in the late 1990's; and through a series of large-scale vented explosion experiments and small-scale confined explosion experiments.
   b. determining whether some modern 'quick-drying' paints affect the characteristic thermal damage of building materials exposed to the passage of a transient flame front through a series of large-scale and small-scale vented explosion experiments.
   c. determining whether the thermal damage associated with the passage of a transient flame front can be used to estimate the depth of a layer of flammable gas/air mixture prior to ignition through the analysis of a series of unpublished, large-scale vented explosion experiments, conducted by MRS and FRS in the early 1980's and by Advantica in the late 1990's.

These objectives will result in a better understanding of the development of an accidental explosion in a dwelling and will provide investigators with the tools required to interpret the forensic evidence found at the scene of an explosion such that the composition and distribution of a fuel/air mixture, prior to its ignition, may be estimated and used to correctly determine the origin and cause of the explosion.

CHAPTER 3
EXPERIMENTAL SET-UP AND MEASUREMENT TECHNIQUES

CHAPTER 3

EXPERIMENTAL SET-UP AND MEASUREMENT TECHNIQUES

3.1. Introduction

Carrying out gas explosion tests, even in a controlled manner, clearly presents some risks that have to be carefully thought through and managed. Safety of people, property and the environment is of the utmost priority. With that in mind, but also considering the objectives of the study, a number of requirements were considered as essential in the selection of test facility, the development of the test programmes and the design and instrumentation of the experimental rigs. These requirements were:

i. the absolute requirement to carry out the gas explosion tests in a safe manner, with due regard to the environment,

ii. the requirement to carry out full-scale tests, wherever possible, to meet the objectives of the individual components of the study, whilst considering credible gas explosion parameters,

iii. the requirement to provide appropriate instrumentation so that the important parameters could be measured,

iv. the requirement to film and photograph the tests, wherever possible, so that explosion development could be monitored,

v. the requirement to meet the budgetary and time constraints of the study.

3.2. Experimental Facilities

During this study, five distinct experimental programmes have been undertaken and/or analysed to determine the effects of parametric variations on accidental gas explosions in dwellings and to characterise the evidential thermal damage that is a consequence of the passage of a transient flame front. Consequently, a number of different test set-ups have been used throughout this study. To avoid confusion over which experimental rig has been used during the various programmes, experimental layouts have been labelled and this reference will be used throughout the thesis. Table 3-1 details the test facility, its location and the experimental rig that was used.

Table 3-1 Location of test facilities and experimental rig

Experimental Programme	Location and Test Facility	Experimental Rig
1	FRS Explosion Research facility at Cardington	A
2	DNV GL Major Hazard Research and Testing facility at Spadeadam	B
3	DNV GL Major Hazard Research and Testing facility at Spadeadam	C
4	DNV GL Major Hazard Research and Testing facility at Spadeadam	C
5	University of Leeds Explosion Hazards – High Pressure Test Facility	D

In order to ensure the essential requirements listed in Section 3.1 were adhered to, a number of Hazard Identification Studies (HAZID) and Operational and Experimental Requirements Studies were carried out. As a consequence of these studies, it was determined that the test facilities should be located in an area where security could be maintained, adequate exclusion zones could be enforced and fuel supplies could be stored safely. It was also determined that the experimental rig should consist of:

- an explosion chamber,
- high voltage and low voltage power supplies,
- fuel gas supplies (natural gas and propane),
- a nitrogen or air supply for the control of pneumatic valves (where used),
- a gas filling, mixing and purging system,
- a gas sampling and analysis system,
- an ignition system (including safety interlocks),
- instrumentation,
    - vent and interconnecting door failure,
    - overpressure,
    - flame speed,
- photography and video equipment,
- a control and data acquisition system, and
- firefighting equipment.

3.2.1. FRS Explosion Research Facility

The FRS explosion research facility was located at the Building Research Establishment (BRE) site at Cardington in Bedfordshire. The FRS explosion chamber was situated within one of two former airship hangars (see Figure 3-1). In the early 1970s FRS needed a large facility in which to carry out gas explosion research following concerns about gas explosions in buildings as a result of the collapse of Ronan Point in 1968. As the 1930s airship sheds at RAF Cardington had been largely unused for some years, FRS was granted permission to use one of the hangers for explosion and high rack storage fire research.

The former airship hangars were approximately 247 m in length x 80 m in width x 55 m maximum height and were constructed from steel sections which were clad with corrugated steel sheeting. The explosion chamber was sited at the North-northeast end of airship hangar No. 2 (right sided hangar Figure 3-1), located in an area 40 m x 25 m which could be cordoned-off from the rest of the airship hangar for safety purposes during explosion tests.

Figure 3-1 Airship hangers at BRE Cardington

3.2.2. DNV GL Major Hazard Research and Testing Site at Spadeadam

The DNV GL explosion research facility was located on an active Ministry of Defence (MOD) site at Spadeadam in Cumbria. The Spadeadam research and test site is one of the world's leading full-scale major hazard test facilities, occupying some 50 hectares of land (Figure 3-2) in a remote part of northern England. The sheer size and remoteness of the facility means that appropriate exclusion zones may be enforced, thus allowing full-scale tests such as vapour cloud explosions, rapid crack propagation, BLEVE's, confined vented explosions etc. to be undertaken.

Figure 3-2 DNV GL Major Hazard Research and Testing Site at Spadeadam

3.2.3. University of Leeds Explosion Hazards – High Pressure Test Facility

The University of Leeds explosion research facility was located in room B11 (basement) of the Houldsworth Building (Figure 3-3). The test facility consisted of a number of explosion vessels that could be used for confined explosion tests, either totally confined or vented.

Figure 3-3 Explosion Hazards – High Pressure Test Facility

This small-scale test facility has been operational since 1997 and consists of two adjoining rooms in a secure part of the building. A concrete partition safety wall separates the main test room and the control room (Figure 3-4).

Access into the main test room was controlled by two safety doors which were interlocked to the control system thereby preventing ignition from being initiated whilst either of the doors are open. These interlocked doors are an essential component in the safe operation of the facility by isolating power to the explosion chambers ignition system and thereby minimising the risk of a person being in the main test room when an explosion test was undertaken.

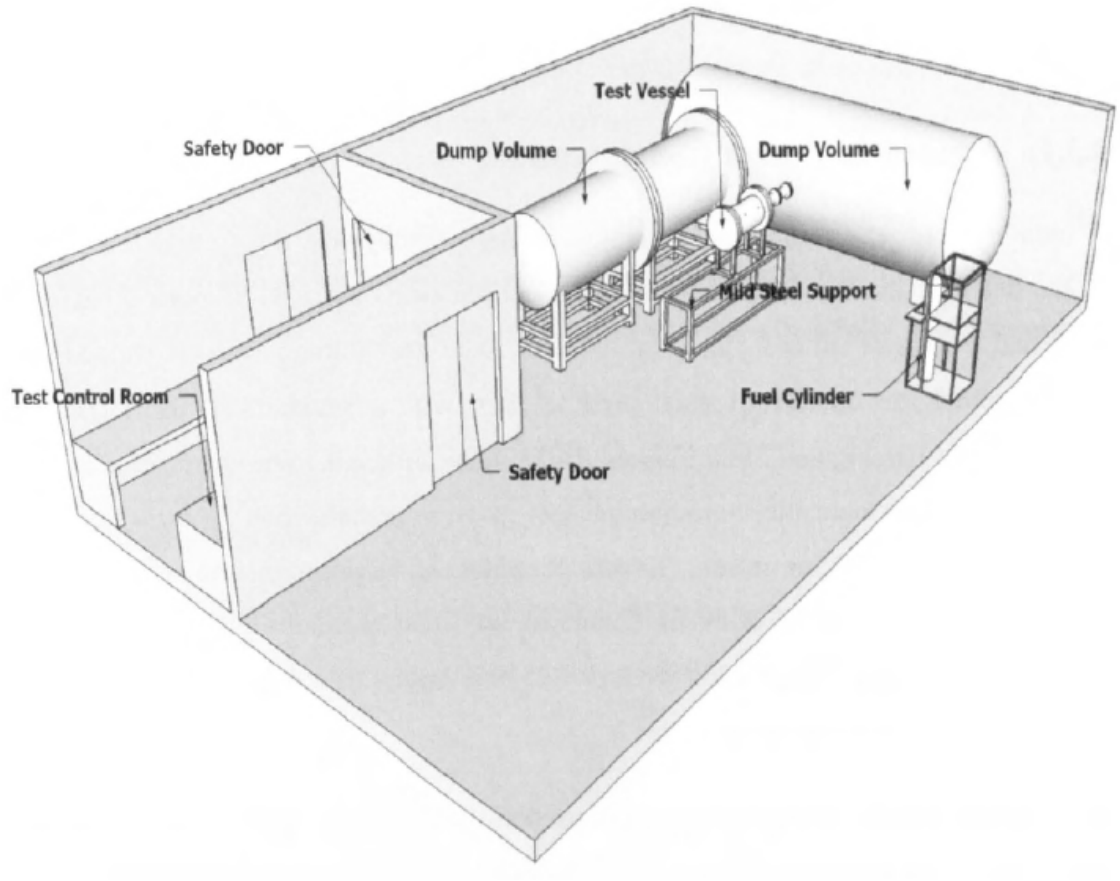

Figure 3-4 Explosion Hazards – High Pressure Test Facility (taken from Willacy [388])

3.3. Explosion Chambers

3.3.1. The FRS Explosion Chamber (Rig A)

The explosion chamber was sited inside one of the airship hangars so that it was protected during adverse weather conditions (Figure 3-5). During explosion experiments the hangar doors were opened.

The explosion chamber was constructed on a solid concrete plinth that was approximately 7.6 m in width, 5 m in length and 0.46 m thick. The concrete plinth was sunk into the concrete floor of the hangar to a depth of 0.36 m, leaving a raised platform approximately 0.1 m above the hangar floor.

The gross dimensions of the explosion chamber were 7.2 m in width x 4.8 m in length x 2.4 m in height. It was designed and constructed to ensure maximum flexibility, consisting of a series of steel columns with steel plates fitted in-between, to form removable walls and doorways. Consequently, the volume of the chamber could be varied between 10 m^3 and 80 m^3.

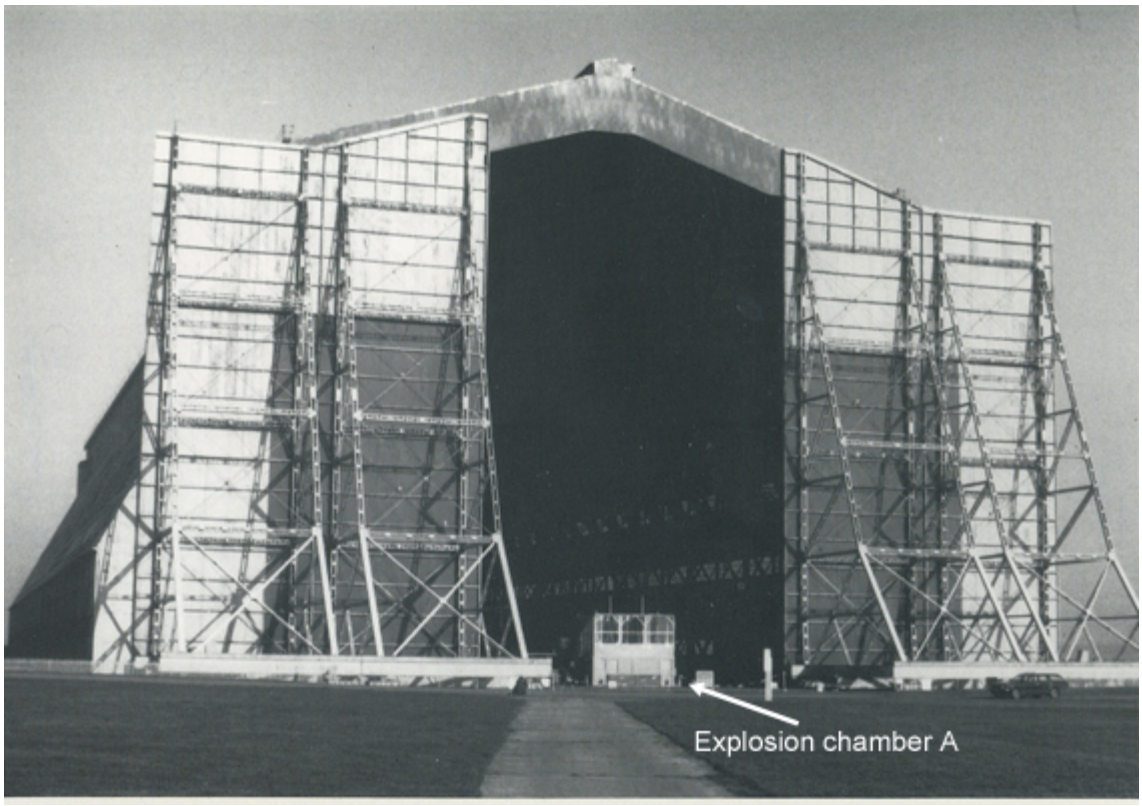

Figure 3-5 Location of the FRS explosion chamber

In the sides and rear of the explosion chamber, provision was made for the introduction of gas mixtures, for the outflow of displaced air during filling, and for purging the chamber of combustion products after each explosion test. This was achieved by the installation of the following:

- for filling - a 3” British Standard Pipe (BSP) connection, located at the centre of the rear wall, at a point 4” from the roof;
- for outflow of air - 3 x 3” BSP connections installed at high level on one side of the chamber (0.75 m, 1.8 m and 3.5 m from the rear wall, at a height of 1.1 m from the top of the chamber) and 2 x 3” BSP connections installed at low level on the opposite side of the chamber (0.8 m and 3.5 m from the front of the chamber, at a height of 0.5 m from the floor);
- for purging – a 3” BSP connection which was connected to the delivery pipe of a centrifugal fan on the side of the explosion chamber nearest the control room.

The inlet and outlet connections on the explosion chamber were actuated by compressed air, controlled by 3” electro-magnetic solenoid valves situated in an ‘intermediate control station’ located at a safe distance from the explosion chamber. The solenoid valves were energised by 2-way electrical switches incorporated in the control room.

In the roof of the chamber, provision was made for fitting gas sampling probes. The roof, which had safety rails positioned around its perimeter, was accessible via two fixed ladders located either side of the explosion chamber (see Figure 3-6).

Although the explosion chamber was sited inside the hangar, a weatherproof cover was fitted to protect the gas sampling equipment when the hangar doors were open. A control room was sited at a distance of 12.5 m from the side of the explosion chamber.

The explosion chamber may be considered as being comprised of three sections:

i. the columns and roof,

ii. the moveable wall-plates and doorways, and,

iii. the front face of the chamber and vent openings.

Figure 3-6 The FRS explosion chamber (Rig A)

The explosion tests undertaken in this facility were for the purpose of determining the effects of interconnected rooms on accidental explosions in dwellings and the characteristics of evidential thermal damage. The geometry of the explosion chamber was configured such that there were two enclosures of equal dimensions, with a corridor running along the back and sides (see Figure 3-7). Each enclosure measured 2.4 m in width x 3.6 m in length x 2.4 m in height, giving a volume of 20.7 m^3.

Periodically, the explosion chamber was tested for leaks using smoke from a smoke generator which created a positive pressure in the enclosure of approximately 1 mbar. Any leaks that were found were sealed with fire retardant silicone sealant.

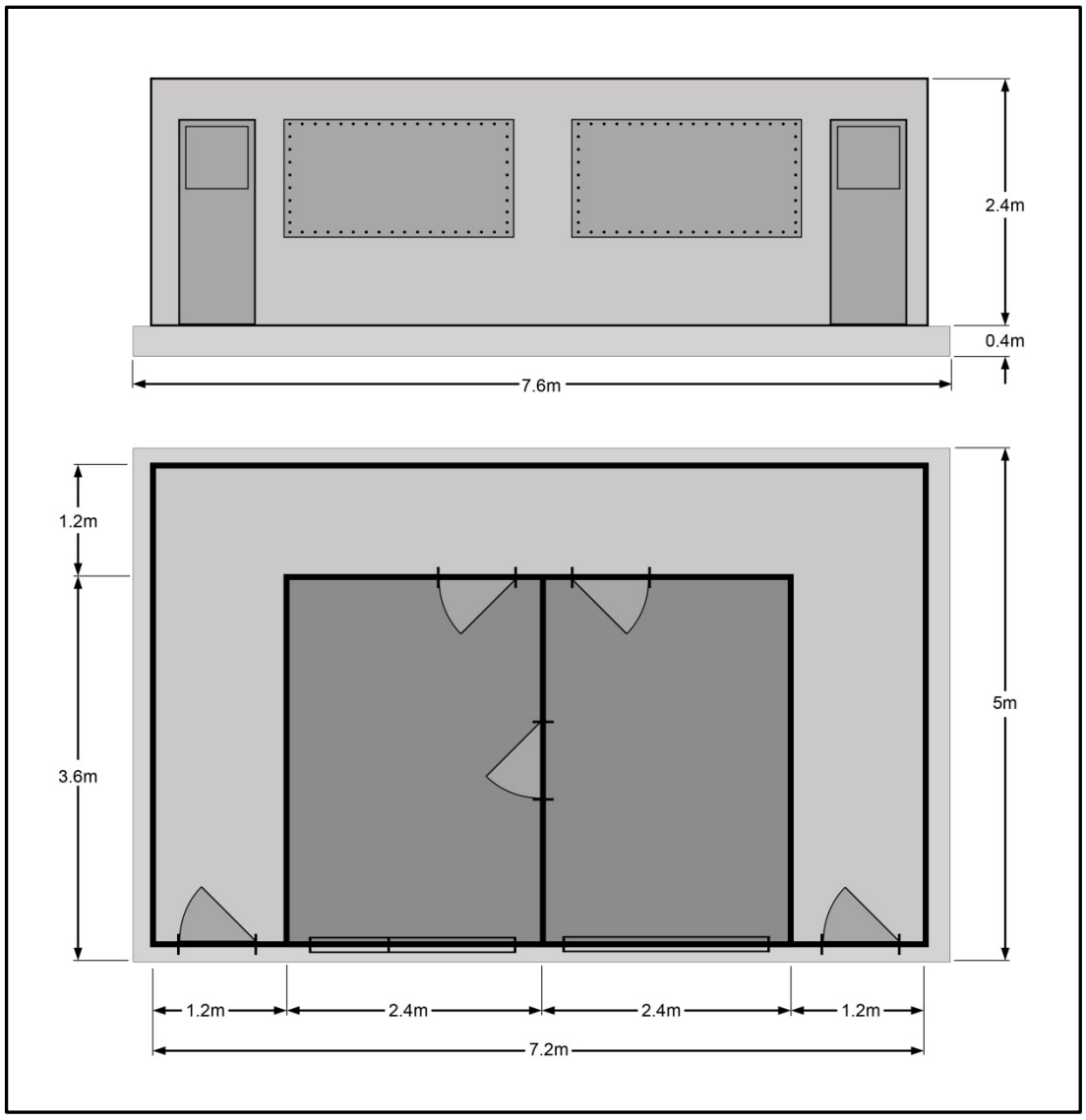

Figure 3-7 Explosion chamber configuration (Rig A)

The Columns and Roof

Twenty-nine, 200 mm steel columns were set into the concrete plinth to provide the vertical structure for the explosion chamber. Five roof beams were then bolted to their corresponding upright steel columns to complete the basic chamber design. The steel columns were fitted with 75 mm flanges, which were drilled with clearance holes (to take M12 threaded bolts) at 150 mm centres so that they would align with holes on the removable steel plate walls.

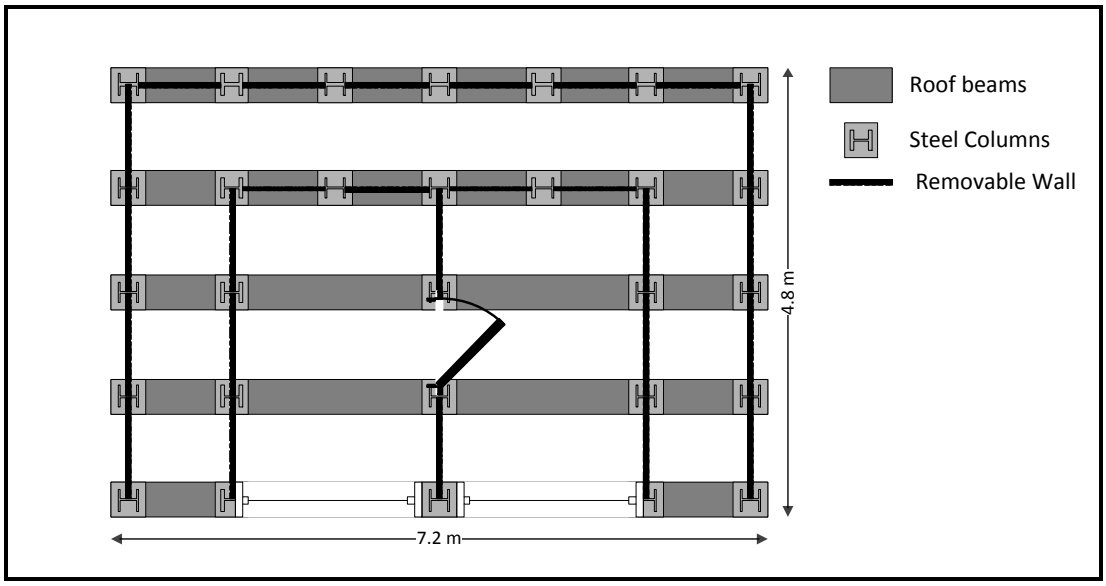

Figure 3-8 Structural design of the FRS explosion chamber (Rig A)

The Moveable Wall-plates and Doorways

The walls and ceiling of the enclosure were made from reinforced 6 mm steel plates. These plates had holes drilled into them such that they aligned with the columns and beams and were secured using M12 bolts, nuts and washers. The roof and wall plate joints were strengthened using either 6 mm plate or angle drilled to match the bolt holes. The steel plates were 1.2 m in width but were of various height in order to allow additional sections to be added, if required (e.g. observation panels etc.).

Access to the enclosures was via a doorway fitted into the rear enclosure wall (Figure 3-7). The door frames were constructed from steel plate bolted to the columns. The two rear enclosure doors were constructed of two 18 mm thick sheets of plywood, bolted together using six lengths of M14 studding. The doors were hung so that the explosion load was against the doorframe. In order to provide a gas-tight seal to the enclosure, an adhesive foam gasket was laced around the door and frame, and the doors were held shut by bolting three sections of steel channel over the door studding and tightening against the doorframe.

The two enclosures were connected by a standard size doorway, 1.98 m in height x 0.76 m in width, with a steel door jamb bolted to the steel column. The door frame was adjustable such that the door could be hinged to open into either the left or right chambers, and fitted with several types of latch. This was important as the direction in which the door was oriented and the force required to initially open the door were believed to play some part in the development of the explosion.

In tests where the door was scheduled to be open, no door was fitted and the doorway was left ‘clear’. In most experiments where the door was closed (in most cases

completely, but in a small number, partially), a lightweight semi-hollow door with an ‘egg-box’ core for stability was fitted. In some of the latter experiments, a heavier, fire door was used. The door was normally hinged such that it would open into the right room. However, in a small number of tests, the door was hinged so that it would open into the left room. In addition, in a small number of tests, different latch types were used to secure the door closed.

The Front Face of the Chamber and Vent Openings

The front face of the chamber was constructed in a manner similar to the walls and roof. However, each enclosure had a vent in the upper half of its front face so that explosion reliefs (designed to simulate a failing window), could be fitted to either enclosure (Figure 3-9). The vent sizes used during the experimental tests were 2.48 m^2, 1.49 m^2 and 0.74 m^2, which corresponded to vent coefficient values, K_A, defined as the ratio of the area of the face containing the vent to the area of the vent itself, of approximately 2.4, 4 and 8 respectively. The vent opening in each enclosure was adjustable such that three different sizes of vent could be selected. The K_A = 4 reliefs could also be fitted at either the left or right side of the upper front face of each enclosure (see Figure 3-9).

Figure 3-9 The front face of the chamber (Rig A)

The material covering the vent openings (explosion relief, which in a dwelling would most likely be glazing) was clamped over the vents behind a steel strip, using the mechanism shown in Figure 3-10. In all but two of the experimental tests, 12.5 mm fibreboard was used as the relief material. In the remaining two experiments single panel glass was used.

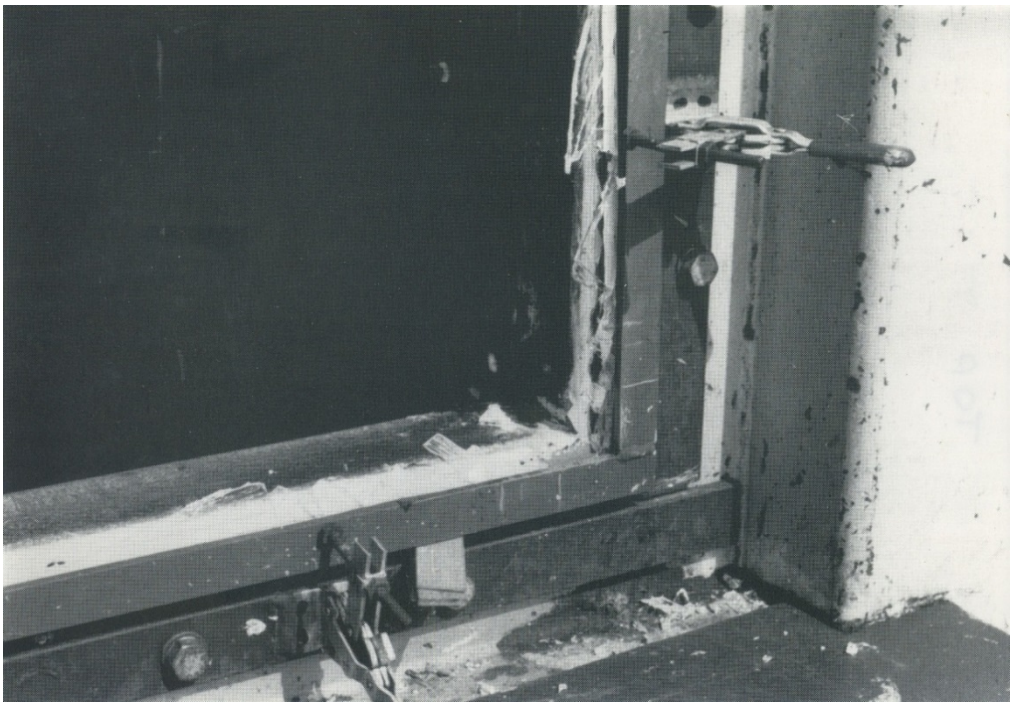

Figure 3-10 Vent relief clamping mechanism (Rig A)

3.3.2. The DNV GL Explosion Chamber (Rig B)

Explosion chamber B, located at the DNV GL Spadeadam Test Site, was a 182 m^3 enclosure constructed of steel with a 2:1:1 aspect ratio (Figure 3-11). The explosion chamber, of dimensions 9.0 m in length x 4.5 m in width x 4.5 m in height, was constructed of 10 mm thick steel plates braced on the outside by regularly spaced I-beams. The explosion chamber, weighing over 60 tonnes, was positioned on a concrete pad and anchored to two buried steel vessels filled with concrete in order to prevent movement during explosion tests.

Figure 3-11 Spadeadam explosion chamber (Rig B)

The rear face of the chamber was constructed of two hinged pressure relief panels, with a failure pressure of 4 bar, to protect the explosion chamber from damage during the experiments. On one side wall of the chamber, 2 x 0.5 m steel pneumatic flap valves were fitted for filling and mixing. These will be described in Section 3.5.

The Front Face of the Explosion Chamber and Vent Openings

The size of the opening on the front face of the explosion chamber could be varied by attaching one of a series of 10 mm thick steel fascia plates to the explosion chamber via a number of threaded M24 steel bolts. These fascia plates incorporated a variety of sizes of vent opening. The vent openings were either 20.25 m^2, 10.13 m^2, 5.06 m^2 or 2.25 m^2. Correspondingly, the vent coefficients (K_A), defined as the area of the front face of the chamber divided by the area of the vent opening, were approximately 1, 2, 4 or 9. The opening was covered by a polythene sheet (low failure pressure) to prevent the gas/air mixture escaping during filling.

Internal Congestion

Obstacle supports were attached to the side walls of the explosion chamber such that eight pipe arrays, each capable of supporting up to ten horizontal pipes, of 4.5 m in length and 0.18 m in diameter, could be positioned perpendicular to the direction of flame propagation (Figure 3-12).

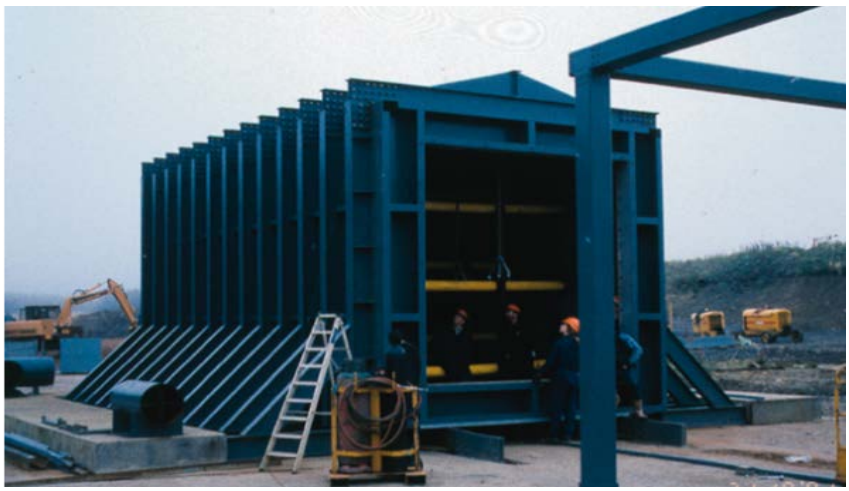

Figure 3-12 Internal obstacles (Rig B)

The arrays were positioned at 1 m intervals along the length of the explosion chamber, with the 1st array positioned 1 m from the rear wall. This meant that a maximum of 80 x 180 mm diameter pipes could be positioned within the chamber providing a maximum area blockage (AB) of approximately 40% and a maximum volume blockage (VB) of approximately 5%. The area blockage was calculated as the percentage of the cross-sectional area of the explosion chamber occupied by the pipes in a single array. The

volume blockage was calculated as the percentage of the total volume of the chamber occupied by the pipes in all arrays. The number of obstacles and the separation distance between obstacles (pitch) was varied during the experiments so the effects of volume blockage and pitch on flame speed and overpressure could be investigated (Figure 3-13).

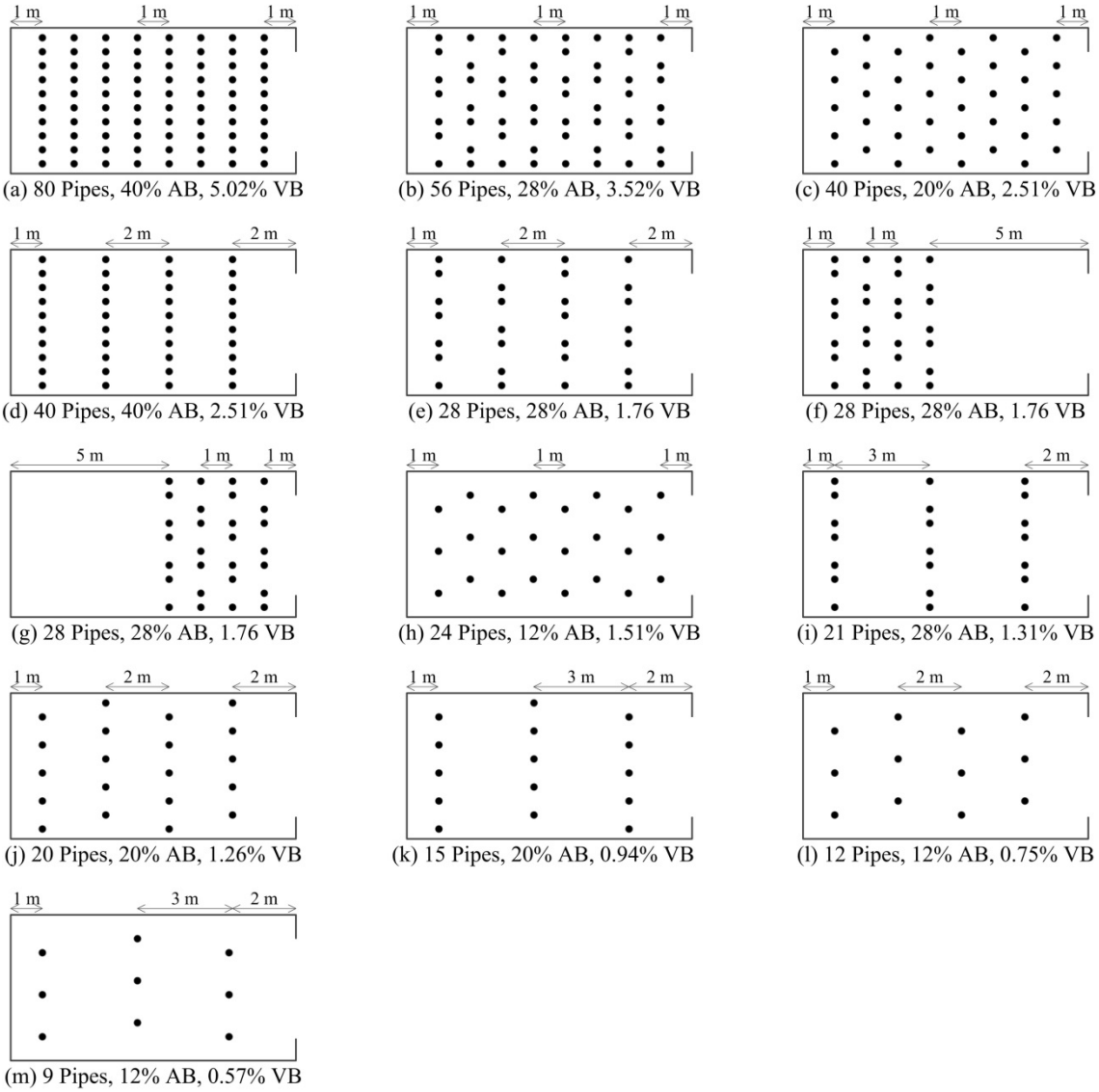

Figure 3-13 Internal congestion configurations (Rig B)

(N.B.: For ease of reference, a seperate copy of this diagram may be found inserted in the pocket on the rear cover of the Thesis).

3.3.3. The DNV GL Explosion Chamber (Rig C)

Explosion chamber C, located near test pad C at the DNV GL Spadeadam Test Site, was a 70 m^3 enclosure constructed of steel with an approximate L/D ratio of 3:1 (Figure 3-2). The explosion chamber, of dimensions 8.3 m in length x 3 m in width and 2.8 m in height was constructed of 10 mm thick steel plates braced on the outside by regularly spaced I beams (Figure 3-14). It was positioned and anchored onto a 0.5 m thick reinforced concrete pad in order to prevent movement during explosion tests.

Figure 3-14 Spadeadam explosion chamber (Rig C)

The roof and one of the side walls of the chamber had an opening, 0.75 m x 0.75 m, which could be used to attach high speed cameras to allow filming of flame propagation inside the chamber during experiments. On one side wall of the chamber, 2 x 0.5 m steel pneumatic flap valves were fitted for filling and mixing. These will be described in Section 3.5.

The explosion tests undertaken in this chamber during experimental programme 4 were used to determine the effects of non-uniform obstacles on flame propagation and pressure development in accidental gas explosions in dwellings, and also to further characterise evidential thermal damage for new paint materials.

Interconnected Compartments

The explosion tests undertaken in this chamber during experimental programme 3 were carried out for the purpose of characterising evidential thermal damage caused to décor and furnishings by a transient flame front. To meet this objective, it was necessary to consider both the degree of thermal damage sustained by materials present in an enclosure in which there was a flammable gas/air mixture and those present in a connected enclosure in which the atmosphere was not flammable. In order to consider both scenarios, and also the scenario where a 'jetting' flame exits the flammable atmosphere and passes into the non-flammable zone in the neighbouring enclosure, the chamber was divided into two interconnected enclosures by a steel partition wall. The partition wall had a door shaped opening 2 m in height and 0.85 m in width and was located such that one enclosure was 4.3 m in length and the other was 4 m. A schematic of the experimental chamber is presented in Figure 3-15. In experimental programme 4, the explosion chamber was configured as a single room enclosure and consequently the steel partition wall was removed.

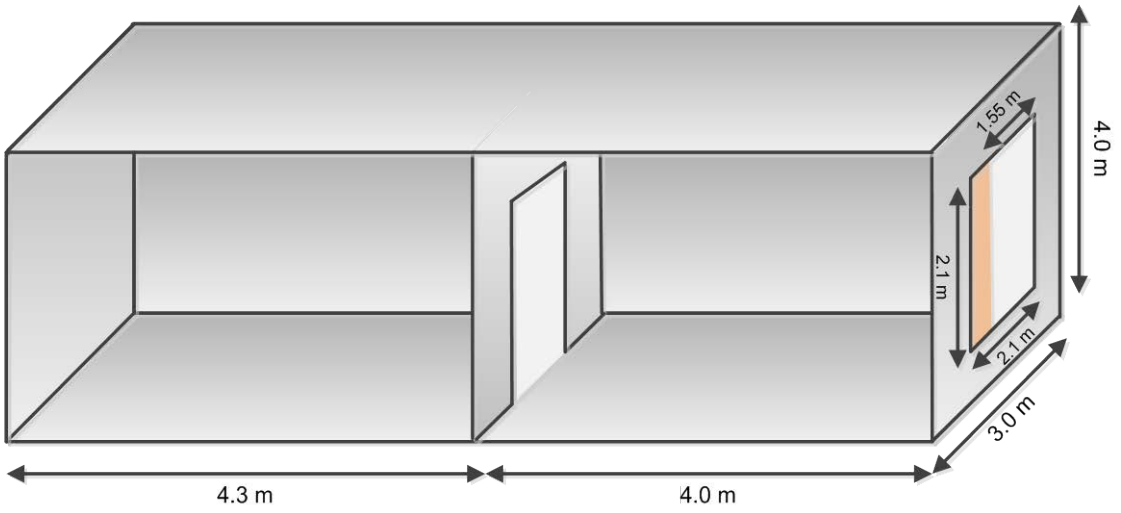

Figure 3-15 Rig C configured as multiple compartment enclosure

The Front Face of the Chamber and Vent Openings

The size of the opening on the front face of the explosion chamber could be varied by attaching one of a series of 10 mm thick steel fascia plates to the explosion chamber via a number of threaded M24 steel bolts (Figure 3-16). These fascia plates incorporated a variety of sizes of vent opening. The opening was covered by either a polythene sheet (low failure pressure) or 12.5 mm fibreboard to prevent the gas/air mixture escaping during filling.

In experimental programme 3, a vent opening of 2.1 m in height x 2.1 m in width was used, which corresponded to an approximate K_A value of 1.9. This vent opening was reduced to 1.55 m in width by a thermal marker-board at position X (increasing the K_A value to approximately 2.5) and covered with polythene sheeting. In experimental programme 4, a vent opening of 2.5 m in width x 1.25 m in height was used, which corresponded to a K_A value of approximately 2.7. The vent opening was covered with 12.5 mm fibreboard to act as the relief material.

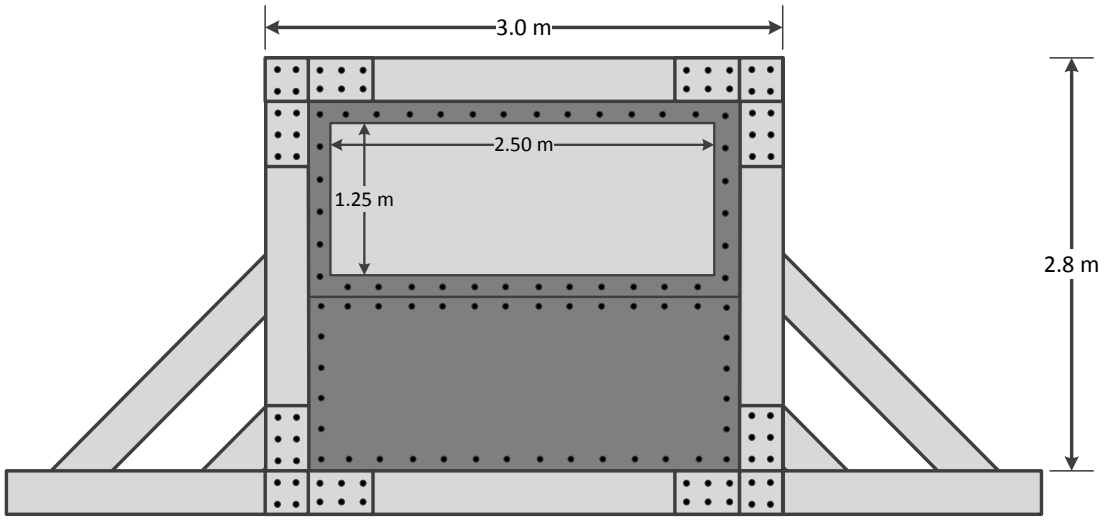

Figure 3-16 Schematic of the front face of explosion chamber (Rig C)

Internal Congestion

The explosion tests undertaken in this chamber during experimental programme 4 were carried out for the purpose of determining the effects of furniture on vented explosions and the characterisation of thermal damage caused to décor and furnishings by a transient flame front. In the average UK home, a doorway may be considered as an opening with a volume blockage of approximately 82% and the average room congestion (by volume) is approximately 17% (estimated using the average UK house size, and data from UK removal companies [389-391]). Inadvertent individual vent openings, in the form of windows, will provide a minimum area vent coefficient (K_A), of 4 where openings are provided on one wall of the room or 8 if windows are provided on more than one wall [392]. To meet the first objective of these tests, it was necessary to source a selection of furniture, including sofas, televisions, storage units etc. The furniture was placed in a layout representative of a typical furnished room (see Figure 3-17) and the volume blockage was calculated for comparison with more idealised experiments carried out in experimental programme 2.

Figure 3-17 Typical furniture layout (Rig C)

3.3.4. The University of Leeds Explosion Chamber (Rig D)

Explosion chamber D, located at the University of Leeds Explosion Hazards – High Pressure Test Facility, was a 1.138 m^3 cylindrical steel vessel with a L/D ratio of 1:1. (Figure 3-18 and Figure 3-19). As the main purpose for the vessel was the explosion characterisation of dust/air and gas/air mixtures, it was designed to meet the specifications of ISO 6184 [393, 394] and was consequently commonly referred to as the ISO 1m^3 (nominal volume) explosion vessel.

The steel vessel was constructed in accordance with BS 5500: 1997 [395]. It consisted of a 1.2 m diameter cylinder with semi-ellipsoidal dished ends. The front dished end had a 0.5 m diameter steel hinged front door that was secured during testing by twenty-four steel bolts tightened using a 678 newton metre (500 pound foot) torque wrench. The design pressure of the vessel was 25 barg and the vessel was periodically hydraulically tested (using water) to a pressure of 35 barg.

Figure 3-18 1m^3 explosion vessel – front elevation (Rig D)

Figure 3-19 1m^3 explosion vessel – side elevation (Rig D)

3.4. Services

3.4.1. General

The experimental facilities were provided with the following services:

- 410 V three-phase power;
- 230 V ac mains power;
- 110 V ac power (external);
- 24 V dc power;
- Air or nitrogen for pneumatic control systems.

3.4.2. Experimental Rig A

Natural Gas

All experiments were undertaken using natural gas/air mixtures of varying concentration. Natural gas (≥ 92% methane by volume) was supplied from Air Products type Y steel cylinders containing 6 m^3 of compressed natural gas at a pressure of 200 bar. The cylinders were fitted with 5/8" cylinder valves manufactured in accordance with BS 341 No. 3.

Air

Air was used, throughout the experimental work, as the fluid to operate the pneumatic control systems. High pressure air was supplied by 82 kg (gross weight) BOC type N cylinders (1.46 m high x 0.23 m diameter) which were positioned in a safe location approximately 30 m from the explosion chambers. The maximum storage pressure in the cylinders was 230 barg (at 15°C) giving a storage volume of 8.85 m^3. A pressure regulator was required in order to reduce the pressure to that required to operate the various pneumatically operated valves and equipment (typically 5.0 barg). BOC 9500 multi-stage high pressure air regulators were chosen to regulate the air pressure as they are designed to give constant, accurate delivery over a range of 0 – 10 bar, without the need for continuous readjustment as the temperature drops due to the Joule-Thomson effect and the cylinder pressure reduces with consumption. The high-pressure regulator has a large surface area first-stage diaphragm that enables the accurate control of pressure and a heavily finned first-stage bonnet which is designed to provide adequate dissipation of any cooling as a result of the pressure reduction of gas, particularly under high-flow conditions. The regulators, which were equipped with two pressure gauges (one reading the cylinder pressure, the other providing the outlet pressure), were connected directly to the cylinders and adjusted such that the outlet pressure was reduced to that required by the control system (typically 5 barg).

Air was distributed to the various pneumatic systems through 8.0 mm (internal diameter) nylon tube which was manufactured to BS 5409, with a maximum operating pressure of 40 bar.

3.4.3. Experimental Rigs B and C

Natural Gas

Natural gas was supplied to the test facilities from the on-site high pressure natural gas storage facility. Liquefied Natural Gas (LNG) was brought to site by road tanker under conditions of atmospheric pressure and a temperature of approximately -164°C. At this temperature, LNG occupies only $1/164^{th}$ of its gaseous volume and consequently large amounts of energy can be stored in relatively small cryogenic tanks. The LNG from the road tanker was either transferred via a pump into cryogenic storage tanks, where it was stored at atmospheric pressure or into the sites high pressure pipe arrays where it was stored at approximately 80 barg (maximum pressure 200 barg). This latter method of storage, where gas was stored in the pipeline, is known as linepack. Gas was then distributed around the site through a gas distribution system (network of underground pipes) with pressure regulating stations strategically located to reduce the pressure. A local pressure regulating station reduced the natural gas pressure from distribution system pressure to 3 barg prior to it being introduced into the explosion chambers mixing system. Further pressure reduction was also used for certain experiments to reduce the gas pressure to ≤ 75 mbarg (typically for layered explosions).

Methane

Methane (G20 Reference Gas - 99.5% methane) was supplied to the explosion chambers via groups of eleven Air Products type n steel cylinders (1.46 m high x 0.23 m diameter), each containing 12 m^3 of compressed natural gas at a pressure of 200 bar (at 15°C), manifolded together and located in secure ‘cages’ (Figure 3-20). The cylinders, which provided 87 kg of gas per cage when full, were each fitted with 5/8” cylinder valves manufactured in accordance with BS 341 No. 3.

Figure 3-20 87 kg methane (G20) cylinders

Propane

Propane was supplied by 47 kg commercial propane cylinders (> 90% propane) which were positioned in a safe location approximately 30 m from the rear of the explosion chamber. A single stage Comap Novacomet BP1813 pressure regulator was connected directly to the cylinder and reduced the pressure from vapour pressure (dependent upon composition and liquid temperature) to 150 mbarg. Gas was distributed to the explosion chamber through an 18.0 mm (outer diameter) propane hose, (manufactured to BS 3212 type 2) which was connected to the outlet of the regulator, via a rotameter and pressure gauge.

Nitrogen

Nitrogen was used, throughout the experimental work, as the fluid to operate the pneumatic control systems. Nitrogen was supplied by 85 kg (gross weight) BOC type W cylinders (1.46 m high x 0.23 m diameter) which were positioned in a safe location approximately 30 m from the explosion chambers (Figure 3-21). The maximum storage pressure in the cylinders was 230 barg (at 15°C) giving a storage volume of 9.78 m^3. BOC multi-stage high pressure nitrogen regulators were chosen to regulate the nitrogen pressure as they are designed to give constant, accurate delivery over the range 0 – 41 bar. The design of the regulator was very similar to the BOC 9500 regulator described in Section 3.4.2. The regulators were adjusted such that the outlet pressure was reduced to that required by the control system (typically 5 barg).

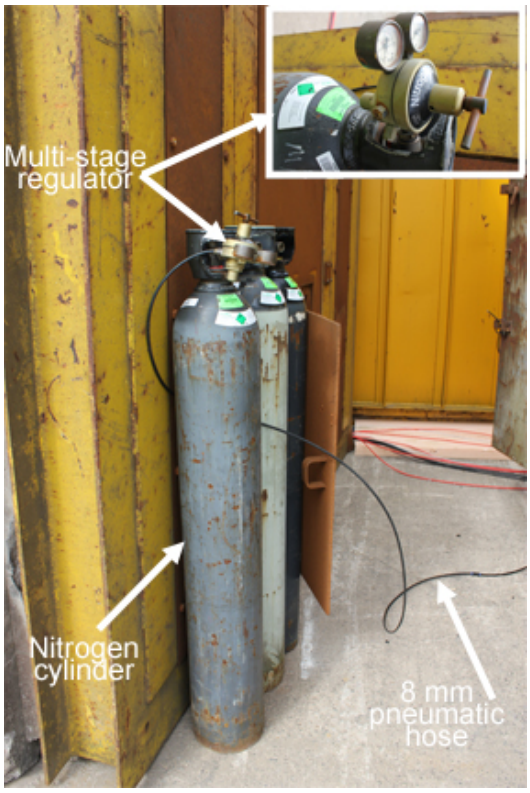

Figure 3-21 Nitrogen supply to pneumatic systems

Nitrogen was distributed to the various pneumatic systems through 8.0 mm (internal diameter) black nylon tube supplied by Pirtek fluid transfer systems (manufactured to BS 5409, with a maximum operating pressure of 40 bar). The nylon tube was directly connected to the outlet of the regulator (Figure 3-21).

3.4.4. Experimental Rig D

Methane

Methane (G20 Reference Gas - 99.5% methane) was supplied to the explosion vessel via a BOC type L steel cylinder (1.64 m high x 0.23 m diameter), containing 13.5 m^3 of compressed natural gas at a pressure of 200 bar (at 15°C). The cylinder, which provided 9 kg of gas when full, was located in the main test room. It was fitted with a 5/8” cylinder valve manufactured in accordance with BS 341 No. 3. The pressure was regulated by a Freshford multi-stage regulator manufactured in accordance with BS EN ISO 2503 (Figure 3-22). Gas was distributed to the explosion vessel via a mixing control system. The mixing control system allowed the correct amount of gas to be added to the explosion vessel through the use of partial pressure measurement.

Figure 3-22 Multi-stage regulator fitted to methane cylinder (Rig D)

Propane

Propane was supplied by a 4.8 kg propane research grade (≥ 99.5% propane) type BA steel cylinder (0.43 m high x 0.27 m diameter) which was located within the main test room. A single stage Comap Novacomet BP1813 pressure regulator was connected directly to the cylinder and reduced the pressure from vapour pressure (dependent upon composition and liquid temperature) to 150 mbarg. Gas was distributed to the explosion vessel through an 18.0 mm (outer diameter) propane hose, (manufactured to BS 3212 type 2) via a mixing control system.

Ethylene

Ethylene (≥ 99.99% ethylene) was supplied to the explosion vessel via a BOC type BC steel cylinder (0.43 m high x 0.10 m diameter), containing 0.05 m^3 of compressed ethylene gas at a pressure of 21 bar (at 15°C). The cylinder was located within the main test room and was fitted with a 5/8” cylinder valve manufactured in accordance with BS 341 No. 3. A two stage HTP1700T regulator was connected directly to the cylinder outlet and reduced the pressure to 150 mbarg. Gas was distributed to the explosion vessel via a mixing control system. The mixing control system allowed the correct amount of gas to be added to the explosion vessel through the use of partial pressure measurement.

Air

Compressed air was used, in addition to ambient air, as the oxidant for the gas/air explosions. A central compressor supplied high pressure air to the University laboratories). A Norgren combined pressure regulator and filter unit, located in the main test room, reduced the pressure to 300 mbar prior to it entering the mixing control system. Air was distributed to the explosion vessel through 8.0 mm (internal diameter) nylon tube which was manufactured to BS 5409, with a maximum operating pressure of 40 bar.

3.5. Gas Filling, Mixing and Purging

3.5.1. Experimental Rig A

The gas supply pressure from the cylinder was reduced via two diaphragm operated pressure regulators to a pressure of 0.7 barg. During periods of high flow in cold weather, the pressure regulating valves were heated in a water bath at 50°C in order to ensure the gas was kept at a reasonable temperature due to the Joule-Thomson effect. Downstream equipment (rotameter, gas meter etc.) in the gas supply line was protected by two pressure relief valves that vented the gas line to atmosphere in the event that a pressure regulator failed and high pressure gas passed through the regulator(s).

The natural gas and air were premixed prior to release into the explosion chamber; filling the chamber by the direct ‘purge’ process. Gas was diverted into a 3” diameter mixing tube, via a 3-way electro-pneumatic valve, which was also used to isolate the gas supply when no further gas was required. Air was delivered by a motor driven centrifugal fan into a 3” supply line which was connected to the mixing tube via a check valve that prevented the flow of gas into the air supply. The fan was capable of delivering air at a flowrate of up to 1.5 m^3/min against a head of 45 mbar. The gas and air mixed by the action of turbulence in the mixing tube. The airflow from the fan was regulated using a needle valve and was isolated using an electro-magnetic valve. The gas/air mixing tube was 3” in diameter and consisted of a mixture sampling point, a flame arrester and an electro-pneumatic isolation valve. It was connected to two gas diffusers (one in each enclosure) by a 3.0” BSP connection located in the centre of the rear wall of the explosion chamber and at a point 4” from the roof. The gas diffusers were 250 mm wide x 250 mm high x 600 mm sheet metal boxes packed with non-flammable mineral wool, and where the upper side was constructed of an open grid mesh. The diffusers were used to minimise further mixing with air already in the

chamber by reducing the efflux velocity of the mixture and encouraging the formation of natural gas/air layers extending downward from the ceiling.

In order to gain the correct gas/air concentration prior to release into the explosion chamber, the relative proportions of gas and air were controlled by the operation of electro-pneumatic operated flow control valves, with gas and air flows metered using rotameters. The natural gas supply also passed through a G6 diaphragm meter (min flowrate 0.6 m^3/hr, max flowrate 10 m^3/hr) to monitor the total gas consumption during a test. A schematic drawing of the filling and mixing system is shown in Figure 3-23.

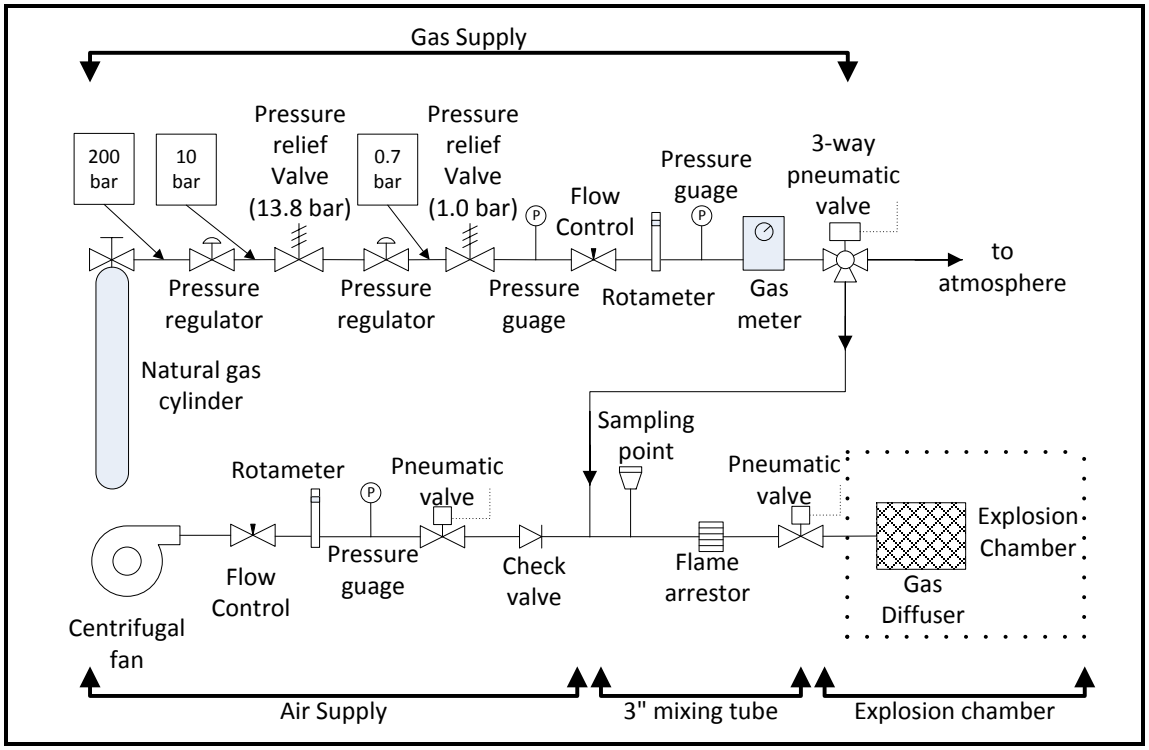

Figure 3-23 Schematic diagram of gas mixing and filling system (Rig A)

The air that was displaced as the gas/air mixture was released into the enclosures was allowed to escape to 'outside' via electro-pneumatic operated ball valves sited near the ground at the front of the explosion chamber. A light indicator system in the control room showed when the valves were open or closed.

To prevent the gas/air mixture composition changing after the desired concentration had been reached in the explosion chamber, the action of isolating power to the fan closed the electro-pneumatic valve in the air line and diverted the 3-way electro-pneumatic valve in the gas line such that no further gas entered the mixing tube.

3.5.2. Experimental Rigs B and C

Three filling and mixing techniques were used during the experiments:

i. Low pressure purge filling (≤ 75 mbarg) – for layered explosions.
ii. Premixed low pressure purge filling (≤ 75 mbarg) – for explosions in multiple compartments.
iii. Recirculation filling.

A PC-based system control and data acquisition (SCADA) system was used to control the gas mixing system by opening and closing pneumatically operated gas and air valves, and by turning on and off the mixing fan.

Purge Filling

Purge-filling is a process by which air in the explosion chamber is displaced by introducing a flammable gas or premixed flammable gas/air mixture of known concentration. For the interconnected enclosure tests, a polyethylene sheet was secured across the partition opening so that only the rear enclosure was filled with gas/air mixture.

The natural gas supply pressure from the distribution pipeline was reduced via a BD-RMG 241 pressure regulator to low pressure (≤ 75 mbar). The pressure regulator assembly included an overpressure shut off device (OPSO) which isolated the gas supply in the event that there was a fault with the regulator and high pressure gas was measured downstream of the device. In order to 'fine tune' the gas concentration within the explosion chamber, the gas supply passed through an electro-magnetic flow control valve with a rotameter before passing through a 3-way electro-pneumatic valve which allowed the gas supply to be isolated to the explosion chamber and the gas line to be vented to atmosphere before a test. A schematic drawing of the purge filling system is shown in Figure 3-24.

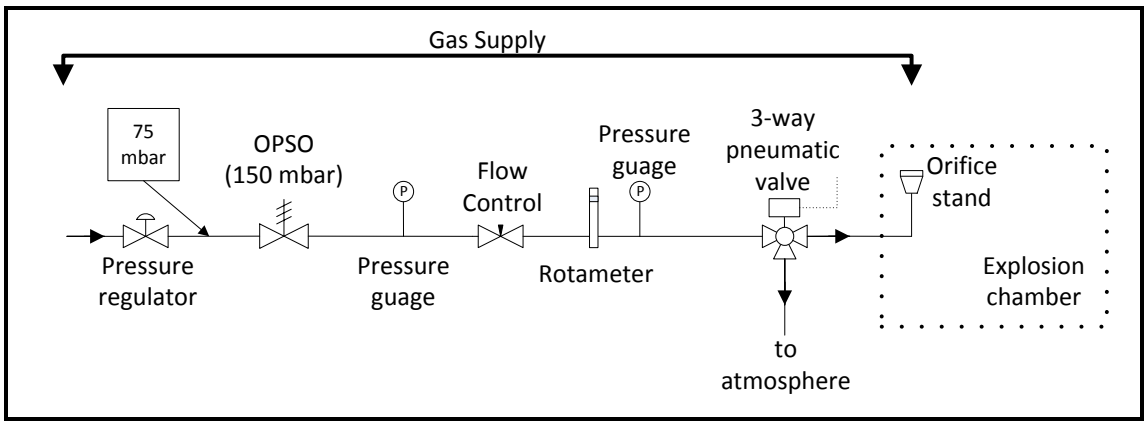

Figure 3-24 Schematic diagram of purge filling system (Rig C)

The supply pipe then passed into the rear enclosure of the explosion chamber where it was connected to a stand which had 4 orifices, at heights of 1 or 2 m above ground level (Figure 3-25).

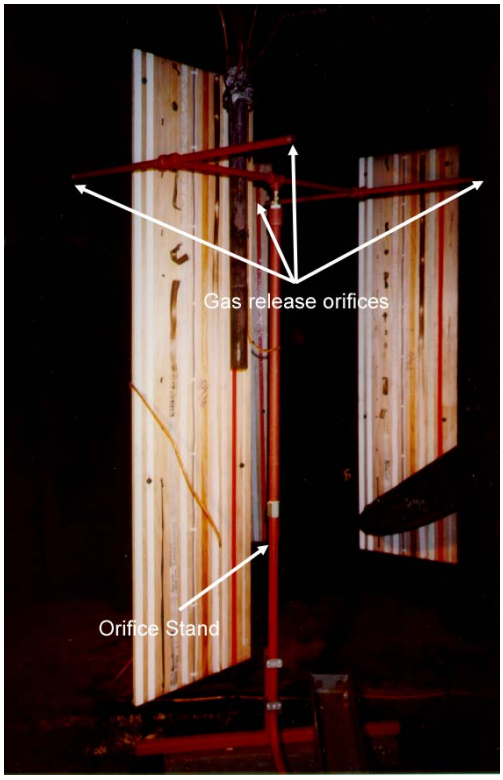

Figure 3-25 Gas release orifices for layered explosion tests

For layered propane experiments, propane was supplied from the 47 kg cylinder into the centre of the rear enclosure at a point 0.3 m above ground level. The tube through which the gas was released was oriented either horizontally or vertically upwards.

During purge filling, a high level natural gas/air layer was then allowed to build up between the points of release (i.e. 1 or 2 m above ground level) and the roof of the rear enclosure or a low level propane/air layer was allowed to build up between the point of release and the floor. The air that was displaced as the gas/air mixture was released into the enclosures was allowed to escape to ‘outside’ via electro-pneumatic operated ball valves sited at high or low level (depending upon the density of the fuel gas) at the rear of the explosion chamber. A light indicator system in the control room showed when the valves were open or closed. To prevent the gas/air mixture concentration changing after the desired concentration had been reached in the explosion chamber, the electro-pneumatic isolation valve was turned-off using the SCADA system and the fuel storage isolation valve was isolated. Prior to ignition, the gas line was vented to atmosphere.

Premixed Purge Filling

For homogenous gas explosion tests in a multiple enclosure, where the rear enclosure was completely filled with a gas/air mixture of a given concentration, the explosion chamber was filled by premixed ‘purge-filling’. A polyethylene sheet was secured across the partition opening so that only the rear enclosure was filled with gas/air mixture. A polythene tube was used to mix the gas with air and convey the mixture to the explosion chamber. It was connected at one end to a 0.6 m diameter steel duct connecter located at low level at the front end of the chamber side wall. The duct connector also housed the pneumatic ram for the flap valve (see Figure 3-26). Opening of the flap valve (controlled by the SCADA system) allowed the gas/air mixture to be released into the explosion chamber. The polythene tube was used as a safety measure to prevent damage to the mixing system in the unlikely event that the flammable mixture was ignited or a jetting flame from the explosion chamber entering the duct.

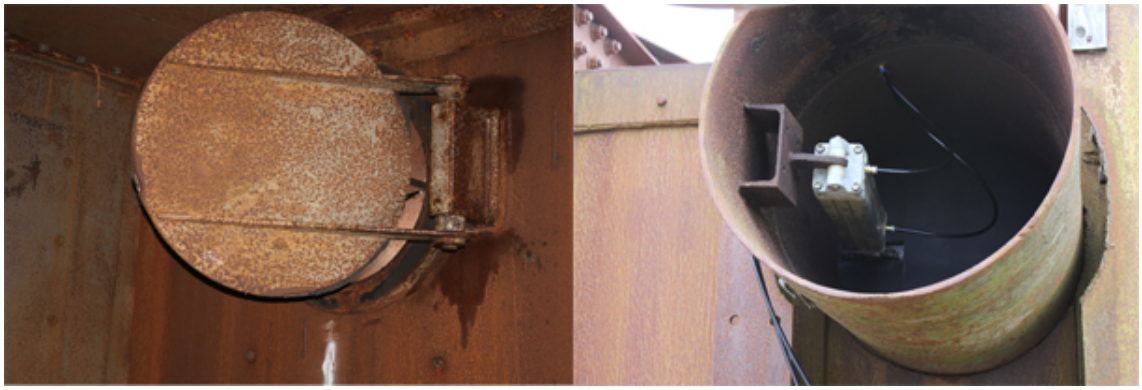

Figure 3-26 Pneumatic flap valve (left) and ram (right)

The polythene tube was connected at the opposite end to a 0.5 m diameter aluminium duct, into which the gas supply (same system as for purge filling) and an air supply, via a check valve, from a motor driven fan were connected. The fan was a Fläkt Woods 5.7 kW, 0.5 m diameter, ATEX compliant (i.e. suitable for use in explosive atmospheres), long cased, axial fan (model No. 50JM ATEX 20/2/6/28, see Figure 3-27).

Figure 3-27 ATEX compliant axial fan

Gas was released into the mixing tube via a pneumatic valve controlled by the SCADA system and air was blown into the tube via the fan. At the rear end of the fan unit, a 300 mm diameter pneumatic blast gate damper (sometimes referred to as a guillotine valve) was installed in order to open or close the mixing duct. Air then passed through the fan unit, past a sampling point and then entered a tee-junction. On one side of the tee-junction a second pneumatic guillotine valve was installed and the other side was connected to the polythene tube. The second guillotine valve was installed so the mixing tube could be purged of gas prior to the explosion test. The volume flow rate of air was controlled by varying the fan speed using the SCADA system and the gas flow rate was controlled by altering the gas valve position. Once the pre-determined gas/air concentration had been reached in the rear enclosure, the flap valve was closed, the gas supply to the chamber was isolated, the guillotine valve(s) closed and the air fan switched off. The mixture was then allowed to become quiescent. A schematic drawing of the premixed purge filling system is shown in Figure 3-28.

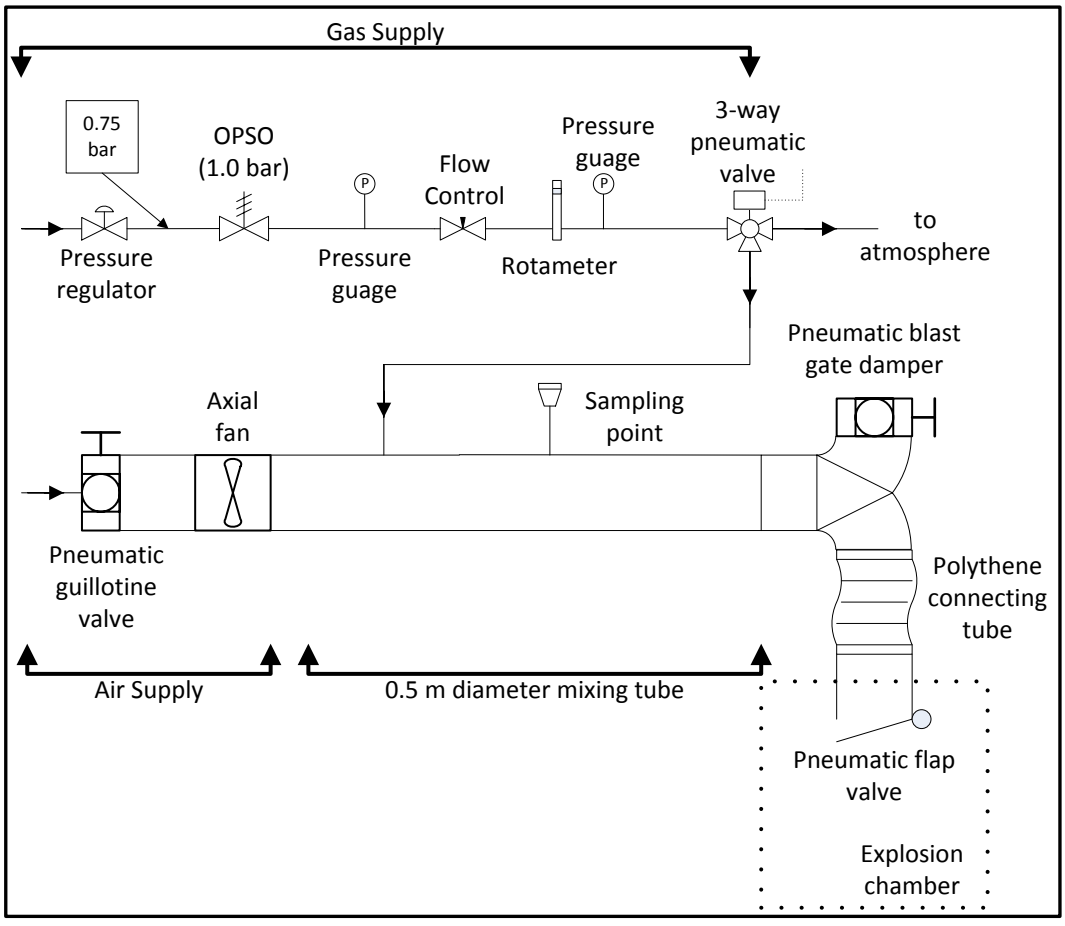

Figure 3-28 Schematic diagram of premixed purge filling system (Rig C)

Recirculation Filling

For a series of homogenous natural gas explosion tests, where the chamber was completely filled with a gas/air mixture of a given concentration, the explosion chamber was filled using a procedure known as 'recirculation filling'. Recirculation filling is a process by which fuel gas is added to a recirculation duct, which is connected to the bottom of one end of a side wall of the explosion chamber and at the top of the opposite end (Figure 3-29). A Fläkt Woods 50JM ATEX 20/2/6/28 fan was used to re-circulate the mixture around the recirculation duct and through the explosion chamber until the gas/air mixture reached its desired gas concentration. This method has been found by MRS to be particularly successful when used in large explosion chambers.

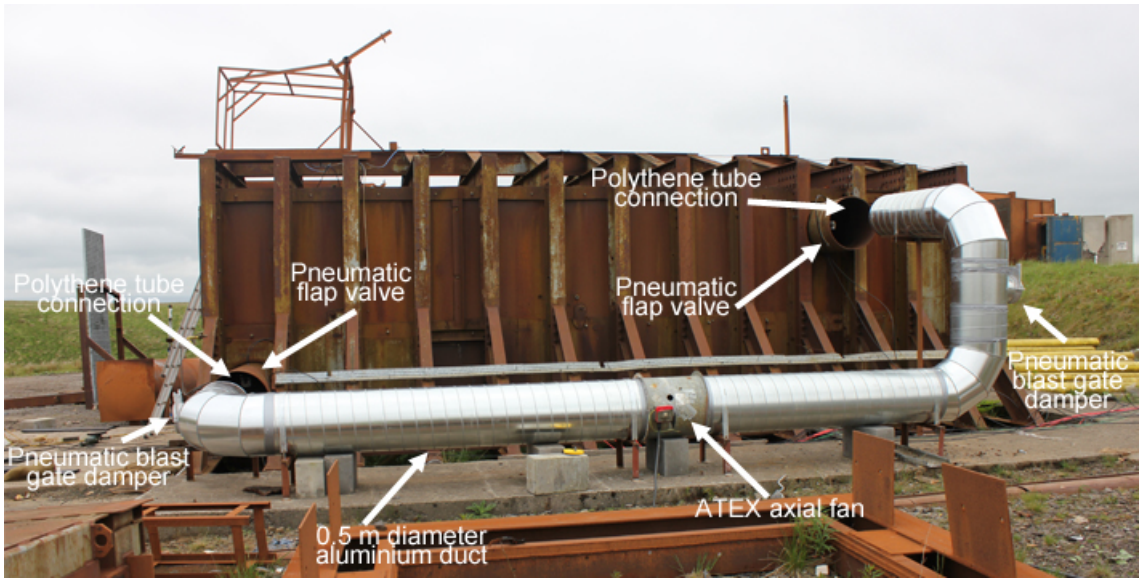

Figure 3-29 Recirculation duct

Gas was taken from the fuel supply via a 25 mm pneumatic isolation valve with a Norton actuator (Figure 3-30).

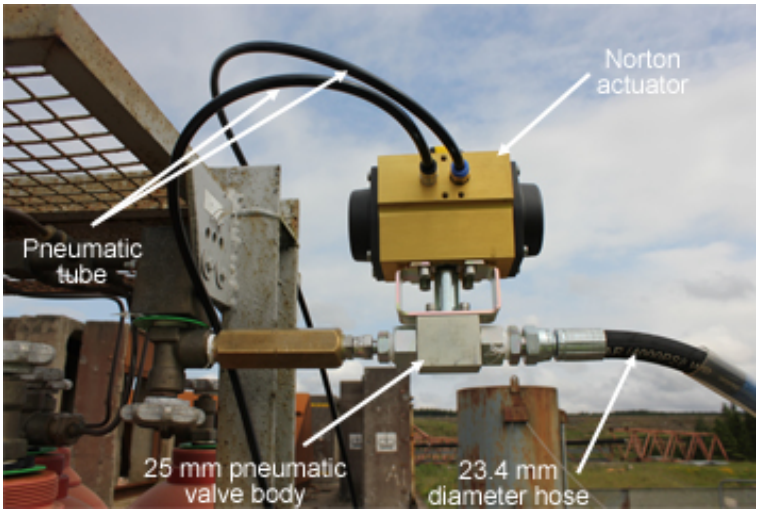

Figure 3-30 Pneumatic isolation valve located adjacent to gas supply

A 23.4 mm gas hose, manufactured in accordance with BS EN 559 conveyed the gas from the supply to the recirculation duct. A further 25 mm pneumatic isolation valve with Norton actuator was located just prior to the gas supply entering the recirculation duct (Figure 3-31). At either end of the mixing duct were 300 mm diameter pneumatic blast gate dampers. The blast gates were fitted to allow air to enter the recirculation system and to purge the recirculation duct of flammable fuel/air mixture prior to carrying out the explosion test.

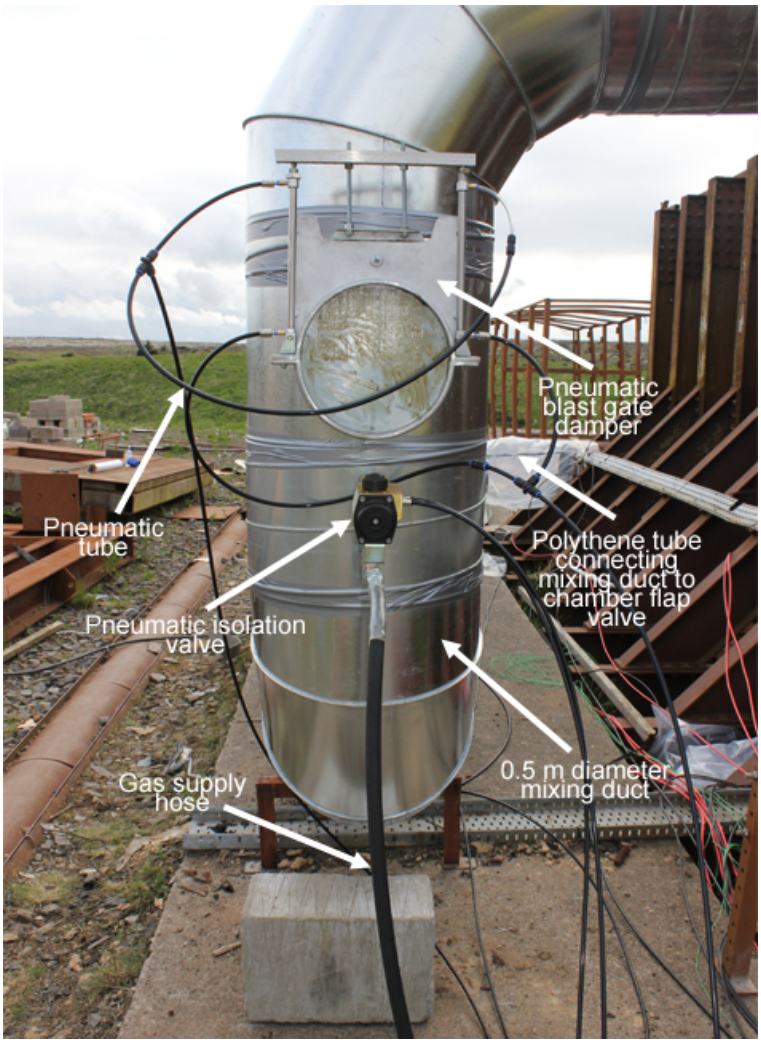

Figure 3-31 Pneumatic isolation valve located at recirculation duct

Prior to filling, the chamber flap valves were opened, Gas was released into the recirculation duct via the two pneumatic valves which were controlled by the SCADA system and the fan was switched on to circulate the gas through the duct and the explosion chamber. Initially, the gas was only mixed with air that was within the explosion chamber. However, if the gas concentration within the chamber became richer than required, then the pneumatic blast gate on the suction side of the fan was opened to allow additional air to enter the recirculation system. The gas flow rate was controlled by adjusting the gas supply regulator and by opening and closing the

pneumatic gas isolation valve. Once the pre-determined gas/air concentration had been reached in the chamber, the flap valves were closed, the gas supply to the chamber was isolated and the air fan switched off. The mixture was then allowed to become quiescent. The pneumatic blast gates were opened and the fan switched on in order to purge the recirculation system of flammable gas/air mixture. A schematic drawing of the recirculation system is shown in Figure 3-32.

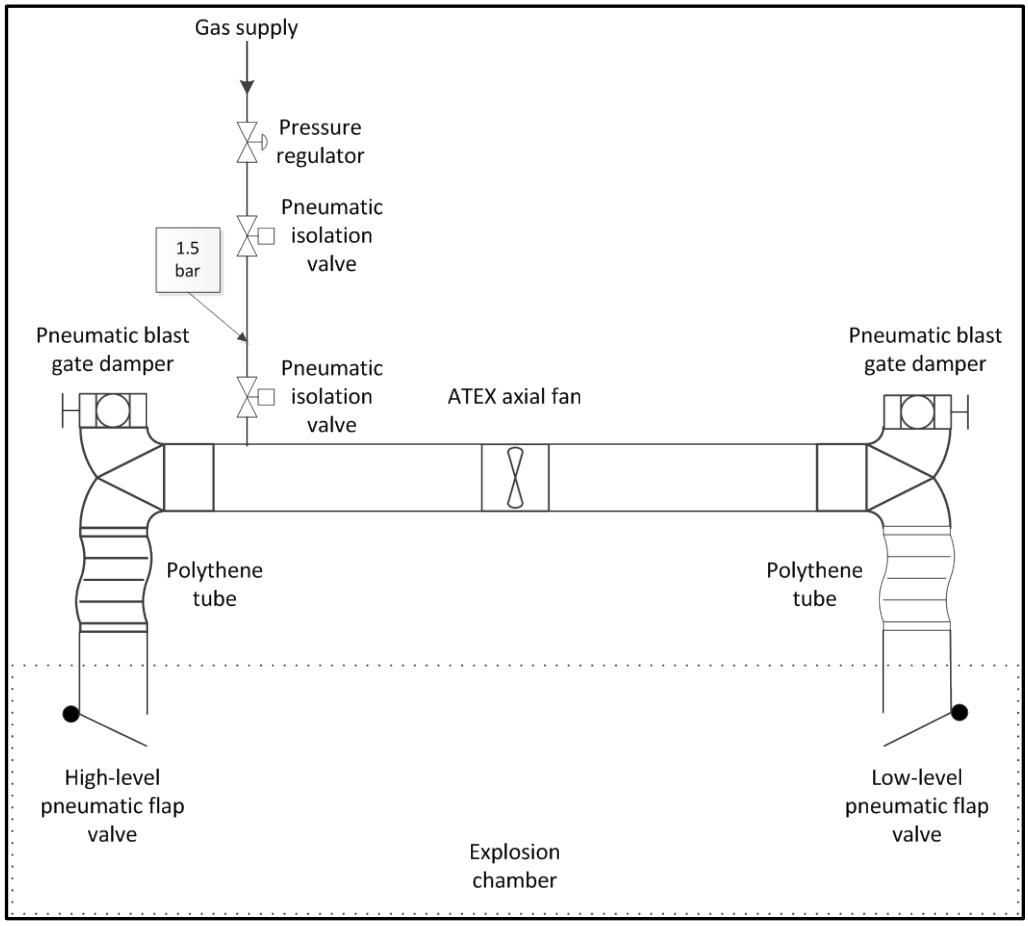

Figure 3-32 Schematic drawing of recirculation system (Rigs B and C)

For homogenous propane experiments, the above procedure was followed, with propane (of at least 97% purity) being supplied from a 47 kg propane cylinder. However, the direction of flow was reversed by rotating the orientation of the mixing fan through 180° such that the fuel/air mixture was entering the top of the explosion chamber and returning into the duct via the bottom of the chamber.

3.5.3. Experimental Rig D

The desired fuel gas/air concentration was obtained by partial pressure measurement using a mixing control system. As the tests were conducted at standard atmospheric pressure (i.e. 1013.25 mbar), to induce a flow from the mixing control system into the explosion vessel, and to facilitate mixing, the pressure within the vessel was reduced to 200 mbar (i.e. a partial vacuum was obtained) with a three-phase Edwards E2M175 two stage oil sealed rotary vane vacuum pump (Figure 3-33). The vacuum pump, which had a maximum displacement of 3.0 m^3/min, was also used for purging the products of combustion from the vessel after the explosion. It was water cooled (from the mains water supply), and had a combined oil trap and filter to prevent oil being released to the atmosphere, and to keep the oil clean and free from deposits. In order to protect dust particulates contaminating the pump, a dust filter was fitted to its inlet connection.

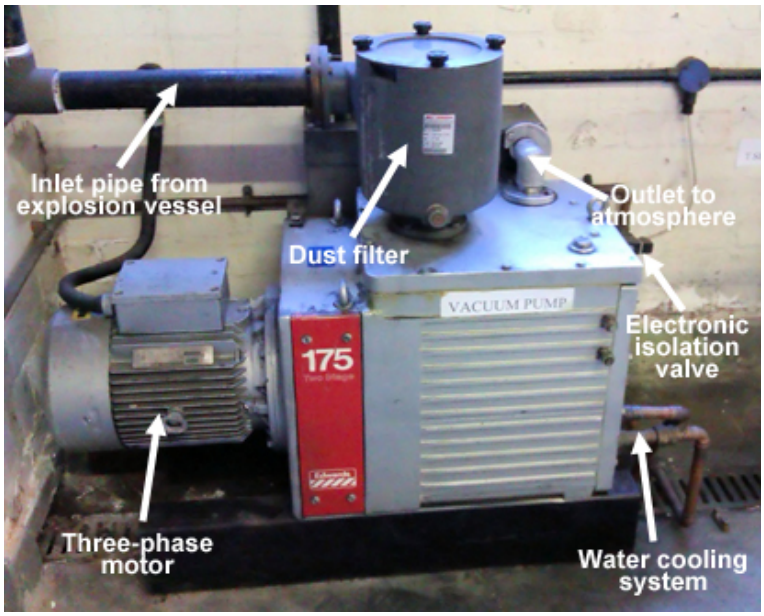

Figure 3-33 Vacuum pump (Rig D)

The vacuum pump line from the explosion vessel to the inlet connection of the vacuum pump, consisted of a Pirtek 1” nominal bore, full vacuum rated, flexible hose, and a section of 1” nominal bore steel pipe. The flexible hose was connected to the explosion vessel to facilitate movement of the vessel (Figure 3-34).

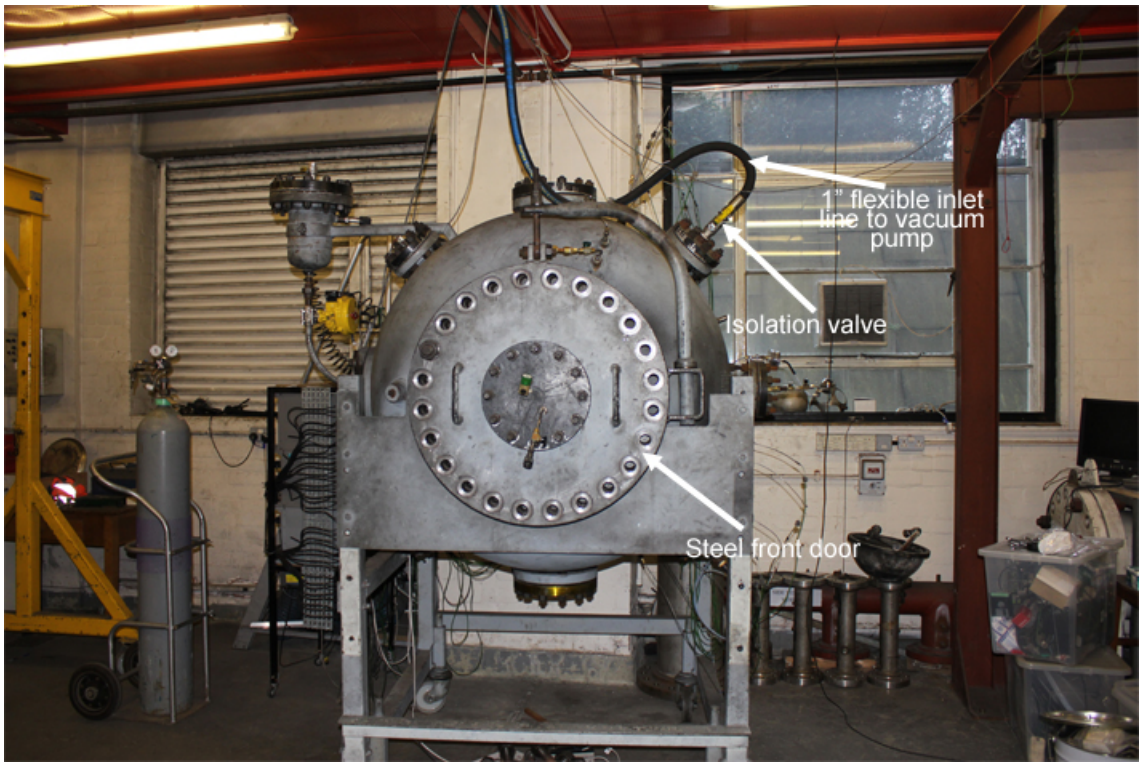

Figure 3-34 Vacuum pump inlet line (Rig D)

The flow of air and of fuel gas into the explosion vessel was controlled by the mixing control system (see Figure 3-35). The control system had a four-way rotary valve which allowed three different gas inlet lines to be connected to a fourth, outlet line, which was connected to the explosion vessel. The rotary valve allowed only a single gas to pass through to the explosion chamber, no mixing was allowed in the valve. During this experimental work, only pure gases were used (i.e. methane, propane and ethylene), and consequently, only two inlet lines were required; namely the fuel line and compressed air, with the fuel source being changed at a quick action connector upstream of the mixing control system.

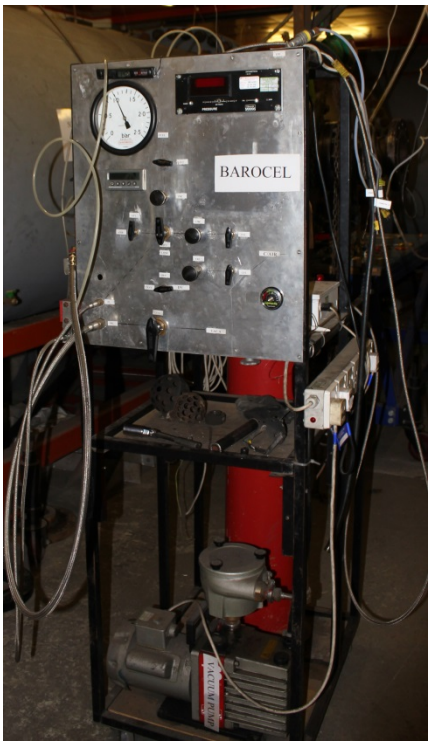

Figure 3-35 Mixing control system (Rig D)

A schematic drawing of the mixing control system is given in Figure 3-36. Fuel gas was taken from the appropriate cylinder at a pressure of 5 bar and passed through a series of controls before entering the four-way valve. Fuel gas was allowed to flow into the vessel through the opening of the appropriate isolation valves and the rate of gas flow through the four-way valve was controlled by adjusting the pressure regulator. The amount of gas required for the desired fuel/air concentration was determined using partial pressure measurement. For example, a natural gas concentration of 10% (by volume), which is slightly rich of stoichiometric, requires 10% of the absolute pressure within the vessel, prior to ignition. As the tests were conducted at standard atmospheric pressure (i.e. 1013.25 mbar), a natural gas pressure of 101.325 mbar, was required. As soon as the desired partial pressure had been reached (i.e. 101.325 mbar + partial vacuum of 200 mbar = 301.325 mbar), the fuel isolation valve was closed.

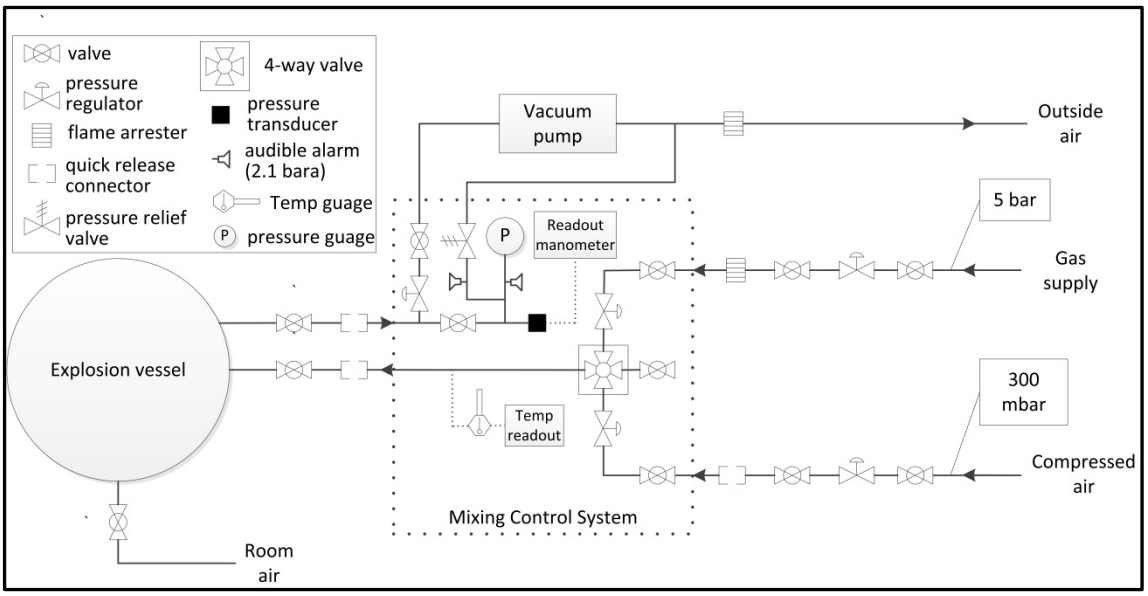

Figure 3-36 Schematic drawing of mixing control system (Rig D)

A BOC Edwards model 600 Barocel absolute vacuum pressure transducer and an absolute pressure gauge (connected in series) were used to monitor the pressure within the explosion vessel during mixture preparation. The DC output of the pressure transducer was converted into a digital display using a BOC Edwards Datametrics 1500 Barocel readout manometer with an accuracy of ± 0.05 mbar. The ambient temperature and pressure measurements were also monitored in the mixing control system.

The fuel/air filling and mixing process was then completed by adding air until the pressure within the explosion vessel was at standard atmospheric pressure. Initially, as the explosion vessel was still under partial vacuum conditions, ambient air was added by opening the isolation valve located at the bottom of the explosion vessel. The addition of a sonic jet of air into the vessel promoted mixing throughout the volume. The filling process was completed by adding compressed air, which was regulated to a pressure of 300 mbar and passed through a series of controls before entering the four-way valve. From this valve, the flow of air into the vessel was controlled until standard atmospheric pressure was attained. The mixture was allowed to stand for approximately 10 minutes for diffusion mixing before the explosion was initiated. The fuel and air supplies were disconnected from the mixing system and the supply line to the vessel was disconnected and isolated prior to ignition. The accuracy of the mixing control system meant that at standard atmospheric conditions, a 10% fuel/air mixture could be prepared to an accuracy of 0.05%.

3.6. Ignition

The main requirement governing the choice of ignition source was that sufficient energy was provided to ignite mixtures of concentrations near the flammability limits and that the mixture should be ignited by a single spark. In Section 2.2.3 it was shown that there is a minimum energy that is required to ignite a gas/air mixture by a spark and that this minimum energy significantly increases as the gas/air mixture diverges towards its flammable limits.

Safety was a critical factor in the design of the ignition system. The systems were designed such that it was not possible to initiate ignition if a number of safety measures had not been completed. These measures included ensuring the safety doors had been closed (in the case of rig D), fuel supply lines had been disconnected, mixing ducts had been purged of flammable mixture and that isolation valves had been closed. In addition to these measures the enforcement of stringent procedures ensured that no-one could be present within prescribed exclusion zones.

3.6.1. Experimental Rig A

Initially an inductive spark was used to ignite the gas mixtures but following difficulties igniting rich mixtures (12% gas in air), ignition was undertaken by a capacitive spark produced by discharging a 60 μF capacitor (charged to 250 V) through a 10 kV transformer (test 28 onwards).

Ignition was initiated in the left chamber (viewed from the front) at a height of 1.22 m down from the ceiling in either a central position or centre of the rear wall.

3.6.2. Experimental Rigs B and C

For tests involving methane or natural gas, the spark was generated by the discharge of a 68 μF capacitor, charged to 160 V dc through the primary windings of a high tension coil. The spark gap was connected to the secondary windings of the coil (Figure 3-37).

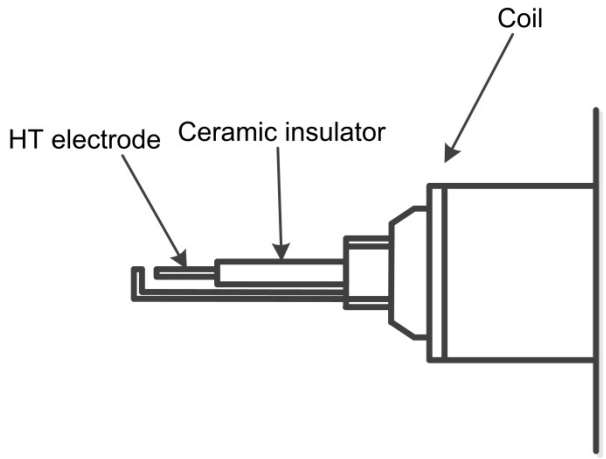

Figure 3-37 Spark ignition (Rigs B and C)

For natural gas or methane tests where the gas/air mixture filled the entire volume of the compartment, from floor to ceiling, the spark was located at mid-height, 1.4 m above the ground in either the centre or the rear of the enclosure. For layered natural gas explosions, the spark was located at the centre of the rear enclosure, at a height of 0.5 m from the roof of the chamber.

For the propane explosions, the spark was generated by putting a 240 V dc, 50 Hz voltage across the primary windings of a Danfoss Trafo type 52L transformer coil. The 8 kV output from the transformer was applied across a spark plug. In the non-layered tests, the spark gap was located at a point 1.5 m above the centre of the rear enclosure and in the layered tests the spark was located at ground level.

A PC using DNV GL bespoke software called ‘TIMER’ controlled the automated timing of the ignition sequence. This sequence triggered the transient recorders, video timers, ionisation probes and the spark igniter with an accuracy of better than 1 ms.

3.6.3. Experimental Rig D

The gas/air mixture was ignited by a 16 J spark generated by a capacitive discharge circuit supplying energy to a conventional automotive spark plug with electrodes that were extended 0.5 m in length in order to ensure its placement in the centre of the vessel. The electrodes were extended by welding stainless steel strips, of the same dimension as the electrode, to the required length. To prevent the electrode arcing at any point along the extension, the central electrode was passed through ceramic beads and secured using electrical insulating tape. The electrode gap at the sparking point was set at 2 mm. The ignition point was located in the geometrical centre of the vessel.

3.7. Measurement of Gas Concentration

3.7.1. General

The concentration of the gas/air mixtures were measured using calibrated Servomex 1400 infra-red absorption analysers. To ensure accuracy of measurement, the analyser was calibrated with a test gas of known composition (e.g. 99.95% methane) prior to each test. In order to sample the gas concentration in the mixing tube (where required), and at different locations within the explosion chambers, without using multiple analysers, a system of separate sampling lines was used, each sampling continuously. Gas samples were drawn from the sample points into the analyser by a KNF diaphragm vacuum pump. The gas flows through the sample lines were diverted in turn through a manifold system which was connected to the analyser via 6.5 mm butyl rubber tubing.

Where natural gas/air mixtures were required, the methane component of the natural gas within the enclosure was measured by a methane calibrated Servomex 1400 infra-red analysers, and thus, knowing the composition of the natural gas, the natural gas concentration was calculated.

3.7.2. Experimental Rig A

The concentration of the gas/air mixture was measured prior to being released into the chamber, thus enabling adjustments to be made to the flow rates at an early stage. The gas concentration in each of the enclosures was measured at the centre point and at various heights through a specially designed sample probe. The gas sampling probe consisted of a hollow stainless steel cylinder, inside which were installed six 8 mm (outer diameter) stainless steel gas sampling tubes [396]. The inner tubes were radially displaced at 30° between adjacent tubes, with the lower ends bent through a right angle such that they terminated flush to the outer cylinder. The uppermost sampling tube terminated at a height of 150 mm from the ceiling, with each further probe terminating at a vertical interval of 300mm.

Prior to ignition, the sampling probes were raised and withdrawn from the chamber using a combined pneumatic/hydraulic lifting system [396]. This was to prevent the probes acting as an obstacle and inducing turbulence.

3.7.3. Experimental Rigs B and C

A PC-based system control and data acquisition (SCADA) system was used to control the gas mixing system by opening and closing pneumatically operated gas and air valves, and by turning on and off the mixing fan. The SCADA system was also used to control the gas sampling stream selection system with the gas concentrations logged. The locations of the gas concentration sampling points for the various experimental tests are shown in Table 3-2.

Table 3-2 Location of gas concentration sampling points

Rig	Enclosure Type	No. Sample Points	Location of Sample Points		
			Height from floor (m)	Distance from front of chamber (m)	Distance from side wall (m)
B	Single enclosure	3	0.5	4.5	0.5
			4.0	4.5	0.5
			2.25	8.5	2.25
C	Single enclosure	1[a]	1.4	7.5	0.5
C	Multi compartment	3	1.5	5.5	1.5
			1.0 (2.3[b])	3.0	0.5
			0.8[b]	5.5[b]	1.5[b]
			0.5[b]	4.0[b]	1.5[b]

[a] Following extensive use with 3 sample points.

[b] For layered explosions.

3.8. Measurement of Pressure

3.8.1. Experimental Rig A

Explosion pressures within the enclosures were measured using eight acceleration compensated piezoelectric pressure transducers (Kistler type 7031), four in each enclosure (labelled P1 to P8, see Figure 3-38). The pressure transducers were calibrated for use in the range 0 – 2.5 bar. Glass wool and silicone sealant were used to protect the transducer diaphragms from flames and heat and transducer leads that were also heat sensitive were protected by steel deflectors and rock wool insulation.

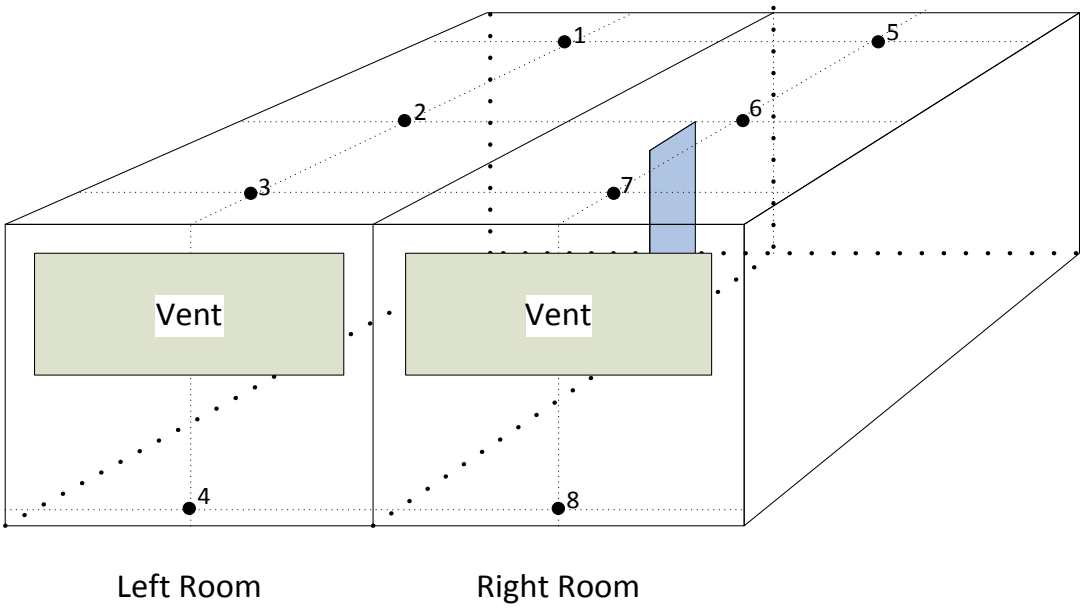

Figure 3-38 Location of pressure transducers

3.8.2. Experimental Rigs B and C

In order to measure the explosion overpressures generated in the experiments, PCB 113A26 piezoelectric pressure transducers were located at various positions both inside and outside the explosion chambers (see Table 3-3). The transducers were located along the centre line of the horizontal axis of the rigs. They were mounted in weatherproof boxes and coated with an insulating layer of silicon grease and aluminium foil to protect them from the effects of flame contact and heat, thereby preventing spurious readings during the later stages of an explosion (Figure 3-39). Transducers located within the vessel or external cloud were secured to the floor (except transducer number six, which was secured to the centre of the sill of the vent opening), whilst those located externally were mounted on transducer stands which were positioned to record the side-on overpressure (Figure 3-40).

The pressure transducers were calibrated prior to the experiments using a PCB model 903B pulse calibrator (0 to 10 barg range). The pressure signals were recorded on a microprocessor controlled Thorn EMI Datatech series 246 transient recorder. The transient recorder was controlled by a sequence timer unit during tests.

Table 3-3 Location of pressure transducers (Rigs B and C)

Rig	Location	Transducer Number	Distance from Rear Wall (m)
B	Inside chamber	T1	0.4
		T2	3.5
		T3	5.6
		T4	7.5
		T5	8.5
	External	T6	13.0
		T7	17.0
		T8	45.0
C	Inside chamber	T1	0.5(l)
		T2	0.5(c)
		T3	0.5(r)
		T4	4.1
		T5	7.9
		T6	8.3
	External	T7	12.3

Figure 3-39 Piezoelectric pressure transducer in weatherproof box

Figure 3-40 External piezoelectric pressure transducer and stand

3.8.3. Experimental Rig D

Explosion pressures were measured using two Keller PAA-11 piezoresistive pressure transducers mounted in the wall of the test vessel. One of the pressure transducers was calibrated for a range of 0-25 bara and other was calibrated for a range of 0-10 bara.

3.9. Opening of the Interconnecting Door

3.9.1. Experimental Rig A

A microswitch was mounted on the door jamb to provide an indication of the position of the interconnecting door during an explosion test (i.e. whether it opened, and if so, at what time). This data was compared with the pressure-time histories on a high resolution storage oscilloscope. Some of the later tests also used an internal high speed video camera to follow the movement of the door during the explosion.

3.10. Failure of the Vent

The time at which the vent failed (for tests using experimental rigs A, B and C) was determined by examining the video footage taken from the high speed cameras.

3.10.1. Experimental Rig C

In addition to using video cameras, a timing wire was fitted to the vent cover. The timing wire was an electrical circuit which consisted of two electrical cables joined by a metallic tape which was stuck onto the front of the vent cover (Figure 3-41). As soon as the vent failed, the metallic tape broke and the time at which the circuit was broken was recorded on the data acquisition system. The accuracy of the time the metallic tape broke is in the region of ± 0.2 ms based nominally on the decay time for the electrical circuitry to discharge to earth after a breakage.

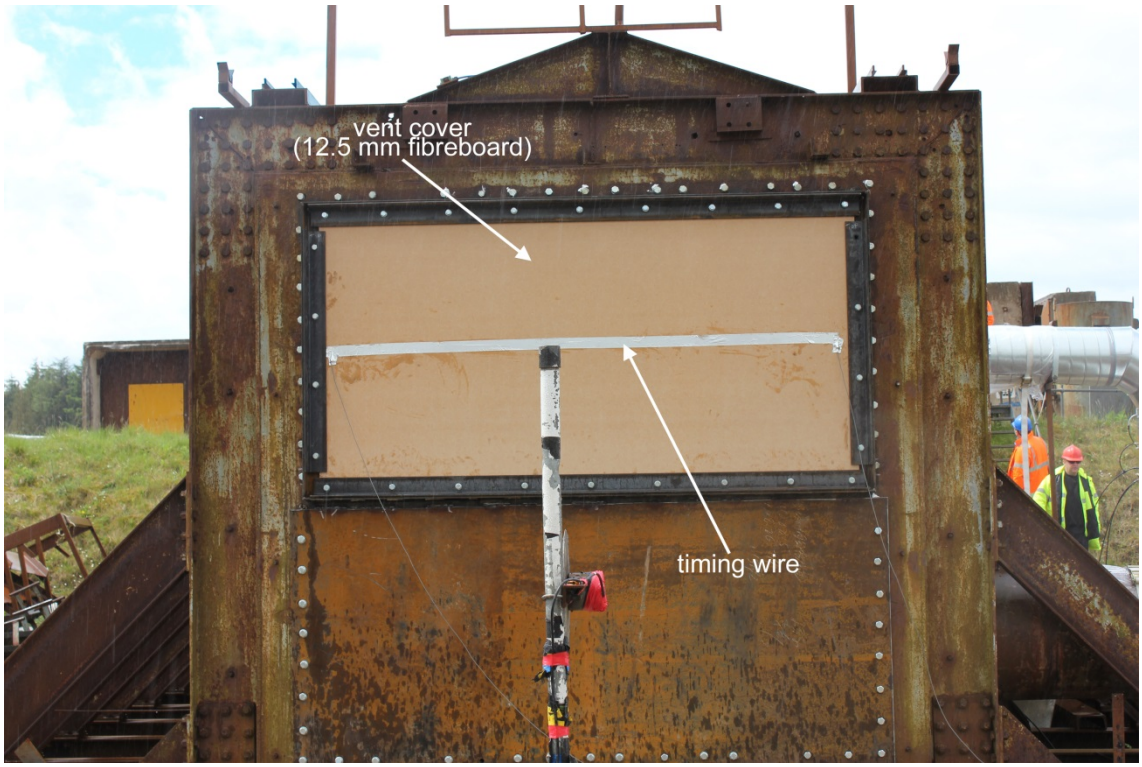

Figure 3-41 Timing wire to record the time of vent failure

3.11. Flame Propagation

3.11.1. Experimental Rig A

Each explosion test was filmed using a video camera positioned outside the explosion chamber. On some of the tests, footage provided by the video camera was supplemented by that of a motor driven Nikon F3 and a Locam cine camera (filming at 200 fps). In several of the later tests, high speed cine cameras were also used to film internal flame propagation in each enclosure. The film records were used to determine the times at which the vent opened, and also the times at which the flame front first appeared at the plane of the vent openings.

3.11.2. Experimental Rigs B and C

The explosion tests were recorded by a Phantom high speed video camera positioned outside the explosion chamber and by two Phantom high speed video cameras located in the walls of the explosion chamber. The film records were used to monitor flame propagation through the explosion chamber and to determine the times at which the vent opened.

3.12. Flame Speed

Thermocouples or flame ionisation probes were used to determine the flame arrival at specific locations within the explosion chambers. When the hot junction of a thermocouple is exposed to something hotter than that of its cold junction, a voltage develops. This potential difference can be calibrated to determine the source temperature. A thermocouple junction placed in the path of a travelling flame will therefore register its arrival as a change in voltage potential across the junction, which can be recorded as a distinct change in the analogue output of the thermocouple. In the context of flame speed, it is not necessary to accurately measure temperature, but rather, register the point at which the flame arrives at the thermocouple through a change in temperature. As thermocouple junctions have an inherent mass, there is a response time to heat. Consequently, it is important to use thermocouples made to the same specification such that response times are identical. The time delay or response time of a thermocouple, usually refers to the time lag for full response to the stimulus and is therefore not directly relevant in the detection of a flame. Providing the distance between two thermocouples or ionisation probes is known, the accurate measurement of the time of this signal change relative to that measured from an adjacent thermocouple or probe, allows the average flame speed to be calculated at the midpoint between the two instruments:

$$S_f = \frac{x_{T_n} - x_{T_{n-1}}}{t_{T_n} - t_{T_{n-1}}} \text{ or } S_f = \frac{x_{IP_n} - x_{IP_{n-1}}}{t_{IP_n} - t_{IP_{n-1}}} \qquad \textbf{(3-1)}$$

Where:

S_f = the flame speed (m/s).

x = the distance from the spark ignition (m).

t = the time of flame arrival (s).

T_n = a numbered thermocouple.

IP_n = a numbered ionisation probe.

When a flame reaches an ionisation probe, which consists of two electrodes separated by a small gap which provides a high resistance, ions in the flame front will lower the electrical resistance of the gap, triggering a voltage output from the electronic circuit. This voltage output may be recorded on a counter device mounted in a PC. Providing the distance between the probes is known, the time difference between the voltage outputs allows the average flame speed to be calculated at the midpoint.

3.12.1. Experimental Rig A

Flame speeds were not measured during experiments undertaken in these rigs.

3.12.2. Experimental Rigs B and C

The time of flame arrival at specific positions inside the chamber was measured using flame ionisation probes (Rig B) and flame ionisation probes and thermocouples (Rig C[1]) (see Table 3-4). Flame arrival times were not measured in the twin compartment arrangement. The flame ionisation probes consisted of two electrodes (the bared ends of two core heat resistance cable) separated by a 5 to 10 mm gap which provided a high resistance to voltage across the cable (Figure 3-42). The presence of ions in the advancing flame front lowered the resistance across the gap and at a pre-set level, triggered a voltage step output from a bespoke electronic timer circuit designed by MRS. This voltage 'spike' terminated counting in registers on a counter board mounted in a PC. The counting was initiated by a sequence timer at the time of ignition, with the count frequency being 100 kHz. Downloading the counter registers after the test, enabled the time of flame arrival to be calculated at each ionisation probe. The IP data were logged using in-house software called IP.

[1] Flame arrival times were not measured in the multiple compartment arrangement.

Table 3-4 Location of flame ionisation probes and thermocouples (Rigs B and C)

Rig	Distance from Rear Wall (m)			
	Ionisation Probe		Thermocouple	
B	IP1	0.900	-	-
	IP2	3.375	-	-
	IP3	3.625	-	-
	IP4	6.375	-	-
	IP5	6.625	-	-
	IP6	7.375	-	-
	IP7	7.625	-	-
	IP8	8.250	-	-
	IP9	8.500	-	-
	IP10	8.750	-	-
C	IP1	0.210	T1	0.470
	IP2	0.470	T2	4.560
	IP3	2.650	T3	5.920
	IP4	3.850	T4	7.450
	IP5	5.260	-	-
	IP6	6.620	-	-
	IP7	8.060	-	-
	IP8	3.850	-	-

The thermocouples used in this experimental rig were exposed junction, mineral insulated type K; supplied by TC Direct (Figure 3-42). The ionisation probes (except IP8, Rig C) and thermocouples (Rig C only) were located along the centre line of the explosion chambers at mid height. As there were likely to be high velocity flows and significant overpressures generated in the explosion tests, the ionisation probes and thermocouples were supported on a suspension wire coated with heat protective tape (Figure 3-43). The exception to this was where an ionisation probe (IP8, Rig C) was located at a distance of 200 mm from the chambers left side wall (looking towards the vent), in order to determine the time at which the flame reached its maximum surface area (Figure 3-43).

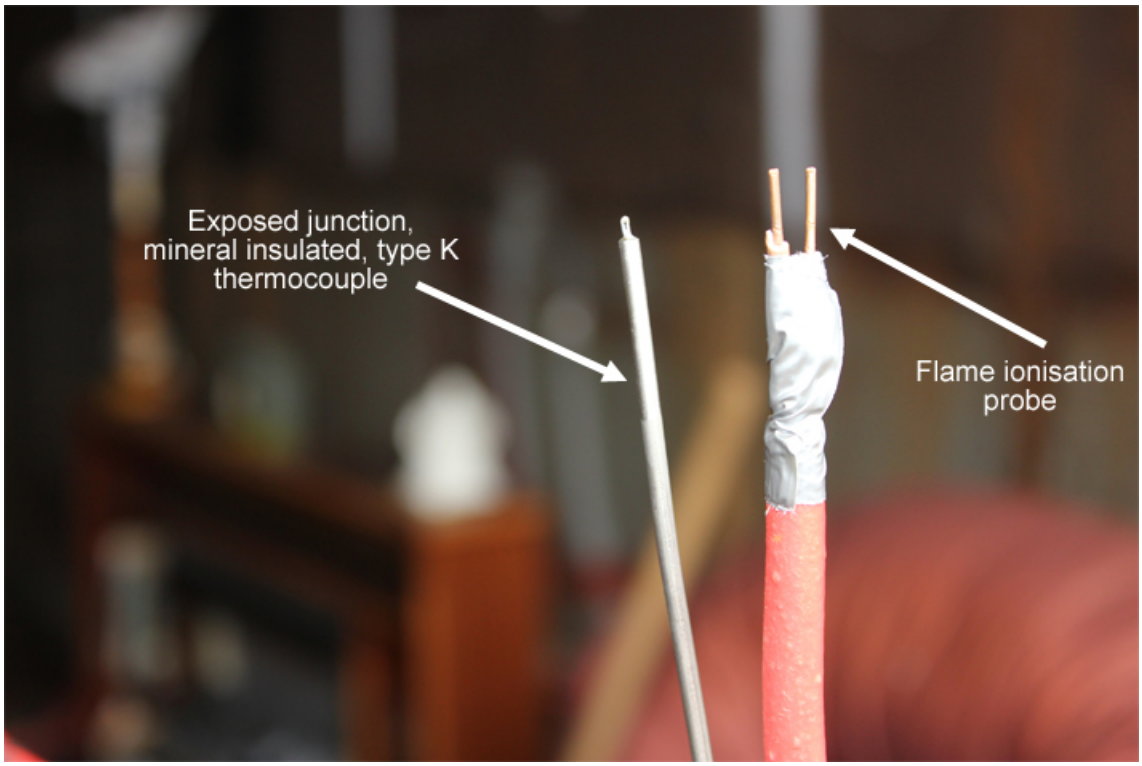

Figure 3-42 Flame ionisation probe and thermocouple (Rig C)

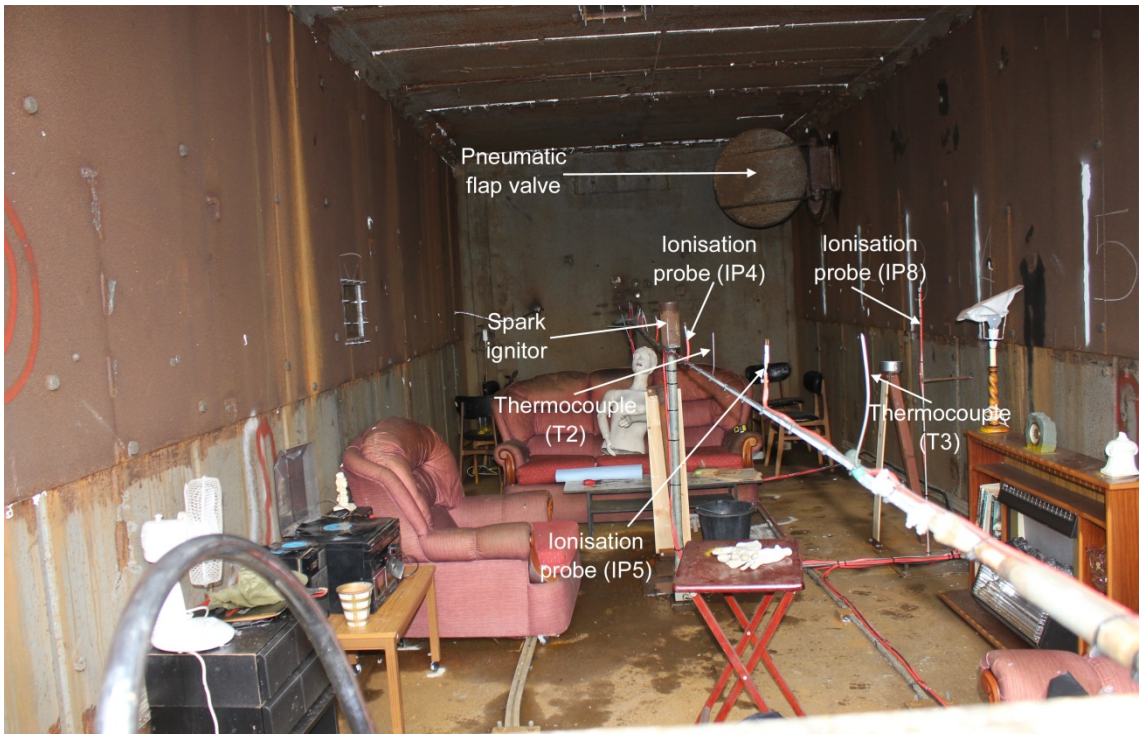

Figure 3-43 Instrumentation to measure flame arrival times (Rig C)

3.12.3. Experimental Rig D

Two arrays of thermocouples were used in this experimental rig in order to detect flame arrival and hence determine the flame speed during the constant pressure period of the explosion. The constant pressure period occurs when the spherical flame propagation is between 0.2 and 0.7 of the vessel radius. Outside of this region, flame propagation is neglected due to the effects of the ignitor in the early stages of the explosion and flame curvature caused by the flame-wall interaction in the latter stages.

The thermocouples used were exposed junction, mineral insulated type K; supplied by TC Ltd. The thermocouple arrays were fitted to the explosion vessel using Swagelock compression fittings with PTFE ferrules (pressure rating of 69 bar) and positioned inside the vessel along its vertical and horizontal axis (see Figure 3-44).

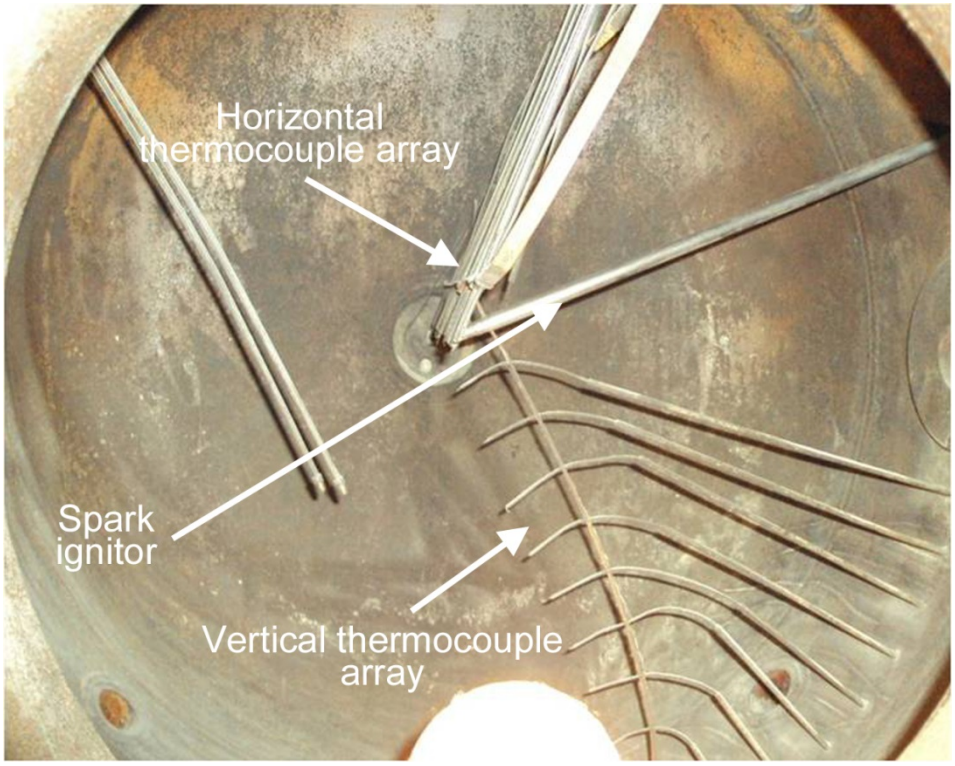

Figure 3-44 Horizontal and vertical thermocouple arrays (Rig D)

In the horizontal axis, the array consisted of thirteen thermocouples located along the centreline of the vessel, twelve of which were positioned either side of the ignition point, providing flame arrival times in the horizontal right and horizontal left directions. In the vertical axis, the array comprised nine thermocouples positioned in the bottom half of the vertical radial centreline (see Figure 3-45 and Table 3-5).

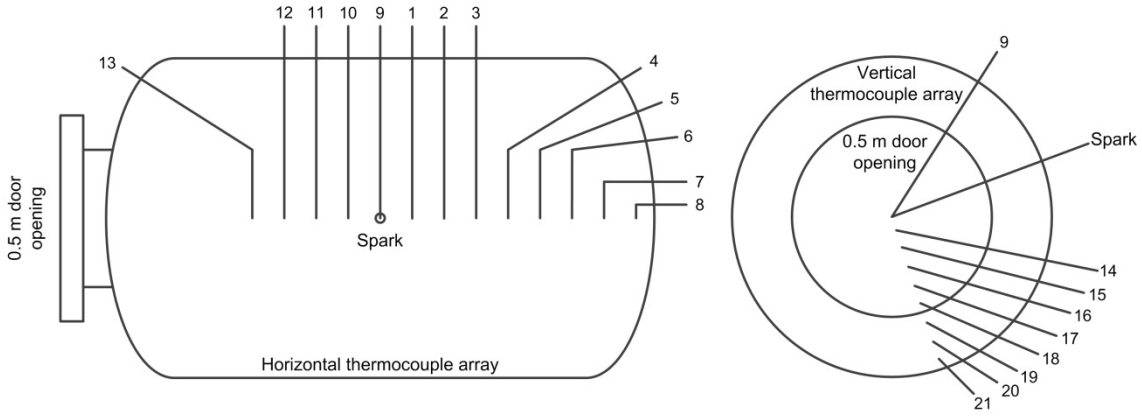

Figure 3-45 Rig D Thermocouple arrangement (taken from Phylaktou et al. [397])

Table 3-5 Location of thermocouples (Rig D)

Horizontal Left		**Horizontal Right**		**Downward Propagation**	
Thermocouple	Distance from spark (mm)	Thermocouple	Distance from spark (mm)	Thermocouple	Distance from spark (mm)
T1	69	T9	25	T14	89
T2	132	T10	93	T15	153
T3	194	T11	155	T16	212
T4	266	T12	224	T17	270
T5	332	T13	292	T18	330
T6	392	-	-	T19	387
T7	460	-	-	T20	452
T8	525	-	-	T21	511
-	-	-	-	T22	574

3.13. Measurement of Thermal Damage

3.13.1. Experimental Rig A

The measurement of thermal damage was carried out by placing thermal marker boards at various points in the two enclosures (see Figure 3-46).

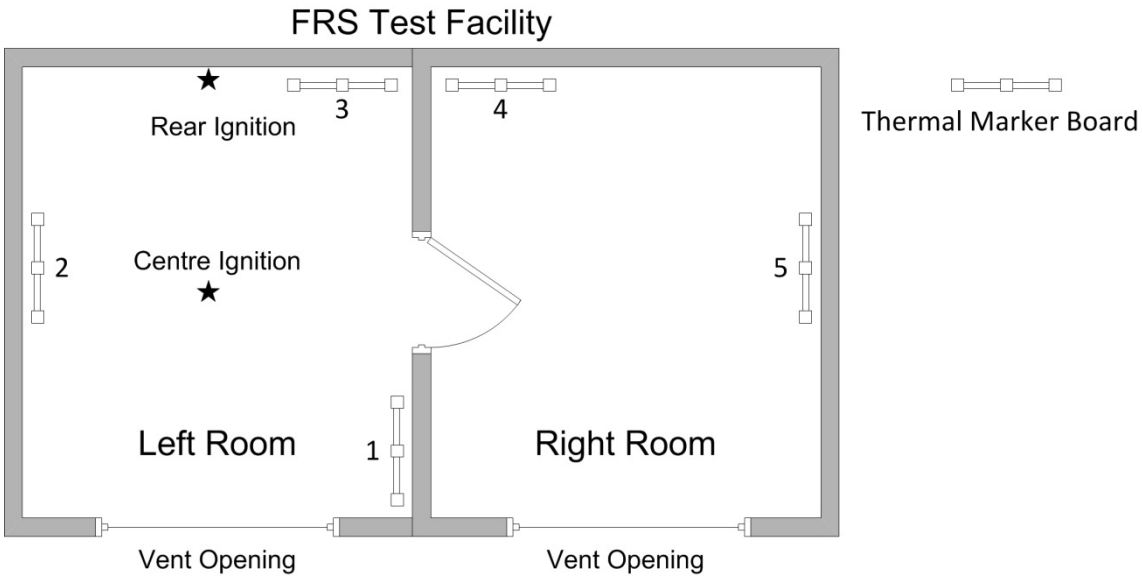

Figure 3-46 Thermal marker boards

The marker boards were 0.6 m in width and were of approximate floor to ceiling height so that thermal damage sustained from layered and full room explosions could be assessed. The boards were constructed such that 3 strips of different material could be attached to them. The materials to be attached to the marker boards were chosen because they represented building or decorative materials that were likely to be found in a typical dwelling. Strips of different material were placed on each marker board prior to each explosion test and were removed for visual examination after the test was completed. As the flame and hot gases propagated during the explosion the thermal strips were subjected to heat (from the hot gases) and short duration flame impingement. Assessment of the degree of thermal damage was undertaken by visual comparison and is reported in Chapter 6.

Seven different materials were selected for the experimental tests. These materials could be broken into two distinct groups, as shown in Table 3-6:

Table 3-6 Selected Materials

Wall Coverings	Wood Surfaces
Ordinary wallpaper on plasterboard	White gloss painted wood
Vinyl wallpaper on plasterboard	Varnished wood
Anaglypta type wallpaper painted with emulsion on plasterboard	Untreated wood
Emulsion painted plasterboard	

All of the material strips were prepared a maximum of 6 months prior to the experimental programme commencing. The wood material strips were 75 mm in width and the length was cut so that they were the approximate height of the explosion chamber. The painted wood was given 1 coat of primer, 1 coat of undercoat and 1 coat of gloss paint. The varnished wood was given 2 coats of polyurethane varnish. The wall covering material strips were approximately 200 mm in width. The location of the strips on the marker boards is shown in Figure 3-47 and the location of the materials during the experimental tests is given in Table 3-7.

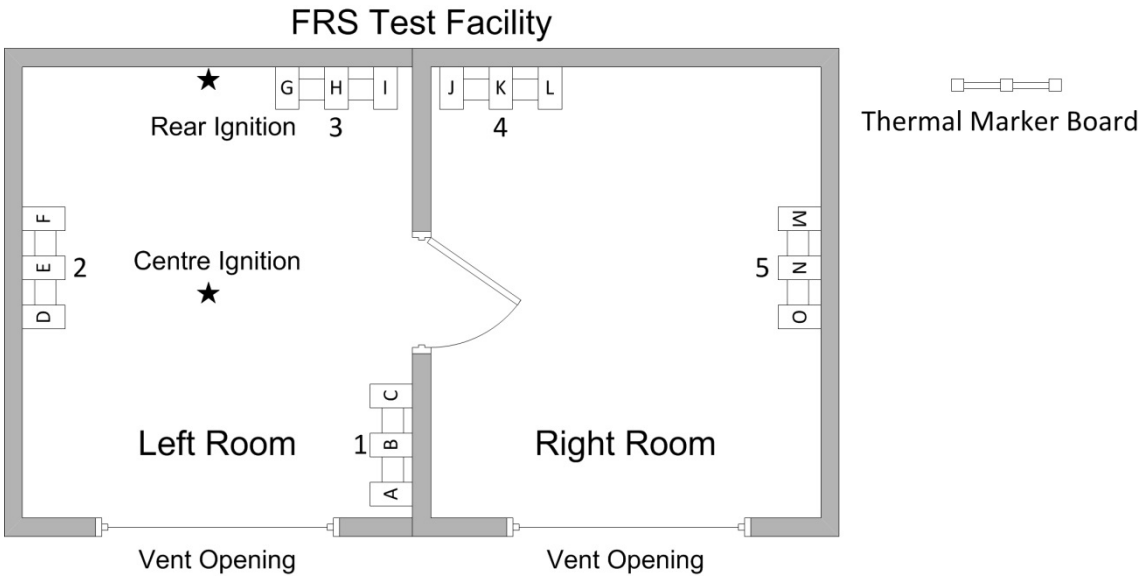

Figure 3-47 Location of material strips on thermal marker boards

Table 3-7 Selected materials and their location on the thermal marker boards

Material	Locations	Test No's.
Ordinary wallpaper	A I J	1 - 19
Vinyl wallpaper	C G L	1 - 19
Anaglypta	F M	1 - 19
Emulsion painted plasterboard	D O	1 - 19
Painted wood	B H K	1 - 19
Varnished wood	E	1 - 19
Untreated wood	N	1 - 19
Painted wood	B H K	23 - 24
Varnished wood	E	23 - 24
Untreated wood	N	23 - 24
Painted wood	E N	25 - 44
Varnished wood	H	25 - 44

3.13.2. Experimental Rig C

The measurement of thermal damage was carried out by placing thermal marker boards at various locations in the explosion chamber. During the multiple compartment tests, the measurement of thermal damage was carried out by placing thermal marker boards at various points in the two enclosures (see Figure 3-48).

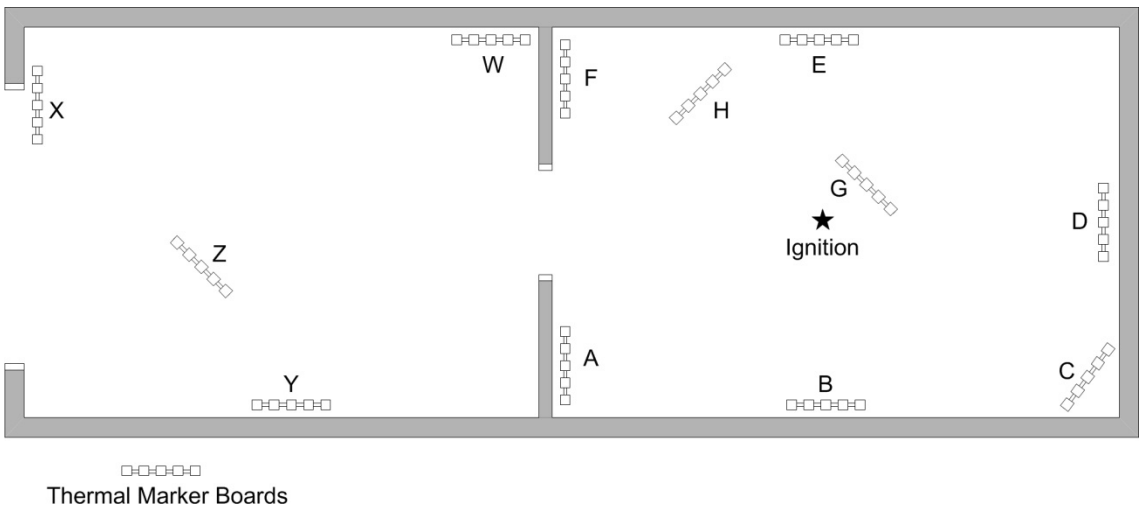

Figure 3-48 Thermal marker board locations

The marker boards were constructed from sheets of plywood 2.2 m in length and 0.6 m in width. A series of 12 samples of materials (see Table 3-8), in the form of strips approximately 3 cm in width, were attached, or painted, to the thermal marker boards (see Figure 3-49). The objective of the design of these boards was to enable the examination of as many materials as practicable (typically used in the decoration or construction of dwellings), in order to try to identify the pattern of thermal damage caused by a gas explosions. The same materials were attached to each marker board and each marker board was used for a single test only. Following completion of an explosion test, the board was removed and assessment of the degree of thermal damage was undertaken by visual examination and, in the case of the tests in the single compartment, by using a Digital SLR camera under consistent laboratory lighting conditions and Axiovision microscopy software.

Table 3-8 Selected materials attached to the thermal marker boards

Material	Description
Backing Board	Plywood sheets 2.2m high x 0.6m wide by 18mm thick
Emulsion paint	Two coats of Leyland vinyl matt emulsion – brilliant white
Gloss paint	One coat of Leyland primer undercoat (white) then one coat of Leyland gloss finish – brilliant white
Polythene sheet	Co-op refuse sacks (60% recycled PE) – black bin liners
Newspaper	Single sheet of newspaper
Heavy-duty wallpaper	Homebase luxury vinyl (Code 736936)
PVC coated electrical cable	Grey 1.5mm^2 twin and earth (type 6242Y) and 0.5mm^2 two core (type 2182Y)
Varnish	Leyland polyurethane varnish – clear
Cotton Strip	Richmond house fine Egyptian cotton (king sized sheets)
Wallpaper	Vymura quality wallpaper (Intaglio stripe, code 61-111 – washable peelable)
PVC Tape	Advance AT7 - flame retardant
Wool	Wendy Aran (25% wool, 75% acrylic)

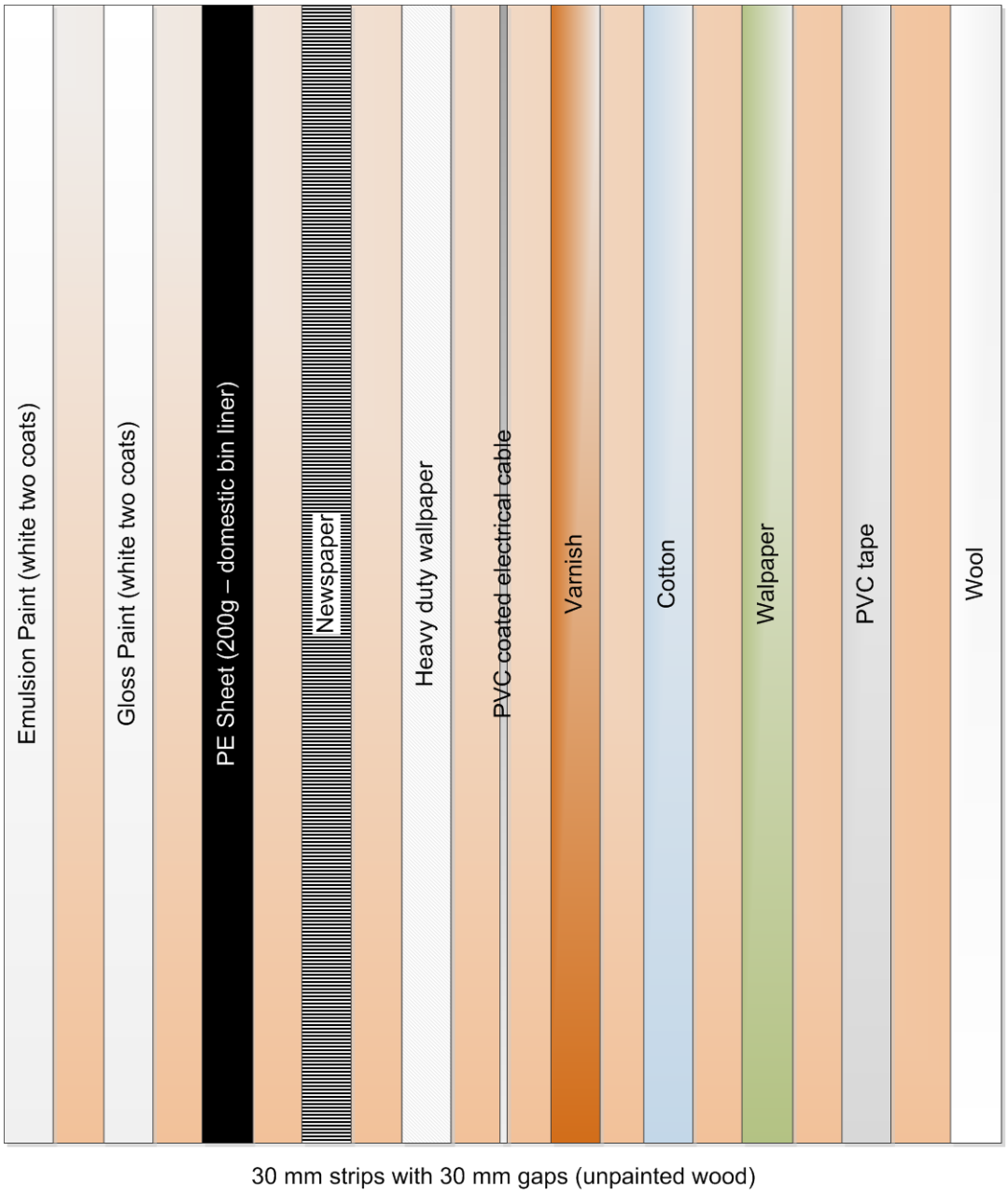

Figure 3-49 Location of material strips on thermal marker boards

In the single compartment tests, two purpose made marker stands were used, each of which secured 2 x softwood panels (Figure 3-50). One panel was placed such that the softwood panels were ‘face-on’ to the propagating flame and one was positioned close to the vessel chamber walls and perpendicular to the propagating flame (see Figure 3-51).

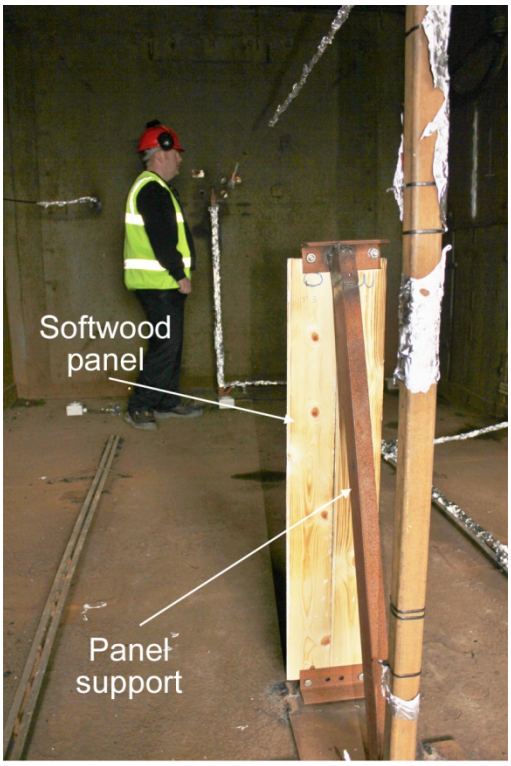

Figure 3-50 Softwood panel support (Rig C)

Figure 3-51 Location of thermal marker stands prior to explosion test (Rig C)

The softwood panels were supplied by Homebase and measured 0.9 m in height x 0.096 m in width x 0.0075 m in depth. Three different finishes were selected for the tests; painted with gloss paint (oil based), painted with quick drying gloss paint (water based) and untreated. Prior to testing, the softwood panels were prepared in the following manner:

i. Gloss painted wood – the softwood was given one coat of primer, one coat of undercoat and one coat of oil based gloss;
ii. Quick drying gloss painted wood - the softwood was given one of coat primer, one coat of undercoat and one coat of water based gloss;
iii. Untreated wood – the sample was left as supplied.

3.13.3. Experimental Rig D

The measurement of thermal damage was carried out by directly placing softwood panel samples on the inside face of the opening door (see Figure 3-52). The softwood panels were identical to that used in Rig D. The softwood panels were cut to a length of 0.25 m such that four samples could fit onto the door during each test. The samples were secured to the steel door using double sided duct tape.

Figure 3-52 Location of softwood samples (Rig D)

Five different finishes were selected for the tests; painted with gloss paint (oil based), painted with quick drying gloss paint (water based), varnished, untreated and covered with wallpaper. For consistency, the softwood panels were prepared in an identical manner to that described in Section 3.13.2, with the addition of varnished wood and wallpaper samples:

i. Gloss painted wood – the softwood was given one coat of primer, one coat of undercoat and one coat of oil based gloss;
ii. Quick drying gloss painted wood - the softwood was given one of coat primer, one coat of undercoat and one coat of water based gloss;
iii. Untreated wood – the sample was left as supplied;
iv. Varnished wood – the softwood was given two coats of polyurethane varnish;
v. Wallpapered – anaglypta wallpaper samples were pasted onto the softwood surface using wallpaper paste.

Following completion of an explosion test, the samples were removed and assessment of the degree of thermal damage was undertaken by visual examination and by scanning electron microscope (SEM).

The SEM was used to analyse the damage at the microscopic level and to determine if this method of analysis could aid explosion investigators. Prior to analysis by SEM the sample must be clean and dry, such that it will not outgas during the examination. Any surface oils should be removed with a solvent and dirt particles must also be removed by compressed gas. To prepare the softwood sample for use in the SEM, a section of each softwood sample was selected and cut to fit within the 25 mm diameter circular specimen stub. After the samples had been selected and cut to size, they were placed under vacuum for twenty-four hours in order to remove any moisture. After the sample was dry, it was fixed to the sample stub using double-sided conductive tape. The perimeter surface of the sample was also coated with carbon paint to ensure continuous conductivity of the sample to the stub. Any dirt on the sample surface was then removed with compressed gas before the sample was sputter coated with gold using an EMSCOPE SC500 SEM specimen vacuum coater to ensure the sample was coated with a thin layer of conductive material.

3.14. Control and Data Acquisition

3.14.1. Experimental Rig A

A transient data capture and recording system was used to record the experimental results. The transient recorder was a Data Laboratories Multitrap DL 6000 modular waveform system. This modular recorder received input from the pressure transducers, amplified and filtered the signals with computer controlled modules, and converted the analogue signals to digital such that they could be recorded on a storage disk.

The transient recorder was fitted with a Tabor 6010 125 MHz universal counter and eight 6024 memory modules. Each module could be used as a four channel recorder giving a capacity of 36 data channels. The maximum recording rate for the 36 channel configuration was 200 kHz at 12 bit resolution, with a maximum recording time of 4 s. The 12 bit analogue to digital conversion gave a resolution of 1 part in 2^{12} (= 4096). The voltage measurement range of the pressure transducers was 0-100 mV. For a pressure measurement range of 0-2.5 bar, the resultant transducer resolution was $\pm$ 0.6 mbar.

The transient recorder was controlled from a PC using the Acquire software package supplied by Data Laboratories. The Pressure-time histories of the 8 pressure transducers were recorded at a rate of 2 kHz for a period of approximately 2 seconds.

3.14.2. Experimental Rigs B and C

In rig B, two 32 channel transient recorders were used to record the experimental results. In rig C, a third 32 channel recorder was used to capture the thermocouple data. The pressure signals from the pressure transducers were amplified by a PCB control unit prior to entering the transient recorders. A Synergy transient recorder operating at 50 kHz at 16 bit resolution was used as the primary data logger for measurement of pressure transducer and flame ionisation probes outputs. The 16 bit analogue to digital conversion gave a resolution of 1 part in 2^{16} (= 65536). For a pressure measurement range of 0-10 bar, the resultant transducer resolution was $\pm$ 0.15 mbar.

The signal from each instrument was recorded on two channels of the transient recorder, the secondary channels covering twice the range of the primary channels. Thus should the pressure generated have exceeded the full scale of the primary channel, the data would also have been logged at lower resolution on the secondary channel. The pressure range for the primary channel was set to cover the anticipated pressure range for the given configuration. A TEAC GX1 transient recorder (with

internal signal conditioning), operating at 50 kHz, was used as a 'backup' data logger such that data would still be recorded in the event of primary equipment failure. A Spartan transient recorder operating at 500 Hz was used to record flame arrival times using thermocouples and gas concentration readings (recorded on the Synergy data logger when the Spartan was not used). A schematic drawing of the data acquisition system (Rig D) is shown in Figure 3-53.

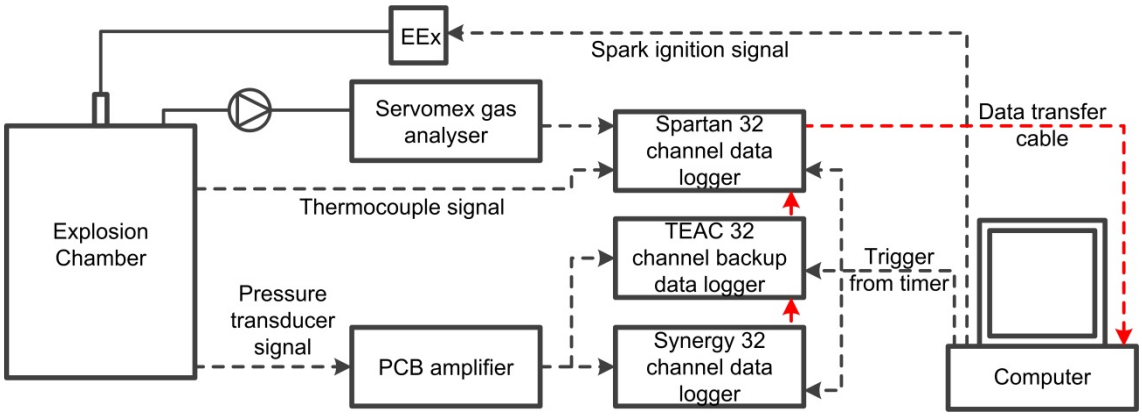

Figure 3-53 Schematic drawing of data acquisition system (Rig D)

The transient recorder and the data collection were controlled by DNV GL bespoke software (TRANSE). The software was used to initiate the control signals and to store the data. After initialising the control signals the test and data capturing process was initiated through an internal time sequence generator which initiated the spark ignition.

3.14.3. Experimental Rig D

A 34 channel Microlink 4000 transient recording system was used to record the experimental results. The Microlink 4000 was a modular data acquisition system that was designed to capture pressure and flame speed data at a sampling frequency of up to 100 KHz per channel. Each channel contained its own amplifier, 12 bit analog to digital converter and memory for the storage of data. A separate channel was used for each pressure transducer and thermocouple such that there was no delay in the transmission of data.

During this experimental programme, the sampling frequency used by the data acquisition system was 5 KHz, meaning that a sample was taken every 0.2 ms. The voltage measurement range of the pressure transducer was 0 – 100 mv and for thermocouples was -100 – 100 mv. The 12 bit analogue to digital conversion gave a resolution of 1 part in 2^{12} (= 4096). For a pressure measurement range of 0-10 bar, the resultant transducer resolution was ± 2.4 mbar. A schematic drawing of the data acquisition system is shown in Figure 3-54.

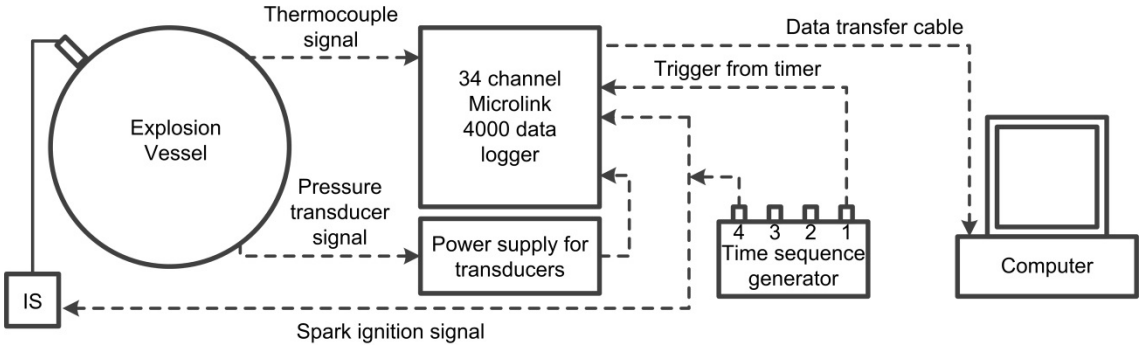

Figure 3-54 Schematic drawing of data acquisition system (Rig D)

Windmill Wavecap software was used to initiate the control signals and to store the data. The software program enabled the sampling frequency and pre and post trigger controls to be varied. After initialising the control signals through Wavecap, the test and data capturing process was initiated through an external trigger (time sequence generator). The trigger mechanism was set by the software to respond on the positive edge of the signal (digital signal transition from low to high, i.e. 0 to 1).

The time sequence generator had four time sequence channels, although in this experimental programme only channels 1 and 4 were used:

- Channel 1: to trigger the data logger;
- Channel 4: to send a signal to the spark ignition system.

Channels 1 and 4 were activated at the same time, when the start button on the sequence generator was activated. The Wavecap software program stored the data in imc FAMOS format (Fast Analysis and Monitoring Of Signals) in preparation for analysis.

3.15. Hazard Identification and Mitigation

It was essential that the risks associated with the explosion tests were thoroughly identified and controlled to an acceptable level. Demonstrating that the risks are at an acceptable level whilst conducting explosion testing requires careful consideration as the normal method of controlling risk (i.e. prevent and mitigate) is clearly not entirely possible given that the purpose of the study is to deliberately cause explosions. However, some of the hazards associated with conducting the experiments may be eliminated. Consequently, the most appropriate method for controlling risks during this study was to identify these potential hazards and to thoroughly assess measures that could be taken to prevent their occurrence (wherever possible) and to mitigate their effects.

A series of hazard identification studies (HAZID) were undertaken to identify hazards that would be present as a consequence of undertaking vented explosion and confined explosion experiments. A HAZID study is a systematic method of identifying hazards associated with the design and operation of hazardous equipment and plant. The studies were undertaken in order to determine the effects of exposure to identified hazards and to implement measures to mitigate the risk of injury or harm to persons or property.

The latter HAZID studies (using Rigs C and D) were undertaken in accordance with BS EN ISO 17776 [398], whilst the earlier studies (using Rigs A, B and C) were conducted in accordance with guidance given by Lee [399]. Due to the structured manner of the HAZID procedure undertaken, the hazards, as well as their possible escalations were identified. A number of reference words were used during the HAZID to prompt identification of hazards. These guidance words are shown in Table 3-9:

Table 3-9 HAZID guidance words

Guidance Words		
leaks and spillages	rough ground	slips, trips and falls
thermal radiation	unignited gas	hot work
overpressure	high pressure gas	pressure testing
non process fires	human factors	proximity of equipment
toxic release	smoke	asphyxiation
transport accidents	venting/depressurisation	missiles
structural failure	aircraft	communications
heavy machinery	noise	lighting
dropped object	overfilling	competence
maintenance	cryogenics	instrumentation & control
extreme weather	multiple activities	burning fragments
emergency response	isolation	electrical

A number of hazards were identified during the HAZID. The preventative and mitigative measures were then considered and a semi quantitative risk assessment undertaken. The results of the HAZID (for all Rigs) are shown in Table 3-10 and the results of the risk assessment (for all Rigs) are shown in Table 3-11.

Table 3-10 Results of HAZID (all Rigs)

Hazard No.	Hazard	Possible Contributing Factors	Safeguards	Consequence	Mitigation
1	Working at height	Sheeting rigs A, B, C and D. Closing/opening Rig D door.	Stairs with hand rails. Harnesses. Safe system of work.	Falls and injury to operators.	PPE. Training for operators.
2	Unintentional Ignition	Ignitor failure. Static ignition.	Two step ignition system. Spark not enabled until required. Written procedure for firing. Enforced exclusion zone during filling and testing.	Unintended explosion. Visitor concern/panic.	Hearing protection worn prior to test (Rigs A, B, C and D).
3	Thermal Radiation	Persons viewing test. Weather conditions.		Burns. Visitors concern/panic.	Visitors and Operators at known safe locations. Briefing before test.
4	Overpressure and noise	Persons viewing test. Weather conditions.		Hearing Damage. Visitors concern/panic.	Visitors and Operators at known safe locations. Briefing before test. Hearing protection.
5	Hot/burning plastic	Persons viewing test. Weather conditions.		Burns. Visitors concern/panic. Grass Fires	Visitors and Operators at known safe locations. Fire brooms and extinguishers available near location. Water misting of local area in dry weather
6	Failed ignition	Ignitor failure.	Procedure for failed ignition - purged through with air.	Delayed test	

Hazard No.	Hazard	Possible Contributing Factors	Safeguards	Consequence	Mitigation
7	Missiles	Overfilling. Structural failure.	Enforced exclusion zones. Warnings with test control. Shutting off of Road (Rigs A, B, C and D).	Injury to operators/visitor. Damage to gas supplies.	Visitors and operators at known safe locations. Raised bank for protecting gas lines (Rigs B, C and D).
8	Fatigue	Repeated pressure cycling of test rig	WSOE. Design, procedures and inspection.	Failure of test rig, missiles, harm to personnel	Visitors and operators at known safe locations.
9	Failure of gas supply lines	Missiles.	Pipes hoses and couplings are suitable for the purpose pressure tested and within their lifespan.	Pressurised gas release. Explosion.	
10	Fire	Dry surrounding area (Rigs B, C and D).		Burns, smoke inhalation.	All persons are briefed on escape routes. Misting of local area. Fire extinguishers & fire engine (Rigs B, C and D).
11	Slips, trips and falls			Injury	Clean area. PPE.

The hazards identified in the HAZID (e.g. 1-11) are shown in the ‘traffic light’ coloured boxes of Table 3-11. The coloured boxes represent the risk presented by the hazard, after preventative and mitigatory measures; with red being unacceptable, amber being tolerable and green being broadly acceptable.

Table 3-11 Semi quantitative risk assessment (all Rigs)

		Consequence/severity				
		Minor Minor injury. No lost time.	Low Injury which requires medical attention. 1-3 days lost time.	Medium Serious injury. Long term absence.	High Life threatening injury. Disruption to business.	Major Fatality or multiple fatalities. Catastrophic business impact.
Likelihood	Very likely[a]					
	Probable[b]	11				
	Possible[c]	6	1, 2			
	Remote[d]		5	4	3, 10	
	Unlikely[e]					7, 8, 9

[a] Almost certain to occur if conditions remain unchanged.
[b] Would not require extraordinary factors to occur at some time.
[c] Could occur at some time.
[d] May only occur under exceptional circumstances.
[e] Could only occur under a freak combination of factors.

Unacceptable (prevent)	Tolerable (mitigate)	Broadly Acceptable

The role of prevention techniques are to eliminate the possible causes for an explosion to occur; for example by ensuring the fuel/air mixture remains outside of its flammable limits, eliminating all potential sources of ignition source or through the use of inerting. The role of protection techniques are to mitigate the effects of an event (protecting people and property/plant), if it is not possible to prevent the event from occurring; for example by designing equipment to withstand explosion overpressures, isolating equipment from the explosion through the use of quick acting valves, suppressing the explosion by the addition of an inertant or by the use of explosion relief.

3.15.1. Firefighting Equipment

During testing in Rigs A, B, C, and D, two dry powder fire extinguishers were positioned outside the control room and were available to extinguish any fire within or outside the explosion chamber. For tests undertaken at the Spadeadam testing and research facility, a fire engine was available should any fire not be controllable through the use of fire extinguishers.

3.16. Operating Procedures

For each of the test rigs, there were six distinct phases to their safe operation, each of which was carried out in a consecutive manner, under the guidance of a written procedure. The phases were:

i. Pre-test instrumentation, data logging and safety checks.
ii. Gas filling and mixing.
iii. Ignition.
iv. Test rig purging.
v. Data check.
vi. Post-test safety checks.

The operational procedures for each of the test rigs are given in Appendix A.

3.17. Experimental Repeatability at Large-Scale

It has been identified previously, that at large-scale, there can be significant variations in the results obtained from two nominally identical experiments [369, 400, 401]. Given the importance of large-scale data in terms of understanding how pressure is generated in explosions, and in the development of guidance to industry and for explosion model evaluation, the HSE commissioned a series of large-scale experiments to study experimental repeatability [402].

There are several factors that can affect the severity of an explosion including the scale of the experiment, the geometry of the explosion chamber (including vent size and congestion arrangement), vent material and fixing, ignition location and fuel reactivity (including fuel type, concentration, oxidant and ambient conditions).

Typically, with large-scale experiments, there will be a small experimental variability in the fuel concentration and ambient conditions (including air temperature, atmospheric pressure and ambient humidity), which can have the effect of changing the average fuel equivalence ratio.

The experimental programme identified that significant variation in the peak overpressures measured at the same location in nominally identical experiments was possible but that the variations were not random across the pressure transducer locations and experiments. That is, if an experiment gave a relatively high peak overpressure at one transducer location compared to the other tests in the series, then the overpressures at all locations in that experiment tended to be higher than those in the other tests. These variations were attributable to shock waves being formed ahead of the flame front. The reflection of these shock waves by obstacles and regions of confinement, and the subsequent interaction with the flame front can produce peak overpressures that are highly variable. The global influence of these variable high pressure regions was considered to be the likely cause of any significant variability between nominally identical experiments. Variations in atmospheric conditions were not found to be of significance.

Confidential research undertaken by MRS [403] into the repeatability of large-scale confined vented explosions demonstrated that relatively slow explosions in empty chambers and explosions with idealised obstacle arrays typically produced overpressures that were within 10% of nominally identical experiments. However, explosions involving highly congested regions had the potential to produce significant variability in a manner similar to that described above.

The repeatability of tests during the experimental programmes is discussed at the relevant section of Chapters 4, 5 and 6. It is shown that, with the exception of one test, the results were within the 10% criteria discussed above.

CHAPTER 4
THE EFFECTS OF INTERCONNECTED ROOMS

CHAPTER 4

THE EFFECTS OF INTERCONNECTED ROOMS

4.1. Introduction

The current knowledge on the development of an explosion in single empty enclosures has been discussed in detail in the literature review (Sections 2.4, 2.5 and 2.6). Whilst a number of studies were found to have demonstrated that reducing the vent size and increasing congestion can affect the flame speed and increase overpressures, the confined and congested situation found in buildings, wherein both adiabatic expansion and turbulent flame acceleration play a role, has received little large-scale attention. Typical modern furnished dwellings will have a pathway, for flame propagation, through the whole structure to the outside, that consists of a number of interconnected rooms, each of which may have significant congestion as well as its own vent area providing relief.

It has been qualitatively recognised for over 45 years (Section 2.6) that the pressure generated by an explosion that propagates from one room to another may be significantly greater than that of a single room of similar volume. Consequently, quantitative experimental research that can develop the understanding of the effects of interconnected rooms on accidental gas explosions is of critical importance.

The experimental programme presented in this chapter represents a substantial body of research, the results of which will be of significant value, not only to those involved in gas explosion investigation, but to standards committees and parties interested in the design and construction of buildings. It details the results of 87 full-scale natural gas explosion tests carried out, on behalf of MRS, at the FRS explosion test facility.

4.2. Experimental Programme

Experiments were undertaken in the two interconnecting rooms at the FRS facility (Figure 3-6 and Figure 3-7). The ‘corridor’ in the explosion chamber was not used in any of the experiments although it was planned to be included in a later study (these plans were later abandoned due to budgetary constraints).

A number of nominally identical tests were undertaken to check repeatability (tests 1 and 2, 3 and 4, 6 and 7, 9 and 10). The results were within the 10% criteria discussed in Section 3.17, except for tests 6 and 7. The reason for this variation is discussed later

in this Chapter (layer variability). As there were a wide range of experimental test combinations used in the experimental programme, it was beneficial to consider the experimental programme as a number of test 'types', conducted in a series of tests. The test type refers to the configuration of the vents. The test types are numbered as follows:

I. Both enclosures had large vent areas of equal size.
II. The enclosures had different vent sizes. The ignition room (L) had a large vent area and the adjoining room (R) had a small vent area.
III. The enclosures had different vent sizes. The ignition room (L) had a small vent area and the adjoining room (R) had a large vent area.
IV. Both enclosures had small vent areas of equal size.

The test series referred to the specific size and location of the vent, the gas concentration in adjoining rooms, and the door type, latching mechanism and orientation. The classification of the types and series of tests is given in Table 4-1. Specific information on each test series is given in the introduction to Sections 4.4, 4.5, 4.6 and 4.7.

Table 4-1 Experimental test classification

Test No.	Test Type	Test series	No. Tests	Vent K_A	
				Ignition Room (L)	Adjoining Room (R)
1 – 22	I	A	22	2.4	2.4
23 – 29 & 42	II	B	8	2.4	4.0(l)
30 – 36	II	C	7	2.4	8.0
37 – 41	II	D	5	2.4	4.0 (r)
43 – 49	III	E	7	4.0 (r)	2.4
50 – 56	III	F	7	8.0	2.4
57 – 59	IV	G	3	4.0 (l)	4.0 (r)
60 – 68	III	H	9	4.0 (r)	2.4
69 – 70	IV	I	2	4.0 (l)	4.0 (r)
71 – 87	III	J	17	4.0	2.4

Table 4-2 Summary of experimental test conditions and results

Test No.	Test Series	Test Type	Gas Conc. (% v/v)		Layer or Full	Layer Depth (m)[a]	Ignition Position	Door Status	K_A		P_V (mbar)	P_{Max} (mbar)	
			Ign (L)	Adj (R)					Ign (L)	Adj (R)		Ign (P4)	Adj (P8)
1	A	I	8	8	Layer	1.2	Rear	Open	2.4	2.4	38	37	38
2	A	I	8	8	Layer	1.2	Rear	Open	2.4	2.4	39	39	39
3	A	I	10	10	Layer	1.2	Rear	Open	2.4	2.4	40	83	103
4	A	I	10	10	Layer	1.2	Rear	Open	2.4	2.4	41	82	85
5	A	I	10	10	Full	2.4	Rear	Open	2.4	2.4	41	138	145
6	A	I	12	12	Layer	1.2	Rear	Open	2.4	2.4	44	152	179
7	A	I	12	12	Layer	1.2	Rear	Open	2.4	2.4	44	76	83
8	A	I	10	10	Full	2.4	Rear	Open	2.4	2.4	44	152	152
9	A	I	10	10	Layer	1.2	Central	Open	2.4	2.4	47	47	47
10	A	I	10	10	Layer	1.2	Central	Open	2.4	2.4	46	44	46
11	A	I	8	8	Layer	1.2	Rear	Closed	2.4	2.4	39	45	48
12	A	I	10	10	Full	2.4	Central	Open	2.4	2.4	44	48	48
13	A	I	8	8	Layer	1.2	Rear	Closed	2.4	2.4	38	37	38
14	A	I	10	10	Layer	1.2	Rear	Closed	2.4	2.4	41	88	88
15	A	I	12	12	Layer	1.2	Rear	Closed	2.4	2.4	66	103	138
16	A	I	10	10	Layer	1.2	Central	Closed	2.4	2.4	47	52	62
17	A	I	10	10	Full	2.4	Rear	Closed	2.4	2.4	44	172	179
18	A	I	10	10	Layer	1.2	Rear	Closed	2.4	2.4	44	97	90
19	A	I	12	12	Layer	1.2	Rear	Closed	2.4	2.4	46	76	103
20	A	I	10	10	Full	2.4	Rear	Closed	2.4	2.4	36	131	138
21	A	I	10	10	Full	2.4	Central	Open	2.4	2.4	40	55	62
22	A	I	10	10	Layer	1.2	Central	Closed	2.4	2.4	40	48	55
23	B	II	8	8	Layer	1.2	Rear	Open	2.4	4l	44	55	62
24	B	II	10	10	Layer	1.2	Rear	Open	2.4	4l	46	83	90
25	B	II	8	8	Layer	1.2	Rear	Closed	2.4	4l	43	179	214
26	B	II	10	10	Layer	1.2	Rear	Closed	2.4	4l	55	317	400
27	B	II	10	10	Layer	1.2	Central	Closed	2.4	4l	55	179	269
28	B	II	12	12	Layer	1.2	Rear	Open	2.4	4l	44	117	145
29	B	II	12	12	Full	2.4	Rear	Closed	2.4	4l	41	172	172
30	C	II	8	8	Layer	1.2	Rear	Open	2.4	8	44	103	131
31	C	II	8	8	Layer	1.2	Rear	Closed	2.4	8	40	131	138
32	C	II	12	12	Layer	1.2	Rear	Open	2.4	8	46	110	152
33	C	II	12	12	Layer	1.2	Rear	Closed	2.4	8	47	138	234
34	C	II	10	10	Layer	1.2	Central	Open	2.4	8	47	152	200
35	C	II	10	10	Layer	1.2	Central	Closed	2.4	8	44	124	207
36	C	II	10	10	Layer	1.2	Rear	Closed	2.4	8	40	283	372
37	D	II	10	10	Layer	1.2	Central	Open	2.4	4r	55	62	76
38	D	II	10	10	Full	2.4	Central	Open	2.4	4r	57	97	117
39	D	II	10	10	Layer	1.2	Central	Closed	2.4	4r	51	103	172
40	D	II	10	10	Full	2.4	Rear	Closed	2.4	4r	41	303	338
41	D	II	10	10	Layer	1.2	Rear	Closed	2.4	4r	50	276	414

Test No.	Test Series	Test Type	Gas Conc. (% v/v)		Layer or Full	Layer Depth (m)[a]	Ignition Position	Door Status	K_A		P_V (mbar)	P_{Max} (mbar)	
			Ign (L)	Adj (R)					Ign (L)	Adj (R)		Ign (P4)	Adj (P8)
42	B	II	10	10	Full	2.4	Rear	Closed	2.4	4l	41	283	317
43	E	III	8	8	Layer	1.2	Rear	Closed	4r	2.4	41	276	234
44	E	III	10	10	Layer	1.2	Rear	Closed	4r	2.4	55	372	338
45	E	III	12	12	Layer	1.2	Rear	Closed	4r	2.4	41	207	207
46	E	III	10	10	Layer	1.2	Central	Closed	4r	2.4	46	76	83
47	E	III	10	10	Layer	1.2	Central	Open	4r	2.4	55	179	186
48	E	III	8	8	Layer	1.2	Rear	Open	4r	2.4	51	69	69
49	E	III	12	12	Layer	1.2	Rear	Open	4r	2.4	51	117	110
50	F	III	8	8	Layer	1.2	Rear	Open	8	2.4	50	103	83
51	F	III	10	10	Layer	1.2	Rear	Open	8	2.4	62	324	234
52	F	III	12	12	Layer	1.2	Rear	Open	8	2.4	47	159	138
53	F	III	8	8	Layer	1.2	Rear	Closed	8	2.4	55	317	276
54	F	III	10	10	Layer	1.2	Rear	Closed	8	2.4	59	462	462
55	F	III	12	12	Layer	1.2	Rear	Closed	8	2.4	48	214	193
56	F	III	10	10	Layer	1.2	Central	Closed	8	2.4	57	97	90
57	G	IV	10	10	Layer	1.2	Rear	Closed	4l	4r	52	159	166
58	G	IV	10	10	Layer	1.2	Rear	Closed	4l	4r	69	283	276
59	G	IV	12	12	Layer	1.2	Rear	Roller Latch	4l	4r	62	179	179
60	H	III	8	8	Layer	1.2	Rear	Roller Latch	4r	2.4	50	290	262
61	H	III	10	10	Layer	1.2	Rear	Roller Latch	4r	2.4	55	428	372
62	H	III	12	12	Layer	1.2	Rear	Roller Latch	4r	2.4	50	393	310
63	H	III	8	8	Layer	1.2	Rear	Fire Door - Unlatched	4r	2.4	50	331	283
64	H	III	10	10	Layer	1.2	Rear	Fire Door - Unlatched	4r	2.4	55	400	386
65	H	III	12	12	Layer	1.2	Rear	Fire Door - Unlatched	4r	2.4	48	407	379
66	H	III	10	10	Layer	1.2	Rear	Fire Door - Roller Latch	4r	2.4	55	501	455
67	H	III	10	10	Layer	1.2	Rear	Mortice Latch	4r	2.4	66	227	214
68	H	III	10	10	Layer	1.2	Rear	Fire Door - Mortice Latch	4r	2.4	72	331	317
69	G	IV	10	10	Layer	1.2	Rear	Fire Door - Roller Latch	4l	4r	14	138	152
70	G	IV	10	10	Layer	1.2	Rear	Fire Door - Roller Latch	4l	4r	83	331	359
71	J	III	8	10	Layer	1.2	Rear	Roller latch	4r	2.4	39	262	193
72	J	III	10	8	Layer	1.2	Rear	Roller latch	4r	2.4	55	400	338
73	J	III	8	12	Layer	1.2	Rear	Roller latch	4r	2.4	55	310	248
74	J	III	12	8	Layer	1.2	Rear	Roller latch	4r	2.4	50	241	193
75	J	III	10	12	Layer	1.2	Rear	Roller latch	4r	2.4	55	276	228

Test No.	Test Series	Test Type	Gas Conc. (% v/v)		Layer or Full	Layer Depth (m)[a]	Ignition Position	Door Status	K_A		P_V (mbar)	P_{Max} (mbar)	
			Ign (L)	Adj (R)					Ign (L)	Adj (R)		Ign (P4)	Adj (P8)
76	J	III	12	10	Layer	1.2	Rear	Roller latch	4r	2.4	50	352	283
77	J	III	6	13	Layer	1.2	Rear	Roller latch	4r	2.4	50	234	186
78	J	III	13	6	Layer	1.2	Rear	Roller latch	4r	2.4	41	290	241
79	J	III	6	10	Layer	1.2	Rear	Roller latch	4r	2.4	41	83	69
80	J	III	10	6	Layer	1.2	Rear	Roller latch	4r	2.4	52	345	276
81	J	III	10	10	Layer	0.3	Rear	Roller latch	4r	2.4	61	103	97
82	J	III	10	10	Layer	0.6	Rear	Roller latch	4r	2.4	58	221	186
83	J	III	10	10	Layer	1.2	Rear	Hinged into left room	4r	2.4	77	262	269
84	J	III	10	10	Layer	1.2	Rear	Hinged into L - 45°	4r	2.4	61	703	655
85	J	III	10	10	Layer	1.2	Rear	Hinged into L - 45°	4r	2.4	39	683	641
86	J	III	10	10	Layer	1.2	Rear	Hinged into L - 90°	4r	2.4	66	345	317
87	J	III	10	0	Layer	1.2	Rear	Roller latch	4r	2.4	44	234	166

[a] Layer depth from ceiling.

The following parameters were investigated in detail:

- gas concentration;
- distribution of the flammable gas/air mixture;
- depth of layer;
- vent opening dimensions and location;
- ignition position;
- the position, orientation and strength of the interconnecting door.

4.2.1. Gas Concentration

Tests were undertaken using the following natural gas/air mixtures:

- 6% gas in air (fuel lean, $\phi = 0.61$);
- 8% gas in air (fuel lean $\phi = 0.83$);
- 10% gas in air (near stoichiometric concentration, $\phi = 1.05$);
- 12% gas in air (fuel rich, $\phi = 1.30$); and
- 13% gas in air (fuel rich, $\phi = 1.42$).

As the development of the explosions were likely to be most marked with fuel/air mixtures slightly richer than stoichiometric, the majority of the explosion tests were undertaken with a concentration of 10% natural gas in air by volume.

4.2.2. Distribution of the Flammable Gas/Air Mixture

In most of the experiments, it was ensured that both of the rooms were filled with gas/air mixture to the same concentration. However, actual gas explosions occur in dwellings where circumstances are such that the gas concentration in neighbouring rooms may vary. Consequently, some of the later experiments were carried out with a different concentration in each of the enclosures. Moreover, in one of the experiments, one of the rooms was given a stoichiometric layer of gas/air mixture and the other room was kept free of gas.

4.2.3. Depth of Layer

In most of the experiments the mixture was distributed to form a high level layer that was half the height of the explosion chamber. Other experiments were conducted using layers of varying depth or with the enclosures completely filled with gas/air mixture.

4.2.4. Vent Opening Dimensions and Location

The façades of typical dwellings in the UK vary widely, ranging from small single fronted terraced houses to large detached double fronted houses. Consequently, it was necessary to consider a wide range of inadvertent explosion reliefs (i.e. a range of window configurations that are representative of common façades of UK dwellings). Therefore, vent coefficients, K_A, of 2.4, 4 and 8 were chosen for the experiments and used in different combinations. The combination $K_A = 8$ in both enclosures was not used as the developed overpressure may have damaged the explosion chamber.

4.2.5. Ignition Position

Two ignition positions were used for all of the experimental tests. The centre of the left room and the centre of the rear wall of the left room. No experiments were undertaken with ignition in the right enclosure.

4.2.6. Interconnecting Door

Experiments were undertaken with both a lightweight and heavyweight interconnecting door, and with the door in the open, partially open and closed positions. The door was normally hinged such that it would open into the adjoining (right) room. In a small number of tests, the door was hinged so that it would open into the ignition (left) room. In addition, in a small number of tests, different latch types were used to secure the door closed.

4.3. General Observations

In almost all of the experiments, the explosion overpressure-time profiles displayed pressure peaks similar to that of an explosion in a single compartment (Section 2.4.2 Figure 2-13); that is, pressure peaks related to the opening of the vent, the onset of burnt gas venting, the external explosion, acoustic and hydrodynamic instabilities and maximum flame area were observed.

In general terms, there were three dominant pressure peaks, not all of which were present in each test but each produced the maximum peak in one or more tests:

i. The first dominant pressure peak was always associated with the removal of one or both of the explosion relief vent panels (in either of the two enclosures) and its magnitude was equal to or slightly greater than the failure pressure of the vent panel. The pressure peak occurred, because initially, combustion was taking place in a totally confined enclosure and the expansion of the hot products of combustion generated a pressure rise. As soon as the vent covers failed, unburnt fuel/air mixture was allowed to escape through the openings causing the pressure to fall and giving rise to a pressure peak, P_V. Interestingly, in many of the type I tests, immediately after the P_V pressure peak, the pressure dropped rapidly to below ambient and then immediately increased to form a second positive peak that was approximately the same value as the negative pressure trough (i.e. if the pressure dropped to -10 mbar, it would then 'bounce back', with a compression wave, to form a peak of approximately +10 mbar [see Figure 4-4)]. The negative pressure phase is caused by the momentum of the outflow of unburnt gas/air mixture, which 'over-vents' the explosion chamber and as the explosion is still in its early stages, the expanding flame front does not generate sufficient pressure to maintain a positive pressure within the chamber. The difference in pressure across the vent opening subsequently causes air and unburnt gas/air mixture to flow back into the vessel which creates turbulence.
ii. The second dominant peak was caused by the external explosion in a similar manner to that of a single compartment explosion.
iii. The third dominant peak, which occurred in many of the explosion tests, and which was observed to produce the maximum pressure in many experiments, was found to be more complex in origin and significantly more variable in its magnitude. The generation of this pressure peak was found to arise from the complex interaction of the combustion in each of the two compartments. This mechanism is discussed in more detail in the next sections.

4.4. Type I Experiments

In the type I tests, undertaken as series A, both the left and right enclosures had the largest vent opening, with a K_A value of 2.4. In all the tests, the vent material used was 12.5 mm fibreboard. Essentially four groups of test were undertaken:

1 Open doorway:
    a. rear ignition,
    b. centre ignition.
2 Closed door:
    a. rear ignition,
    b. centre ignition.

For each of these groups of test, the effects of gas concentration and depth of layer were investigated.

4.4.1. The Effects of Gas Concentration

Test number 1 was undertaken with a layered natural gas/air mixture of 8% concentration (v/v) in each enclosure. The interconnecting doorway was open and ignition was in the rear position. The overpressure-time history is shown in Figure 4-1. The pressure measurements shown in the diagram were taken from pressure transducers P4 and P8. The pressure measurements taken from other transducers had similar profiles.

As the natural gas/air mixture was moderately lean in concentration, there was an initial, relatively slow pressure rise up to approximately 580 ms after ignition, followed by a rapid drop in pressure to below ambient (Figure 4-1). It can be seen that the maximum pressure was generated in the first pressure peak and was recorded at 38 mbar. The video footage showed that both enclosure vents began to fail simultaneously at 540 ± 40 ms and were clear of the vent openings approximately 80 ms later. The pressure peak of 38 mbar at 580 ms therefore corresponds to the vent opening and onset of venting. The flame reaches the plane of the vent opening at 900 ± 40 ms but no significant pressure rise was measured inside the explosion chamber (usually seen shortly after an external explosion). However, bulk oscillations about ambient pressure start very shortly afterwards, at approximately 1 s, and occur at a frequency of approximately 60 Hz. The pressure oscillations recorded for each enclosure appear to have an opposite phase indicating that there is bulk movement between rooms via the doorway. In general terms, the pressure-time profile was similar to that expected of an explosion of a lean mixture in a single enclosure with a similar vent opening and failure pressure.

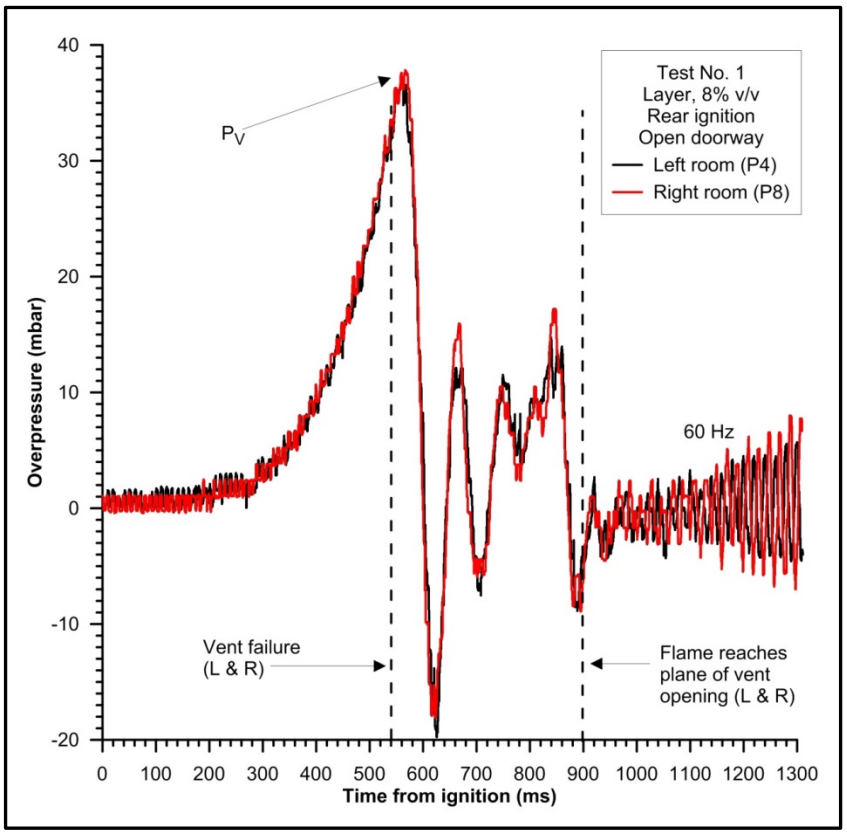

Figure 4-1 Overpressure-time profile for type I test (fuel lean, ϕ = 0.83)

The dominant pressure peak in the fuel lean layered tests generally corresponded to the failure of the vents and the onset of venting, with the external explosion being less influential. This was because the entrainment of air, as the unburnt fuel/air mixture was expelled from the vent openings, diluted the forming cloud to a point where it was either not flammable or the severity of the external explosion was not sufficient to generate further overpressure within the explosion chamber.

Figure 4-2 shows the pressure-time history for test number 4. Test number 4 was undertaken with a layered natural gas/air mixture of 10% concentration (v/v) in each enclosure. The interconnecting doorway was open and ignition was in the rear position. Consequently, the test was identical to test number 1 except the concentration was now slightly rich of stoichiometric. However, in comparison with the overpressure-time history of test number 1, there were a number of significant differences.

The initial pressure rise is considerably more rapid in this test because of the higher burning velocity associated with the near stoichiometric concentration. Observation of the video footage showed that both enclosure vents began to fail simultaneously at approximately 270 ± 40 ms (see Figure 4-3) and were clear of the vent openings approximately 80 ms later.

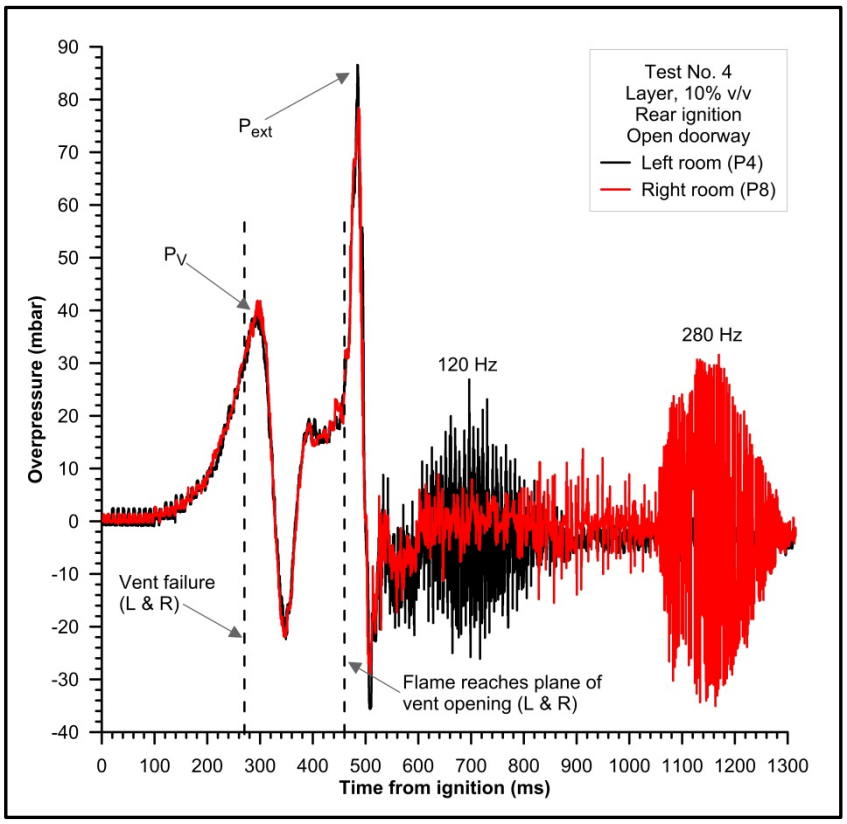

Figure 4-2 Overpressure-time profile for type I test (≈ stoichiometric, ϕ = 1.05)

However, as a consequence of the vent opening, and in a similar manner to test number 1, a rapid pressure drop to below ambient pressure occurred, giving rise to a pressure peak of similar magnitude (approximately 40 mbar) at 300 ms after ignition. Following this pressure drop to below ambient, a number of bulk gas oscillations occurred with flow reversal through the vent opening. However, these oscillations were interrupted by a sudden, very rapid pressure rise beginning at 460 ms, giving rise to a sharp pressure peak of 86 mbar at 480 ms. The video footage indicates that the flame reached the plane of both of the enclosure vent openings at 460 ms ± 40 ms (frame three of Figure 4-3). The sharp pressure peak therefore corresponds to the arrival of the flame at the vent openings and may be attributed to ignition of the flammable cloud expelled from the chamber during venting. In most of the tests observed during this series, there was a slight ‘dip’ in the overpressure-time profile just before the P_{ext} peak. This slight reduction in overpressure was caused by the onset of burnt gas venting.

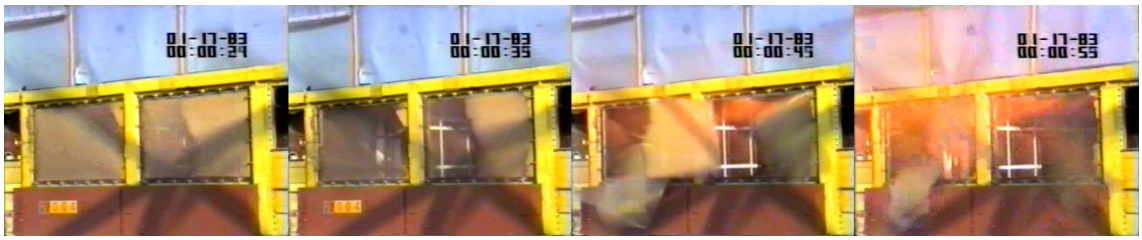

Figure 4-3 Photo sequence from onset of vent opening to external explosion (test No. 4)

Figure 4-4 shows the pressure-time history for test number 7. This test was undertaken with a layered natural gas/air mixture of 12% concentration (v/v) in each enclosure. The interconnecting doorway was open and ignition was in the rear position. Consequently, the test was similar to test numbers 1 and 4 except the concentration was now rich. The timing of vent failure and the flame reaching the plane of the vent opening was similar to that of the slightly rich mixture of stoichiometric test No. 4, with the maximum pressure peak occurring immediately after the flame front had reached the vent opening. This indicates that the pressure peak was caused by the external explosion. Perhaps surprisingly, the magnitude of the maximum pressure peak, caused by the external explosion was similar to that of test No. 4. Previous experimental work has shown that there is a direct correlation between the pressure inside the explosion chamber following an external explosion and increasing gas concentration [34, 35].

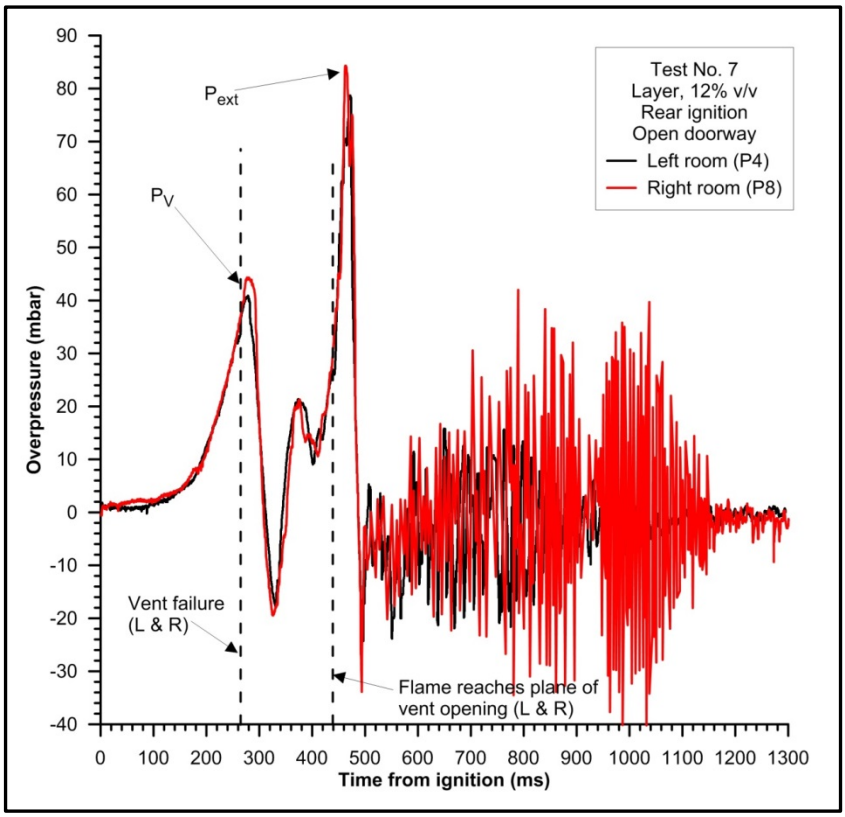

Figure 4-4 Overpressure-time profile for type I test (fuel rich, ϕ = 1.30)

The unburnt gas/air mixture entrains air as it is expelled through the vent opening and therefore stoichiometric mixtures are likely to be fuel lean when ignited by the explosion flame front and fuel rich mixtures are likely to be closer to stoichiometric. An identical test (test No. 6), produced a maximum pressure peak of 179 mbar in the right enclosure, which, in accordance with the previous work of Tite [34, 35], was greater than the results of the near stoichiometric tests.

The results of test number 7 may be understood when it is recognised that the layer of fuel/air mixture within the enclosures, prior to ignition, was only half full and consequently there may have been dilution of the mixture by air in the lower half of the enclosures in addition to entrainment of air during venting.

The effects of gas concentration on maximum overpressure for type I tests with rear ignition and no interconnecting door are summarised in Figure 4-5.

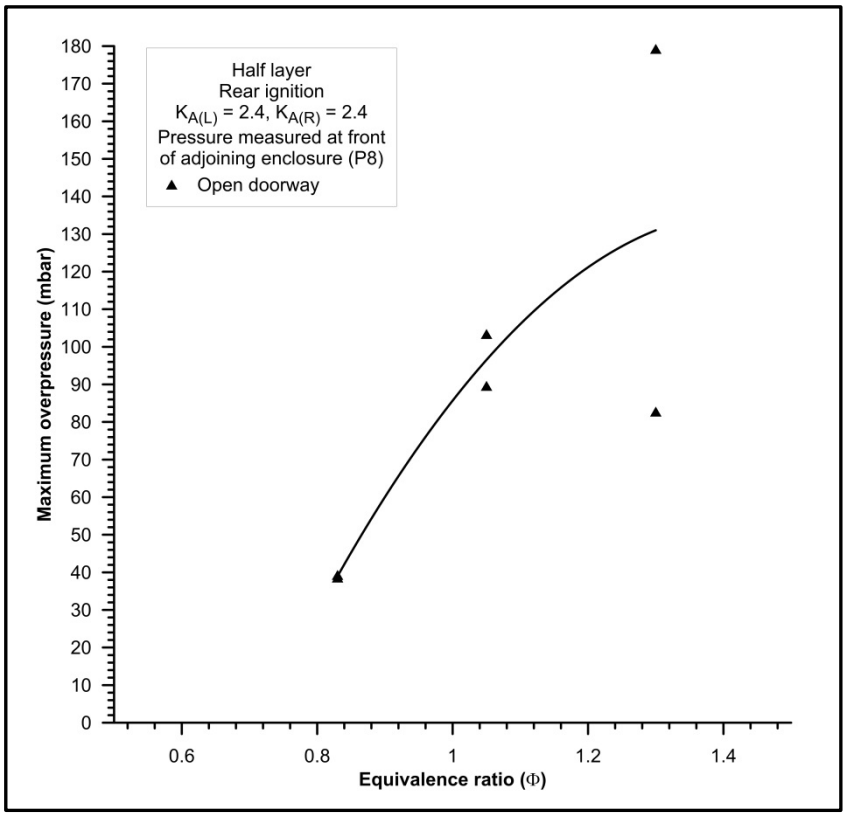

Figure 4-5 Maximum overpressure vs. gas concentration (type I tests, series A)

Interestingly, the maximum overpressure peak for the 8% gas concentration tests corresponded to the failure of the vents, resulting in an overpressure of 39 mbar, whilst both the 10% and 12% maximum peak pressure peaks were related to the external explosion, with maximum values measuring 103 and 179 mbar respectively. The results of the fuel rich tests (No's 6 and 7), show a difference in peak overpressure of 96 mbar. The reason for this has been described above.

4.4.2. The Effects of Layer Depth

The overpressure-time profile comparing half layer and full volume tests is shown in Figure 4-6. In this example, both enclosures contained a fuel/air mixture of 10% gas concentration, ignition was at the rear of the chamber and the doorway was open. It can be noticed that whilst the profile of the two tests are similar (except for the oscillatory combustion), the magnitude of the pressure peaks and the time at which they occur is significantly different. It is clear from the overpressure-time profile that the rate of pressure rise during the early stages of the explosion (up until vent failure) is greater in the full volume test. Furthermore, in the full volume test, the flame arrives at the vent opening sooner (≈ 400 ms vs. 505 ms) indicating that the flame speed was also faster. The rate of pressure rise and flame speed are directly proportional to the flame surface area. In the half layer tests, ignition was initiated in the left chamber, at the centre of the rear wall; a height, which is at the flammable mixture–air interface. Consequently, during the early stages of the explosion, the expanding flame front would have started to propagate in the shape of a quarter-sphere whilst the full volume flame would have propagated in a hemispherical shape. Accordingly, the total surface area of the flame would have been significantly greater in the case of the full volume test, and this is demonstrated by the shorter time taken for the flame front to arrive at the vent opening.

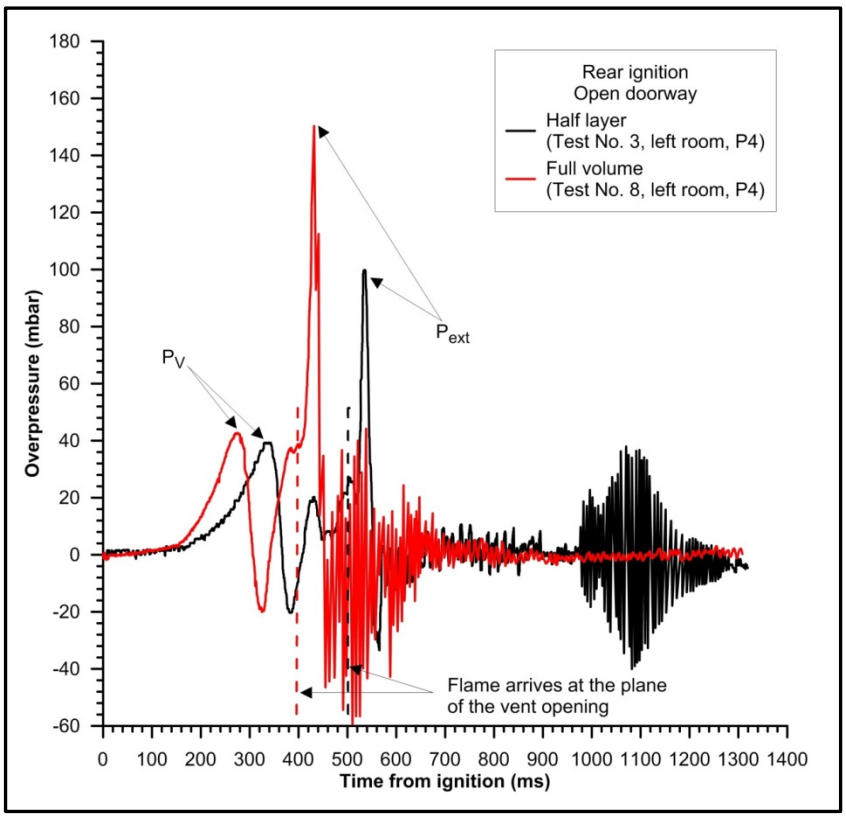

Figure 4-6 The effects of layer depth (type I, series A)

The difference in magnitude of the P_{ext} pressure peak may be explained by a reduction in gas concentration and hence flame speed. Firstly, as the flame propagates through the half layer within the enclosures, the bunt gases expand creating flow. This flow, causes the air in the lower half of the chamber to mix with the fuel/air mixture, diluting its concentration. Secondly, further dilution takes place as the mixture entrains air as it is expelled through the vent opening. It was demonstrated in Chapter 2 that the greatest burning velocity, and hence most violent explosion, occurs just rich of stoichiometric; so it is logical to assume that the greatest overpressure generated outside the chamber will occur with the ignition of a slightly rich flammable cloud. This concentration is more likely to have occurred with a full volume than that of a half layer, and this is demonstrated by the difference in magnitude of the P_{ext} overpressure peaks. It would have been desirable to have a transient record of the changing concentration of the external flammable cloud, but this was outside the scope of this study.

4.4.3. The Effects of Ignition Position

Figure 4-7 shows the overpressure time profile of test number 10 in which a 10% natural gas half layer was ignited at the centre ignition position. No interconnecting door was present. When compared to similar tests with rear ignition, the initial rate of pressure rise in the central ignition test was higher due to the increased flame surface area as the flame propagated hemispherically (centre ignition position is at the mixture/air interface for half layer tests). The rate of pressure rise should be similar to that of a full volume rear ignition test as the flame surface area would, in theory, be similar. Observation of the overpressure-time profile of test number 8 (Figure 4-6) confirms that this theory is correct as the P_V peak occurred at around 280 ms for both tests and there was only a 2 mbar difference in magnitude.

In central ignition tests, a single, sharp P_{ext} pressure peak was not observed. Instead, two separate pressure peaks, generally smaller in magnitude [labelled $P(L)_{ext}$ and $P(R)_{ext}$ in Figure 4-7] occurred, separated by 40 – 50 ms. The observation that the magnitude of the P_{ext} pressure peak was smaller than that associated with rear ignition tests was in agreement with the findings detailed in Chapter 2, where it was illustrated that with central ignition, much less unburnt gas is expelled before the flame front reaches the vents. This is because the flame propagates away from the point of ignition, trapping a quantity of the unburnt gas/air mixture behind the expanding flame front, towards the rear of the chamber. Hence the external cloud is much smaller than in the rear ignition case where a large quantity of unburnt gas/air mixture is expelled ahead of the expanding flame front, and combustion of this smaller cloud gives rise to a much lower maximum overpressure.

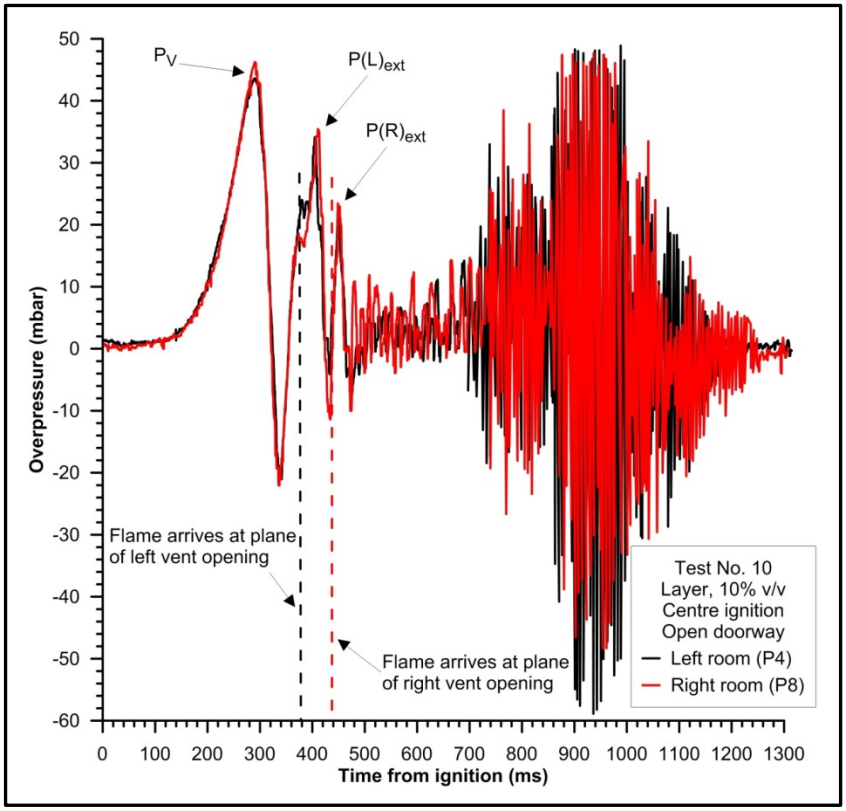

Figure 4-7 Overpressure-time profile for type I test (central ignition)

The two pressure peaks $P(L)_{ext}$ and $P(R)_{ext}$ were recorded by the pressure transducers in both enclosures and occurred immediately after the flame front had reached the left vent and right vent respectively. Observation of the video records showed that there appeared to be two external explosions separated by a short time interval (40 to 50 ms) and this was in agreement with the pressure peaks observed in the overpressure-time profiles. The $P(L)_{ext}$ pressure peak originated from ignition of the unburnt cloud expelled mainly from the vent in the left enclosure, by the flame front as it jetted out of the left vent opening. The $P(R)_{ext}$ pressure peak corresponded to ignition of the unburnt cloud outside the right vent opening. It was not within the scope of this project to determine the actual cause of this mechanism, but it is possible that two separate flammable clouds were formed outside the enclosures, which were separated by a non-flammable gap. Consequently, the flammable clouds were ignited by the flame fronts exiting from each of the enclosures. It is also possible that the expelled flammable cloud from the left vent opening had sufficient momentum to carry it clear of the explosion chamber, preventing the immediate ignition of the unburnt mixture subsequently expelled from the right vent. This second external cloud would then have been ignited some 40 to 50 ms later, by the jetting flame front exiting the right vent opening, and giving rise to the pressure peak $P(R)_{ext}$.

Centre ignition in a type I experiment with both chambers full of a 10% natural gas/air mixture (test number 12) gave rise to a slightly greater rate of pressure rise when compared to half layer tests and slightly larger $P(L)_{ext}$ and $P(R)_{ext}$ pressure peaks. The increased magnitude is in part due to the increased surface area of the spherical flame front but also to the dilution effects associated with a layer that were discussed in Section 4.4.2.

4.4.4. The Effects of an Interconnecting Door

In tests undertaken where an interconnecting door was present, there were some noticeable differences in the overpressure time profiles. Figure 4-8 shows the overpressure-time profile of the right enclosure for test number 14 and Figure 4-9 shows both the left and right enclosure profiles for comparison. In this test a 10% natural gas/air half layer was ignited at the rear ignition position, with the lightweight door in the closed position. The door was pushed closed but was not latched at the time of ignition.

It can be observed from the diagrams that the overpressure-time profiles were significantly different from profiles with an open doorway. Whist, the first pressure peak, P_V, corresponded to the simultaneous failure of both the vents, and was of a similar magnitude (41 mbar) to tests with an open doorway, the second major pressure peak, P_{ext}, was completely different in profile.

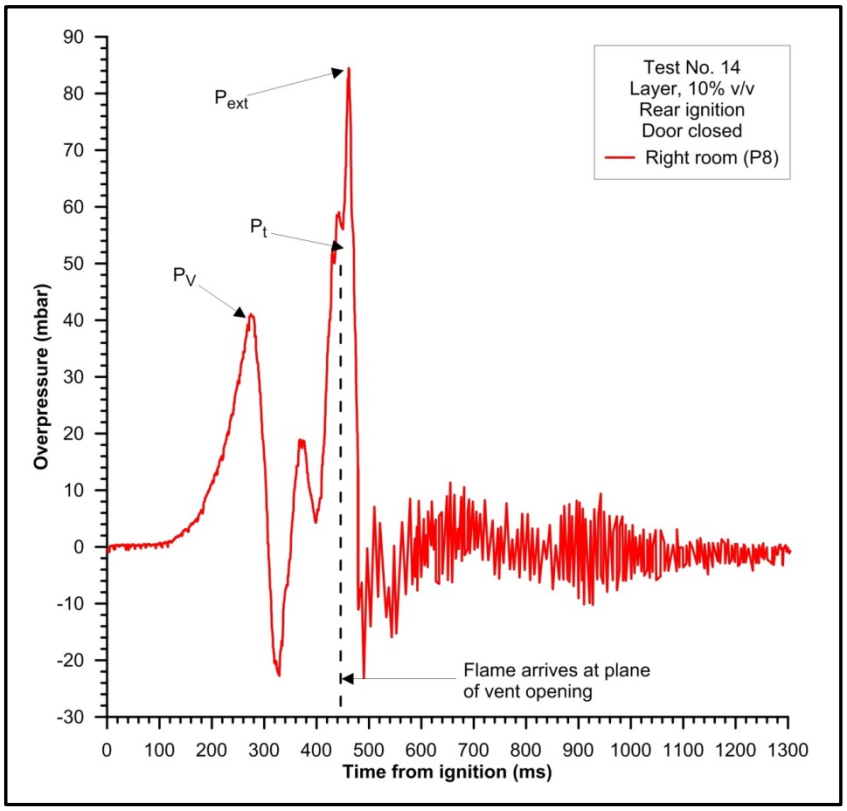

Figure 4-8 The effects of an interconnecting door (type I test, right room)

The pressure rise leading to P_{ext} was considerably slower than in the open door experiments, leading to a peak of approximately twice the duration. A sharp pressure spike, immediately preceded by a slight fall, was superimposed on this broad peak, attaining a maximum pressure of 88 mbar, so the peak was similar in magnitude to those recorded in the open doorway tests. The flame front was observed at the plane of the vent openings at 450 ms after ignition, which was some 40 to 50 ms after the start of the broad duration peak, coinciding with the slight fall in pressure immediately prior to the sharp spike. This indicates that the fall in pressure corresponded to the onset of burnt gas venting and that the spike that was superimposed onto the broad pressure peak was the P_{ext} peak caused by ignition of the cloud of unburnt mixture expelled from the vent openings. However, the cause of the broad pressure peak must be caused by another mechanism. The overpressure time profiles of the left and right enclosures are shown in Figure 4-9.

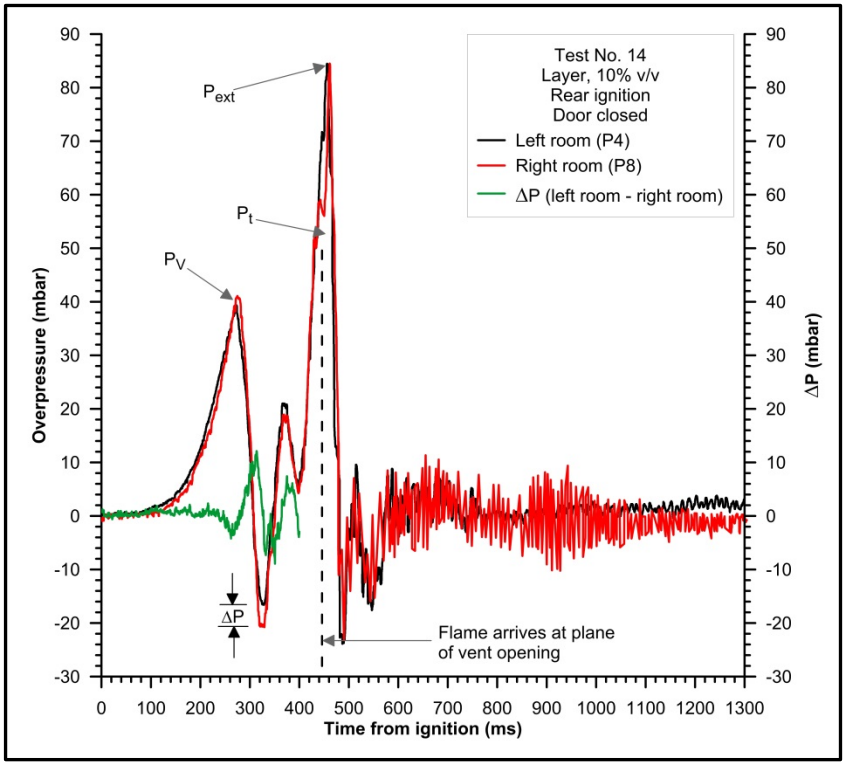

Figure 4-9 The effects of an interconnecting door (left and right rooms)

Although the pressure-time profiles for the two enclosures are very similar, there are time periods where there are differences in magnitude that reflect the development of the explosion and, when the status of the door permits, indicate that there is flow from one room to another. The difference in pressure between the two enclosures is shown from ignition to 400 ms as the plot, ΔP, on the secondary Y axis in Figure 4-9. During, the initial stage of the explosion, the expanding flame kernel in the ignition enclosure caused the pressure to rise but did not increase the pressure in the adjoining room as

the door was initially closed. Examination of video records shows that at approximately 150 ms after ignition, the interconnecting door began to swing open into the right enclosure. The overpressure time profiles indicate that the pressure differential at that time was in the order of a few mbar, which was sufficient to overcome the inertia of the lightweight door that was not latched. Consequently, there was a mass flow of unburnt gas/air mixture from the left enclosure into the right enclosure which caused the pressure to rise until it equalised across the two rooms. The process of the door swinging open and the subsequent mass flow into the right enclosure created turbulence, which caused an increase in the burning velocity and a mass combustion rate that was greater than that of the initially quiescent stage of combustion in the left enclosure.

In addition to this effect, the propagating flame front would have become ‘stretched’ as it approached the interconnecting doorway and propagated into the adjoining room. Because of the turbulence in this room and because of the increased surface area of the flame front caused by distortion as it passed through the doorway, a rapid rise in combustion rate would have occurred, resulting in a significant increase in pressure. This pressure rise would clearly have occurred before the flame front reached the vent openings and that is demonstrated in the rapid increase in pressure which commenced at 400 ms after ignition. The broad part of this pressure peak has been labelled P_t to reflect the turbulent combustion, but it is also clear from the overpressure-time profiles, and the video records, that the external explosion also contributes to the magnitude of the pressure peak. Consequently, they are both marked on the diagrams.

In order to investigate the effect of the door opening, the pressure differential between the enclosures and the volume flowrate though the doorway (from the time the door opened until the flame front reached the doorway), are plotted in Figure 4-10. The volume flowrate has been calculated using the equation for the flow through an orifice [Equation (2-43)], taking the pressure differential across the door from the overpressure-time profiles. As the position of the door was not accurately known, it has been assumed to be fully open for the purposes of the calculations.

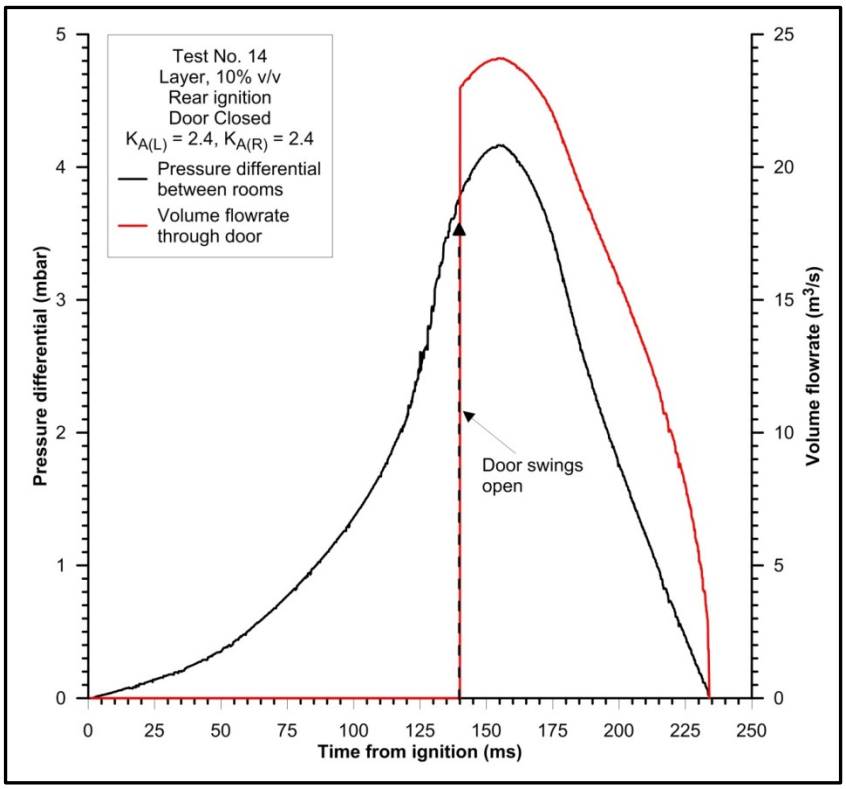

Figure 4-10 Potential volume flowrate though open doorway (test 14)

It can be seen that the maximum flowrate that could have passed through a doorway that opened instantaneously would have been 24.5 m^3/s. Correspondingly, the calculated maximum velocity through the doorway would have been 16 m/s. As some flow would have been directed towards the partition wall, the mean velocity, U, may be determined by multiplying the maximum flow velocity by the door area blockage ratio, ABR (0.174), giving a mean velocity of 2.8 m/s towards the partition wall. If the open doorway is assumed to be a large grid type obstacle, then Equation (2-64) may be used to calculate the turbulence intensity. The C_T value required in Equation (2-64) was calculated to be 0.225, based on the t/d ratio for the door opening (Section 2.5.3), and the pressure loss coefficient, K, also required in Equation (2-64), was determined using Equation (2-66), assuming a C_d value of 0.61. The turbulence intensity, u′/U was calculated to be 0.22, giving a root mean square (rms) of the fluctuating component of velocity, u', a value of 0.63 m/s. This clearly demonstrates that turbulence is being generated. Similar values of turbulence were calculated for the peaks at 320 ms and 360 ms.

It should be noted that there are some assumptions used in the above calculation of the turbulence within the right enclosure that are not strictly valid but are representative of the levels of turbulence within the room for comparative purposes. The calculation assumes that the flame front is fully developed within the left enclosure and just about to enter the right enclosure. This is not an accurate representation of the condition as

the explosion involved a layer of flammable/air mixture and the flame would not have been fully developed. However, as the same assumption will be made for three of the test types, the calculations provide a sufficient accuracy for comparative purposes.

In general terms, explosions involving less reactive mixtures, provided sufficient time for turbulent combustion to develop in the secondary enclosure before the flame arrived at the vent opening, and consequently P_t tended to dominate. However, in the faster flame speed tests (ϕ = 1.05), the flame front reached the vent opening before combustion of the turbulent mixture at the rear of the enclosure and P_{ext} tended to dominate.

In a few tests involving more reactive mixtures, the flame arrived at the plane of the vent opening after the P_t peak and there was no significant P_{ext} peak produced (Figure 4-11). In these tests, the flame front reached the doorway at approximately the same time as the vents failed. This resulted in the flame front in the right enclosure being distorted towards the vent opening.

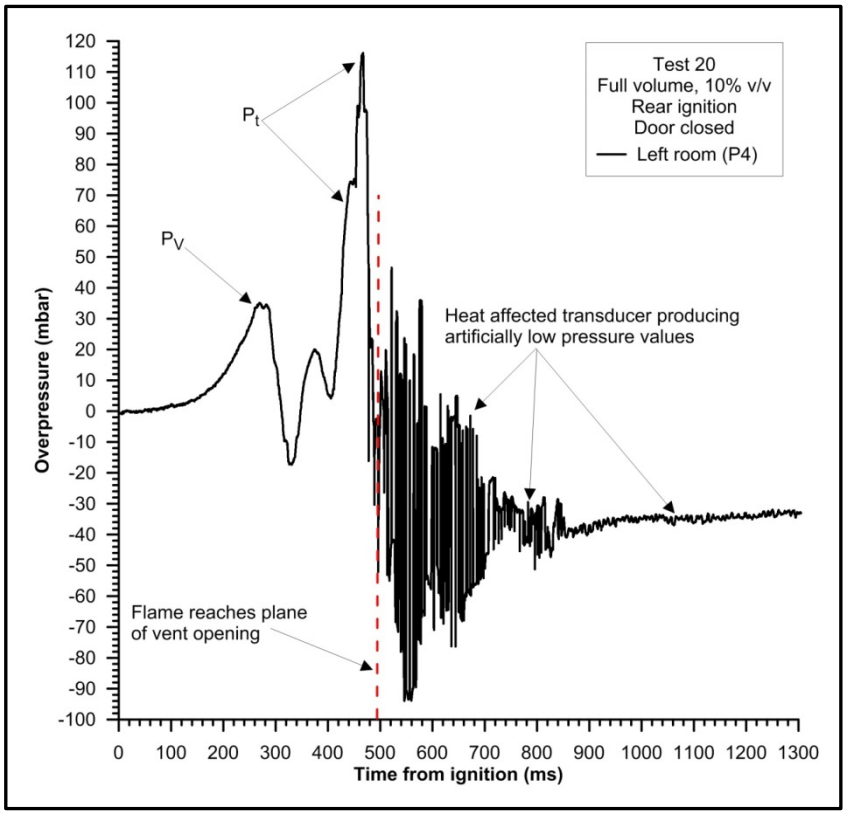

Figure 4-11 Overpressure-time profile showing late flame arrival at the vent

4.4.5. Proposed Mechanism for Explosion Development

Whilst the turbulent combustion mechanism noted in these tests was extremely important (in terms of explosion development), and occurred in all tests where a door was present, it did not result in a maximum pressure greater than that observed in the open doorway tests. A proposed mechanism for the type I tests with a closed door is given in Figure 4-12.

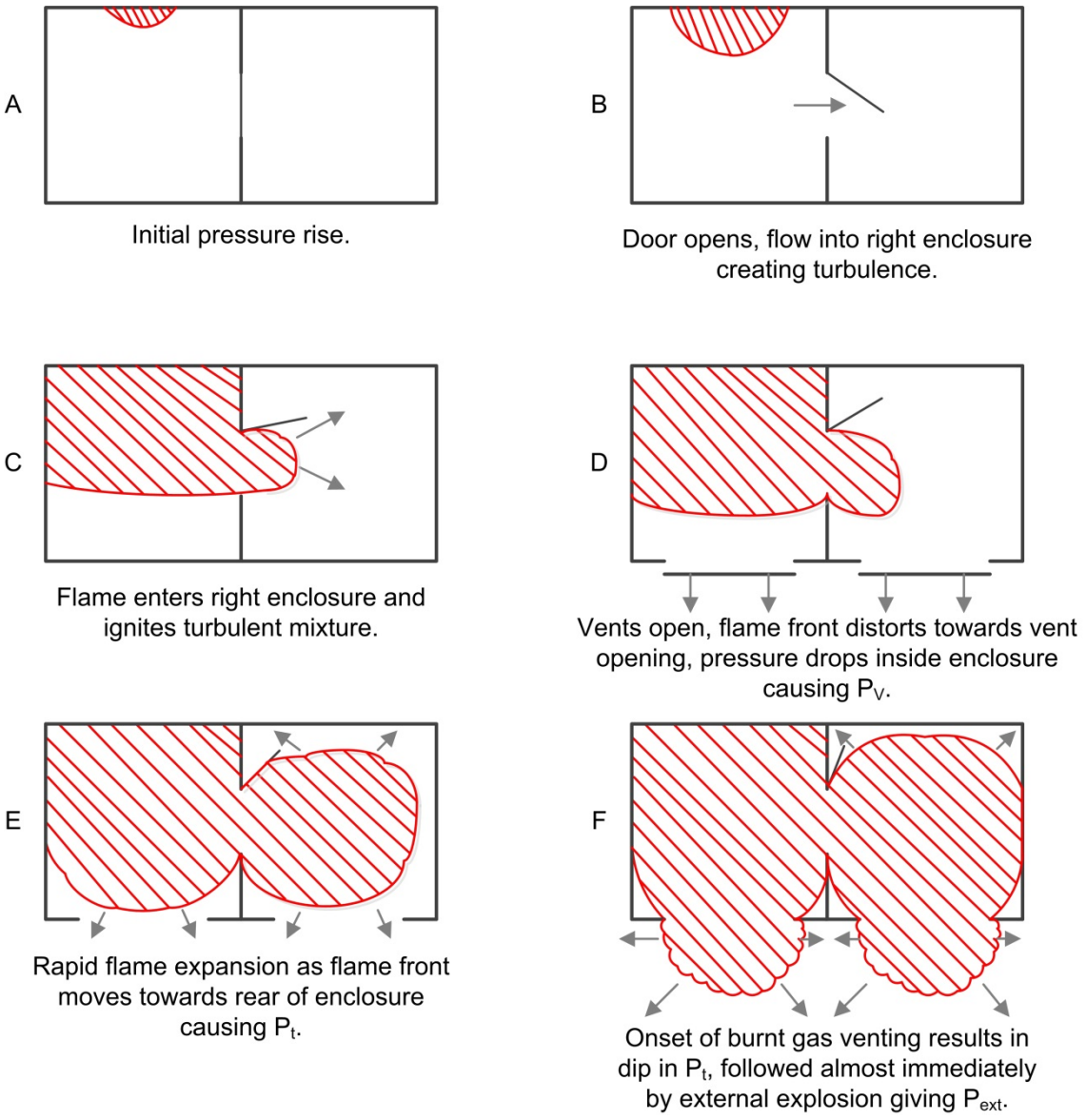

Figure 4-12 Proposed mechanism for type I tests (door closed)

4.4.6. Summary of Findings of Type I Tests

With the exception of some tests involving fuel lean layers, the overpressure-time profiles were characterised by two dominant pressure peaks. The first of these peaks, occurred in all tests and corresponded to the failure, often simultaneously, of the explosion vents. The second peak corresponded to either the external explosion or turbulent combustion as a consequence of the interaction between adjoining rooms.

In tests where there was an open doorway, the second dominant peak tended to correspond to the external explosion. The magnitude of the pressure peak generated by the external explosion was comparable to previous experiments conducted in a single compartment of the same explosion chamber [179]. It therefore appears that the adjoining room does not have a significant effect on the overpressure if there is an open doorway between the rooms and the vent areas are similar in both enclosures.

The situation in which a closed interconnecting door was present between the enclosures, may be considered as two adjoining rooms connected via a very low failure pressure vent. In experiments of this scenario, the delayed opening of the door caused a pressure differential to develop between the rooms, which initiated flow from the ignition room (L) to the adjoining room (R) when the door swung open. The action of the door swinging open and the flow between the rooms (until the pressure equalised) generated turbulence, which resulted in a rapid pressure rise (P_t) once combustion was established. In some instances (12% layer, or 10% full volume), the flame arrived at the plane of the vent opening after the P_t peak and there was no significant P_{ext} peak produced, and consequently, P_t dominated.

In vented explosions, any parameter that affects the rate of mass combustion can influence the development of the explosion. Varying the gas concentration, layer depth and ignition position all influenced the overpressure-time profiles. As each of the above parameters alter the mass burning rate, either by changing the burning velocity (concentration) or the flame surface area (layer depth and ignition position), they each affect the rate of pressure generation and its magnitude. Thus, altering any of the parameters influenced the time taken, from ignition, to reach the first pressure peak. Furthermore, all three parameters affected the magnitude of the P_{ext} pressure peak because they each influenced the size and composition of the external cloud.

A summary of the time taken for vent failure, the maximum overpressure generated and the dominant mechanism for the maximum pressure peak is given in Table 4-3.

Table 4-3 Summary of type I test conditions and results

Test No.	Gas in air (% volume)		Layer or Full	Layer Depth (m)	Ignition Position	Door Status	Time taken for flame to reach vent (ms)	Max Pressure (mbar)	Dominant Peak
	Ign (L)	Adj (R)							
1	8	8	Layer	1.2	Rear	Open	540	38	P_V
2	8	8	Layer	1.2	Rear	Open	580	39	P_V
3	10	10	Layer	1.2	Rear	Open	330	103	P_{ext}
4	10	10	Layer	1.2	Rear	Open	270	85	P_{ext}
5	10	10	Full	2.4	Rear	Open	250	145	P_{ext}
6	12	12	Layer	1.2	Rear	Open	275	179	P_{ext}
7	12	12	Layer	1.2	Rear	Open	250	83	P_{ext}
8	10	10	Full	2.4	Rear	Open	250	152	P_{ext}
9	10	10	Layer	1.2	Central	Open	260	47	P_V
10	10	10	Layer	1.2	Central	Open	270	46	P_V
11	8	8	Layer	1.2	Rear	Closed	450	48	P_t
12	10	10	Full	2.4	Central	Open	260	48	P_{ext}
13	8	8	Layer	1.2	Rear	Closed	480	38	P_V
14	10	10	Layer	1.2	Rear	Closed	260	88	$P_t + P_{ext}$
15	12	12	Layer	1.2	Rear	Closed	180	138	P_{ext} [a]
16	10	10	Layer	1.2	Central	Closed	240	62	P_{ext}
17	10	10	Full	2.4	Rear	Closed	250	179	P_{ext}
18	10	10	Layer	1.2	Rear	Closed	280	97	P_{ext}
19	12	12	Layer	1.2	Rear	Closed	260	103	P_t [a]
20	10	10	Full	2.4	Rear	Closed	260	138	P_t
21	10	10	Full	2.4	Central	Open	250	62	P_{ext}
22	10	10	Layer	1.2	Central	Closed	240	55	P_{ext}

[a] Test ignited with Ce-Mg fuses – failed to ignite with spark.

4.5. Type II Experiments

The type II tests, undertaken as series B, C and D, had a larger vent in the left (ignition) enclosure, $K_{A(L)} = 2.4$, and the right enclosure had a smaller vent:

- Series B, $K_{A(R)} = 4(l)$ (i.e. the vent was fitted in the left side of the fascia panel).
- Series C, $K_{A(R)} = 8$ (fitted to the centre of the fascia panel).
- Series D, $K_{A(R)} = 4(r)$ (i.e. the vent was fitted in the right side of the fascia panel).

In all the tests, the vent material used was 12.5 mm fibreboard. Similarly to type I tests, the same four group of tests were undertaken by varying the ignition and door position. For each of these groups of test, the effects of gas concentration and depth of layer were investigated.

4.5.1. Proposed Mechanism for Explosion Development

Figure 4-13 shows the overpressure-time profile for test number 26. In this test, a 10% natural gas half layer was ignited at the rear ignition position and the doorway was closed with an unlatched lightweight door. Figure 4-13 shows the profile for the both enclosures separately, with a further plot to show the two curves superimposed. It also shows the difference in overpressure between the two enclosures (ΔP on the Y axis). Though at first glance, the overpressure-time profile looks very similar to that of the type I profile, there are a number of significant differences.

Whilst in the type I tests the first pressure peak was caused by the simultaneous failure of both vents (in most tests), the first pressure peak in the type II test corresponded to the failure of the left vent ($K_{A(L)} = 2.4$) only. Measuring 55 mbar, it was also appreciably greater in magnitude. The second dominating pressure peak measured 400 mbar in test 26, which is over double the highest value attained in any type I experiment.

In the very early stages of the layered explosion (< 50 ms), the flame front begins to propagate in the shape of a quarter-sphere and a slight pressure differential is developed between the rooms, caused by the presence of the closed door. This continued to build and at approximately 180 to 200 ms the inertia of the door was overcome by the pressure differential and the interconnecting door swung open, allowing unburnt gas/air mixture to flow into the right enclosure. The action of the door swinging open and the flow into the room generated turbulence. At approximately 220 ms, the pressure had equalised between the two compartments and flow between them would have ceased. A proposed mechanism, generalising the events observed in the type II tests is given in Figure 4-14.

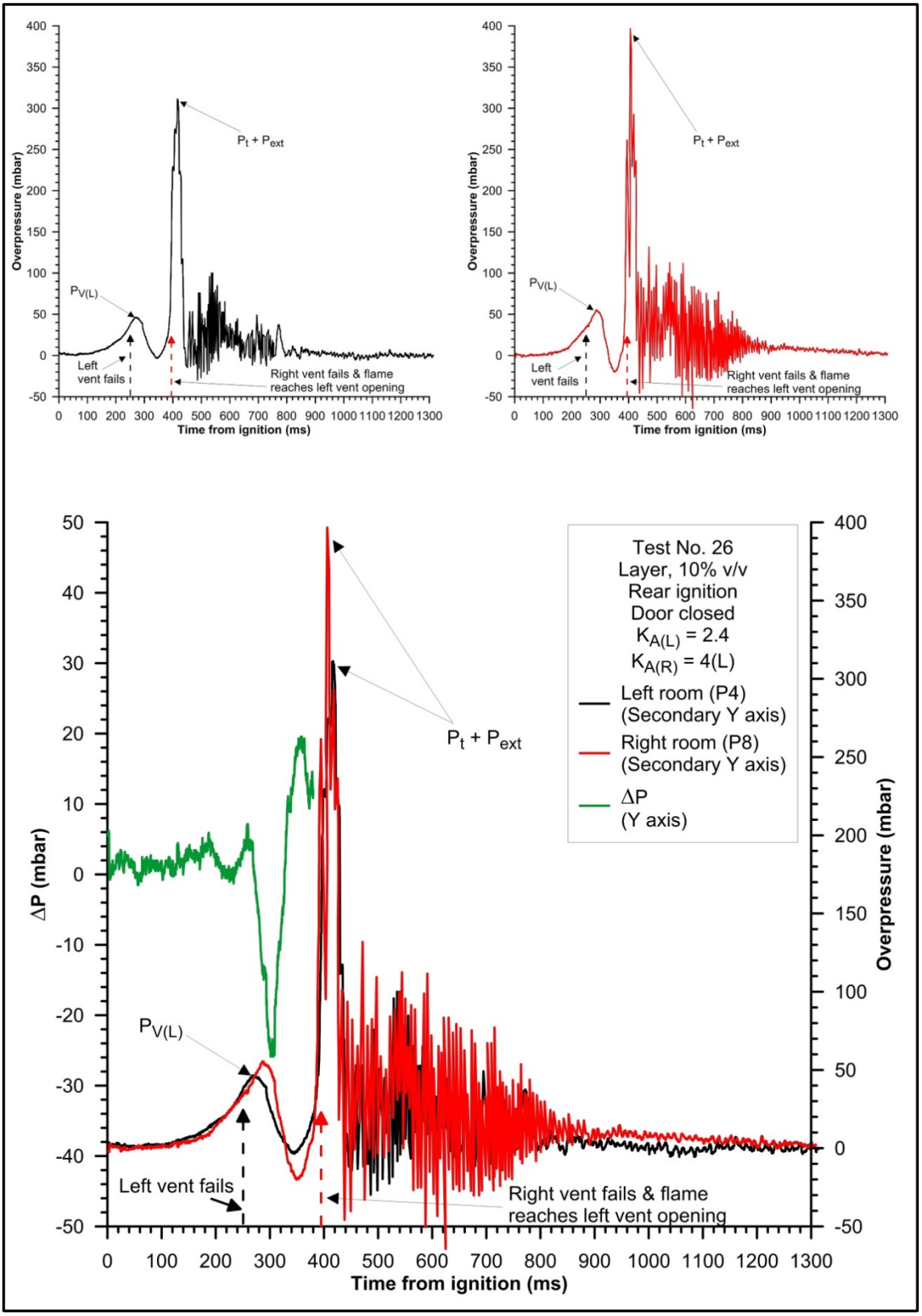

Figure 4-13 Overpressure-time profiles for type II test

At 250 ms the pressure in the enclosure was of sufficient magnitude that the left enclosure vent failed, allowing unburnt gas/air mixture to be rapidly expelled, giving rise to the pressure peak $P_{V(L)}$ in the left enclosure some 20 ms later, with a magnitude of 48 mbar. The expanding flow, distorts the flame front in the left room (ignition) towards the doorway such that at a similar time to the vent failure, combustion has begun in the right enclosure. The right enclosure vent, being smaller in size, had a greater failure pressure and remained intact at this time. The pressure in the left enclosure then dropped, passing through ambient at 350 ms and, as it was very early in the explosion, reaching a slightly negative value due to over-venting. Combustion in the right enclosure was rapid at this point, due to the turbulent mixture, so the pressure in the right enclosure continued to rise after $P_{V(L)}$ had occurred in the left enclosure, producing a $P_{V(L)}$ pressure peak in the right enclosure at approximately 290 ms, with a value of 55 mbar. Thus $P_{V(L)}$ occurred 20 ms later in the right enclosure than in the left. As a positive pressure differential had now developed between the right enclosure and the left enclosure, the flow reversed through the doorway and the flame front was ‘pulled’ back towards the door. The sudden venting of the right enclosure into the left, caused the pressure to drop to 20 mbar below ambient at 350 ms, whilst the pressure decrease in the left enclosure was less marked because the venting losses were somewhat offset by the inward flow from the right enclosure. It is clear to see, that even in these early stages of the explosion, the mechanism is extremely complex with flow reversing between the rooms, and into and out of the enclosure, as the pressure differential changed. This would have generated significant turbulence.

Whilst the venting of the right room was occurring, at approximately 330 ms, the pressure differential had now reversed again which caused the flow to reverse through the doorway into the right enclosure. The pressure in both rooms then began to rise again, slightly faster in the right enclosure, so that at 390 ms the pressures had again equalized. At this point, combustion of a highly turbulent mixture in the right enclosure was fully established. The very rapid combustion, coupled with the restricted venting through the doorway, caused a very rapid rise in pressure to occur, such that at 400 ms the right vent failed. Examination of the video records indicated that the flame front first appeared at the left hand vent immediately after the start of the second peak and this initiated the external explosion. Thus a significant pressure peak was generated, which was somewhat higher in the right enclosure than the left, and was attributed to both turbulent combustion and the external explosion. The pressure peaks were measured as 400 mbar in the right enclosure and 317 mbar in the left.

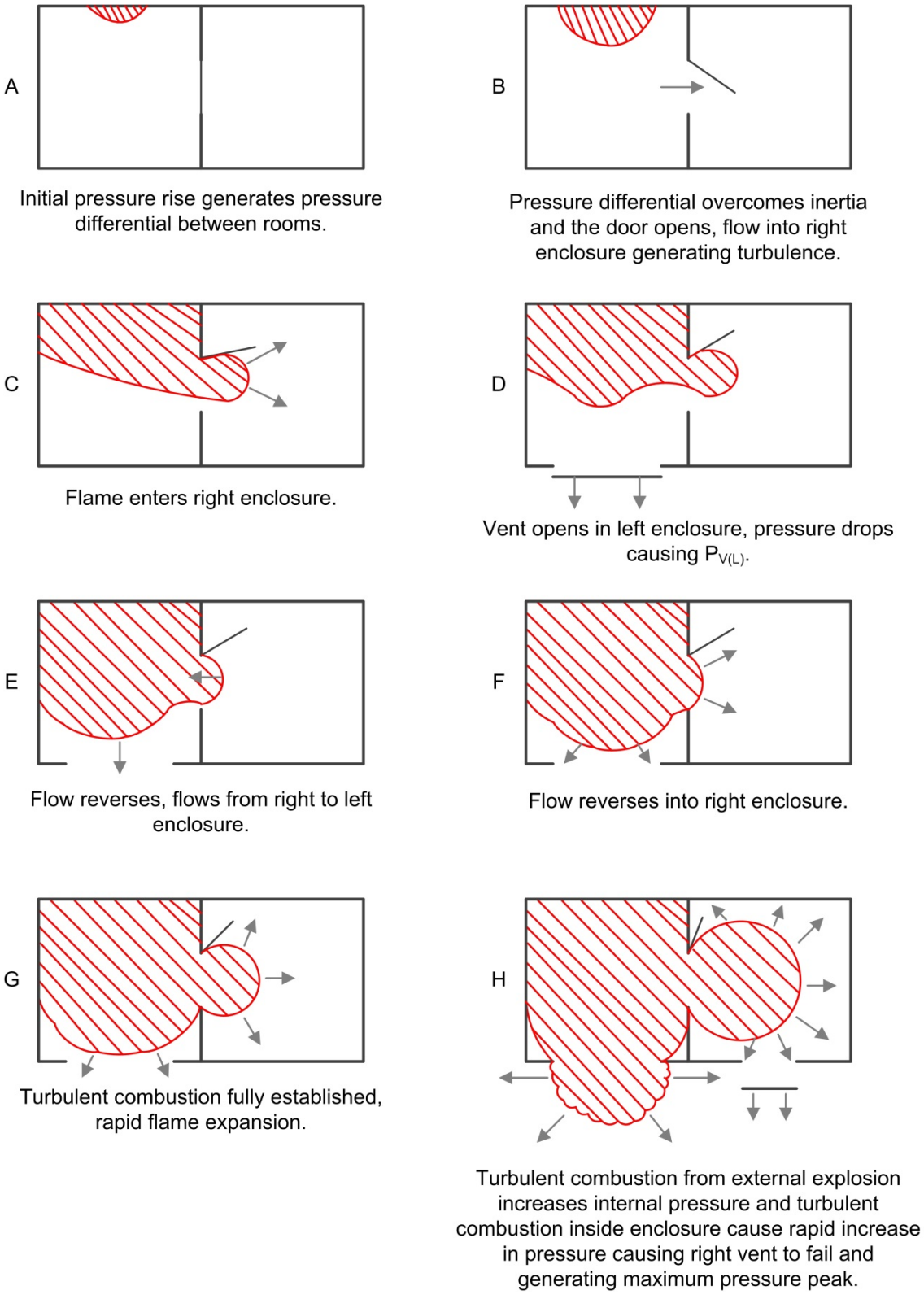

Figure 4-14 Proposed mechanism for type II tests (rear ignition, door closed) (adapted from the observational notes of Skippon and Field [404])

The video records and overpressure-time profiles for type II tests demonstrate that whilst the external explosion plays an important role in the development of the maximum explosion overpressure, the dominating factor was the turbulent combustion. The effect of this turbulent combustion was significantly more influential than in the type I experiments, because it takes place under a much higher degree of confinement. In the type I experiments the right enclosure is relieved through the doorway and the $K_{A(R)}$ = 2.4 right vent during the whole of the turbulent combustion phase, whilst in the type II experiments, relief occurs only through the doorway, and at a late stage through a much smaller $K_{A(R)}$ = 4 or $K_{A(R)}$ = 8 vent. Furthermore, a series of flow reversals created a significantly greater degree of turbulence than would have been generated in the type I experiments, giving rise to overpressures more than double that measured in type I tests. Previous studies of interconnected vessels have identified that that expanding flame front in the ignition vessel can precompress the fuel/air mixture in the secondary vessel leading to significantly increased overpressures [154, 207, 241, 249, 251, 256-262]. However, this work demonstrates that the situation is in fact more complicated in vented explosions with interconnected rooms, since it is apparent that a number of flow reversals across the doorway occur. Moreover, in Figure 4-13, it can be seen that at 350 ms, between the first and second pressure peaks, that the pressure in the right enclosure falls below ambient and any precompression that occurred between 350 ms and 390 ms, when the flame re-entered the right room and turbulent combustion was fully established, was small and would not account for the magnitude of the second pressure peak.

4.5.2. The Effects of Gas Concentration

The effects of concentration on maximum overpressure are shown in Figure 4-15. Both the closed door and open doorway results are given for tests involving a half layer and rear ignition. It has already been discussed in Section 4.5.1 that the maximum pressure corresponds to a combination of turbulent combustion and the external explosion with the former being the dominant factor. Consequently, there is a direct correlation between the magnitude of the pressure peak and the turbulent burning velocity; and as the burning velocity is dependent upon gas concentration, it would be expected, with closed door tests, that tests with 10% concentration produced the maximum overpressures. Figure 4-15 confirms this hypothesis. However, for open doorway tests, the degree of turbulence was less influential and the external explosion became more significant (Figure 4-16). Consequently, in these tests, the maximum overpressures would be expected to occur with fuel rich concentrations; Figure 4-15 confirms this observation.

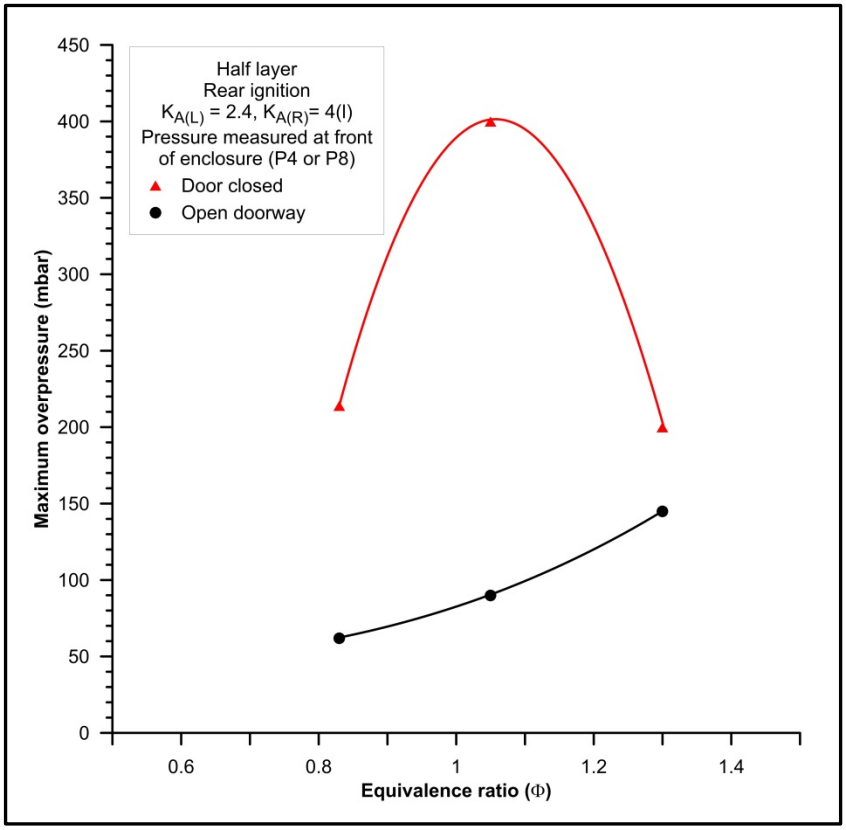

Figure 4-15 The effects of gas concentration (type II tests, series B)

4.5.3. The Effects of an Interconnecting Door

Where an interconnecting door was absent, the degree of turbulence generated in the right enclosure must have been significantly less than when the door was closed. Some turbulence would have been generated as the expanding flame front in the left enclosure initiated flow through the doorway, but in comparison, there would not have been a sudden flow as the door was opened and neither would the door have acted as a turbulence generating obstacle. Consequently, turbulent combustion in the right enclosure was less influential on the maximum overpressure developed within the explosion chamber, and the contribution of the external explosion played a more significant role.

In test number 28 (Figure 4-16), which was a fuel rich test with an open doorway, at approximately 400 ms, the pressure starts to increase rapidly due to the turbulent combustion. However, immediately after the flame front arrived at the left vent opening, there was a sharp pressure rise corresponding to the external explosion, which produced a sharp spike on top of the P_t pressure peak. This contribution from the external explosion is the reason for the increase in maximum overpressure, as a function of gas concentration seen in Figure 4-15.

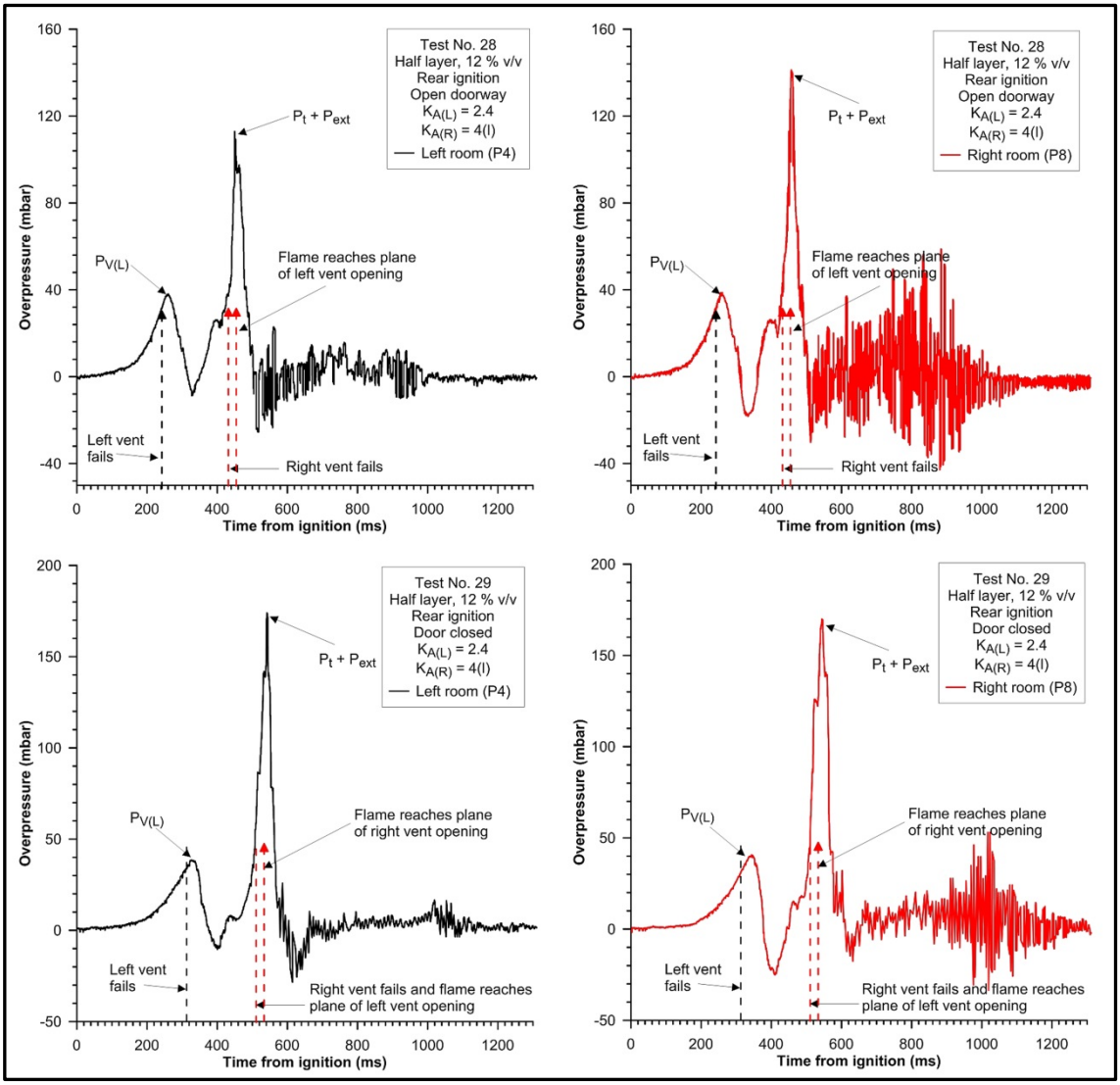

Figure 4-16 Comparison of tests with open doorway and closed door

Closing the door had a significant effect on the maximum overpressure and on the development of the explosion, as discussed in Section 4.5.1. This effect can be clearly seen in Figure 4-16, which allows for two identical tests (except for the door position) to be compared. The test with the open doorway generated a maximum overpressure of 145 mbar whilst closing the door increased the maximum pressure to 172 mbar. The presence initially obstructs flow between the rooms and allows a pressure differential to build up. Once the door is opened, significant turbulence is created resulting in higher maximum overpressures.

Surprisingly, in Figure 4-16, it can be seen that it took less time for the left vent (ignition enclosure) to fail in test 28 (open doorway) than in test 29. This observation did not occur in any other tests undertaken in the series. It would be expected for closed door tests, given that more turbulent combustion occurs, that the pressure rise more rapidly, causing the vent to fail earlier than it would in a corresponding test with an open

doorway. The difference in time taken to reach the pressure peak indicates that in this case, combustion was taking place more rapidly in the test with the open doorway. Consequently, the possible causes for this surprising observation are that the flame distorted through the open doorway, increasing the flame surface area significantly, or that there was an error in the recording of the gas concentration of either test.

4.5.4. The Effects of Ignition Position

The overpressure-time profiles of a central ignition test and a comparable rear ignition test are given in Figure 4-17. In this experimental arrangement, a 10% half layer was used, the vent sizes were $K_{A(L)}$ = 2.4 and $K_{A(R)}$ = 4(l), and the doorway was closed by an unlatched lightweight door. Observation of the profiles reveals two significant differences. The first difference is that the magnitude of the second pressure peak is greater with rear ignition. The second difference is that the onset of both major pressure peaks begins slightly earlier with central ignition (approximately 30 ms).

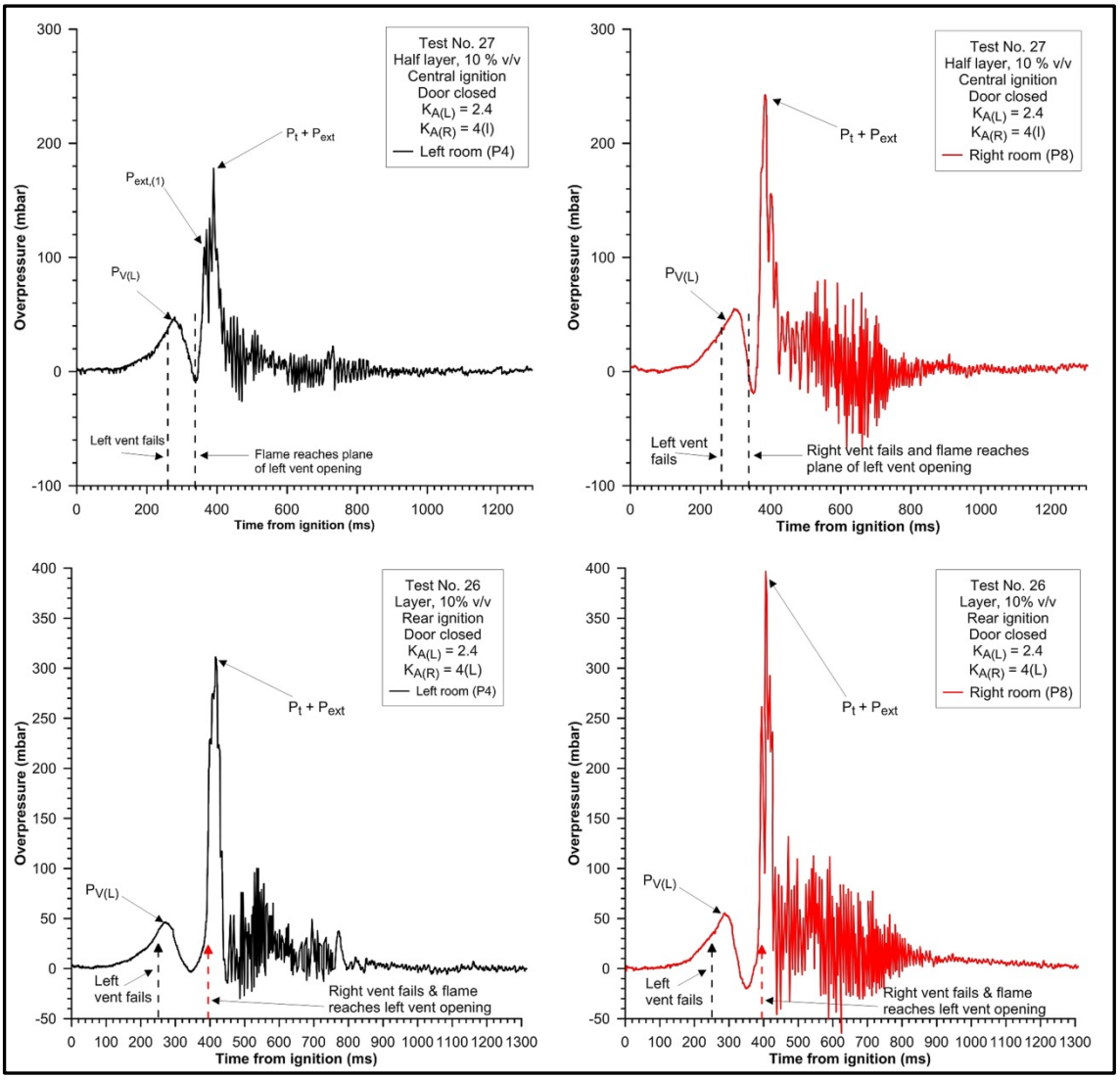

Figure 4-17 Comparison of tests with rear and central ignition

The proposed sequence of events during central ignition tests is shown schematically in Figure 4-18. Early in the explosion, the flame front is expanding from the centre ignition position in a spherical (full volume) or hemispherical shape (half layer), which causes the pressure to rise in the left enclosure and because the door is closed a pressure differential is developed. As the flame continues to expand, the pressure rises in the left room and overcomes the inertia of the door, causing it to swing open. The flame distorts towards the doorway and because of the pressure differential, unburnt gas/air mixture flows into the right enclosure generating turbulence.

The flame enters the right enclosure much earlier than is the case with rear ignition because it has a shorter distance to travel. Consequently, the interval between the door opening and the flame front entering the room is short, so the period of turbulence generation is also shorter than is the case with rear ignition. The pressure in the left enclosure continues to rise, which causes the left enclosure vent to fail, generating the $P_{V(L)}$ pressure peak in the left enclosure. Unburnt gas/air mixture are expelled through the left vent opening generating a flammable cloud. Combustion is already well established in the right enclosure.

Shortly after the failure of the left vent, the pressure drops in the left enclosure. This causes the flow to reverse through the doorway causing the pressure to drop in the right enclosure. Meanwhile the flame front in the left enclosure distorts towards the vent and when it reaches the opening, it ignites the external cloud causing the external explosion. This pressure wave restricts outflow through the vent and creates the second, intermediate pressure peak labelled $P_{ext,(1)}$ in the left enclosure (see Figure 4-17).

The pressure wave from the external explosion propagates through the vent opening into the explosion chamber, which has the effect of ‘pushing’ the flame front farther into the right enclosure. The turbulent combustion (along with the external explosion) creates the second, and maximum, pressure peak. There is a shorter interval between the first and second pressure peaks because the flame front is being driven into the right enclosure by the external explosion. The rapid pressure rise causes the right vent to fail, expelling unburnt gas/air mixture through the vent. This may be ignited when the flame front in the right enclosure reaches the vent opening. However, at this stage in the explosion there is a relatively small quantity of unburnt gas/air mixture within the enclosure.

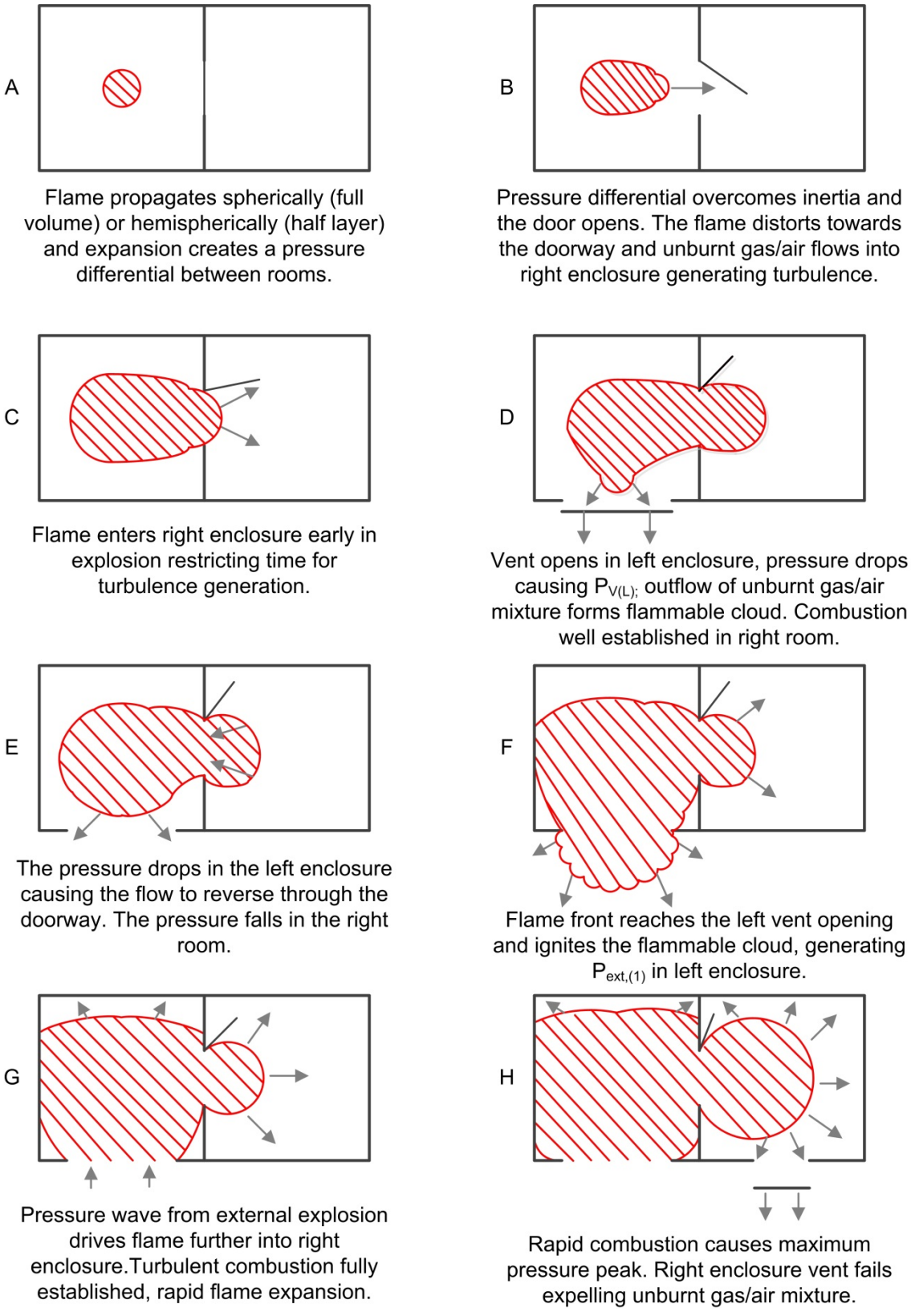

Figure 4-18 Proposed mechanism for type II tests (central ignition, door closed) (adapted from the observational notes of Skippon and Field [404])

4.5.5. The Effects of Vent Size in the Adjoining Enclosure

The effect of changing the size of the vent in the adjoining (right) enclosure on maximum overpressure is given in Figure 4-19. In the diagram, the maximum overpressure generated within the enclosure is plotted against K_A for both central and rear ignition. In all tests $K_{A(L)}$ = 2.4. For completeness, the $K_{A(R)}$ value of 2.4 from test type I is included in this plot. In most of the type I tests, the maximum pressure corresponded to the external explosion, whereas, in the type II tests, the maximum overpressure was generally dominated by turbulent combustion.

It can be seen that decreasing the right vent size from $K_{A(R)}$ = 2.4 to $K_{A(R)}$ = 4 or 8 increased the maximum overpressure for both central ignition and rear ignition tests. It can also be observed, that whilst decreasing the right vent size from $K_{A(R)}$ = 2.4 to $K_{A(R)}$ = 4 had a significant effect on the maximum overpressure, a further decrease in vent size did not result in a further increase in overpressure. Work undertaken by MRS [187] has shown that if an enclosure has more than one vent, each with different failure pressures, the venting process takes place predominately through the vent with the lower failure pressure. In these tests, the right enclosure may be considered as a room with two vents, the first vent is the $K_{A(R)}$ = 4 or $K_{A(R)}$ = 8, and the second is the lightweight door, with a failure pressure of a few mbar. Consequently, the main contribution to pressure relief in the right enclosure would have been venting through the doorway and out of the left vent opening. Additionally, the area of the doorway was greater than that of the smaller $K_{A(R)}$ = 4 and $K_{A(R)}$ = 8 vents.

Figure 4-20 shows the overpressure-time profiles for tests 26 ($K_{A(R)}$ = 4) and 36 ($K_{A(R)}$ = 8). It can be seen that the $K_{A(R)}$ = 4 vent fails sooner than the $K_{A(R)}$ = 8 vent. This is because the $K_{A(R)}$ = 4 vent is larger, and as both vents are constructed of the same material, it has a lower failure pressure. It can also be seen that the P_V peak is of greater magnitude and that the flame reaches the plane of the left vent opening sooner in the $K_{A(R)}$ = 4 test. These observations indicate that there is more turbulence being generated in test 26 and provides some explanation of the greater overpressure developed. Furthermore, the longer time taken for the failure of the $K_{A(R)}$ = 8 vent means that there was more venting through the doorway and out of the left enclosure opening in comparison with the $K_{A(R)}$ = 4 test.

In the experiments where $K_{A(R)}$ = 4, the vent could be fitted at either the left side or the right side of the front fascia panel. This was found to have no significant effect on either the maximum overpressure or the shape of the overpressure-time profile.

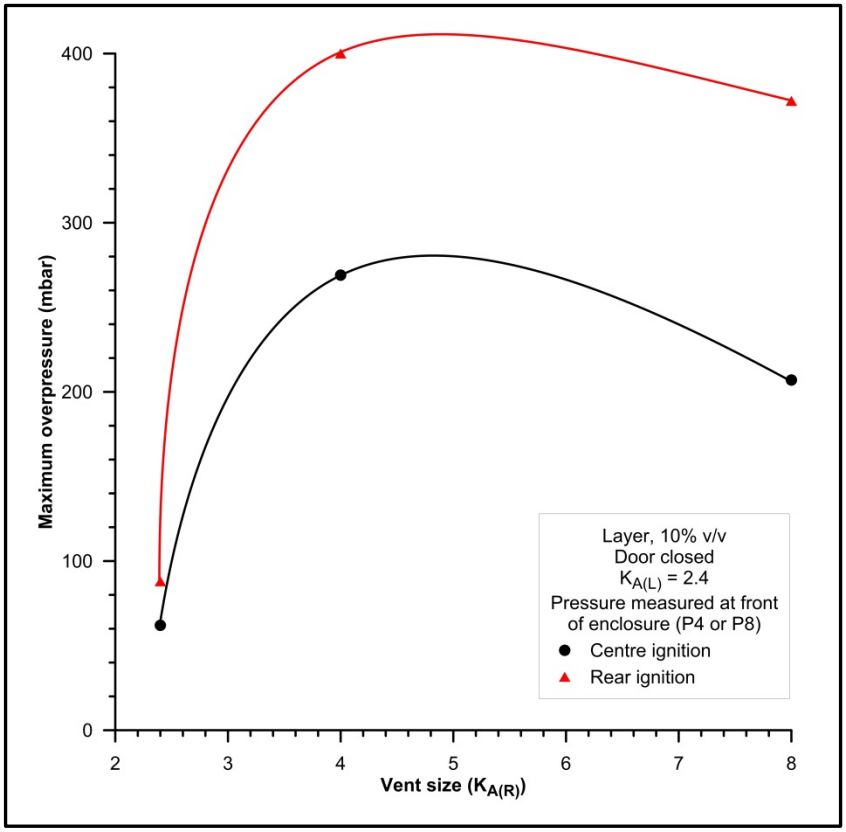

Figure 4-19 Maximum overpressure vs. vent size (type II tests)

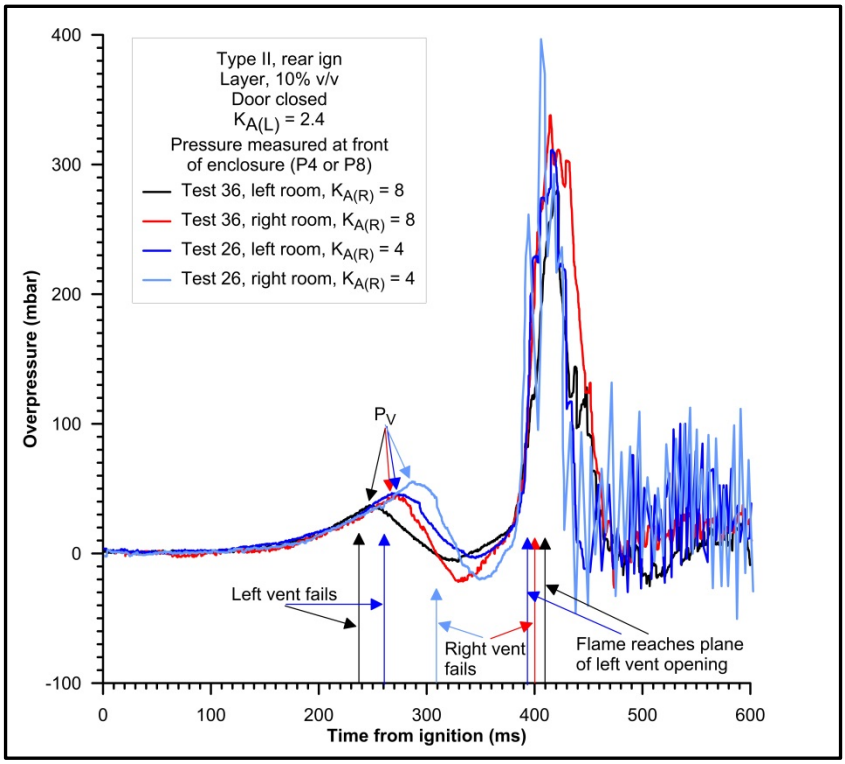

Figure 4-20 The effects of adjoining enclosure vent size (type II tests)

4.5.6. Summary of Findings of Type II Tests

The highest overpressure recorded in type II experiments was 414 mbar. Similarly to type I tests, the type II experiments were characterised by two dominant pressure peaks. The first peak always corresponded to the failure of the left (ignition enclosure) vent, which was recorded in both enclosures (right enclosure always recorded the event later than the left). The second pressure peak was considerably higher than the comparable peak observed in the type I tests. In most cases, this was caused by the rapid turbulent combustion of the fuel/air mixture in the right (secondary) enclosure. The mixture had become turbulent due to the complex flow interaction between enclosures via the connecting doorway and its effect on pressure generation was enhanced due to the increased confinement.

In tests where there was an open doorway, less turbulence was generated, and the dominant influence, particularly with fuel rich explosions, was the external explosion. In these instances, the maximum overpressure was produced by tests involving a 12% natural gas concentration. However, when an interconnecting door was present, significant turbulence was generated in the fuel/air mixture in the right enclosure leading to high peak overpressures (sufficient to cause structural damage to buildings). Not surprisingly, due to the higher burning velocity, the 10% concentration tests produced greater overpressures than either the 8% or 12% concentrations.

With central ignition tests, the flame entered the right enclosure much earlier than was the case with rear ignition tests because it had a shorter distance to travel. Consequently, the interval between the door opening and the flame front entering the room was short, so the period of turbulence generation was also shorter than was the case with rear ignition. In addition, due to the position of ignition, after the door opened, the turbulent flow through the doorway was of shorter duration meaning that the turbulent burning velocity would have been lower than corresponding tests with rear ignition. Consequently, the maximum pressure generated within the enclosure was of lower magnitude.

The use of a smaller vent in the right enclosure had a significant effect on the maximum overpressure and the mechanism of the explosion development. However, altering the size from $K_{A(R)} = 4$ to $K_{A(R)} = 8$ had little overall effect. This was largely due to the greater generation of turbulence with $K_{A(R)} = 4$ and the venting process at this stage of the explosion which predominantly occurred via the doorway and through the left vent opening.

A summary of the time of flame arrival at the vent opening, the maximum overpressure and the dominant pressure generation mechanism is given in Table 4-4.

Table 4-4 Summary of type II test conditions and results

Test No.	Gas in air (% volume)		Layer or Full	Ignition Position	Door Status	Vent Size (K_A)		Time of flame at vent (ms)		Max Pressure (mbar)	Main cause of dominant Peak
	Ign (L)	Adj (R)				Ign (L)	Adj (R)	Ign (L)	Adj (R)		
23	8	8	Layer	Rear	Open	2.4	4l	740	740	62	P_t
24	10	10	Layer	Rear	Open	2.4	4l	-	-	90	P_{ext}
25	8	8	Layer	Rear	Closed	2.4	4l	560	560	214	P_t
26	10	10	Layer	Rear	Closed	2.4	4l	390	-	400	P_t
27	10	10	Layer	Central	Closed	2.4	4l	340	-	269	P_t
28	12	12	Layer	Rear	Open	2.4	4l	460	-	145	P_{ext}
29	12	12	Full	Rear	Closed	2.4	4l	510	530	172	P_t
30	8	8	Layer	Rear	Open	2.4	8	-	-	131	P_t
31	8	8	Layer	Rear	Closed	2.4	8	-	-	138	P_t
32	12	12	Layer	Rear	Open	2.4	8	620	-	152	P_{ext}
33	12	12	Layer	Rear	Closed	2.4	8	510	550	234	P_t
34	10	10	Layer	Central	Open	2.4	8	400	470	200	P_t
35	10	10	Layer	Central	Closed	2.4	8	400	440	207	P_t
36	10	10	Layer	Rear	Closed	2.4	8	420	460	372	P_t
37	10	10	Layer	Central	Open	2.4	4r	360	400	76	P_{ext}
38	10	10	Full	Central	Open	2.4	4r	350	430	117	P_t
39	10	10	Layer	Central	Closed	2.4	4r	340	380	172	P_t
40	10	10	Full	Rear	Closed	2.4	4r	430	430	338	P_t
41	10	10	Layer	Rear	Closed	2.4	4r	390	430	414	P_t
42	10	10	Full	Rear	Closed	2.4	4l	-	-	317	P_t

4.6. Type III Experiments

The type III tests, undertaken as series E, F, H and J, had a smaller vent in the left (ignition) enclosure and a larger, $K_{A(R)}$ = 2.4 vent in the right enclosure. The left enclosure was vented as follows:

- Series E, $K_{A(L)}$ = 4(r) (i.e. the vent was fitted in the right side of the left enclosure fascia panel).
- Series F, $K_{A(L)}$ = 8.
- Series H, $K_{A(L)}$ = 4(r).
- Series J, $K_{A(L)}$ = 4(r).

In all of the tests, the vent material used was 12.5 mm fibreboard. However, in this test type, a number of parameters were varied, namely, gas concentration in the enclosures such that in some tests (Series J) the gas concentration in adjoining rooms was different, the door type, the room into which the door hinged, the door latching mechanism and the angle that the door was open. The test arrangements are summarised in Table 4-5. In addition, in a small number of tests, the depth of flammable layer was varied (Series J). The results of these tests are reported in Section (4.6.6).

Table 4-5 Door type and orientation for type III tests

Test No.	Gas Concentration (% v/v)		Door Type	Door Status[a]	Latching Mechanism
	Ign (L)	Adj (R)			
43	8	8	Lightweight	Closed	Unlatched
44	10	10	Lightweight	Closed	Unlatched
45	12	12	Lightweight	Closed	Unlatched
46	10	10	Lightweight	Closed	Roller latch
47	10	10	Lightweight	Open	Roller latch
48	8	8	Lightweight	Open	Unlatched
49	12	12	Lightweight	Open	Unlatched
50	8	8	Lightweight	Open	Unlatched
51	10	10	Lightweight	Open	Unlatched
52	12	12	Lightweight	Open	Unlatched
53	8	8	Lightweight	Closed	Unlatched
54	10	10	Lightweight	Closed	Unlatched
55	12	12	Lightweight	Closed	Unlatched
56	10	10	Lightweight	Closed	Unlatched
60	8	8	Lightweight	Closed	Roller latch
61	10	10	Lightweight	Closed	Roller latch
62	12	12	Lightweight	Closed	Roller latch
63	8	8	Fire door	Closed	Unlatched
64	10	10	Fire door	Closed	Unlatched
65	12	12	Fire door	Closed	Unlatched
66	10	10	Fire door	Closed	Roller latch
67	10	10	Lightweight	Closed	Mortice latch
68	10	10	Fire door	Closed	Mortice latch
71	8	10	Lightweight	Closed	Roller latch
72	10	8	Lightweight	Closed	Roller latch
73	8	12	Lightweight	Closed	Roller latch
73	12	8	Lightweight	Closed	Roller latch
75	10	12	Lightweight	Closed	Roller latch
76	12	10	Lightweight	Closed	Roller latch
77	6	13	Lightweight	Closed	Roller latch
78	13	6	Lightweight	Closed	Roller latch
79	6	10	Lightweight	Closed	Roller latch
80	10	6	Lightweight	Closed	Roller latch
81	10	10	Lightweight	Closed	Roller latch
82	10	10	Lightweight	Closed	Roller latch
83	10	10	Lightweight	Hinged into left room – open at 45°	Unlatched
84	10	10	Lightweight	Hinged into left room – open at 45°	Unlatched
85	10	10	Lightweight	Hinged into left room – open at 45°	Unlatched
86	10	10	Lightweight	Hinged into left room – open at 90°	Unlatched
87	10	0	Lightweight	Closed	Tubular latch

[a] Door hinges into right (adjoining room) unless otherwise stated.

4.6.1. Proposed Mechanism for Explosion Development

Figure 4-21 shows the overpressure-time profile and pressure differential between enclosures for test 44, which was a half layer test of 10% concentration, ignited at the rear ignition position. A lightweight door was closed and unlatched. The right vent ($K_{A(R)}$ = 2.4) was larger than the left vent ($K_{A(L)}$ = 4). Continuing the trend of test types I and II, there are two major pressure peaks, with the second being of considerably greater magnitude than the first.

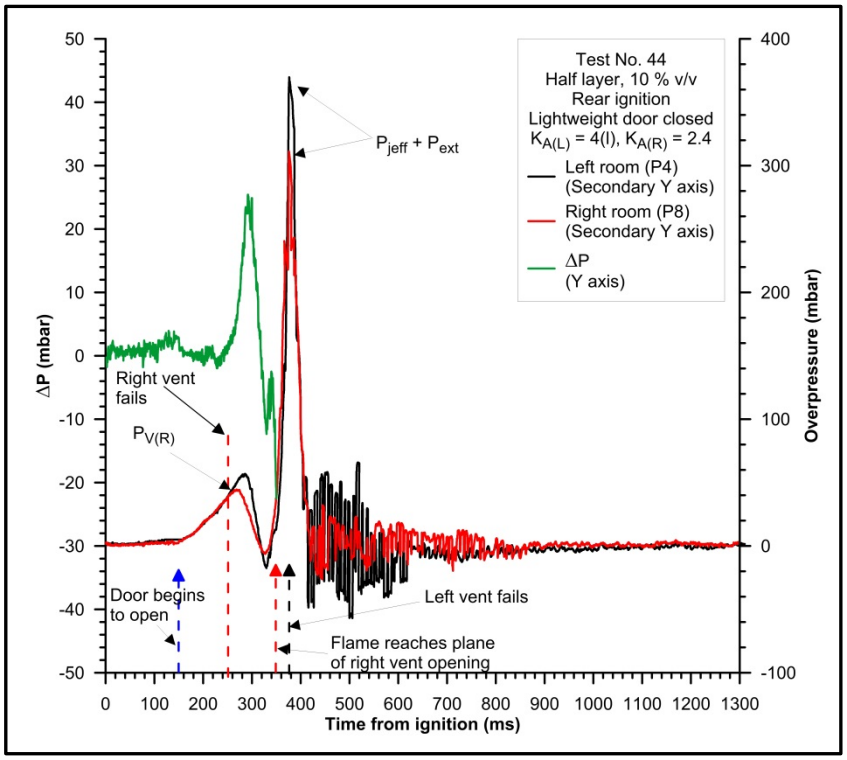

Figure 4-21 Overpressure-time profile for type III test

Additionally, as in test types I and II, the presence of a closed door made a difference to the maximum overpressure and the development of the explosion, although it was less pronounced than the type II tests in particular. A proposed mechanism for type III explosions is given in Figure 4-22. In the very early stages of the explosion, the flame propagates in the left (ignition) enclosure, assuming the shape of a quarter-sphere and the expanding hot gases generate pressure in the left enclosure (A). As the interconnecting door is closed, a pressure differential is developed, which at approximately 150 ms is sufficient to start to swing the door open (B). Due to the pressure difference, unburnt gas/air mixture flows into the right enclosure, generating turbulence and causing the flame front to distort towards the doorway. Approximately 50 ms later, the pressure in the enclosures equalise, but by this time the flame front has reached the interconnected doorway and started to further distort, increasing the rate of combustion through an already turbulent mixture (C). The vent in the right

enclosure fails, generating the P_V pressure peak, which in the case of test 44 ($K_{A(R)}$ = 2.4) was recorded at 270 ms and measured approximately 40 mbar in the right enclosure (D). The P_V peak is registered in the left enclosure some 20 ms later because it is only able to vent through the doorway, and consequently attains a greater magnitude (55 mbar in test 44). Due to the onset of venting, the pressure in both enclosures then falls below ambient. The flow through the doorway 'drives' the flame front towards the right vent opening and this sudden expanding flame front, rapidly increases the rate of combustion, generating a fast rise in pressure within the adjoining enclosure, which creates a pressure peak (E and F), labelled P_{jeff}, due to its correspondence with the jetting expanding flame front. The P_{jeff} pressure peak in test 44 occurred at approximately 370 ms and attained values of 314 mbar in the right enclosure and 370 mbar in the left. The left vent ($K_{A(L)}$ = 4) failed during the generation of this pressure peak.

It can be seen that the second major pressure peak is dominated by the rapid increase in flame surface area, which has been initiated through the complex flow interaction between rooms when a door is initially closed, and the venting process through the adjoining room. The external explosion (F) contributes to the magnitude of this second peak but is not the dominating influence. A key feature of the type III explosions however, is the 'jetting' of the flame front into the adjoining enclosure, driven by the venting process. This causes a significant increase in the rate of combustion which is greater than that seen in type II tests. Consequently, the maximum pressure peaks occur earlier and are of greater magnitude.

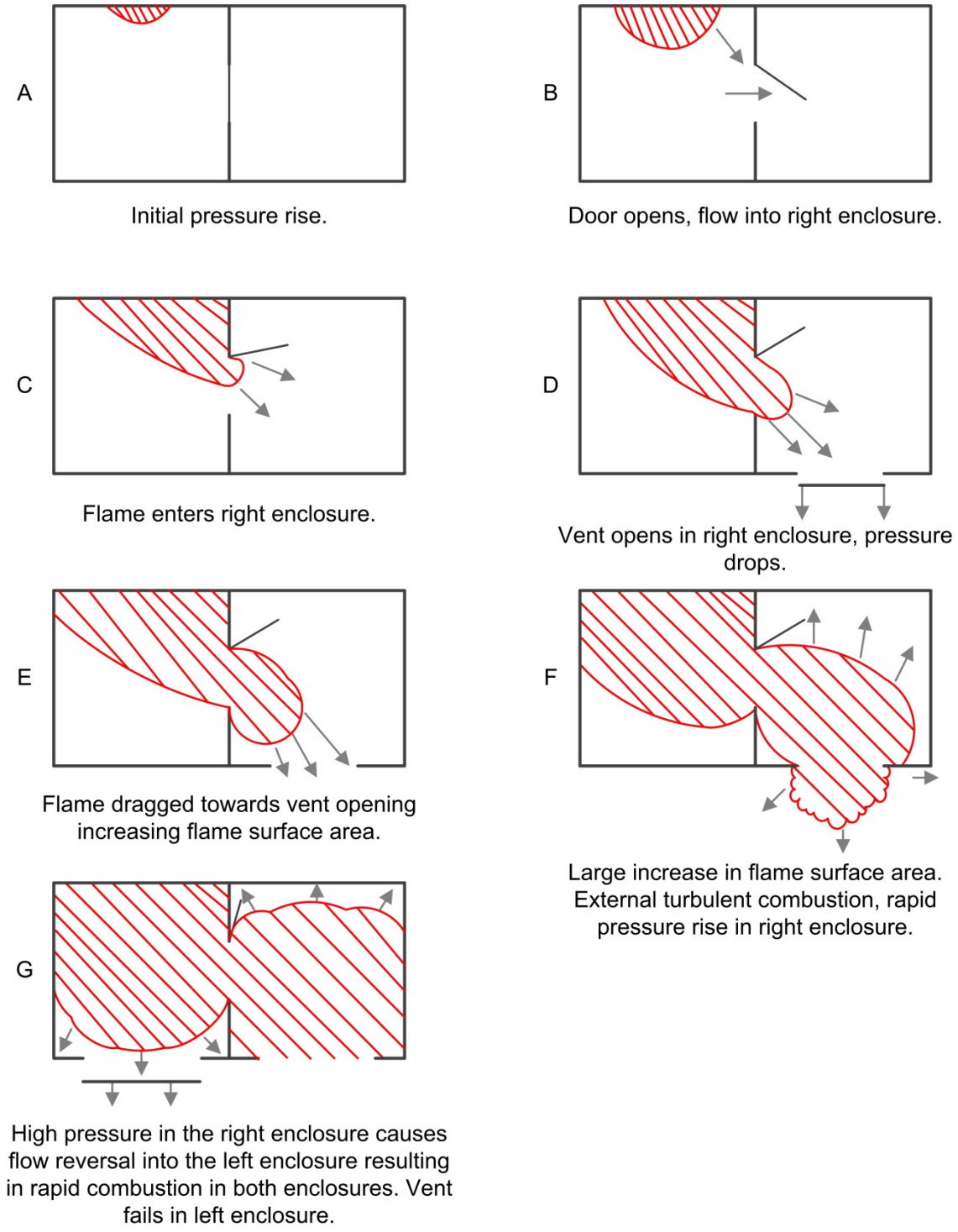

Figure 4-22 Proposed mechanism for type III tests (rear ignition, door closed) (adapted from the observational notes of Skippon and Field [404])

4.6.2. The Effects of Gas Concentration

The effect of gas concentration on the maximum overpressure generated within the enclosure is given in Figure 4-23. This diagram highlights the effects of gas concentration on half layer tests with the door initially both open and closed. Rather differently from the type I and II test, the curves for both an open and closed door, follow the variation of burning velocity with gas concentration. This further demonstrates that the dominating factor in pressure generation in type III tests was turbulent combustion within the enclosure, rather than the external explosion. In the case where the external explosion was most influential, the fuel rich concentration would produce the greatest overpressure.

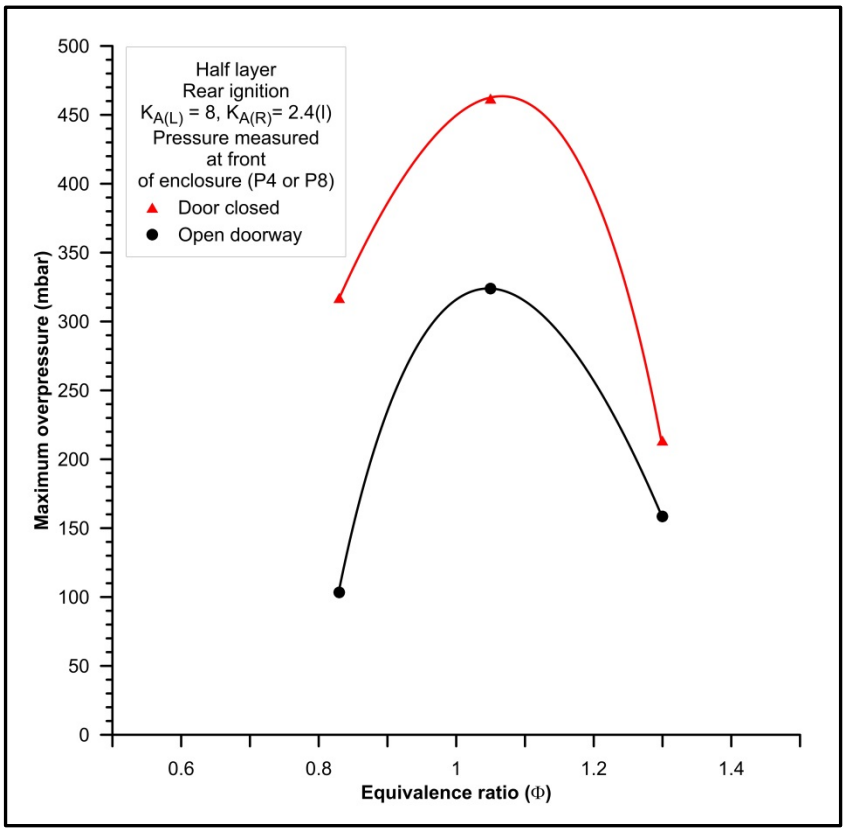

Figure 4-23 The effects of gas concentration (type III tests, series F)

4.6.3. The Effects of an Interconnecting Door

The effect of the interconnecting door on maximum overpressure is also highlighted in Figure 4-23. It can be seen that the presence of an interconnecting door clearly has a positive effect on the pressure attained during the explosion, but in comparison to type II tests, the difference is not as marked. The reason for this may be explained by the explosion mechanism in these tests, where the venting process occurs predominantly through the right enclosure. Consequently, whilst the presence of the door increased the generation of turbulence, it had little effect on the jetting expanding flame front being driven towards the vent opening. This process produced very rapid combustion that was faster than the turbulence enhanced combustion seen in type II tests, producing maximum pressures of over 300 mbar in tests with an open doorway.

4.6.4. The Effects of Vent Size in the Left Enclosure

The effect of the vent size (in the ignition enclosure) on maximum overpressure is shown in Figure 4-24. The data is taken from type III tests involving half layers of 10% concentration, ignited at the centre and rear of the enclosure, with a vent size of $K_{A(R)}$ = 2.4 in the adjoining (right) enclosure, and with a lightweight unlatched door covering the interconnecting doorway. For completeness, data points for K_A = 2.4 have been taken from corresponding the type I tests. However, it should be noted that the maximum pressure for the type I tests are caused by the external explosion, whereas the type III tests are caused by the turbulent jet driven flame front.

In the proposed mechanism described in Section 4.6.1, the jetting flame being driven towards the vent opening in the adjoining enclosure would occur for any vent size in the ignition enclosure, so long as the ignition room vent is strong enough to survive the pressure peak caused by the failure of the larger vent in the adjoining enclosure. This is because, once the jetting flame mechanism has occurred, the pressure within the ignition enclosure is predominantly relieved though the doorway and the larger vent in the adjoining enclosure. Therefore, the mechanism suggests that there would be a significant increase in the maximum pressure when the vent size in the left enclosure is reduced from $K_{A(L)}$ = 2.4 to $K_{A(L)}$ = 4 (or the vent material is stronger such that there is an equivalent increase in failure pressure), but a smaller difference if is further decreased in size to $K_{A(L)}$ = 8. This is exactly what can be seen in Figure 4-24.

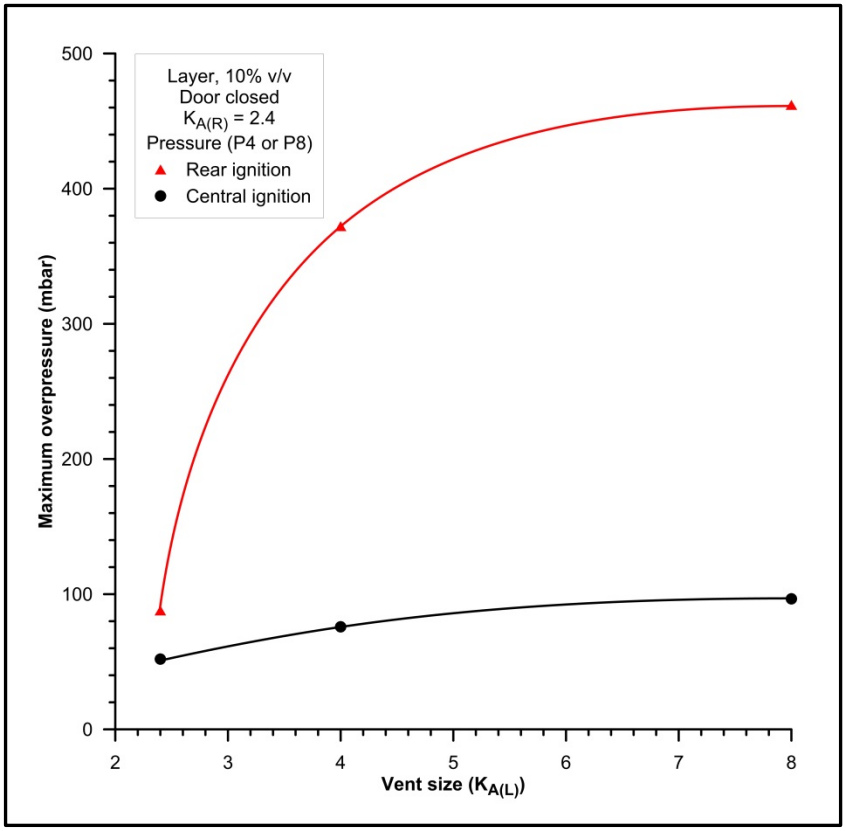

Figure 4-24 Maximum overpressure vs. vent size (type III tests)

4.6.5. The Effects of Ignition Position

Figure 4-24 also highlights the effect of ignition position on maximum overpressure. It can be seen that central ignition tests produce much lower overpressures than comparable rear ignition tests. There are a number of reasons for the cause of this difference. Firstly, the duration between ignition and the point at which the flame front enters the right enclosure is shorter, because of the shorter travel distance, and consequently there is less time to generate turbulence. Secondly, the flame surface area would be much greater at the time the right vent failed, thus the jetting driven flame front would be less significant. Thirdly, in the case of the $K_{A(R)}$ = 2.4 results, where the maximum pressure is dependent upon the external explosion, there is less unburnt gas/air mixture expelled during the venting process because the flame front is closer to the vent opening.

4.6.6. The Effects of Layer Depth

A small number of type III tests were conducted in order to examine the behaviour of natural gas/air ceiling layers of differing depth. This is representative of real gas explosion scenarios, for example, when a cooker hob is switched on and not ignited. The experiments were conducted with 10% natural gas/air layers with a nominal depth from the ceiling of 0.3 m, 0.6 m and 1.2 m, vent sizes of $K_{A(L)}$ = 4 and $K_{A(R)}$ = 2.4, rear

ignition, and a lightweight interconnecting door secured in a closed position with a roller latch. The maximum overpressure is plotted as a function of layer depth in Figure 4-25. It can be seen that the maximum overpressure increases linearly with layer depth. Although, this limited data set shows a strong dependence on the layer depth, this is not as strong as that in the work of Butlin and Tonkin [160] in a single enclosure of the same explosion chamber, where they identified that the relationship between overpressure and layer depth was quadratic. Further work is required in this area.

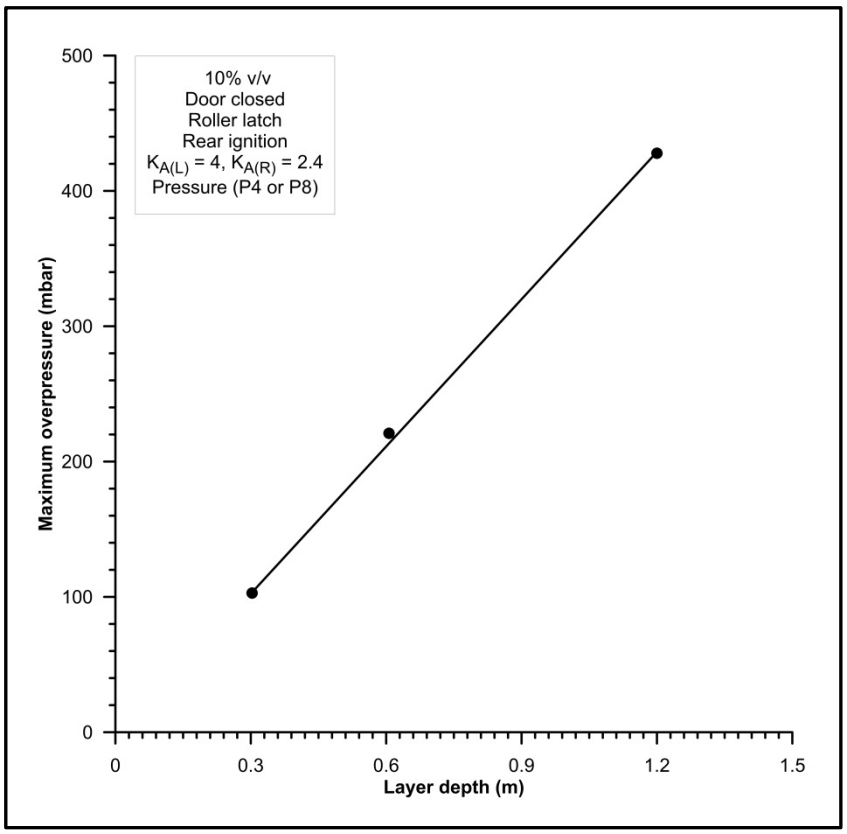

Figure 4-25 Maximum overpressure vs. layer depth

4.6.7. Interconnecting Enclosures with Different Gas Concentrations

In an accidental gas explosion, it is entirely possible that conditions surrounding the gas release and subsequent build-up to a flammable mixture, result in different concentrations being present in adjoining rooms. Consequently, in order to investigate realistic situations where a gas explosion propagates from one room to another, some tests were undertaken where the concentrations were different in the two enclosures. The experiments were conducted as series J, with a half layer in each enclosure, rear ignition, $K_{A(L)}$ = 4 and $K_{A(R)}$ = 2.4 and a lightweight door secured in the closed position by a roller latch. The results of the tests are shown in Table 4-6.

Table 4-6 Results of tests involving different gas concentrations

Test No.	Gas Concentration (% v/v)		P_V (mbar)	P_{max} (mbar)	
	Ign (L)	Adj (R)		Ign (L)	Adj (R)
61	10	10	55	428	372
71	8	10	39	262	193
72	10	8	55	400	338
73	8	12	55	310	248
74	12	8	50	241	193
75	10	12	55	276	228
76	12	10	50	352	283
77	6	13	50	234	186
78	13	6	41	290	241
79	6	10	41	83	69
80	10	6	52	345	276
87	10	0	44	234	166

Figure 4-26 shows a comparison of the maximum overpressure as a function of concentration in the interconnected enclosures. It is evident, that in all tests the maximum overpressures attained occurred in the left (ignition) enclosure. The left graph plots the overpressure against the concentration in the left enclosure, for a number of tests where the concentration in the right enclosure was fixed at 10%. It can be seen that when the ignition enclosure had a lean layer of 6%, the maximum overpressure was relatively low, at 83 mbar (left enclosure). However, this increased significantly to a maximum of 428 mbar as the concentration in the ignition enclosure reached 10%, before decreasing to 352 mbar at 12%. These results demonstrate that the maximum overpressure is strongly dependent on the gas concentration in the ignition enclosure.

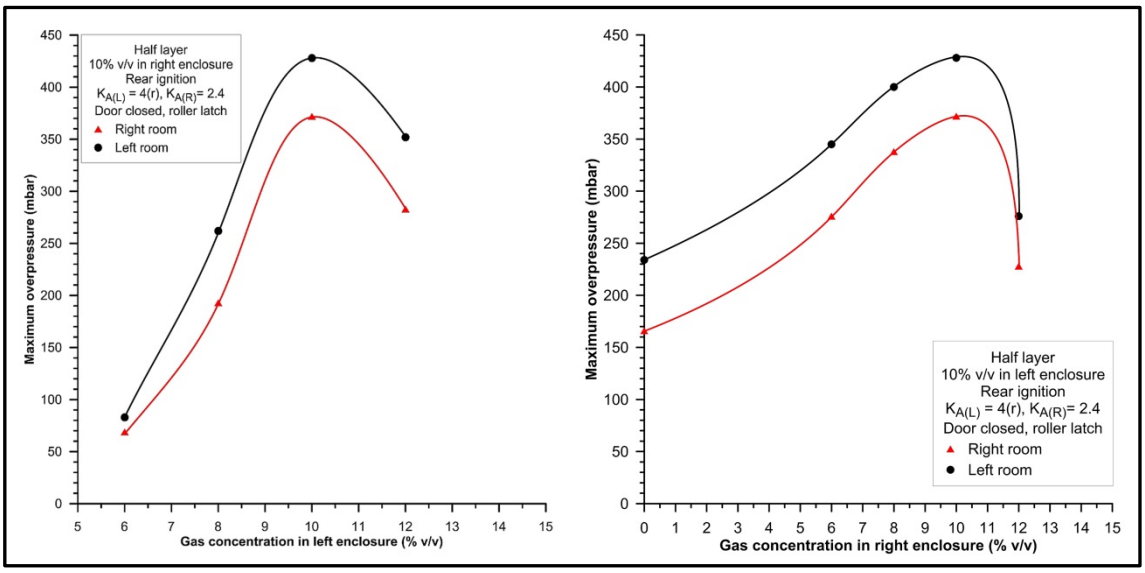

Figure 4-26 Maximum overpressure vs. differing concentration in enclosures

Contrastingly, the right graph plots the overpressure against the concentration in the adjoining (right) enclosure, for a number of tests where the concentration in the left (ignition) enclosure was fixed at 10%. Similarly, to the left graph, the curves peak at a concentration of 10% and fall as the concentration becomes richer, but they fall to values lower than that recorded with lean mixtures of 6% and 8%. This was unexpected and suggests that some mixing of unburnt gas was taking place in the ignition enclosure as the flow was initially reversed. The recorded overpressures for lean concentrations in the adjoining enclosure are also interesting. Overpressures of 234 and 165 mbar were recorded in the left and right enclosures respectively when there was no gas present in the right enclosure at the time of ignition. This finding is important as the second major pressure peak recorded in the type III tests was derived initially from turbulent combustion of mixture in the adjoining enclosure as the flame jets into the room from the interconnecting doorway. Due to budgetary constraints, no further tests were undertaken where the adjoining enclosure has no gas present. It is recommended that further experimental work is undertaken, which should include tests where the concentration in the ignition enclosure is varied across the flammable range.

It is possible that following the opening of the interconnecting door, the flow of unburnt mixture from the left enclosure into the right would result in some mixing of the mixture already present in the right room. Consequently, the magnitude of the maximum pressure peak would be dependent upon the mean concentration of the two enclosures, weighted towards that of the adjoining enclosure because not all of the flammable mixture in the ignition enclosure would be available for mixing. If however, the situation occurred where the flow from the ignition enclosure simply displaced the original mixture from the adjoining enclosure, then the maximum pressure developed in

the explosion would be independent of the original concentration in the adjoining enclosure.

Figure 4-27 plots the maximum overpressure results against the gas concentration in the adjoining room. The black curve represents the tests where the concentration of a natural gas layer was fixed at 10% in the (ignition) left enclosure whilst the concentration of the layer in the adjoining enclosure was varied. The red curve represents the tests where the concentration of a natural gas layer was fixed at 10% in the adjoining (right) enclosure whilst the concentration of the layer in the ignition enclosure was varied.

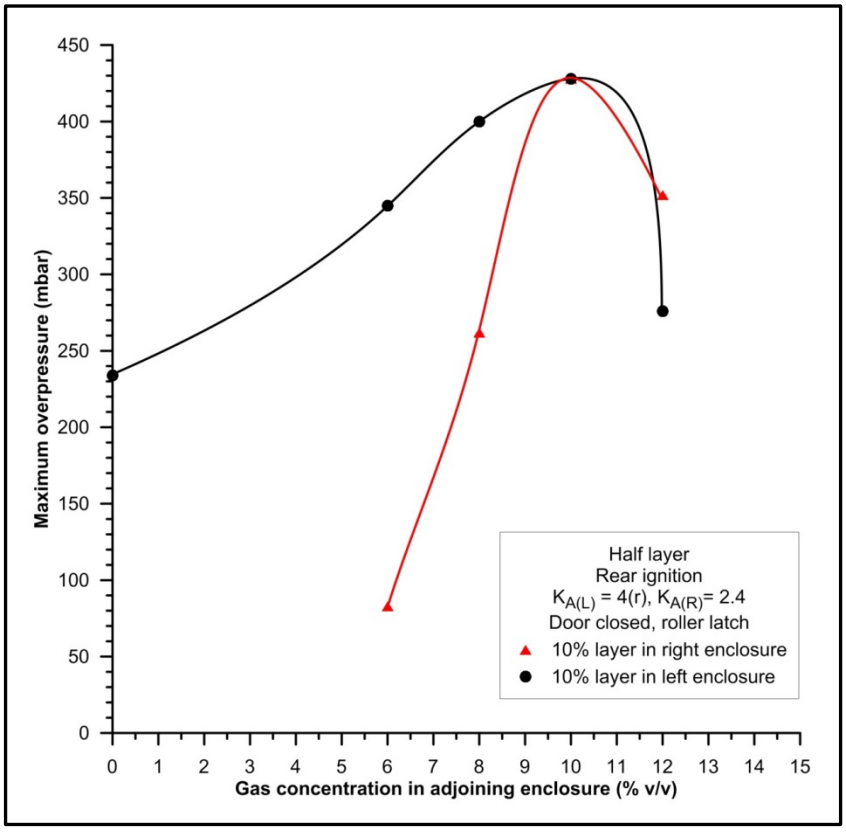

Figure 4-27 Maximum overpressure vs. concentration in adjoining enclosure

The x-axis represents the concentration in the adjoining enclosure (i.e. for the curve of 10% in the right enclosure, the x-axis represents the concentration in the left enclosure and vice versa). This diagram suggests that whilst the magnitude of the maximum (second) pressure peak was strongly dependent upon the concentration in the ignition enclosure, it was affected by the concentration in the adjoining (right) enclosure. Thus, in respect of the behaviour of the mixtures in the adjoining enclosure, with the limited data available, it appears that both mixing of the mixture, and displacement of the original mixture must be taking place.

4.6.8. The Effects of Different Door and Latch Types

A number of tests were undertaken with different door and latch types. Two door types were used; the lightweight, 'egg-box' type internal door and an internal fire door. Three types of latching mechanism were used; unlatched (i.e. door pushed closed), a roller latch and a stronger mortice latch. In these experiments, the vent sizes were $K_{A(L)}$ = 4(r) and $K_{A(R)}$ = 2.4, and the ignition was in the rear position. The results of these tests are given in Table 4-7.

Table 4-7 Results of tests involving different door and latch types

Test No.	Gas Conc. (% v/v)	Door type	Latch type	P_V (mbar)	P_{max} (mbar)		Time to $P_{max,(L)}$ (ms)
					Ign (L)	Adj (R)	
43	8	Lightweight	Unlatched	41	276	234	500
44	10	Lightweight	Unlatched	55	372	338	375
45	12	Lightweight	Unlatched	41	207	207	470
59	12	Lightweight	Roller latch	62	179	179	625
60	8	Lightweight	Roller latch	50	290	262	580
61	10	Lightweight	Roller latch	55	428	372	375
62	12	Lightweight	Roller latch	50	393	310	430
63	8	Fire door	Unlatched	50	331	283	540
64	10	Fire door	Unlatched	55	400	386	365
65	12	Fire door	Unlatched	48	407	379	485
66	10	Fire door	Roller latch	55	501	455	375
67	10	Lightweight	Mortice latch	66	227	214	425
68	10	Fire door	Mortice latch	72	331	317	400
69	10	Fire door	Roller latch	14	138	152	485
70	10	Fire door	Roller latch	83	331	359	425

Figure 4-28 shows the overpressure-time profiles for six tests. Test 44 and 61 show the profiles for a lightweight door, unlatched and with a roller latch. Tests 64 and 66 show the profiles for a fire door, unlatched and with a roller latch, and tests 67 and 68 show the effects of a mortice lock. It is evident from Figure 4-28 that for both door types higher maximum overpressures were generated when roller latches were fitted rather than being left unlatched. The latch mechanism would have increased the failure pressure of the door, thus creating a greater pressure differential between enclosures. Consequently, when the door opened a greater level of turbulence would have been generated.

For each latch type, higher maximum overpressures were also observed with fire doors than with lightweight 'egg-box' doors. In a manner similar to the effect of the roller latch, it would have required a greater pressure differential to overcome the inertia of a fire door, which results in a higher level of turbulence. Figure 4-28 shows that the test involving a fire door combined with a roller latch produced the greatest maximum overpressure of the test series (500 mbar).

Surprisingly, when either door type was fitted with a mortice latch, the strongest of the latching mechanisms, lower overpressures were produced than in comparable tests with unlatched doors or with a roller latch. It would be expected that the greater pressure differential created by this high failure pressure door and latch, would result in very high levels of turbulence.

Figure 4-29 shows the overpressure-time profile for a test undertaken with a lightweight door and a mortice latch. Typical of a vented explosion, after ignition the pressure began to rise relatively slowly, whilst the pressure in the adjoining enclosure stayed at ambient. Accordingly, a pressure differential was developed between the two enclosures. However, the strength of the door and latch was not overcome until approximately 250 ms after ignition, by which time the pressure differential had reached approximately 45 mbar. As soon as the door failed open, there was a sudden turbulent flow into the right enclosure, causing the pressure in the left enclosure to relieve, such that by 300 ms the pressure was close to ambient. Correspondingly, the pressure in the right enclosure had risen to over 40 mbar which was sufficient for the vent to fail in the right enclosure. The action of the door failing corresponded to a new first pressure peak, which is labelled $P_{d.}$

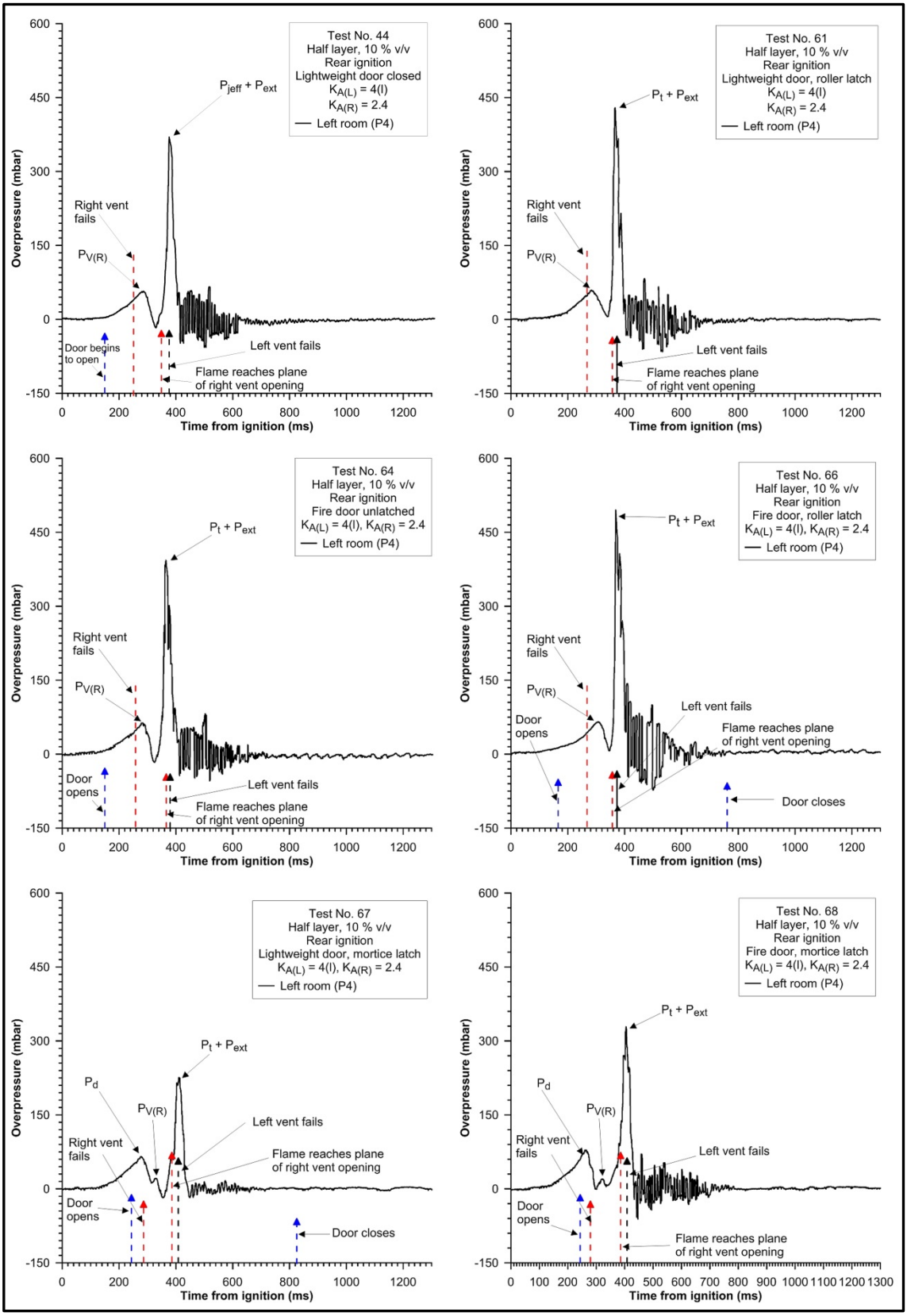

Figure 4-28 The effects of door type and latch mechanism

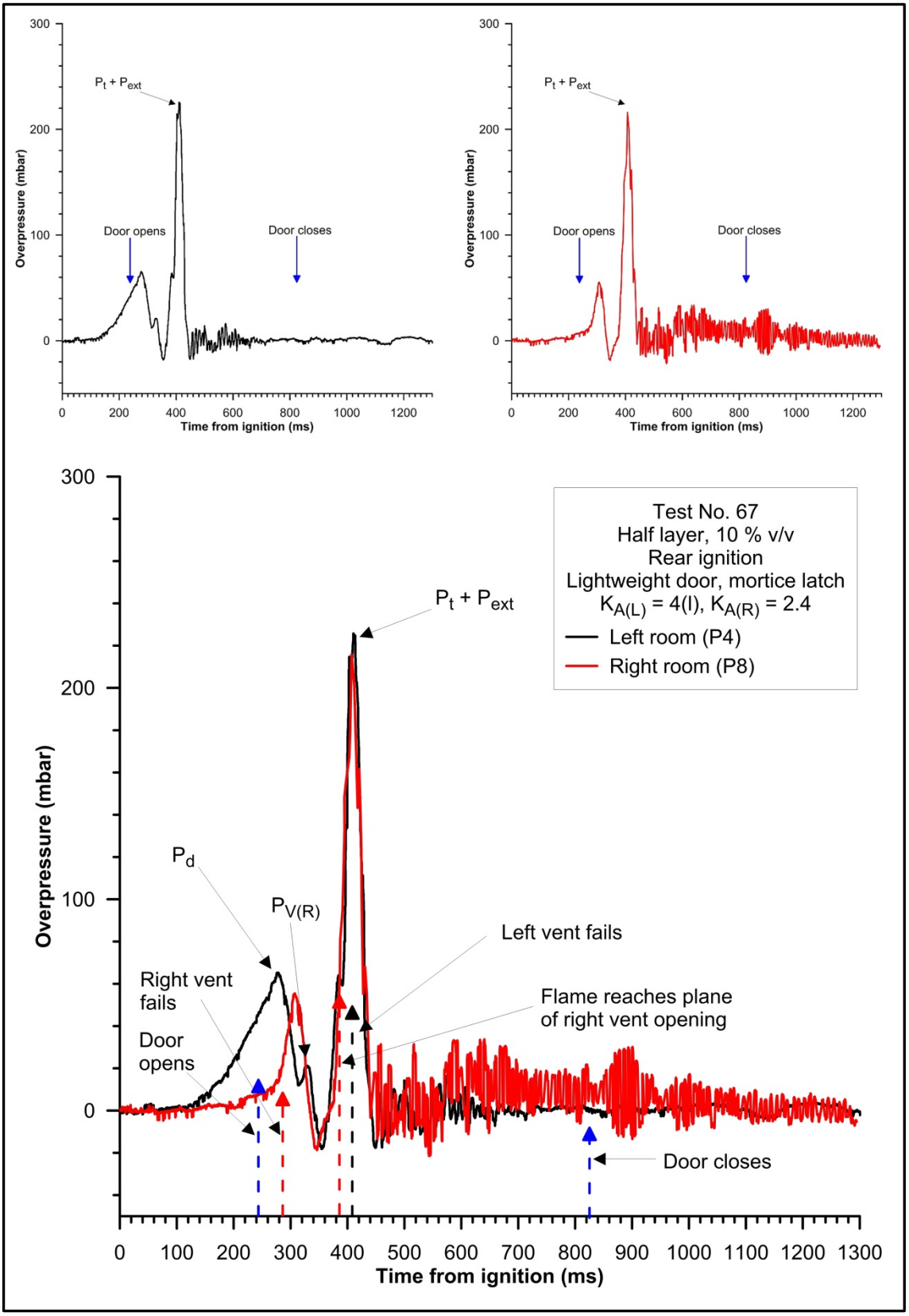

Figure 4-29 Overpressure-time profiles for tests involving a mortice latch

A key difference in the behaviour of this type of explosion is that the failure of the right vent did not cause a ‘jetting’ driven flame toward the right vent opening. This is because of the large pressure that remained in the right enclosure. Venting of this pressure subsequently occurred through the right vent opening and through a sudden flow reversal back through the doorway because of the reversed pressure differential between the enclosures. This sudden flow reversal would prevent the jetting mechanism from occurring. In test 68, a similar test with a mortice latch, a series of damped oscillations occurred shortly after this sudden flow reversal, resulting in the flow reversing through the doorway several times. This was not evident in test 67. However, in both instances, following this, turbulent flow was established in the right enclosure and a P_t peak was generated. This rapid spike in pressure was sufficient to cause the left enclosure vent to fail.

This series of experiments indicate that the failure pressure of the interconnecting door is critical to the development of the explosion and the maximum overpressure that will be generated. In these instances, the dominant factor is turbulent combustion. A proposed mechanism for explosion development in type III explosions with a high strength interconnecting door is given in Figure 4-30.

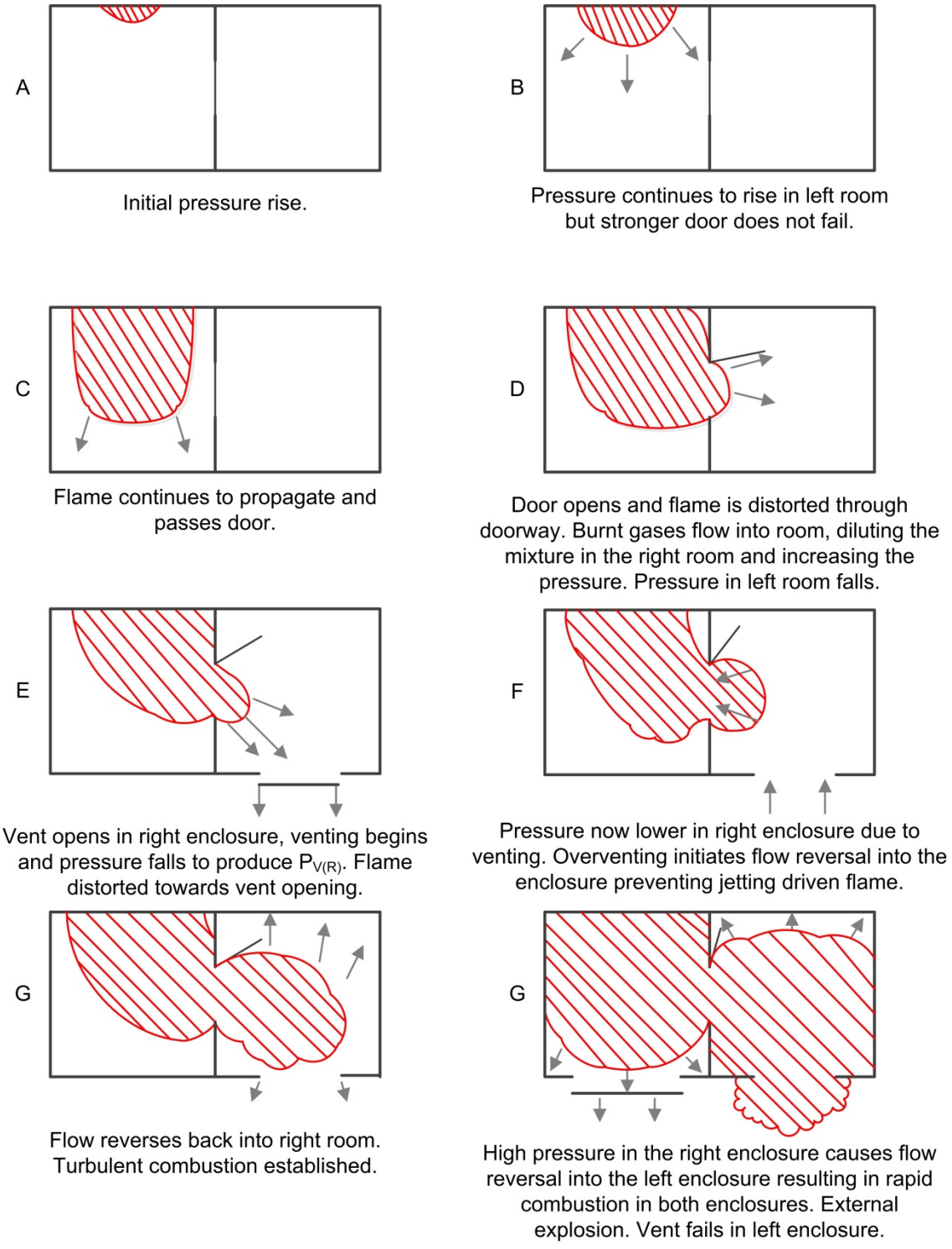

Figure 4-30 Proposed mechanism for type III tests (high strength door)

4.6.9. Experiments with Door Hinged to Open into the Ignition (Left) Enclosure

Four experiments were undertaken where the door hinged into the ignition (left) enclosure. The purpose of these tests was to investigate situations where the door closed against the door jamb. This would effectively increase the force required to open the door. Furthermore, it was likely that the door would 'break', rather than open.

Figure 4-31 shows the overpressure-time profile for test 83, in which a lightweight door was utilised with a roller latch. The door hinged into the left enclosure and was closed at time of ignition.

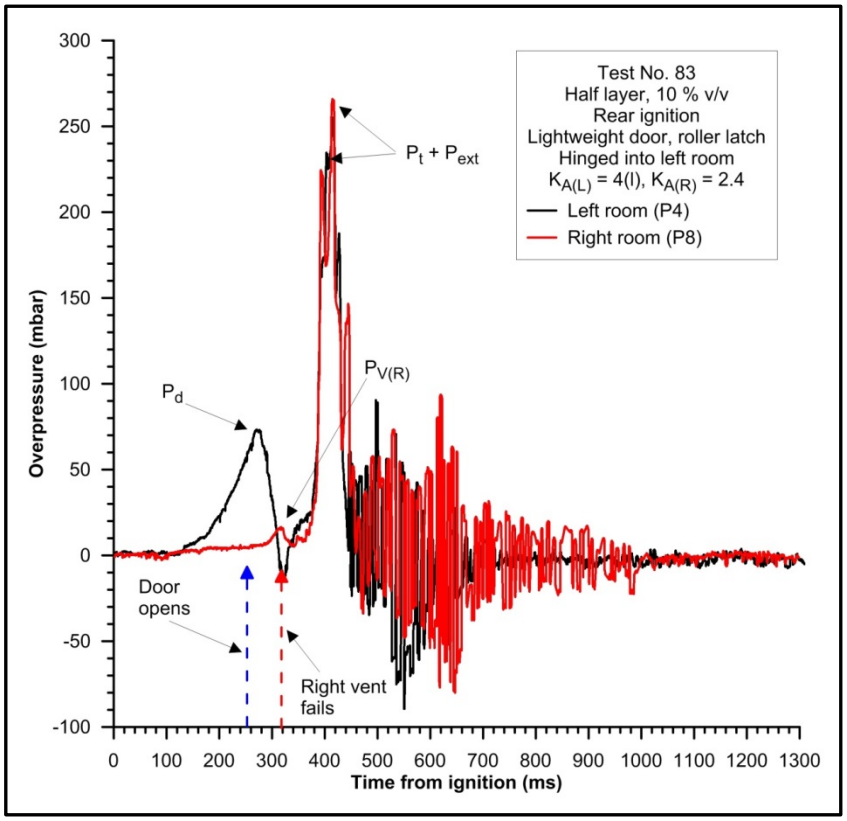

Figure 4-31 Overpressure-time profile for test with door hinged into left room

Not surprisingly, the overpressure-time profiles are similar to profiles of tests where the door was fitted with a mortice latch, with the high failure pressure of the door causing a similar explosion development. In this instance, there were a series of damped oscillations that occurred just after the P_d and $P_{V(R)}$ pressure peaks that caused flow reversals between the interconnecting rooms and restricted the jetted flame process. Consequently, the maximum overpressure that was attained (270 mbar), was considerably lower than the corresponding test where the door hinged into the right enclosure (428 mbar, test 61).

A very interesting finding occurred with an identical experimental set-up to test 83, except that the door was left partially open, at an angle of 45° into the left enclosure (test 84). In this instance, the magnitude of the second pressure peak 703 mbar is over twice the pressure generated in test 83, where the door was initially closed. This test was repeated in test 85, producing a similar overpressure-time profile, with a maximum overpressure of 683 mbar (Figure 4-32). This type of test (test 84) produced the highest pressure measurement of the whole experimental programme.

Figure 4-32 shows the overpressure-time profiles for test 85. As the pressure peak was of a high magnitude, three of the plots are shown using a broken scale Y axis, so that the first major pressure peak and intermediate peak can be more clearly seen. The complete second major pressure peak, for the left room, is shown in isolation as a separate image (fourth plot).

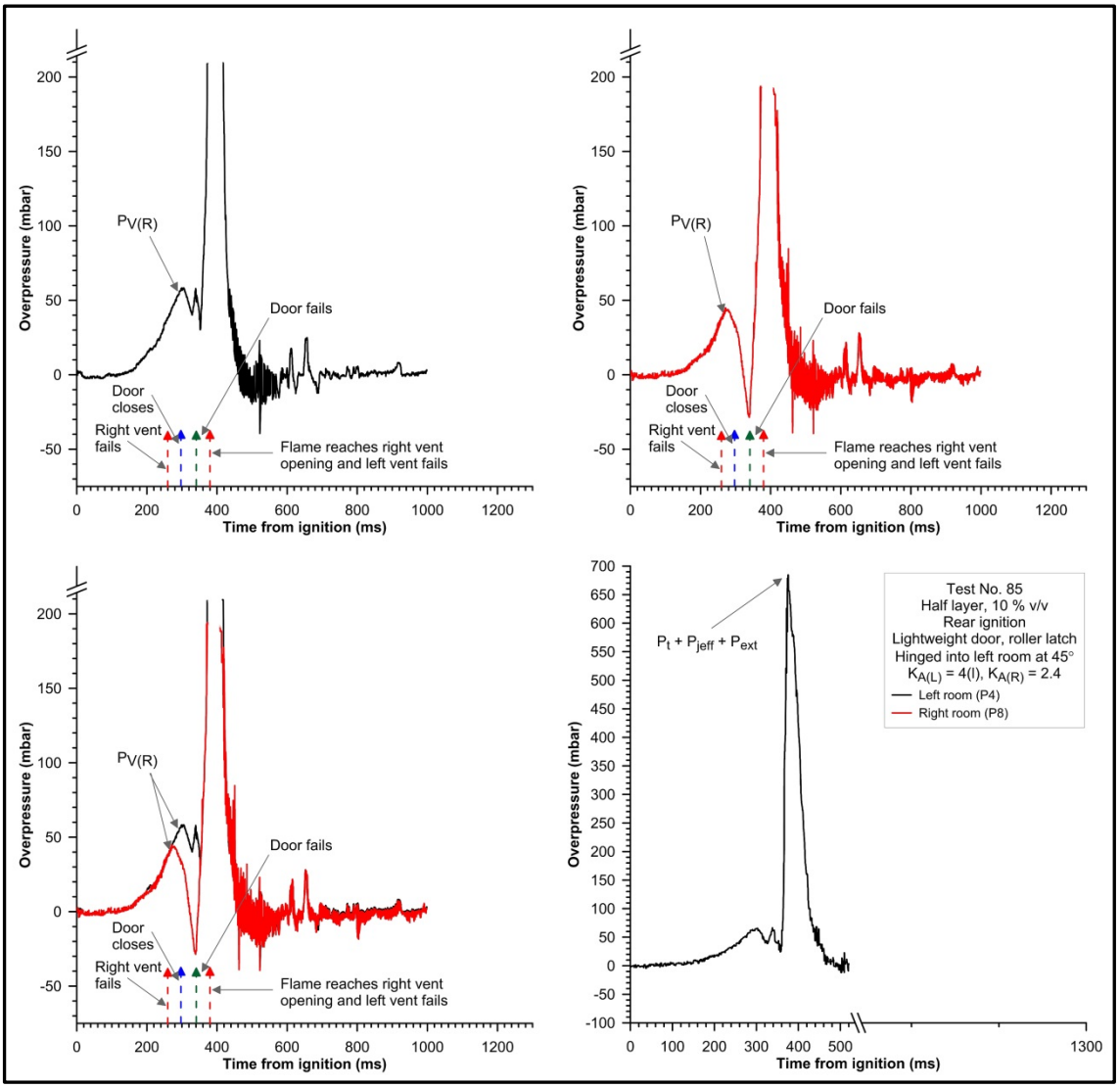

Figure 4-32 Overpressure-time profile for test with door open at 45° into left room

The door was initially open at an angle of 45° and consequently during the initial stages of the explosion the pressure in the two enclosures was equal. As the flame continued to propagate the pressure increased in both enclosures until, at 260 ms, the pressure in the right enclosure reached 40 mbar and the right vent failed. As soon as the right vent failed, the rapid flow towards the doorway (relieving the pressure in the left enclosure), pushed the door closed before the flame front was able to enter the right enclosure. As a consequence of the door closing, the right enclosure was able to continue venting, thus reducing the pressure, but the pressure in the left enclosure began to rise again, following an initial drop after the failure of the right vent ($P_{V(R)}$).

Evidence from cine film, taken from inside the explosion chamber clearly showed that the door had closed before the flame front reached the doorway, and that subsequently the door burst (breaking into several fragments) into the right enclosure (Figure 4-33). Almost instantaneously, a violent jet of flame was then seen to propagate into the right enclosure. This sequence, can be explained from the pressure-time profile.

Figure 4-33 Failure of the door and jetting expanding flame front (test 85)

When the pressure in the ignition (left) enclosure reached approximately 60 mbar, the door burst open, and because of the significant pressure differential created between the two rooms, the flame front was driven violently into the adjoining (right) enclosure. The relief of the pressure in left room, via the right enclosure, caused the pressure to fall, generating a small pressure peak in between the two major pressure peaks (Figure 4-32). The jetting flame front propagating towards the vent opening, resulted in an extremely rapid rise in flame surface area, generating a rapid pressure rise which resulted in the dominant pressure peak, which corresponds to both turbulent combustion and the jetting expanding flame front. Consequently, the peak has been

labelled $P_t + P_{jeff}$. Very quickly the flame reaches the plane of the right vent opening generating the external explosion, which also contributes to the magnitude of the second major pressure peak. The pressure wave produced by the turbulent combustion then propagated back through the doorway, greatly increasing the rate of combustion in the left enclosure, and the left vent fails.

This can be seen in Figure 4-34, which is a photo of the external combustion at the right vent opening during test 85. The left enclosure vent can be seen failing and being pushed clear of the opening at this point.

Figure 4-34 External explosion during test 85 (400 ms after ignition)

An external video camera was directed towards the right vent in order to try to capture the flame propagation after the vent had failed. Once the vent was clear of the opening, it was possible to track the flame as it propagated from the doorway to the vent opening. Whilst this was not an accurate method of measuring flame speed, it was possible, using the time record captured on the video, to estimate the average flame speed during this phase of the explosion. The flame was estimated to be travelling at a speed of approximately 130 m/s. For comparison, using cine film footage taken inside the left enclosure, the flame speed during the initial pressure rise leading to the failure of the right vent opening was estimated to be approximately 6 m/s.

A proposed mechanism for the type III explosions with a door open at 45°, and hinged into the left enclosure is given in Figure 4-35.

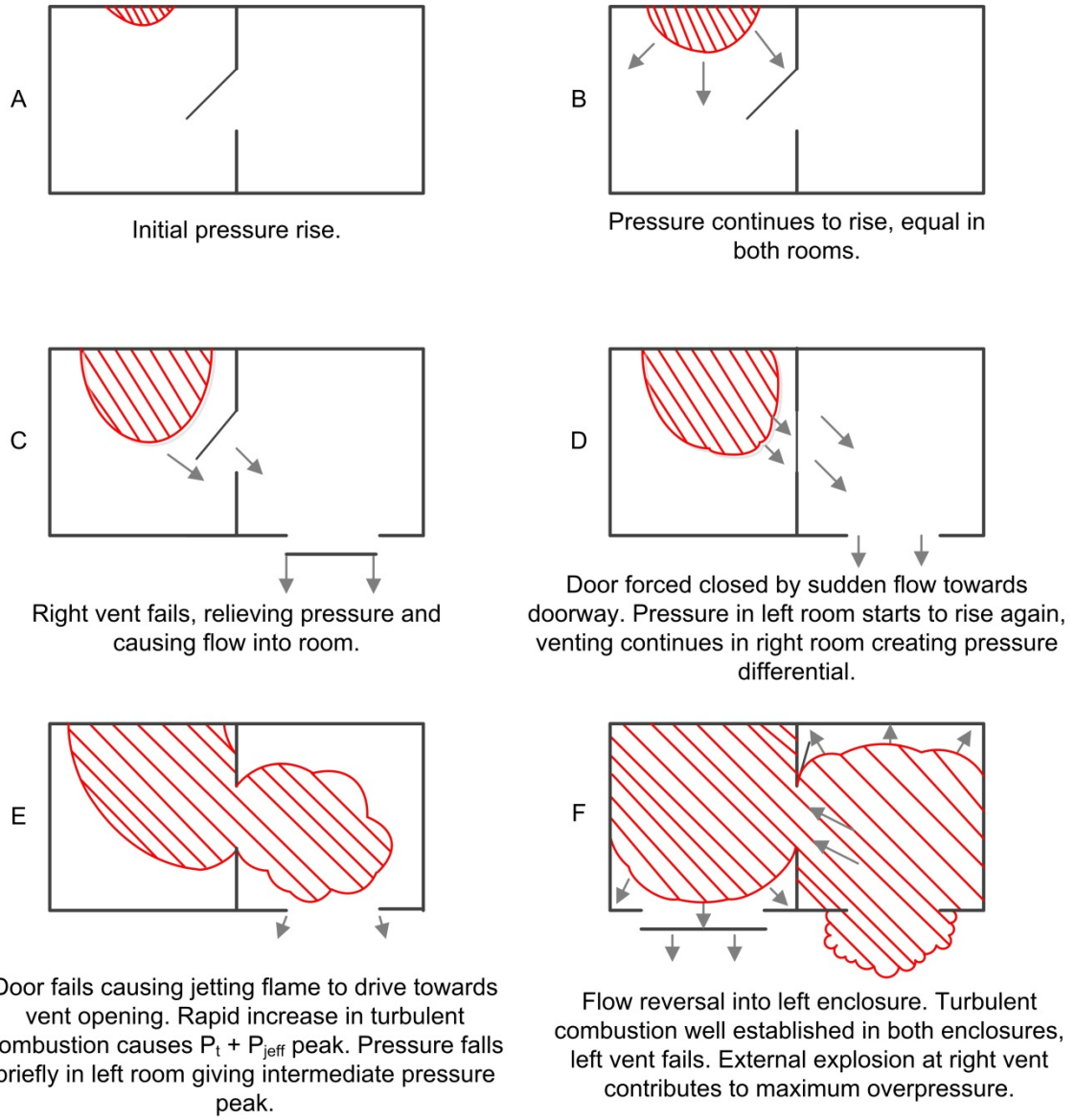

Figure 4-35 Proposed mechanism for type III tests (door open at 45°)

Test 84 and 85 were repeated in test 86, with the slight difference that the door was left open at an angle of 90° into the left enclosure. The maximum overpressure generated in this test however was 345 mbar, approximately half of that observed when the door was open at a 45° angle. Observations taken from the pressure-time profiles also revealed that there was no intermediate pressure peak between the P_V and P_t peaks. The cine footage taken inside the left enclosure revealed that the door did not close following the failure of the right vent and that the flame front passed through the interconnecting doorway. It is likely that the position of the door presented a greater inertia to overcome than is the case with a 45° angle. The rapid pressure rise following turbulent combustion in the right enclosure prevented the door from closing and demolished it before it could reach the door frame. Thus, the jetting flame from the left enclosure into the right enclosure was not enhanced, as would have happened if the

door had been pushed closed, and the magnitude of the P_t peak was reduced significantly.

This series of tests demonstrated the importance of the position of the interconnecting door, and the direction the door swings. Moreover, it can be one of the most significant factors in the development of the explosion and the generation of overpressure. As a limited number of experiments were undertaken, further large-scale experimental work is recommended.

4.6.10. Combustion Driven Oscillations

In Section 2.4.2, the effects of low frequency oscillations and high frequency acoustic oscillations were discussed. It was determined that the role that pressure oscillations play in accidental explosions in buildings was insignificant. Consequently, this section of the chapter only briefly discusses pressure oscillations observed during the tests.

In all of the tests, pressure oscillations were observed relatively late in the explosion (typically later than 600 ms), with each pressure transducer often recording a different magnitude, frequency and duration. However, a number of discrete frequencies, in the range of 60 to 480 Hz were observed during the experiments.

Several previous large-scale studies (see above referenced section) identified that acoustic pressure driven oscillations can be significant in vented explosions, often corresponding to the maximum overpressure developed. The pressure oscillations observed during this experimental programme did not correlate to any significant pressure peak. This was as expected for the reasons outlined in Section 2.4.2.

One important inference from the observation of combustion driven oscillations in the type I tests, was described in Section 4.4.1 and shown in Figure 4-1. In this case, the pressure oscillations occurred at the same time and had a similar magnitude and duration, but were out of phase by 180°. This suggested that the cause of the oscillations was bulk movement between the rooms via the doorway.

4.6.11. Summary of Findings of Type III Tests

A characteristic of the type III tests, in agreement with the findings of type I and II tests, was the exhibition of two major pressure peaks on the overpressure-time profiles. The first of these peaks corresponded to the failure of the vent in the right enclosure and was always recorded later in the left enclosure. The second major peak was found to be considerably greater in magnitude than the comparable peak in types I and slightly higher than type II. This pressure peak corresponded to the highly turbulent combustion in the right enclosure, caused by the venting driven ‘jetting’ flame, propagating into the adjoining enclosure and towards the right vent opening.

Analysis of the overpressure-time profiles revealed that whilst the presence of a closed door generated considerable turbulence, it has little effect on the maximum overpressure because the jetting flame was significantly more prominent. Consequently, although the maximum pressures produced in tests with a closed door were higher than those with an open doorway, the difference was not as significant as comparable tests of type II. However, the failure pressure of the interconnecting door, and its inertia, have been observed to be key factors in the generation of turbulence, resulting in some of the highest overpressures attained during the experimental programme. In addition, the complex nature of the interaction between the flow fields in the adjoining enclosures means that the turbulent combustion and jetting mechanisms are highly sensitive to the position of the door prior to ignition and the direction in which the door hinges.

As the dominant mechanism for generating pressure was turbulent combustion, the greatest overpressures were recorded with tests of 10% natural gas concentration. This is because the burning velocity is dependent upon concentration and is at its maximum, at concentrations slightly rich of stoichiometric, reducing as the concentration diverges towards its flammable limits.

Significantly higher overpressures were recorded with rear ignition tests. This is because the turbulent combustion process was less significant in central ignition tests.

The size of the left vent had little effect on the magnitude of the maximum overpressure as long as it had a greater failure pressure than the right vent. This is because the venting process occurred through the doorway and the vent opening in the adjoining enclosure.

In tests involving a concentration in the ignition enclosure that was different to the concentration in the adjoining enclosure, it was found that the maximum overpressure was strongly dependent upon the original mixture in the ignition enclosure, but had some dependence upon the mixture in the adjoining enclosure.

A summary of the type III test results is given in Table 4-8.

Table 4-8 Summary of type III test conditions and results

Test No.	Gas Conc. (% v/v)		Layer depth	Ignition Position	Door type	Latch	Door Status	Vent Size (K_A)		Max Pressure (mbar)
	Ign (L)	Adj (R)						Ign (L)	Adj (R)	
43	8	8	1.2	Rear	Lightweight	Unlatched	Closed	4r	2.4	276
44	10	10	1.2	Rear	Lightweight	Unlatched	Closed	4r	2.4	372
45	12	12	1.2	Rear	Lightweight	Unlatched	Closed	4r	2.4	207
46	10	10	1.2	Central	Lightweight	Unlatched	Closed	4r	2.4	83
47	10	10	1.2	Central	Lightweight	Unlatched	Open	4r	2.4	186
48	8	8	1.2	Rear	Lightweight	Unlatched	Open	4r	2.4	69
49	12	12	1.2	Rear	Lightweight	Unlatched	Open	4r	2.4	117
50	8	8	1.2	Rear	Lightweight	Unlatched	Open	8	2.4	103
51	10	10	1.2	Rear	Lightweight	Unlatched	Open	8	2.4	324
52	12	12	1.2	Rear	Lightweight	Unlatched	Open	8	2.4	159
53	8	8	1.2	Rear	Lightweight	Unlatched	Closed	8	2.4	317
54	10	10	1.2	Rear	Lightweight	Unlatched	Closed	8	2.4	462
55	12	12	1.2	Rear	Lightweight	Unlatched	Closed	8	2.4	214
56	10	10	1.2	Central	Lightweight	Unlatched	Closed	8	2.4	97
60	8	8	1.2	Rear	Lightweight	Roller latch	Closed	4r	2.4	290
61	10	10	1.2	Rear	Lightweight	Roller latch	Closed	4r	2.4	428
62	12	12	1.2	Rear	Lightweight	Roller latch	Closed	4r	2.4	393
63	8	8	1.2	Rear	Fire door	Unlatched	Closed	4r	2.4	331
64	10	10	1.2	Rear	Fire door	Unlatched	Closed	4r	2.4	400
65	12	12	1.2	Rear	Fire door	Unlatched	Closed	4r	2.4	407
66	10	10	1.2	Rear	Fire door	Roller latch	Closed	4r	2.4	501
67	10	10	1.2	Rear	Lightweight	Mortice latch	Closed	4r	2.4	227
68	10	10	1.2	Rear	Fire door	Mortice latch	Closed	4r	2.4	331
71	8	10	1.2	Rear	Lightweight	Roller latch	Closed	4r	2.4	262
72	10	8	1.2	Rear	Lightweight	Roller latch	Closed	4r	2.4	400
73	8	12	1.2	Rear	Lightweight	Roller latch	Closed	4r	2.4	310
74	12	8	1.2	Rear	Lightweight	Roller latch	Closed	4r	2.4	241
75	10	12	1.2	Rear	Lightweight	Roller latch	Closed	4r	2.4	276
76	12	10	1.2	Rear	Lightweight	Roller latch	Closed	4r	2.4	352
77	6	13	1.2	Rear	Lightweight	Roller latch	Closed	4r	2.4	234
78	13	6	1.2	Rear	Lightweight	Roller latch	Closed	4r	2.4	290
79	6	10	1.2	Rear	Lightweight	Roller latch	Closed	4r	2.4	83
80	10	6	1.2	Rear	Lightweight	Roller latch	Closed	4r	2.4	345
81	10	10	0.3	Rear	Lightweight	Roller latch	Closed	4r	2.4	103
82	10	10	0.6	Rear	Lightweight	Roller latch	Closed	4r	2.4	221
83	10	10	1.2	Rear	Lightweight	Unlatched	Hinged into L (closed)	4r	2.4	262
84	10	10	1.2	Rear	Lightweight	Unlatched	Hinged into L - 45°	4r	2.4	703
85	10	10	1.2	Rear	Lightweight	Unlatched	Hinged into L - 45°	4r	2.4	683
86	10	10	1.2	Rear	Lightweight	Unlatched	Hinged into L - 90°	4r	2.4	345
87	10	0	1.2	Rear	Lightweight	Roller latch	Closed	4r	2.4	234

4.7. Type IV Experiments

The type IV tests, undertaken as series G, had two K_A = 4 vents. In the left enclosure the vent was fitted to the left side of the fascia panel [$K_{A(L)}$ = 4(l)] and in the right enclosure it was fitted to the right side [$K_{A(R)}$ = 4(r)].

There were only five tests undertaken of this type. All the tests were undertaken with a layer, rear ignition and the door closed. However, in these series, different doors, latching mechanisms and vent materials were used in a manner similar to test type III. The specific set up of the test series is given in Table 4-9.

Table 4-9 Door type and vent material for type IV tests

Test No.	Gas Concentration (% v/v)		Door Type	Latching Mechanism	Vent Material
	Ign (L)	Adj (R)			
57	10	10	Lightweight	Unlatched	12 mm fibreboard
58	10	10	Lightweight	Unlatched	12 mm fibreboard
59	12	12	Lightweight	Unlatched	12 mm fibreboard
69	10	10	Fire door	Roller latch	3 mm single pane glass
70	12	12	Fire door	Roller latch	4 mm single pane glass

4.7.1. General

The maximum overpressures generated during these tests were, in general terms, of a range in between that of the type I and type II tests. In some tests (57, 69 and 70) the left vent failed first, generating the $P_{V(L)}$ pressure peak and resulting in overpressure-time profiles similar to the type II tests whereas in the other tests the vents failed simultaneously to give $P_{V.}$

The K_A = 4 vents had a failure pressure of approximately 70 mbar. Because both of the enclosures utilised these higher failure pressure vents, the duration of the flow between rooms was longer than in the type I tests, generating more turbulence, such that P_t dominated the second major pressure peak. In general terms, the type IV tests represented an intermediate case between type I and type II tests.

4.7.2. Experiments with a Single Pane Glass Vent

Two experiments, test numbers 69 and 70, were conducted with single paned glass as the vent material instead of the 12.5 mm fibreboard. In test 69, the glass was 3 mm thick and in test 70, the glass was 4 mm thick.

During both of these tests, the left vent failed first, producing $P_{V(L),}$ but at that time the right vent remained intact. Consequently, these experiments can be likened to the type II tests. However, the 3mm glass failed at a much lower pressure than the 12.5 mm fibreboard and hence a much lower P_V overpressure was produced (see Figure 4-36).

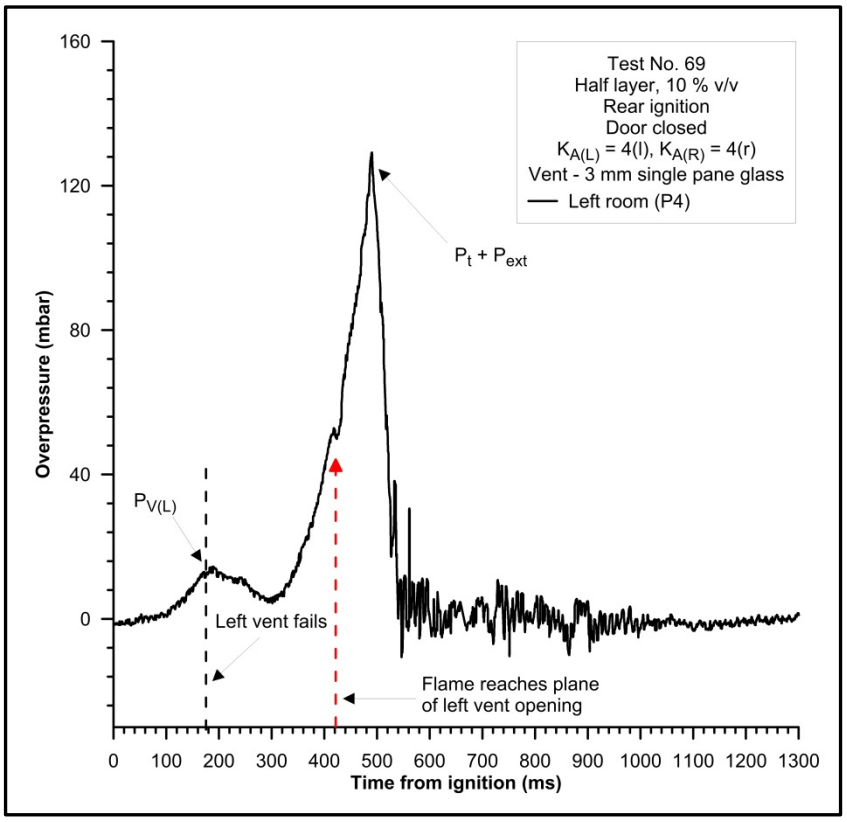

Figure 4-36 Overpressure-time profile for test with 3 mm single pane glass vent

Figure 4-37 shows the failure of the right window. The window was made of single pane glass, 4 mm thick. It can be seen that the left vent had already failed and that there is a secondary external explosion at the right vent opening. This secondary external explosion has transpired because the gas/air mixture was expelled through the right vent opening after the external explosion at the left vent had occurred.

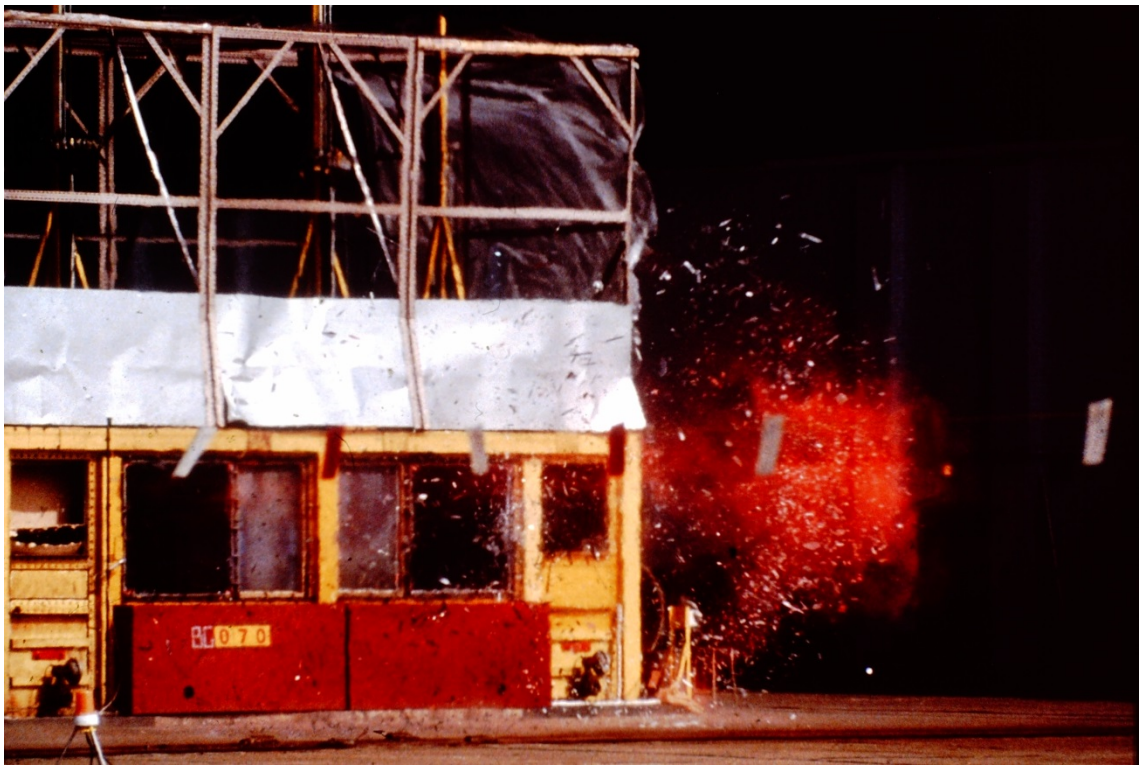

Figure 4-37 Failure of the right 4 mm single glass pane vent and secondary external explosion (taken from DNV GL archive)

4.8. Comparison of Experimental Results

It is apparent that there are four main mechanisms for the development of the maximum pressure peak:

1. The external explosion – this occurs in situations where the failure pressure of the vent relief is the same in adjoining rooms.
2. The sudden turbulent combustion in the adjoining room – this occurs where the failure pressure of the vent relief is higher in the adjoining room and where there is an interconnecting door that is initially closed.
3. The sudden increase in flame surface area as a consequence of a jetting flame into the adjoining room – this occurs where the failure pressure of the vent relief is lower in the adjoining room and where there is an interconnecting door that is closed.
4. A combination of turbulent combustion and a rapid increase on flame surface area as a consequence of a jetting flame into the adjoining room – this occurs where the failure pressure of the vent relief is lower in the adjoining room and where there is an interconnecting door that is partially open.

4.8.1. Maximum Overpressure

In the literature review, it was identified that most of the vented explosion research has been undertaken in single empty chambers that are not representative of gas explosions in buildings. However, four correlations were identified, that were developed from the research conducted after the Ronan Point explosion. For completeness, the predicted overpressures from these correlations have been compared to the explosion data from this study. The correlation of Astbury et al. was omitted from this comparison as one of the input parameters was the maximum pressure developed in the ignition room and this was found to be dependent upon the interaction between the enclosures.

In Figure 4-38 a comparison is made of the experimental results from the work described in this thesis and the correlations derived by Rasbash [Equation (2-74)], Rasbash et al. [Equation (2-75) and (2-76)], Cubbage and Marshall [Equation (2-78)] and Dragosavic [Equation (2-83)]. In respect of the experimental results, the maximum overpressures (irrespective of test type) have been plotted and, in addition, the maximum overpressures produced for each test type have been averaged and plotted against equivalence ratio. The predicted maximum overpressure from Equation [(2-78)] has been plotted for the corresponding equivalence ratios by selecting appropriate values for the laminar burning velocity. It was not possible to predict the maximum overpressure against equivalence ratio using the Dragosavic or Rasbash correlations.

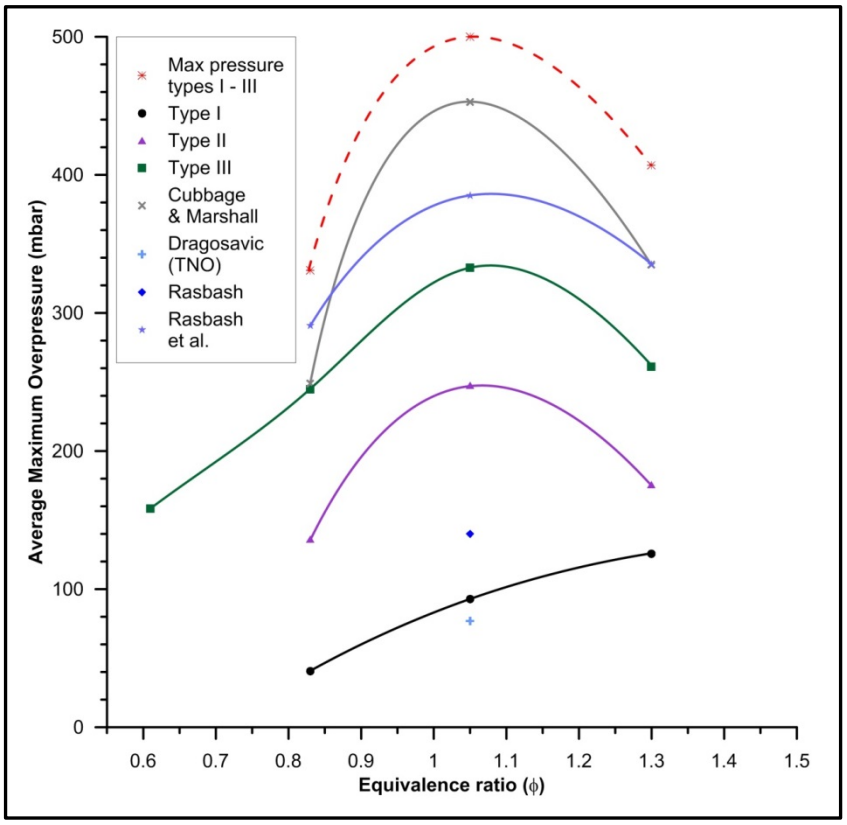

Figure 4-38 Comparison of experimental results

It can be seen from Figure 4-38 that the average maximum overpressure for type I test increases with concentration, showing that there is a dependence upon gas concentration. This demonstrates that the dominating factor in type I tests is the external explosion, with fuel rich mixtures more likely to produce a near stoichiometric flammable cloud outside the vent opening. The curves for the type II and III experiments do not follow this trend due to the dominance of turbulent combustion and/or a rapid increase in flame surface area due to the jetting expanding flame front. Consequently, the curves for these tests are similar to the burning velocity curve, where it peaks at an equivalence ratio of approximately 1.05 and diverges towards the flammable limits.

The Dragosavic correlation underpredicts the average maximum overpressure for all the test types. This is perhaps not surprising as the correlation was developed to simulate the two pressure peaks that were a feature of the TNO experimental results. However, whilst the first pressure peak was identical to that of this experimental programme, the second pressure peak was caused by oscillations towards the end of the explosion and was most commonly lower in magnitude than the first peak. The failure pressure of the vent was therefore a key factor in the magnitude of the overpressure.

The correlation of Rasbash et al. and Cubbage and Marshall overpredict the average maximum pressure developed but underpredict the maximum pressure for all equivalence ratios. However, the correlations of Rasbash et al. and Cubbage and Marshall are interesting as they follow the type II and III profiles remarkably well. This is largely due to the fact that the correlation is dependent upon the turbulent burning velocity and the type II and III tests are dominated by turbulent combustion. Given, that the correlations are also dependent upon a turbulence ‘factor’ it is recommended that further work be undertaken to investigate whether this correlation could be refined in light of the findings of this study.

Mannan [405] in reference to the Rasbash et al. and Cubbage and Marshall correlations states that the Cubbage and Marshall correlation is limited to methane/air mixtures as the dependency on the square of the burning velocity tends to give overestimates of the maximum pressure for gases with high burning velocity. The results presented in this chapter suggests that this is likely not the case as the correlation is underpredicting the maximum pressure for methane/air concentrations but overpredicting the average maximum overpressures for all test types.

In terms of overpressure-time profile, the prediction of Molkov (Figure 2-36) is not in agreement with the findings of this work. The time taken to reach both pressure peaks

occurs far too quickly and the pressure-time curve bears little resemblance to that seen in the during the experiments. Furthermore, the second pressure peak was not caused by “mixture burnout”, but rather, was caused by the external explosion, turbulent combustion or the jetting flame.

Structural Damage

In the literature review it was identified, that overpressures greater than 200 mbar could structurally damage a building. One of the objectives of this study was to determine if significant pressure damage could be produced by fuel lean and/or fuel rich flammable gas/air mixtures. Table 4-10 details the tests where the maximum overpressure exceeded this value. It is clear from the results, that damaging overpressures can be produced by mixtures across the flammable range, given the right set of circumstances. This is an important finding and is not in agreement with the most widely used reference sources used in the investigation of gas explosions [12, 15, 16].

Table 4-10 Tests capable of causing structural damage to a building

Test Type	Test No.	Gas Conc. (% v/v)	Layer or Full	Ignition Position	Door Status	P_{max}
II	25	8	Layer	Rear	Closed	214
II	26	10	Layer	Rear	Closed	400
II	27	10	Layer	Rear	Closed	269
II	33	12	Layer	Rear	Closed	234
II	34	10	Layer	Central	Open	200
II	35	10	Layer	Central	Closed	207
II	36	10	Layer	Rear	Closed	372
II	40	10	Full	Rear	Closed	338
II	41	10	Layer	Rear	Closed	414
II	42	10	Full	Rear	Closed	317
III	43	8	Layer	Rear	Closed	276
III	44	10	Layer	Rear	Closed	372
III	45	12	Layer	Rear	Closed	207
III	51	10	Layer	Rear	Open	324
III	53	8	Layer	Rear	Closed	317
III	54	10	Layer	Rear	Closed	462
III	55	12	Layer	Rear	Closed	214
IV	58	10	Layer	Rear	Closed	283
III	60	8	Layer	Rear	Roller latch	290
III	61	10	Layer	Rear	Roller latch	428
III	62	12	Layer	Rear	Roller latch	393
III	63	8	Layer	Rear	Fire door unlatched	331
III	64	10	Layer	Rear	Fire door unlatched	400
III	65	12	Layer	Rear	Fire door unlatched	407
III	66	10	Layer	Rear	Fire door roller latch	501
III	67	10	Layer	Rear	Mortice latch	227
III	68	10	Layer	Rear	Fire door mortice latch	331
IV	70	10	Layer	Rear	Fire door roller latch	359
III	71	8	Layer	Rear	Roller latch	262
III	72	10	Layer	Rear	Roller latch	400
III	73	8	Layer	Rear	Roller latch	310
III	74	12	Layer	Rear	Roller latch	241
III	75	10	Layer	Rear	Roller latch	276
III	76	12	Layer	Rear	Roller latch	352
III	77	6	Layer	Rear	Roller latch	234
III	78	13	Layer	Rear	Roller latch	290
III	80	10	Layer	Rear	Roller latch	345
III	81	10	Layer	Rear	Roller latch	103
III	82	10	Layer	Rear	Roller latch	221
III	83	10	Layer	Rear	Hinged into left room	269
III	84	10	Layer	Rear	Hinged into left room 45°	703
III	85	10	Layer	Rear	Hinged into left room 45°	683
III	86	10	Layer	Rear	Hinged into left room 90°	345
III	87	10	Layer	Rear	Roller latch	234

4.8.2. The Influence of Turbulence

A number of calculations were made to determine the turbulence intensity for the range of test types and to relate this information to the explosion development mechanisms that have been identified in this study. Some of these results are presented In Table 4-11, where values are given for the maximum overpressure, turbulence intensity and rms velocity of the flow. The key mechanism for the development of the maximum pressure is included as it provides a useful appraisal of the calculated turbulence values and the proposed mechanisms for pressure development.

Table 4-11 Calculated values of turbulent flow

Test Type	Test No.	Q_{max} (m^3/s)	U_{max} (m/s)	U	u′/U	u′ (m/s)	P_{max} (mbar)	Dominant Peak
I	14	24.50	16.28	2.84	0.221	0.62	88	P_{ext}
II	26	53.69	35.68	6.21	0.221	1.38	400	P_t
III	44	50.93	33.85	5.89	0.221	1.31	372	P_{jeff}
III	67	80.53	53.52	9.32	0.221	2.07	227	P_t
III	85	103.97	69.09	12.03	0.221	2.67	683	$P_t + P_{jeff}$

The results in the table are informative and provide additional support to the qualitative analysis undertaken as the main body of work in this chapter. It can be seen that the type I tests produce some turbulence, but it was not significant, and this is corroborated by the qualitative analysis that shows the dominating mechanism, under these circumstances, to be the external explosion. The type II tests produced much more turbulence and this is substantiated by the high overpressure produced and the observations that these type of tests were turbulence dominated. It can also be seen that the type III test (test 44), produced a slightly lower level of turbulence than the type II test. This is in agreement with the observations that turbulence had less influence on this type of explosion and the sharp pressure rise corresponded to the rapidly expanding flame front due to the jetting flame. However, significant levels of turbulence were produced by some of the type III explosions. Relatively high levels of turbulence occurred when the interconnecting door had a high failure pressure (i.e. fire door or latched), and most prominently, situations where the door hinged into the room in which ignition occurred and was partly open (45°angle).

4.9. Conclusions

The results presented in this chapter represent a substantial amount of new large-scale explosion data, which has been interpreted to provide a better understanding of how gas explosions develop in buildings and how this information can be applied during the subsequent origin and cause investigation.

A number of mechanisms have been proposed, providing new knowledge and understanding of the manner in which gas explosions propagate from one room to another. This knowledge provides a valuable new insight into how complex a vented explosion in a typical building can be, and how the design and construction of a building can affect the magnitude of the explosion (e.g. the selection of windows, the use of heavy doors, doors that hinge into rooms with significant ignition sources etc.).

It is clear from the results of this programme that gas explosions that propagate from one room to another have the potential to generate significantly higher overpressures than would be the case of an explosion in a single room of the same total volume and vent area.

With the exception of some tests involving fuel lean layers, the overpressure-time profiles were characterised by two dominant pressure peaks. The first of these peaks, occurred in all tests and corresponded to the failure, of one or both of the vents. The second peak corresponded to the external explosion or turbulent combustion as a consequence of the interaction between adjoining rooms. For the vast majority of the tests, the second major pressure peak produced the maximum overpressures. The maximum pressures recorded during the programme ranged from 38 mbar (type I test) to 703 mbar (type III test). Several major mechanisms for the development of the high overpressures have been identified:

i. The ignition of a flammable cloud outside the vent opening(s) (i.e. the external explosion).
ii. The sudden increase in mass combustion as the turbulised mixture in the secondary compartment is ignited by the propagating flame front emerging through the interconnecting doorway.
iii. The highly turbulent ‘jetting’ flame, driven by the venting process, propagating from the interconnecting doorway and towards the vent opening in the secondary enclosure.

The relative influence of the different explosion development mechanisms was strongly dependent upon the configuration of the explosion chamber and the ignition position. In terms of the configuration of the explosion chamber, the key factors were the failure

pressures of the respective vents, and the status (including the direction of hinge), failure pressure and inertia of the interconnecting door, prior to ignition.

Where both enclosures had large, low failure pressure vents, the maximum pressure peak was dominated by the external explosion. The external explosion caused a rapid pressure rise of short duration (≈ 50 ms), which restricted the outflow from the vent, thereby raising the pressure within the enclosure. The pressure wave also propagated back into the enclosure and, in type II and III tests, could cause turbulent combustion in the adjoining enclosure. The magnitude of the pressure wave was found to be directly dependent upon the concentration, increasing over the range 8% to 12%. This was due to the dilution of the flammable cloud that had formed outside the explosion chamber. Consequently, the maximum overpressure recorded, that was solely due to an external explosion, corresponded to a 12% half layer (179 mbar). It should be noted that a test involving a 10% gas/air mixture produced a pressure a peak pressure of identical magnitude but involved an enclosure that was full of flammable mixture (as opposed to a layer).

In type II tests, where the enclosure in which ignition was initiated had a vent of lower failure pressure than the adjoining enclosure, and the interconnecting door failed prior to either of the vents, turbulence was created in the adjoining enclosure by flow through the doorway. The flow was set-up by the development of a pressure differential due to the presence of the door. In addition, the action of the opening of the door into the adjoining enclosure caused turbulence. The turbulence had the effect of increasing the burning velocity, and hence the mass combustion rate, so large overpressures were developed when the flame front propagated from the ignition room into the secondary enclosure. In addition, the flame front distorted as it passed through the doorway, increasing the flame surface area and hence the mass burning rate. Overpressures produced by this mechanism, corresponded to the second major peak and were recorded as high as 414 mbar for a 10% layered explosion.

It was discussed in the report following the Potters Marston experiments [27] that ‘back-relief’ could limit the maximum overpressure developed in an explosion where the flame could propagate from one room to another. However, if you consider the open doorway and vent in the neighbouring room as ‘back-relief’, then this experimental work has demonstrated that a type II explosion could produce overpressures that would cause structural damage to a building. This appears to contradict one of the conclusions of the Potters Marston work. However, the discrepancy may be explained as both compartments at Potters Marston had very

large vent panels of low failure pressure, whereas in these experiments, the adjoining enclosure had a small vent with a relatively high failure pressure.

In type III tests, where the enclosure in which ignition was initiated had a vent of greater failure pressure than the adjoining enclosure, flow through the interconnecting doorway caused turbulence in the secondary chamber. When the vent in the adjoining enclosure failed, pressure in the left enclosure was relieved as unburnt gas/air mixture flowed, and the flame front propagated, through the doorway and towards the vent in the right enclosure. This rapid venting process caused the flame front to 'jet' through the secondary enclosure towards the vent. The flame front expanded rapidly and combustion was highly turbulent, so high overpressures were attained (462 mbar). Higher overpressures still, over 700 mbar, were attained when the door was hinged into the left enclosure (ignition) and left open at a 45° angle.

Due to the complex interaction of flow between the interconnected rooms, it was found that in some circumstances unburnt gas/air mixture in the secondary chamber could be either mixed with combustion products, or expelled through the vent opening during flame jetting. This meant that the maximum overpressure was much more strongly dependent on the mixture in the left enclosure than that in the adjoining room.

As expected, the ignition position had a significant effect on the maximum overpressure and the mechanism of explosion development. The magnitude of the external explosion is dependent upon its concentration and mass. With rear ignition, a greater volume of unburnt gas/air mixture is expelled through the opening. Consequently, explosions dominated by the external explosion produced higher pressure peaks with rear ignition than with central ignition. In the case of the turbulent combustion and jetting flame mechanisms, the ignition location determines the time between ignition and flame entry into the adjacent enclosure. Consequently, shorter travel distances, such as with central ignition, will result in the flame front reaching the doorway faster than with rear ignition, resulting in less turbulent combustion and lower overpressures.

The most important findings, in terms of the objectives of this study, are that under the right conditions, fuel lean and fuel rich explosions can cause overpressures that have the potential to structurally damage buildings (> 200 mbar). For example, in test 53, an 8% natural gas/air layer produced an overpressure of 317 mbar and in test 62, a 12% layer caused an overpressure of 393 mbar. These results are of considerable importance to gas explosion investigators involved in the interpretation of forensic evidence at the scene of a gas explosion in a building, since extensive pressure damage is not usually associated with either lean or rich mixtures.

CHAPTER 5
THE EFFECTS OF IDEALISED OBSTACLES AND FURNITURE

CHAPTER 5

THE EFFECTS OF IDEALISED OBSTACLES AND FURNITURE

5.1. Introduction

In Chapter 4, it was identified that turbulence and the jetting expanding flame front play a key role in gas explosions in buildings, initiated by the complex flow interaction through interconnected rooms. However, turbulence can also be generated by the interaction of flow with obstacles, such as furniture.

Typical modern furnished dwellings will have a pathway, for flame propagation, that consists of a number of interconnected rooms, each of which may have significant congestion. In Chapter 3, it was identified that the average UK home would have room congestion of the order of 17% (by volume), with living rooms of the order of 5 – 10%. To understand the effects of furniture, in the development of accidental explosions in buildings, two large-scale experimental programmes were undertaken at the DNV GL Spadeadam Test Site. The results of these confined vented explosion programmes are discussed in this chapter.

5.2. Experimental Programmes

The experimental programmes (programmes 2 and 4) were designed to investigate a wide range of parameters that were likely to influence the development of the explosion and the maximum overpressure. Experimental programme 2 was conducted in Rig B and consisted of thirty eight natural gas/air vented explosion tests with idealised obstacle arrays. Experimental programme 4 was carried out in Rig C and consisted of seventeen methane/air tests, of which eleven had furniture within the explosion chamber.

5.3. Experiments Involving Idealised Obstacle Arrays (Rig B)

The main variables of interest in this study were vent size (i.e. representative of differing window sizes in buildings) and the degree of congestion within the explosion chamber (investigated in terms of the area and volume blockage).

5.3.1. Test conditions and Data (experimental programme 2, Rig B)

A summary of the experimental test conditions and data gathered from the thirty-eight explosion tests is contained in Table 5-1 All the tests were ignited at the centre of the rear chamber wall, using full volume, natural gas/air mixtures of 10% concentration (v/v). Due to budgetary constraints, and that this explosion chamber had been used for a large number of explosions involving pipe arrays where repeatability had been demonstrated, only a small number of nominally identical experiments were undertaken to check repeatability (tests 12 and 13, and tests 33, 34 and 35). The peak overpressure in tests 33, 34 and 35 was found to vary by approximately 5%, which was within the 10% limit identified by MRS [403]. However, tests 12 and 13 were found to have variability exceeding this limit (15%). Tests 12 and 13 involved the highest degree of confinement and consequently it was possible for these tests to exhibit significant variability in maximum overpressure for the reasons described in Section 3.17 [402].

Table 5-1 Summary of test conditions and experimental data.

Test No.	K_A	Congestion			P_V[b] (mbar)	P_b[b] (mbar)	P_{ext}[b] (mbar)	P_{mfa}[b] (mbar)	P_{max}[b] (mbar)	Flame Speed[c] (m/s)
		Type[a]	AB (%)	VB (%)						
1	1	-	0.0	0.00	14	22	69	44	69	35
2	1	m	12.0	0.57	14	81	155	120	155	88
3	1	l	12.0	0.75	14	112	135	157	157	86
4	1	k	20.0	0.94	14	108	145	119	145	83
5	1	j	20.0	1.26	11	203	246	-	246	89
6	1	l	28.0	1.31	13	365	380	368	380	145
7	1	h	12.0	1.51	13	309	336	285	336	152
8	1	e	28.0	1.76	11	374	393	418	418	149
9	1	c	20.0	2.51	20	547	713	715	715	192
10	1	d	40.0	2.51	20	-	903	815	903	210
11	1	b	28.0	3.52	21	1350	1425	1296	1425	262
12	1	a	40.0	5.02	18	2793	2992	2272	2992	395
13	1	a	40.0	5.02	-	3367	3474	2941	3474	-
14	2	-	0.0	0.00	12	23	92	-	92	143
15	2	m	12.0	0.57	14	301	477	671	671	86
16	2	l	12.0	0.75	20	320	677	405	677	102
17	2	j	20.0	1.26	21	555	1079	790	1079	111
18	2	h	12.0	1.51	18	-	719	1036	1036	109
19	2	f	28.0	1.76	20	686	678	1614	1614	125
20	2	e	28.0	1.76	15	661	780	1281	1281	109
21	2	g	28.0	1.76	-	691	1073	969	1073	66
22	2	c	20.0	2.51	17	1162	1259	1937	1937	172
23	2	d	40.0	2.51	-	1641	1934	1979	1979	176
24	2	b	28.0	3.52		1801	1986	2273	2273	185
25	4	-	0.0	0.00	20	96	183	132	183	132
26	4	l	12.0	0.75	-	-	-	1058[d]	1058	103
27	4	j	20.0	1.26	-	-	-	1397[d]	1397	114
28	4	c	20.0	2.51	-	1293	-	2152[d]	2152	115
29	4	b	28.0	3.52	-	2185	2508	2992[d]	2992	203
30	9	-	0.0	0.00	26	-	-	353[d]	353	417
31	9	l	12.0	0.75	-	-	-	1598[d]	1598	64
32	9	k	20.0	0.94	-	1406	-	2006[d]	2006	72
33	9	j	20.0	1.26	-	-	-	2134[d]	2134	88
34	9	j	20.0	1.26	-	-	-	2262[d]	2262	-
35	9	j	20.0	1.26	-	-	-	2162[d]	2162	-
36	9	h	12.0	1.51	-	-	-	2098[d]	2098	70
37	9	c	20.0	2.51	-	-	-	2996[d]	2996	-
38	9	b	28.0	3.52	-	-	-	3700[d]	3700	-

[a] See Figure 3-13 for the specific pipe array layout for each congestion type.
[b] Measurement taken from a piezoelectric pressure transducer located 0.4 m from the spark igniter.
[c] Flame speed calculated at a distance 7.5 m from the spark igniter.
[d] Relatively long duration peak, combination of P_{ext} and P_{mfa}.

5.3.2. General

In Figure 5-1, a pressure-time profile is shown for an explosion in an empty enclosure with a vent size of K_A = 1; four distinct pressure peaks are evident.

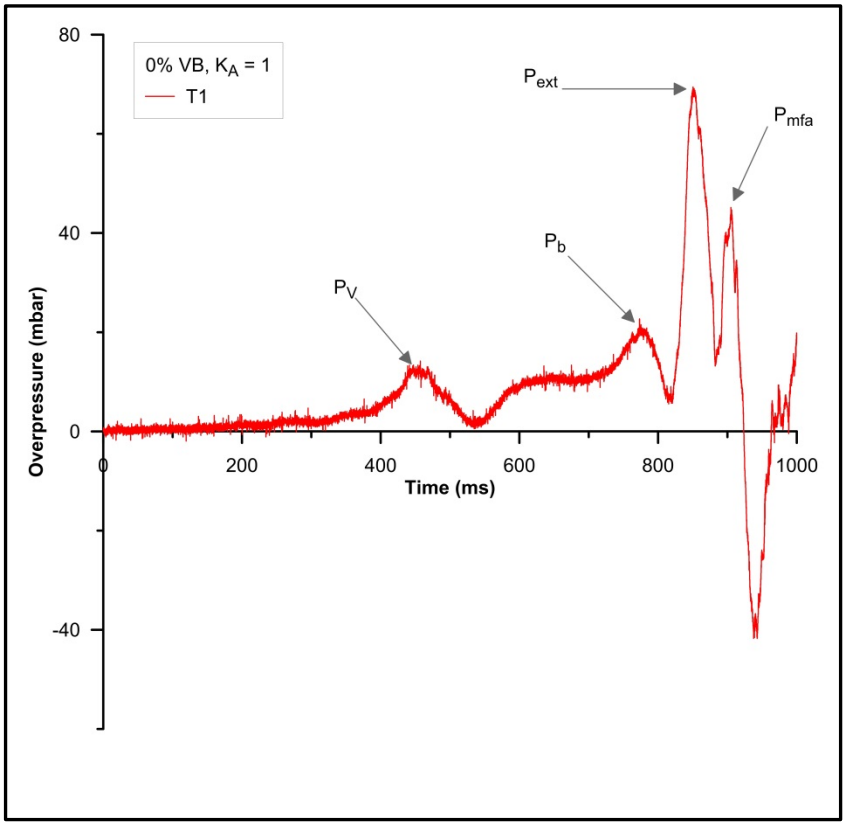

Figure 5-1 Overpressure-time profile for test number 1

The first pressure peak, P_V, corresponds to the failure of the polythene sheet at a time of around 450 ms after ignition. The polythene sheet failed at an overpressure of approximately 14 mbar and as this does not represent a significant pressure gradient across the vent opening, the rate of unburnt gas/air outflow is relatively low. The second pressure peak, P_b, corresponds to the onset of burnt gas venting at a time of approximately 775 ms and was recorded as the time that the flame front reached the plane of the vent opening. With the onset of burnt gas venting, the volumetric outflow rate increases dramatically as the volumetric flow through the vent is inversely proportional to the square root of the density of the gas being vented. This significant increase in outflow manifests itself as a drop in pressure on the pressure-time profile resulting in the pressure peak P_b. The third pressure peak corresponds to the external explosion, which occurs when the previously vented unburned gas/air mixture is ignited by the flame front when it exits the vent opening.

In Figure 5-2, a pressure-time profile, recorded on pressure transducers T1 and T6, is shown for test number 2. Transducer T1 was located 0.4 m from the rear of the explosion chamber and transducer T6 was located 4 m outside the vent opening

resulting in a distance of 12 m between the transducers (Table 3-3). The speed of sound in the combustion products of a stoichiometric methane/air was calculated to be 992 m/s meaning that if the pressure wave generated by the external explosion was propagating into the explosion chamber, giving rise to a pressure peak, P_{ext}, it would be recorded at transducer T1, 12 ms after it was recorded at T6.

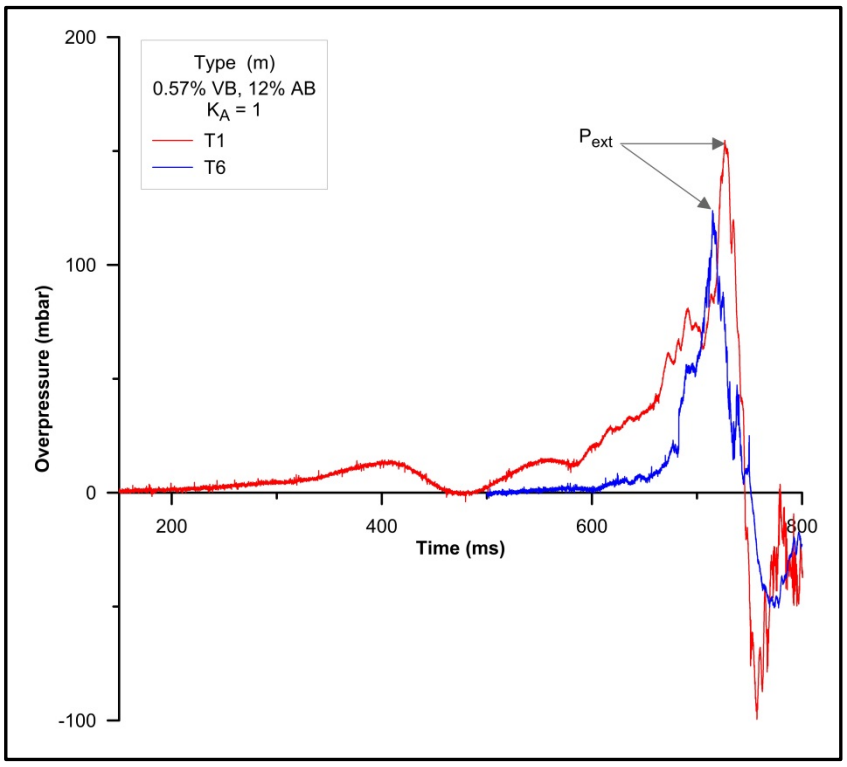

Figure 5-2 Pressure-time profile showing the effects of the external explosion

In Figure 5-2 it can be seen that the external explosion was recorded on T6 at 715 ms, generating a pressure peak of 123 mbar. The corresponding pressure peak on T1, identical in its profile but of greater magnitude, was recorded at 727 ms and generated a pressure peak of 155 mbar. Importantly, in all but two of the experiments (test no's 3 and 5, where the pressure peak was of the same magnitude), the magnitude of the pressure inside the enclosure was greater than that recorded outside. Consequently, the external combustion event cannot be solely attributable to the pressure peak generated within the explosion chamber, and whilst it was evident that the pressure peak was triggered by the external explosion, its magnitude was caused by a combination of the propagation of the external pressure wave into the enclosure, the temporary restriction to the outflow of gases caused by the reduced pressure differential across the vent opening following the external combustion, and by increases in the rate of combustion caused by turbulence and Taylor instabilities. In Figure 5-1, the fourth pressure peak corresponds to the time at which the flame surface area was at its greatest, giving rise to the pressure peak, P_{mfa}. This peak was seen on a number of tests to be superimposed onto the P_{ext} pressure peak.

Taylor instabilities are hydrodynamic instabilities introduced when the less dense burned gases are accelerated into the denser unburned gas/air mixture, thereby creating a large increase in flame surface area (Section 2.2.5). Taylor instabilities are most commonly observed with central ignition and are a contributor to the low frequency oscillatory combustion frequently observed with vented explosions. During the early stage of burnt gas venting, the flame front was accelerated outside of the enclosure creating a 'pear' shaped flame front (in the case of central ignition). When the flame front was accelerated in this direction, the Taylor effect stabilised the rear of the flame front, inside the enclosure, resulting in a reduced mass combustion rate, causing a fall in pressure. This fall in pressure triggered an acceleration of the flame front in the opposite, Taylor unstable direction, thereby increasing the flame surface area and causing a pressure rise in the enclosure. This low frequency oscillatory combustion may continue until all the fuel is consumed. A similar effect may be observed with rear ignition (although less marked), where, following the external explosion, Taylor instabilities are introduced as the burned gases are accelerated into the unburned gas/air mixture trapped in the corners of the explosion chamber.

Although the type of pressure-time profile shown in Figure 5-1 was exhibited on a significant number of the explosion tests, there were a number of experiments where the maximum pressure peak was of longer duration (caused by a combination of the P_b, P_{ext}, and P_{mfa} pressure peaks) and the P_V and P_b pressure peaks were not obvious as a consequence of the magnitude of the maximum pressure peak.

The series of tests produced peak explosion overpressures of between 70 mbar (K_A = 1 and no congestion) to 3.7 bar (K_A = 9 and 3.52% VB) with corresponding maximum flame speeds in the range 35 - 395 m/s at a distance of 7 m from the ignition point. Flame speeds in excess of 600 m/s were consistently recorded close to the vent opening during tests with area blockages of 20% or greater combined with a volume blockage greater than 1.5%. One test configuration (Type a), was only utilised for tests with a vent opening of K_A = 1, as the overpressures predicted for tests involving a vent opening of K_A = 2, 4 or 9, based on earlier experiments, exceeded the design strength of the explosion chamber.

It is clear from the results of these experiments that the presence of congestion can significantly increase the overpressures generated, often by more than an order of magnitude. High and damaging overpressures can be generated even from relatively benign confined explosions in empty (no internal congestion) chambers with large vent areas. The significance of these results is that they confirm that the size of the vent opening and the degree of congestion within a building are key factors in whether or not a building will sustain structural damage following a gas explosion.

The tests demonstrated that is was possible to generate overpressures capable of causing structural damage in empty chambers if the vent openings do not allow sufficient outflow (i.e. $K_A = 9$). Furthermore, with volume blockages of as little as 0.57%, overpressures greater than 200 mbar were generated in all tests where $K_A > 1$.

It is recognised that the effect of area blockage and obstacle array separation distance may play a more important role in the development of fast flames than volume blockage. However, unlike chemical, process and storage facilities, where congested region layouts or designs will be readily available, populated buildings will have congested and confined areas that are not predictable, and, as a consequence, it is easier to use volume blockage as a criteria. Consequently, for the purpose of this study, the volume blockage was the main variable when designing the congestion configuration. However, further large-scale experimental tests, investigating the effects of area blockage and separation distance are recommended.

5.3.3. Effect of Vent Size

Effect on Overpressure

In Figure 5-3, the effect of vent size (i.e. confinement) on overpressure is shown for explosions with no congestion. It can be seen that the overpressure and the duration of the maximum pressure peak increases as the vent size is reduced. Furthermore, the maximum pressure peak on the $K_A = 9$ pressure-time profile is significantly longer in duration, has a shallower gradient than tests with larger vent openings and also exhibits a number of oscillatory peaks. These observations are attributed to the influence of turbulence and Taylor instabilities caused by the significant amount of unburnt gas that gets ‘trapped’ in the corners of the explosion chamber.

It was also noted that as the vent size was increased, the magnitude of P_b decreased because unburnt gas venting was not significantly restricted by the vent opening and the external explosion, P_{ext}, was dominant. However, as the size of the vent was reduced, the outflow through the vent was restricted, which increased the magnitude of P_b, and the external explosion became less significant, and in some instances, typically with $K_A = 9$, resulted in its pressure peak, P_{ext} merging with the pressure peak P_b, to produce a single broad peak (sometimes also merging with P_{mfa}). It was also evident that it triggered Taylor instabilities.

The effect of vent size on empty enclosures with regard to maximum overpressures was also very interesting. The magnitude of the $K_A = 9$ maximum overpressure was found to be twice that of the corresponding value for $K_A = 4$, four times that of $K_A = 2$ and five times that of $K_A = 1$.

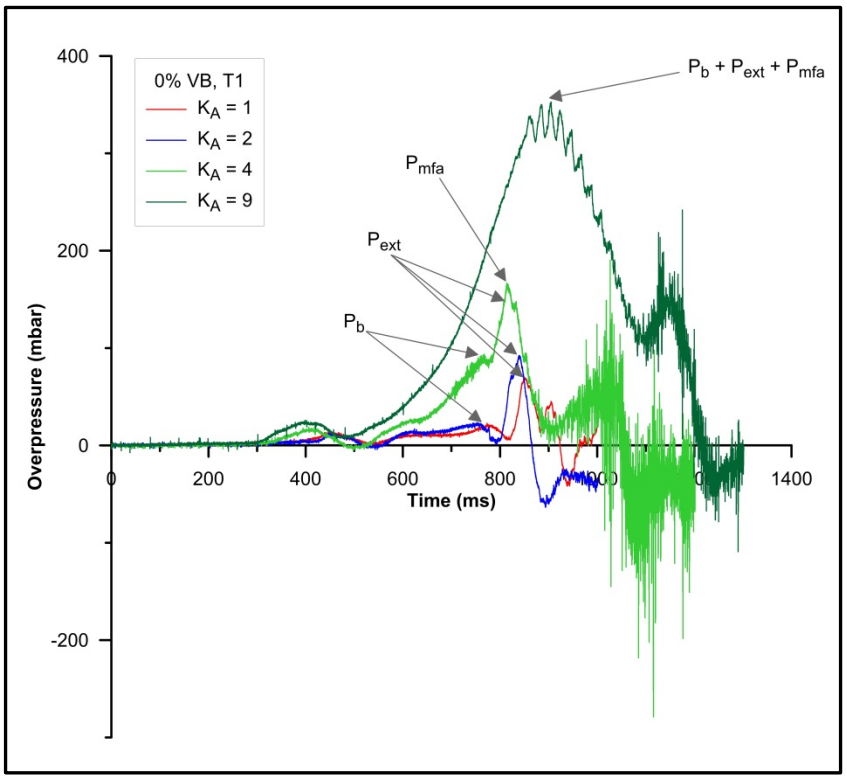

Figure 5-3 The effect of vent size on overpressure (no congestion)

In Figure 5-4, the effect of vent size on overpressure is shown for tests where congestion was present in the enclosure. It can be seen that as the vent size was decreased, the magnitude of the maximum pressure peak increased. In a similar manner to tests without congestion, the influence of the external explosion, on the pressure generated within the enclosure, reduced with decreasing vent size and increasing congestion, with the pressure peak P_{ext}, merging with the pressure peaks P_b and P_{mfa} to produce a single broad peak. Furthermore, the average rate of pressure rise, $(dP/dt)_{avg}$, from the onset of the maximum pressure peak, ranged from 2.8 bar/s for K_A = 1, to 17.4 bar/s for K_A = 9 indicating that there is a direct correlation between both the rate of pressure rise and maximum overpressure with reducing vent size.

It was observed that in tests conducted with a larger vent size (i.e. K_A = 1), the flame typically emerged from the vent as a narrow jet and a few metres from the plane of the vent opening, the jetting flame front ignited the unburnt gas/air mixture and flame propagated rapidly in a ‘mushroom’ shape, giving rise to the peak external overpressure. As the vent size was decreased, the pressure at which flame venting occurred increased and as a consequence the emerging jet velocity increased and the unburnt gas/air mixture was distributed farther from the vent opening. These increased jet velocities cause higher shear and would be expected to promote better mixing with external air, resulting in a leaner external cloud.

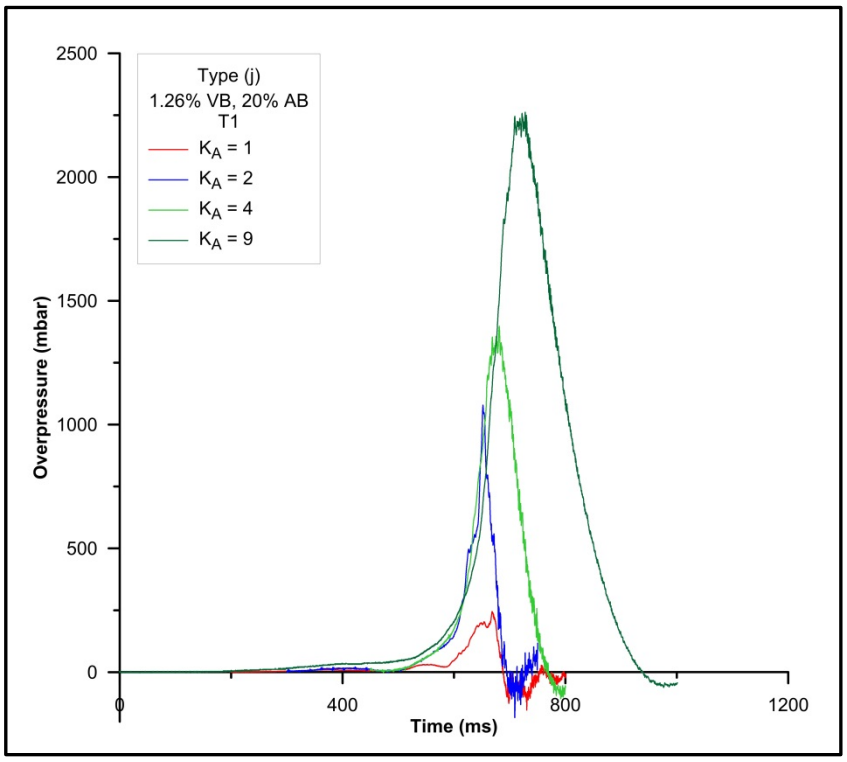

Figure 5-4 The effect of vent size on overpressure (type (j) congestion)

In addition, the time taken for flame venting increased as the vent area was decreased, allowing more time for the vented gases to travel farther from the vent opening. In these instances, the external flame propagation did not appear mushroom shaped, but rather, was elongated, with the centre of the external explosion typically being several metres from the plane of the vent opening. For this reason, and because the smaller vent opening limits the size of the pressure wave that can propagate back into the enclosure, the influence of the external explosion was observed to be greater with larger vent openings. However, due to the reasons described above, it is possible that very rich mixtures inside a chamber with a small vent could result in a strong external explosion. This should be the subject of further research.

The effect of vent size on the pressure generated outside the explosion chamber is shown in Figure 5-5. This diagram shows the maximum overpressure recorded, as a consequence of the external explosion, by the transducers located outside the explosion chamber. The results show that decreasing the size of the vent gives rise to an increase in external overpressures. This increase in pressure is a result of the small vent area causing flammable unburnt gas/air mixture ahead of the flame front to be vented at far higher velocities than is the case for larger vent areas. This high efflux velocity causes greater turbulence within the external flammable gas cloud, which causes faster burning velocities (and hence flame speeds) and higher external overpressures, though of shorter duration. The plot also highlights the effect of

decreasing vent size discussed above, with the K_A = 9 tests with congestion registering a greater overpressure at the T7 location than at T6 (see Table 3-3 for location data).

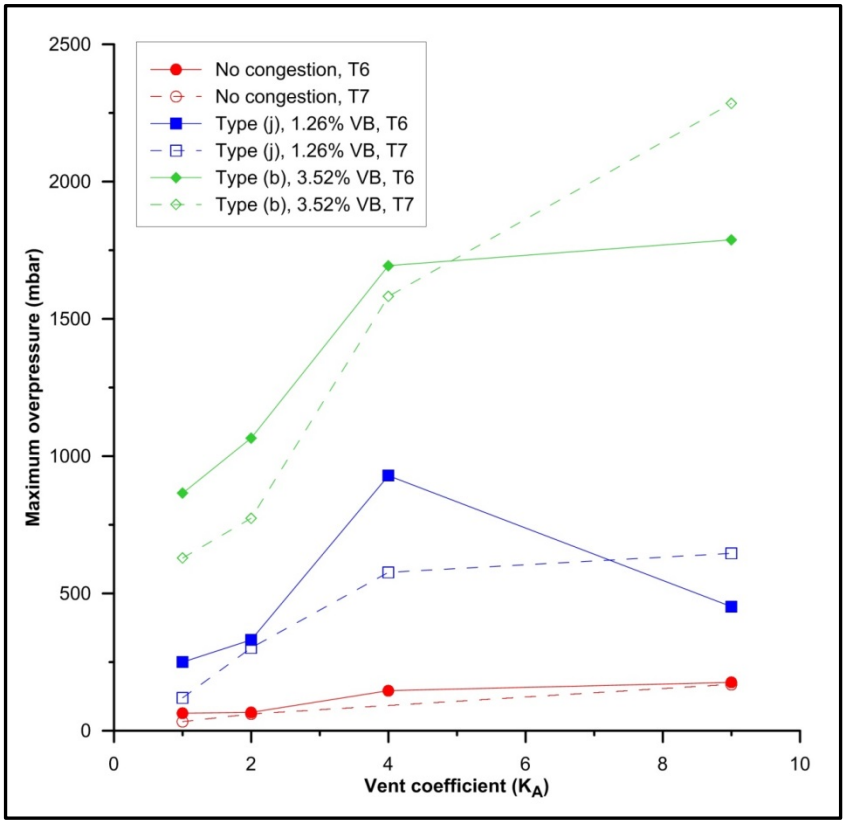

Figure 5-5 The effect of vent size on external pressure

Effect on Flame Speed

In Figure 5-6, the effect of vent size on flame speed is shown for explosions with no congestion. As the flame speed is a combination of the rate of combustion and the induced flow velocity, a change in either alters its magnitude. However, the two properties are not independent, as combustion generates pressure, and pressure generates flow (Schelkin Mechanism). The 'induced' flow, in terms of turbulent vented explosions, is typically of the order of 80 – 85% of the flame speed [103], and consequently, any change in outflow velocity will significantly affect the flame speed. As seen in Figure 5-6 , reducing the vent size resulted in increased flame speeds as the flame approaches the vent, suggesting that for explosions without congestion, there is an indirect correlation between flame speed and vent size. It should be noted that the flame speeds are measured along the centreline and that reducing the vent size increases the internal pressure giving rise to greater flow velocities. This has the effect of producing greater distortion of the flame, particularly along the centreline.

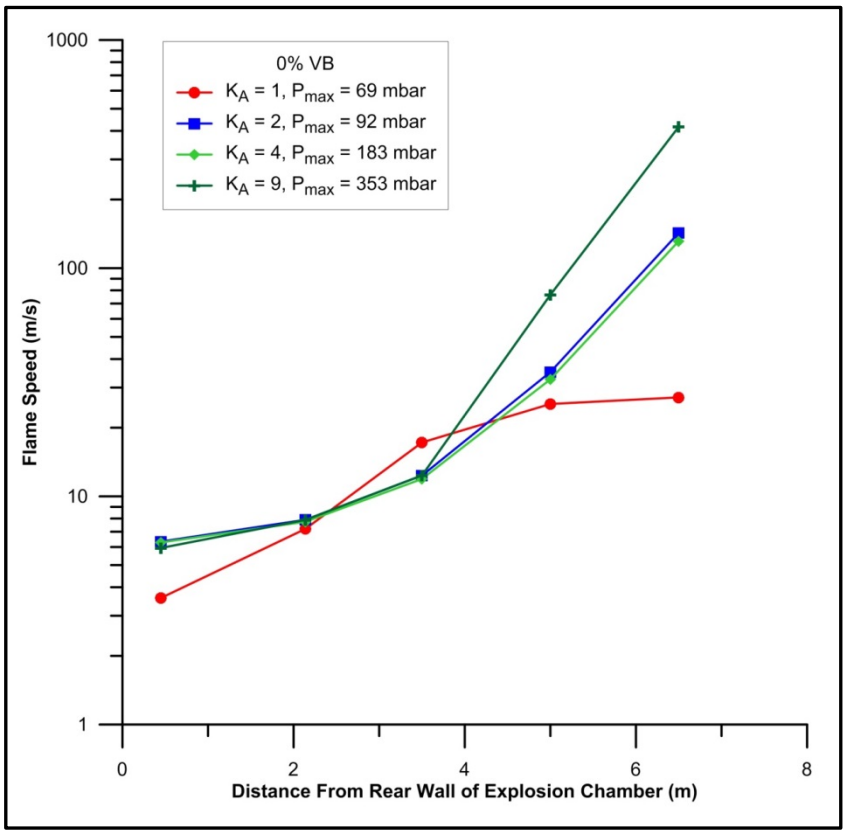

Figure 5-6 The effect of vent size on flame speed (no congestion)

The effect of varying the vent size where congestion is present in the enclosure is shown in Figure 5-7 and Figure 5-8. Figure 5-7 shows the calculated flame speed for tests with 0.75% volume blockage and Figure 5-8 plots the calculated flame speeds for tests with 1.26% volume blockage. It can be seen in Figure 5-7 that in the early stages of the explosions (flame travel $\leq$ 5 m), the flame speeds are significantly faster than those tests where no congestion was present, and that, unlike the results shown in Figure 5-6, reducing the vent size resulted in reduced flame speeds. However, as the flame approached the vent opening, the flame speeds increased rapidly long the centreline of the vent opening. The effect of vent size on reduced flame speed was most significant when the volume blockage was greater than 2%, with the fastest flame speeds being generated in the K_A = 1 tests (Figure 5-8). Reducing the vent opening (i.e. increasing confinement) tended to reduce the speeds of the flowing mixture inside the chamber, except in regions close to the opening, which reduces the flame speed. In certain instances, choked flow conditions occurred. Choked flow occurs in vented explosions when the unburnt gas/air mixture and/or burnt gases passing through the vent opening are initially subsonic (upstream of the vent opening), and the principles of the conservation of mass require the fluid to increase in velocity as it flows through the reduced cross-sectional area of the vent opening. This increase in velocity will continue until the limiting conditions of choked flow are reached. This limiting condition occurs

when the fluid approaches the local speed of sound (i.e. Mach number 1) and consequently the velocity cannot be increased by increasing the upstream pressure or reducing the downstream pressure. However, the mass flow rate may be increased by increasing the upstream pressure, which will increase the density of the fluid across the vent opening, but will not increase its velocity. The onset of choked flow may be estimated in vented natural gas/air explosions as the condition occurs when the critical pressure ratio, that is the ratio of the absolute pressure immediately upstream of the vent opening to the absolute pressure immediately downstream of the vent opening is approximately 1.89 for the unburnt gas/air mixture and 1.80 for the burnt gases under stoichiometric conditions. Consequently, choked flow conditions cannot occur at overpressures, within the enclosure, less than 900 mbar.

It may be concluded therefore, that reducing the vent size, for a given level of congestion, results in increased flame speeds up until the point where the fluid velocity through the vent opening reaches the local speed of sound. After this point, reducing the vent opening results in the flame speed being reduced, except in the region of the vent opening. In addition, the reduction in flow velocity will result in comparatively lower levels of turbulence in the wake of obstacles and this will result in less enhancement of combustion rates and hence comparatively low flame speeds.

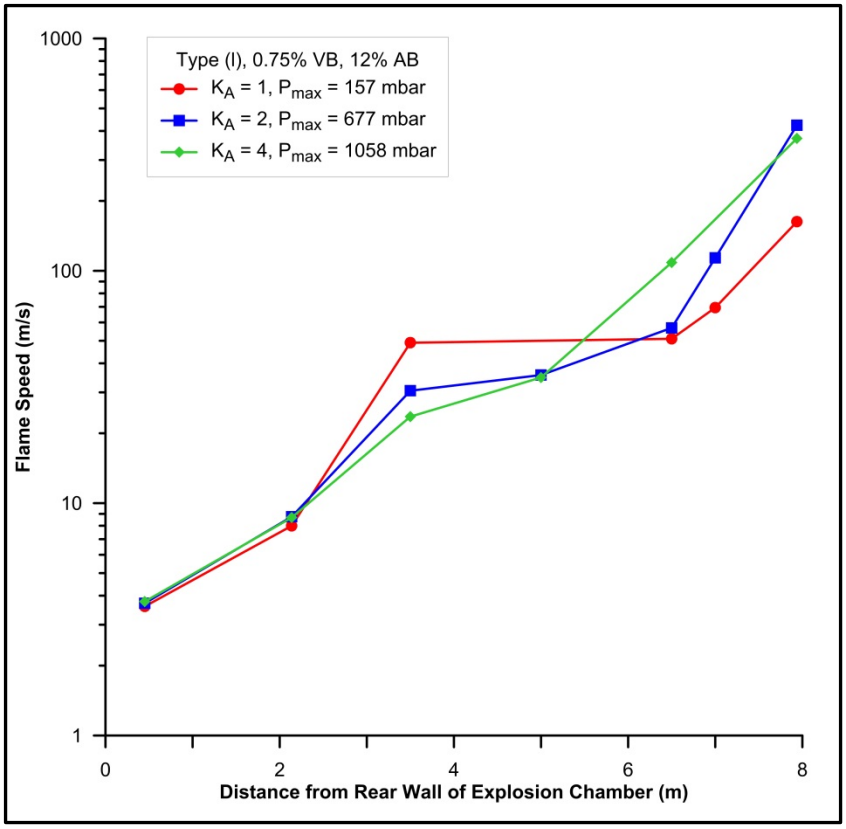

Figure 5-7 The effect of vent size on flame speed (type (I) congestion)

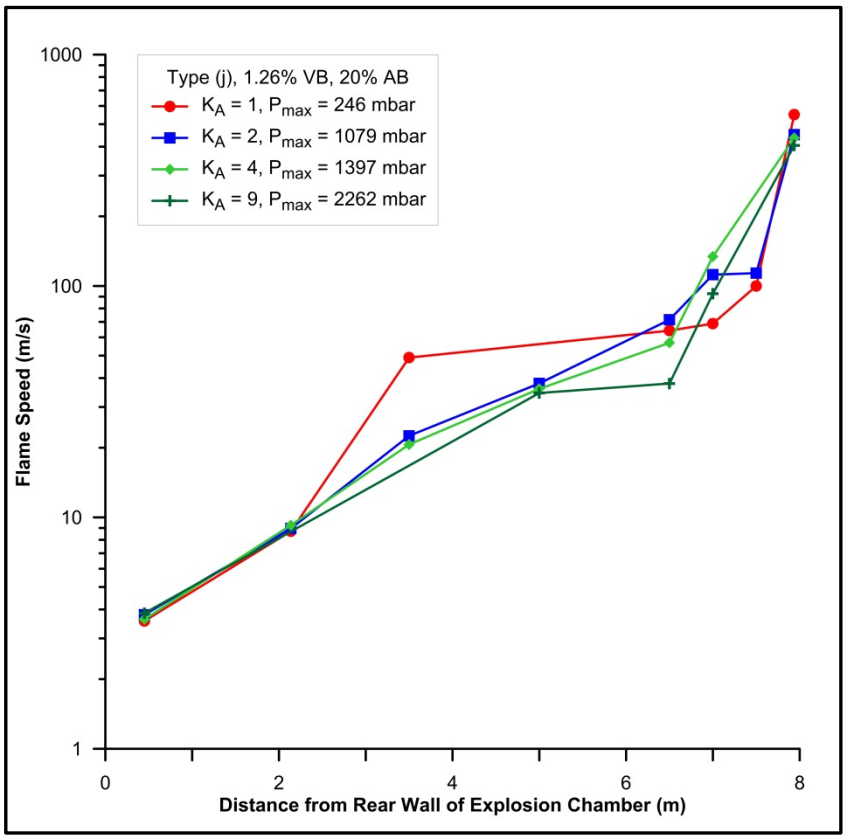

Figure 5-8 The effect of vent size on flame speed (type (j) congestion)

5.3.4. Effect of Congestion

Congestion increases the flame speed, and consequently, the overpressure as a result of three mechanisms. Firstly, the flame surface area increases due to the distortion of the flame as it flows around the obstacles that form the congested region. This leads to an increase in the overall mass burning rate, thereby increasing the flame speed. Secondly, the unburnt mixture being pushed ahead of the flame will create turbulence in the wake of the obstruction. Thirdly, when the flame front reaches this turbulent region there is an increase in the rate of heat and mass transfer within the reaction zone, the burning velocity is therefore enhanced and this also increases the flame speed, setting up the positive feedback process. This results in the faster production of combustion products, which further enhances the flow and initiates a change from laminar to turbulent conditions. The first mechanism was found to be more significant in the early stages of the explosion process when the flame front is moving relatively slowly and few turbulence generating obstacles have been encountered. By contrast, the second mechanism will be more significant when the flame speed is already high as the higher flow speeds cause increased levels of turbulence to be created in the wake of obstacles. Therefore turbulence will be more significant later in the explosion process when the flame will have progressed farther along the enclosure.

Effect of Volume Blockage

A pressure-time profile for an explosion involving a type (j) obstacle configuration with a vent size of K_A = 1 is shown in Figure 5-9. This configuration consisted of four arrays, each containing five pipes. The first array was located 1 m from the rear of the enclosure and the pitch between arrays was set at 2 m. The times at which the flame front arrived at the obstacle arrays have been plotted on the graph so that the effects of obstacles on overpressure may be observed; three distinct pressure peaks are evident.

The first pressure peak occurs approximately 360 ms after ignition and corresponds to the flame passing through the 1st obstacle array but also may be associated with the failure of the polythene sheet. This peak occurs at an overpressure of approximately 14 mbar, and as this does not represent a significant pressure gradient across the vent opening, the rate of unburnt gas/air outflow is relatively low and the pressure peak is not significant. The second pressure peak occurs at approximately 560 ms and corresponds to the flame arrival at the second pipe array (located at 3 m). At this point the flame speed was in the order of 50 m/s but with the downstream obstacle array 2m away, the enhanced combustion in the wake of the second array did not extend the full gap between the arrays and the flame speed started to decrease, resulting in the pressure falling, giving the second pressure peak.

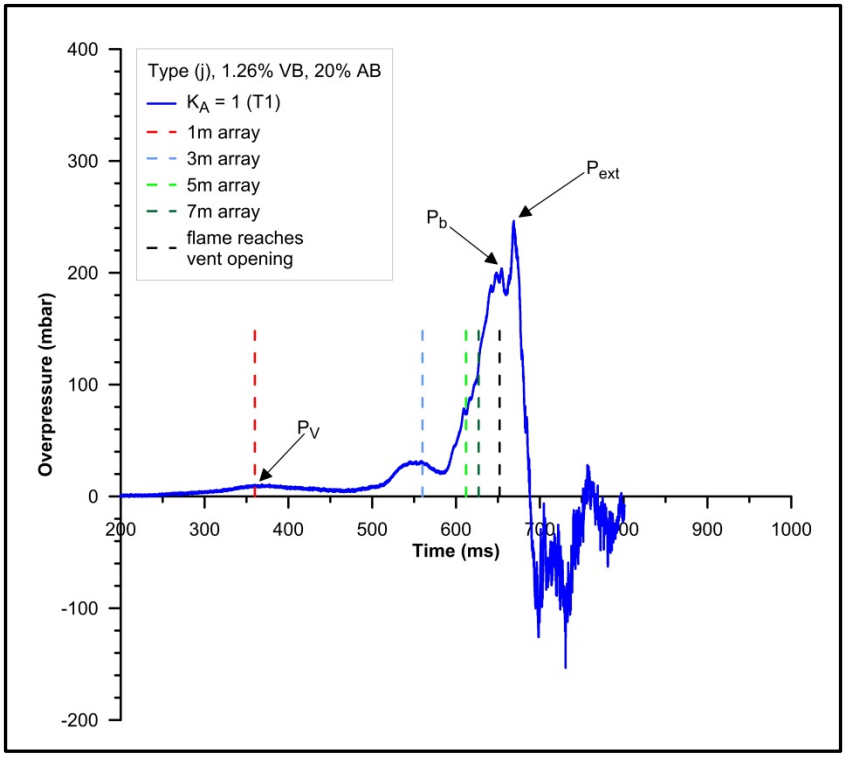

Figure 5-9 Overpressure-time profile for type (j) explosion, K_A = 1

The influence of the 5 m and 7 m obstacle arrays are evident as changes in the gradient of the pressure-time curve, indicating that the flame speed is increasing. The third pressure peak, P_b, corresponds to the onset of burnt gas venting at a time of approximately 680 ms. The fourth pressure peak corresponds to the external explosion, which occurs when the previously vented unburned gas/air mixture is ignited by the flame front when it exits the vent opening.

An overpressure-time profile for an explosion involving a type (a) obstacle configuration with a vent size of $K_A = 1$ is shown in Figure 5-10. This configuration consisted of eight arrays, each containing ten pipes and was the most congested set-up that was used in the experimental programme. It was only used on the largest vent size in order to prevent damage to the explosion chamber. The first array was located 1 m from the rear of the enclosure and the pitch between arrays was set at 1 m. The time at which the flame front arrived at the first seven of the eight obstacle arrays is plotted on the graph so the effects of congestion on overpressure can be observed. It was not possible to plot the flame arrival at the final array as the ionisation probe triggered early, possibly due to the high flow speeds. The flame speed in the region of the vent opening however, was in excess of 600 m/s. The effect of the 1st obstacle array is not immediately obvious on the pressure time profile but it is important as it has established flow within the chamber.

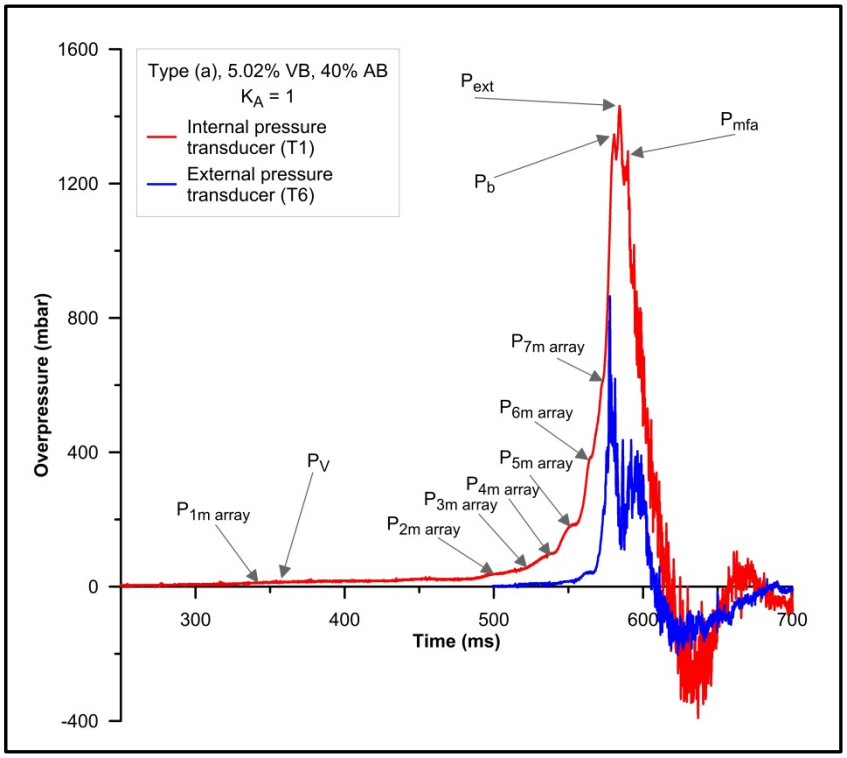

Figure 5-10 Overpressure-time profile for type (a) explosion, $K_A = 1$

The P_V pressure peak has a magnitude of 18 mbar and occurred at approximately 355 ms, a similar time to that of the type (j) test shown in Figure 5-9. However, the pressure peak is not obvious on the pressure-time graph due to the magnitude of the maximum pressure peak. It can be seen in Figure 5-10 that the influence of the onset of burnt gas venting is significantly less than that of a type (j) explosion, which has less congestion. This observation was consistent throughout the experimental programme. The flame arrival at the second and then subsequent arrays is seen as an increase in gradient on the pressure-time curve indicating that the flame front is accelerating and interacting with obstacles immediately downstream to cause further turbulence, thereby setting up a positive feedback mechanism.

An overpressure-time profile for an explosion involving a type (c) obstacle configuration with a vent size of $K_A = 4$ is shown in Figure 5-11. This configuration consisted of eight arrays, each containing five pipes. The first array was located 1 m from the rear of the enclosure and the pitch between arrays was set at 1 m. However, the arrays were offset (see Figure 3-13) such that the horizontal distance between each individual pipe was 2 m. The maximum overpressure generated in this explosion was 2.15 bar, considerably more than that generated in explosions with more congestion but with larger vent openings. It appears that the horizontal spacing between consecutive obstacles has affected the development of the explosion. Clearly, the generation of pressure is a combination of flame acceleration due to congestion and the degree of confinement, and it may be concluded that both congestion and confinement (i.e. less inadvertent venting) will tend to increase the observed overpressures in accidental explosions in buildings. Interestingly, with this type of configuration and vent size, the external explosion is of less influence, for the reasons described in Section 5.3.3. There is a noticeable pressure differential from the rear of the chamber to the vent opening in tests involving the larger vent sizes, which is not apparent with tests of vent size K = 9.

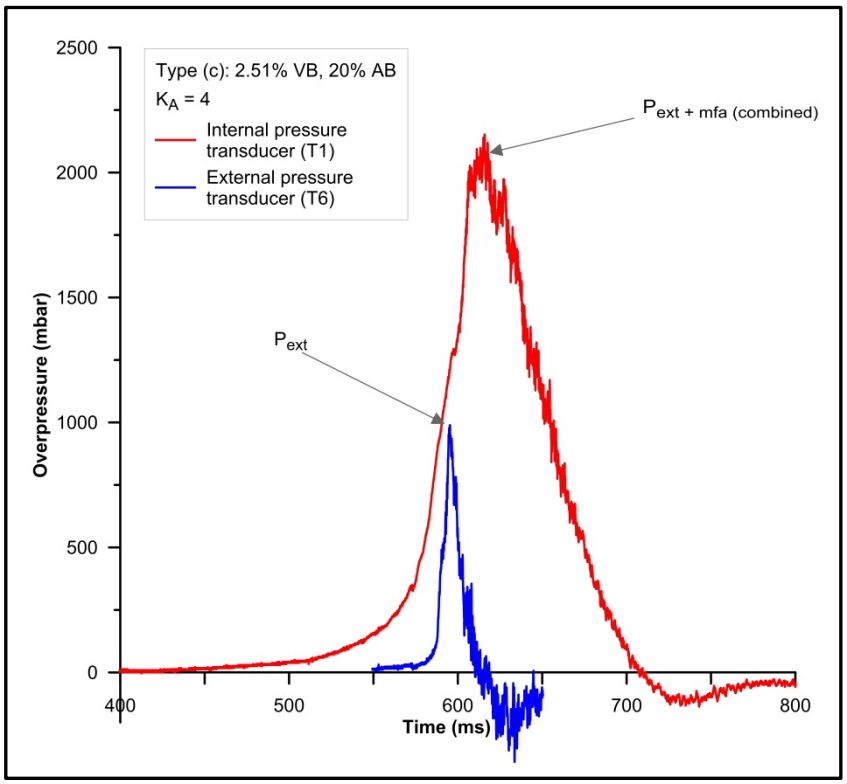

Figure 5-11 Overpressure-time profile for type (c) explosion, K_A = 4

The effect of volume blockage on internal explosion overpressures is shown in Figure 5-12 and Figure 5-13. It can be seen that, in general terms, with the vent size remaining constant, the observed maximum overpressures increased as the volume blockage was increased and the maximum pressure peak occurred earlier in the explosion. This is to be expected as explosion overpressures increase with flame speed and an increasing level of congestion resulted in a higher flame speed for a given vent size (see Figure 5-14). In addition, the effect of decreasing the vent size (higher vent coefficient) is to increase the overpressure because it reduces the venting rate.

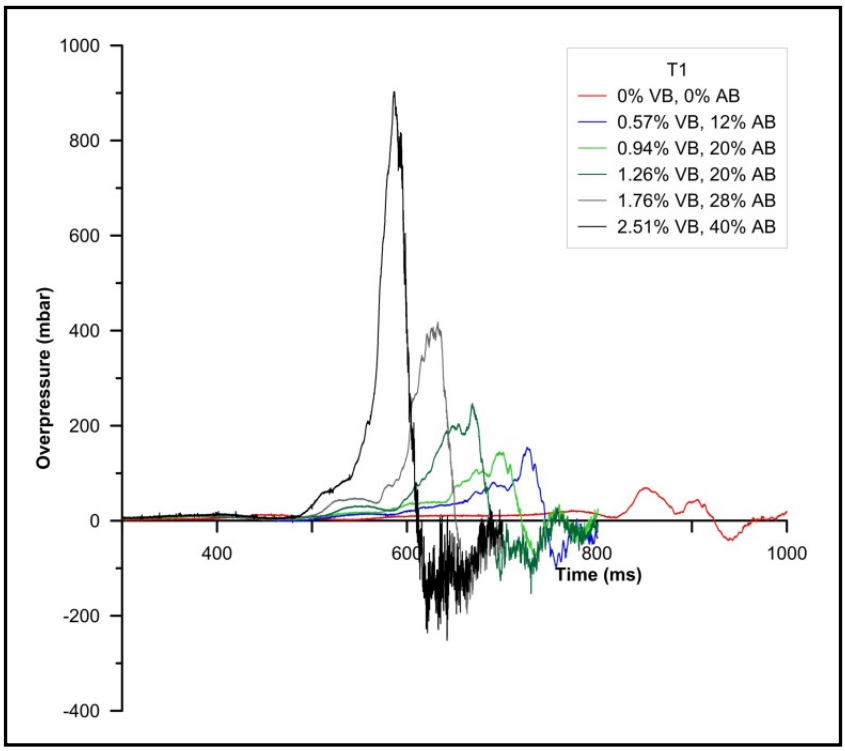

Figure 5-12 The effect of volume blockage on overpressure, $K_A = 1$

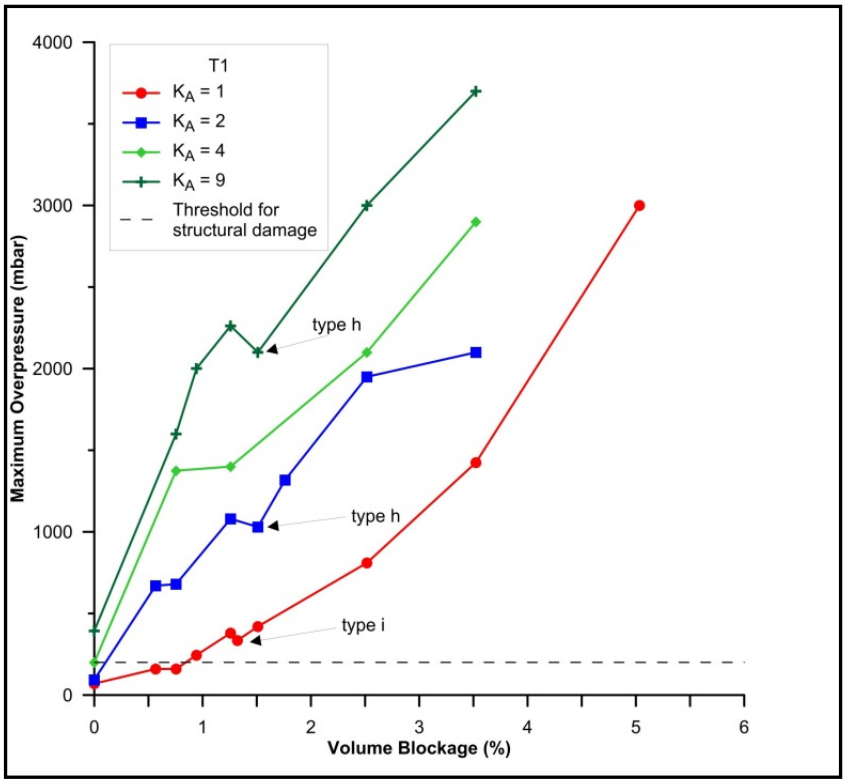

Figure 5-13 The effect of volume blockage on maximum overpressure

For any given congestion level, reducing the vent size always resulted in an increased pressure. Whilst a larger vent resulted in increased flow and turbulence, it did not overcome the effects of reducing the confinement. The noticeable reduction in overpressure observable in Figure 5-13 occurs with the type (i) and type (h) congestion

configurations. The type (i) configuration has three arrays and a 3.0 m pitch and the type (h) configuration has a reduced area blockage. It is therefore apparent that the area blockage and pitch play an important role in the development of fast flames and overpressure.

Interestingly, increasing the level of congestion affects the influence of the vent size on overpressure. In Section 5.3.3, it was observed that reducing the vent size, for experiments with no congestion, gave rise to overpressures for K_A = 9 that were twice that of the corresponding value for K_A = 4, four times that of K_A = 2 and five times that of K_A = 1. Table 5-2 shows the comparison with experiments involving congestion.

Table 5-2 Effects of congestion and vent size on overpressure

Test Type	Max Pressure (bar)				Maximum Pressure Ratio					
	Vent Coefficient (K_A)				$\left(\frac{K_A=9}{K_A=4}\right)$	$\left(\frac{K_A=9}{K_A=2}\right)$	$\left(\frac{K_A=9}{K_A=1}\right)$	$\left(\frac{K_A=4}{K_A=2}\right)$	$\left(\frac{K_A=4}{K_A=1}\right)$	$\left(\frac{K_A=2}{K_A=1}\right)$
	1	2	4	9						
0% VB	0.07	0.09	0.18	0.35	1.9	3.9	5.0	2.0	2.6	1.3
m	0.16	0.67			-	-	-	-	-	4.2
l	0.16	0.68	1.37	1.6	1.2	2.4	10.0	2.0	8.6	4.3
k	0.15			2.01	-	-	13.4	-	-	-
j	0.25	1.08	1.4	2.26	1.6	2.1	9.0	1.3	5.6	4.3
h	0.34	1.04		2.1	-	2.0	6.2	-	-	3.1
e	0.42	1.28			-	-	-	-	-	3.0
c	0.72	1.94	2.15	3	1.4	1.5	4.2	1.1	3.0	2.7
d	0.9	1.98	2.92		-	-	-	1.5	3.2	2.2
b	1.43	2.27		3.7	-	1.6	2.6	-	-	1.6

It can be seen that for all tests, excluding K_A = 1, the addition of congestion reduces the relative influence of the vent size when compared to experiments without congestion. However, when comparing tests involving K_A = 1, the opposite is found to occur for the lower levels of congestion; with the magnitude of overpressure for a type (k) test with a vent size of K_A = 9, over thirteen times greater than the comparative test with K_A = 1, indicating that the level of congestion (generating turbulence) is insufficient to overcome the effects of the reduction in confinement (larger vent). This is not surprising as the pressure developed within an enclosure during a vented explosion is a balance

between the rate at which expanding combustion products are produced and the rate of outflow through the vent opening. Consequently, any restriction in outflow through a reduction in vent size will result in higher overpressures within the enclosure; the effect of which will be enhanced if the congestion is increased. This effect is further highlighted in Figure 5-14, where the effect of vent size on maximum overpressure is plotted. In Figure 5-13 and Figure 5-14, a line is plotted to indicate the overpressure threshold for structural damage. It can be seen that tests without congestion (K_A > 4), and tests involving congestion below the levels typically found in residential buildings, developed overpressures greater than that for structural damage for a typical building. This may suggest that most buildings involved in gas explosions would suffer significant damage. However in practice, this is not the case, as the flammable gas/air mixture is often ignited at non-stoichiometric conditions (e.g. a permanent source of ignition ignited the mixture as soon as it became flammable) such that lower flame speeds are developed, thereby allowing more time for venting and consequently constraining the overpressure developed.

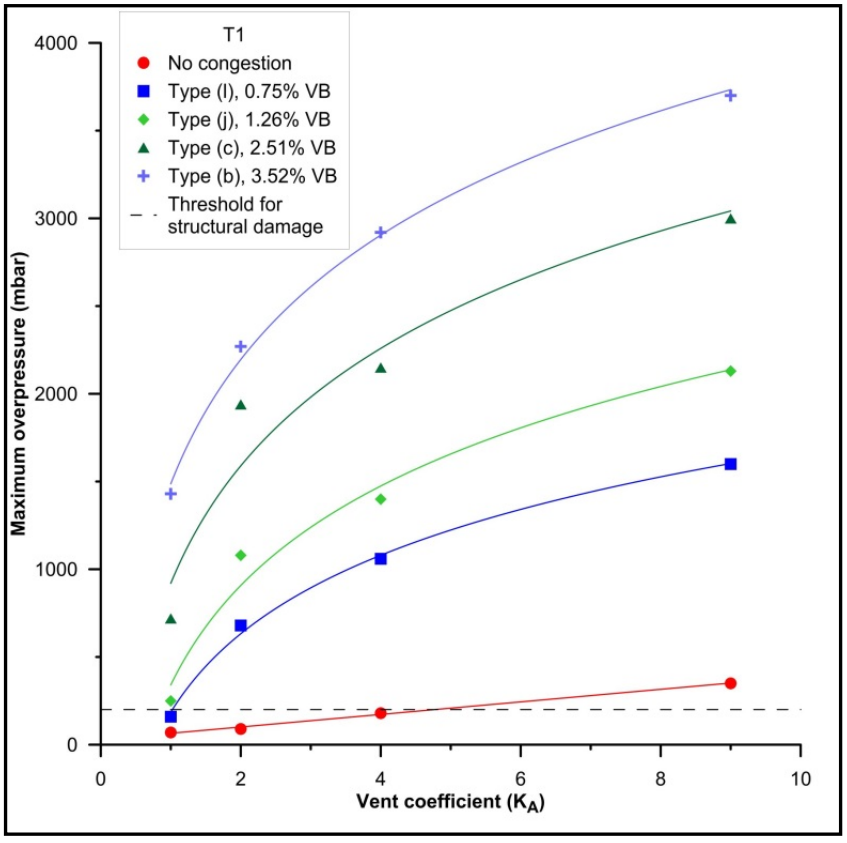

Figure 5-14 The effect of vent size on maximum overpressure

The effect of volume blockage on flame speed is shown in Figure 5-15 for explosion tests where the pitch was set at 2.0 m. It can be seen that the flame speed rises as the volume blockage within the enclosure is increased, irrespective of vent size.

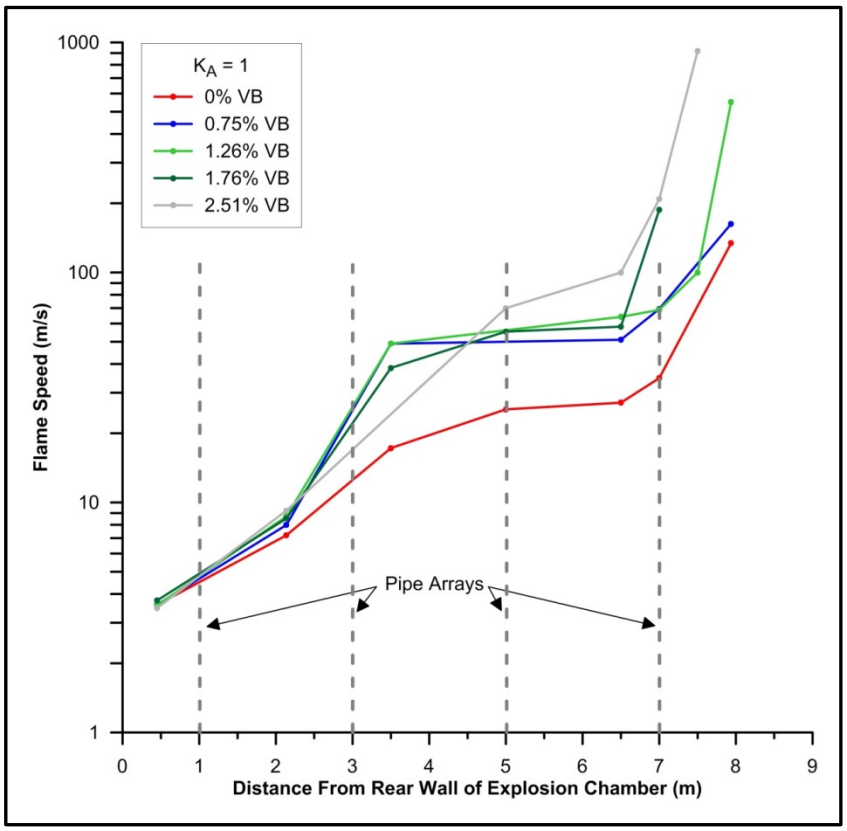

Figure 5-15 Flame speed vs. blockage ratio

Effect of Area Blockage and Pitch

The effects of the obstacle array separation distance (pitch) has received little systematic study in the literature [406]. In turbulent explosions, the maximum burning rate, and therefore the highest rate of pressure generation for a given vent size, will occur at the position of maximum turbulence intensity. It has been shown [406, 407], that the turbulence intensity increases downstream of an obstacle array until it reaches a maximum value some distance after it, and it then begins to decay at an approximately steady rate over a relatively long distance. Consequently, if a flame front is propagating towards a series of obstacle arrays, the maximum flame speed, and hence overpressure, might be generated if the arrays were separated by the 'critical' distance. That is, each successive array is located just downstream of the position of maximum turbulence intensity, so that it receives the flame front at its peak speed, and thereby, it generates the maximum possible turbulence intensity downstream, so that the peak flame speed is received by the next obstacle, and so on. If the pitch of a series of arrays is too large or too small, then the downstream array would not be affected by the peak turbulence generated from the upstream array, resulting in an explosion of lesser severity.

During this experimental programme, a number of experiments were undertaken where the pitch and/or the area blockage were altered. However, no experiments were

undertaken where the volume blockage and area blockage were constant and the pitch was altered. However, as some of the results were interesting, a brief description is detailed in this section.

A few experiments were undertaken where the area blockage and vent size were constant and the volume blockage was altered by varying the separation distance between arrays. In Figure 5-16, the effect of pitch on overpressure is shown for tests where the area blockage was 20%, the vent size was K_A = 1 and the pitch was varied between 1.0, 2.0 and 3.0 m by altering the volume blockage. It can be seen that the greatest overpressures, and fastest flame speeds are being generated by the arrays with a pitch of 1.0 m, and the lowest overpressure is being generated where the pitch of the arrays is 3.0 m. This may simply be because the rig represents that with the largest volume blockage and largest number of repeat arrays but further large-scale study is recommended.

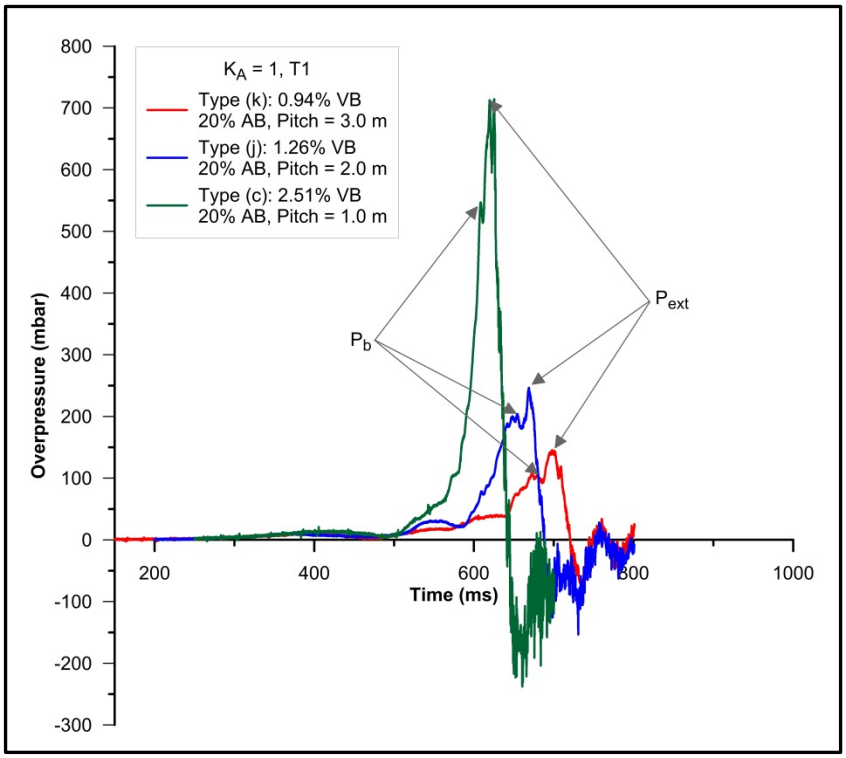

Figure 5-16 The effect of pitch on overpressure

A small number of experiments were undertaken where the volume blockage and vent size were constant and the area blockage and the separation distance between arrays was altered. The effect of area blockage and pitch on overpressure is shown in Figure 5-17 for tests where the volume blockage was 2.51%, the vent size was K_A = 1 and the pitch was varied between 1.0 and 2.0 m. It can be seen that the greatest overpressures and fastest flame speeds were generated when the area blockage was greatest. Further large-scale studies into the effect of area blockage are recommended.

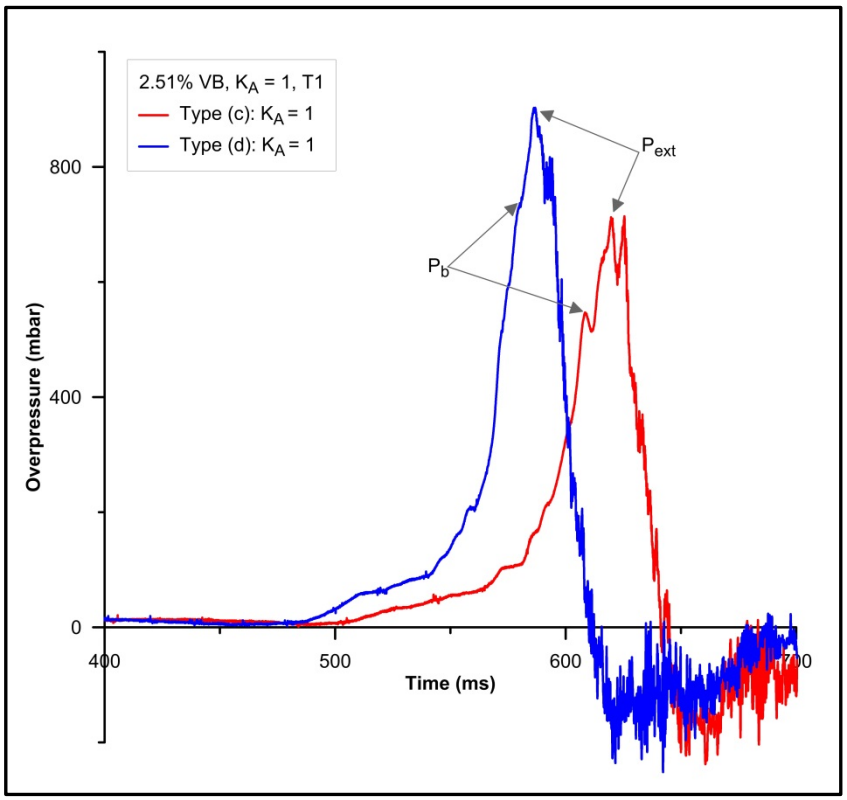

Figure 5-17 The effect of area blockage and pitch on overpressure

5.3.5. Summary of Findings from the Idealised Obstacle Tests

The series of tests produced peak explosion overpressures of between 70 mbar (K_A = 1 and no congestion) to 3.7 bar (K_A = 9 and 3.52% VB) with corresponding maximum flame speeds in the range 35 - 395 m/s at a distance of 7 m from the ignition point. Flame speeds in excess of 600 m/s were consistently recorded close to the vent opening during tests with area blockages of 20% or greater combined with a volume blockage greater than 1.5%. One test configuration [Type (a)], was only utilised for tests with a vent opening of K_A = 1, as the overpressures predicted for tests involving a vent opening of K_A = 2, 4 or 9, based on earlier experiments, exceeded the design strength of the explosion chamber.

A number of important observations were made in terms of the vent size. For any given congestion level, reducing the vent size always resulted in an increased pressure. The vent size was also found to significantly affect the external explosion, with larger vents tending to produce higher overpressures within the chamber.

The results of these large-scale experiments show that high and damaging overpressures can be generated even from explosions in empty (no internal congestion) enclosures if the vent opening is such that it prevents sufficient outflow (K_A > 4). The presence of congestion was found to significantly increase the overpressures generated, often by more than an order of magnitude. With volume blockages of as

little as 0.57%, overpressures greater than 200 mbar were generated in all tests where $K_A > 1$. The significance of these results is that they confirm that the size and failure pressure of potential vent openings, and the degree of congestion within a building, are key factors in whether or not a building will sustain structural damage following a gas explosion. Given that the average volume blockage in a room in a UK dwelling is in the order of 17% (living rooms are less, circa 5 – 10%), it is clear that without the use of large windows of low failure pressure, residential buildings will continue to be susceptible to significant structural damage during an accidental gas explosion.

5.4. Experiments Involving Furniture (experimental programme 4, Rig C)

There were two main objectives of this part of the experimental work. The first objective was to understand the effect of furniture on overpressure, for a volume blockage that was typical of the average UK room. The second objective was to build upon the idealised work reported in Section 5.3 and to investigate whether there was any correspondence between the results of experiments with idealised obstacle arrays and those involving non-uniform obstacles in the form of furniture.

5.4.1. Test Conditions and Data

The experimental programme was undertaken in Rig C with a fixed vent size of K_A = 2.7. Seventeen methane/air tests were undertaken in this programme, of which ten involved furniture. The main variables of interest in this study were different furniture configurations, of which there were four, and the gas concentration. All but one of the tests were undertaken with rear ignition, the remaining test was ignited centrally.

A number of ‘baseline’ tests were undertaken to check for repeatability, prior to undertaking the tests with furniture. As the majority of tests with furniture were undertaken with 10% methane/air mixtures, four of the seven baseline tests were undertaken at this concentration. The results were in agreement with the 10% criteria described in Section 3.17.

A summary of the experimental variables and data gathered from the seventeen vented explosion tests is contained in Table 5-3.

Table 5-3 Summary of test conditions and data

Test No.	Concentration (% v/v)	Ignition	Furniture	VB (%)	P_{max} (mbar)
1	10	Rear	No	0	209
2	10	Rear	No	0	196
3	10	Rear	No	0	186
4	10	Rear	No	0	172
5	6	Rear	No	0	-
6	7.5	Rear	No	0	112[a]
7	12.5	Rear	No	0	310
8	10	Rear	Yes	5	509
9	10	Rear	Yes	5	497
10	7.5	Rear	Yes	5	164
11	9.5	Rear	Yes	5	463
12	10	Rear	Yes	3	236
13	9.5	Rear	Yes	8	501
14	10	Rear	Yes	7	293
15	12.5	Rear	Yes	7	929
16	11.5	Rear	Yes	7	821
17	10	Central	Yes	7	247

[a] Vent did not fail, gases vented around vent panel, pressure-time profile incorrect.

5.4.2. Baseline Tests in an Empty Chamber

Rows 1 – 7 of Table 5-3 provide the maximum overpressures recorded in the empty enclosure tests. Test 5, which was a lean (6%) methane/air mixture, proved difficult to ignite, with the vent failing to open following ignition. No overpressure data was generated but analysis of the internal video footage revealed an unusual combustion process (for explosions). A thin blue flame appeared to propagate along the axially located suspension wire, which secured the ionisation probes and thermocouples (Figure 5-18). This unusual manner of flame propagation during an explosion may be attributed to the suspension wire, around which aluminium foil had been wrapped in order to provide additional heat protection to the ionisation cables. Whilst the ignition energy was not sufficient to sustain a propagating flame, it appears that aluminium and iron oxide from the suspension wire and its metallic wrapping may be catalysing the oxidation of methane [408, 409].

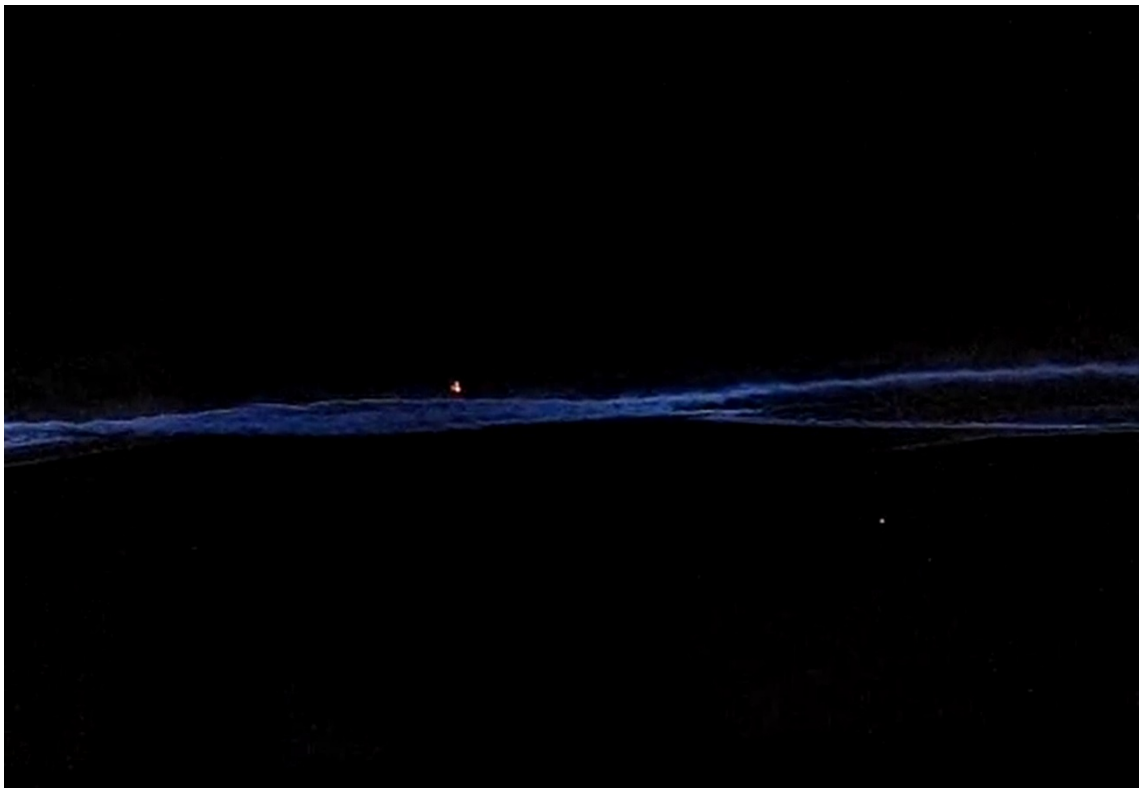

Figure 5-18 Aluminium and iron oxide from the suspension wire catalysing the oxidation of methane (6% methane/air test)

Figure 5-19 shows the overpressure-time profile for a 10% natural gas/air explosion carried out as a baseline test. It is immediately apparent that there are two major pressure peaks in this explosion. By comparison, Figure 5-20 shows the profile with that of test 1 in Rig B, which displays four pressure peaks. In both cases the explosion chambers were empty but the volumes of the explosion chamber, the vent area and vent failure pressure were different. In the case of Rig B, the failure pressure of the vent was low, whereas Rig C had a smaller vent of significantly higher failure pressure.

The timing wire broke at 504 ms indicating that the 12.5 mm fibreboard vent had failed; this is marked on the plot (Figure 5-19). Shortly after the vent failed, and due to the onset of venting, the pressure within the chamber dropped, causing the P_V pressure peak. This was measured at 209 mbar and was the maximum overpressure attained in the explosion. Analysis of the video records show that the flame reached the plane of the vent opening at 600 $\pm$ 10 ms. Immediately after this point, a small peak may be observed on the plot indicating the onset of burnt gas venting, but this was instantaneously followed by a rapid pressure rise due to the external explosion (coinciding with maximum flame surface area).

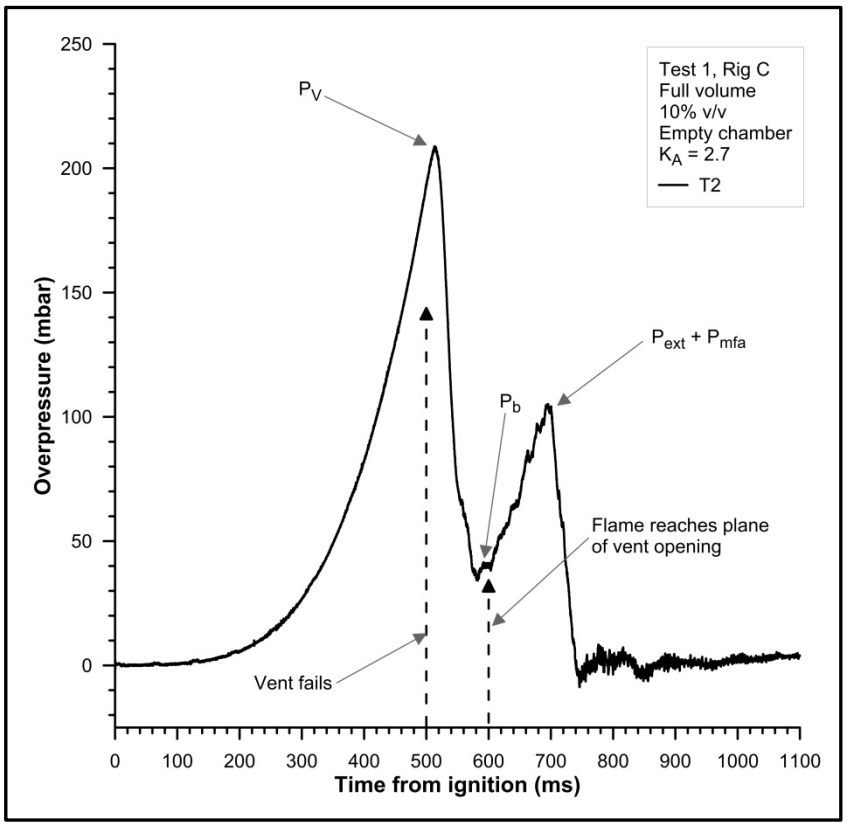

Figure 5-19 Overpressure-time profile for empty chamber

The reason there are only two apparent pressure peaks in test 1 conducted in Rig C, was due to the relatively high failure pressure of the vent. This means that the flame was already well developed by the time the vent failed, and consequently, there was less gas/air mixture left in the chamber. This is also demonstrated by the relatively low pressure peak from the external explosion. The flame front arrived at the vent opening shortly after the vent failed, which would have resulted in less gas/air mixture being expelled through the opening and subsequently being available for combustion. The pressure rise was also not as rapid as other examples of the external explosion. In this instance, the pressure rise was largely driven by the reduction in pressure difference across the vent opening, thereby reducing the rate of outflow during the burnt gas venting phase.

The flame speeds, along the centre-line, for a 10% methane/air explosion in an empty chamber are shown in Figure 5-21. These were determined from the flame arrival times recorded by the ionisation probes and thermocouples (Table 3-4 and Figure 3-43).

The maximum flame speed attained in this experiment in an empty chamber of volume 70 m^3 and L/D ≈ 3:1 was calculated as 65 m/s. In comparison with Figure 5-6, which is an equivalent explosion in Rig B (182 m^3 volume, L/D 2:1), the results are broadly similar, with the slightly lower flame speeds in test 3 being explained by the difference in chamber size and vent failure pressures.

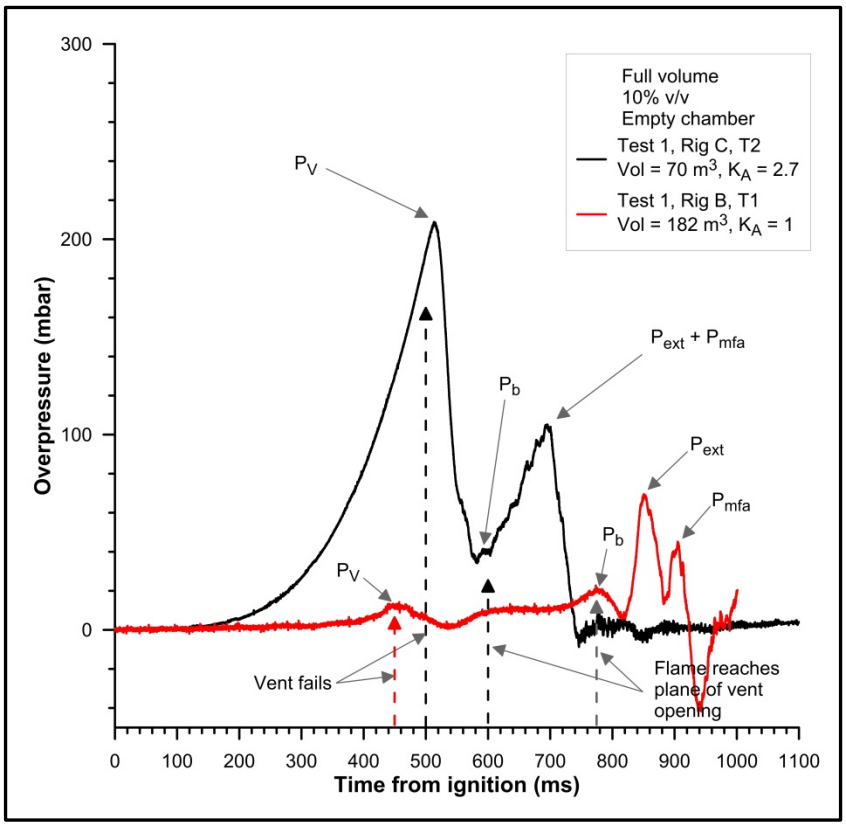

Figure 5-20 Comparison of overpressure-time profiles for tests in empty chamber chambers (Rigs B & C)

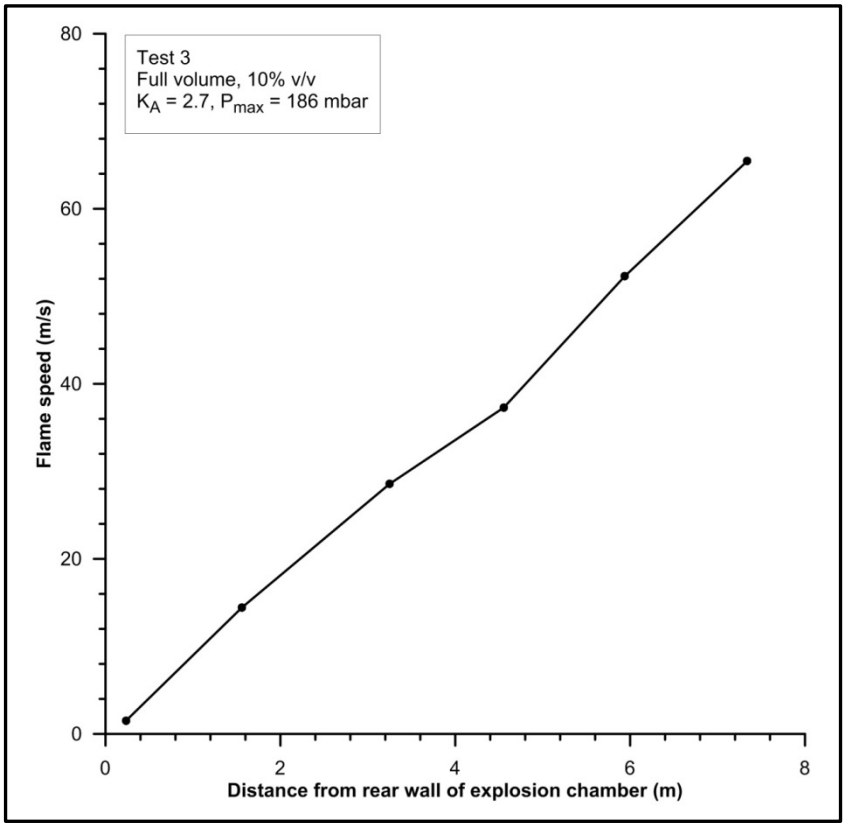

Figure 5-21 Flame speed for a 10% methane/air explosion in an empty chamber

The External Explosion

A photo sequence taken during test 4 (Figure 5-22) illustrates the later stages of a 10% methane/air explosion in an empty chamber, from vent failure through to the external explosion. The photo sequence has been taken from video footage at 30 frames per second (fps). Consequently, each frame represents approximately 33 ms. Frame 1 is taken just before the vent starts to fail; and in frame 2, the vent can be seen 'bowing' outwards. In frame 3, the vent has failed but is still largely in place, restricting outflow. In frames 4 and 5 the vent has been removed and is being pushed clear of the vent, such that in frame 6, the vent is clear of the opening, allowing full outflow of unburnt gas/air mixture. In frames 7 and 8, the vent can be seen breaking into pieces and being pushed farther away from the vent opening. In frame 9, the flame has just reached the plane of the vent opening and in frame 10, a jet of flame can be seen exiting the vent. In frame 11, the jetting flame can be seen igniting the unburnt gas/air mixture, which had accumulated approximately 6 – 8 m from the vent opening.

Figure 5-22 Photo sequence showing the later stages of a 10% methane/air explosion in an empty chamber

Figure 5-23 shows a photo sequence for a 12% methane/air explosion in an empty chamber (test 7). The maximum pressure generated in this explosion, measured at 310 mbar, was greater than that of the 10% explosion (test 1, Figure 5-19). This maximum pressure peak (P_{ext}) was caused by the external explosion. The pressure peak was considerably greater than the P_V peak which was approximately 200 mbar. The difference in the external explosion of a stoichiometric concentration compared to a fuel rich mixture may be visualised by comparing Figure 5-22 and Figure 5-23. The external explosion of the fuel rich mixture appears more visible, with the jetting flame being more luminous (relatively, the apparent luminosity may be due to background light).

Figure 5-23 Photo sequence showing the later stages of a 12.5% methane/air explosion in an empty chamber

In an identical manner to that of Figure 5-22, the photo sequence in Figure 5-23 has been taken from video footage at 30 fps. Frame 1 is taken just before the vent starts to fail, and in frame 2, the vent can be seen ‘bowing’ outwards. In frame 3, the vent has failed, but is still partially in place, restricting outflow. In frame 4, the vent is clear of the opening, thus allowing the full outflow of unburnt gas/air mixture. In frames 5, 6 and 7 the vent can be seen breaking into pieces and being pushed farther away from the vent opening, whilst the unburnt gas/air mixture is diluting and forming a flammable cloud that is likely close to stoichiometric concentration. In frame 8, the flame front reaches the plane of the vent opening and exits as a jet in frame 9. In frame 10, the jetting flame

ignites the flammable cloud that has accumulated some 6 – 8 m from the vent opening. The external explosion is clearly visible throughout the rest of the frames.

The jetting external explosion was a key factor in the development of the explosion during this programme. Due to confinement, there is a build-up of pressure which, if it was sufficiently high enough, could cause unburnt gas/air mixture to be vented at high velocity through the vent opening. This turbulent transient jet has a characteristic 'mushroom' shape appearance with a high velocity stalk (see Figure 2-32). At some point, after the venting stage of the explosion, the expanding flame front will reach the jet, and as the centre of the jet is intensely turbulent (see Section 5.3.3), the flame front is accelerated due to the combined influence of turbulence and flame stretch. If the concentration of the external jet has not been reduced below the lower flammable limit and the time-scale of the turbulence does not cause flame quenching, the jetting flame front will ignite the 'mushroom' shaped jet head and give rise to an external explosion. This can be clearly seen in Figure 5-23. Jetted external explosions can correspond to the dominant pressure peak in some vented explosions (Chapter 4), restricting venting within the chamber and causing a pressure wave to propagate back towards and into the chamber itself. The effectiveness of this process is governed by the magnitude of the pressure developed during the external explosion (dependent upon concentration of the external cloud) and the distance of the external explosion to the vent opening. If combustion within the chamber is still ongoing at the time of the external explosion, the pressure can rise by a factor of two or more than would have occurred if there was not an external explosion.

5.4.3. Tests with Furniture

A number of pieces of furniture had been sourced from a local house clearance business. These pieces of furniture were used to create realistic 'mock ups' of a typical UK living room. A drawing showing the layout of the first mock up is given in Figure 5-24 and a photograph taken before test 8 is shown in Figure 5-25.

Tests 8 – 11 (5% VB)

The items used during the experimental programme, and their calculated volume, are given in Appendix B. The furniture layout used in tests 8 to 11 had a volume blockage of 5%.

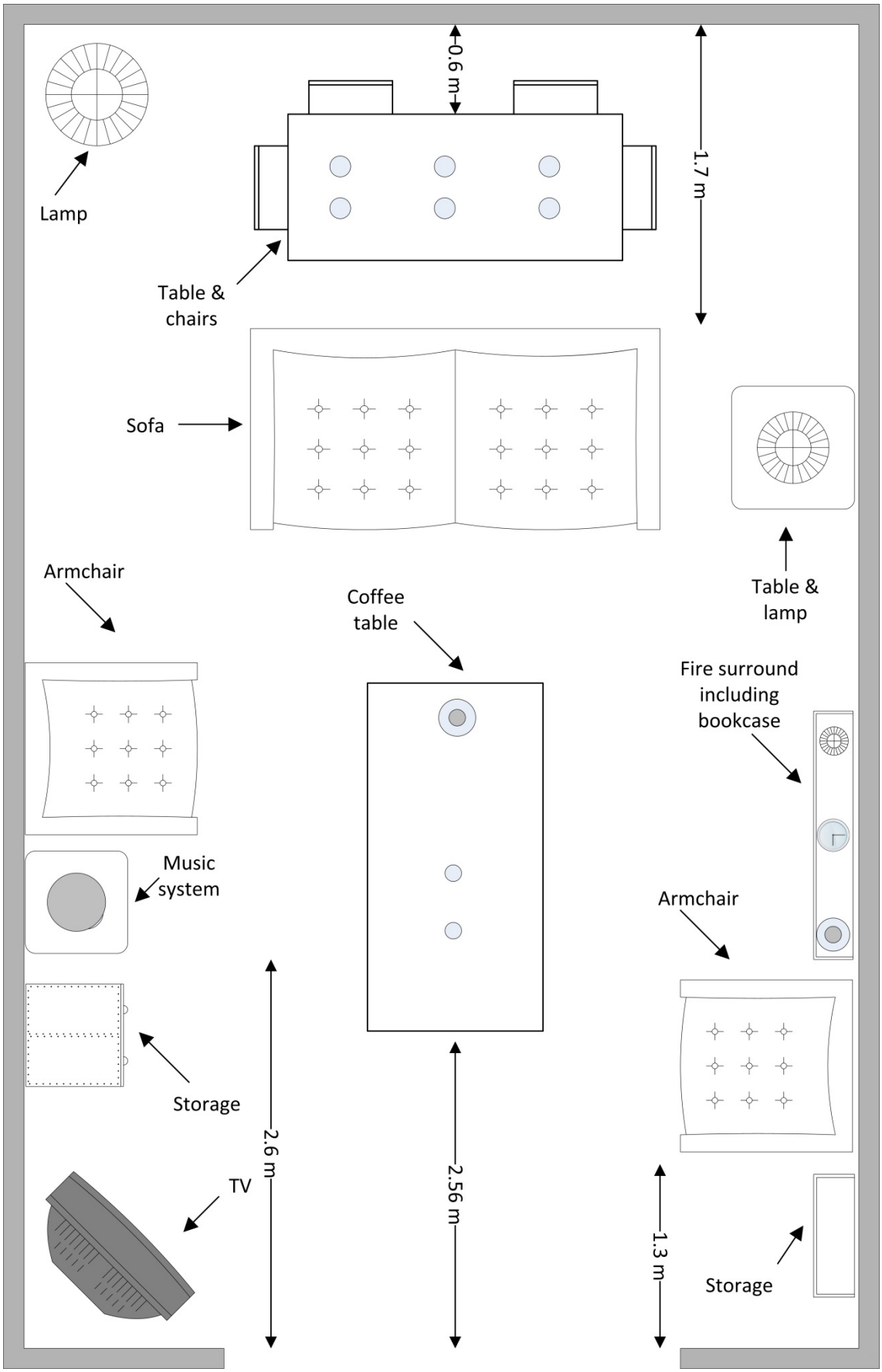

Figure 5-24 Layout of furniture for tests 8 to 11

Figure 5-25 Furniture layout for tests 8 to 11

Figure 5-26 shows the overpressure-time profile for test 8, which was a 10% methane/air explosion. It can be seen that there are two main pressure peaks, but unlike the corresponding test in the empty chamber, the second peak was dominant. The timing wire on the vent broke at 450 ms, indicating that the vent had failed. Analysis of the video records showed that the flame reached the vent opening at 525 ms. In Figure 5-26, at 525 ms there is a slight dip in the overpressure-time curve, which corresponds to the onset of burnt gas venting. However, approximately 30 ms later, there was a rapid pressure rise due to the external explosion. Consequently the P_b pressure peak is barely noticeable. The external explosion was measured as 509 mbar which is over double that recorded in the corresponding test in an empty chamber.

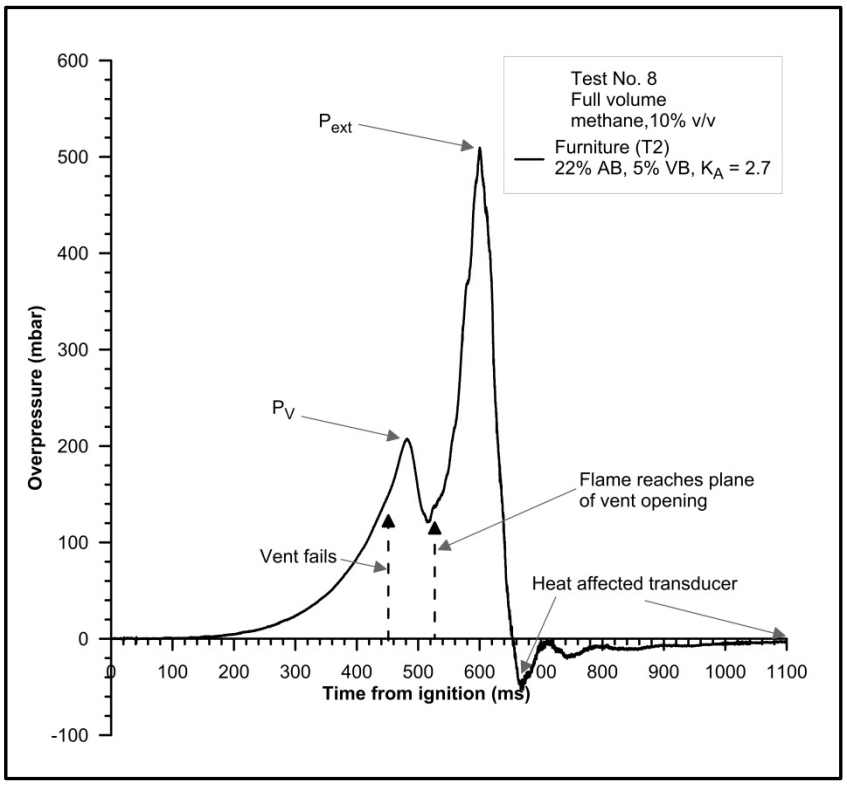

Figure 5-26 Overpressure-time profile for test 8

Figure 5-27 shows the overpressure-time profiles for tests 8 and 10. It compares the pressure development between stoichiometric and fuel lean mixtures. There are several noticeable differences on the pressure traces. Firstly, the stoichiometric explosion has two main pressure peaks, whilst the fuel lean has three. Secondly, the duration of the explosion is considerably longer for the fuel lean explosion, which corresponds to the lower burning velocity. Thirdly, the stoichiometric explosion is dominated by the external explosion, whilst the fuel lean explosion is dominated by the P_V peak, and also generated a peak corresponding to the maximum flame area.

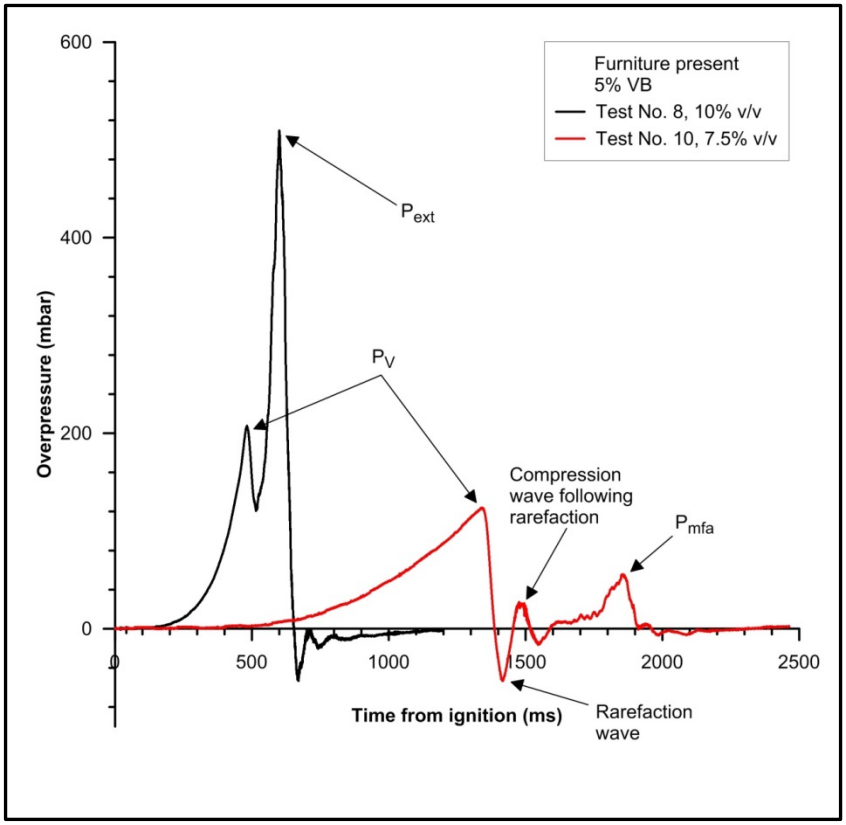

Figure 5-27 Overpressure-time profiles for tests 8 and 10

Interestingly, in a similar manner to some of the experiments with interconnected rooms, the fuel lean explosion generated a peak shortly after the rarefaction wave, which followed the P_V peak as a consequence of overventing. No external explosion occurred during the fuel lean explosion, which correlates with the lack of a P_{ext} peak on the overpressure-time profile. It is perhaps better demonstrated by the photo sequence shown in Figure 5-28. The sequence starts 30 ms before vent failure, no external flame is observed.

Figure 5-28 Photo sequence showing the later stages of a 7.5% methane/air explosion with 5% VB from furniture

An additional observation of note is that the vents fail at different pressures, even though the size, material of the vent panel, and its fixing were identical. As discussed in Section 1.6 pressure damage is dependent upon the magnitude of the pressure generated and the relationship between the duration of the imposed pressure load and the natural period of vibration of the structure. In this case, whilst the pressure was lower, in the case of the fuel lean explosion, the duration was significantly longer.

Due to budgetary constraints, only two experiments were conducted with methane/air concentrations of 7.5%. Neither of these tests produced an overpressure of magnitude sufficient to cause structural damage to a building. However, the addition of furniture in

the second test did cause the maximum pressure to increase. It is therefore clear, that an explosion of a fuel lean mixture, in a building with interconnected rooms that were furnished, would be capable of causing structural damage. Further work is recommended with fuel lean explosions, where the explosion chamber has both interconnected rooms and furniture.

Tests 12 (3% VB)

For test 12, the armchairs and the coffee table were removed (see Figure 5-24), reducing the volume blockage to 3%. In addition, the sofa was moved towards the vent such that it was 2.65 m from the rear of the explosion chamber. The test was undertaken with a 10% methane/air mixture and generated a maximum overpressure of 236 mbar. The cause of the relatively low overpressure was attributed to the low level of congestion and greater distance between the ignition source and largest turbulence generating obstacle.

Test 13 (8% VB)

For test 13, a number of items were added along the edges of the side walls and the armchairs were repositioned (see Figure 5-29). This was carried out to increase the volume blockage in the enclosure, in a manner that was representative of realistic furnishing of rooms (i.e. furniture is typically positioned against the walls of a room). Following the changes to the room layout, the volume blockage was calculated to be 8%; this was the maximum blockage used during this experimental programme.

Figure 5-30 shows the overpressure-time profile for test 13 (9.5% methane/air) and compares it to that of test 8 (10% v/v and 5% VB). Whilst the profiles look very similar, perhaps surprisingly (even though there was a slightly higher laminar burning velocity due to concentration), the test with the lower blockage ratio attained a slightly higher maximum overpressure and a considerably higher pressure peak corresponding to the vent opening. In addition, it reached the 1st peak sooner. These findings are easily explained, and in some way, set the scene for the effects of furniture. Whilst the volume blockage was increased, the additional furniture was placed against the walls of the chamber and not in the direct path of the propagating flame front. Consequently, turbulent flow due to these additional obstacles was limited. Furthermore, they had the effect of reducing the potential maximum flame surface area, also acting to cool the flame slightly earlier. In terms of the time taken to reach the first peak, the sofa was moved farther from the source of ignition, which meant its influence occurred later in the explosion. Consequently, in test 8, flame acceleration due to turbulence generated by the sofa, occurred earlier, and the pitch of the downstream obstacles was such that it did not further affect pressure development.

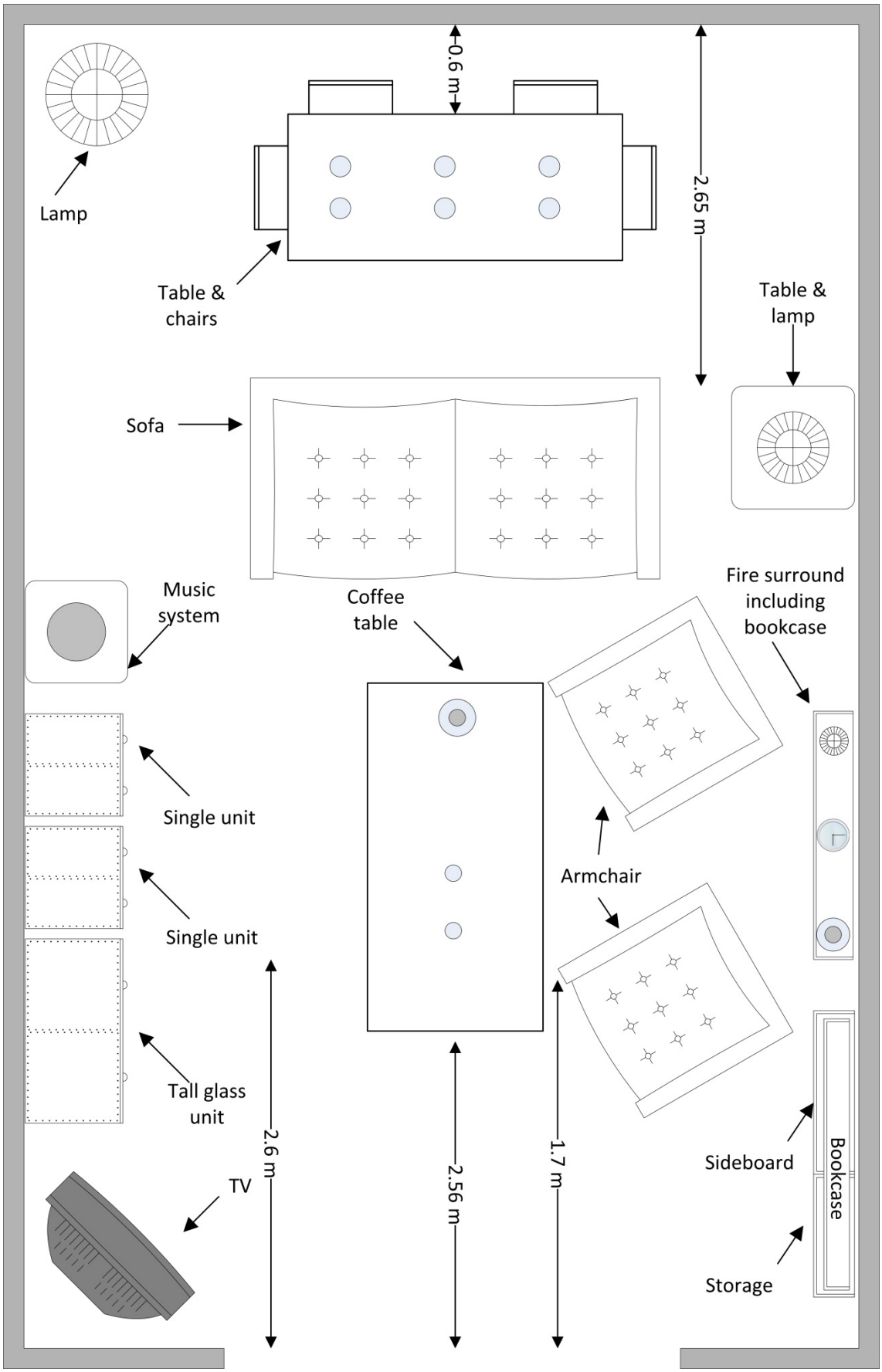

Figure 5-29 Layout of furniture for test 13

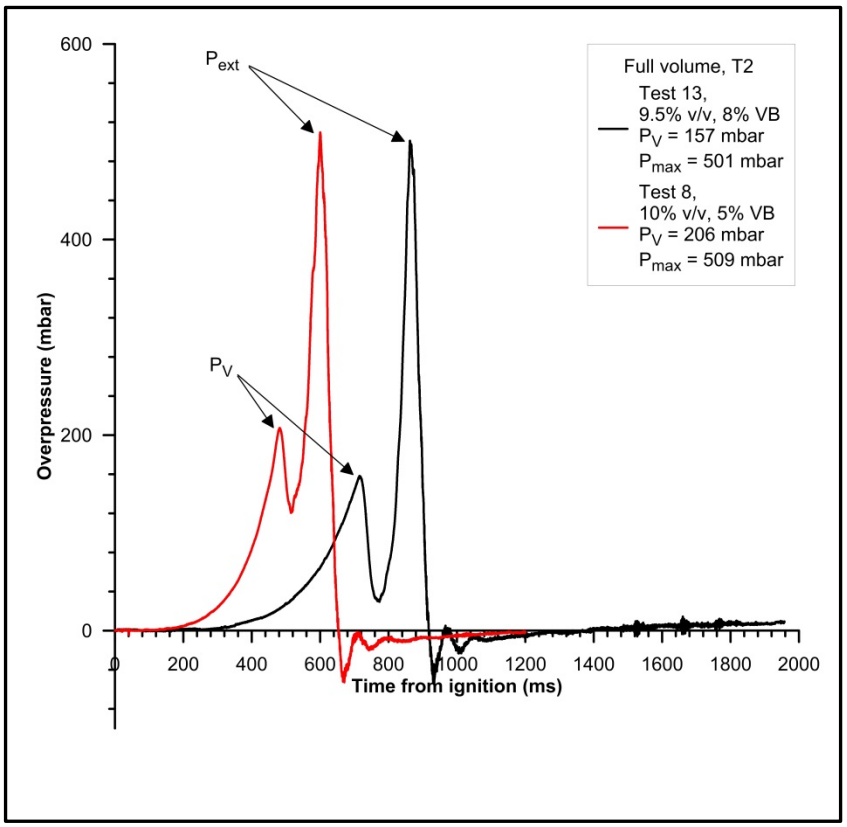

Figure 5-30 The effect of volume blockage

Pressure Damage

Figure 5-31 and Figure 5-32 show the damage to the furniture layout following 10% methane/air explosions. Test 12 had a volume blockage of 3% and generated a maximum pressure of 236 mbar. It can be seen that some of the furniture had been 'overturned' and some moved during the explosion. It is relatively common during the investigation of gas explosions in buildings to see an apparent lack of damage to furniture and household items. The propagating flame front and flow ahead of the flame will flow around the obstacle wherever possible. Items may also 'bounce' as the pressure rise within enclosures causes flexible suspended floors (e.g. floorboards etc.) to momentarily bow before returning to their original shape (although in some instances the flooring may be permanently deformed). However, items such as storage units, appliances etc. which present a confined space where gas can accumulate, may suffer significant damage. Furthermore, in general terms, there will be large scale damage in situations where the building walls and floors collapse.

Figure 5-31 Damage following test 12

Figure 5-32 Damage following test 13

Test 13 had a volume blockage of 8% and generated a maximum pressure of 501 mbar. It can be seen that there are more items of furniture that have been overturned. This degree of pressure generation in a building would have caused significant structural damage and the distribution of furniture would have been far more

widespread. It can also be seen in Figure 5-32 that the sofa has suffered extensive fire damage. This was a cumulative effect as a result of several explosions.

Tests 14 to 17 (7% VB)

As a consequence of the damage to the sofa, the furniture was changed prior to test 14. In addition, the volume blockage was altered to 7%. The layout for tests 14 to 17 is given in Figure 5-33 and Figure 5-34.

Figure 5-33 Photo of furniture layout for tests 14 to 17

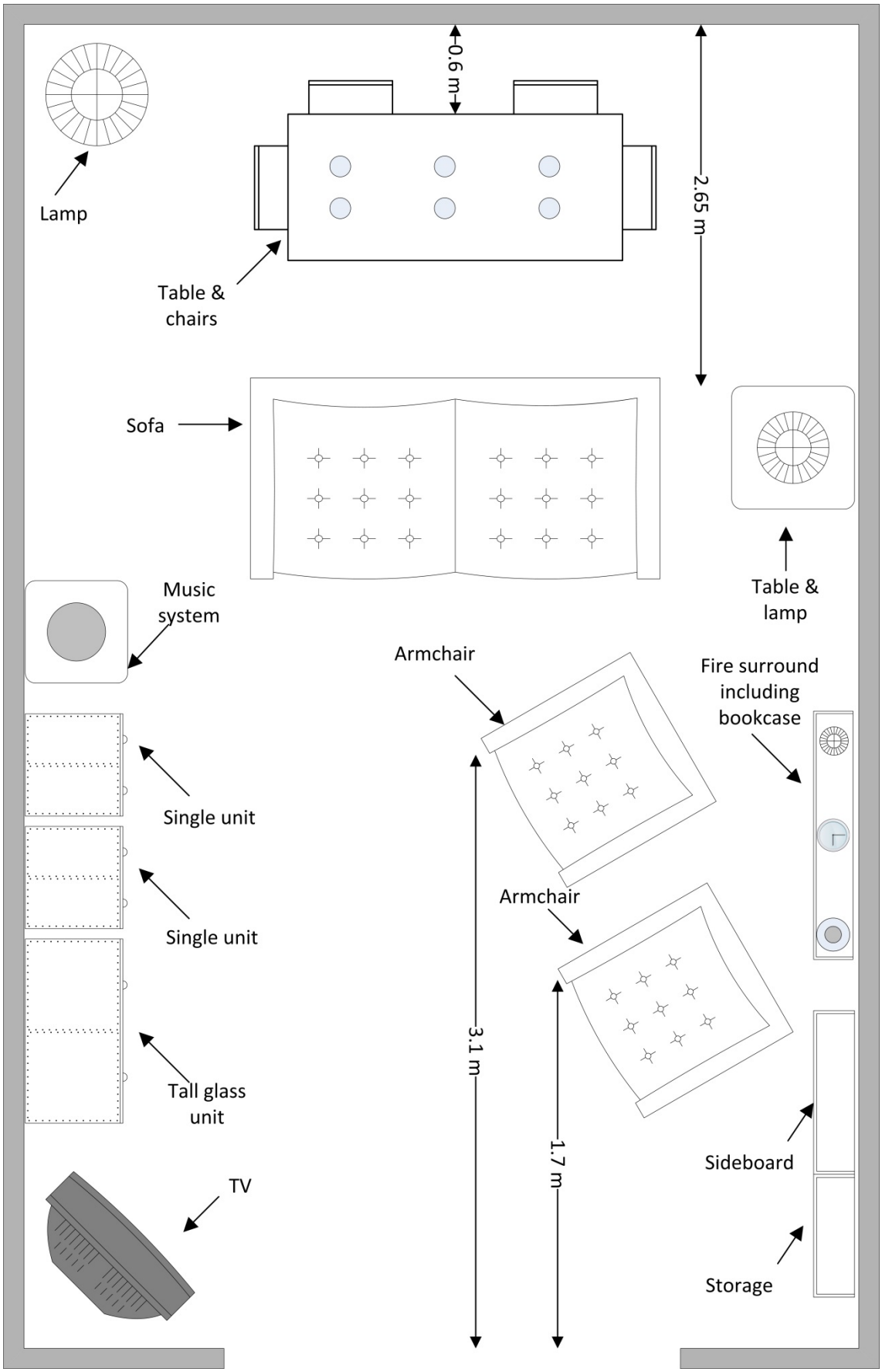

Figure 5-34 Layout of furniture for tests 14 to 17

Figure 5-35 shows the calculated flame speed for test 15, which for comparative purposes is shown against plots for test numbers 3 and 13. For clarity, some of the more significant pieces of furniture, directly in the path of the propagating flame front, are plotted on the diagram.

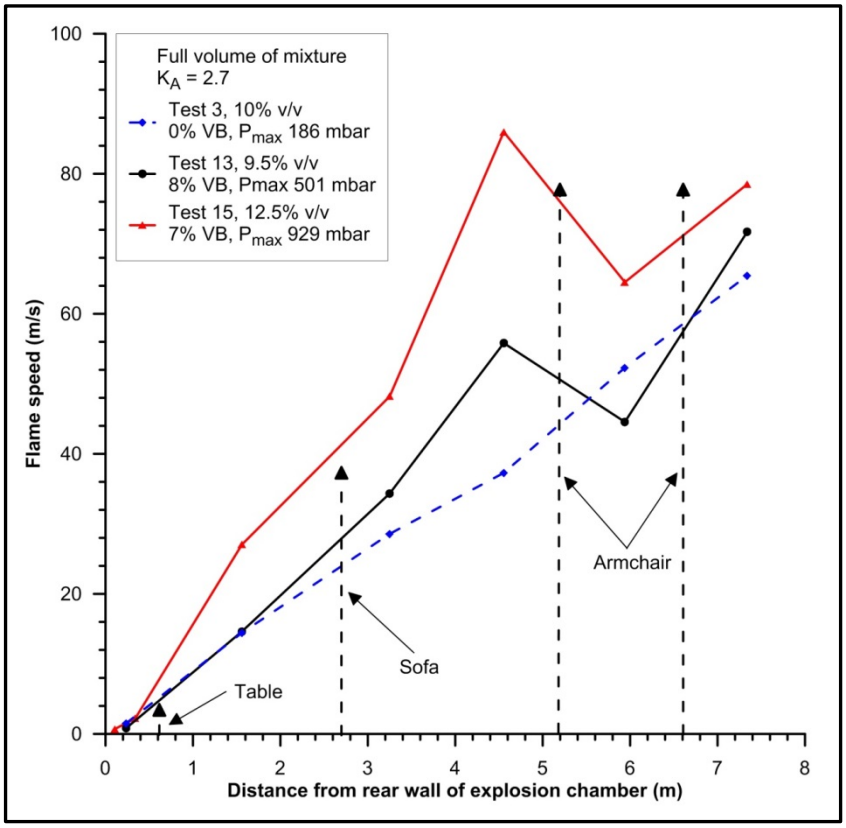

Figure 5-35 Comparison of centreline flame speeds (tests 3, 13 and 15)

As discussed in Section 5.3.4, congestion increases the flame speed, and consequently, the overpressure. In these experiments, where the experimental set-up is attempting to represent realistic conditions in which an accidental gas explosion may occur; the acceleration of the flame front is a consequence of a complex interaction between the propagating flame front, the local obstruction and its position, and the size and geometry of the enclosure. This can be clearly seen in Figure 5-35, where the increase in flame speed is approximately linear for the test with no congestion; whilst with congestion it is clear that additional mechanisms are affecting the flame speed.

However, the comparisons between the tests carried out with furniture are somewhat surprising. The fuel rich mixture (test 15, ϕ = 1.3, VB = 7%) produced higher flame speeds than that of the stoichiometric concentration (test 13, ϕ = 1.0, VB = 8%). It also generated a significantly higher maximum overpressure; which was largely attributable to the external explosion. Nevertheless, the inconsistency still remains that higher flame speeds were attained by a concentration with a lower laminar burning velocity, and in an enclosure with a lower volume blockage. The volume blockage discrepancy

may be explained with the same reasoning as discussed earlier in this chapter. To develop turbulence, the obstacle must be in the path of the propagating flame front and the separation distance between downstream obstacles is also critical. If the obstacles are spaced either too close, or too far apart, the turbulence intensity will be reduced and the explosion will be less severe. In this instance, the additional furniture was positioned at the edge of the enclosure and the sofa was positioned farther from the ignition source. It seems plausible that this could, to some degree, explain the discrepancy.

Scrutiny has been given to the reliability of the ionisation probe and thermocouple measurements as the explosion process is extremely turbulent and in some instances the flame front was recorded at an instrument downstream before it was recorded at the adjacent, upstream position. However, test 14 (also 10% methane/air) was undertaken with the same furniture layout as tests 15 and 16 (11.5% methane/air), and again it produced a lower maximum overpressure and lower flame speeds (see Figure 5-36). Furthermore, the argument regarding the accuracy of the flame arrival measurements is invalid as the overpressure-time profiles clearly demonstrate that the pressure peaks were being generated faster with the fuel rich mixture; and the time at which the pressure peaks are generated is a function of flame speed.

Clearly, erroneous gas concentration measurements have to be considered. However, the gas filling process was robust with the gas analyser being calibrated against a test gas of known composition prior to each test. A single sampling point was used in Rig C, but this was considered adequate as the gas was recirculated during this experimental programme. To check the accuracy of this system, a small number of additional tests were undertaken using four sample points (not included in this thesis). The gas concentration measurements taken using a single sample point compared favourable to those taken from the four point system. Furthermore, the difference in mixture concentration is clearly visible from inspection of internal and external video records (see Figure 5-22, Figure 5-23 and Figure 5-28), where the fuel rich flames are more luminous than those of stoichiometric concentration. There is also a distinct difference between stoichiometric and fuel lean images.

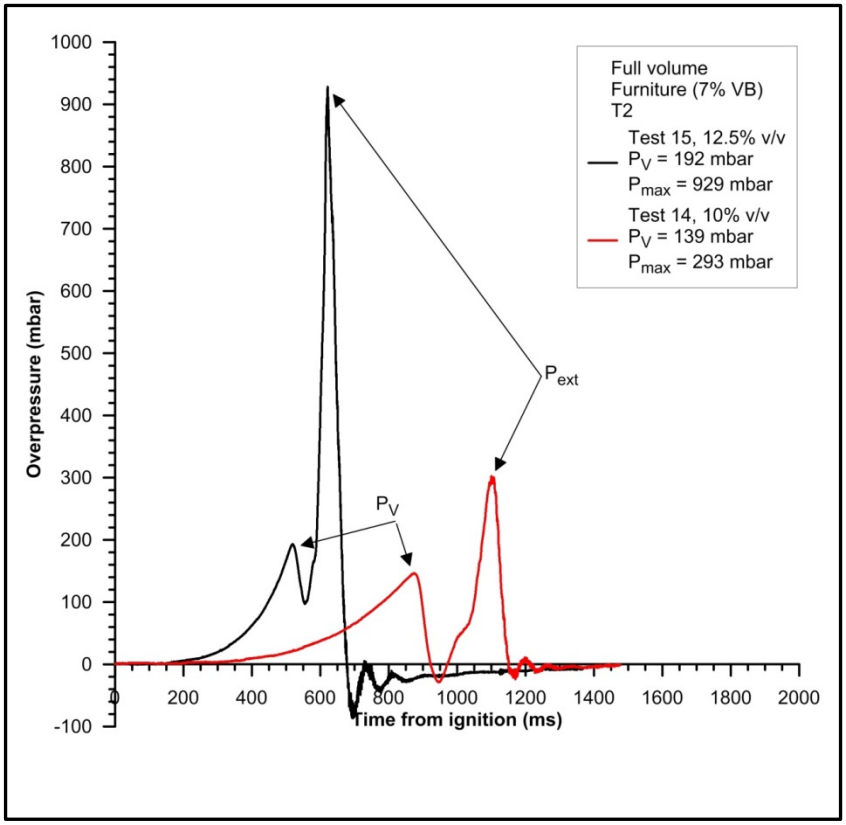

Figure 5-36 Overpressure vs. gas concentration (tests 14 and 15)

Accepting that the gas concentrations are valid, what plausible explanation could there be for the discrepancy in flame speed? The answer lies in the internal video records. Figure 5-37 shows the flame development of tests 14 and 15 taken at 470 ms after ignition. Test 14 is in the left frame. The flame can be seen to be developing in a hemispherical shape and appears to be laminar. Contrastingly, test 15, in the right frame is clearly cellular and wrinkled in its nature, with an increased surface area. The flame stretch and curvature would have resulted in a Markstein number, Ma < 0, with a consequent increased mass burning rate. Hence the flame front arrives at the 1st obstacle (table and chairs), early in the explosion, generating flow and creating turbulence. This turbulence enhances the burning rate, which creates more flow, and so on. It therefore appears that the cause of the flame speed discrepancy is due to the fuels rich mixtures early development of a cellular flame structure. The author is not aware of this finding being reported elsewhere in the literature and consequently it necessitates further work.

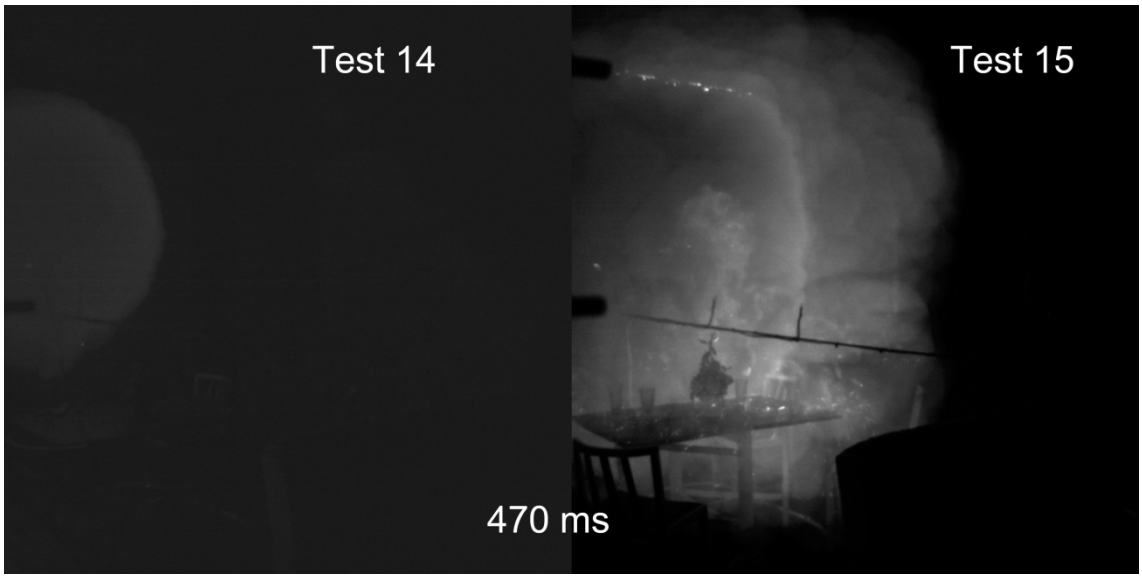

Figure 5-37 Flame development (tests 14 and 15)

Accepting the difference in flame structure with the fuel rich mixture, in general terms, the development of the flame front witnessed in the experiments was similar to that observed in small-scale experiments of Masri et al. [44]. The explosion develops in two distinct ways. Firstly, the initially laminar flame distorts as it impinges upon the obstacle, increasing the flame surface area, thereby increasing the mass combustion rate and the flame speed (Figure 5-38, 340 – 440 ms).

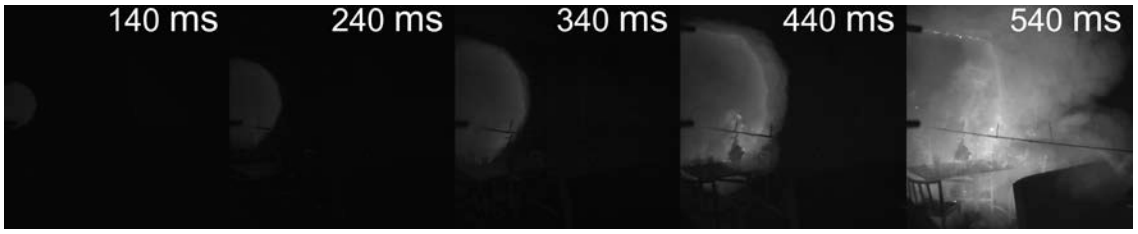

Figure 5-38 Explosion development showing increase in flame surface area as advancing flame front propagates around table

Secondly, the explosion is significantly influenced by the changes in the flow field induced by the obstacle. The unburnt mixture pushed ahead of the flame creates turbulence in the wake of the obstruction. The flame interacts with the modified flow field, with the geometry and size of the obstacle determining the turbulence levels and length scales. This can further enhance the mass combustion rate, thereby increasing the flame speed and setting up a positive feedback process (Figure 5-38, 540 ms).

The location of obstacles, their shape and separation distance was found to be important. These factors govern the manner of the flow around the obstruction, the intensity of the re-circulation zone which was formed, and whether any unburnt gas was trapped in the wake of the obstruction. Flat type obstacles (sofa etc.), which

typically present the larger blockage area in the flame path, tended to give rise to the most rapid increase in combustion rate. Conversely, flows were seen to pass smoothly around cylindrical type obstacles. In certain circumstances, obstacles can result in pockets of gas being formed downstream. The flame front will follow the easiest path around these obstacles and will burn in these pockets, which if they are confined may generate pressure pulses.

The large obstacles and their position sets up a complex interaction between the propagating reaction front and the flow fields around the obstructions. In some instances, particularly where the obstacle was positioned against the wall of the chamber, the velocities were reduced and little turbulence was generated. Furthermore, the flame area was also reduced as it has reached the edge of the flammable mixture. These factors result in lower overpressures. In other instances, if the separation distance was in an ‘optimum’ region, local flame acceleration in the form of jetting occurred. The motion of gas movement around the obstacles creates both turbulence by vortex shedding and local wake/recirculation which can cause the flame to ‘fold’ on itself, to form a vortex shape flame. This folding, increases the flame surface area available for combustion but may produce localised flame quenching. A colour image of a folded flame front is given in Figure 5-39. This image of a vortex shaped flame was captured at the point at which the flame front propagated around the thermal marker board, which represented a flat type obstacle. In this example, the flame was still in the early stages of development and was laminar prior to reaching the obstacle.

Figure 5-39 Folded flame front producing a vortex shaped flame

The External Explosion

In the tests involving furniture, the maximum overpressure typically corresponded to the external explosion. The exception to this was the test carried out with a 7.5% methane/air mixture. The magnitude of the external explosion, in agreement with the findings of Chapter 4 and Section 5.3, was dependent upon the gas concentration; with fuel rich mixtures generating the largest overpressures within the explosion chamber. Figure 5-40 shows the overpressure-time profile for test 15. The key stages of the external explosion are plotted on the diagram. The breaking of the timing wire and analysis of the video records (see Figure 5-41) show that the vent failed 515 ms after ignition and some 20 ms later was clear of the vent opening. It can be seen in the video record that the expanding flame front had just passed over the 1st obstacle (kitchen table and chairs) when the vent failed. At 594 ms, the flame front was observed to have arrived at the plane of the vent opening, immediately igniting the high velocity unburnt gas/air mixture expelled from the chamber to form a jetting flame (see Figure 5-42).

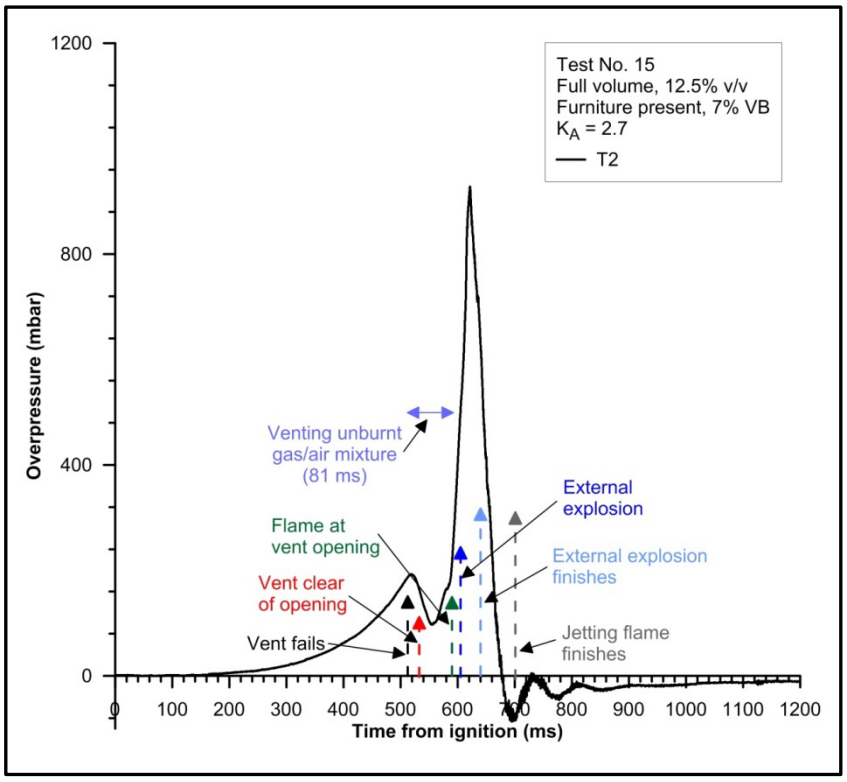

Figure 5-40 Overpressure-time profile for fuel rich mixture (test 15)

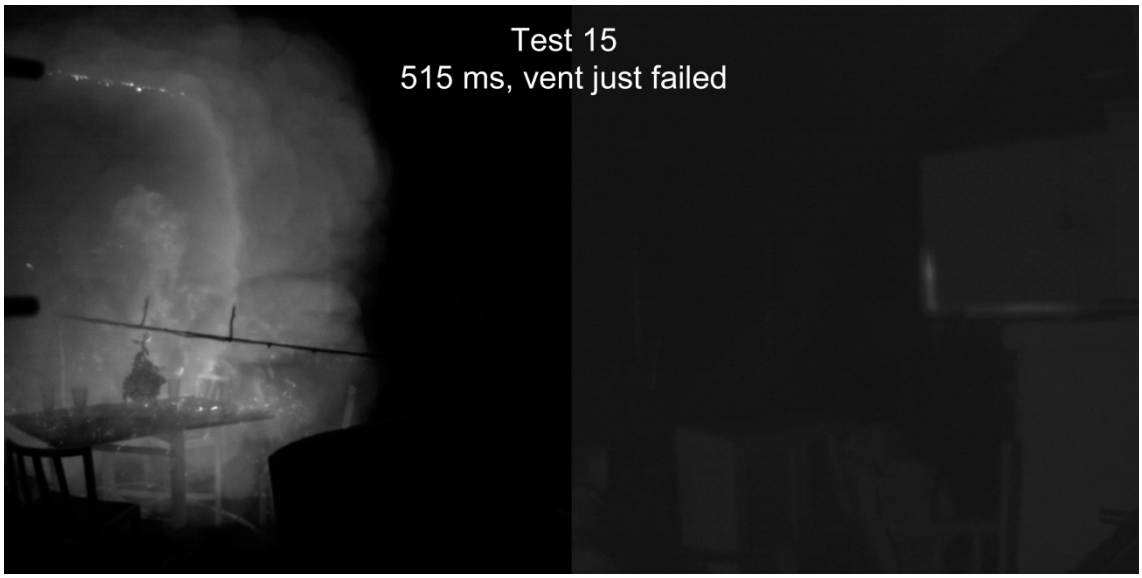

Figure 5-41 Video record from a high speed camera showing the explosion development and time of vent failure (test 15)

These observations indicate that unburnt gas/air mixture was being expelled, at high velocity, for 81 ms. At 607 ms, the jetting flame reached the ‘mushroom’ shaped tip of the jetting outflow and ignited it, generating the external explosion. The magnitude of the external explosion caused the pressure to peak within the chamber at 929 mbar. At 644 ms the external explosion stopped and the jetting flame ceased at 706 ms.

Figure 5-42 Development of the external explosion for fuel rich mixture (test 15)

Figure 5-43 shows a plot of the calculated methane/air mixture outflow through the vent opening during the venting stage of the explosion. It has been calculated using the equation for the flow through an orifice [Equation (2-43)], taking the pressure differential across the vent from the overpressure-time profiles. It has been assumed that the flow is incompressible and that the temperature of the mixture is constant. Clearly these assumptions are not strictly correct, but they are deemed as adequate for providing an estimate of the volume of gas expelled from the vent opening to form a flammable cloud. The total volume of gas expelled is of the order of 48 m^3.

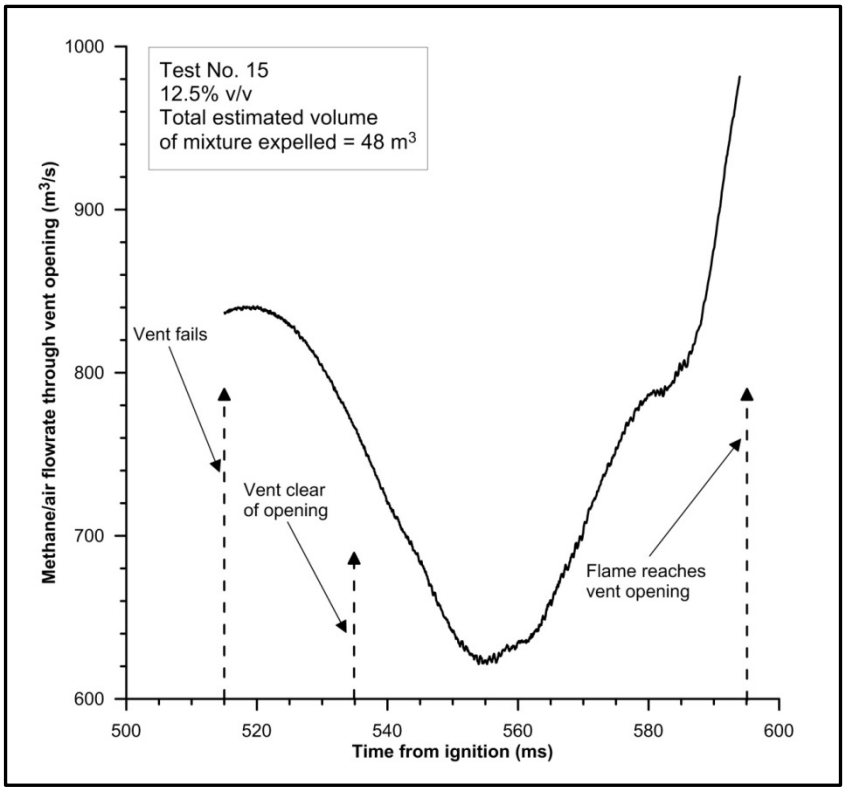

Figure 5-43 Calculated outflow of methane/air mixture through the vent opening

Central Ignition

A single test (test 17) was undertaken with central ignition. The test was undertaken with a 10% methane/air mixture and a volume blockage of 7%. Figure 5-44 shows the overpressure-time profile. In agreement with the typical pressure-time profile of a rear ignition test, there are two pressure peaks. The first pressure peak corresponds to the vent failure and the second peak corresponds to the external explosion and maximum flame area. This explosion also exhibited pressure oscillations during the latter stages of the explosion. This mechanism is initiated because central ignition causes the flame to propagate from the centre of the chamber outwards in an approximately spherical shape. Consequently, unburnt gas/air mixture becomes trapped at the rear of the chamber and is burnt towards the end of the explosion.

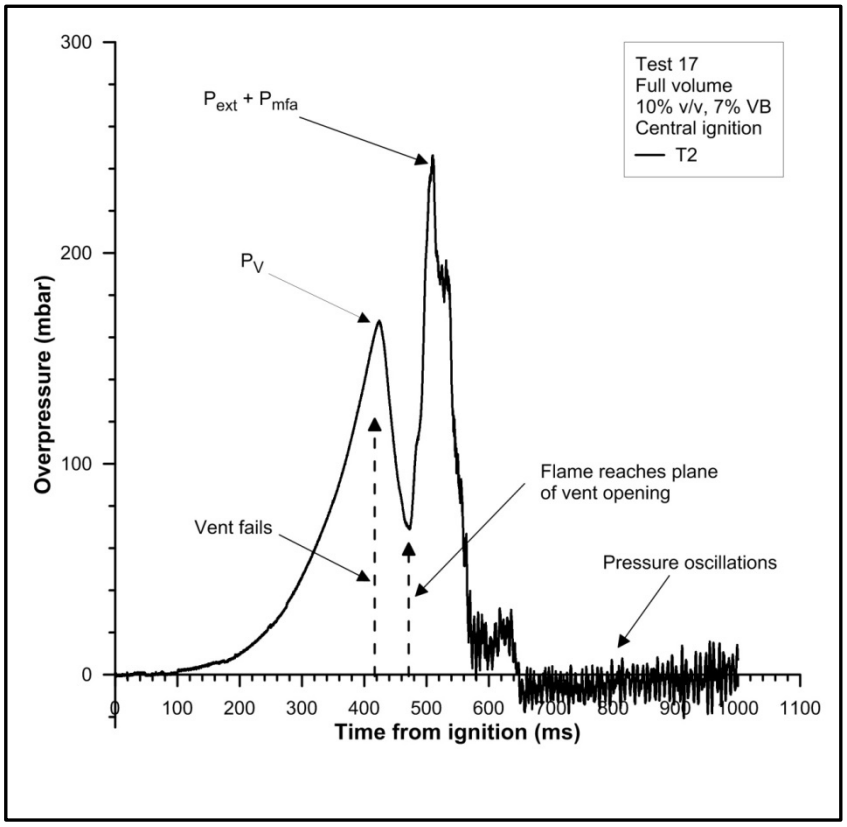

Figure 5-44 Overpressure-time profile for central ignition test (No. 17)

The external explosion also behaves in a different manner to rear ignition tests. Figure 5-45 shows three images taken from the high speed camera. In the first frame, the spherical flame can be seen developing. In the second frame, the vent is just beginning to fail, but the flame front is already close to the vent opening. In the third frame, the flame can be seen distorting towards the vent opening as it ignites the jetting outflow of unburnt gas/air mixture.

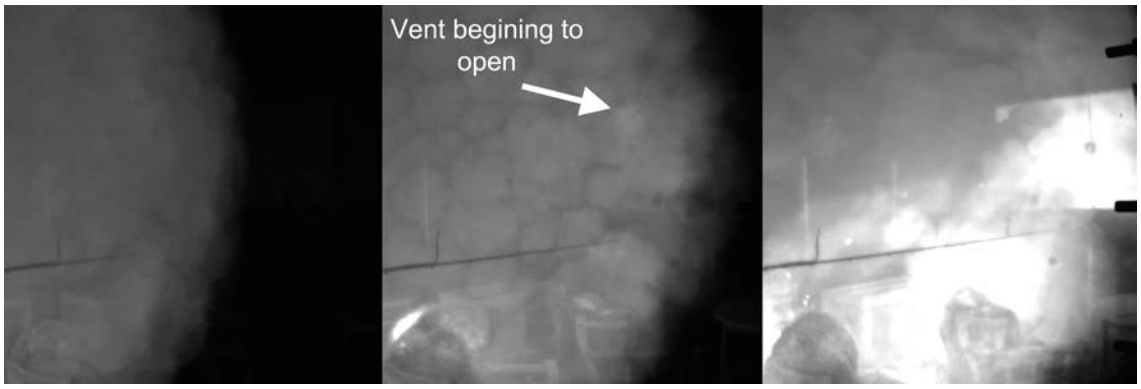

Figure 5-45 Explosion development – central ignition (test No. 17)

A photo sequence of the external explosion is given in Figure 5-46. There are some interesting differences between the external explosion from a centrally ignited explosion and that of rear ignition. Firstly, the initiation of the jetting flame is almost immediately followed by the external explosion. Secondly, the external explosion occurs closer to the vent opening because there is a shorter distance for the flame front to travel to the vent opening, and consequently, the flame front reaches the vent opening very quickly after the vent fails. Thirdly, there is a reduced volume of gas expelled through the vent opening, again, due to the position of the flame front. Lastly, the jetting flame continues after the external explosion for a significant time. This is because, with central ignition, there is more unburnt gas/air mixture left within the chamber.

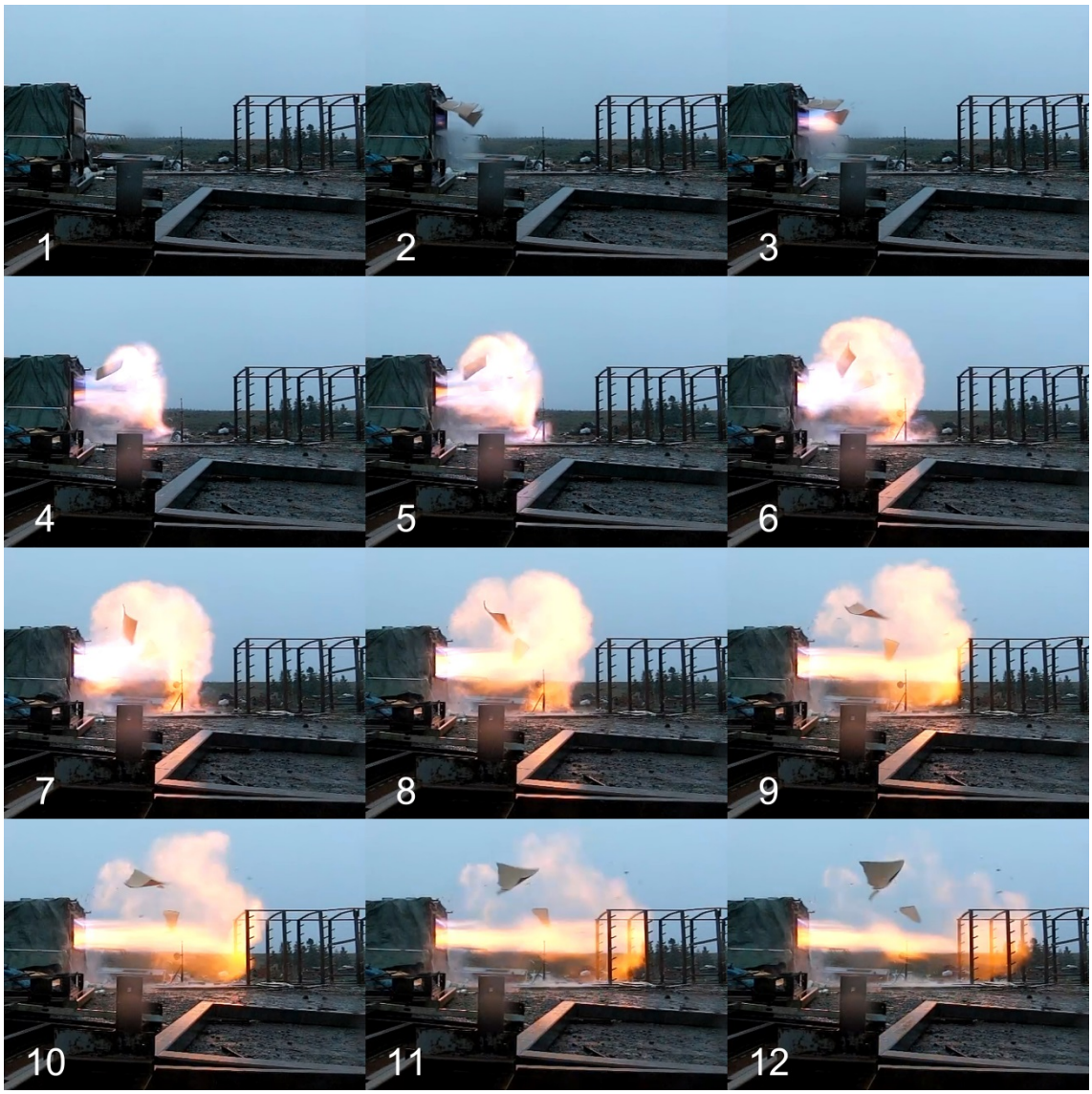

Figure 5-46 Photo sequence of external explosion – central ignition (test No. 17)

5.4.4. Comparison of Results

Comparison with Experiments Involving Idealised Obstacle Arrays

For comparative purposes, Figure 5-47 shows the overpressure-time profile of an experiment involving furniture and two experiments with idealised obstacles. The test involving furniture consisted of a layout that provided an area blockage of 22% and a volume blockage of 5%, whilst the idealised obstacle tests had area blockages of 20% and 12%, and volume blockages of 1.26% and 0.75% respectively.

Care should be taken when comparing these results as the explosion chambers are of different volume, the vent openings are of different size and the vent material has a different failure pressure. However, some interesting observations can be made. The second pressure peak on the overpressure-time profiles are similar in shape, with the

difference in shape of the first pressure peak caused by the difference in vent failure pressure and effects of inertia. It can also be seen that the both tests involving idealised obstacles produced higher maximum overpressures than the experiment involving furniture; with the idealised obstacle configuration that provided a similar area blockage (20%), producing a considerably greater maximum overpressure (1079 mbar). The idealised obstacle set-ups had uniform separation distances between obstacle arrays, whilst the furniture layout consisted of several obstacles that were not directly in the path of the propagating flame front and consequently would not have generated significant turbulence.

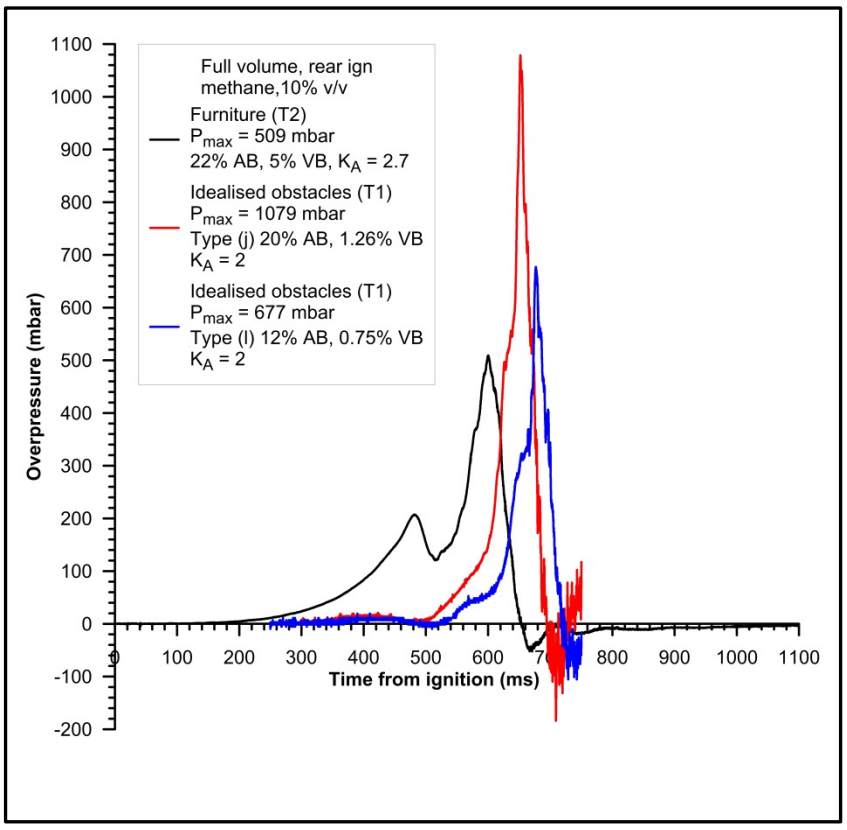

Figure 5-47 Comparison of overpressure-time profiles for tests involving furniture and idealised obstacles

Figure 5-48 shows the effects of volume blockage on the maximum overpressure. It compares the results of some of the experiments involving idealised obstacle arrays with those using furniture. There are three plots on the graph and a dotted line to indicate the threshold for structural damage. The first plot represents the results of the tests with idealised obstacle arrays, the second represents the tests involving furniture and the third represents the volume blockage of furniture directly in the path of the propagating flame front (all furniture positioned against the walls of the chamber has been discounted from the volume blockage calculation).

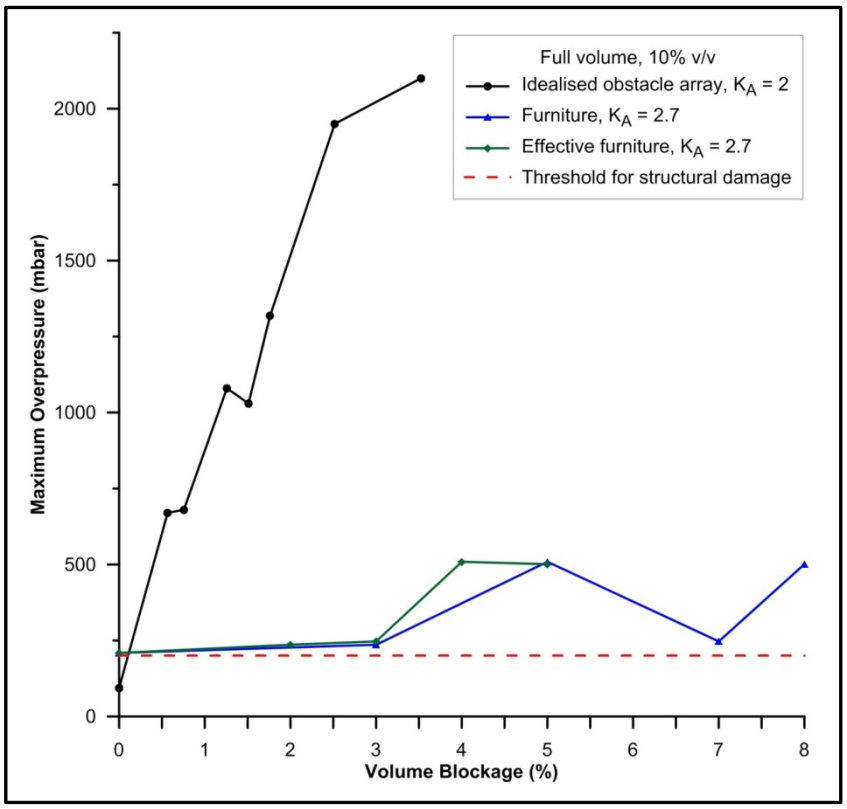

Figure 5-48 Maximum overpressure vs. volume blockage

It can be seen that consistently higher maximum overpressures were recorded during the idealised obstacle array tests. This is not surprising as the importance of separation distance between obstacles in the development of pressure has already been discussed in this chapter. The idealised obstacle arrays had more obstacles in the path of the flame and the separation distance between obstacles was uniform.

The plot that represents the furniture that was positioned in the path of the flame front, and therefore considers the volume of furniture that is effective in generating turbulence, shows that the maximum pressure increased with increasing volume blockage. However, the difference in the magnitude of the maximum overpressures between the idealised obstacles and furniture demonstrates that volume blockage is just one parameter that needs to be considered. It is clear from the two experimental programmes that area blockage is a more effective measure for turbulence generation and that obstacle separation distance is critical. Notwithstanding this, gas explosion investigators would realistically only be able to measure congestion in terms of volume blockage, so the relationship between this simple parameter and overpressure is important. In terms of explosion investigation, the most important finding from Figure 5-48 is that tests with all tests (except the empty chamber, Rig B) generated pressures greater than that required to cause structural damage to a building. The volume

blockage can be seen to play a significant role in generating pressure in all cases except for volume blockages of 3% and 7% involving furniture.

The encouraging finding of the work is that the overpressures with furniture and realistic obstacles produce significantly lower overpressures than idealised obstacle arrays with similar volume blockage. Given that the results for tests involving idealised obstacles and those of furniture produced such different results, it is important that further large-scale experimental work involving furniture be conducted. Furthermore, given the findings with fuel rich tests, it is of significant importance that this work be conducted with a wide range of concentrations. An experimental programme to conduct some 300 explosion tests, in a purpose built two-storey building that will contain furnished interconnected rooms, has been developed. The experimental programme, which has been estimated to cost £2.5m and take two years to complete, is in the final stages of negotiation with OFGEM regarding its suitability for funding through the Network Innovation Allowance (NIA) and/or Network Innovation Competition (NIC) research schemes. It is hoped that these essential programmes will commence in 2015.

Comparison with Other Large-Scale Experiments

Bimson et al. [48] observed a transition from normal self-wrinkling behaviour to flame distortion as the flame front interacted with the obstacle, leading to rapid flame acceleration. This process ‘drove’ unburnt gas/air mixture ahead of the flame and out through the vent opening in a ‘mushroom’ shaped vortex. The authors hypothesised that the prolonged outflow after the main and external explosion was due, inter alia, to the combustion of unburned gas/air held up in the front corners of the enclosure.

The results of this work are in agreement with the work of Bimson et al. [48], where similar effects of air entrainment on the external explosion were noted. It was observed that there was a rich mixture at which entrained air produced an external cloud of optimum concentration, generating peak overpressures within the enclosure. Initial unburnt gas/air richer or leaner than this concentration, produced external flammable clouds above or below this optimum mixture respectively ($\phi \approx 1.05$), resulting in reduced external and internal overpressures. Their results, for particular vent coefficients, were in the region of 5 – 10% dilution of the concentration prior to ignition. Similar effects were observed in this work, where initial equivalence values of $\phi = 1.3$ produced greater overpressures than those of $\phi = 1.05$.

The observations related to external explosions in this work were also similar to that observed by Harrison and Eyre [133] with an emerging jet igniting a ‘mushroom’ shaped cloud. The external explosion also influenced pressure generation within the

enclosure in the same manner. Firstly, through the reduction, or reversal, of the pressure gradient across the vent opening, thereby reducing the outflow through the vent and increasing the quasi-static internal pressure. Secondly, the acoustic pressure wave generated by the external explosion was also observed to propagate through the vent opening and into the explosion chamber, thereby increasing the internal overpressure. This wave was also reflected at the rear of the enclosure, with the coincidence of the incident and reflected waves resulting in pressure peaks that were larger and narrower than those recorded elsewhere in the enclosure. Thirdly, in some instances, the external explosion triggered instabilities that resulted in low frequency oscillatory pressure generation.

Comparison with Identified Correlations

In the literature review, two correlations were identified that accounted for turbulence (via a turbulence factor) and also allowed the maximum overpressure to be plotted against gas concentration. In Figure 5-49, a comparison is made of the experimental results from this work and the correlations derived by Rasbash et al. [Equation (2-75) and (2-76)] and Cubbage and Marshall [Equation (2-78)]. In respect of the experimental results, the maximum overpressures produced for each test with furniture have been averaged and plotted against equivalence ratio. The predicted maximum overpressures from Equation (2-75) and Equation (2-78) have been plotted for the corresponding equivalence ratios by selecting appropriate values for the laminar burning velocity.

It can be seen from Figure 5-49 that the maximum overpressure in the experiments increases with concentration. This suggests that the dominating factor is the external explosion, with fuel rich mixtures more likely to produce a near stoichiometric flammable cloud outside the vent opening. However, the surprising finding that fuel rich flames, due to the early development of a cellular structure, were propagating at faster speeds than that of stoichiometric mixtures, is also contributing to the overpressures in these instances.

The predictions of both correlations follow a typical burning velocity curve which does not follow the trend of the experimental results, whilst also overpredicting the lean and stoichiometric overpressures and underpredicting those of fuel rich concentrations. This reason for the underprediction of fuel rich overpressures is because the correlations do not account for the effects of the external explosion.

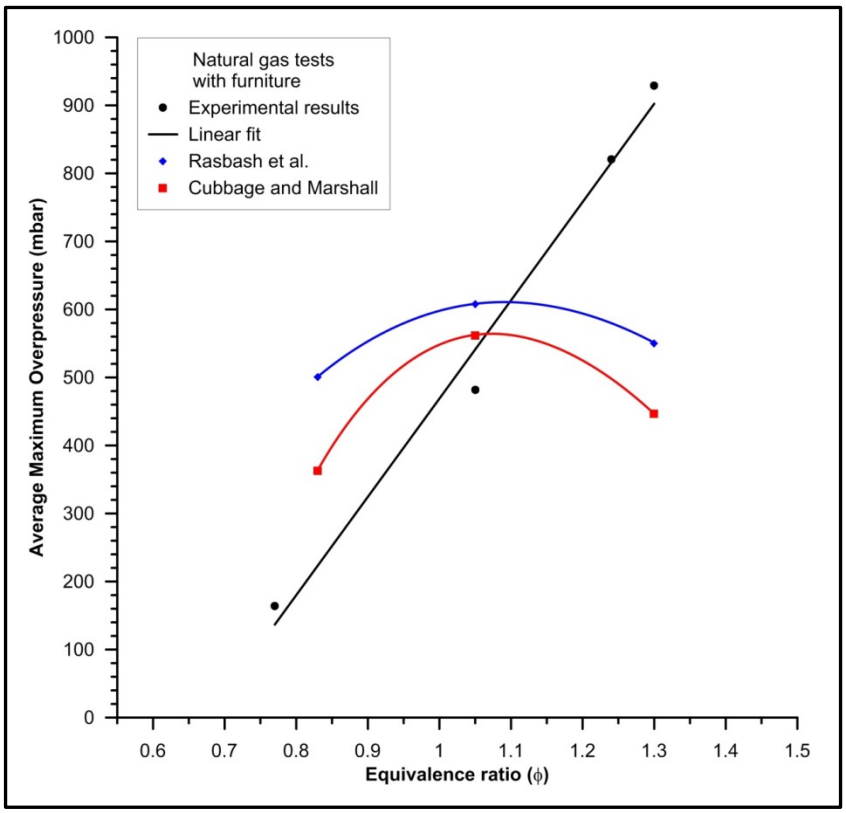

Figure 5-49 Comparison of experimental results with the correlations of Rasbash et al. [Equation (2-75)] and Cubbage and Marshall [Equation (2-78)]

5.4.5. Summary of Findings from the Furniture Tests

The series of tests produced peak overpressures between 164 mbar (7.5% methane/air) and 929 mbar (12.5% methane/air).

With the exception of a fuel lean test, experiments involving furniture generated two pressure peaks, with the dominant peak corresponding to the external explosion. The first pressure peak was always associated with the failure of the vent. The external explosions involving furniture produced pressure peaks that were over double that of corresponding tests in an empty chamber.

The jetting external explosion was a key factor in the development of the explosion during this programme. Confinement and turbulence caused a pressure build-up which caused unburnt gas/air mixture to be expelled through the vent opening at high velocity. This was subsequently ignited by the flame front as it exited the vent opening, producing a jetting flame which then ignited the ‘mushroom’ shaped cloud to initiate the external explosion. The maximum overpressures produced in the programme corresponded to the external explosion of an initially fuel rich methane/air mixture (12.5%).

Two fuel lean tests were undertaken in this programme (7.5% methane/air), neither produced pressures capable of causing structural damage. All other tests involving furniture produced explosions capable of causing structural damage to a building.

It was found that there was not a satisfactory correlation relating the actual volume blockage of a room to the maximum overpressure. Most importantly, it was the blockage in the path of the flame front that was important. Furthermore, the separation distance between turbulence generating obstacles was also significant.

In general terms, the expanding flame front was observed to develop in two distinct ways. Firstly, the flame distorted as it impinged upon an obstacle, increasing the flame surface area. Secondly, the unburnt mixture pushed ahead of the flame created turbulence in the wake of the obstruction. The flame then interacts with the modified flow field, which can further enhance the mass combustion rate, thereby increasing the flame speed and setting up a positive feedback process.

Fuel rich mixtures were found to develop cellular flame structures very early in the explosion giving rise to increased mass burning rates and generating flow which created turbulence downstream of obstacles. Surprisingly, these burning rates were faster than that of corresponding near stoichiometric mixtures. Further work is recommended to investigate this observation.

A central ignited test produced a different overpressure-time profile, with a different characteristic external explosion. In this case, the flame reached the flame front soon after the vent had failed and consequently, the external explosion occurred close to the vent opening.

The results of these large-scale experiments show that high and damaging overpressures can be generated from explosions involving congestion in the form of furniture.

5.5. Conclusions

Similarly to Chapter 4, the results presented in this chapter represent a substantial amount of new large-scale explosion data, which can be readily interpreted and applied to the development and subsequent investigation of gas explosions in buildings.

It was shown that it was possible to generate overpressures capable of causing structural damage in empty (no internal congestion) enclosures if the vent openings do not allow sufficient outflow. The presence of congestion was found to significantly increase the overpressures generated, often by more than an order of magnitude. Furthermore, with volume blockages of as little as 0.57%, overpressures greater than 200 mbar were generated in all tests where $K_A > 1$. However, the obstacle geometry, and its location to other obstacles and the enclosure, are critical in the development, or otherwise, of damaging overpressures. Consequently, volume blockage, as a parameter for determining the maximum overpressure, has to be interpreted carefully.

A number of findings were presented, providing new knowledge and understanding of the manner in which gas explosions develop in the presence of furniture. This knowledge provides further insight into how complex a vented explosion in a typical building can be, and how the degree of congestion in the form of furniture, and its layout within a room, can affect the magnitude of the explosion.

All of the pressure peaks identified in the literature review were observed during this experimental programme. The P_V peak was always the first pressure peak and corresponded to the failure of the vent. In some tests, however, where there was a vent of low failure pressure, and considerable congestion, the peak was not immediately evident. The P_b pressure peak associated with the onset of burnt gas venting was seen in some of the results but more often was masked by the rapid pressure increase due to the external explosion. The P_{ext} peak, corresponding to the external explosion was the dominant factor in most of the tests reported in this chapter.

It was determined, that for any given congestion level, reducing the vent size always resulted in an increased pressure. Whilst a larger vent resulted in increased flow and turbulence, it did not overcome the effects of reducing the confinement.

The size of the vent was also found to significantly affect the external explosion. In tests with larger vents, a jetting flame emerged and ignited the external flammable cloud, forming a mushroom shaped flame and giving rise to the peak external overpressure. As the vent size was decreased, the emerging jet velocity increased and the unburnt gas/air mixture was distributed farther from the vent opening. In these instances, the external flame propagation did not appear mushroom shaped, but rather,

was elongated, with the centre of the external explosion typically being several metres from the plane of the vent opening. Consequently, the influence of the external explosion was observed to be greater with larger vent openings.

In terms of flame speed it was found that reducing the vent size, for a given level of congestion, resulted in increased flame speeds up until the point where the fluid velocity through the vent opening reached the local speed of sound. After this point, reducing the vent opening resulted in the flame speed being reduced, except in the region of the vent opening. In addition, this reduction in flow velocity reduced the levels of turbulence in the wake of obstacles, thereby lessening the enhancement of combustion rates and producing relatively low flame speeds.

Similarly to the behaviour observed with idealised obstacles, two important processes were observed in the development of an explosion involving furniture. Firstly, an initially laminar flame distorts as it impinges upon the obstacle, increasing the flame surface area. Secondly, the explosion is significantly influenced by the changes in the flow field induced by the obstacle. When the flame arrives at the obstacle, it interacts with the modified flow field, with the geometry and size of the obstacle determining the turbulence levels and length scales. Consequently, the separation distance between obstacles and their location was found to be important. When the volume blockage in the path of a propagating flame front increases, the gaps between the obstructions and the enclosure will decrease resulting in increased gas velocities around the obstacle, which may increase the reaction rate.

The effect that the shape of the obstruction and its location within the enclosure appeared to be significant. It governed the manner of the flow around the obstruction, the intensity of the re-circulation zone which was formed, and whether any unburnt gas was trapped in the wake of the obstruction. The introduction of large obstacles and their position sets up a complex interaction between the propagating reaction front and the flow fields around the obstructions. In some instances, particularly where the obstacle was positioned against the walls of the chamber, flow velocities were reduced and little turbulence was generated. In other instances, if the separation distance was in an ‘optimum’ region, local flame acceleration in the form of jetting occurred. The motion of gas movement around the obstacles creates both turbulence by vortex shedding and local wake/recirculation which can cause the flame to ‘fold’ on itself, to form a vortex shaped flame, resulting in increased combustion rates.

It is recognised that the effect of area blockage and obstacle array separation distance may play a more important role in the development of fast flames than volume blockage. However, unlike chemical, process and storage facilities, where congested

region layouts or designs will be readily available, populated buildings will have congested and confined areas that are not predictable, and, as a consequence, it is appropriate to use volume blockage as a criteria. Consequently, for the purpose of this study, the volume blockage was the main variable when designing the congestion configuration. However, further large-scale experimental tests, investigating the effects of area blockage and separation distance are recommended. This should be linked to a programme that investigates the complex interaction caused when flames propagate from one furnished room to another. In addition, due to the surprising findings in some of the fuel rich tests, further work should also be carried out to investigate the development of cellular flames which were found to increase mass burning rates and generate turbulence downstream of obstacles.

It is clear from the results of this experimental programme, and those reported in Chapter 4, that gas explosions that propagate from one furnished room to another have the potential to generate overpressures capable of inflicting significant structural damage on buildings. The significance of the results presented in this chapter, is that they confirm that the size and failure pressure of potential vent openings, and the degree of congestion within a building, are key factors in whether or not a building will sustain structural damage following a gas explosion. Given that the average volume blockage in a room in a UK dwelling is in the order of 17%, it is clear that without the use of large windows of low failure pressure, residential buildings will continue to be susceptible to significant structural damage during an accidental gas explosion.

CHAPTER 6
THE INTERPRETATION OF THERMAL DAMAGE

CHAPTER 6

THE INTERPRETATION OF THERMAL DAMAGE

6.1. Introduction

When a flammable gas is released within, or migrates into, a building and mixes with air to form a flammable gas/air mixture which is ignited; a flame front will propagate through the mixture, wherever possible in an approximate spherical geometry, releasing energy in the form of heat, light and pressure.

In Chapter 1 it was discussed that the damage sustained by a building, and its decor, during an explosion can provide forensic evidence that is important in the accurate determination of the origin and cause of the incident. The severity and extent of thermal damage to surfaces such as door frames, window-sills, wallpaper etc. may be used to provide an indication of the relative density of the fuel gas, its concentration in the explosive mixture prior to ignition, its distribution throughout the building and the depth of any flammable layer. This information may then be used to determine any credible sources of gas by calculating or measuring the release rate and estimating whether an escape of this magnitude is capable of mixing with air to form a flammable layer, or completely full mixture, which is in agreement with the scorching patterns.

There are numerous materials, typically found at the scene of explosion incidents that are susceptible to thermal damage and hence may be used as ‘markers’ by explosion investigators. These materials include paints, polyethylene sheeting, wallpaper, paper, wool, cotton, plywood, varnished wood, PVC coated electrical cable etc.

In Chapter 2 it was determined that whilst there was a plethora of literature relating to the response of people and materials exposed to heat, the majority of this work focused on the intensity of hydrocarbon fires and the behaviour of materials exposed to compartment fires. little work was found in the literature relating to the heat flux of a vented explosion.

Of the few studies in the literature concerning thermal damage from an explosion, the most relevant work saw a variety of fibres exposed to an electric heating plate set to 350°C (to ensure the fabric melting point was exceeded) and a gas burner (Section 2.7.3). The fibres were exposed to the heat sources for a duration of 30 s except for acrylic, polyester, silk and wool materials, where the duration was shortened to 15 s due to the very rapid melting/charring of the fibre samples. The samples were

subsequently analysed through an optical microscope and SEM. The initial change in the fibre, that occurred with either heat source, and which was particularly prevalent in cellulosic materials, was a discolouration from yellowish initially through to brown. The fibre ends of nylon, polyester, acrylic and wool were found to have melted and fused together to form 'bulb-like' ends. Cotton fibres, after contact with the flame were found to lose their normal appearance and take on a lacelike, delicate charred consistency. Whilst these results are of relevance to this study, they need to be treated with caution as the experiments are not fully representative of the conditions of an explosion, particularly in terms of duration and flame temperature.

The objectives of this aspect of the research were to determine the effect of an explosion within a building on specific markers that were most likely to be found at the scene of an explosion and to determine to what extent these thermal damage markers could be used as forensic evidence in the investigation to determine the origin of the explosion and the most likely source of gas release. In particular, the intention was to identify if the materials and surfaces exposed to a propagating flame could provide reliable evidence that could be used to:

i. determine the relative density of the fuel gas (and hence likely fuel type);
ii. estimate the distribution of flammable mixture throughout the building;
iii. determine the depth of any flammable layer; and
iv. estimate the concentration of fuel gas in the explosive mixture prior to ignition.

6.2. The Experimental Programmes

The experimental work was undertaken in four separate programmes. The 1st set of tests were conducted in conjunction with the interconnected room tests undertaken at the FRS facility. The 2nd and 3rd set of tests were undertaken at DNV GL Spadeadam and the final set of tests was undertaken at the University of Leeds. The first two sets of tests were analysed by visual comparison and the third and fourth set using various laboratory techniques. These techniques are discussed later in this chapter. A number of tests were undertaken under nominally identical conditions to check repeatability. Whilst assessment of thermal damage is subjective, the results were considered to be satisfactory.

6.2.1. The FRS Experimental Programme

Test numbers 1 – 19 and 23 – 44 of the interconnected room tests were, in addition to being used to determine the effects of interconnecting rooms, also used to analyse the thermal damage that occurs to typical materials found in dwellings, as a consequence of exposure to a transient flame front and the movement of hot combustion products.

The marker boards were positioned adjacent to the walls of the chambers (see Figure 3-46, Figure 3-47 and Table 3-7). This location was chosen for two reasons; firstly, because it represented the position that the materials were most likely to be found in a building, and secondly, because the location would not significantly affect the development of the explosion (e.g. by creating turbulence).

As the flame and hot gases propagated during the explosion the thermal strips were subjected to heat (from the hot gases) and short duration flame impingement. Assessment of the vertical distribution and severity of thermal damage was undertaken by measurement and visual comparison. The lowest vertical position on each strip, at which scorching was observed, was measured from floor level and recorded. This information was used to compare the observed damage with the initial depth of the gas/air mixture. The severity of thermal damage was assessed by visually comparing the degree of scorching of each test strip with other strips of the same material and to a reference non-exposed strip. Each strip was graded on a 'relative damage number' scale of 0 – 5, where 0 represented no evidence of scorching and 5 represented the worst case of damage to that particular type of material. Differences in the sensitivity of the various materials to thermal damage were taken into account by using a separate damage number scale for each type of material. Table 6-1 shows the criteria used for assessing the severity of thermal damage and the assignment of a damage number.

Table 6-1 The criteria for assessing thermal damage (FRS)

Damage Number	Severity of Damage
0	No evidence of thermal damage
1	Material showed signs of discolouration
2	Material exhibited significant discolouration
3	Material showed evidence of charring
4	Material presented significant charring
5	Material exhibited blistering, blackening or burning

A summary of the experimental test conditions and data gathered from the 45 explosion tests conducted is contained in Table 6-2. A range of experimental parameters were used during the tests and their effects on the severity and extent of thermal damage to the test materials are discussed in this chapter. The main variables studied during these experimental tests, in terms of thermal damage, were the gas concentration, initial depth of the natural gas/air ceiling layer and ignition position.

Table 6-2 Summary of test conditions and experimental data

Test No.	Gas Conc. (% v/v)	Layer Depth[a] (m)	Ignition Position	Door	K_A		Average Damage Number[b]	Lowest Scorching from Ceiling[c] (m)
					L	R		
1	8	1.2	Rear	Open	2.4	2.4	1.1	1.1
2	8	1.2	Rear	Open	2.4	2.4	1.2	1.2
3	10	1.2	Rear	Open	2.4	2.4	2.1	1.4
4	10	1.2	Rear	Open	2.4	2.4	1.8	1.4
5	10	Full	Rear	Open	2.4	2.4	2.8	2.2
6	12	1.2	Rear	Open	2.4	2.4	2.6	1.8
7	12	1.2	Rear	Open	2.4	2.4	2.6	1.8
8	10	Full	Rear	Open	2.4	2.4	2.6	2.1
9	10	1.2	Central	Open	2.4	2.4	2.6	1.6
10	10	1.2	Central	Open	2.4	2.4	3.2	1.7
11	8	1.2	Rear	Closed	2.4	2.4	1.3	1.4
12	10	Full	Central	Open	2.4	2.4	3.0	2.2
13	8	1.2	Rear	Closed	2.4	2.4	1.3	1.4
14	10	1.2	Rear	Closed	2.4	2.4	1.6	1.7
15	12	1.2	Rear	Closed	2.4	2.4	1.7	1.3
16	10	1.2	Central	Closed	2.4	2.4	3.1	1.5
17	10	Full	Rear	Closed	2.4	2.4	2.5	2.3
18	10	1.2	Rear	Closed	2.4	2.4	1.6	1.2
19	12	1.2	Rear	Closed	2.4	2.4	2.0	1.4
23	8	1.2	Rear	Open	2.4	4l	1.3	1.6
24	10	1.2	Rear	Open	2.4	4l	2.5	1.3
25	8	1.2	Rear	Closed	2.4	4l	1.0	1.5
26	10	1.2	Rear	Closed	2.4	4l	2.7	1.6
27	10	1.2	Central	Closed	2.4	4l	2.7	1.3
28	12	1.2	Rear	Open	2.4	4l	4.0	1.4
29	12	Full	Rear	Closed	2.4	4l	2.3	2.2
30	8	1.2	Rear	Open	2.4	8	2.0	1.6
31	8	1.2	Rear	Closed	2.4	8	1.0	1.4
32	12	1.2	Rear	Open	2.4	8	3.0	1.4
33	12	1.2	Rear	Closed	2.4	8	2.3	1.5
34	10	1.2	Central	Open	2.4	8	2.0	1.3
35	10	1.2	Central	Closed	2.4	8	2.7	1.7
36	10	1.2	Rear	Closed	2.4	8	2.7	1.2
37	10	1.2	Central	Open	2.4	4r	3.0	1.6
38	10	Full	Central	Open	2.4	4r	1.3	2.1
39	10	1.2	Central	Closed	2.4	4r	2.7	1.6
40	10	Full	Rear	Closed	2.4	4r	2.0	2.2
41	10	1.2	Rear	Closed	2.4	4r	2.7	1.8
42	10	Full	Rear	Closed	2.4	4r	3.3	2.2
43	8	1.2	Rear	Closed	4r	2.4	1.8	1.4
44	10	1.2	Rear	Closed	4r	2.4	2.1	1.6
45	12	1.2	Rear	Closed	4r	2.4	2.3	1.5
46	10	1.2	Central	Closed	4r	2.4	2.7	1.6
81	10	0.3	Rear (0.3)[d]	Closed	4r	2.4	2.3	0.6
82	10	0.6	Rear (0.6)[d]	Closed	4r	2.4	2.2	0.8

[a] Measured from the ceiling.

[b] Weighted average of all the materials used in the test.

[c] To an accuracy of ± 20 cm.

[d] Height of spark ignitor from ceiling.

6.2.2. The Spadeadam Experimental Programmes

Two experimental programmes were carried out in Rig C at Spadeadam. The measurement of thermal damage was carried out by placing thermal marker boards at various locations in the explosion chamber(s) (for programme three, see Figure 3-48). During experimental programme four, two purpose made marker stands were used, each of which held 2 x softwood panels in place during the explosion. One panel was placed such that the softwood panels were 'face-on' to the propagating flame and one was positioned close to the vessel chamber walls and perpendicular to the propagating flame (Figure 3-51). A summary of the test conditions and data is given in Table 6-3.

In programme three, similarly to the FRS experiments, the severity of thermal damage was assessed by visually comparing the degree of scorching of each test strip with other strips of the same material. However, in this case, each strip was graded on a 'relative damage number' scale of 0 - 10 where 0 represented no evidence of scorching and 10 represented the worst case of damage to that particular type of material. Differences in the materials sensitivity to thermal damage were taken into account by using a separate damage number scale for each type of material (see Table 6-4).

The purpose of the homogenous natural gas explosions was to simulate the ignition of a uniform flammable mixture in a room, which had built-up over a significant time following the onset of a low momentum gas release, and to determine the subsequent thermal damage. A number of natural gas layered explosions were also undertaken to simulate relatively common accidental natural gas explosions in dwellings.

The purpose of the propane release experiments was to simulate an accidental explosion following a high momentum vertical propane release into a room, which was subsequently ignited shortly after the release commenced. This would represent a common cause of propane explosions in dwellings, that where a single-stage propane regulator fails and allows gas to escape, at high momentum, through appliance controls. In addition, a single propane layer test was undertaken [3(8)].

In the propane tests, the fuel/air mixtures were found to be inhomogeneous. In tests (3)5 to (3)7, the central region of the inner-chamber was relatively fuel rich compared to the outer portion of the chamber. This was confirmed by comparing the gas concentration measured at 2.3 m high with gas build-up calculations (taken from Harris [16]), assuming uniform mixing of the total gas entering the vessel through the entire volume of the inner-chamber. The discrepancy between the calculated and measured value was found to be greatest in experiment (3)7, most likely because the mixing efficiency was reduced due to the low efflux velocity of the propane entering the chamber. A summary of results is given in Table 6-5.

Table 6-3 Summary of test conditions

Test No.[a]	Explosion Test Groupings	Release Height[b] (m)	Orientation	Flowrate (m^3/h)	Duration of Release	Ignition Position	Gas Conc. (% v/v)		
							0.8 m[b]	1.5 m[b]	2.3 m[b]
(3)1	Homogeneous natural gas	-	-	-	-	Centre[c]	-	7.7	-
(3)2		-	-	-	-	Centre[c]	-	11.8	-
(3)3		-	-	-	-	Centre[c]	-	9.7	-
(3)4		-	-	-	-	Centre[c]	-	8.9	-
(3)5	Propane	0.3	Up	17	240	Centre[c]	-	3.8	-
(3)6		0.3	Up	16	480	Centre[c]	-	7.4	3.3
(3)7		0.3	Up	6	240	Centre[c]	-	5.7	1.9
(3)8		0.3	Horizontal	12	480	Centre[c]	-	1	4.8
(3)9	Layered natural gas	1	Horizontal	-	-	Centre[c]	0.4	7.3	8.1
(3)10		1	Horizontal	-	-	Centre[c]	0.1	8.7	9.4
(3)11		1	Horizontal	-	-	Centre[c]	0.2	4.7	6.1
(3)12		1	Horizontal	-	-	Centre[c]	0.5	10.2	12.4
(3)13		2	Horizontal	-	-	Centre[c]	0.1	0.1	9.0
(3)14		2	Horizontal	-	-	Centre[c]	0.1	0.1	7.4
(3)15		2	Horizontal	-	-	Centre[c]	-	-	12.3
(4)1	Homogeneous methane	-	-	-	-	Rear	-	10	-
(4)2		-	-	-	-	Rear	-	10	-
(4)3		-	-	-	-	Rear	-	10	-
(4)4		-	-	-	-	Rear	-	10	-
(4)5		-	-	-	-	Rear	-	6	-
(4)6		-	-	-	-	Rear	-	7.5	-
(4)7		-	-	-	-	Rear	-	12.5	-
(4)8		-	-	-	-	Rear	-	10	-
(4)10		-	-	-	-	Rear	-	7.5	-
(4)11		-	-	-	-	Rear		9.5	-

[a] The experimental programme number is given in parentheses.
[b] Measured from floor level.
[c] Centre of the rear chamber.

Table 6-4 The criteria for assessing thermal damage (Spadeadam Rig C)

Damage Number	Material												
	Marker-boards	Emulsion	Gloss	PE Sheet	Newspaper	Heavy-Duty Wallpaper	PVC Cable	Varnish	Cotton	Wallpaper	PVC Tape	Wool
0	No damage	No damage	No damage	No damage	No damage	No damage	No damage	No damage	No damage	No damage	No damage	No damage
1							Scorching to one corner					Faint yellowing
2	Slight scorching			Slightly wilted	Edges scorched	Raised areas slightly browned		Slight discolouring	Edges burnt	Some blotches or discolour	Some blisters	Slight browning
3		Some blistering	Some blistering				Both corners damaged					
4	Thoroughly scorched			Wrinkled				Browned	Starting to go brown	Larger or more dense blotches	More blisters or burnt blisters	More obvious browning
5					Slightly browned	Raised areas well browned and some damage to rest						Burnt through
6	Well browned	Heavy blistering	Heavy blistering	Curled edges			Coating well damaged	Well browned	Well browned, some white	Covered in blotches	Heavily blistered and blisters blackened	
7					Well browned	Thoroughly browned						Heavily browned but no melting
8	Blackened			Very curled edges			Plastic melted	Dark brown	Mostly blackened, some white	Heavily browned	Completely covered in blisters and mostly black	Melting
9						Raised areas burnt			Mostly black, no white			
10	Completely burnt	Completely blackened	Completely blackened	Completely melted	Burnt away	Completely burnt	All plastic melted and wire blackened	Completely blackened	Completely blackened	Completely blackened	Peeled away or completely blackened	Burnt/melted away

Table 6-5 Average damage number results (tests (3)1 to (3)15)

Test No.	Test Type	Backboard[a]			Matt Emulsion Paint[a]			PVC Coated Wiring[a]			Varnish[a]		
		High	Mid	Low	High	Mid	Low	High	Mid	Low	High	Mid	Low
(3)1	Homogeneous natural gas	0.0	0.0	0.0	0	0	0	1.3	0.8	0.4	0.5	0	0
(3)2		0.3	1.8	0.8	0.5	1	0.5	1.7	0.8	1.0	1	4	3.5
(3)3		0.0	0.0	0.0	0	0	0	1.0	2.0	1.2	0	0	0
(3)4		0.5	1.3	1.5	0	0	0	1.0	1.8	0.8	0	2	3
(3)5	Propane	0.0	0.0	0.0	0.0	0.2	0.2	0.0	0.0	0.0	0.0	0.0	0.4
(3)6		0.0	0.2	0.4	0.2	0.4	0.2	0.0	0.4	0.8	0.0	0.4	1.0
(3)7		0.0	0.0	0.0	0.0	0.0	0.0	0.0	0.0	0.0	0.0	0.0	0.0
(3)8		0.0	0.0	0.0	0.0	0.0	0.0	0.0	0.0	0.2	0.0	0.0	0.2
(3)9	Layered natural gas	0.0	0.0	0.0	0.0	0.0	0.0	0.0	1.5	1.0	0.0	2.0	0.0
(3)10		1.0	2.0	0.5	0.0	0.0	0.0	0.0	1.0	1.0	1.0	1.5	0.0
(3)11		0.0	0.0	0.0	0.0	0.0	0.0	0.0	0.0	0.0	0.0	0.0	0.0
(3)12		1.0	1.7	1.0	0.0	0.0	0.0	0.0	1.5	1.0	1.0	1.3	0.5
(3)13		0.0	0.0	0.0	0.0	0.0	0.0	0.0	0.0	0.0	0.0	0.0	0.0
(3)14		0.0	0.0	0.0	0.0	0.0	0.0	0.0	0.0	0.0	0.0	0.0	0.0
(3)15		0.0	0.0	0.0	0.0	0.0	0.0	0.0	0.0	0.0	0.0	0.0	0.0
Test No.	**Test Type**	**Gloss Paint[a]**			**Polyethylene[a]**			**Cotton Strip[a]**			**Wallpaper[a]**		
		High	Mid	Low	High	Mid	Low	High	Mid	Low	High	Mid	Low
(3)1	Homogeneous natural gas	0.0	0.0	0.0	10.0	10.0	10.0	6.0	6.7	6.3	0	0.5	0
(3)2		0.5	1.3	0.5	10.0	10.0	10.0	7.7	7.7	7.7	2.5	4	3
(3)3		0.5	1.0	0.5	9.7	10.0	10.0	7.3	7.3	7.0	0	0.5	0
(3)4		0.0	1.0	0.5	10.0	10.0	10.0	6.7	8.0	7.7	0	1.5	0.5
(3)5	Propane	2.2	2.8	2.8	8.8	9.0	8.2	5.4	3.2	3.6	0.0	0.0	0.0
(3)6		0.2	1.6	2.0	10.0	10.0	10.0	4.0	7.8	6.6	0.0	0.2	0.0
(3)7		0.0	0.0	0.0	9.4	8.8	9.0	0.0	0.2	0.6	0.0	0.0	0.0
(3)8		0.0	0.0	0.2	9.0	9.6	10.0	0.0	2.8	7.6	0.0	0.0	0.4
(3)9	Layered natural gas	2.2	2.4	1.3	10.0	10.0	10.0	6.2	6.6	2.8	0.0	0.0	0.0
(3)10		1.8	1.4	0.5	10.0	10.0	10.0	8.4	7.8	3.8	0.0	1.0	0.0
(3)11		0.0	0.0	0.0	10.0	7.2	2.8	0.8	0.0	0.0	0.0	0.0	0.0
(3)12		2.0	1.8	0.7	10.0	10.0	10.0	4.4	5.4	3.0	0.0	0.0	0.0
(3)13		2.0	1.0	0.0	10.0	10.0	8.0	4.0	1.3	0.0	0.5	0.0	0.0
(3)14		1.0	0.0	0.0	10.0	10.0	6.0	2.6	0.5	0.0	0.0	0.0	0.0
(3)15		1.0	1.0	0.0	10.0	10.0	7.2	4.6	2.4	0.0	0.0	0.0	0.0
Test No.	**Test Type**	**Newspaper[a]**			**Heavy Duty Wallpaper[a]**			**PVC Tape[a]**			**Wool[a]**		
		High	Mid	Low	High	Mid	Low	High	Mid	Low	High	Mid	Low
(3)1	Homogeneous natural gas	7.0	7.0	7.0	1.3	2.7	1.0	0.5	1.7	0.5	4.0	5.7	4.3
(3)2		9.7	9.7	10.0	2.0	4.3	3.0	2.3	4.7	3.3	4.5	6.0	5.5
(3)3		10.0	7.3	7.3	2.0	2.7	1.0	1.0	1.7	1.0	2.3	4.0	2.7
(3)4		10.0	10.0	9.7	2.3	3.7	3.7	2.0	2.3	1.3	3.7	7.3	7.3
(3)5	Propane	5.8	5.0	5.0	0.4	0.4	1.0	1.0	1.2	1.2	6.6	4.8	3.6
(3)6		9.0	10.0	10.0	1.2	2.4	3.4	1.4	3.0	3.8	8.0	9.2	9.8
(3)7		0.4	2.0	2.8	0.0	0.2	0.4	0.0	0.0	0.0	0.2	0.2	0.2
(3)8		0.4	5.6	9.4	0.0	1.2	2.0	0.0	0.4	2.2	0.0	2.2	4.8
(3)9	Layered natural gas	9.8	10.0	7.2	2.6	3.2	1.5	3.0	4.2	2.0	9.6	9.6	4.6
(3)10		10.0	10.0	9.0	3.0	3.8	1.8	3.4	4.8	1.6	10.0	9.8	3.8
(3)11		2.6	1.0	0.0	1.0	0.0	0.0	0.7	0.0	0.0	3.4	1.3	0.0
(3)12		10.0	10.0	8.8	2.2	3.8	1.4	3.2	4.4	1.8	9.6	10.0	7.4
(3)13		9.4	5.0	0.5	1.8	1.0	0.0	1.8	1.3	0.0	5.4	2.4	0.0
(3)14		8.4	3.3	0.0	1.5	1.0	0.0	0.8	0.0	0.0	3.0	0.8	0.0
(3)15		9.2	7.5	0.5	1.6	2.4	0.5	1.4	2.0	0.0	9.2	3.6	0.7

[a] Average thermal damage number.

6.2.3. The University of Leeds Experimental Programme

Seventeen explosion tests were undertaken in the $1m^3$ explosion chamber. The purpose of these tests was to undertake a comparison with the large-scale tests, under the more controlled conditions possible at small-scale. It was also useful to carry out some experiments under completely confined conditions in a near spherical explosion chamber. This would make it possible to determine if venting affected the pattern of thermal damage.

Explosions were undertaken using methane, propane and ethylene at varying concentration. The material samples were placed on the door of the explosion vessel and secured using double sided tape. Similarly to the Spadeadam experiments, the severity of thermal damage was assessed by visually comparing the degree of scorching of each test strip with other strips of the same material and graded using the same 'relative damage number' scale (see Table 6-6). In addition, samples from this set of experiments were also assessed for thermal damage by SEM. A summary of the experimental test conditions and data is given in Table 6-7.

Table 6-6 The criteria for assessing thermal damage by visual examination (University of Leeds)

Damage Number	Material				
	Untreated Wood	**Oil Based Gloss Paint**	**Water Based Gloss Paint**	**Varnish**	**Wallpaper**
0	No damage	No damage	No damage	No damage	No damage
1					
2	Slight discolouring			Slight discolouring	Some blotches or discolour
3		Some blistering	Some blistering		
4	Browned			Browned	Larger or more dense blotches
5					
6	Well browned	Heavy blistering	Heavy blistering	Well browned	Covered in blotches
7					
8	Dark brown			Dark brown	Heavily browned
9					
10	Completely blackened	Completely blackened	Completely blackened	Completely blackened	Completely blackened

Table 6-7 Summary of experimental test conditions and data

Test No.[a]	Fuel	Gas Conc. (% v/v)	Equivalence Ratio (ϕ)	Ignition Position	P_{max} (barg)	Average Damage Number				
						Gloss Paint[b]	Bare Wood	Gloss Paint[c]	Varnish	Wallpaper
TDM1	Methane	7	0.72	Centre	4.84	6	4.5	0.8	6	6
TDM2		8	0.83	Centre	6.40	7	7	1	7	8
TDM3		10	1.06	Centre	7.37	8	8	2	8	9
TDM4		12	1.30	Centre	6.12	7	6.5	0.6	7	7
TDM5		13	1.42	Centre	4.58	5.5	6	0.8	5	6.5
TDM6		8	0.83	Centre	6.37	7	6.5	1	6.5	7.5
TDM7		10	1.06	Centre	7.35	8	8	2	8	8.5
TDM8		8	0.83	Centre	6.28	7	6.5	1.5	8	7
TDM9		10	1.06	Centre	7.92	8	8	1	7	8.5
TDM10		12	1.30	Centre	6.17	6.5	6	1	7	6.5
TDP1	Propane	3	0.74	Centre	5.94	6.5	7	2	6	6
TDP2		4.5	1.13	Centre	8.14	9	9	3	9	9
TDP3		7	1.81	Centre	-	4	4	1	7	7
TDP4		7	1.81	Centre	4.92	4.5	4.5	1.5	7	8
TDE1	Ethylene	6.5	1.00	Centre	8.94	8	8.5	2	6	9
TDE2		4	0.60	Centre	5.37	5	4	1	4	5
TDE3		6.5	1.00	Centre	8.88	9	9	2	9	9
TDE4		8.6	1.35	Centre	8.47	8	8	1	7	8

[a] The numbering scheme is derived as follows: TD stands for thermal damage. The third letter denotes the fuel type (M = methane, P = propane and E = ethylene).
[b] Oil based paint.
[c] Water based paint.

6.3. Sensitivity to Thermal Damage (all Rigs)

Thermal damage to the material samples was typically exhibited in a mottled pattern (Figure 6-1).

With homogeneous (full volume) explosions, the thermal damage sustained during the explosion was distributed fairly uniformly along the length of the samples, although in the large-scale tests (Rigs A and C) a slight increase in damage was noticeable in the middle section, approximately corresponding to the elevation of the ignition position. This information may prove useful in the determination of the ignition source.

Figure 6-1 Typical mottled pattern of thermal damage (Rig C)

The large-scale layered natural gas explosion tests (Rigs A and C) produced thermal damage that was distributed relatively uniformly to the middle and upper sections of the samples (approximately corresponding to the layer depth), whilst the propane layer experiment produced damage that was distributed to the bottom section of the sample (again corresponding to the approximate layer depth). This suggests that the density of the fuel, and hence likely fuel type, may be determined in layered explosions. It also suggests that the approximate height of the gas release may be determined.

In the twin compartment tests in Rig C, marker boards in the outer enclosure displayed a greater degree of damage than a comparable board in the inner enclosure. Analysis of the video records demonstrated that this was because some of the boards in the outer enclosure were in the path of the venting flame front and hot combustion gases.

Figure 6-2 shows a comparison of the average damage number (taken from the material samples of the Spadeadam tests in Rig C) against critical heat flux values taken from Babrauskas [410]. It should be noted that the critical heat flux values taken for the gloss paint, varnish, and polyethylene samples have been taken from experiments where the material was fixed to a wood backboard (substrate) and this is not an accurate representation of the Spadeadam experimental conditions. The results show that there does not appear to be a correlation between the critical heat flux and the observed thermal damage sustained by materials during a gas explosion.

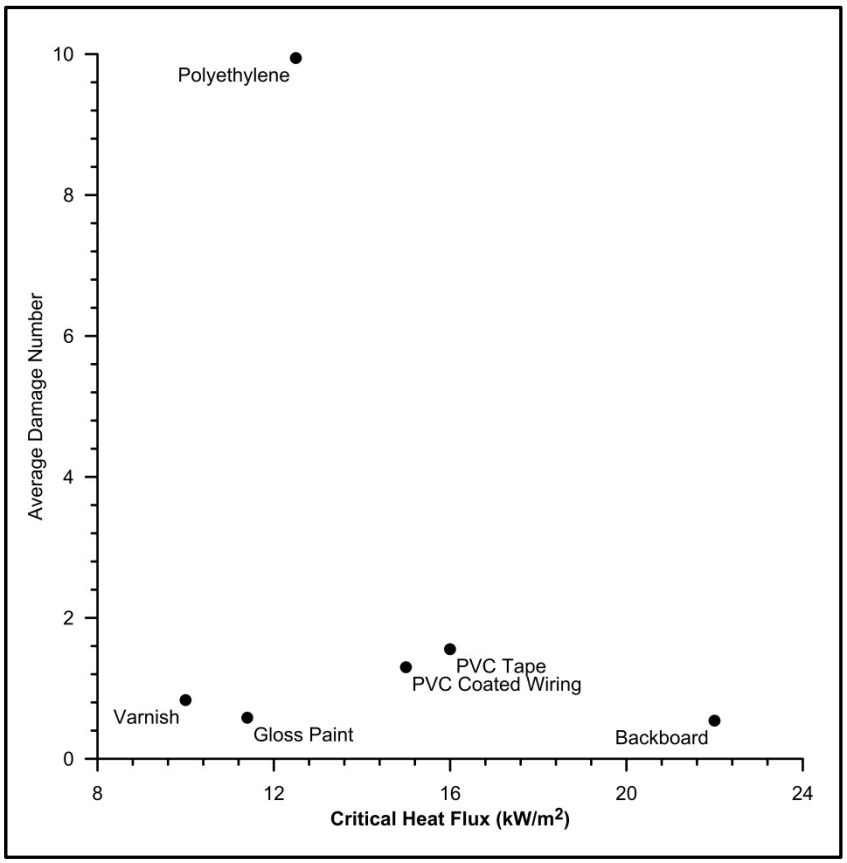

Figure 6-2 Comparison of damage number vs. critical heat flux (Rig C, critical heat flux data taken from Babrauskas table 19 [410])

The reason for this disagreement is due to the fact that thermal damage from explosions is often exhibited in the coating or covering of a wood surface. Work undertaken by Burrell and Hare [343] on behalf of the HSE and by Staggs et al. [354] identified that non-specialised coatings (i.e. paints, varnishings etc.) tend to burn off at low heat fluxes but do not produce volatiles of sufficient concentration to initiate flaming combustion. Consequently, once the coating is removed, the ignition properties of the substrate remain unchanged. As energy is required to 'drive off' volatiles from the coating, the critical heat flux of the coated wood sample increases [343, 354]. Therefore, if critical heat flux is to be used as a measure for the susceptibility of coatings to thermal damage, further experimental work is required to derive critical heat flux values for the materials themselves (i.e. without the substrate).

6.3.1. Wallcoverings (all Rigs)

The damage sustained by wallcoverings during the explosion tests was generally exhibited as scorching, a discolouration of the materials surface due to the transient flames radiative and contact heat transfer, with the severity of the discolouration depending on the flame temperature and the duration of its exposure/contact with the

surface. Little or no scorching was evident on the emulsion painted plasterboard test strips.

In the FRS and Spadeadam tests, several alternative types of ordinary and vinyl wallpapers were used in certain tests. Each exhibited its own scorching and damage characteristics, and consequently, the different types of wallpaper were not generally comparable. Insufficient samples of each of these types were used to enable consistent damage number scales to be established and so the data should be used carefully. An example of typical damage sustained by vinyl wallpaper during the FRS tests is shown in Figure 6-3.

In certain tests, some of the wallpapers (particularly vinyl types) also exhibited blistering on their surfaces (as can be seen in the right sided test strip in Figure 6-3). The presence of scorched blisters, was found to be prevalent where the quality of the papering was poor and air bubbles were trapped behind the paper. The extent of blistering, therefore, was not initially considered to be as reliable a damage indicator as the degree of scorching.

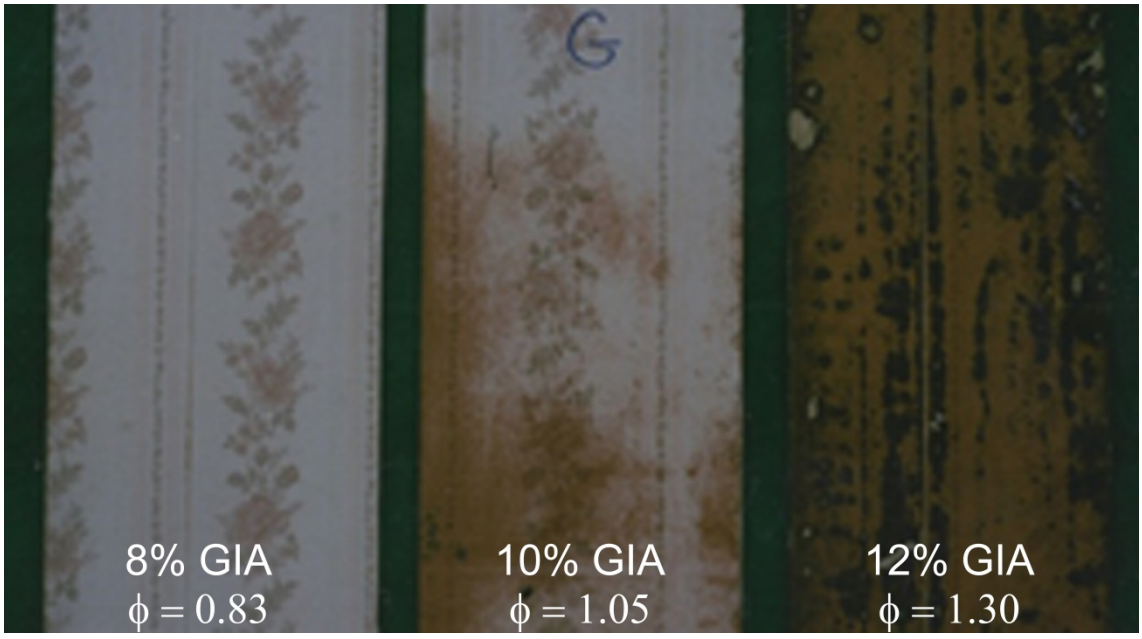

Figure 6-3 Typical thermal damage sustained by vinyl wallpaper (FRS)

Damage to Anaglypta type wallpaper tended to pick out the raised pattern on the paper (Figure 6-4 FRS, and Figure 6-5 University of Leeds), most probably because these areas were less able to lose heat through conduction to the backing, and so scorched much more readily than the surrounding depressions.

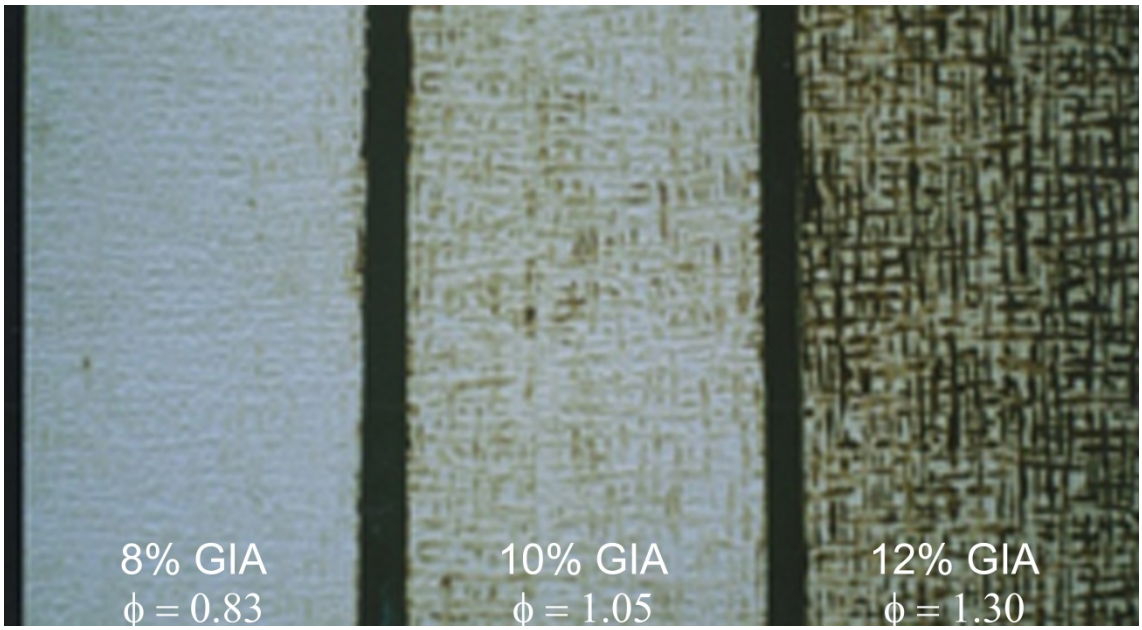

Figure 6-4 Thermal damage to raised areas of anaglypta type wallpaper (FRS)

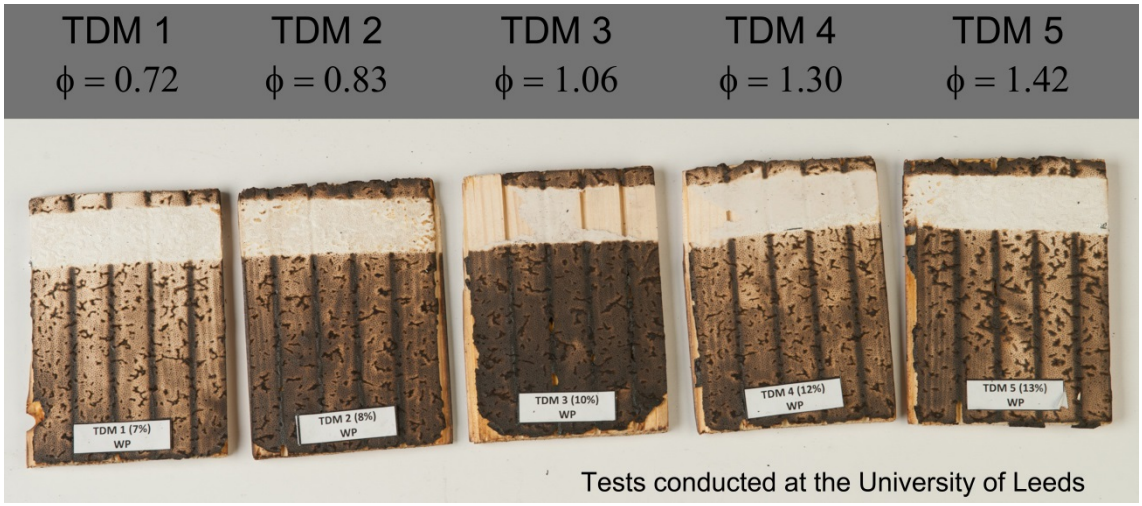

Figure 6-5 Thermal damage to wallpaper (confined explosion – Leeds)

6.3.2. Wood Surfaces (all Rigs)

The typical thermal damage that was sustained by gloss painted and varnished wood surfaces during the explosion tests is illustrated in Figure 6-6 (University of Leeds) and Figure 6-7 (FRS) respectively. The scorching showed the typical mottled blistering but also tended to pick out the grain in the wood in a manner similar to that displayed by Anaglypta type wallpaper. It was evident that painted or varnished woods were more susceptible to scorching than untreated softwood. Varnished and white-gloss painted softwood provided the greatest repeatability of any of the surfaces tested.

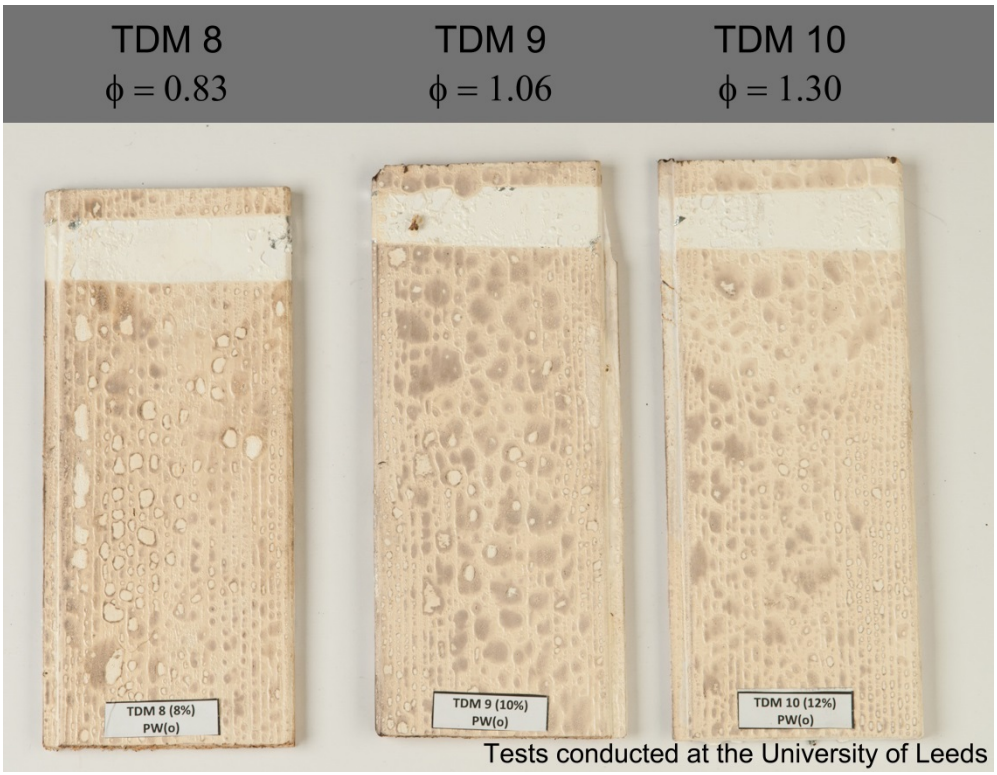

Figure 6-6 Typical thermal damage to white gloss painted wood (Leeds)

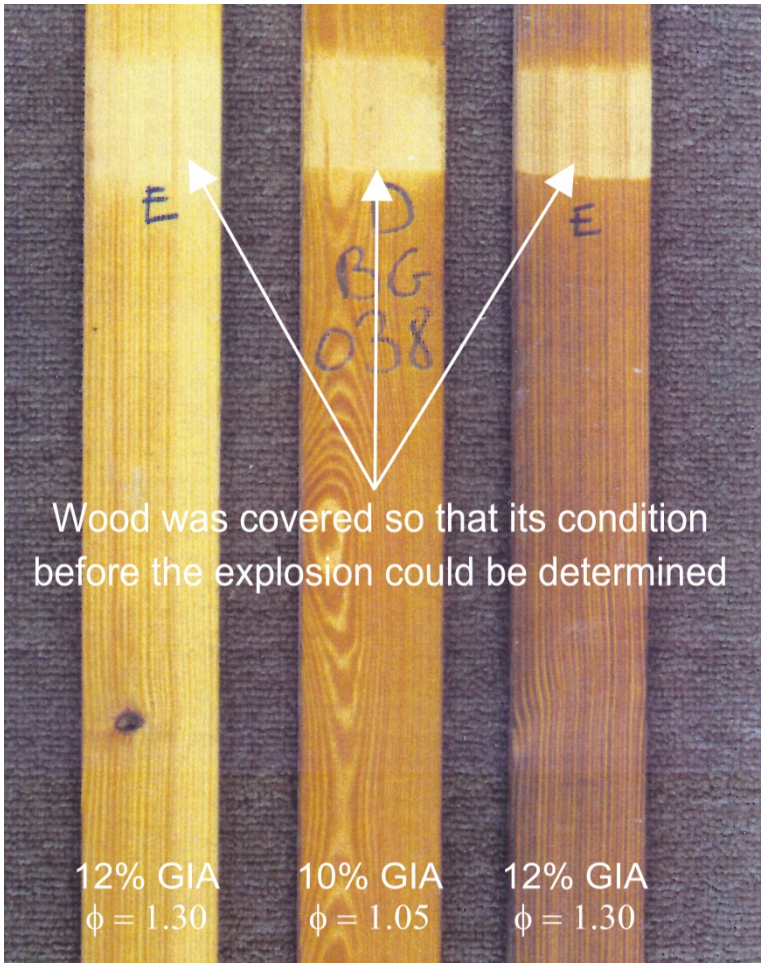

Figure 6-7 Typical thermal damage to varnished softwood (FRS)

Figure 6-8 (University of Leeds) shows some examples of wood painted with quick drying gloss. Unlike wooden surfaces painted with oil based gloss, those painted with quick drying gloss or emulsion (both water based) displayed very little damage to the naked eye. For comparison Figure 6-9 (Spadeadam) shows the thermal marker board in Rig C, with painted wood samples, before and after a stoichiometric explosion. The sample on the left is painted with water based (quick drying) gloss and the sample on the right is painted with oil based gloss. The results are startling, the sample painted with the water based gloss suffered very little thermal damage, yet the oil based sample had significant scorching.

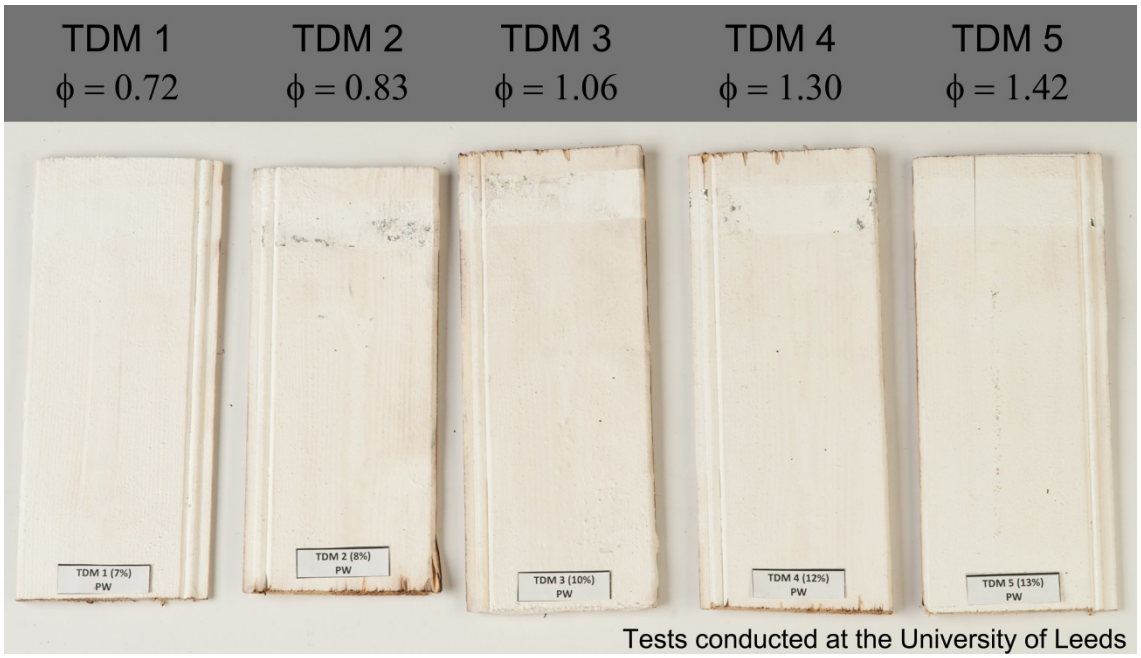

Figure 6-8 Wood samples painted with quick drying gloss (Leeds)

This finding is very interesting; if an accidental explosion occurred in a modern building, which has been decorated using quick drying paints, and the investigator is following guidance given in the standard reference texts (Sections 1.2 and 1.6), the evidence would be suggesting that a fuel lean mixture had caused the explosion. Although this evidence may be contrary to the pressure damage the building has sustained, it is plausible that the evidence would be misinterpreted, possibly resulting in an incorrect interpretation of the origin and cause of the explosion.

An observation that occurred consistently in all painted samples, was that evidence of thermal damage was more evident in sections of the wood where a knot was present (Figure 6-10, Spadeadam, Rig C). The thermal damage would present itself in the form of scorching or discoloration in the exact shape of the knot. Even if the knot was not visible through the painted surface, but a small area of scorching was present, examination of the rear side of the sample consistently demonstrated that the damage

corresponded to the area of wood where a knot was present. Knots are imperfections in the wood (where branches used to grow) that allow the sap (resin) within the wood to 'bleed' out. This resin is an oil based substance that is prone to scorching. This finding gives investigators a useful tip, because in all cases where a transient flame passed over a knot in a sample of wood, either scorching or discolouration was evident.

In order to see if there was a more robust method for detecting thermal damage in the form of discoloration, UV lighting was used to examine the samples. It was found that this was useful in looking at areas where little scorching was visible to the naked eye (see Section 6.10.1).

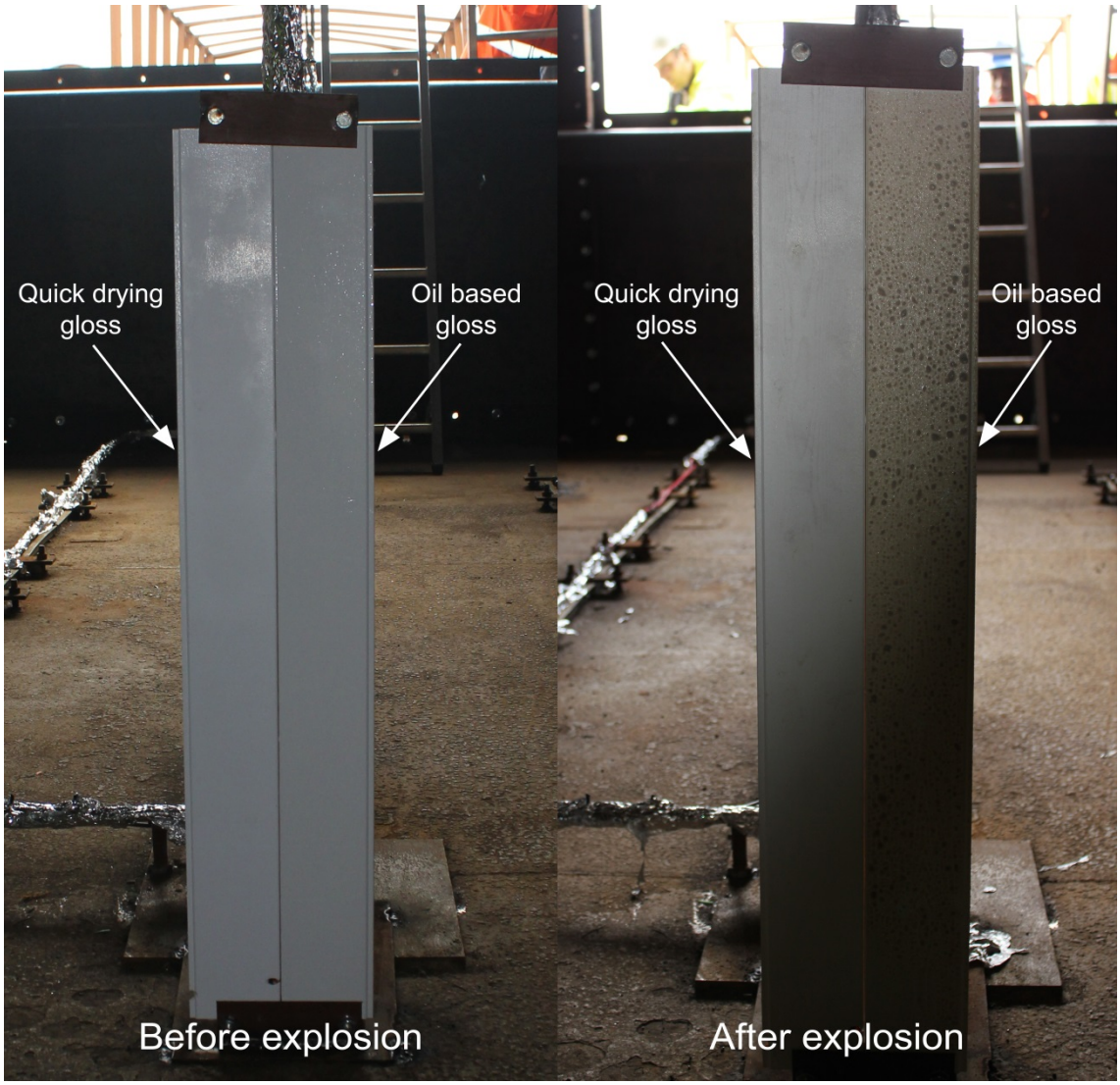

Figure 6-9 Thermal damage to painted wood samples (Spadeadam, Rig C)

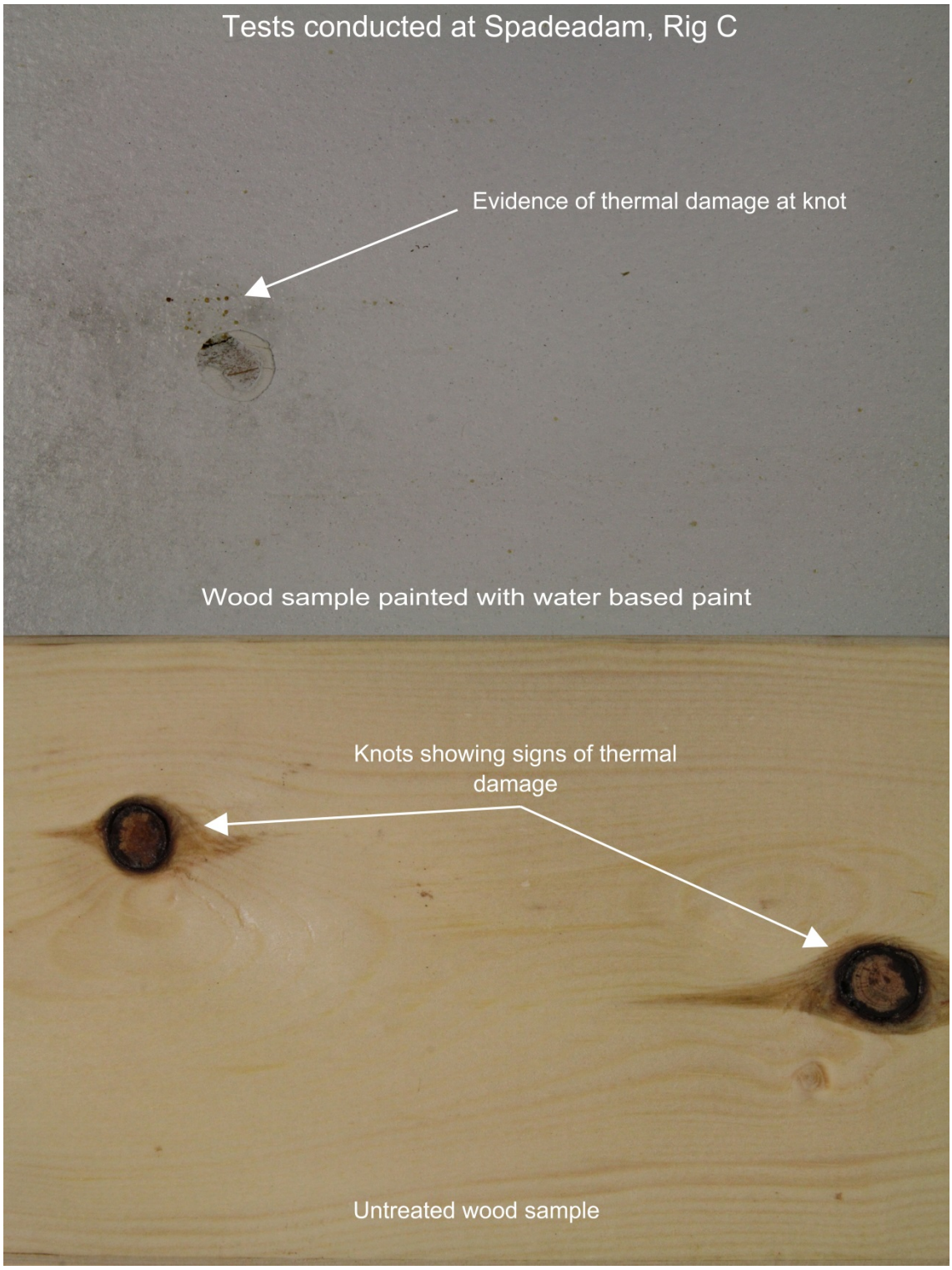

Figure 6-10 Thermal damage to knots in wood (Spadeadam, Rig C)

6.3.3. Newspaper (Spadeadam, Rig C)

Newspaper exhibited significant scorching in all of the tests and often was completely destroyed. This is not surprising given it is a very thermally thin cellulosic material. An example of a sample taken following a homogenous natural gas explosion (Spadeadam, Rig C) is given in Figure 6-11. Where the newspaper was not completely destroyed, it displayed a characteristic blackening around the edges. It was typically graded between 7 and 10 on the damage scale. Note that the damage appears most pronounced at approximately the height of the ignition source.

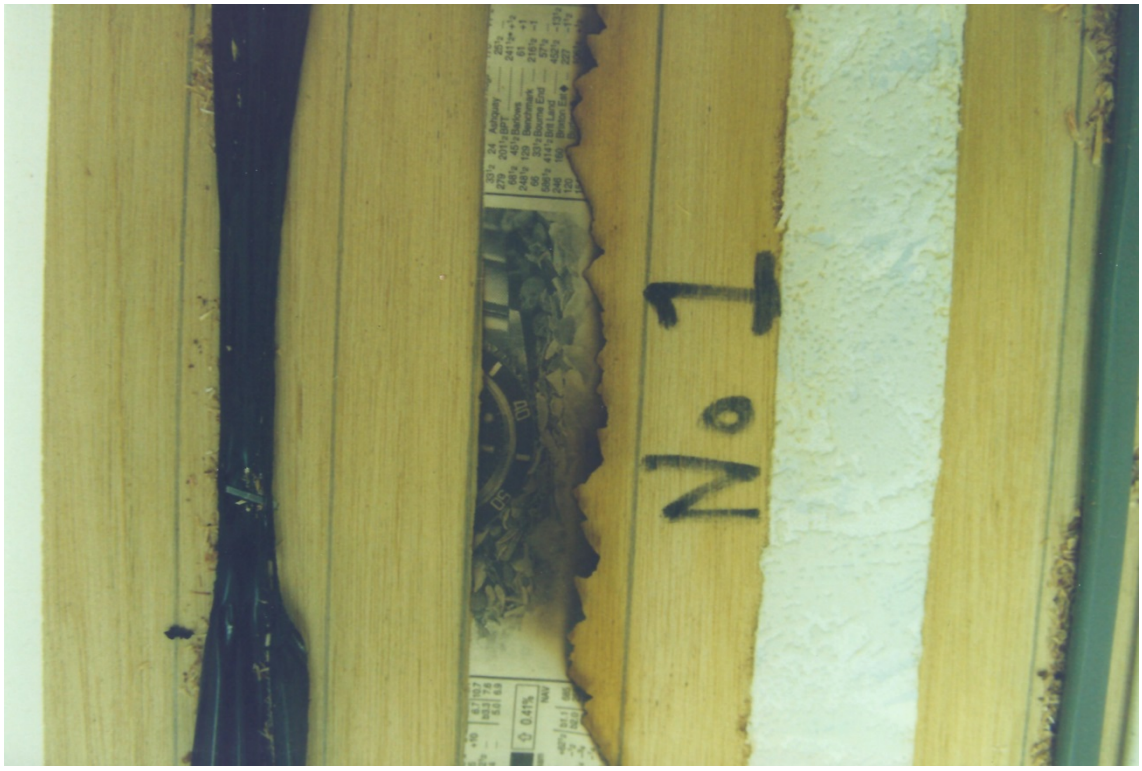

Figure 6-11 Thermal damage to newspaper (Spadeadam, Rig C)

6.3.4. Polythene sheet (Spadeadam, Rig C)

The polythene sheet samples represented a number of materials found in households (e.g. bin bags, carrier bags etc.). When subjected to the passage of a transient flame, the polythene sheet melted and shrank. This was consistently seen throughout the programme (see Figure 6-12, Spadeadam, Rig C). It was typically graded between 8 and 10 on the damage scale.

Figure 6-12 Thermal damage to polythene sheet (Spadeadam, Rig C)

6.3.5. Electrical Cable and Insulating Tape (Spadeadam, Rig C)

The PVC covered electrical cable and the PVC tape displayed similar characteristics. The PVC covering or tape often blistered and then burnt (see Figure 6-13, Spadeadam, Rig C). The tape often exhibited a mottled effect throughout its length.

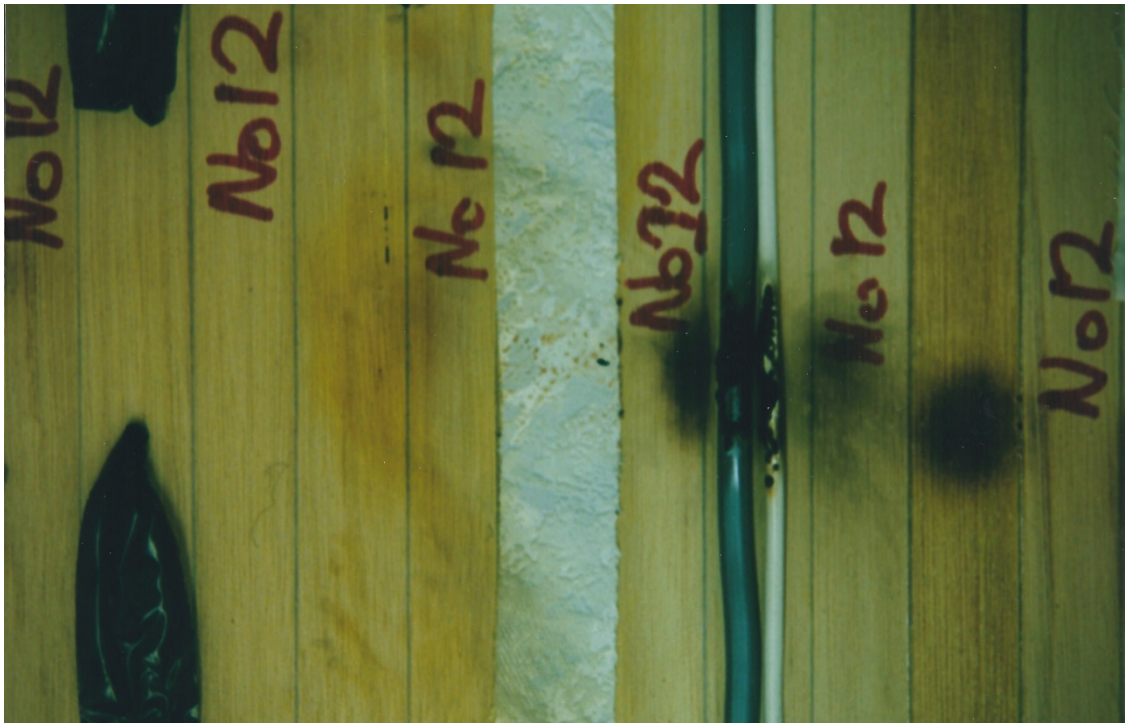

Figure 6-13 Thermal damage to electrical cable (Spadeadam, Rig C)

6.3.6. Cotton Wool (Spadeadam, Rig C)

Figure 6-14 shows an example of thermal damage to cotton wool, where fibre ends have melted and fused together to form blackened 'bulb-like' ends, in a manner similar to that observed by Wąs-Gubala and Krauß (see Section 2.7.3). The cotton wool samples consistently showed significant thermal damage with uneven amounts of blackening throughout its length; which in some instances, and in accordance with other evidence, was most pronounced at the height of the ignition source. In a number of tests, the cotton was nearly completely destroyed and was typically graded as 9 on the damage scale.

Figure 6-14 Thermal damage to cotton wool (Spadeadam, Rig C)

6.4. The Effect of Initial Mixture Composition (all Rigs)

Figure 6-15 shows the effect of equivalence ratio on the intensity of thermal damage. A series of plots of average thermal damage number against equivalence ratio are shown for a series of homogenous natural gas tests undertaken at Spadeadam in Rig C during experimental programme three. It can be seen, in general terms, the average damage number increases with increasing equivalence ratio and hence gas concentration. The result of the tests from the University of Leeds are shown in a different diagram (Figure 6-17). The damage numbers from the Leeds results are not directly comparable to the damage number results from the Spadeadam tests as some of the materials used were different (e.g. varnish used in the Spadeadam tests was

water based polyurethane whilst the Leeds tests used oil based polyurethane varnish) and the materials were mounted on different substrates (e.g. wood backboard). For this reason, the order of susceptibility of materials to thermal damage is different in the two experimental programmes.

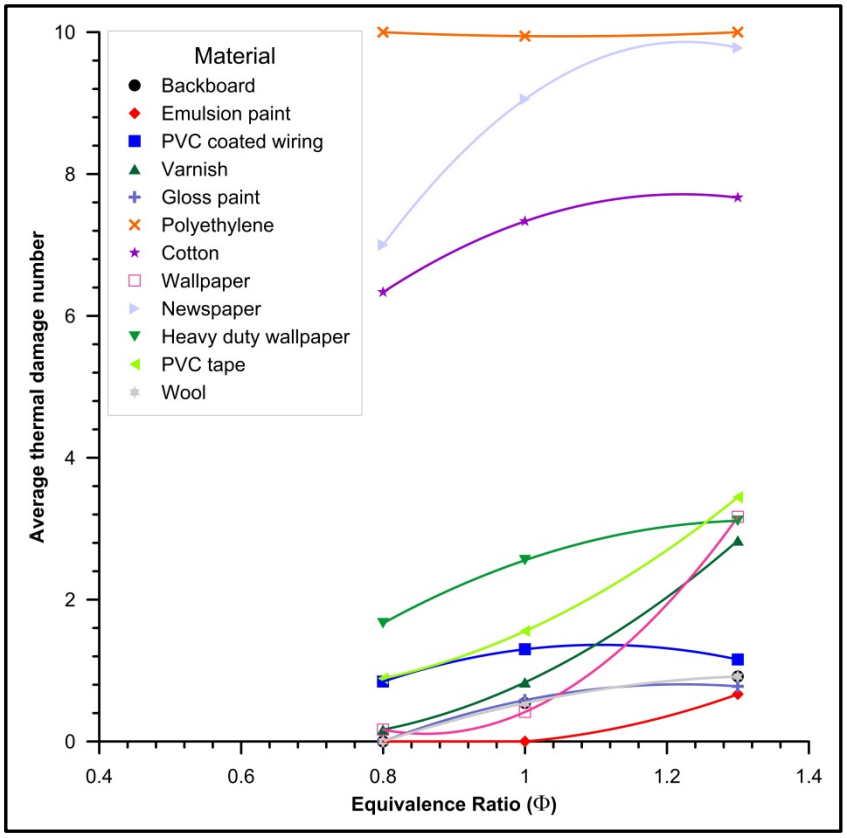

Figure 6-15 The effects of gas concentration on various materials (Spadeadam, Rig C)

Figure 6-16 provides an example of the degree of thermal damage corresponding to vented explosions of concentrations of 8, 10 and 12% natural gas in air (taken from Spadeadam tests, Rig C).

Examination of the test results demonstrated that there was a direct correlation between the degree of thermal damage and the concentration of the flammable gas/air mixture prior to ignition, with the severity of thermal damage increasing with gas concentration over this range (8% – 12%). This is also shown in Figure 6-3, Figure 6-4, and Figure 6-7, which are also representative examples of thermal damage sustained in vented explosions. However, a few additional vented explosion tests (not included in the summary data) were conducted Spadeadam at concentrations of 6% and 13% natural gas in air. No scorching was evident on most of the test samples at 6%, and the damage at 13% natural gas was slightly less than that observed at 12%.

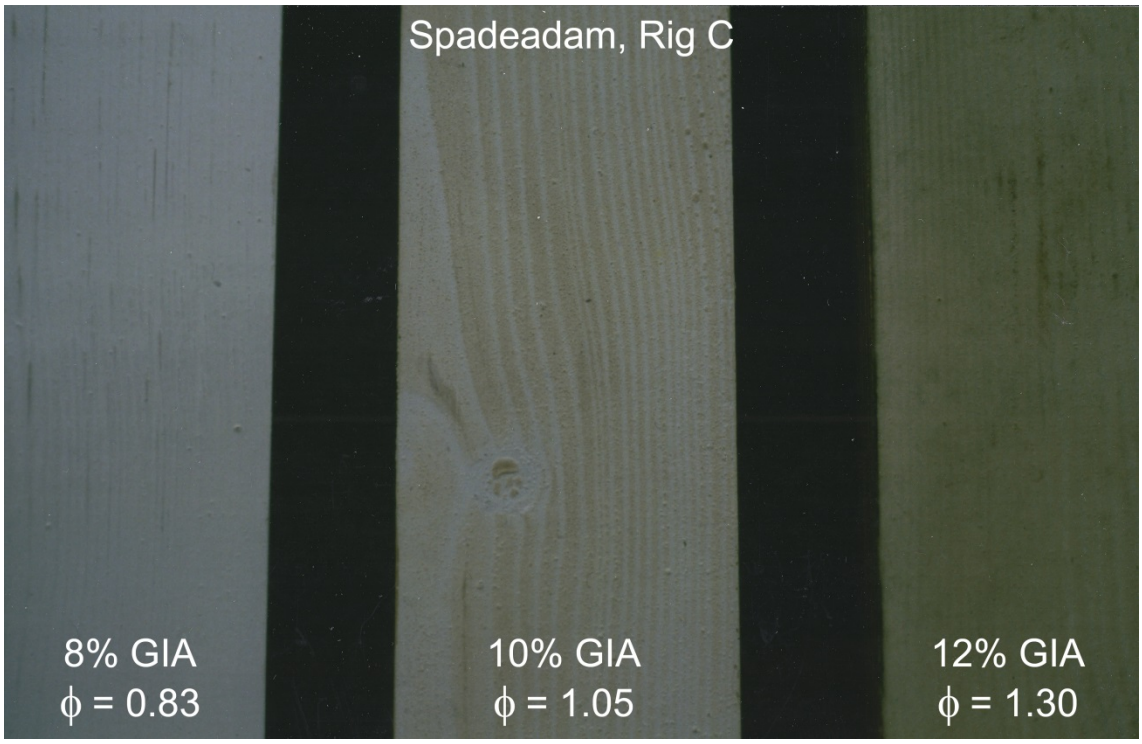

Figure 6-16 The effects of gas concentration on unfinished softwood (Spadeadam, Rig C)

The findings of the tests undertaken at the University of Leeds in the confined explosion rig were interesting. Consistently, and unlike the experiments undertaken in large-scale vented explosion chambers, the thermal damage was most intense at around stoichiometric concentration and became less intense as the concentration diverged towards the flammable limits (see Figure 6-17 and Figure 6-18). This suggests there is a direct correlation between flame temperature and the intensity of thermal damage. The question is then raised, why are the results different in a vented explosion. The answer to this question may be found in information gathered during the literature review.

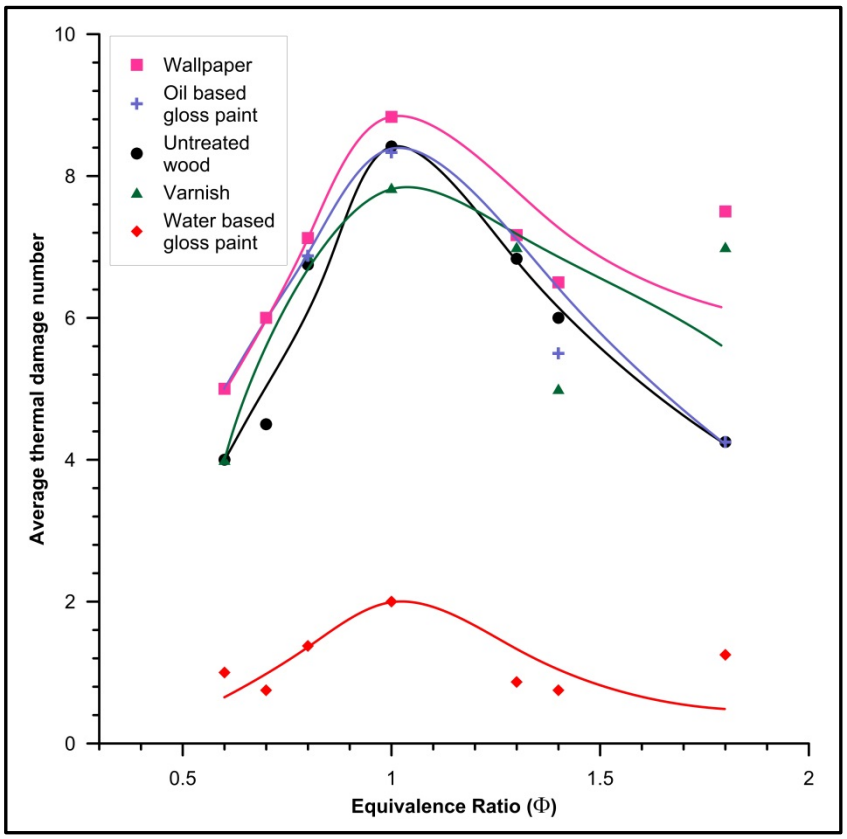

Figure 6-17 The effects of gas concentration on various materials (confined explosions – University of Leeds)

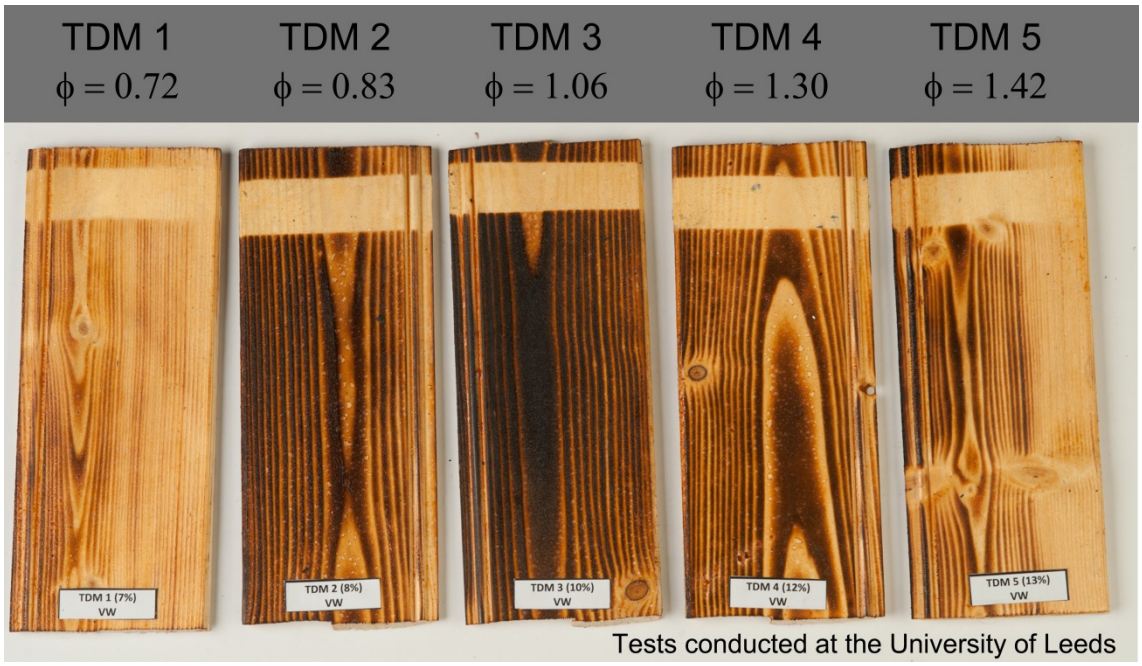

Figure 6-18 The effects of gas concentration on varnished wood (confined explosion – University of Leeds)

In Section 2.2.4, it was determined that stoichiometric hydrocarbon/air flames have an adiabatic flame temperature, at conditions of constant pressure, of approximately 2150 – 2250 K, but the flame temperature decreases as the gas/air concentration diverges towards its flammable limits. During confined explosions, the pressure increases, resulting in an increased flame temperature because the unburnt gas/air mixture is heated by compression.

In Section 2.2.5, it was shown that the burning velocity of a particular flammable gas is also strongly dependent upon the concentration of the gas/air mixture, with the maximum laminar burning velocity value for any fuel gas being typically found just on the 'rich' side of the stoichiometric concentration and reducing in value as the concentration diverges towards its flammable limits. It was also shown that the burning velocity value decreases as the pressure increases. However, although there is a decrease in the rate of combustion in volumetric terms, the mass burning rate is increased due to the increased density of the gas.

Additionally, in Section 2.2.5, it was established that the flame thickness increases as the gas concentration diverges towards the flammable limits and is at its maximum under fuel rich conditions. However, the flame thickness decreases with increasing pressure and temperature; the dependency on pressure being larger than that of temperature.

If it is accepted that the degree of thermal damage is a function of flame temperature and contact duration. Then, in a confined explosion, where the peak flame temperature occurs just rich of stoichiometric and increases, the mass combustion rate increases, and the flame thickness decreases; the flame contact duration will be less than that in a vented explosion and the flame temperature will be the dominant factor.

In vented explosions, whilst the maximum flame temperature still occurs at just rich of stoichiometric, at fuel rich concentrations, the flame thickness is greater and the burning velocity is lower. This means that the flame contact duration is greater than at stoichiometric conditions and consequently scorching can be more marked. These effects are what have been observed during the experiments.

The effect of radiation on thermal damage should also be contemplated and was considered as a reason for the discrepancy in results between vented and confined explosions (fuel rich mixtures being more radiative). Whilst radiation clearly plays some part in producing thermal damage, the duration of an explosion is so short that its effects are limited and consequently flame contact is dominant. This is corroborated by the lack of thermal damage during layered explosions to areas of material outside the nominal layer depth (see Section 6.5). If radiation was playing a significant role in

producing thermal damage, some visible damage would be apparent on all surfaces visible to the flame front. The minor effect of radiation in terms of thermal damage during vented explosions is not surprising as the time period of maximum flame intensity is in the order of a few hundred milliseconds and consequently radiation would be expected to play a less important role (Section 2.7.3).

As a consequence of these findings, it is presented by the author, that an explosion investigator, by observing the severity of the thermal damage, may be able to estimate the natural gas concentration prior to ignition, to the nearest 2%, over the concentration range 6% to 12%. However, at a natural gas concentration of 13% the severity of thermal damage is difficult to distinguish from that at 12%. Thermal damage to wooden surfaces resulting from fuel lean explosions may be difficult to observe at the scene of an explosion. In such circumstances, the observation of superficial melting or fusing of plastic materials and fibres provides evidence of exposure to a transient flame front.

6.5. The Effect of layer Depth (FRS, Rig A and Spadeadam, Rig C)

During experimental programme 3 (Spadeadam, Rig C), a number of layered explosion tests were undertaken. Photographs of layered natural gas tests during this programme clearly showed buoyant flames propagating through the high level flammable layer. Figure 6-19 provides an example of a flame propagating through a natural gas layer of depth 1.8 m (measured from the ceiling). As a consequence of natural gas layered explosions, thermal damage was observed on the material samples above the nominal layer boundary, indicating exposure to a transient flame front.

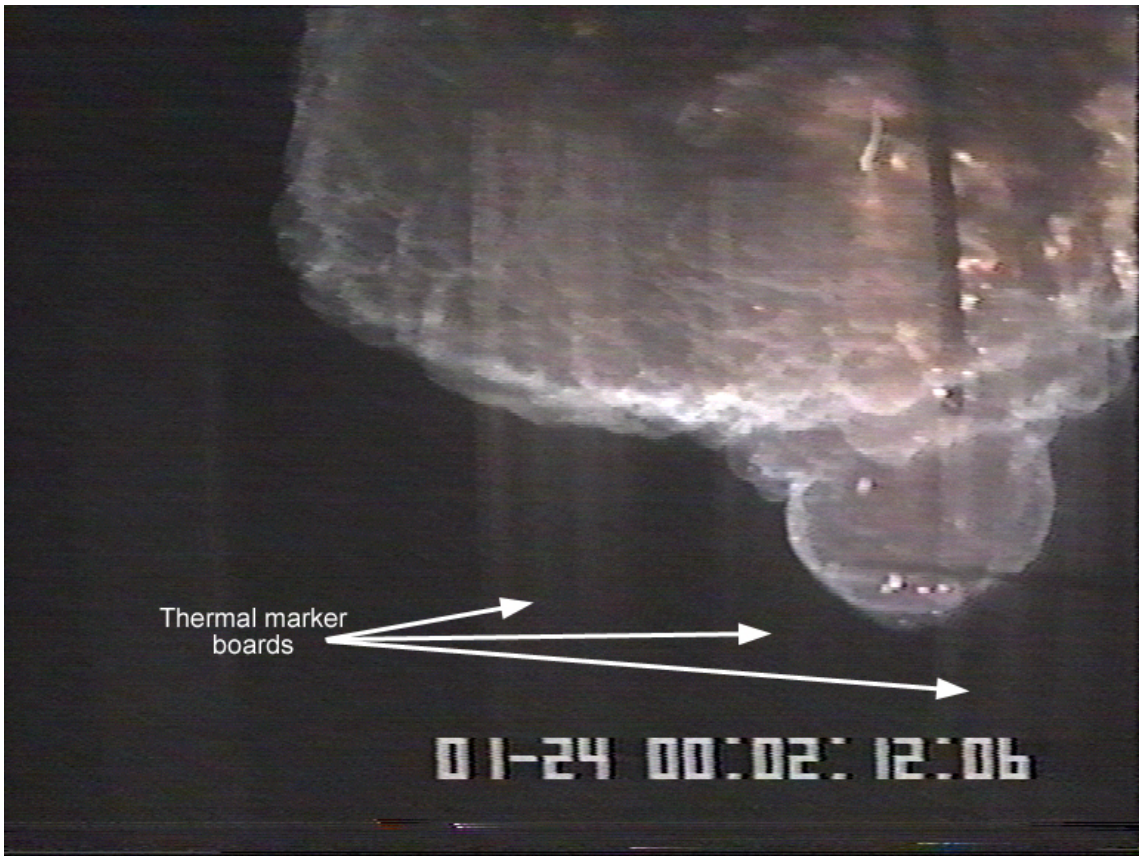

Figure 6-19 Flame propagation during a layered natural gas explosion (Rig C)

During experimental programme 1 (FRS, Rig A), the average height, above floor level, of the lowest scorch marks was measured in each test and compared with the initial depth of the buoyant gas/air mixture layer prior to ignition.

Figure 6-20 (taken from tests conducted at FRS, Rig A) shows the average values for all materials, for each explosion test, plotted against the nominal layer depth from the ceiling. Where a flammable natural gas layer was present initially, thermal damage was observed above the nominal layer boundary, with the material strips showing a well-defined transition region, typically 30 cm in height, between the scorched and unscorched area of the strip. The discolouration generally extended down to the height at which the concentration had been 8% ± 1% and followed an approximate trend of extending 15 cm for each percentage gas concentration above eight. Thus there was little scorching below the nominal layer depth for 8% layered explosions but for 10% layers, scorching could be found 30 cm below the nominal layer boundary and for 12% layers, scorching could be found up to 60 cm below the nominal layer boundary.

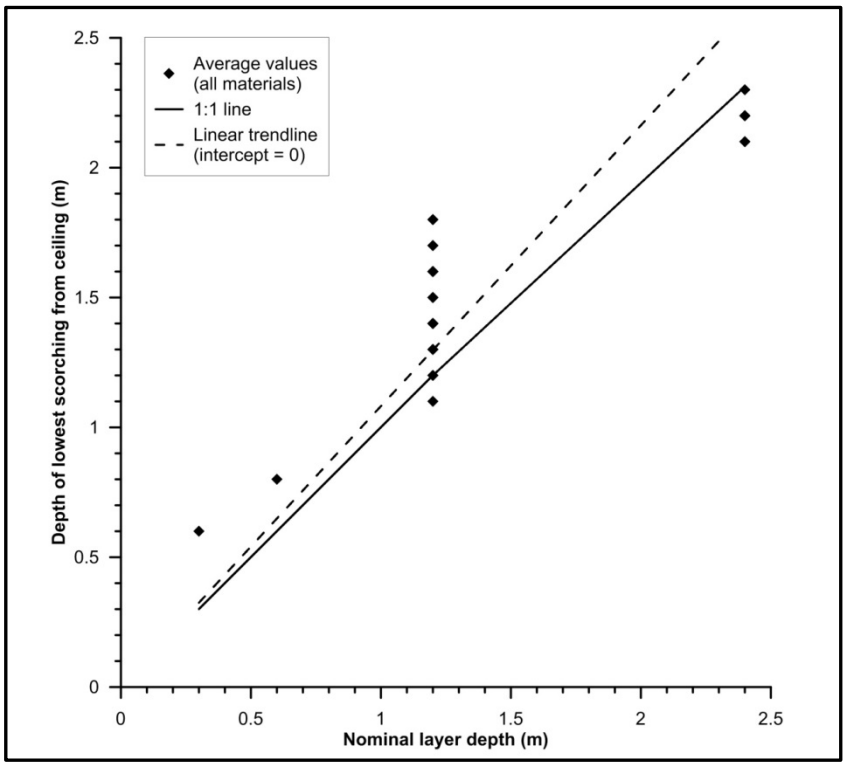

Figure 6-20 Presence of scorching with the depth of flammable layer (FRS)

In contrast to the location of thermal damage in a natural gas explosion, explosions involving layers of heavier than air gases, such as LPG, exhibit thermal damage at low level, from the point of leakage down to floor level. In these situations, more burning should be evident at low level, such as scorching to carpets, furniture etc., than at ceiling level.

Figure 6-21 is a photograph of thermal damage to the upper section of an internal door. It was taken during the investigation of a gas explosion in an occupied building and provides an indication of exposure to a transient flame front propagating through a lighter than air flammable layer. In this particular incident, the fuel involved was natural gas.

Figure 6-21 Evidence of scorching on the upper section of an internal door (taken from DNV GL archive)

6.6. The Effect of Fuel Type (University of Leeds, Rig D)

As the thermal damage is a function of flame temperature and contact duration, hydrocarbon fuels other than natural gas/methane should present similar results. Whilst the flame temperature, burning velocities and flame thicknesses are different for different fuels, as discussed in Chapter 2, they have similar flame temperature, burning velocity and flame thickness characteristics. Consequently, it was expected that the degree of thermal damage for both propane and ethylene would follow the same trend, but most probably with slightly more damage. To demonstrate this, a number of tests were undertaken with propane and ethylene at the University of Leeds. Figure 6-22 shows some of the results of the experiments. The results for propane and ethylene are in broad agreement with those of methane, and the reasoning given above.

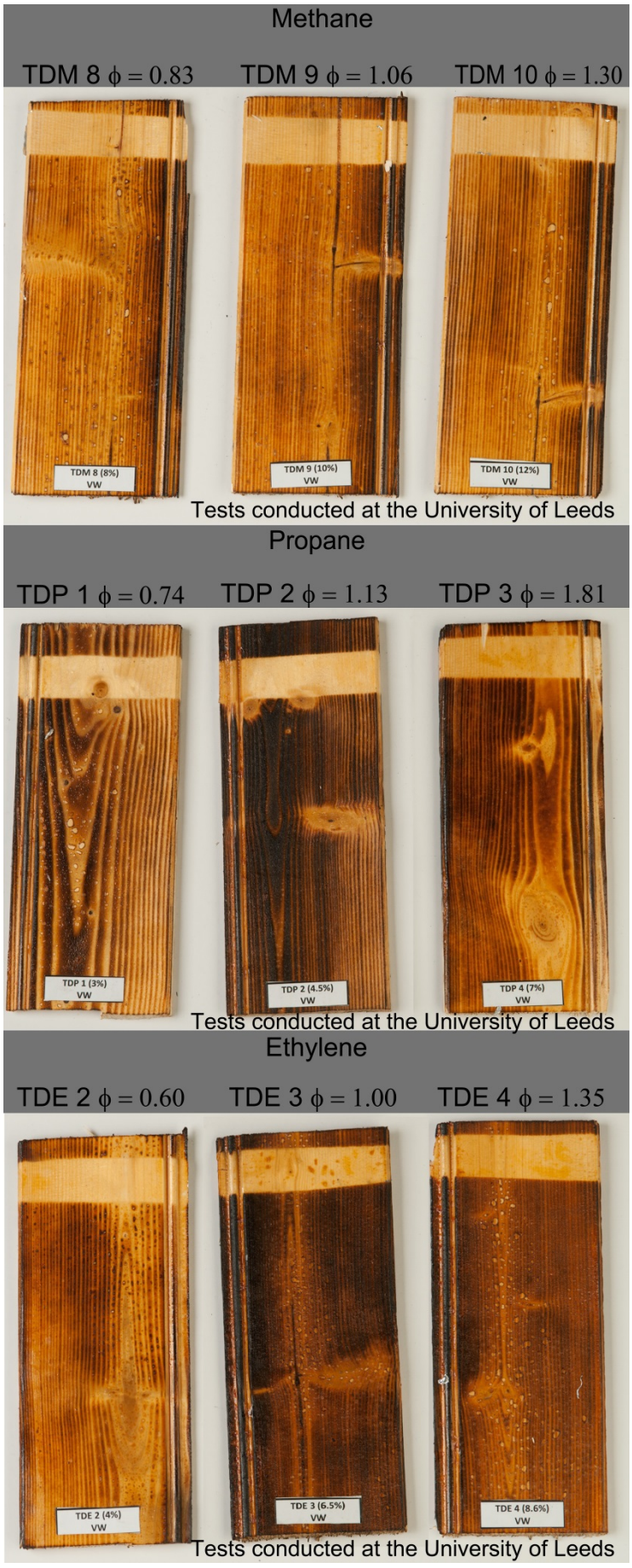

Figure 6-22 The effects of fuel type on varnished wood (Leeds)

6.7. The Effect of Ignition Position (FRS, Rig A)

The effect of ignition position was considered for tests undertaken at FRS during experimental programme 1. The thermal damage sustained during central ignition tests was found to be more spatially uniform than in rear ignition tests. All marker boards in the left room were located approximately equidistant from the central point of ignition, and exhibited a similar severity of thermal damage, meaning that it was possible to quite accurately determine the initial flammable mixture concentration (as thermal damage was consistent). However, with rear ignition, marker boards at positions A, B, and C, at the front of the left room, tended to suffer relatively light damage, whilst others exhibited more significant thermal damage. Examination of the video records showed that once venting was established, rapid flow through the vent impeded the flame front from reaching the two front corners of the room. A consequence of this was that it was more difficult to accurately estimate the initial mixture concentration, or in other terms, the lack of thermal damage could lead investigators to underestimate the gas concentration prior to ignition. This finding also provides further evidence that it is flame contact that causes the majority of thermal damage.

6.8. The Effect of Flame Speed (Spadeadam, Rig C)

As the degree of thermal damage is dependent upon contact duration, it follows that if the temperature remains constant but the flame speed increases, less thermal damage should be evident. A small number of tests were undertaken to investigate this during experimental programme 4. Figure 6-23 shows the results of two tests. The first test result (shown on the left) was a test undertaken with a gas concentration of 10% with furniture giving a 5% volume blockage (test number 8). For comparison, the results of test number 1 are shown alongside (10% concentration, no furniture). For consistency both photographs have been taken with a Canon EOS 7D DSLR under laboratory conditions with optimum lighting. It is clear, that the test without furniture has considerably more thermal damage . This result was consistent with the limited number of other comparable tests undertaken with and without furniture. The results suggest that faster flames result in a reduced contact duration and consequently materials exposed to the transient flame suffer less thermal damage. This finding is significant and could be a further reason for the conflicting evidence gathered during explosion investigations. Further work in this area is recommended.

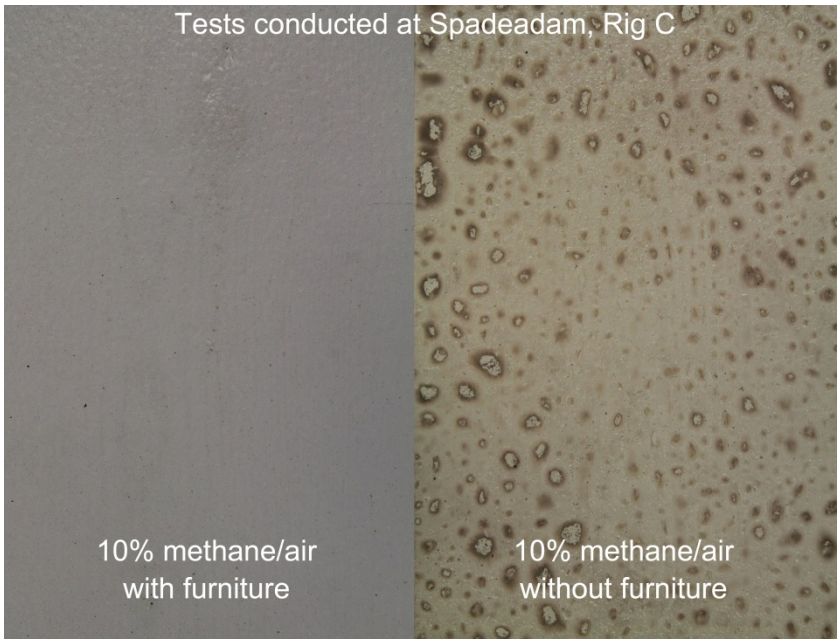

Figure 6-23 The effect of flame speed on thermal damage

6.9. The Effect of Door Position (FRS, Rig A)

In the explosion tests (experimental programme 1) where the interconnecting door was initially closed, it acted as a very low failure pressure explosion relief, venting from the ignition room to the secondary room. This process led to the generation of turbulence or the jetting of the flame front, both of which resulted in larger flame areas. In some cases, more extensive scorching damage was noticeable, particularly on wood surfaces. This additional damage was caused by the flame extending below the original boundary layer resulting in more extensive scorching damage as the flame was able to come into contact with parts of the marker board which were below the original layer boundary. Further large-scale experimental work is recommended in this area.

6.10. The Interpretation of Thermal Damage

The interpretation of thermal damage discussed so far in this chapter has largely been through subjective evaluation. This is consistent with the reality of how the majority of gas explosions are currently investigated. The determination of origin and cause, in terms of thermal damage, is typically based on photographic evidence taken on site and the knowledge and experience of the investigator (see Figure 6-24). Consequently, a number of additional methodologies were used to determine if there was a more scientific method for classifying thermal damage.

Figure 6-24 Evidence of thermal damage to crisp packets

For clarity, this aspect of the study was not intended to be exhaustive. Its purpose was to determine if other readily available and cost effective methodologies for evaluating the intensity of thermal damage were effective and practicable. The results of experimental programme number four (Spadeadam, Rig C), were therefore subjected to three additional methodologies:

i. UV lighting.
ii. Stereo microscopy.
iii. Digital imaging microscopy software.

6.10.1. UV lighting (Spadeadam Rig C)

All of the test samples from experimental programme four were transferred to the DNV GL laboratory at Loughborough for further analysis. Samples were placed under a UV bench light and photographed. This technique was not particularly successful in distinguishing the degree of thermal damage between samples subjected to explosions of different concentration or flame speed. An example of a sample (test 10) subjected to UV light is given in Figure 6-25. Whilst thermal damage is clearly visible on the surface of the painted wood sample, there are areas of thermal damage that are more evident under UV light. The use of UV light may therefore be of some value during the on-site investigation or in a laboratory, where UV light may aid the investigator in identifying samples that have suffered thermal damage which otherwise may not have been visible to the naked eye (i.e. thermal damage from fuel lean explosions).

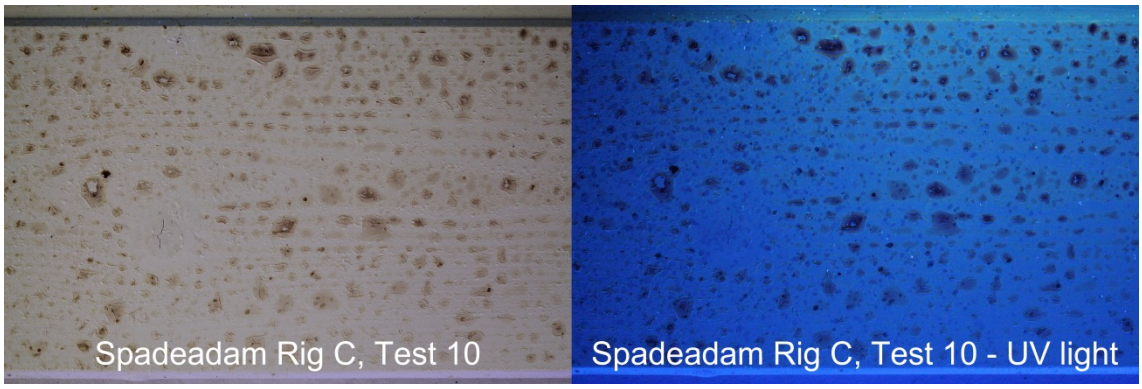

Figure 6-25 Painted wood sample subjected to examination by UV light

6.10.2. Stereo Microscopy (Spadeadam Rig C)

It was initially believed that the best determination of the degree of thermal damage would be gained through the use of a stereo microscope. However, this was dismissed as it became apparent that in order to make a credible determination of the gas concentration before ignition and the depth of any flammable layer, from the thermal damage a surface had suffered, an assessment of a relatively large area of the sample was required. The majority of the samples examined had at least one small area of more significant damage and thus erroneous evaluations were possible. An example of the image of thermal damage through a stereo microscope is given in Figure 6-26.

Figure 6-26 Stero microscope image of a sample of painted wood (Spadeadam Rig C, test 2)

6.10.3. Digital Imaging Measurement (Spadeadam Rig C)

Following the findings outlined in Section 6.10.2, it was decided to seek a methodology using digital imaging. It was believed that digital photographic imaging and analysis may present an accurate and efficient method of analysing thermal damage.

The samples were sorted into batches according to their coating (e.g. oil based paint etc.), their location in the explosion chamber, orientation and gas concentration. Each

sample was then photographed (in three sections of identical length) using a Canon EOS 7D camera under studio conditions to ensure the colour, white balance etc. was consistent. The digital images were then analysed using Axiovision image measurement and analysis software. The software package allows manual, semi-automated and fully automated analysis. The experiment samples were analysed for total area damaged and percentage area damaged using the fully automatic function. An example of the damage captured by Axiovision software is given in Figure 6-27.

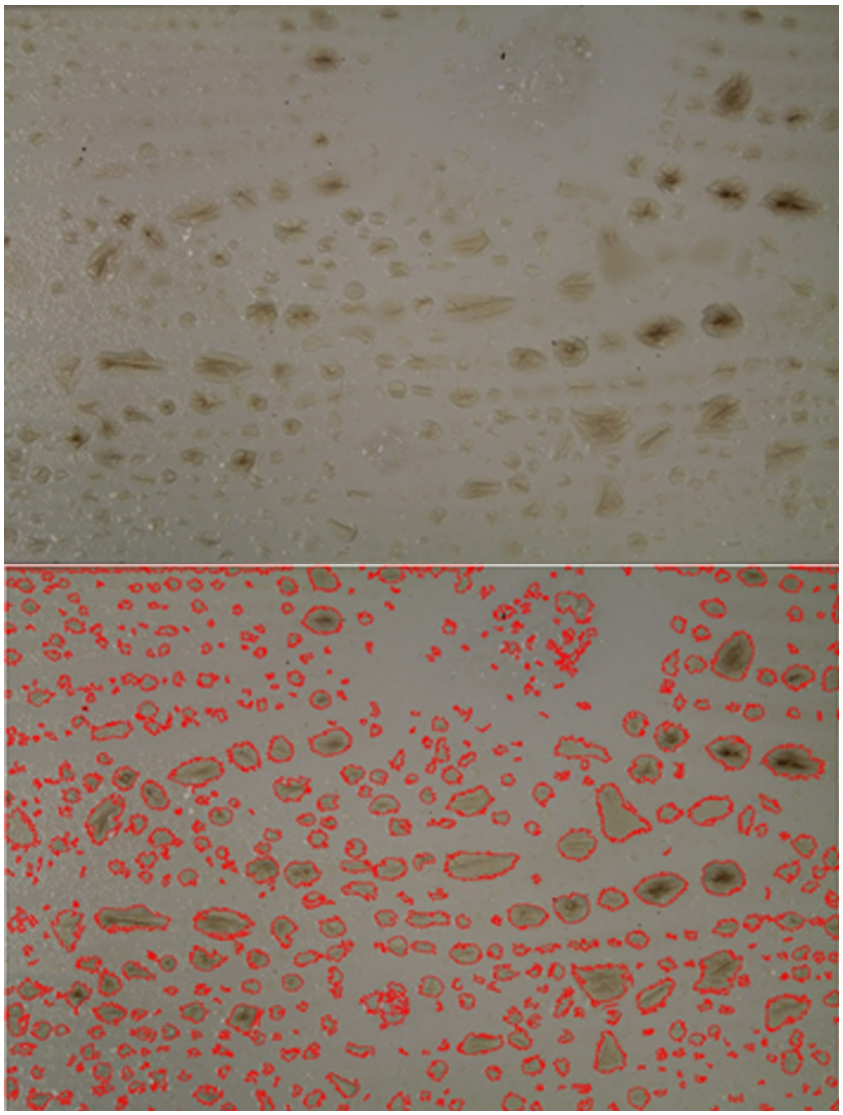

Figure 6-27 Fully automated damage capture from Axiovision (Spadeadam Rig C, test 5)

It can be seen from Figure 6-27 that this type of imaging software has the potential to offer objective determinations of the degree of thermal damage a material has suffered. However, the number of experiments that were carried out with this methodology was limited. Consequently, further work is recommended.

With this analysis, the results were measured in terms of percentage surface area that was damaged, per unit length of sample. The average area subjected to thermal damage for 10% tests was 28.9% for tests with furniture and 45.8% for tests without furniture, demonstrating the effect of flame speed. Interestingly, a comparison of marker boards directly in the path of the propagating flame front (40.1% thermal damage) and those side-on to the flame (52.0% thermal damage) showed that objects side-on to the flame may be subjected to the flame front for a longer duration.

6.10.4. Scanning Electron Microscopy

The results of the small-scale experiments undertaken at the University of Leeds were also analysed using a Scanning Electron Microscope (SEM). With an identical argument to that given in Section 6.10.2, the methodology was dismissed due to the constraints surrounding the sample size. However, for completeness some of the results are presented in this section.

SEM analysis was undertaken for various samples with magnification ranging from x 50 to x 1000. An example is shown in Figure 6-28 for a 10% methane/air explosion, where analysis of a vanished wood sample before and after the explosion is shown. The magnification levels in this example are x 50. It can be seen that the work is really useful, not surprisingly, for understanding the effects of the explosion on the material at the microscopic level.

Analysis of the various images of painted and varnished samples showed small blisters where pyrolysed volatiles had become trapped or broken through the surface of the coating.

The wallpaper samples prior to the explosion revealed imperfections (bubbles) under the surface caused by the quality of the wallpaper pasting. After the explosion, there was evidence of cellulosic fibre damage and bubbles and blisters caused through pyrolysis.

It was difficult to distinguish the thermal damage on the bare wood samples with the SEM.

Overall, the results of the SEM analysis were not particularly useful in terms of identifying the degree of damage and relating that to the depth of flammable layer or gas concentration.

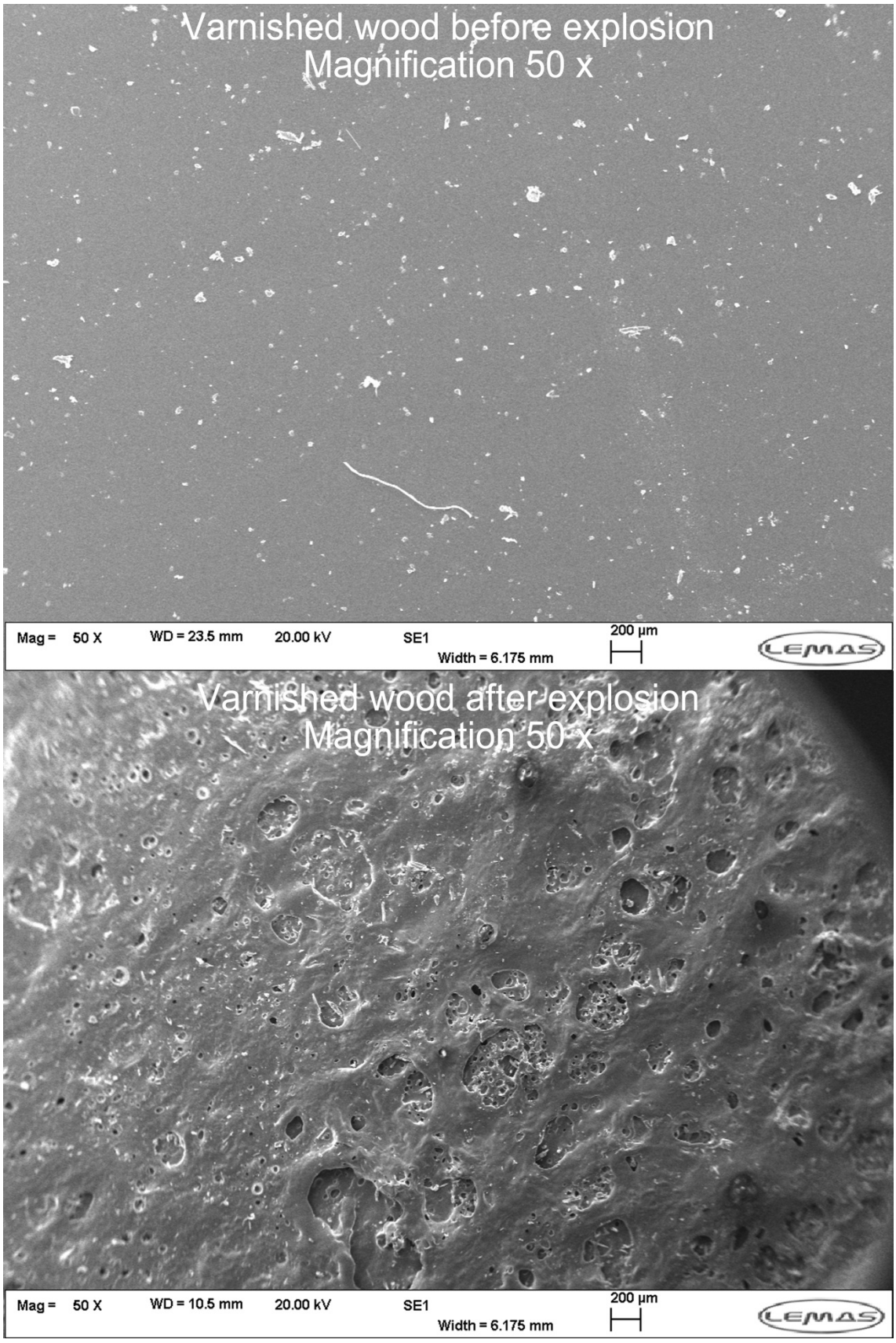

Figure 6-28 SEM analysis for varnished wood

6.11. Summary of Findings

The experiments demonstrated that materials commonly found in residential buildings exhibit characteristic thermal damage patterns that enables the path of a transient flame front, and consequently, the distribution of flammable gas within a building, to be determined. Most commonly, the samples displayed blistering or mottled scorching patterns.

Thermal damage in all cases was most intense at approximately the same height as the ignition source. This may aid investigators in determining the source of ignition.

Varnished or painted wooden surfaces (with oil based paint) produced the greatest repeatability during the tests and consequently appear to be the most reliable material for assessing thermal damage in explosion investigations. Wooden surfaces painted with quick drying paints (water based) displayed very little thermal damage to the naked eye. Knots in wood always displayed thermal damage if exposed to a transient flame front.

Polythene sheeting shrank and melted, displaying a characteristic thermal damage pattern. PVC covered materials tended to blister and burn, often displaying a mottled effect.

There was a direct correlation, in vented explosions, between gas concentration and the degree of thermal damage (in the natural gas range of 8 to 12%), with the most significant damage occurring under fuel rich conditions. This pattern was not seen in confined explosion tests where the degree of thermal damage followed the flame temperature curve. These thermal damage characteristics were also observed during propane and ethylene tests.

Where a flammable natural gas layer was present initially, thermal damage was observed above the nominal layer boundary, with the material strips showing a well-defined transition region, typically 30 cm in height, between the scorched and unscorched area of the strip. This information means that investigators would be able to estimate the depth of flammable gas layer to within typically 30 cm.

Tests undertaken with furniture produced less thermal damage than comparable tests without furniture. This suggests that there is an indirect correlation between flame speed and thermal damage.

It was possible to gain objective thermal damage assessments using digital imaging software.

6.12. Conclusions

The results presented in this chapter represent a substantial amount of new data; which can be readily interpreted during the investigation of gas explosions in buildings. A number of findings were presented, providing new knowledge and understanding of the thermal damage exhibited by various materials when subjected to a propagating flame front. This knowledge provides insight into why some explosions exhibit significant thermal damage and others, of very similar nature, display very little.

During a gas explosion investigation, there are often a number of potential sources of gas that could have caused the explosion. Some of these sources may have been present before the explosion (i.e. potential causes) and others may be present as a consequence of the explosion. The need to determine the concentration of the gas/air mixture is of critical importance to an explosion investigator as this information is used to eliminate or identify the source of the gas release [i.e. can potential release sources lead to a build-up of gas of the required concentration within the enclosure(s)]. The experiments conducted in these programmes have demonstrated that it is possible to use the severity and extent of thermal damage to wooden surfaces (e.g. window-frames, windowsills, doorframes etc.), wall coverings and furniture, sustained during a gas explosion, to provide useful information on the gas concentration, its distribution throughout the building prior to ignition and the depth of any flammable layer.

The presence of blistering was observed on all types of surfaces, with the severity of blistering increasing with natural gas concentration (up to 12%). However, blistering also depends on factors other than flame temperature and contact duration (e.g. the material age and quality of wallpaper hanging etc.). Consequently, the overall discolouration of a surface perhaps represents a more reliable thermal damage indicator. Other fuel types displayed similar characteristics.

Whilst wallpaper surfaces exhibited a distinct scorching pattern, the wide variety available, and their wide variation in thermal properties, makes them much less useful as forensic indicators, and probably only useful in indicating the distribution of gas and the passage of a transient flame front. The most suitable materials, in terms of forensic indicators, appear to be softwood covered with either gloss varnish or white oil based gloss paint. Such surfaces are common in buildings as door frames, window frames, etc.

Under controlled experimental conditions it was possible to assess the severity of the thermal damage to various materials and estimate the natural gas concentration (over the range 8% to 12%) prior to the explosion to the nearest 2%. However, when

investigating an actual gas explosion incident, this degree of accuracy is unlikely because of the large number of other factors involved. Though it should be possible in most cases to distinguish between lean, (5% to 8%), close to stoichiometric conditions (9% to 11%) and rich (12% to 15%) natural gas/air mixtures.

It is currently common practice for buildings to be decorated using water based quick drying paints. These paints are less susceptible to thermal damage and may cause the misinterpretation of evidence, which could lead to an incorrect diagnosis of the origin and cause of an explosion. The work presented in this chapter will assist explosion investigators in understanding the behaviour of various materials when subjected to a propagating flame front, and provide guidance on the analysis of the events that led up to the explosion. A UV light may be a simple aid on-site that would enable thermal damage to wood surfaces painted with water based paint to be more readily identified, even if it may not be possible to determine the gas concentration from that particular piece of evidence.

Where a flammable gas/air layer was present, thermal damage was observed above the nominal layer boundary (for natural gas), down to the lowest level where the concentration was originally above 8% ± 1%. It was possible to estimate the layer depth from the damage to an accuracy of approximately 30 cm. In practical situations this accuracy would probably be decreased because of the effects of obstacles such as furniture causing large scale turbulence during the explosion, breaking up the layer.

Whilst mixtures containing a lighter than air fuel gas are known to form ceiling layers of the type witnessed with the natural gas experiments, those containing heavier than air fuel gases will form low level layers. These two cases should be distinguishable from the vertical distribution of thermal damage, so that observation of such damage should assist in the identification of the fuel gas involved in an explosion.

Some of the explosion experiments in the twin enclosure, caused significant thermal damage in the adjoining chamber. Analysis of video records confirmed that this was caused by the distorted (sometimes jetting) flame front during the venting and external explosion stages.

The results of the experimental programmes presented in this chapter, provide evidence that the guidance used by explosion investigators worldwide is incomplete at best and incorrect in certain areas. The knowledge that little evidence of thermal scorching is not necessarily indicative of a fuel lean mixture, is a key finding that will change the manner in which explosions are investigated, and is of considerable importance to gas explosion investigators involved in the interpretation of forensic evidence at the scene of a gas explosion in a building.

CHAPTER 7
CONCLUSIONS

CHAPTER 7

CONCLUSIONS

7.1. Conclusions

This research is related to the investigation of accidental gas explosions in dwellings. In particular it considers how forensic evidence, in terms of pressure and thermal damage, found at the scene of an explosion may be used to determine the likely composition and distribution of the fuel/air mixture, prior to its ignition.

An understanding of the magnitude of pressure generated during the explosion, and an assessment of the thermal damage sustained by the building and its décor, will assist an experienced investigator in determining the fuel type, its reactivity, the distribution of the mixture throughout the building and the depth of any flammable layer. This information is required in order to establish the most credible source of gas release and to correctly determine the origin and cause of the explosion.

Studies have shown that an overpressure generated by a gas explosion, in the region of 200 mbar, has the potential to cause significant structural damage to a properly designed and constructed building (Section 1.6). Current guidance (Sections 1.2 and 1.6) suggests that extensive pressure damage is caused by near stoichiometric concentrations and is not usually associated with either lean or rich mixtures. The same guidance also states that extensive thermal damage to decor, furnishings etc. is associated with fuel/air mixtures of stoichiometric or greater concentrations, whilst an explosion involving a fuel lean concentration will exhibit little signs of thermal damage.

However, there have been gas explosions where the building has suffered significant structural damage but there has been very little, and in some cases, no evidence of thermal damage (Section 1.6). Three key questions arise from these observations:

1. Can fuel lean or fuel rich explosions cause significant structural damage?
2. Is it possible to determine the gas concentration prior to ignition from the severity of the thermal damage?
3. Do materials exposed to a transient flame front always exhibit thermal damage?

Following the tragic gas explosion at Ronan Point in 1968, a significant body of research into the causes, mechanisms and effects of gas explosions in buildings was undertaken. It was believed that the cause of the widespread damage to the tower block was largely produced by the propagation of a flame from one room to another,

generating higher overpressures than would have been expected if the explosion had been confined to a single room. Whilst the research (Section 2.6) demonstrated that higher pressures could be generated in these so called ‘cascade’ explosions, the mechanism for producing these overpressures was not fully understood.

The insightful work of Stretch [239] and Rasbash [229, 236] (Section 2.6.1) was found to be especially important to this study as it recognised the role that both interconnected rooms and furniture play in the development of an accidental gas explosion and the necessity for research into their effects. They concluded that large-scale experimental work was required to determine pressure-time curves for single sets of rooms containing furniture. They noted that whilst full-scale experiments were difficult to carry out with a high degree of reliability and were expensive, when the investment and risks involved were considered, further experimental work was quite clearly demanded. To date, some forty-five years after this recommendation, no work of this nature had been published

The majority of the literature related to thermal damage was found to have been conducted in terms of fire investigation and was concerned with the ignition, pyrolysis, burning and charring behaviour of wood and textiles. Consequently, there was little directly relevant material regarding the scorching of fabrics and materials following an explosion and no information to relate the degree of thermal damage to the gas concentration prior to ignition or to the depth of any flammable layer.

In Chapter 4, a considerable amount of large-scale data was presented on the propagation of a natural gas explosion from one enclosure to another. It provides new knowledge and understanding relating to the development of gas explosions in buildings where there has been a build-up of flammable gas/air mixture in more than one room.

A number of mechanisms have been proposed, detailing the manner in which gas explosions propagate from one room to another. This knowledge provides a valuable new insight into how complex a vented explosion in a typical building can be, and how the design and construction of a building can affect the magnitude of the explosion. It is clear from the results of this study that gas explosions that propagate from one room to another have the potential to generate significantly higher overpressures than would be the case of an explosion in a single room of the same total volume and vent area.

Several causes of the development of high overpressures have been identified:

i. The ignition of a flammable cloud outside the vent opening(s) (i.e. the external explosion).

ii. The sudden increase in mass combustion as the turbulised mixture in the secondary compartment is ignited by the propagating flame front emerging through the interconnecting doorway.
iii. The highly turbulent ‘jetting’ flame, driven by the venting process, propagating from the interconnecting doorway and towards the vent opening in the secondary enclosure.

The relative influence of the different explosion development mechanisms was found to be strongly dependent upon the configuration of the building and the ignition position. The key factors being the failure pressures of the respective vents, the failure pressure and inertia of the interconnecting door and the position of the door (including the direction of hinge) prior to ignition.

The most important findings presented in Chapter 4, in terms of the objectives of this study, are that under the right conditions, fuel lean and fuel rich explosions can cause overpressures that have the potential to structurally damage buildings (> 200 mbar). These results are of considerable importance to gas explosion investigators involved in the interpretation of forensic evidence at the scene of a gas explosion in a building, since extensive pressure damage has not typically been associated with either lean or rich mixtures.

The most effective interconnected enclosure design, in terms of mitigating the effects of a gas explosion, would consist of adjoining rooms that have windows that are large, of low failure pressure and equal size, with a lightweight interconnecting door that hinges away from the room that presents the most likely ignition source. Of course, this design would not be ideal in terms of fire protection, so careful consideration would be required.

In Chapter 5, a substantial amount of new large-scale explosion data was presented on the effects of congestion in the form of idealised obstacle arrays and furniture. A number of findings were presented, providing new knowledge and understanding of the manner in which gas explosions develop in the presence of furniture. This knowledge provides further insight into how complex a vented explosion in a typical building can be, and how the degree of furniture, and its layout within a room, can affect the magnitude of the explosion.

It was shown that it was possible to generate overpressures capable of causing structural damage in empty (no internal congestion) enclosures if the vent openings do not allow sufficient outflow (i.e. K_A > 4). The presence of congestion was found to significantly increase the overpressures generated, often by more than an order of magnitude. Furthermore, with volume blockages of as little as 0.57%, overpressures

greater than 200 mbar were generated in all tests where $K_A > 1$. However, the obstacle geometry, and its location to other obstacles and the enclosure, were found to be critical in the development, or otherwise, of damaging overpressures.

It was determined, that for any given congestion level, reducing the vent size would always result in an increased pressure. There was therefore no point in this study where the increased flow and turbulence caused by a larger vent actually overcome the effects of reducing the confinement. This represents an important piece of information for the designers of buildings in that increasing the size of the windows will always reduce the maximum overpressure that could be developed in the event of an explosion, and consequently, it reduces the likelihood of the building being structurally damaged.

The size of the vent was also found to significantly affect the external explosion. As the vent size was decreased, the emerging jet velocity increased and the unburnt gas/air mixture was distributed farther from the vent opening. Consequently, the influence of the external explosion was observed to be greater with larger vent openings.

Two important processes were observed in the development of an explosion involving furniture. Firstly, an initially laminar flame was distorted as it impinged upon the obstacle, increasing the flame surface area. Secondly, the explosion was significantly influenced by the changes in the flow field induced by the obstacle. When the flame arrived at the obstacle, it interacted with the modified flow field, with the geometry and size of the obstacle determining the turbulence levels and length scales. Consequently, the separation distance between obstacles and their location was found to be important.

The effect that the shape of the obstruction and its location within the enclosure appeared to be significant. The introduction of large obstacles and their position sets up a complex interaction between the propagating reaction front and the flow fields around the obstructions. In some instances, particularly where the obstacle was positioned against the wall of the chamber, the velocities were reduced and little turbulence was generated. Furthermore, the flame area was also reduced as it has reached the edge of the flammable mixture. In other instances, if the separation distance was in an ‘optimum’ region, local flame acceleration in the form of jetting occurred.

In Chapter 6, a substantial amount of new data was presented, which can be readily interpreted in the investigation of gas explosions in buildings. These findings provide new knowledge and understanding of the thermal damage exhibited by various materials when subjected to a propagating flame front. This knowledge provides insight

into why some explosions exhibit significant thermal damage and others, of very similar nature, display very little.

The thermal damage sustained by a building, and its decor, during an explosion has been shown to provide useful forensic evidence in the investigation of a gas explosion. The experiments have demonstrated that it is possible to use the severity and extent of thermal damage to wall coverings and wood surfaces, sustained during a gas explosion, to provide useful information on the gas concentration, its distribution throughout the building prior to ignition and the depth of any flammable layer.

It was demonstrated that it was possible to assess the severity of the thermal damage to various materials in order to estimate the natural gas concentration (over the range 8% to 12%) prior to the explosion to the nearest 2%.

The presence of blistering was observed on all types of surfaces, with the severity of blistering increasing with natural gas concentration (up to 12%). However, as blistering also depends on factors other than flame temperature and contact duration, the overall discolouration of a surface was found to represent a more reliable thermal damage indicator.

Whilst wallpaper surfaces exhibited a distinct scorching pattern, the wide variety available, and their wide variation in thermal properties, makes them much less useful as forensic indicators, and probably only useful in indicating the distribution of gas and the passage of a transient flame front. The most suitable materials, in terms of forensic indicators, appear to be softwood covered with either gloss varnish or white oil based gloss paint. Such surfaces are common in buildings as door frames, window frames, etc.

It is currently common practice for buildings to be decorated using water based quick drying paints. These paints have been found to be less susceptible to thermal damage and may cause the misinterpretation of evidence which could lead to an incorrect diagnosis of the origin and cause of an explosion. The knowledge that little evidence of thermal scorching is not necessarily indicative of a fuel lean mixture is a key finding that will change the manner in which explosions are investigated, and is of considerable importance to gas explosion investigators involved in the interpretation of forensic evidence at the scene of a gas explosion in a building. Consequently, during explosion investigations where little evidence of scorching to painted surfaces is exhibited, the investigator should undertake a more detailed examination of other materials susceptible to thermal damage (e.g. wallcoverings, furnishings, carpets etc.) before concluding that the explosion is attributed to the ignition of a fuel lean mixture.

Where a flammable gas/air layer was present, thermal damage was observed above the nominal layer boundary (for natural gas), down to the lowest level where the concentration was originally above 8% ± 1%. It was possible to estimate the layer depth from the damage to an accuracy of approximately 30 cm.

Whilst mixtures containing a lighter than air fuel gas are known to form ceiling layers of the type witnessed with the natural gas experiments, those containing heavier than air fuel gases will form low level layers. These two cases should be distinguishable from the vertical distribution of thermal damage, so that observation of such damage should assist in the identification of the fuel gas involved in an explosion.

Overall, it has been clearly demonstrated that under the right conditions, fuel lean and fuel rich explosions can cause overpressures that have the potential to structurally damage buildings (> 200 mbar), contrary to the current guidance and investigation practice. It was shown that it is possible to determine the gas concentration from the severity of explosion damage to the nearest 2%. It was also demonstrated that certain coatings can significantly affect the degree of thermal damage that a material exhibits. Careful interpretation of the evidence is critical. It is hoped that this study will significantly assist in this matter.

7.2. Limitations of the Study

It was recognised that the effect of area blockage and obstacle separation distance may play a more important role in the development of fast flames than volume blockage. However, unlike chemical, process and storage facilities, where congested region layouts or designs will be readily available, populated buildings will have congested and confined areas that are not predictable, and, as a consequence, it is easier to use volume blockage as a criterion. Consequently, for the purpose of this study, the volume blockage was the main variable when designing the congestion configuration. However, further large-scale experimental tests, investigating the effects of area blockage and separation distance are recommended. This should be linked to a programme that investigates the complex interaction caused when flames propagate from one furnished room to another.

Whilst the experiments conducted into the effects of thermal damage were substantial, the range of materials used in the study, in comparison to the materials that may be encountered during an explosion investigation, was limited. Consequently, further research is recommended.

It was demonstrated in this study, that under controlled conditions, that it was possible to assess the severity of the thermal damage to various materials in order to estimate

the natural gas concentration prior to the explosion to the nearest 2% (over the range 8% to 12%). However, when investigating an actual gas explosion incident, this degree of accuracy is unlikely because of the large number of other factors involved. Though it should be possible in most cases to distinguish between lean, (5% to 8%), close to stoichiometric conditions (9% to 11%) and rich (12% to 15%) natural gas/air mixtures.

It was also demonstrated that it was possible to estimate the depth of a flammable layer from the damage to an accuracy of approximately 30 cm. In practical situations this accuracy would probably be decreased because of the effects of obstacles such as furniture causing large scale turbulence during the explosion, breaking up the layer.

7.3. Recommendations for Future Work

During the course of this study, a number of findings were identified that necessitate more investigation. Consequently, the following are suggestions for future large-scale experimental work:

1. Further tests should be carried out with furnished rooms. These tests should be conducted across a wide range of fuel/air concentration.
2. Experiments should be carried out in a two-storey explosion chamber with interconnected rooms to further investigate the turbulence intensity generated during the complex flow interaction between interconnected rooms.
3. Experimental work should be carried out to investigate the combined effect of interconnected rooms and furniture for fuel lean mixtures. Fuel lean explosions are capable of producing damaging overpressures if the flame front propagates from room to room. However, in the limited fuel lean tests carried out with furniture, damaging overpressures were not produced.
4. Experimental work should be undertaken to further investigate the situation where the ignition room has a flammable mixture but the adjoining room has no gas present. The programme should include tests where the concentration in the ignition enclosure is varied across the flammable range and where the adjoining enclosure has either no gas present, or a concentration up to the lower flammable limit.
5. Tests should be undertaken to investigate the effect of reducing the vent size in an adjoining enclosure. This is to determine the size of vent at which any further reduction in vent size does not result in an increased overpressure.
6. Tests should be undertaken to investigate the effects of area blockage and separation distance. This work should be conducted with multiple arrays, of differing shape, and where the area blockage and volume blockage are

constant. Ideally, this work should be linked to a programme that investigates the complex interaction caused when flames propagate from one furnished room to another.

7. Tests should be carried out to measure the transient concentration of the outflow of unburnt gas/air mixture that forms an external flammable cloud. This will help researchers better understand the role that the external explosion plays and the mechanism that generates overpressure within the explosion chamber. It would also help validate the concentrations predicted by CFD type models.
8. Experiments should be carried out to investigate the cause of possible separate external explosions where the explosion chamber has more than one vent. This should include the determination of whether two separate distinct flammable clouds are formed outside each vent.
9. Experiments should be carried out to investigate the effect of decreasing vent size with fuel rich explosions. These tests should be conducted to determine if strong external explosions can be produced as a consequence of high jet velocities and shear mixing outside the vent opening.
10. The effect of layer depth on maximum overpressure should be further investigated. Tests should be carried out with lighter and heavier than air fuels.
11. Further thermal damage experiments should be undertaken in interconnecting rooms to better establish the effect of turbulence and jetting flames on the ability to accurately determine the layer depth and gas concentration prior to ignition.
12. The compilation of a comprehensive photographic library of examples of thermal damage, for comparative purposes, would be of significant value to explosion investigators, enabling them to confidently predict the gas concentration prior to ignition.
13. Further examination of a wide variety of materials exposed to a transient flame front should be undertaken using digital imaging software to develop a robust methodology for the objective assessment of thermal damage.
14. Experimental work should be undertaken to determine critical heat flux values for materials commonly used as forensic evidence during explosion investigations (e.g. paints, varnishes etc.). This will help determine if the susceptibility of materials to thermal damage can be categorised by critical heat flux.

7.4. Final Remarks

This study started as a quest to answer questions related to the interpretation of evidence at the scene of an accidental gas explosion. At that time, it was believed by the author and other members of the DNV GL incident investigation team and the wider scientific community, that there was potential for the origin and cause of gas explosions to be incorrectly determined due to a lack of meaningful, or worse still, incorrect, guidance in the literature.

This research has resulted in a clearer understanding of how gas explosions develop in furnished buildings and has certainly answered those early questions. It is hoped that this knowledge may be used to better interpret evidence such that the likelihood of incorrect origin and cause determination is greatly reduced.

Mark Twain said, during his 'Disappearance of Literature' speech in New York on 20th November 1900, "it's a 'classic', something that everybody wants to have read and nobody wants to read". Whilst I can be confident that this thesis will not become a 'classic', I sincerely hope that students, scholars and industry recognise and appreciate its contribution to knowledge and understanding of gas explosions in dwellings, and want to read it.

REFERENCES

REFERENCES

1. Gas Safe Register. *Gas Safe Register Legislation and Standards document list* [online]. 2014. [Accessed]. Available from: www.engineers.gassaferegister.co.uk/doc/AccessToStandards/TB%20999%20Gas%20Safe%20Register%20Normative%20Document%20list.pdf.
2. Health and Safety Executive. *Incidents relating to the supply and use of flammable gas* [online]. 2009/10 - 2013/14. [Accessed]. Available from: http://www.hse.gov.uk/statistics/tables/index.htm#gas.
3. Office for National Statistics. *Families and Households* [online]. 2013. [Accessed]. Available from: http://www.ons.gov.uk/ons/rel/family-demography/families-and-households/2013/stb-families.html.
4. Health and Safety Executive. *Major Hazard Safety Performance Indicators in the UK Onshore Gas and Pipelines Industry* [online]. 2013. [Accessed]. Available from: www.hse.gov.uk/pipelines/annual-report12-13.pdf.
5. Office for National Statistics. *Deaths Registered in England and Wales* [online]. 2013. [Accessed]. Available from: http://www.ons.gov.uk/ons/rel/vsob1/mortality-statistics--deaths-registered-in-england-and-wales--series-dr-/2012/stb-deaths-registered-in-england-and-wales-in-2012-by-cause.html.
6. Scotland, G.R.O.f. *Births, Deaths and Other Vital Events* [online]. 2013. [Accessed]. Available from: http://www.gro-scotland.gov.uk/statistics/theme/vital-events/general/bmd-preliminary/index.html.
7. Office for National Statistics. *Population* [online]. 2013. [Accessed]. Available from: http://www.ons.gov.uk/ons/taxonomy/index.html?nscl=Population.
8. Health and Safety Executive. *Health and Safety at Work etc Act 1974* [online]. [Accessed]. Available from: http://www.hse.gov.uk/legislation/hswa.htm.
9. Health and Safety Executive. *The Gas Safety (Management) Regulations 1996* [online]. [Accessed]. Available from: http://www.hse.gov.uk/pubns/books/l80.htm.
10. Burgoyne, J.H. The scientific investigation of occurrences of fire. *Fire Safety Journal*, 1981, **4**(3), pp.159-162.
11. Burgoyne, J.H. Accident investigation. *Journal of Occupational Accidents*, 1982, **3**(4), pp.289-297.
12. NFPA. *NFPA 921 Guide for Fire & Explosion Investigations.* Maryland: NFPA, 2011.
13. IGEM. *IGE/GL/8 Edition 2 - Reporting and investigation of gas related incidents.* UK: IGEM, 2010.
14. Bjerketvedt, D., J.R. Bakke and K. van Wingerden. Gas explosion handbook. *Journal of Hazardous Materials*, 1997, **52**(1), pp.1-150.
15. Foster, C.D. Investigation of Gas Phase Explosions. *In:* A. Beveridge, ed. *Forensic Investigation of Explosions*. 2nd ed. London: CRC Press, 2011, pp.349-404.
16. Harris, R.J. *The Investigation and Control of Gas Explosions and Heating Plant.* London: E & F Spon Ltd, 1983.
17. IAAI. *User's Manual for NFPA 921: Guide for Fire and Explosion Investigations.* 2nd ed. NFPA, 2006.
18. Noon, R.N. *Engineering Analysis of Fires and Explosions.* London: CRC Press, 1995.
19. Yallop, H.J. *Explosion investigation.* Edinburgh: Forensic Science Society; Scottish Academic Press, 1980.
20. DeHaan, J.D. and D.J. Icove. *Kirk's Fire Investigation.* 7th ed. Prentice Hall, 2011.

21. Kennedy, P.M. and J. Kennedy. *Explosion Investigation and Analysis - Kennedy on Explosions.* Chicago: The Investigations Institute, 1990.
22. Kuchta, J.M. *Investigation of Fire and explosion Accidents in the Chemical, Mining, and Fuel-Related Industres - A Manual*. Bulletin 680. Washington, DC, United States: Bureau of Mines, 1985.
23. Griffiths, H., Sir A Pugsley and Sir O Saunders. *Report of the Inquiry into the Collapse of Flats at Ronan Point, Canning Town*. London, 1968.
24. Glasstone, S. *The effects of nuclear weapons.* Revised ed. Washington: U.S. Atomic Energy Commission, 1964.
25. Astbury, N.F., H.W.H. West, H.R. Hodgkinson, P.A. Cubbage and R. Clare. *Gas Explosions in Load-Bearing Brick Structures*. Special Publication No. 68. The British Ceramic Research Association, 1970.
26. Rasbash, D.J., K.N. Palmer, Z.W. Rogowski and S. Ames. *Gas Explosions in Multiple Compartments*. Fire Research Note No. 847. Fire Research Station, 1970.
27. Astbury, N.F., H.W.H. West and H.R. Hodgkinson. *Experimental Gas Explosions: Report of Further Tests at Potters Marston*. Special Publication No. 74. The British Ceramic Research Association, 1972.
28. Solberg, D.M., J.A. Pappas and E. Skramstad. *Gas explosions in confined or partly confined spaces*. Norwegian Maritime Research, No. 4, 1979.
29. Solberg, D.M., J.A. Pappas and E. Skramstad. Experimental investigations on flame acceleration and pressure rise phenomena in large scale vented gas explosions. *In: 3rd International Symposium on Loss Prevention and Safety Promotion in the Process Industries.*, Basle, Switz. Swiss Soc of Chem Ind, 1980, pp.16/1295-16/1303.
30. Solberg, D.M., J.A. Pappas and E. Skramstad. Observations of flame instabilities in large scale vented gas explosions. *In: 18th International Symposium on Combustion*, 17-22 August, University of Waterloo, Canada. 1980.
31. Solberg, D.M., J.A. Pappas and E. Skramstad. Observations of flame instabilities in large scale vented gas explosions. *Symposium (International) on Combustion*, 1981, **18**(1), pp.1607-1614.
32. Solberg, D.M., E. Skramstad and J.A. Pappas. *Experimental Investigations on Partly Confined Gas Explosions: Analysis of Pressure Loads, Part I*. 79-0483. Det Norske Veritas, 1979.
33. MacFadyen, N.K. and J.P. Tite. *Oscillatory Pressure Peaks in Vented Explosions - An Interim Report*. MRS I 2798. Midlands Research Station, 1981.
34. Tite, J.P. *An Experimental Study of Explosion Overpressures Produced by the Combustion of Natural Gas/Air and Manufactured Gas/Air Mixtures in a Vented Enclosure*. MRS I 2795. Midlands Research Station, 1981.
35. Tite, J.P. *Overpressure-Time Profiles Produced by Gas/Air Explosions in Vented Enclosures Fitted with Low Failure Pressure Explosion Reliefs*. MRS I 2797. Midlands Research Station, 1981.
36. Hammond, S. *Investigations of First Peak Pressures Generated in Vented Explosions*. MRS I 2796. Midlands Research Station, 1981.
37. Zalosh, R.G. Gas explosion tests in room-size vented enclosures. *In: AIChE Loss Prevention Symposium*, Houston, TX, USA. AIChE, 1980, pp.98-110.
38. Andrews, G.E., P. Herath and H.N. Phylaktou. The influence of flow blockage on the rate of pressure rise in Large L/D cylindrical closed vessel explosions. *Journal of Loss Prevention in the Process Industries*, 1990, **3**(3), pp.291-302.
39. Phylaktou, H., A. Alexiou and G. Andrews. *Interaction of Fast Explosions with an Obstacle*. OTI 94 625. Health and Safety Executive, 1995.
40. Phylaktou, H. and G.E. Andrews. The acceleration of flame propagation in a tube by an obstacle. *Combustion and Flame*, 1991, **85**(3–4), pp.363-379.

41. Phylaktou, H. and G.E. Andrews. Prediction of the maximum turbulence intensities generated by grid-plate obstacles in explosion-induced flows. *Symposium (International) on Combustion*, 1994, **25**(1), pp.103-110.
42. Phylaktou, H.N. *Gas Explosions in Long Closed Vessels with Obstacles: A turbulent combustion study applicable to industrial explosions*. PhD thesis, University of Leeds, 1993.
43. Ibrahim, S.S., G.K. Hargrave and T.C. Williams. Experimental investigation of flame/solid interactions in turbulent premixed combustion. *Experimental Thermal and Fluid Science*, 2001, **24**(3-4), pp.99-106.
44. Masri, A.R., S.S. Ibrahim, N. Nehzat and A.R. Green. Experimental study of premixed flame propagation over various solid obstructions. *Experimental Thermal and Fluid Science*, 2000, **21**(1–3), pp.109-116.
45. Bauwens, C.R., J. Chaffee and S. Dorofeev. Effect of Ignition Location, Vent Size, and Obstacles on Vented Explosion Overpressures in Propane-Air Mixtures. *Combustion Science and Technology*, 2010, **182**(11), pp.1915 - 1932.
46. Hjertager, B.H., K. Fuhre and M. Bjørkhaug. Concentration Effects on Flame Acceleration by Obstacles in Large-Scale Methane-Air and Propane-Air Vented Explosions. *Combustion Science and Technology*, 1988, **62**(4), pp.239 - 256.
47. Moen, I.O., J.H.S. Lee, B.H. Hjertager, K. Fuhre and R.K. Eckhoff. Pressure development due to turbulent flame propagation in large-scale methane-air explosions. *Combustion and Flame*, 1982, **47**, pp.31-52.
48. Bimson, S.J., D.C. Bull, T.M. Cresswell, P.R. Marks, A.P. Masters, A. Prothero, J.S. Puttock, J.J. Rowson and B. Samuels. An experimental study of the physics of gaseous deflagration in a very large vented enclosure. *In: 14th International Colloquium on the Dynamics of Explosions and Reactive Systems*, , Coimbra, Portugal. 1993.
49. Bauwens, C.R., J.L. Chaffee and S. Dorofeev. Experimental and Numerical Study of Methane-air Deflagrations in a Vented Enclosure. *In: Ninth International Symposium on Fire Safety Science*, 2009, pp.1043-1054.
50. Bauwens, C.R., S. Dorofeev and F. Tamanini. Effects of Aspect Ratio and Ignition Location on Vented Explosion Pressures. *In: Proceedings of the 5th International Seminar on Fire and Explosion Hazards*, 23-27 April 2007, Edinburgh, UK. 2007.
51. Binding, T.M. *Vented Explosions in Vessels with Dimension Ratios in the Range 6:1:1 to 15:1:1*. MRS I 5428. Midlands Research Station, 1991.
52. DeGood, R. and K. Chatrathi. Comparative analysis of test work studying factors influencing pressures developed in vented deflagrations. *Journal of Loss Prevention in the Process Industries*, 1991, **4**(5), pp.297-304.
53. Di Sarli, V., A. Di Benedetto and G. Russo. Using Large Eddy Simulation for understanding vented gas explosions in the presence of obstacles. *Journal of Hazardous Materials*, 2009, **169**(1-3), pp.435-42.
54. Greening, K. and J.P. Tite. *The Correlation of Overpressure Development with Flame Propagation in Vented Explosions*. MRS I 4667. Midlands Research Station, 1988.
55. Gubba, S.R., S.S. Ibrahim, W. Malalasekera and A.R. Masri. LES Modelling of Premixed Deflagrating Flames in a Small-Scale Vented Explosion Chamber with a Series of Solid Obstructions. *Combustion Science and Technology*, 2008, **180**(10), pp.1936 - 1955.
56. Lowesmith, B.J., C. Mumby, G. Hankinson and J.S. Puttock. Vented confined explosions involving methane/hydrogen mixtures. *International Journal of Hydrogen Energy*, 2011, **36**(3), pp.2337-2343.
57. Park, D.J., Y.S. Lee and A.R. Green. Prediction for vented explosions in chambers with multiple obstacles. *Journal of Hazardous Materials*, 2008, **155**(1-2), pp.183-92.

58. Park, D.J., Y.S. Lee and A.R. Green. Experiments on the effects of multiple obstacles in vented explosion chambers. *Journal of Hazardous Materials*, 2008, **153**(1-2), pp.340-50.
59. Proust, C. and E. Leprette. The dynamics of vented gas explosions. *Process Safety Progress*, 2010, **29**(3), pp.231-235.
60. Scheid, M., A. Geisler and U. Krause. Experiments on the influence of pre-ignition turbulence on vented gas and dust explosions. *Journal of Loss Prevention in the Process Industries*, 2006, **19**(2-3), pp.194-199.
61. Solberg, D.M. and J.A. Pappas. Modelling of vented gas deflagrations. *In: Colloque International - Berthelot-Vieille-Mallard-Le Chatelier, 1st Specialists Meeting (International) of the Combustion Institute.*, Bordeaux, Fr. Combust Inst, Fr Sect, 1981, pp.25-30.
62. Sutton, P. and J.P. Tite. *Vented Explosions in Vessels with Side Lengths in the Ratio 3:1:1*. MRS I 5038. Midlands Research Station, 1990.
63. Tamanini, F. and J.L. Chaffee. Turbulent vented gas explosions with and without acoustically-induced instabilities. *Symposium (International) on Combustion*, 1992, **24**(1), pp.1845-1851.
64. Cooper, M.G., M. Fairweather and J.P. Tite. On the mechanisms of pressure generation in vented explosions. *Combustion and Flame*, 1986, **65**(1), pp.1-14.
65. Beveridge, A. *Forensic Investigation of Explosions.* International Forensic Science and Investigation Series. 2nd ed. London: CRC Press, 2011.
66. Marshall, M.R. and G. Pool. *Build-Up of Gas-Air Mixture in a Two-Room Enclosure from Subsonic Natural Gas Releases*. GRC R 0097. BG Research and Technology, 1994.
67. Marshall, M.R. and G. Pool. *Build-Up of Natural Gas-Air and Propane-Air Mixtures in Single Room Enclosures under Ventilated Conditions*. GRC R 0098. BG Research and Technology, 1994.
68. Pool, G. *An Experimental Study of Natural Gas Accumulation Following Subsonic Releases under Unventilated Conditions*. GRC R 0095. BG Research and Technology, 1994.
69. Pool, G. and M.R. Marshall. *A Large-Scale Experimental Study of Natural Gas Accumulation Following Low Pressure Releases into Multi-Room Enclosures - Appendix*. GRC R 0985. BG Research and Technology, 1995.
70. Pool, G. *An Experimental Study of Natural Gas Accumulation Following Sonic Releases under Unventilated Conditions*. GRTC R 0094. BG Research and Technology, 1996.
71. Pool, G. and R.W. Hill. *An Experimental Study of the Build-Up and Dispersal of Natural Gas in a 2-Storey, Multi-Room Enclosure*. GRTC R 1797. BG Research and Technology, 1997.
72. Astbury, N.F. and G.N. Vaughan. *Motion of Brickwork Structure Under Certain Assumed Conditions*. Technical Note No. 191. The British Ceramic Research Association, 1972.
73. West, H.W.H., H.R. Hodgkinson and W.F. Webb. *The Resistance of Clay Brick Walls to Lateral Loading*. Technical Note No. 176. The British Ceramic Research Association, 1971.
74. West, H.W.H., H.R. Hodgkinson and W.F. Webb. *The Resistance of Brick Walls to Lateral Loading*. The British Ceramic Research Association, 1971.
75. Wong, C.W. and M. Karamanoglu. Modelling the response of masonry structures to gas explosions. *Journal of Loss Prevention in the Process Industries*, 1999, **12**(3), pp.199-205.
76. Lewis, B. and G. von Elbe. *Combustion, Flames and Explosions of Gases.* Third ed. London: Acadmic Press Inc., 1987.
77. Griffiths, J.F. and J.A. Barnard. *Flame and combustion.* 3rd ed. London: Blackie, 1995.
78. Williams, F.A. *Combustion theory.* 2nd ed. New York: Westview Press, 1985.
79. Strehlow, R.A. *Combustion fundamentals.* London: McGraw-Hill, 1984.

80. Mishra, D. *Fundamentals of combustion.* PHI Learning Pvt. Ltd., 2007.
81. Drysdale, D. *An Introduction to Fire Dynamics.* 3rd ed. London: Wiley-Blackwell, 2011.
82. Kuo, K.K. *Principles of combustion.* 2nd ed. New Jersey: Wiley, 2005.
83. Kuo, K.K. and R. Acharya. *Fundamentals of Turbulent and Multiphase Combustion.* 1st ed. New Jersey: Wiley, 2012.
84. Zabetakis, M.G. *Flammability characteristics of combustible gases and vapors*. Bulletin 627. Washington, DC, United States: United States Bureau of Mines, 1965.
85. Coward, H.F. and G.W. Jones. *Limits of flammability of gases and vapors*. Bulletin 503. Washington, DC, United States: United States Bureau of Mines, 1952.
86. Andrews, G. Fire and explosion stoichiometry. *In: Fire flammability and explosions*. University of Leeds, 2002.
87. Crowl, D.A. *Understanding Explosions.* New York: Center for Chemical Process Safety of the American Institute of Chemical Engineers, 2003.
88. Morley, C. *Gaseq* [online]. [Accessed]. Available from: http://www.gaseq.co.uk/.
89. J.W, L. Methods of measuring burning velocities. *Symposium (International) on Combustion*, 1953, **4**(1), pp.20-35.
90. Andrews, G.E. and D. Bradley. Determination of burning velocities: A critical review. *Combustion and Flame*, 1972, **18**(1), pp.133-153.
91. Rallis, C.J. and A.M. Garforth. The determination of laminar burning velocity. *Progress in Energy and Combustion Science*, 1980, **6**(4), pp.303-329.
92. Hattwig, M. and H. Steen. *Handbook of explosion prevention and protection.* Cambridge: Wiley-VCH, 2004.
93. Gibbs, G.J. and H.F. Calcote. Effect of Molecular Structure on Burning Velocity. *Journal of Chemical Engineering Data*, 1959, **5**(226).
94. Lewis, B. *Selected combustion problems.* AGARD, 1954.
95. Egerton, A. and A.H. Lefebvre. Flame Propagation: The Effect of Pressure Variation on Burning Velocities. *Proceedings of the Royal Society of London. Series A, Mathematical and Physical Sciences*, 1954, **222**(1149), pp.206-223.
96. Dugger, G.L. *Effect of initial mixture temperature on flame speed of methane-air, propane-air, and ethylene-air mixtures*. Washington, DC, United States: National Advisory Committee for Aeronautics, 1952.
97. Andrews, G.E. and D. Bradley. The burning velocity of methane-air mixtures. *Combustion and Flame*, 1972, **19**(2), pp.275-288.
98. Dixon-Lewis, G. and S.M. Islam. Flame modelling and burning velocity measurement. *Symposium (International) on Combustion*, 1982, **19**(1), pp.283-291.
99. Heravi, H.M., A. Azarinfar, S.I. Kwon, P.J. Bowen and N. Syred. Determination of Laminar Flame Thickness and Burning Velocity of Methane-Air Mixture. *In: Third European Combustion Meeting*, 11-13 April 2007, Chania, Crete. The Combustion Institute, 2007.
100. Hazlehurst, J. *Tolley's Basic Science and Practice of Gas Service.* Gas Service Technology: Vol 1. 5th ed. London: Newnes, 2009.
101. *Essential Gas Safety: Domestic.* Basingstoke: CORGI Services Limited, 2010.
102. Treloar, R.D. *Gas Installation Technology.* 2nd ed. Sussex: Wiley-Blackwell, 2010.
103. Harris, R.J. and M.J. Wickens. Understanding vapour cloud explosions - an experimental study. 1989, **IGE Communication 1408**.
104. Markstein, G.H. Interaction of flame propagation and flow disturbances. *Symposium on Combustion and Flame, and Explosion Phenomena*, 1949, **3**(1), pp.162-167.
105. Mitani, T. and F.A. Williams. Studies of Cellular Flames in Hydrogen-Oxygen-Nitrogen Mixtures. *Combustion and Flame*, 1980, **39**(2), pp.169-190.

106. Manton, J., G. von Elbe and B. Lewis. Nonisotropic propagation of combustion waves in explosive gas mixtures and the development of cellular flames. *The Journal of Chemical Physics*, 1952, **20**(1), pp.153-157.
107. Palm-Leis, A. and R.A. Strehlow. On the propagation of turbulent flames. *Combustion and Flame*, 1969, **13**(2), pp.111-129.
108. Ronney, P.D. Premixed-Gas Flames. *In:* H. Ross, ed. *Microgravity Combustion: Fires in Free Fall*. London: Academic Press, 2001, pp.35-82.
109. Darrieus, G. Propagation d'un front de flame: assai de théorie des vitesses anomales de deflagration par developpement spontanné de la turbulence. *In: Sixth International Congress of Applied Mathematics*, Paris. 1946.
110. Landau, L.D. and E.M. Lifshitz. *Fluid mechanics.* Oxford: Pergamon Press, 1987.
111. Ciccarelli, G. and S. Dorofeev. Flame acceleration and transition to detonation in ducts. *Progress in Energy and Combustion Science*, 2008, **34**(4), pp.499-550.
112. Markstein, G.H. *Non steady flame propagation.* Pergamon Press, 1964.
113. Clavin, P. and F.A. Williams. Effects of molecular diffusion and thermal expansion on the structure and dynamics of premixed flames in turbulent flows of large scale and low intensity. *Journal of Fluid Mechanics*, 1981, **116**, pp.252–282.
114. Joulin, G. and P. Clavin. Linear stability of nonadiabatic flames: Thermal-diffusional model. 1979, pp.139-145.
115. Pelce, P. and P. Clavin. Influence of hydrodynamics and diffusion upon the stability of laminar premixed flames. *Journal of Fluid Mechanics*, 1982, **124**, pp.219–237.
116. Abdel-Gayed, R.G., D. Bradley and F.K.K. Lung. Combustion regimes and the straining of turbulent premixed flames. *Combustion and Flame*, 1989, **76**(Compendex), pp.213-218.
117. Andrews, G.E., D. Bradley and S.B. Lwakabamba. Turbulence and turbulent flame propagation-A critical appraisal. *Combustion and Flame*, 1975, **24**, pp.285-304.
118. Bradley, D. Instabilities and flame speeds in large-scale premixed gaseous explosions. *Philosophical Transactions of the Royal Society of London Series a-Mathematical Physical and Engineering Sciences*, 1999, **357**(1764), pp.3567-3581.
119. Bradley, D. Turbulent Combustion. *In: Explosion Prediction and Mitigation*. University of Leeds, 2002.
120. Gu, X.J., M.Z. Haq, M. Lawes and R. Woolley. Laminar burning velocity and Markstein lengths of methane-air mixtures. *Combustion and Flame*, 2000, **121**(1-2), pp.41-58.
121. Karlovitz, B., D.W. Denniston, D.H. Knapschaefer and F.E. Wells. Studies on turbulent flames. *Fourth Symposium (International) on Combustion*, 1953.
122. Bradley, D., P.H. Gaskell and X.J. Gu. Burning velocities, Markstein lengths, and flame quenching for spherical methane-air flames: A computational study. *Combustion and Flame*, 1996, **104**(1-2), pp.176-198.
123. Buckmaster, J. The quenching of two-dimensional premixed flames. *Acta Astronautica*, 1979, **6**(5-6), pp.741-769.
124. Matalon, M. On Flame Stretch. *Combustion Science and Technology*, 1983, **31**(3-4), pp.169-181.
125. Chung, S.H. and C.K. Law. An invariant derivation of flame stretch. *Combustion and Flame*, 1984, **55**(1), pp.123-125.
126. Clavin, P. and G. Joulin. Premixed flames in large scale and high intensity turbulent flow. *J. Physique Lett.*, 1983, **44**(1), pp.1-12.
127. Lord Kelvin (Thomson, W.,). Hydrokinetic solutions and observations. *Philosophical Magazine Series 4*, 1871, **42**(281), pp.362-377.

128. von Helmholtz, H. On discontinuous movements of fluids. *Philosophical Magazine Series 4*, 1868, **36**(244), pp.337-346.
129. Taylor, G. The Instability of Liquid Surfaces when Accelerated in a Direction Perpendicular to their Planes. I. *Proceedings of the Royal Society of London. Series A. Mathematical and Physical Sciences*, 1950, **201**(1065), pp.192-196.
130. Lord Rayleigh (Strutt, J.W.,). Investigation of the Character of the Equilibrium of an Incompressible Heavy Fluid of Variable Density. *Proceedings of the London Mathematical Society*, 1882, **s1-14**(1), pp.170-177.
131. Searby, G. and D. Rochwerger. A parametric acoustic instability in premixed flames. *Journal of Fluid Mechanics*, 1991, **231**, pp.529-543.
132. van Wingerden, C.J.M. and J.P. Zeeuwen. On the role of acoustically driven flame instabilities in vented gas explosions and their elimination. *Combustion and Flame*, 1983, **51**, pp.109-111.
133. Harrison, A.J. and J.A. Eyre. External Explosions as a Result of Explosion Venting. *Combustion Science and Technology*, 1987, **52**(1), pp.91 - 106.
134. Bradley, D. Evolution of Flame Propagation in Large Diameter Explosions. *In: 2nd International Seminar on Fire & Explosion Hazards of Substances and Venting of Deflagrations*, August 11-15, Moscow, Russia. 1997, pp.51-59.
135. AIChE. *Guidelines for vapour cloud explosion, pressure vessel burst, BLEVE and flash fire hazards.* Second ed. New York: American Institute of Chemical Engineers, 2010.
136. Phylaktou, H. and G.E. Andrews. Application of turbulent combustion models to explosion scaling. *Process Safety and Environmental Protection: Transactions of the Institution of Chemical Engineers, Part B*, 1995, **73**(1), pp.3-10.
137. Catlin, C.A. and D.M. Johnson. Experimental scaling of the flame acceleration phase of an explosion by changing fuel gas reactivity. *Combustion and Flame*, 1992, **88**(1), pp.15-27.
138. Pappas, J.A., T.E. Foyn, E. Skramstad and D.M. Solberg. *Report from the 1982 Experiments*. Gas Explosion Research Programme, 82-1090. Det Norske Veritas, 1982.
139. Pappas, J.A., T.E. Foyn and D.M. Solberg. Combustion Instabilities and the Scaling of Vented Gas Deflagrations. *In: 9th International Colloquium on Dynamics of Explosions and Reactive Systems*, July 1983, Poiter, France. 1981.
140. Pappas, J.A., T.E. Foyn, D.M. Solberg and E. Skramstad. *Data Report from the 35 m^3 Tests*. Gas Explosion Research Programme, 82-1237. Det Norske Veritas, 1983.
141. Pappas, J.A., T.E. Foyn, D.M. Solberg, E. Skramstad and S. Mann. *Data Report from the 425 m^3 Experiments*. Gas Explosion Research Programme, 82-1169. Det Norske Veritas, 1982.
142. Pappas, J.A., D.M. Solberg and T.E. Foyn. *Final Report*. Gas Explosion Research Programme, 83-1334. Det Norske Veritas, 1984.
143. Rinnan, A., E. Skramstad and D.M. Solberg. *Gas Explosions: Description of Test Site and Experimental Set-UP*. 79-0119. Det Norske Veritas, 1979.
144. Rogers, M. and J.P. Tite. *The Effect of Vessel Volume on Pressures Generated in Natural Gas-Air Explosions in Cubical Vessels*. MRS I 5071. Midlands Research Station, 1992.
145. van Wingerden, C.J.M. *Experimental Study of the Influence of Obstacles and Partial Confinement on Flame Propagation*. EUR 9541 EN/I I. Commission of the European Communities for nuclear science and technology, 1984.
146. Hjertager, B.H., K. Fuhre and M. Bjørkhaug. Gas explosion experiments in 1:33 and 1:5 scale offshore separator and compressor modules using stoichiometric homogeneous fuel/air clouds. *Journal of Loss Prevention in the Process Industries*, 1988, **1**(4), pp.197-205.
147. Mercx, W.P.M., C.J.M. van Wingerden and H.J. Pasman. Venting of gaseous explosions. *Process Safety Progress*, 1993, **12**(1), pp.40-46.

148. Solberg, D.M. Gas explosions - and the problem of scaling. *Veritas No. 103 - II*, 1981, **27th Volume**.
149. Mercx, W.P.M. *Modelling and Experimental Research into Gas Explosions: Overall Final Report on the MERGE Project.* Commission of the European Communities Report. Contract STEP-CT-011 (SSMA), 1993.
150. Mercx, W.P.M., D.M. Johnson and J. Puttock. Validation of scaling techniques for experimental vapor cloud explosion investigations. *Process Safety Progress*, 1995, **14**(2), pp.120-130.
151. Taylor, P.H. and W.J.S. Hirst. The Scaling of Vapour Cloud Explosions: a Fractal Model for Size and Fuel Type. *In: 22nd International Symposium on Combustion*, 1988.
152. F.C, G. An application of fractals to modeling premixed turbulent flames. *Combustion and Flame*, 1987, **68**(3), pp.249-266.
153. Samuels, B. Explosion Hazard Assessment of Offshore Modules using l/12th Scale Models. *In: Major Hazards I IChemE Symposium Series No. 130*, 20–22 October 1992: IChemE, 1992.
154. Bartknecht, W. *Explosions, course prevention protection.* New York: Springer-Verlag, 1981.
155. NFPA. *NFPA 68 Standard on Explosion Protection by Deflagration Venting.* Maryland: NFPA, 2013.
156. van Wingerden, C.J.M. On the venting of large-scale methane–air explosions. *In: Sixth international symposium of loss prevention and safety promotion in the process industries*, Oslo. 1989.
157. van Wingerden, C.J.M. and J.P. Zeeuwen. Venting of gas explosions in large rooms. *In: 4th International Symposium on Loss Prevention and Safety Promotion in the Process Industries (EFCE Event n 290). Volume 3: Chemical Process Hazards.*, Harrogate, England. IChemE, 1983, pp.F38-F47.
158. Solberg, D.M. and J.A. Pappas. Modelling of Vented Gas Deflagrations. *In: First Specialists Meeting (International) of the Combustion Institute*, 20-24 July, Bordeaux. 1981.
159. Chao, J., C.R. Bauwens and S.B. Dorofeev. An analysis of peak overpressures in vented gaseous explosions. *Proceedings of the Combustion Institute*, 2011, **33**(2), pp.2367-2374.
160. Butlin, R.N. and P.S. Tonkin. *Pressures Produced by Gas Explosions in a Vented Compartment*. Fire Research Note No. 1019. Fire Research Station, 1974.
161. Eckhoff, R.K., K. Fuhre, C.M. Guirao and J.H.S. Lee. Venting of turbulent gas explosions in a 50 m^3 chamber. *Fire Safety Journal*, 1984, **7**(2), pp.191-197.
162. Forcier, T. and R. Zalosh. External pressures generated by vented gas and dust explosions. *Journal of Loss Prevention in the Process Industries*, 2000, **13**(3–5), pp.411-417.
163. Pappas, J.A., T.E. Foyn and D.M. Solberg. *Interim Report from the 35 m^3 Experiments*. Gas Explosion Research Programme, 83-1025. Det Norske Veritas, 1983.
164. Cubbage, P.A. and W.A. Simmonds. An investigation of explosion reliefs for industrial drying ovens, I—top reliefs in box ovens. *The Gas Council Research Communication GC23*, 1955.
165. Cubbage, P.A. and W.A. Simmonds. An investigation of explosion reliefs for industrial drying ovens, II—Back reliefs in box ovens, reliefs in conveyor ovens. *The Gas Council Research Communication GC43*, 1957.
166. *Final Report 1957, Swedish Committee for Explosion Testing*. Stockholm, 1958.
167. Catlin, C.A. *Modelling the Effect of External Combustion on the Internal Overpressures Developed During a Confined Vented Explosion*. MRS I 4499. Midlands Research Station, 1987.
168. Fakandu, B.M., G.E. Andrews and H.N. Phylaktou. Impact of non-central vents on vented explosion overpressures. *In: Tenth International Symposium on*

Hazards, Prevention, and Mitigation of Industrial Explosions (X ISHPMIE), 10-14 June, Bergen, Norway. 2014.
169. van Wingerden, C.J.M. *An Experimental Study into the Venting of Gaseous Explosions: Part 1 - Experimental Results*. PML 1984 - 29. TNO, 1984.
170. Fakandu, B.M., Z.X. Yan, H.N. Phylaktou and G.E. Andrews. The Effect of Vent Area Distribution in Gas Explosion Venting and Turbulent Length Scale Influence on the External Explosion Overpressure. *In: Seventh International Seminar on Fire & Explosion Hazards (ISFEH7)*, May 5-10, Providence, Rhode Island. 2013, pp.1-10.
171. Fakandu, B.M. *Vented Gas Explosions*. PhD thesis, University of Leeds, 2014.
172. Lunn, G.A. *Venting gas and dust explosions - A review.* IChemE, 1984.
173. Burgoyne, J.H. and M.J.G. Wilson. The relief of pentane vapour—air explosions in vessels. *In: Symposium on Chemical Process Hazards*: Institution of Chemical Engineers, 1960.
174. Donat, C. *VDI Berichte Nr. 165.* Dusseldorf, 1971.
175. Jiang, X., B. Fan, J. Ye and G. Dong. Experimental investigations on the external pressure during venting. *Journal of Loss Prevention in the Process Industries*, 2005, **18**(1), pp.21-26.
176. Lee, Y., S. Ahn and J. Ahn. External pressure characteristics generated by vented gas explosions a partially confined chamber. *In: European Safety and Reliability Conference 2006, ESREL 2006 - Safety and Reliability for Managing Risk, 18 - 22 September, 2006*, Estoril, Portugal. Taylor and Francis/Balkema, 2006, pp.2009-2012.
177. Palmer, K.N. and P.S. Tonkin. External pressures caused by venting gas explosions in a large chamber. *In: 3rd International Symposium on Loss Prevention and Safety Promotion in the Process Industries.*, Basle, Switz. Swiss Soc of Chem Ind, 1980, pp.16/1274-16/1294.
178. Walker, D.G. Confidential Report. *Vented Turbulent Premixed Combustion in an Axisymmetric Tube containing Baffles and constrained by a Vent containing a Flame Arrester*. British Gas Research and Technology, 1995.
179. Thorne, P.F., Z.W. Rogowski and P. Field. Performance of Low Inertia Explosion Reliefs Fitted to a 22 m^3 Cubical Chamber. *In: 4th International Symposium on Loss Prevention and Safety Promotion in the Process Industries*: Pergamon Press, 1983.
180. Dragosavic, M. *In: BRE Symposium on Buildings and the Hazard of Explosion, Paper No. 3*, 1972.
181. McCann, D.P.J., G.O. Thomas and D.H. Edwards. Gasdynamics of vented explosions part I: Experimental studies. *Combustion and Flame*, 1985, **59**(3), pp.233-250.
182. Kasmani, R.M., G.E. Andrews and H.N. Phylaktou. The influence of vessel volume and equivalence ratio in vented gas explosions. *In: 4th International Conference on Safety and Environment in Process Industry, CISAP4, March 14, 2010 - March 17, 2010*, Florence, Italy. Italian Association of Chemical Engineering - AIDIC, 2010, pp.463-468.
183. Kasmani, R.M. *Vented Gas Explosions*. PhD thesis, University of Leeds, 2008.
184. Rasbash, D.J. and Z.W. Rogowski. Gaseous explosions in vented ducts. *Combustion and Flame*, 1960, **4**, pp.301-312.
185. Rasbash, D.J. and Z.W. Rogowski. Gaseous Explosions in Propane/Air Mixtures Moving in a Straight Unobstructed Duct. *In: Second Symposium on Chemical Process Hazards with Special Reference to Plant Design*, London. IChemE, 1963.
186. Alexiou, A., H. Phylaktou and G.E. Andrews. The Effect of Vent Size on Pressure Generation in Explosions in Large L/D Vessels. *Combustion Science and Technology*, 1996, **113**(1), pp.645 - 652.
187. Hammond, S. *An Interim Report on the Definition of Vent Coefficient in Vented Explosions*. MRS I 2799. Midlands Research Station, 1981.

188. Buckland, I.G. Explosions of gas layers in a room size chamber. *Institution of Chemical Engineers Symposium Series*, 1980.
189. Cubbage, P.A. and M.R. Marshall. Pressures generated by explosions of gas–air mixtures in vented enclosures. *Inst. Gas Engineers Communication No. 926*, 1973.
190. Harris, R.J., M.J. Wickens and D.M. Johnson. *The Effect of Explosion Pressures on Structures and Structural Components*. MRS E 450. London: British Gas Research & Development, 1985.
191. Ferrara, G., S.K. Willacy, H.N. Phylaktou, G.E. Andrews, A. Di Benedetto and M.C. Mkpadi. Duct-vented propane/air explosions with central and rear ignition. *In: Proceedings of the International Association for Fire Safety Science Symposium,*, Beijing, China. IAFSSS, 2005.
192. Kindracki, J., A. Kobiera, G. Rarata and P. Wolanski. Influence of ignition position and obstacles on explosion development in methane-air mixture in closed vessels. *Journal of Loss Prevention in the Process Industries*, 2007, **20**(The Institution of Engineering and Technology), pp.551-61.
193. Ponizy, B. and J.C. Leyer. Flame dynamics in a vented vessel connected to a duct: 1. Mechanism of vessel-duct interaction. *Combustion and Flame*, 1999, **116**(1-2), pp.259-271.
194. Ponizy, B. and J.C. Leyer. Flame dynamics in a vented vessel connected to a duct: 2. Influence of ignition site, membrane rupture, and turbulence. *Combustion and Flame*, 1999, **116**(1-2), pp.272-281.
195. Binding, T.M. *The Effect of External Relief Ducting on Overpressures Generated in Vented Natural Gas Explosions*. MRS I 5081. Midlands Research Station, 1989.
196. Chow, S.K. *Detailed Analysis of Vented Explosions in a Cylindrical Vessel*. MRS I 5657. British Gas Research and Technology, 1992.
197. Willacy, S., H. Phylaktou, G. Andrews and G. Ferrara. Stratified Propane–Air Explosions in a Duct Vented Geometry Effect of Concentration, Ignition and Injection Position. *Process Safety and Environmental Protection*, 2007, **85**(2), pp.153-161.
198. Bray, K.N.C. The interaction between turbulence and combustion. *Symposium (International) on Combustion*, 1979, **17**(1), pp.223-233.
199. Bray, K.N.C. The challenge of turbulent combustion. *Symposium (International) on Combustion*, 1996, **26**(1), pp.1-26.
200. Paul, C. Dynamic behavior of premixed flame fronts in laminar and turbulent flows. *Progress in Energy and Combustion Science*, 1985, **11**(1), pp.1-59.
201. Buckmaster, J., P. Clavin, A. Liñán, M. Matalon, N. Peters, G. Sivashinsky and F.A. Williams. Combustion theory and modeling. *Proceedings of the Combustion Institute*, 2005, **30**(1), pp.1-19.
202. Abdel-Gayed, R.G. and D. Bradley. Criteria for turbulent propagation limits of premixed flames. *Combustion and Flame*, 1985, **62**(1), pp.61-68.
203. Poludnenko, A.Y. and E.S. Oran. The interaction of high-speed turbulence with flames: Turbulent flame speed. *Combustion and Flame*, 2011, **158**(2), pp.301-326.
204. Gülder, Ö.L. Turbulent premixed flame propagation models for different combustion regimes. *Symposium (International) on Combustion*, 1991, **23**(1), pp.743-750.
205. Chan, C., I.O. Moen and J.H.S. Lee. Influence of confinement on flame acceleration due to repeated obstacles. *Combustion and Flame*, 1983, **49**(1-3), pp.27-39.
206. Phylaktou, H., G.E. Andrews, N. Mounter and K.M. Khamis. Spherical Explosions Aggravated by Obstacles. *In: Major Hazards I IChemE Symposium Series No. 130*, 20–22 October 1992: IChemE, 1992.
207. Solberg, D.M. Industrial gas explosion problems. *Plant/Operations Progress*, 1982, **1**(4), pp.243-248.

208. Phylaktou, H. and G.E. Andrews. Gas Explosions in Long Closed Vessels. *Combustion Science and Technology*, 1991, **77**(1-3), pp.27-39.
209. Phylaktou, H. and G.E. Andrews. The effect of obstacles on enclosed gas explosions. *In: International Conference on Industrial Fire and Explosion Hazards*: The Institute of Energy, 1991, pp.63-73.
210. Reynolds, O. An Experimental Investigation of the Circumstances Which Determine Whether the Motion of Water Shall Be Direct or Sinuous, and of the Law of Resistance in Parallel Channels. *Philosophical Transactions of the Royal Society of London*, 1883, **174**(ArticleType: research-article / Full publication date: 1883 / Copyright © 1883 The Royal Society), pp.935-982.
211. Reynolds, O. On the Dynamical Theory of Incompressible Viscous Fluids and the Determination of the Criterion. *Proceedings: Mathematical and Physical Sciences*, 1895, **451**(1941), pp.5-47.
212. Lighthill, M.J. Osborne Reynolds and Engineering Science Today. *In: Turbulence*. New York: Manchester University Press Barnes and Noble Inc., 1970.
213. Taylor, G.I. The Spectrum of Turbulence. *Proceedings of the Royal Society of London. Series A, Mathematical and Physical Sciences*, 1938, **164**(919), pp.476-490.
214. Taylor, G.I. Statistical Theory of Turbulence. *Proceedings of the Royal Society of London. Series A, Mathematical and Physical Sciences*, 1935, **151**(873), pp.421-444.
215. Dryden, H.L. A review of the statistical theory of turbulence. *Quarterly Journal of Applied Mathematics*, 1943, **1**(1), pp.7–42.
216. Kolmogorov, A.N. Equations of turbulent flow of an incompressible viscous liquid. *Journal of Physics*, 1942, **6**(5), pp.227-228.
217. Damköhler, G. The effect of turbulence on the flame velocity in gas mixtures. *Z.F. Electrochem*, 1940, **46**, p.601.
218. Cates, A. and B. Samuels. A simple assessment methodology for vented explosions. *Journal of Loss Prevention in the Process Industries*, 1991, **4**(5), pp.287-296.
219. Chamberlain, G.A. and J.J. Rowson. Gas Explosion Experiments in Congested Plant Partially Filled with Fuel-Air Mixtures. *In: International Conference: Major Hazards Offshore - Practical Safety Implications*: ERA Technology, 2000.
220. Fairweather, M., G.K. Hargrave, S.S. Ibrahim and D.G. Walker. Studies of premixed flame propagation in explosion tubes. *Combustion and Flame*, 1999, **116**(4), pp.504-518.
221. Fairweather, M., S.S. Ibrahim, H. Jaggers and D.G. Walker. Turbulent premixed flame propagation in a cylindrical vessel. *Symposium (International) on Combustion*, 1996, **26**(1), pp.365-371.
222. Sakthitharan, V. *Time-resolved measurements of flame propagation over baffle-type obstacles*. PhD thesis, Imperial College London, 1995.
223. Lindstedt, R.P. and V. Sakthitharan. Time resolved velocity and turbulence measurements in turbulent gaseous explosions. *Combustion and Flame*, 1998, **114**(3-4), pp.469-483.
224. Ibrahim, S.S. and A.R. Masri. The effects of obstructions on overpressure resulting from premixed flame deflagration. *Journal of Loss Prevention in the Process Industries*, 2001, **14**(3), pp.213-221.
225. Dorofeev, S.B. Flame acceleration and explosion safety applications. *Proceedings of the Combustion Institute*, 2011, **33**(2), pp.2161-2175.
226. Hall, R., A. Masri, P. Yaroshchyk and S. Ibrahim. Effects of position and frequency of obstacles on turbulent premixed propagating flames. *Combustion and Flame*, 2009, **156**(2), pp.439-446.
227. Mercx, W.P.M., A.C. van den Berg, C.J. Hayhurst, N.J. Robertson and K.C. Moran. Developments in vapour cloud explosion blast modeling. *Journal of Hazardous Materials*, 2000, **71**(1-3), pp.301-319.

228. Catlin, C.A. Scale effects on the external combustion caused by venting of a confined explosion. *Combustion and Flame*, 1991, **83**(3-4), pp.399-411.
229. Rasbash, D.J. *The Relief of Gas and Vapour Explosion in Domestic Structures*. Fire Research Note No. 759. Fire Research Station, 1969.
230. Rasbash, D.J., D.D. Drysdale and N. Kemp. Design of an explosion relief system for a building handling liquefied fuel gases. *In: IChemE Symposium Series No. 47*: IChemE, 1976.
231. Dörge, K.J., D. Pangritz and H.G. Wagner. Experiments on velocity augmentation of spherical flames by grids. *Acta Astronautica*, 1976, **3**(11–12), pp.1067-1076.
232. Dragosavic, M. Structural Measures Against Natural-Gas Explosions in Highrise Blocks of Flats. *Heron*, 1973, **19**(4).
233. Harris, G.F.P. The effect of vessel size and degree of turbulence on gas phase explosion pressures in closed vessels. *Combustion and Flame*, 1967, **11**(1), pp.17-25.
234. Andrews, G. *Laminar and Turbulent Flame Propagation*. PhD thesis, University of Leeds, 1972.
235. Andrews, G.E., D. Bradley and S.B. Lwakabamba. Measurement of turbulent burning velocity for large turbulent Reynolds numbers. *Symposium (International) on Combustion*, 1975, **15**(1), pp.655-664.
236. Rasbash, D.J. Explosions in Domestic Structures. *In: Joint meeting of the Institution of Structural Engineers and the Institution of Heating and Ventilating Engineers*, 23 October 1969, 11 Upper Belgrave Street, London SW1. 1969.
237. Cubbage, P.A. and W.A. Simmonds. The Design of Explosion Reliefs for Industrial Drying Ovens. *In: IChemE Symposium on Process Hazards*, 1960.
238. Rasbash, D.J. and Z.W. Rogowski. Relief of explosions in duct systems. *In: Proc. of the Symposium on Chemical Process Hazards with Special Reference to Plant Design*, London. IChemE, 1961.
239. Stretch, K.L. The Relationship Between Containment Characteristics and Gaseous Reactions. *In: Joint meeting of the Institution of Structural Engineers and the Institution of Heating and Ventilating Engineers*, 23 October 1969, 11 Upper Belgrave Street, London SW1. 1969.
240. Molkov, V.V. Explosions in buildings: modeling and interpretation of real accidents. *Fire Safety Journal*, 1999, **33**(1), pp.45-56.
241. Abdullin, R.K., V.S. Babkin and P.K. Senachin. Combustion of gas in connected vessels. *Combustion, Explosion, and Shock Waves*, 1988, **24**(2), pp.123-132.
242. Di Benedetto, A. and E. Salzano. CFD simulation of pressure piling. *Journal of Loss Prevention in the Process Industries*, 2010, **23**(4), pp.498-506.
243. Di Benedetto, A., E. Salzano and G. Russo. Modeling Explosion In Compartmented Vessels. *In: Joint Meeting of The Scandinavian-Nordic and Italian Sections of The Combustion Institute*, Napoli - Italy. 2003.
244. Di Benedetto, A., E. Salzano and G. Russo. Predicting pressure piling by semi-empirical correlations. *Fire Safety Journal*, 2005, **40**(3), pp.282-298.
245. Holbrow, P., S. Andrews and G.A. Lunn. Dust explosions in interconnected vented vessels. *Journal of Loss Prevention in the Process Industries*, 1996, **9**(1), pp.91-103.
246. Holbrow, P., G.A. Lunn and A. Tyldesley. Dust explosion protection in linked vessels: guidance for containment and venting. *Journal of Loss Prevention in the Process Industries*, 1999, **12**(3), pp.227-234.
247. Lunn, G.A., P. Holbrow, S. Andrews and J. Gummer. Dust explosions in totally enclosed interconnected vessel systems. *Journal of Loss Prevention in the Process Industries*, 1996, **9**(1), pp.45-58.
248. Maremonti, M., G. Russo, E. Salzano and V. Tufano. Numerical simulation of gas explosions in linked vessels. *Journal of Loss Prevention in the Process Industries*, 1999, **12**(3), pp.189-194.

249. Phylaktou, H. and G.E. Andrews. Gas explosions in linked vessels. *Journal of Loss Prevention in the Process Industries*, 1993, **6**(1), pp.15-19.
250. Razus, D., D. Oancea, F. Chirila and N.I. Ionescu. Transmission of an explosion between linked vessels. *Fire Safety Journal*, 2003, **38**(2), pp.147-163.
251. Singh, J. Gas explosions in inter-connected vessels: pressure piling. *Process Safety and Environmental Protection: Transactions of the Institution of Chemical Engineers, Part B*, 1994, **72**, pp.220-228.
252. Wang, Z.R., M.Y. Pan and J.C. Jiang. Experimental investigation of gas explosion in single vessel and connected vessels. *Journal of Loss Prevention in the Process Industries*, 2013, **26**(6), pp.1094-1099.
253. Willacy, S.K., H.N. Phylaktou, G.E. Andrews and M.C. Mkpadi. Partially filled interconnected vessel explosions: methane-air in the lean to stoichiometric range. *Journal of the Energy Institute*, 2006, **79**(3), pp.152-157.
254. You, M.-W., J.-C. Jiang, Y. Yu and Z.-R. Wang. Experimental study on effect of venting area on premixed flammable gas explosion venting in linked vessels. *Shiyan Liuti Lixue/Journal of Experiments in Fluid Mechanics*, 2011, **25**(5), pp.51-54.
255. Butlin, R.N. *A Review of Information on Experiments Concerning the Venting of Gas Explosions in Buildings*. Fire Research Note No. 1026. Fire Research Station, 1975.
256. Beyling, E. *Tests for Determining the Safety of Specially Protected Electric Motors and Apparatus Against Explosion from Firedamp (translated).* Glückauf 42: pp 97–99 and 129–138. 1906.
257. Rogstadkjernet, L. *Combustion of Gas in Closed, Interconnected Vessels: Pressure Piling*. Candidatus Scientiarum thesis, University of Bergen, 1993.
258. Singh, J. *Gas Explosions in Single and Compartmented Vessels*. PhD thesis, Imperial College London, 1978.
259. Singh, J. Gas explosions in compartmented vessels: pressure piling. *Chemical Engineering research and Design Transactions of the Institution of Chemical Engineers, Part A*, 1984, **62, No. 6**.
260. Brown, T.J.A. *Pressure piling in compartmented vessels*. Technical Report D/T 109. The British electrical and allied industrial research association, 1959.
261. Grice, C.S.W. and R.V. Wheeler. *Firedamp explosions within closed vessels: "pressure piling".* H.M. Stationary Office, 1929.
262. Gleim, E.J. and J.F. Marcy. *A study to determine factors causing pressure piling in testing explosion-proof enclosures.* US Bureau of Mines, Report of investigations 4904, 1952.
263. Molkov, V.V. Unified correlations for vent sizing of enclosures at atmospheric and elevated pressures. *Journal of Loss Prevention in the Process Industries*, 2001, **14**(6), pp.567-574.
264. Konishi, T. Experimental And CFD Investigations On Compartment Explosion With Ignition And Fuel Sources Located In Different Compartment. *In: Eighth International Symposium on Fire Safety Science*.
265. Mannan, S. Chapter 16 - Fire. *In:* S. Mannan, ed. *Lees' Loss Prevention in the Process Industries (Fourth Edition)*. Oxford: Butterworth-Heinemann, 2012, pp.1075-1366.
266. Hottel, H.C. and A.F. Sarofim. *Radiative transfer.* McGraw-Hill, 1967.
267. Leckner, B. Spectral and total emissivity of water vapor and carbon dioxide. *Combustion and Flame*, 1972, **19**(1), pp.33-48.
268. Howell, J.R., R. Siegel and P. Menguc. *Thermal Radiation Heat Transfer, 5th Edition.* Taylor & Francis, 2010.
269. Bejan, A. and A.D. Kraus. *Heat Transfer Handbook.* Wiley, 2003.
270. Cowley, L.T. OTI 92 596. Offshore Technology Information. *Current Fire Research: Experimental, Theoretical and Predictive Modelling Resources*. Steel Construction Institute OTI 92 598, OTI 92 598. HSE, 1992.

271. Cowley, L.T. OTI 92 597. Offshore Technology Information. *Behaviour of Oil and Gas Fires in the Presence of Confinement and Obstacles*. Steel Construction Institute OTI 92 597, OTI 92 597. HSE, 1992.
272. Cowley, L.T. and A.D. Johnson. OTI 92 596. Offshore Technology Information. *Oil and Gas Fires: Characteristics and Impact*. Steel Construction Institute OTI 92 596, OTI 92 596. HSE, 1992.
273. Chamberlain, G.A. Developments in Design Methods for Predicting Thermal Radiation from Flares. *Chemical Engineering Research and Design*, 1987, **65**(4), pp.299-309.
274. Chamberlain, G.A. Experimental study of large-scale compartment fires. *Process Safety and Environmental Protection: Transactions of the Institution of Chemical Engineers, Part B*, 1994, **72**(4), pp.211-219.
275. Chamberlain, G.A. Hazards posed by large-scale pool fires in offshore platforms. *In: Major Hazards II: Major Hazards Onshore and Offshore II*, 24-26 October, UMIST, Manchester, UK. Inst of Chemical Engineers, 1995, pp.213-226.
276. Chamberlain, G.A. Recent developments in evaluating and designing against offshore fire and explosion. *In: Proceedings of the 1997 7th International Offshore and Polar Engineering Conference. Part 4 (of 4), May 25, 1997 - May 30, 1997*, Honolulu, HI, USA. Int Soc of Offshore and Polar Engineerns (ISOPE), 1997, pp.807-814.
277. Chamberlain, G.A. Controlling Hydrocarbon Fires in Offshore Structures. *In: Offshore Technology Conference, May 6, 2002 - May 9, 2002*, Houston, TX, United states. Offshore Technology Conference, 2002, pp.1211-1218.
278. Chamberlain, G.A. Management of Large LNG Hazards. *In: 23rd World Gas Conference*, Amsterdam. 2006.
279. Chamberlain, G.A. Experimental Research on Fire Loading and its Implications. *In: Oil and Gas UK Piper 25 FABIG Session: Advances in Fire & Explosion Engineering*, Aberdeen, UK. FABIG, 2013.
280. Lowesmith, B.J., G. Hankinson, M.R. Acton and G. Chamberlain. An overview of the nature of hydrocarbon jet fire hazards in the oil and gas industry and a simplified approach to assessing the hazards. *Process Safety and Environmental Protection*, 2007, **85**(3 B), pp.207-220.
281. Wickens, M.J. and B.J. Lowesmith. Fire and explosion hazards—large scale experiments to assess and mitigate their effects. *In: Institution of Gas Engineers, Eastern Section.* 1993.
282. Eisenberg, N.A., C.J. Lynch and R.J. Breeding. *Vulnerability model: a simulation system for assessing damage resulting from marine spills*. CG-D-137-75. Department of Transportation, United States Coast Guard, Office of Research and Development, 1975.
283. Hymes, I., W. Boydell and B. Prescott. *Thermal Radiation: Physiological and Pathological Effects.* Institution of Chemical Engineers, 1996.
284. Rew, P.J. *LD_{50} equivalent for the effect of thermal radiation on humans*. CRR 129/1977. HSE, 1997.
285. Babrauskas, V. Ignition of Wood: A Review of the State of the Art. *In: Interflam 2001: 9th International Fire science and Engineering Conference*, 17-19 September, Edinburgh, Scotland. Interscience Communications Limited, 2001.
286. Babrauskas, V. Charring rate of wood as a tool for fire investigations. *Fire Safety Journal*, 2005, **40**(6), pp.528-554.
287. Babrauskas, V. and J. Krasny. *Fire Behaviour of Upholstered Furniture.* NBS Monograph 173. Gaithersburg, USA: National Engineering Laboratory Center for Fire Research, National Bureau of Standards, US Department of Commerce, 1985.
288. Delichatsios, M., B. Paroz and A. Bhargava. Flammability properties for charring materials. *Fire Safety Journal*, 2003, **38**(3), pp.219-228.

289. Goynes, W.R. and B.J. Trask. Effects of Heat on Structures of Cotton, Polyester, and Wool Fibers in a Triblended Fabric With and Without Flame Retardant. *Textile Research Journal*, 1987, **57**(9), pp.549-554.
290. Gratkowski, M.T., N.A. Dembsey and C.L. Beyler. Radiant smoldering ignition of plywood. *Fire Safety Journal*, 2006, **41**(6), pp.427-443.
291. Hilado, C.J. Combustion of Polymers. *Chemische Technik*, 1972, **2**(4), pp.232-238.
292. Hilado, C.J., K.E. Atkins and J.A. Fisher. Fire Studies of Furniture Materials. *Journal of Fire and Flammability/Consumer Product Flammability, Supplement*, 1975, **2**, pp.154-169.
293. Hilado, C.J. and D.P. Brauer. Ignitability by Radiant Heat of Furniture Upholstery Fabrics. 1978, **5**(4), pp.217-237.
294. Hilado, C.J., H.J. Cumming and R.M. Murphy. Flash-Fire Propensity of Plastics and Elastomers. *Journal of Elastomers and Plastics*, 1979, **11**(3), pp.239-243.
295. Hilado, C.J., H.J. Cumming and R.M. Murphy. Flash-Fire Propensity of Pyrolysis Gases from Materials. *SAMPE Quarterly*, 1979, **10**(2), pp.29-31.
296. Hilado, C.J. and P.A. Huttlinger. Fire Behavior of Building Contents: A Bibliography - 2. *Journal of consumer product flammability*, 1980, **7**(3), pp.203-209.
297. Hilado, C.J. and P.A. Huttlinger. Ignition of Fabric-Cushion Systems. *Journal of Coated Fabrics*, 1981, **11**(2), pp.63-72.
298. Hilado, C.J. and K.L. Kosola. Laboratory Technique for Determining Ignition Temperatures of Materials. *Fire Technology*, 1978, **14**(4), pp.291-296.
299. Hilado, C.J. and R.M. Murphy. Screening Materials for Ignitability. *Modern Plastics*, 1978, **55**(10), pp.52, 54-52, 54.
300. Hopkins Jr, D. and J.G. Quintiere. Material fire properties and predictions for thermoplastics. *Fire Safety Journal*, 1996, **26**(3), pp.241-268.
301. Horrocks, A.R. An Introduction to the Burning Behaviour of Cellulosic Fibres. *Journal of the Society of Dyers and Colourists*, 1983, **99**(7-8), pp.191-197.
302. Horrocks, A.R. and S.C. Anand. *Handbook of Technical Textiles.* Cambridge, UK: Woodhead Publishing Ltd., 2011.
303. Lawson, D.I. and D.L. Simms. Ignition of wood by radiation. *British Journal of Applied Physics*, 1952, **3**(12), p.394.
304. Lawson, D.I., P.H. Thomas and D.L. Simms. *The Thermal Properties of Skin*. F.R. Note No. 224/1955. Fire Research Station, 1955.
305. Leung, E.H. and D.X. Halliday. "Flashburning" - Interpreting the presence of heat damage to a suspect's clothing and footwear in the investigation of fires. *Science & Justice*, 2010, **50**(4), pp.187-191.
306. Madrzykowski, D. and D.W. Stroup. Flammability Hazard of Materials. *In: Fire Protection Handbook*. Maryland: NFPA, 2008.
307. McLean, A.D. Burns and Military Clothing. *Journal of the Royal Army Medical Corps*, 2001, **Vol 147**, pp.97-106.
308. Mehta, A.K. and F. Wong. *Measurement of Flammability and Burn Potential of Fabrics*. NSF-RA-E-73-191. Fuels Research Laboratory, Massachusetts Institute of Technology, 1973.
309. Morse, H.L., J.G. Thompson, K.J. Clark, K.A. Green and C.B. Moyer. *Analysis of the Thermal Response of Protective Fabrics*. AD-759 525. California, USA: Aerotherm Division/Acurex Corporation, 1973.
310. Mouritz, A.P. and A.G. Gibson. *Fire Properties of Polymer Composite Materials.* Physica-Verlag, 2007.
311. Moysey, E.B. and W.E. Muir. Pilot ignition of building materials by radiation. *Fire Technology*, 1968, **4**(1), pp.46-50.
312. Naveda, O.A. *Study of the Actual Ignition Sources of Clothing*. MSc thesis, Georgia Institute of Technology, 1974.
313. Ndubizu, C.C. and P. Durbetaki. Modeling radiative ignition of fabrics in air. *Fire Safety Journal*, 1978, **1**(4–5), pp.281-290.

314. Schroeder, R.A. *Post-fire analysis of construction materials*. 9966561 thesis, University of California, Berkeley, 1999.
315. Schroeder, R.A. and R.B. Williamson. Post-fire analysis of construction materials—gypsum wallboard. *Fire and Materials*, 2000, **24**(4), pp.167-177.
316. Schroeder, R.A. and R.B. Williamson. Application of Materials Science to Fire Investigation. *In: Fire and Materials 2001: 7th International Conference and Exhibition*, 22-24 January, San Antonio, Texas. Interscience Communications Limited, 2001.
317. Scott, R.A. *Textiles for Protection.* Elsevier Science, 2005.
318. Shafizadeh, F. Pyrolysis and Combustion of Cellulosic Materials. *In:* L.W. Melville and R.S. Tipson, eds. *Advances in Carbohydrate Chemistry*. Academic Press, 1968, pp.419-474.
319. Simms, D.L. Experiments on the Ignition of Cellulosic Materials by Radiation. *Fire Research Notes 423*, 1960.
320. Simms, D.L. Ignition of cellulosic materials by radiation. *Combustion and Flame*, 1960, **4**(0), pp.293-300.
321. Simms, D.L. Experiments on the ignition on celluslosic materials by thermal radiation. *Combustion and Flame*, 1961, **5**(0), pp.369-375.
322. Simms, D.L. Damage to cellulosic solids by thermal radiation. *Combustion and Flame*, 1962, **6**(0), pp.303-318.
323. Simms, D.L. On the pilot ignition of wood by radiation. *Combustion and Flame*, 1963, **7**(0), pp.253-261.
324. Simms, D.L. and M. Law. The ignition of wet and dry wood by radiation. *Combustion and Flame*, 1967, **11**(5), pp.377-388.
325. Stoll, A.M. and M.A. Chianta. *Heat Transfer Through Fabrics*. NADC-MR-7017. Pennsylvania, USA: Naval Air Development Center, 1970.
326. Stoll, A.M. and M.A. Chianta. Heat Transfer Through Fabrics as Related to Thermal Injury. *Transactions of the New York Academy of Sciences*, 1971, **33**(7 Series II), pp.649-670.
327. Stoll, A.M., M.A. Chianta and L.R. Munroe. Flame-Contact Studies. *Journal of Heat Transfer*, 1964, **86**(3), pp.449-456.
328. Stoll, A.M., M.A. Chianta and J.R. Piergallini. Prediction of threshold pain skin temperature from thermal properties of materials in contact. *Aviat Space Environ Med*, 1982, **53**(12), pp.1220-3.
329. Stoll, A.M. and L.C. Greene. *Relationship between pain and tissue damage due to thermal radiation.* 1959.
330. Theuns, E., B. Merci, J. Vierendeels and P. Vandevelde. Critical evaluation of an integral model for the pyrolysis of charring materials. *Fire Safety Journal*, 2005, **40**(2), pp.121-140.
331. Thomas, P.H. and D.L. Simms. *Thermal Damage to Solids by Radiation and Thermal Decomposition*. F.R. Note No. 331/1958. Fire Research Station, 1955.
332. Thomas, P.H. and D.L. Simms. *Thermal Damage to Fabrics at High Intensities of Radiation*. F.R. Note No. 392/1959. Fire Research Station, 1959.
333. Thomas, P.H., D.L. Simms and M. Law. *The Rate of Burning of Wood*. F.R. Note No. 657/1967. Fire Research Station, 1967.
334. Torvi, D.A. *Heat Transfer in Thin Fibrous Materials Under High Heat Flux Conditions*. PhD thesis, University of Alberta, 1997.
335. Torvi, D.A. and J.D. Dale. Effects of Variations in Thermal Properties on the Performance of Flame Resistant Fabrics for Flash Fires. *Textile Research Journal*, 1998, **68**(11), pp.787-796.
336. Torvi, D.A. and J.D. Dale. Heat Transfer in Thin Fibrous Materials Under High Heat Flux. *Fire Technology*, 1999, **35**(3), pp.210-231.
337. Torvi, D.A. and G.V. Hadjisophocleous. Institute for Research into Construction. *Research Needs in Protective Clothing for Fire Fighters*. Internal Report No. 751. Canada's Construction Technology Centre, National Research Council, 1997.

338. Wichman, I.S. A Review of the Literature of Material flammability, combustion, toxicity and fire hazard in transportation. *Progress in Energy and Combustion Science*, 2003, **29**(3), pp.247-299.
339. Yang, L., X. Chen, X. Zhou and W. Fan. The pyrolysis and ignition of charring materials under an external heat flux. *Combustion and Flame*, 2003, **133**(4), pp.407-413.
340. Hockey, S.M. and P.J. Rew. *Review of Human Response to Thermal Radiation*. CRR 97/1996. HSE, 1996.
341. Backer, S., G.S. Tesoro, T.Y. Toong and N.A. Moussa. *Textile Fabric Flammability.* MIT Press, 2003.
342. Babrauskas, V. Ignition of Wood: A Review of the State of the Art. *Journal of Fire Protection Engineering*, 2002, **12**(3), pp.163-189.
343. Burrell, G. and J. Hare. *Review of HSE Building Ignition Criteria*. HSL/2006/33. HSL, 2006.
344. Technica Ltd. *Manual of Industrial Hazard Assessment Techniques*. Office of Environmental and Scientific Affairs, World Bank, 1988.
345. OGP. *Risk Assessment Data Directory: Vulnerability of Humans*. Report No. 434 – 14.1. International Association of Oil & Gas Producers, 2010.
346. Daycock, J.H. and P.J. Rew. *Thermal radiation criteria for vulnerable populations*. CRR 285/2000. HSE, 2000.
347. Rew, P.J. and I.P. McKay. Derivation of Fatality Criteria for Humans Exposed to Thermal Radiation. *In: Advances in Safety & Reliability: proceedings of the ESREL'97 International Conference on Safety and Reliability*, June 1997, Lisbon, Portugal. 1997.
348. Rew, P.J., H. Spencer and T. Maddison. The Sensitivity of Risk Assessment of Flash Fire Events to Modelling Assumptions. *In: Hazards XIV: Cost Effective Safety*, 10-12 November, UMIST, Manchester, UK. 1998.
349. Spearpoint, M.J. and J.G. Quintiere. Predicting the piloted ignition of wood in the cone calorimeter using an integral model — effect of species, grain orientation and heat flux. *Fire Safety Journal*, 2001, **36**(4), pp.391-415.
350. Thunman, H. and B. Leckner. Thermal conductivity of wood—models for different stages of combustion. *Biomass and Bioenergy*, 2002, **23**(1), pp.47-54.
351. Wesson, H.R., J.R. Welker and C.M. Sliepcevich. The piloted ignition of wood by thermal radiation. *Combustion and Flame*, 1971, **16**(3), pp.303-310.
352. Shen, D.K. and M.X. Fang. Ignition of Wood-Based Materials by Thermal Radiation. *International Journal on Engineering Performance-Based Fire Codes*, 2006, **Volume 8**(Number 2), pp.pp. 69-83.
353. Shen, D.K., M.X. Fang, Z.Y. Luo and K.F. Cen. Thermal Degradation and Ignition of Wood by Thermal Radiation. *International Association for Fire Safety Science*, 2007.
354. Staggs, J.E., H.N. Phylaktou and R.E. McCreadie. The Effect of Paint on the Ignition Resistance of Plywood and Chipboard. *Fire Safety Science, Proceedings of the 7th International Symposium*, 2003.
355. Wąs, J. Identification of thermally changed fibres. *Forensic Science International*, 1997, **85**(1), pp.51-63.
356. Wąs-Gubala, J. and W. Krauß. Textile damage caused by vapour cloud explosions. *Science & Justice*, 2004, **44**(4), pp.209-215.
357. Wąs-Gubala, J. and W. Krauß. Damage caused to fibres by the action of two types of heat. *Forensic Science International*, 2006, **159**(2-3), pp.119-126.
358. Wąs-Gubała, J. and W. Krauß. Damage caused to fibres by vapour cloud explosions. *Forensic Science International*, 2004, **141**(2–3), pp.77-83.
359. Devon & Somerset Fire & Rescue Service. *Facts and Figures about Arson* [online]. 2014. [Accessed]. Available from: http://www.dsfire.gov.uk/YourSafety/Arson/FactsAndFigures/Index.cfm?siteCategoryId=4&T1ID=40&T2ID=126.

360. Wąs-Gubala, J. and W. Krauß. Damage caused to fibres by vapour cloud explosions. *Forensic Science International*, 2004, **141**(2-3), pp.77-83.
361. Bounds, W.L. *Design of Blast-resistant Buildings in Petrochemical Facilities: Second Edition.* American Society of Civil Engineers, 2010.
362. Cormie, D., G.C. Mays and P.D. Smith. *Blast Effects on Buildings.* 2nd ed. London: Thomas Telford, 2009.
363. Dusenberry, D.O. *Handbook for Blast Resistant Design of Buildings.* Wiley, 2010.
364. Harris, R.J., M.R. Marshall and D.J. Moppett. The Response of Glass Windows to Explosion Pressures. *In: IChemE Symposium No. 49*, 1977.
365. Mainstone, R.J. *The Breakage of Glass Windows by Gas Explosions*. 26/71. Building Research Station.
366. West, H.W.H. *A Note on the the Resistance of Glass Windows to Pressures Generated by Gaseous Explosions*. Fourth Symposium on Loadbearing Brickwork. British Ceramic Research Association, 1971.
367. West, H.W.H. *The Resistance of Glass Windows to Pressures Generated by Gaseous Explosions*. Technical Note No. 192. The British Ceramic Research Association, 1972.
368. De Matteis, G., I. Langone and F.M. Mazzolani. Structural integrity of buildings with precast load bearing walls under gas explosion. *In:* C. Schauer*, et al.*, eds. *Improvement of Buildings' Structural Quality by New Technologies: Proceedings of the Final Conference of COST Action C12, 20-22 January 2005, Innsbruck, Austria*. Routledge, 2005, pp.91 - 104.
369. Johnson, D.M., R.P. Cleaver and M.R. Acton. *Blast and Fire Engineering for Topside Structures: Confined Vented Explosions*. Work Package No. BL2. Midlands Research Station, 1981.
370. Na'inna, A.M., H.N. Phylaktou and G.E. Andrews. Acceleration of Flames in Tube Explosions with Two Obstacles as a Function of the Obstacle Separation Distance: The Influence of Mixture Reactivity. *In: Proc. of the Seventh International Seminar on Fire & explosion Hazards (ISFEH7)*, Providence, USA. 2013, pp.627-636.
371. Na'inna, A.M., H.N. Phylaktou and G.E. Andrews. The acceleration of flames in tube explosions with two obstacles as a function of the obstacle separation distance. *Journal of Loss Prevention in the Process Industries*, 2013, **26**(6), pp.1597-1603.
372. Oh, K.H., H. Kim, J.B. Kim and S.E. Lee. A study on the obstacle-induced variation of the gas explosion characteristics. *Journal of Loss Prevention in the Process Industries*, 2001, **14**(6), pp.597-602.
373. Park, D.J., A.R. Green and Y.C. Chen. Analysis of Local Flame Propagation in Gas Explosions with Multiple Obstacles. *In: 15th Australasian Fluid Mechanics Conference*, 13-17 December 2004, Sydney, Australia. 2004.
374. Park, D.J., A.R. Green, Y.S. Lee and Y.-C. Chen. Experimental studies on interactions between a freely propagating flame and single obstacles in a rectangular confinement. *Combustion and Flame*, 2007, **150**(1–2), pp.27-39.
375. Park, D.J., Y.S. Lee and A.R. Green. Experiments on the effects of multiple obstacles in vented explosion chambers. *Journal of Hazardous Materials*, 2008, **153**(1–2), pp.340-350.
376. Pritchard, D.K., D. Hedley and N.K. Webber. *Effect of Obstacles on Flame Acceleration and Explosion Development*. GE/97/02. HSL, 2002.
377. Steel Construction Institute. *Buncefield Explosion Mechanism Phase 1 (Volumes 1 and 2)*. Research Report 718. HSE, 2009.
378. van Wingerden, C.J.M. and J.P. Zeeuwen. Flame propagation in the presence of repeated obstacles: Influence of gas reactivity and degree of confinement. *Journal of Hazardous Materials*, 1983, **8**(2), pp.139-156.

379. Di Sarli, V., A. Di Benedetto and G. Russo. Using Large Eddy Simulation for understanding vented gas explosions in the presence of obstacles. *Journal of Hazardous Materials*, 2009, **169**(1–3), pp.435-442.
380. Gamezo, V.N., T. Ogawa and E.S. Oran. Flame acceleration and DDT in channels with obstacles: Effect of obstacle spacing. *Combustion and Flame*, 2008, **155**(1-2), pp.302-315.
381. Gubba, S.R., S.S. Ibrahim, W. Malalasekera and A.R. Masri. Measurements and LES calculations of turbulent premixed flame propagation past repeated obstacles. *Combustion and Flame*, 2011, **158**(12), pp.2465-2481.
382. Hall, R., A.R. Masri, P. Yaroshchyk and S.S. Ibrahim. Effects of position and frequency of obstacles on turbulent premixed propagating flames. *Combustion and Flame*, 2009, **156**(2), pp.439-446.
383. Hjertager, B.H., K. Furhe and M. Bjorkhaug. *Effects of Concentration by Obstacles on Large-Scale Methane-Air and Propane-Air Explosions*. Bergen: Chr. Michelson Institute, 1984.
384. Molkov, V., V. Agafonov and S. Aleksandrov. Deflagration in a vented vessel with internal obstacles. *Combustion, Explosion, and Shock Waves*, 1997, **33**(4), pp.418-424.
385. Park, D.J., Y.S. Lee and A.R. Green. Prediction for vented explosions in chambers with multiple obstacles. *Journal of Hazardous Materials*, 2008, **155**(1–2), pp.183-192.
386. Tomlin, G.B. and D.M. Johnson. A Large Scale Study of the Venting of Confined Explosions into Unobstructed and Congested Flammable Vapor Clouds. *In: Seventh International Seminar on Fire and Explosion Hazards (ISFEH)*, 5 – 10 May 2013, Providence, RI, USA. 2013.
387. Cronin, P. and M.J. Wickens. *A Large Scale Experimental Study of the Conditions Required for Sustained High Speed Flame Propagation in a Flammable Vapour Cloud*. MRS I 4348. Midlands Research Station, 1986.
388. Willacy, S. *Homogeneous and Stratified Vented Gas Explosions*. PhD thesis, University of Leeds, 2008.
389. Admirals Storage. *How much space do I need* [online]. [Accessed]. Available from: http://www.admiralstorage.co.uk/how%20much%20space.html.
390. BBC news. *'Shoebox homes' become the UK norm* [online]. 2011. Available from: http://www.bbc.co.uk/news/uk-14916580.
391. Drury, A., J. Watson, R. Broomfield, D. Levitt and R. Tetlow. Mayor of London. *Housing Space Standards*. HATC Ltd, 2006.
392. Greater London Authority. Mayor of London. *Housing: supplementary planning guidance*. 2012.
393. International Organization for Standardization. *ISO 6184-1:1985 Explosion protection systems -- Part 1: Determination of explosion indices of combustible dusts in air*. Geneva, 1985.
394. International Organization for Standardization. *ISO 6184-2:1985 Explosion protection systems -- Part 2: Determination of explosion indices of combustible gases in air*. Geneva, 1985.
395. British Standards Institution. *BS 5500:1997 Specification for unfired fusion welded pressure vessels*. London, 1997.
396. Buckland, I.G., R.N. Butlin and D.J. Annable. *Gas Explosions in Buildings: Part VI. Remotely Controlled Gas Sampling Probe and Closure Valves for a Gas Explosion Chamber*. Fire Research Note No. 1052. Fire Research station, 1976.
397. Phylaktou, H.N., C.L. Gardner and G.E. Andrews. Flame Speed Measurements in Dust Explosions. *In:* D. Bradley, G. Makhviladze and V. Molkov, eds. *Proceedings of the Sixth International Seminar on Fire and Explosion Hazards*, 11-16 April 2010, Weetwood Hall Conference Centre, Leeds, UK. Leeds Research Publishing, 2010.

398. British Standards Institution. *BS EN ISO 17776:2002 Petroleum and natural gas industries — Offshore production installations — Guidelines on tools and techniques for hazard identification and risk assessment*. London, 2002.
399. Lee, F.P. *Lees' Loss Prevention in the Process Industries: Hazard Identification, Assessment and Control.* London: Butterworth-Heinemann, 1980.
400. Johnson, D.M., R.P. Cleaver and M.R. Acton. *Blast and Fire Engineering for Topside Structures: Explosions in Highly Congested Volumes*. Work Package No. BL3. Midlands Research Station, 1981.
401. Selby, C.A. and B.A. Burgan. *Blast and Fire Engineering Project for Topside Structures Phase 2, Final Report*. Steel Construction Institute, 1998.
402. Health and Safety Executive. Offshore Technology Report. *The Repeatability of Large Scale Explosion Experiments*. OTO 1999 042. HSE, 1999.
403. Johnson, D.M. *Repeatability of Large-Scale Explosions*. British Gas Research and Technology (MRS), (Confidential Report), 1998.
404. Field, P. and M.S. Skippon. *Personal Communication - observational notes on large-scale explosion tests conducted in the FRS explosion chamber*, 1983.
405. Chapter 17 - Explosion. *In:* S. Mannan, ed. *Lees' Loss Prevention in the Process Industries (Fourth Edition)*. Oxford: Butterworth-Heinemann, 2012, pp.1367-1678.
406. Na'inna, A.M., H.N. Phylaktou and G.E. Andrews. Effects of Obstacle Separation Distance on Gas Explosions: The Influence of Obstacle Blockage Ratio. *Procedia Engineering*, 2014, **84**(0), pp.306-319.
407. Baines, W.D. and E.G. Peterson. Investigation of flow through screens. *American Society of Mechanical Engineers - Transactions*, 1951, **73**(5), pp.467-477.
408. Sazonov, V.A., Z.R. Ismagilov and N.A. Prokudina. Catalytic combustion of lean methane–air mixtures. *Catalysis Today*, 1999, **47**(1–4), pp.149-153.
409. Barbosa, A.L., J. Herguido and J. Santamaria. Methane combustion over unsupported iron oxide catalysts. *Catalysis Today*, 2001, **64**(1–2), pp.43-50.
410. Babrauskas, V. *Ignition Handbook.* Issaquah, USA: Fire Science Publishers, 2003.

APPENDIX A

Operational Procedures

Rig A

1 Ensure that operating personnel are aware of their duties and location during the test.
2 Place marker boards as required
3 Secure vent covers.
4 Ensure that the air supply for pneumatic systems is turned on.
5 Ensure that the natural gas supply is connected correctly and that the manually operated gas flow valve and pneumatic isolation valve on the gas supply line to the rig are closed.
6 Check operation of instrumentation.
7 On satisfactory completion of the above items, ensure that personnel in the area around the test enclosure are aware that testing of the main enclosure functions is about to commence.
8 The operation of the fan shall be checked.
9 Operation of the pneumatically operated rig gas isolation, purge and gas inlet valves shall be checked.
10 Check operation of the gas sampling system.
11 After ensuring the area around them is clear, the operation of the explosion chamber purge valves shall be checked for satisfactory opening and closing.
12 Check the operation of the ignition spark.
13 Calibrate gas analyser and check computer timing.
14 Conduct a visual check of the surrounding area outside the main test zone.
15 Ensure that all personnel are evacuated from the exclusion zone and that all barriers leading to the exclusion zone are closed. Carry out a further visual check on the area outside the main test zone.
16 Ensure that all personnel associated with the test are aware of their required location for the filling and firing sequences of the test.
17 Ensure that all test rig valves are closed.
18 Check that the explosion chamber purge valves are closed.
19 Open the manual isolation valves on the high pressure natural gas supply.

20 The needle valve on the gas supply (located immediately downstream of the gas supply shall be opened by a maximum ¼ turn to ensure the gas enters the system at a relatively slow rate.

21 When the Engineer in charge is satisfied that all preparations are complete, contact Test Control and request clearance to proceed further.

22 When clearance to proceed has been granted, contact the test control room and ask for the pneumatically operated rig gas isolation valve to be opened.

23 Open the pneumatically operated gas and air inlet valves.

24 Turn on the fan and gas supply to the mixing system and adjust flow using flow valves and rotameters.

25 During filling, monitor the site and ensure that personnel remain at their designated positions.

26 As filling proceeds; the Engineer-in-charge shall, as appropriate, notify Test Control that the test is ready to proceed at 10 minutes prior to the test. Three long klaxon blasts will sound and a spoken warning will be issued over the radio system.

27 When the gas/air mixture is at its desired concentration the Engineer-in-charge shall notify Test Control.

28 Shut-off the gas supply to the rig by closing the pneumatic gas inlet and gas isolation valves.

29 Shut off the fan and close pneumatic valves on air supply.

30 Open the gas purge valve to depressurise the gas supply line and then close the gas purge valve.

31 Raise the gas sampling system.

32 Gain clearance from Test Control to proceed with the test. Two long klaxon blasts will sound 1 minute before the test and a spoken warning will be given. Five short klaxon blasts will sound 30 s before the test followed by a countdown from 10 to ignition.

33 If the test fails to ignite. The Engineer-in-charge shall ensure that all personnel remain at their designated locations unless instructed to the contrary, whilst an assessment of the cause of failure is conducted. The enclosure shall be made safe by the following method:

Open the explosion chamber purge valves and allow the gas/air mixture to vent to atmosphere. The Engineer-in-charge shall ensure that the gas concentration is less than 20% of the lower explosion limit prior to approaching the explosion chamber. Any repairs that can be safely

carried out may be undertaken and the filling sequence may then be re-initiated.

34 Following firing or aborting the test, the Engineer-in-charge shall inform Test Control that the test is complete or aborted as appropriate.

35 One long klaxon blast will be given and the “all clear” will be given over the radio system.

36 The Engineer-in-charge shall approach the area; ensure that any fires are extinguished and that the rig enclosure is safe. All other test personnel shall remain at their designated positions until the area has been declared safe.

37 The manual valves on the gas supply line shall be closed. The gas filling line to the enclosure shall be vented.

38 The Engineer-in-charge shall notify Test Control that the area is safe and open the gates to the exclusion zone.

39 If, as a result of the explosion, the rig is in a damaged condition and may be considered dangerous to personnel, warning signs should be issued advising as such and action taken to make the rig safe.

40 Check data results.

Rigs B and C (premixed purge and recirculation filling)

1 Ensure that operating personnel are aware of their duties and location during the test.
2 Fit polythene tube over gas recirculation ductwork.
3 Place congestion (furniture/obstacles) as required
4 Secure vent cover.
5 Ensure that the nitrogen bottles for pneumatic systems are turned on.
6 Check operation of instrumentation.
7 Calibrate gas analyser using test gas.
8 Ensure that the methane/ propane supply is connected correctly and that the manually operated gas flow valve and pneumatic isolation valve on the gas supply line to the rig are closed.
9 On satisfactory completion of the above items, ensure that personnel in the area around the test enclosure are aware that testing of the main enclosure functions is about to commence.
10 After ensuring the area around them is clear, the operation of the explosion chamber flap valves and gas recirculation/purge system blast gate dampers shall be checked for satisfactory opening and closing.
11 The operation of the fan shall be checked.
12 Operation of the pneumatically operated rig gas isolation, purge and gas inlet valves shall be checked.
13 Check the operation of the ignition spark.
14 Calibrate gas analyser and check computer timing.
15 Conduct a visual check of the surrounding area outside the Spadeadam Site Boundary (CCTV cameras) and inform the RAF and Forestry Commission of the test.
16 Ensure that all personnel are evacuated from the exclusion zone and that all barriers leading to the exclusion zone are closed. Carry out a further visual check on the area outside the Spadeadam Site Boundary.
17 Ensure that all personnel associated with the test are aware of their required location for the filling and firing sequences of the test.
18 Ensure that all test rig valves are closed.
19 Open the explosion chamber flap valves.
20 Turn the fan on and check that it is operating.
21 Open the manual isolation valves on the high pressure methane or propane gas supply.

22 The needle valve on the gas supply (located immediately downstream of the gas supply shall be opened by a maximum ¼ turn to ensure the gas enters the gas recirculation system at a relatively slow rate.

23 When the Engineer in charge is satisfied that all preparations are complete, contact Test Control and request clearance to proceed further.

24 Test Control shall obtain clearance to test from RAF Range Controller and confirm this to the Engineer-in-charge.

25 When clearance to proceed has been granted, contact the test control room and ask for the pneumatically operated rig gas isolation valve to be opened.

26 Open the pneumatically operated gas inlet valve.

27 During filling, monitor the site and ensure that personnel remain at their designated positions.

28 The required gas concentration will be achieved by regulating the gas flow valve and/or opening and closing the pneumatic gas valve. The air flow may be regulated by controlling the fan speed.

29 As filling proceeds; the Engineer-in-charge shall, as appropriate, notify Test Control that the test is ready to proceed at 15 minutes and 5 minute prior to the test. These will be broadcast over the Spadeadam site radio system and acknowledged by Test Control.

30 When the gas/air mixture is at its desired concentration and weather conditions are correct for the test, the Engineer-in-charge shall allow the attendees to approach the viewing area.

31 Ensure that all personnel at the viewing area fit hearing protection before commencing further, a two minute warning of firing shall be given over the Spadeadam Site radio and Test Control will sound the alarm 3 times.

32 Shut-off the gas supply to the rig by closing the pneumatic gas inlet and gas isolation valves.

33 Close the explosion chamber flap valves and turn off the fan.

34 Open the gas purge valve to depressurise the gas supply line and then close the gas purge valve.

35 Open the recirculation system blast gate dampers and turn on the fan for 15 seconds. Turn off the fan.

36 Gain clearance from Test Control to proceed with the test.

37 A five second countdown shall be given over the Spadeadam Site radio and upon ‘fire’ ignition will initiated.

38 If the test fails to ignite. The Engineer-in-charge shall ensure that all personnel remain at their designated locations unless instructed to the contrary,

whilst an assessment of the cause of failure is conducted. The enclosure shall be made safe by the following method:

With the fan on, the recirculation system purge valves and the explosion chamber flap valves shall be opened to allow purging of the enclosure with air. The Engineer-in-charge shall ensure that the gas concentration is less than 20% of the lower explosion limit prior to approaching the explosion chamber. Any repairs that can be safely carried out may be undertaken and the filling sequence may then be re-initiated.

39 Following firing or aborting the test, the Engineer-in-charge shall inform Test Control that the test is complete or aborted as appropriate.

40 The Engineer-in-charge shall approach the area; ensure that any fires are extinguished and that the rig enclosure is safe. All other test personnel shall remain at their designated positions until the area has been declared safe.

41 The manual valves on the gas supply line shall be closed. The gas filling line to the enclosure shall be vented.

42 The Engineer-in-charge shall notify Test Control that the area is safe and open the gates to the exclusion zone.

43 If, as a result of the explosion, the rig is in a damaged condition and may be considered dangerous to personnel, warning signs should be issued advising as such and action taken to make the rig safe.

44 The Engineer-in-charge shall ensure that any buildings or cabins within the exclusion zone damaged during tests are inspected and any necessary actions undertaken such that they do not present a hazard to personnel.

45 The attendees can leave the exclusion zone.

46 Check data results.

Rigs B and C (purge filling)

1 Ensure that operating personnel are aware of their duties and location during the test.
2 Place marker boards as required.
3 Secure vent cover.
4 Ensure that the nitrogen bottles for pneumatic systems are turned on.
5 Ensure that the methane/ propane supply is connected correctly and that the manually operated gas flow valve and pneumatic isolation valve on the gas supply line to the rig are closed.
6 Check operation of instrumentation.
7 On satisfactory completion of the above items, ensure that personnel in the area around the test enclosure are aware that testing of the main enclosure functions is about to commence.
8 Operation of the pneumatically operated rig gas isolation, purge and gas inlet valves shall be checked.
9 After ensuring the area around them is clear, the operation of the explosion chamber flap valves shall be checked for satisfactory opening and closing.
10 Check the operation of the ignition spark.
11 Calibrate gas analyser and check computer timing.
12 Conduct a visual check of the surrounding area outside the Spadeadam Site Boundary (CCTV cameras) and inform the RAF and Forestry Commission of the test.
13 Ensure that all personnel are evacuated from the exclusion zone and that all barriers leading to the exclusion zone are closed. Carry out a further visual check on the area outside the Spadeadam Site Boundary.
14 Ensure that all personnel associated with the test are aware of their required location for the filling and firing sequences of the test.
15 Ensure that all test rig valves are closed.
47 Check that the explosion chamber flap valves are closed.
16 Open the manual isolation valves on the high pressure methane or propane gas supply.
17 The needle valve on the gas supply (located immediately downstream of the gas supply shall be opened by a maximum ¼ turn to ensure the gas enters the system at a relatively slow rate.
18 When the Engineer in charge is satisfied that all preparations are complete, contact Test Control and request clearance to proceed further.

19 Test Control shall obtain clearance to test from RAF Range Controller and confirm this to the Engineer-in-charge.

20 When clearance to proceed has been granted, contact the test control room and ask for the pneumatically operated rig gas isolation valve to be opened.

21 Open the pneumatically operated gas inlet valve.

48 The required gas concentration will be achieved by regulating the gas flow valve and/or opening and closing the pneumatic gas valve.

22 During filling, monitor the site and ensure that personnel remain at their designated positions.

23 As filling proceeds; the Engineer-in-charge shall, as appropriate, notify Test Control that the test is ready to proceed at 15 minutes and 5 minute prior to the test. These will be broadcast over the Spadeadam site radio system and acknowledged by Test Control.

24 When the gas/air mixture is at its desired concentration and weather conditions are correct for the test, the Engineer-in-charge shall allow the attendees to approach the viewing area.

25 Ensure that all personnel at the viewing area fit hearing protection before commencing further, a two minute warning of firing shall be given over the Spadeadam Site radio and Test Control will sound the alarm 3 times.

26 Shut-off the gas supply to the rig by closing the pneumatic gas inlet and gas isolation valves.

27 Open the gas purge valve to depressurise the gas supply line and then close the gas purge valve.

28 Gain clearance from Test Control to proceed with the test.

29 A five second countdown shall be given over the Spadeadam Site radio and upon ‘fire’ ignition will initiated.

30 If the test fails to ignite. The Engineer-in-charge shall ensure that all personnel remain at their designated locations unless instructed to the contrary, whilst an assessment of the cause of failure is conducted. The enclosure shall be made safe by the following method:

Open the explosion flap valves and allow the gas/air mixture to vent to atmosphere. The Engineer-in-charge shall ensure that the gas concentration is less than 20% of the lower explosion limit prior to approaching the explosion chamber. Any repairs that can be safely carried out may be undertaken and the filling sequence may then be re-initiated.

31 Following firing or aborting the test, the Engineer-in-charge shall inform Test Control that the test is complete or aborted as appropriate.

32 The Engineer-in-charge shall approach the area; ensure that any fires are extinguished and that the rig enclosure is safe. All other test personnel shall remain at their designated positions until the area has been declared safe.

33 The manual valves on the gas supply line shall be closed. The gas filling line to the enclosure shall be vented.

34 The Engineer-in-charge shall notify Test Control that the area is safe and open the gates to the exclusion zone.

35 If, as a result of the explosion, the rig is in a damaged condition and may be considered dangerous to personnel, warning signs should be issued advising such and action taken to make the rig safe.

36 The Engineer-in-charge shall ensure that any buildings or cabins within the exclusion zone damaged during tests are inspected and any necessary actions undertaken such that they do not present a hazard to personnel.

37 The attendees can leave the exclusion zone.

38 Check data results.

Rig D

1 Undertake safety checks, power on the data logging system and the gas mixing system, load the Wavecap software.
2 Check all instrumentation is functioning correctly.
3 Record the ambient temperature, pressure and humidity.
4 Close the explosion vessel door (using a non-asbestos gasket), and tighten all bolts (sequence of opposites) using the 4R Torque Wrench set to 500 lbf.ft.
5 Check all valves in the vessel are closed.
6 Connect barocel pressure line to the vessel, open one of the ambient valves in the vessel (located in the front door) and record ambient pressure, temperature and humidity.
7 Close the ambient valve and evacuate the vessel to 200 mbar. Allow pressure to settle. If pressure does not settle a special procedure is required to check for leak sources and the test should be abandoned if the leak is not found.
8 Fill the vessel with the required test gas to reach the required concentration using the partial pressure method.
9 Fill the vessel with air such that the gas/air mixture reaches atmospheric conditions (typically 1013.3 mbar).
10 Disconnect barocel pressure line.
11 Connect ignition lead and power spark box.
12 Check the test room is clear of people and leave test room.
13 Set time delay sequence in sequence generator
14 RUN and ARM data logger
15 Activate sequence in sequence generator (pressing START)
16 Reset sequence generator and save data.
17 Enter test room and disconnect ignition lead and power to spark box.
18 Perform oxygen gas analysis.
19 Purge the system:
    a. Turn on vacuum pump;
    b. Open evacuating valve;
    c. After two minutes open ambient valve in the vessel for combustion gas and clean air mixing under vacuum (no combustion gases can be discharged into the test room);
    d. After 10-15 minutes, stop vacuum pump.
20 Open the explosion vessel door.
21 Check data results.
22 Inspect explosion vessel and equipment.

APPENDIX B

Calculations of the Furniture Volume

Table B-1 Furniture layout 1 (tests 8 – 11)

Item No.	Description	Model Used	Volume Item (m^3)	No. Items	Total Volume (m^3)
1	Tall Lamp				
	Lamp shade	Total cone	0.010497		
		Small cone	0.001416		
		Vol frustum	0.009081		
		Vol stand	0.000100		
		Total volume (ign base)	**0.009181**	**1**	**0.009181**
2	Kitchen table chair	Seat	0.004725		
		Back rest	0.003150		
		Legs	0.001350		
		Back rest supports	0.000675		
		Total volume	**0.009900**	**4**	**0.039600**
3	Kitchen table	Table top	0.022500		
		Legs	0.008250		
		Total volume	**0.030750**	**1**	**0.030750**
4	Glasses (tumblers 35cl)	**Total volume**	**0.000350**	**5**	**0.001750**
5	Vase & flowers	Cylinder	**0.014451**	**1**	**0.014451**
6	Sofa	Rectangle 1 (seat)	0.475200		
		Sides	0.234000		
		Back	0.540000		
		Total volume	**1.249200**	**1**	**1.249200**
7	Small table	Table top	0.004230		
		Legs	0.001500		
		Total volume	**0.005730**	**1**	**0.005730**
8	Picture frame	**Total volume**	**0.000375**	**1**	**0.000375**
9	Small lamp	Total cone	0.004562		
		Small cone	0.000003		
		Vol frustum	0.004558		
		Vol stand	0.001810		
		Total Volume	**0.006368**	**1**	**0.006368**
10	Armchair	Rectangle 1 (seat)	0.224400		
		Sides	0.234000		

Item No.	Description	Model Used	Volume Item (m^3)	No. Items	Total Volume (m^3)
		Back	0.255000		
		Total volume	**0.713400**	**1**	**0.713400**
11	Small table	Table top	0.007600		
		Legs	0.000860		
		Total volume	**0.008460**	**1**	**0.008460**
12	Stereo	Stereo	0.033300		
		Speakers	0.014040		
		Total volume	**0.047340**	**1**	**0.047340**
13	Flower table	Table top	0.010925		
		Legs	0.000700		
		Total volume	**0.011625**	**1**	**0.011625**
14	Glasses (15cl)	**Total volume**	**0.000150**	**3**	**0.000450**
15	Vase	Cylinder	**0.004712**	**1**	**0.004712**
16	Fire surround	Rectangle	**0.163200**	**1**	**0.163200**
17	small lamp	Total cone	0.007548		
		Small cone	0.000825		
		Vol frustum	0.006723		
		Vol stand	0.000126		
		Total Volume(ign base)	**0.006849**	**1**	**0.006849**
18	Small clock	Rectangle	0.001105	1	0.001105
19	Vase	Cylinder	0.004712	1	0.004712
20	stereo cabinet	Rectangle	0.048298		
	drawers	Rectangle	0.031668		
		Total volume	**0.079966**	**1**	**0.079966**
21	Armchair	Rectangle 1 (seat)	0.224400		
		Sides	0.234000		
		Back	0.255000		
		Total volume	**0.713400**	**1**	**0.713400**
22	TV	Rectangle	0.196365	1	0.196365
	Room	**Total volume**			**3.3 m^3**
		Chamber volume			**68 m^3**
		Volume blockage			**5%**

Table B-2 Furniture layout 2 (test 12)

Item No.	Description	Model Used	Volume Item (m^3)	No. Items	Total Volume (m^3)
1	Tall Lamp				
	Lamp shade	Total cone	0.010497		
		Small cone	0.001416		
		Vol frustum	0.009081		
		Vol stand	0.000100		
		Total volume (ign base)	**0.009181**	**1**	**0.009181**
2	Kitchen table chair	Seat	0.004725		
		Back rest	0.003150		
		Legs	0.001350		
		Back rest supports	0.000675		
		Total volume	**0.009900**	**4**	**0.039600**
3	Kitchen table	Table top	0.022500		
		Legs	0.008250		
		Total volume	**0.030750**	**1**	**0.030750**
4	Glasses (tumblers 35cl)	**Total volume**	**0.000350**	**5**	**0.001750**
5	Vase & flowers	Cylinder	**0.014451**	**1**	**0.014451**
6	Sofa	Rectangle 1 (seat)	0.475200		
		Sides	0.234000		
		Back	0.540000		
		Total volume	**1.249200**	**1**	**1.249200**
8	Picture frame	**Total volume**	**0.000375**	**1**	**0.000375**
9	Small lamp	Total cone	0.004562		
		Small cone	0.000003		
		Vol frustum	0.004558		
		Vol stand	0.001810		
		Total Volume	**0.006368**	**1**	**0.006368**
12	Stereo	Stereo	0.033300		
		Speakers	0.014040		
		Total volume	**0.047340**	**1**	**0.047340**
13	Flower table	Table top	0.010925		
		Legs	0.000700		
		Total volume	**0.011625**	**1**	**0.011625**
14	Glasses (15cl)	**Total volume**	**0.000150**	**3**	**0.000450**
15	Vase	Cylinder	**0.004712**	**1**	**0.004712**
16	Fire surround	Rectangle	**0.163200**	**1**	**0.163200**
17	small lamp	Total cone	0.007548		
		Small cone	0.000825		

Item No.	Description	Model Used	Volume Item (m^3)	No. Items	Total Volume (m^3)
		Vol frustum	0.006723		
		Vol stand	0.000126		
		Total Volume (ign base)	**0.006849**	**1**	**0.006849**
18	Small clock	Rectangle	0.001105	1	0.001105
19	Vase	Cylinder	0.004712	1	0.004712
20	stereo cabinet	Rectangle	0.048298		
	drawers	Rectangle	0.031668		
		Total volume	**0.079966**	**1**	**0.079966**
22	TV	Rectangle	0.196365	1	0.196365
	Room	**Total volume**			**1.9 m^3**
		Chamber volume			**68 m^3**
		Volume blockage			**3%**

Table B-3 Furniture layout 3 (test 13)

Item No.	Description	Model Used	Volume Item (m^3)	No. Items	Total Volume (m^3)
1	Tall Lamp				
	Lamp shade	Total cone	0.010497		
		Small cone	0.001416		
		Vol frustum	0.009081		
		Vol stand	0.000100		
		Total volume (ign base)	**0.009181**	**1**	**0.009181**
2	Kitchen table chair	Seat	0.004725		
		Back rest	0.003150		
		Legs	0.001350		
		Back rest supports	0.000675		
		Total volume	**0.009900**	**4**	**0.039600**
3	Kitchen table	Table top	0.022500		
		Legs	0.008250		
		Total volume	**0.030750**	**1**	**0.030750**
4	Glasses (tumblers 35cl)	**Total volume**	**0.000350**	**5**	**0.001750**
5	Vase & flowers	Cylinder	**0.014451**	**1**	**0.014451**
6	Sofa	Rectangle 1 (seat)	0.475200		
		Sides	0.234000		
		Back	0.540000		
		Total volume	**1.249200**	**1**	**1.249200**
8	Picture frame	**Total volume**	**0.000375**	**1**	**0.000375**
9	Small lamp	Total cone	0.004562		
		Small cone	0.000003		
		Vol frustum	0.004558		
		Vol stand	0.001810		
10	Armchair	Rectangle 1 (seat)	0.135000		
		Sides	0.432000		
		Back	0.216000		
		Total volume	**0.783000**	**2**	**1.566000**
11	Small table	Table top	0.007600		
		Legs	0.000860		
		Total volume	**0.008460**	**1**	**0.008460**
12	Stereo	Stereo	0.033300		
		Speakers	0.014040		
		Total volume	**0.047340**	**1**	**0.047340**
13	Flower table	Table top	0.010925		
		Legs	0.000700		

Item No.	Description	Model Used	Volume Item (m^3)	No. Items	Total Volume (m^3)
		Total volume	**0.011625**	**1**	**0.011625**
14	Glasses (15cl)	**Total volume**	**0.000150**	**3**	**0.000450**
15	Vase	Cylinder	**0.004712**	**1**	**0.004712**
16	Fire surround	Rectangle	**0.163200**	**1**	**0.163200**
17	small lamp	Total cone	0.007548		
		Small cone	0.000825		
		Vol frustum	0.006723		
		Vol stand	0.000126		
		Total Volume (ign base)	**0.006849**	**1**	**0.006849**
18	Small clock	Rectangle	0.001105	1	0.001105
19	Vase	Cylinder	0.004712	1	0.004712
20	stereo cabinet	Rectangle	0.048298		
	drawers	Rectangle	0.031668		
		Total volume	**0.079966**	**1**	**0.079966**
22	TV	Rectangle	0.196365	1	0.196365
22	Sideboard	model as rectangle	0.356250	1	0.356250
23	Book case	model as rectangle	0.197400	1	0.197400
24	Tall glass unit	model as two rectangles	0.900852	1	0.900852
25	Single wooden unit	model as rectangle	0.162000	1	0.162000
26	Single glass unit	model as rectangle	0.119070	1	0.119070
27	Single floor unit	model as rectangle	0.069540	1	0.069540
	Room	**Total volume**			**5.2 m^3**
		Chamber volume			**68 m^3**
		Volume blockage			**8%**

Table B-4 Furniture layout 4 (test 14 - 17)

Item No.	Description	Model Used	Volume Item (m^3)	No. Items	Total Volume (m^3)
1	Tall Lamp				
	Lamp shade	Total cone	0.010497		
		Small cone	0.001416		
		Vol frustum	0.009081		
		Vol stand	0.000100		
		Total volume (ign base)	**0.009181**	**1**	**0.009181**
2	Kitchen table chair	Seat	0.004725		
		Back rest	0.003150		
		Legs	0.001350		
		Back rest supports	0.000675		
		Total volume	**0.009900**	**4**	**0.039600**
3	Kitchen table	Table top	0.022500		
		Legs	0.008250		
		Total volume	**0.030750**	**1**	**0.030750**
4	Glasses (tumblers 35cl)	**Total volume**	**0.000350**	**5**	**0.001750**
5	Vase & flowers	Cylinder	**0.014451**	**1**	**0.014451**
6	Sofa	Rectangle 1 (seat)	0.515625		
		Sides	0.450000		
		Back	0.375000		
		Total volume	**1.340625**	**1**	**1.340625**
8	Picture frame	**Total volume**	**0.000375**	**1**	**0.000375**
9	Small lamp	Total cone	0.004562		
		Small cone	0.000003		
		Vol frustum	0.004558		
		Vol stand	0.001810		
		Total Volume (ign base)	**0.006849**	**1**	**0.006849**
10	Armchair	Rectangle 1 (seat)	0.135000		
		Sides	0.432000		
		Back	0.216000		
		Total volume	**0.783000**	**2**	**1.566000**
11	Small table	Table top	0.007600		
		Legs	0.000860		
		Total volume	**0.008460**	**1**	**0.008460**
12	Stereo	Stereo	0.033300		
		Speakers	0.014040		
		Total volume	**0.047340**	**1**	**0.047340**

Item No.	Description	Model Used	Volume Item (m^3)	No. Items	Total Volume (m^3)
14	Glasses (15cl)	**Total volume**	**0.000150**	**3**	**0.000450**
15	Vase	Cylinder	**0.004712**	**1**	**0.004712**
16	Fire surround	Rectangle	**0.163200**	**1**	**0.163200**
17	small lamp	Total cone	0.007548		
		Small cone	0.000825		
		Vol frustum	0.006723		
		Vol stand	0.000126		
		Total Volume (ign base)	**0.006849**	**1**	**0.006849**
18	Small clock	Rectangle	0.001105	1	0.001105
19	Vase	Cylinder	0.004712	1	0.004712
20	stereo cabinet	Rectangle	0.048298		
	drawers	Rectangle	0.031668		
		Total volume	**0.079966**	**1**	**0.079966**
22	TV	Rectangle	0.196365	1	0.196365
22	Sideboard	model as rectangle	0.356250	1	0.356250
24	Tall glass unit	model as rectangle	0.391140	1	0.391140
25	Single wooden unit	model as rectangle	0.162000	1	0.162000
26	Single glass unit	model as rectangle	0.119070	1	0.119070
27	Single floor unit	model as rectangle	0.069540	1	0.069540
	Room	**Total volume**			**5 m^3**
		Chamber volume			**68 m^3**
		Volume blockage			**7%**

Table B-5 Effective Furniture layout 1 (tests 8 – 11)

Item No.	Description	Model Used	Volume Item (m^3)	No. Items	Total Volume (m^3)
2	Kitchen table chair	seat	0.004725		
		back rest	0.003150		
		legs	0.001350		
		back rest supports	0.000675		
		Total Volume	**0.009900**	**4**	**0.039600**
6	Kitchen table	tabletop	0.022500		
		legs	0.008250		
		Total volume	**0.030750**	**1**	**0.030750**
7	Glasses (tumblers 35cl)	**Total volume**	**0.000350**	**5**	**0.001750**
8	Vase & flowers	**model as cylinder**	**0.014451**	**1**	**0.014451**
9	Sofa	Rectangle 1 (seat)	0.475200		
		Sides	0.234000		
		Back	0.540000		
		Total volume	**1.249200**	**1**	**1.249200**
13	Armchair	Rectangle 1 (seat)	0.224400		
		Sides	0.234000		
		Back	0.255000		
		Total volume	**0.713400**	**1**	**0.713400**
16	Flower table	tabletop	0.010925		
		legs	0.000700		
		Total volume	**0.011625**	**1**	**0.011625**
17	Glasses (15cl)	**Total volume**	**0.000150**	**3**	**0.000450**
18	Vase	**model as cylinder**	**0.004712**	**1**	**0.004712**
24	Armchair	Rectangle 1 (seat)	0.224400		
		Sides	0.234000		
		Back	0.255000		
		Total volume	**0.713400**	**1**	**0.713400**
25	TV	**model as rectangle**	**0.196365**	**1**	**0.196365**
	Room	**Total volume**			**3.0 m^3**
		Vessel volume			**68 m^3**
		Effective volume blockage			**4%**

Table B-6 Effective Furniture layout 2 (test 12)

Item No.	Description	Model Used	Volume Item (m^3)	No. Items	Total Volume (m^3)
2	Kitchen table chair	seat	0.004725		
		back rest	0.003150		
		legs	0.001350		
		back rest supports	0.000675		
		Total Volume	0.009900	4	0.039600
6	Kitchen table	tabletop	0.022500		
		legs	0.008250		
		Total volume	0.030750	1	0.030750
7	Glasses (tumblers 35cl)	Total volume	0.000350	5	0.001750
8	Vase & flowers	model as cylinder	0.014451	1	0.014451
9	Sofa	Rectangle 1 (seat)	0.475200		
		Sides	0.234000		
		Back	0.540000		
		Total volume	1.249200	1	1.249200
16	Flower table	tabletop	0.010925		
		legs	0.000700		
		Total volume	0.011625	1	0.011625
17	Glasses (15cl)	Total volume	0.000150	3	0.000450
18	Vase	model as cylinder	0.004712	1	0.004712
25	TV	model as rectangle	0.196365	1	0.196365
	Room	Total volume			1.5 m^3
		Vessel volume			68 m^3
		Effective volume blockage			2%

Table B-7 Effective Furniture layout 3 (test 13)

Item No.	Description	Model Used	Volume Item (m^3)	No. Items	Total Volume (m^3)
2	Kitchen table chair	seat	0.004725		
		back rest	0.003150		
		legs	0.001350		
		back rest supports	0.000675		
		Total Volume	0.009900	4	0.039600
6	Kitchen table	tabletop	0.022500		
		legs	0.008250		
		Total volume	0.030750	1	0.030750
7	Glasses (tumblers 35cl)	Total volume	0.000350	5	0.001750
8	Vase & flowers	model as cylinder	0.014451	1	0.014451
9	Sofa	Rectangle 1 (seat)	0.475200		
		Sides	0.234000		
		Back	0.540000		
		Total volume	1.249200	1	1.249200
13	Armchair	Rectangle 1 (seat)	0.135000		
		Sides	0.432000		
		Back	0.216000		
		Total volume	0.783000	2	1.566000
16	Flower table	tabletop	0.010925		
		legs	0.000700		
		Total volume	0.011625	1	0.011625
17	Glasses (15cl)	Total volume	0.000150	3	0.000450
18	Vase	model as cylinder	0.004712	1	0.004712
25	TV	model as rectangle	0.196365	1	0.196365
	Room	Total volume			3.1 m^3
		Vessel volume			68 m^3
		Effective volume blockage			5%

Table B-8 Effective Furniture layout 4 (tests 14 - 17)

Item No.	Description	Model Used	Volume Item (m^3)	No. Items	Total Volume (m^3)
2	Kitchen table chair	seat	0.004725		
		back rest	0.003150		
		legs	0.001350		
		back rest supports	0.000675		
		Total Volume	0.009900	4	0.039600
6	Kitchen table	tabletop	0.022500		
		legs	0.008250		
		Total volume	0.030750	1	0.030750
7	Glasses (tumblers 35cl)	Total volume	0.000350	5	0.001750
8	Vase & flowers	model as cylinder	0.014451	1	0.014451
13	Armchair	Rectangle 1 (seat)	0.135000		
		Sides	0.432000		
		Back	0.216000		
		Total volume	0.783000	2	1.566000
25	TV	model as rectangle	0.196365	1	0.196365
		Total volume			2 m^3
		Vessel volume			68 m^3
		Volume blockage			3%